

# Macro-ion Characterization



ACS SYMPOSIUM SERIES 548

# Macro-ion Characterization

## From Dilute Solutions to Complex Fluids

**Kenneth S. Schmitz**, EDITOR  
*University of Missouri—Kansas City*

Developed from a symposium sponsored  
by the Divisions of Polymer Chemistry, Inc.,  
and Colloid and Surface Chemistry  
at the 205th National Meeting  
of the American Chemical Society,  
Denver, Colorado,  
March 28–April 2, 1993



American Chemical Society, Washington, DC 1994

In Macro-ion Characterization; Schmitz, K.;  
ACS Symposium Series; American Chemical Society: Washington, DC, 1993.



## Library of Congress Cataloging-in-Publication Data

Macro-ion characterization: from dilute solutions to complex fluids /  
Kenneth S. Schmitz, editor.

p. cm.—(ACS symposium series, ISSN 0097-6156; 548)

“Developed from a symposium sponsored by the divisions of Polymer Chemistry, Inc., and Colloid and Surface Chemistry at the 205th National Meeting of the American Chemical Society, Denver, Colorado, March 28–April 2, 1993.”

Includes bibliographic references and index.


ISBN 0-8412-2770-5

1. Polyelectrolytes—Congresses.

I. Schmitz, Kenneth S., 1943— . II. American Chemical Society.  
Division of Polymer Chemistry. III. American Chemical Society.  
Division of Colloid and Surface Chemistry. IV. Series.

QD382.P64M33 1994  
547.7'04572—dc20

93-39732  
CIP

The paper used in this publication meets the minimum requirements of American National Standard for Information Sciences—Permanence of Paper for Printed Library Materials, ANSI Z39.48-1984. 

Copyright © 1994

American Chemical Society

All Rights Reserved. The appearance of the code at the bottom of the first page of each chapter in this volume indicates the copyright owner's consent that reprographic copies of the chapter may be made for personal or internal use or for the personal or internal use of specific clients. This consent is given on the condition, however, that the copier pay the stated per-copy fee through the Copyright Clearance Center, Inc., 27 Congress Street, Salem, MA 01970, for copying beyond that permitted by Sections 107 or 108 of the U.S. Copyright Law. This consent does not extend to copying or transmission by any means—graphic or electronic—for any other purpose, such as for general distribution, for advertising or promotional purposes, for creating a new collective work, for resale, or for information storage and retrieval systems. The copying fee for each chapter is indicated in the code at the bottom of the first page of the chapter.

The citation of trade names and/or names of manufacturers in this publication is not to be construed as an endorsement or as approval by ACS of the commercial products or services referenced herein; nor should the mere reference herein to any drawing, specification, chemical process, or other data be regarded as a license or as a conveyance of any right or permission to the holder, reader, or any other person or corporation, to manufacture, reproduce, use, or sell any patented invention or copyrighted work that may in any way be related thereto. Registered names, trademarks, etc., used in this publication, even without specific indication thereof, are not to be considered unprotected by law.

PRINTED IN THE UNITED STATES OF AMERICA

**American Chemical  
Society Library**  
9155 16th St., N.W.  
Washington, D.C. 20036

# 1993 Advisory Board

## ACS Symposium Series

M. Joan Comstock, *Series Editor*

- |   |   |
|---|---|
| V. Dean Adams<br>University of Nevada—<br>Reno                | Bonnie Lawlor<br>Institute for Scientific Information                         |
| Robert J. Alaimo<br>Procter & Gamble<br>Pharmaceuticals, Inc. | Douglas R. Lloyd<br>The University of Texas at Austin                         |
| Mark Arnold<br>University of Iowa                             | Robert McGorin<br>Kraft General Foods   |
| David Baker<br>University of Tennessee                        | Julius J. Menn<br>Plant Sciences Institute,<br>U.S. Department of Agriculture |
| Arindam Bose<br>Pfizer Central Research                       | Vincent Pecoraro<br>University of Michigan                                    |
| Robert F. Brady, Jr.<br>Naval Research Laboratory             | Marshall Phillips<br>Delmont Laboratories                                     |
| Margaret A. Cavanaugh<br>National Science Foundation          | George W. Roberts<br>North Carolina State University                          |
| Dennis W. Hess<br>Lehigh University                           | A. Truman Schwartz<br>Macalaster College                                      |
| Hiroshi Ito<br>IBM Almaden Research Center                    | John R. Shapley<br>University of Illinois<br>at Urbana–Champaign              |
| Madeleine M. Joullie<br>University of Pennsylvania            | L. Somasundaram<br>DuPont   |
| Gretchen S. Kohl<br>Dow-Corning Corporation                   | Peter Willett<br>University of Sheffield (England)                            |

# Foreword

THE ACS SYMPOSIUM SERIES was first published in 1974 to provide a mechanism for publishing symposia quickly in book form. The purpose of this series is to publish comprehensive books developed from symposia, which are usually “snapshots in time” of the current research being done on a topic, plus some review material on the topic. For this reason, it is necessary that the papers be published as quickly as possible.

Before a symposium-based book is put under contract, the proposed table of contents is reviewed for appropriateness to the topic and for comprehensiveness of the collection. Some papers are excluded at this point, and others are added to round out the scope of the volume. In addition, a draft of each paper is peer-reviewed prior to final acceptance or rejection. This anonymous review process is supervised by the organizer(s) of the symposium, who become the editor(s) of the book. The authors then revise their papers according to the recommendations of both the reviewers and the editors, prepare camera-ready copy, and submit the final papers to the editors, who check that all necessary revisions have been made.

As a rule, only original research papers and original review papers are included in the volumes. Verbatim reproductions of previously published papers are not accepted.

*M. Joan Comstock*  
Series Editor

# Preface

**POLYELECTROLYTES** remain one of the least-understood states of condensed matter, in contrast to neutral polymer solutions. Although bulk properties like osmotic pressure and viscosity have been studied for many years, an understanding of the behavior of polyelectrolytes is lacking. This problem is especially critical because of the fundamental importance of many of the prototypical polyelectrolytes such as, for example, DNA.

Few meetings have focused on polyelectrolytes since the NATO meeting two decades ago. Consequently, the response to the symposium on which this book is based was overwhelming. The participants represented a scientific diversity that covered both theory and experiment, from synthesis to physical properties in (and of) gels, and from nonperturbative methods to the application of external electric fields. The backgrounds of the participants spanned academia and industry; synthetic polymers and biopolymers; and the departments of physics, chemistry, polymers, material sciences, and biological sciences. The participants came from all parts of the world.

The chapters are divided into six major subject areas: theory, synthesis and characterization, condensation and complexation, solution structure, surface adsorption and interfaces, and gels. The objective in making these classifications was to proceed from the more fundamental and simplest cases to the most complex system, with respect both to the organization of the major headings and also to the ordering of the chapters within these sections. The chapters describe a wide variety of techniques as applied to the understanding of these complex systems.

## Acknowledgments

Paul Dubin and Ray Farinato put in a tremendous effort in originating and organizing the symposium on which this book is based. I also acknowledge the cooperation of everyone involved in bringing this volume into existence, including the authors, the reviewers, and the people at the American Chemical Society Books Department. I give special thanks to Anne Wilson, whose electronic-mail messages were inspirational. I also thank Julie Fisher for designing and drawing the roller coaster illustration in Chapter 1. Finally, I acknowledge those who were also influential in

the organization of this volume: Candace, wherever she may be; Julie Fisher, for her courage; and DAX, may his principles survive.

KENNETH S. SCHMITZ  
Department of Chemistry  
University of Missouri  
Kansas City, MO 64110

August 6, 1993



# Chapter 1

## An Overview of Polyelectrolytes

Six Topics in Search of an Author

Kenneth S. Schmitz

Department of Chemistry, University of Missouri—Kansas City,  
Kansas City, MO 64110

Interests in solutions and suspension of macroions has been renewed in the past few years, as evidenced by the mini symposium upon which this present volume is based. Presented in this introductory chapter is a brief presentation of a selection of six topics that I believe deserves further consideration regarding these complex systems: 1) the definition of the screening parameter; 2) the mathematical form of the pairwise electrostatic energy between macroions; 3) the phenomenon of counterion condensation and its application to specific molecular geometry; 4) the use of the Gibbs versus the Helmholtz free energy in describing the thermodynamics of these charged systems; 5) the calculation of the electrostatic component to the persistence length of flexible polyions; and 6) the splitting of relaxation modes as detected by dynamic light scattering measurements.

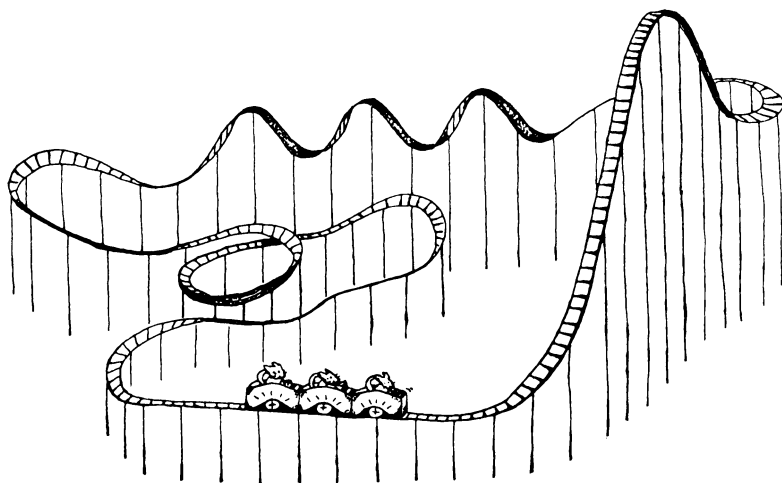
Studying polyelectrolytes is like taking a roller coaster ride. In the beginning one knows nothing about the field and therefore faces a steep upward learning curve. At some point one reaches a degree of understanding of the field and begins to publish the new results. Further investigations into the field have their ups and downs, sometimes even being thrown for a loop when unexpected results are obtained. Eventually, however, the excursion through the field of polyelectrolytes returns one to the starting point. To illustrate the above metaphor one only has to follow the history of a simple basic question: "Is the interaction between the charged macroions attractive or repulsive?"

In 1938 Langmuir treated a solution of micelles in a manner similar to that of a simple salt crystal. He thus considered the counterions between the micelles as part of the interaction energy, which led to a major result (*I*):

The interaction of these charges, just as in the sodium chloride crystal, gives an excess of attractive force and in order to have equilibrium it will be necessary not to have an additional *attractive* force, such as the van der Waals force postulated by Hamaker, but some new kind of *repulsive* force.

In contrast to the conclusion of Langmuir, the currently accepted paradigm for the majority of the practitioners in the colloid field is the DLVO (Derjaguin-Landau-

0097-6156/94/0548-0001\$06.50/0  
© 1994 American Chemical Society



Verwey-Overbeek) model (2). The attractive part of the DLVO potential is the van der Waals contribution that becomes significant at relatively close distances, viz., less than 20 Å. The repulsive part of the DLVO potential is a pairwise screened Coulomb interaction between two colloidal particles of radius  $R_S$  and charge  $q_p = Z_p q_e$  ( $q_e$  is the magnitude of the electron charge) separated by a distance  $R$  is,

$$U_{\text{elec}}^{\text{DLVO}} = \left( \frac{e^{\kappa_{\text{DH}} R_S}}{1 + \kappa_{\text{DH}} R_S} \right)^2 \frac{q_p^2}{\epsilon} \frac{e^{-\kappa_{\text{DH}} R}}{R} = X_{\text{DLVO}}^2 \frac{q_p^2}{\epsilon} \frac{e^{-\kappa_{\text{DH}} R}}{R} \quad (1)$$

where the Debye-Hückel screening parameter  $\kappa_{\text{DH}}$  is defined by the m<sub>add</sub> different species of added electrolyte ions at concentrations  $\langle n_j \rangle_u$  [uniform (bulk) concentration in particles/mL] and charge  $Z_j q_e$ ,

$$\kappa_{\text{DH}}^2 = \frac{4\pi q_e^2}{\epsilon k_B T} \sum_{j=1}^{m_{\text{add}}} Z_j^2 \langle n_j \rangle_u = 4\pi \lambda_B \sum_{j=1}^{m_{\text{add}}} Z_j^2 \langle n_j \rangle_u \quad (2)$$

where  $\epsilon$  is the dielectric constant,  $k_B$  is Boltzmann's constant, and  $\lambda_B$  is the Bjerrum length. Note that only the added electrolyte ions contribute to the screening parameter in the DLVO theory as in the Debye-Hückel theory of simple salts, which is why the subscript "DH" is include in equation 2. The reason for the apparent universal acceptance of the DLVO potential lies in its qualitative success in explaining most phenomena in colloidal systems even though the apparent charge required to fit the data is generally smaller than the anticipated value of the charge based on the chemical composition of the macroion.

For more than two decades, however, Ise and co-workers (3-10) have emphasized that there exists some form of long range attractive interaction between macroions that is not consistent with the standard DLVO potential. More specifically, video movies taken through an ultramicroscope clearly showed two distinct regions in a suspension of latex particles; a highly kinetic region in which the particles undergo Brownian motion, and a relatively static ordered region (5, 9) which has embedded regions of stable voids (9). Sogami and Ise (11) thus developed a model based on the Gibbs free energy that exhibited a stable minimum at macroion separation distances

on the order of several thousand angstroms, as experimentally observed. Overbeek (12), however, criticized this model on the basis that the electrical contribution of the solvent exactly canceled the term  $\kappa_{\text{DH}}^2(\partial A/\partial\kappa_{\text{DH}}^2)_{\text{V,T,Z}}$  that gave rise to the minimum in the Sogami-Ise potential, where  $A$  is the Helmholtz free energy. From the Gibbs-Duhem relationship Overbeek (12) derived the solvent contribution,

$$\langle n_o \rangle_u \left[ \frac{\partial A}{\partial \langle n_o \rangle_u} \right]_{\text{V,T,Z}} = -\kappa_{\text{DH}}^2 \left[ \frac{\partial A}{\partial \kappa_{\text{DH}}^2} \right]_{\text{V,T,Z}} \quad (3)$$

where  $\langle n_o \rangle_u$  is the uniform distribution of the solvent. Overbeek thus concluded:

The claim in Sogami's and Ise's papers that  $\text{Ge}^{\text{I}}$  leads to an attraction between particles is incorrect. The experimental data presented in papers 1 through 7 and in other similar publications will have to be explained in a different manner.

This conclusion is thus diametrically opposite of the conclusion of Langmuir as to whether an additional attractive or repulsive force, respectively, must be postulated to explain the stability of colloidal systems.

The story does not end here, however. Ise and co-workers (10) point out in a footnote that Overbeek misapplied the Gibbs-Duhem expression by *not also including the macroion contribution*. Citing Verwey and Overbeek (2) in regard to the specific terms that comprise the electrical contribution in the DLVO theory, Smalley (13) points out that the Overbeek solvent correction likewise cancels the electrical contribution to the DLVO potential. Smalley thus concluded that in the DLVO theory with the solvent term (13):

there is *no* energy associated with the electrical double layers.

Since experimental data clearly establishes that there are electrical interactions between charged particles in solution and colloidal suspension one must conclude from the symmetric application of the solvent contribution term of Overbeek to both the DLVO and SI potentials that either the DLVO theory is wrong or that the nature of the electrical interaction between charge macroions under the most dilute conditions is not well understood.

It may be suggested from the previous paragraph that we appear to have returned to the beginning of the roller coaster ride, i.e., knowing nothing about the fundamental interactions between macroions in these complex systems. This statement is not entirely true, however, since certain concepts have been developed towards the understanding the basic nature of macroionic systems. The illusion of truth in that sentence, however, is manifested in the literature by varying usage of these concepts in the description of the asymmetrically charged systems of polyions and simple salts. The following few paragraphs address some of these problems, with the intent to stimulate further discussion on these matters and not to resolve their differences.

### The Screening Parameter

The most fundamental concept in systems of charged particles is the screening parameter, generically denoted by the symbol  $\kappa$ . In the Debye-Hückel theory of simple electrolytes  $\kappa$  is defined in terms of all of the electrolyte species present since only one of the ions is selected as the "test" ion.

**Definition of the Screening Parameter in Macroionic Systems.** In macroionic systems the contribution of the macroions and associated counterions are not included

in the DLVO theory, where the screening length as defined by equation 2. The justification for the omission of the macroion and associated counterion contributions is that the concentration of these components is sufficiently small that they can be ignored. This result is clearly indicated in the mean spherical approximation (MAS) to the Ornstein-Zernike equation, as shown for example by Median-Noyola and McQuarrie (14). In the coupled mode theory of Lin, Lee, and Schurr (15), however, the total screening parameter naturally results from the solution to the cubic secular equation for the polyion-added electrolyte system, viz.,

$$\kappa_{\text{tot}}^2 = 4\pi\lambda_B \left( Z_1^2 \langle n_1 \rangle_u + Z_2^2 \langle n_2 \rangle_u + Z_3^2 \langle n_3 \rangle_u \right) \quad (4)$$

where the polyion, counterion, and coion are denoted by 1, 2, and 3, respectively, and the electroneutrality constraint is employed,

$$\langle n_2 \rangle_u = - \frac{Z_1 \langle n_1 \rangle_u + Z_3 \langle n_3 \rangle_u}{Z_2} \quad (5)$$

There is a third definition of the screening parameter that is intermediate between those defined by equations 2 and 4 and employed, for example, by Beresford-Smith and coworkers (16) and by Belloni (17). In this definition the counterions from the macroion are included in the concentration of the common ion from the added electrolyte but the contribution of the macroion is omitted, viz.,

$$\kappa_{\text{interm}}^2 = 4\pi\lambda_B \left[ Z_2^2 \left( \langle n_{2,\text{add}} \rangle_u + |Z_1| \langle n_1 \rangle_u \right) + Z_3^2 \langle n_3 \rangle_u \right] \quad (6)$$

The consequences of the choice of the screening parameter are discussed in more detail in the section of interaction potentials.

**"Global" and "Local" Screening Parameters.** The screening parameters defined by equations 2, 4, and 6 may be referred to as "global" values since they are a function of the uniform concentrations of the ions. The electrolyte ions, however, are not uniformly distributed throughout the solution. The distribution of electrolyte ions about a polyion, however, is strongly dependent upon the magnitude and distribution of surface charge of the polyion. Counterions are preferentially drawn to the vicinity of the polyion whereas coions are repelled from this region. For the Boltzmann distribution is easily shown that in the limit of weak polyion charge that the excess number of counterions exactly cancels the deficit number of coions and the screening parameter (for symmetric electrolyte ions) truly takes on a "global" character.

In their cell model for the electrolyte ion distribution about a charged cylinder, Alexandrowicz and Katchalsky (18) partitioned the problem into two regions. The "inner region" was assumed to contain only the counterions since it was presumed that the high charge density prohibited the coions from accumulating in significant concentrations. The solution to the Poisson equation thus employed only the local concentration of counterions at this boundary. Because of symmetry the upper limit of the "outer region" was defined at the mid-distance between the aligned rods. The linearized Debye-Hückel solution to the Poisson equation was assumed to be valid in this region, where the counterion concentration was necessarily larger than the coion concentration. Russel (19) pointed out that the parallel aligned cylinders in the Alexandrowicz and Katchalsky calculation was not realistic, and that at the outer boundary should be defined by the thickness of the ion cloud. Hence the periodic boundary conditions were replaced with a random distribution of neighboring macroions. The Alexandrowicz - Katchalsky model in the cylindrical system therefore set a precedence to the assumption of "local screening parameters" in the Sogami-Ise (11) and Sogami (20) theories for the interaction between charged spheres. It has also been proposed that the local screening parameter for the

interaction between discrete charges on a cylinder be computed as a "linear average" of the relative concentrations of "inner" (sheath) and "outer" (bulk) counterion concentrations (21).

**Comments on Screened Electrical Interactions.** There is a universal agreement that electrical interactions between charged particles are screened. The screening of interactions between two macroions originates from the principle that the electrolyte ions are mobile in the solution or suspension. Because of the complexity of the many-body problem, however, the computations generally involve only three particles, viz., the two particles of interest at a fixed separation distance while the integration is carried out over the coordinates of a mobile third particle. Hence both the correlations between the mobile particles and the contributions of the other macroions are neglected. A more focused study of electrolyte correlations and distributions about the macroions and the resulting effects on the macroion-macroion interactions should be initiated. These results could then be compared with the results of the *ad hoc* operational definitions of the screening parameter.

### Pairwise Electrostatic Energy Between Macroions

Introduced in this section are selected forms of the pairwise electrostatic interaction potential between two identical macroions. Those given in the first subsection are based on the electrostatic Helmholtz free energy, and the second subsection presents the Sogami-Ise result (11) based on the Gibbs free energy. The discussion regarding the use of the Helmholtz or the Gibbs free energy depends upon concepts related to counterion condensation given in the following section. Hence the Helmholtz versus Gibbs free energy is postponed until then.

**Helmholtz Free Energy.** Since the screening parameter in the DLVO potential is dependent only on the concentration of added electrolyte and independent of the macroion charge and concentration, the DLVO potential is said to be a "true" pairwise interaction potential. That is, the value of  $U_{\text{elec}}^{\text{DLVO}}$  is independent of the polyion concentration. In contrast other pairwise interaction potentials presented herein are dependent upon the polyion concentration.

Using the "Jellum Approximation" of uniformly distributed spherical macroions, Beresford-Smith, Chan, and Mitchell (16) obtained the pairwise interaction potential,

$$U_{\text{elec}}^{\text{BSCM}} = \left[ \frac{e^y(1 + \phi_1)}{1 + y} \right]^2 \frac{q_1^2 e^{-\kappa_{\text{interm}}R}}{\epsilon R} = X_{\text{BSCM}}^2 \frac{q_1^2 e^{-\kappa_{\text{interm}}R}}{\epsilon R} \quad (7)$$

where  $\phi_1$  is the volume fraction of the polyion,  $y = \kappa_{\text{interm}}R_S$ , and  $\kappa_{\text{interm}}$  is defined by equation 6. Note that at fixed R increasing the concentration of the polyion the potential in equation 7 becomes more repulsive than in the DLVO potential due, primarily, to the differences in the definition of the screening parameter.

Belloni (17) pointed out that the Jellum Approximation was not needed since the MSA solution to the Ornstein-Zernike equation yielded an exact solution for the hard sphere potential. Belloni obtained for the pairwise interaction potential,

$$U_{\text{elec}}^{\text{B}} = X_{\text{B}}^2 \frac{q_1^2 e^{-\kappa_{\text{interm}}R}}{\epsilon R} \quad (8)$$

where

$$X_B = \cosh(y) + [y \cosh(y) - \sinh(y)] \left[ \frac{3\phi_1}{y^3(1-\phi_1)} - \frac{\gamma}{y} \right] \quad (9)$$

and  $\gamma$  is a "screening function" that depends upon  $\phi_1$  and the MSA Coulombic screening parameter whose precise form is of no consequence in this discussion.

Sogami and Ise (11) approached the macroion-electrolyte ion problem on the same footing as the quantum mechanical description of chemical bonding. Using the adiabatic approximation for separation of macroion and electrolyte ion contributions, they expressed the charge density in the Poisson equation as two parts, that which was due to the macroions and that which was due to the electrolyte ions. Hence there was an interdependence of the distribution of both the electrolyte ions and the macroions. They then employed the usual charging procedure as in the DLVO theory and obtained the resulting expression for the Helmholtz interaction potential,

$$U_{\text{elec}}^{\text{SI}} = \left[ \frac{\sinh(y)}{y} \right]^2 \frac{q_1^2 e^{-\kappa_{\text{interm}} R}}{\epsilon R} = X_{\text{SI}}^2 \frac{q_1^2 e^{-\kappa_{\text{interm}} R}}{\epsilon R} \quad (10)$$

Sogami (20) proposed a model based on the linearized Debye-Hückel potential of interaction between two charged spheres with a two-state electrolyte ion distribution. Region I was defined in terms of the macroion and the associated ion cloud of thickness  $\lambda_C$ . The effective radius of the kinetic unit,  $R_S^*$ , is therefore  $R_S + \lambda_C$ . Region II was the solution intermittent to the two kinetic units. Since the kinetic unit was assumed to be charged it followed that for region II,

$$\frac{N_2^{\text{II}} q_2 + N_3^{\text{II}} q_3}{v^{\text{II}}} \neq 0 \quad (11)$$

The value of the screening parameter  $\kappa_{\text{II}}$  was then computed from the number concentrations in equation 11. Sogami then obtained for the interaction potential,

$$U_{\text{elec}}^{\text{S}} = X_{\text{S}}^2 \frac{q_1^2 e^{-\kappa_{\text{II}} R}}{\epsilon R} \quad (12)$$

where

$$X_{\text{S}} = \frac{q_1}{q_1} \left\{ 1 - \frac{q_1 - q_1^*}{q_1^*} \left[ 2 - \frac{1}{4} \left( \frac{N_2^{\text{II}} - N_3^{\text{II}}}{N_2^{\text{II}} + N_3^{\text{II}}} \right) \left( e^{-2\kappa_{\text{II}} R_S^*} - 1 + 2\kappa_{\text{II}} R_S^* - \kappa_{\text{II}} R \right) \right] \right\}^{1/2} \quad (13)$$

and

$$q_1^* = \frac{\sinh(\kappa_{\text{II}} R_S^*)}{\kappa_{\text{II}} R_S^*} (q_1 + N_2^{\text{I}} q_2 + N_3^{\text{I}} q_3) \quad (14)$$

All of the above forms of the Helmholtz electrostatic interaction potential have the Yukawa form [i.e.,  $\exp(-aR)/R$ ] multiplied by a model specific form  $X^2$ . At this stage of discussion only the Sogami model for the Helmholtz electrical interaction potential has the property of exhibiting a minimum. The reason for this minimum is found in the expression for the location of the minimum (20),

$$R_{\min} = \frac{4 \left( \frac{N_2^{\text{II}} + N_3^{\text{II}}}{N_2^{\text{II}} - N_3^{\text{II}}} \right) \left( \frac{3q_1^* - 2q_1}{q_1 - q_1^*} \right) + e^{-2\kappa_{\text{II}}R_S^*} + 2\kappa_{\text{II}}R_S^*}{\kappa_{\text{II}}} \quad (15)$$

It now becomes transparent that the presence of a minimum at finite separation distances is a result of a difference in the counterion and coion concentration in the Region II. Hence the situation is reminiscent of, but not identical to, the Alexandrowicz and Katchalsky (18) model discussed in the previous section. By setting  $N_2^{\text{II}} = N_3^{\text{II}}$  the Sogami potential reduces to the same form of the DLVO potential with the location of the minimum at infinity. This transformation is thus similar in concept to the transformation from the Alexandrowicz-Katchalsky model (18) to the model of Russel (19) for charged cylinders.

**Gibbs Free Energy.** Sogami and Ise (11) proposed a theory of the interaction potential between two macroions based on the Gibbs free energy. The interaction potential is obtained from equation 10 using the operator  $2 + \kappa^2(\partial/\partial\kappa^2)$ , viz.,

$$G_{\text{elec}}^{\text{SI}} = U_{\text{elec}}^{\text{SI}} [1 + y \coth(y) - \kappa_{\text{interm}} R] \quad (16)$$

where  $U_{\text{elec}}^{\text{SI}}$  is defined by equation 10. A minimum in  $G_{\text{elec}}^{\text{SI}}$  occurs at (11),

$$R_{\min} = \frac{y \coth(y) + 1 + \left\{ [y \coth(y) + 1][y \coth(y) + 3] \right\}^{1/2}}{\kappa_{\text{interm}}} \quad (17)$$

Sogami and Ise (11) estimated that  $R_{\min} \approx 5.47R_S$ .

**Comments on the Pairwise Interaction Potential.** The DLVO potential is a "true" pairwise potential since it is independent of the concentration of the macroions. The remaining potentials discussed in this section reduce to the DLVO potential in the limit of vanishing macroion concentration and uniform electrolyte concentration. Hence the differences in these potentials arise from the *ad hoc* assumptions regarding the disposition of the macroion contributions at finite concentration and their effect on the electrolyte ion distribution. Regardless of the choice of potential used in the analysis of experimental data, a common result is that the apparent charge of the macroion is considerably smaller than that anticipated on the basis of chemical analysis and titration curves. This discrepancy in charge values has not been vigorously addressed in the literature, but partially "justified" by postulating "charge renormalization" concepts or redefining the structural unit as the macroion and tightly associated counterions.

The primary problem with the aforementioned potentials is that they are mean potentials developed from the Debye-Hückel limiting expressions. The situation with macroion systems is therefore reminiscent of the Faraday discussion in 1927 regarding deviations of experimental data on the simple salt systems from the predictions of the Debye-Hückel theory. For example, the Debye-Hückel potential obtained from the linearized Poisson-Boltzmann equation is consistent with the fundamental principles of the Gibbs phase integral in statistical mechanics as long as fluctuations in the mean potential of simple electrolyte systems are negligible (22). The possibility arises that fluctuations in the mean potentials are of even greater significance for the highly asymmetric system of macroions and electrolyte ions.

### Counterion condensation: the Oosawa-Manning theories

Oosawa and co-workers (23-27) employed the Poisson-Boltzmann equation to study the interaction of small ions with the geometry of charged spheres, rods, and coils. They proposed two types of small ion association mechanisms; those localized at specific chemical groups on the polyion ("P-binding") and those delocalized within a volume (which we denote as  $v_c$ ) of the polyion (" $\psi$ -binding") (24). A major conclusion of these studies was that if the charge parameter  $\lambda_c$  was greater than unity, then the average extent of dissociation,  $\langle\lambda_d\rangle$ , of the cylindrical polyion was,

$$\langle\lambda_d\rangle = \frac{1}{\lambda_c} = \frac{b}{|z_1 Z_s| \lambda_B} \quad (\lambda_c > 1) \quad (18)$$

where  $z_1$  is the charge on the monomer group for the polyion,  $b$  is the distance between groups, and  $Z_s$  is the charge of the symmetric electrolyte.

Manning (28-34) developed a "two-state" model for counterion condensation about an infinitely long line charge. The primary assumption in the Manning model was that the reduction in electrical free energy between the *charged groups on the line charge* due to condensation of counterions was counterbalanced by the entropy of mixing. The sum of these two contribution was then minimized to obtain the critical fraction of bound sites by the counterions,  $\theta_b^c$ . Because of the linear geometry and infinite chain length assumptions the summation over electrostatic energy states resulted in a logarithmic expression for the electrostatic free energy. In order to eliminate the divergence in the free energy expression as the counterion concentration went to zero, the coefficient of the term  $\ln(<n_2 >_u)$  was set equal to zero. Hence,

$$|Z_2| \theta_b^c = 1 - \frac{b}{|Z_2| \lambda_B} \quad (19)$$

The relationship between the Oosawa and Manning models is,

$$\langle\lambda_d\rangle = 1 - |Z_s| \theta_b^c = \frac{1}{|Z_s| \xi_{OM}} \quad (20)$$

where the Oosawa-Manning parameter  $\xi_{OM}$  is defined as,

$$\xi_{OM} \equiv \frac{\lambda_B}{b} \quad (21)$$

The physical meaning of the Oosawa-Manning parameter is that it represents the maximum charge density that can be supported by the solvent. If  $\xi_{OM} < 1$  then the average spacing between the charges on the rodlike polyion is simply the charge spacing as determined, for example, by titration and  $\langle b \rangle = b$ . On the other hand if  $\xi_{OM} > 1$  then counterions will condense onto the linear surface until the condition  $\xi_{OM} = 1$  is met, i.e.,  $\langle b \rangle = \lambda_B$ . The same conclusion results if the nonlinear Poisson-Boltzmann equation is solved (19).

The Oosawa and Manning theories are reminiscent of the Bjerrum model for simple salts. Those counterions that are "condensed" onto the polyion surface are "thermodynamically removed" from the bulk solution and also effectively reduce the charge of the polyion. Caution must be exercised, however, in the application of the



Oosawa-Manning condensation results to linear polyions of finite length and thickness, to polyions with geometric shapes other than the line charge, to site specific binding systems, and to ligands of finite size. The assumption of a line charge, for example, appears to be valid for extremely low ionic strength solvents (large  $\lambda_{DH}$ ) but fails at moderate to high ionic strength solvents (35-37). Skolnick and Grimmelmann (38) show that in the infinite length approximation may be valid for finite chain length only if  $\lambda_{DH}$  is small relative to the length of the line. Using the Mayer cluster integrals Woodbury and Ramanathan (39) conclude that *counterions do not condense onto finite length line charges*. If the dielectric constant of the polyion differs from that of the bulk solvent then projection of the actual charge distribution onto a line may lead to difficulties in the application of the Oosawa-Manning condensation theories. Skolnick and Fixman (40) show that charges placed on the same side of a cylinder *enhanced* the site-site interactions relative to the reference condition of two charges in the solvent, whereas the interaction was decreased if the two charges were placed on opposite sides of the cylinder. Dewey (41) notes that the "condensation" volume goes to infinity as the electrolyte concentration goes to zero for finite chain lengths because the electrostatic instability for the infinite chain length no longer exists. According to Dewey (41),

Since this instability no longer exists for finite length polymers, retention of the condensation free energy term now causes an instability in the system.

A problem remains in the "operational definition" of the condensed counterions. NMR measurements on the association of  $^{23}\text{Na}^+$  to DNA indicates that the cation is mobile, and thus "territorially" bound and rapidly exchanges with those in the bulk solution (42,43). On the other hand NMR studies indicate that  $^{25}\text{Mg}^{2+}$  binds in a more complex manner, having an "inner sphere" with an accompanying hydration change and an "outer sphere" with no hydration change (44, 45). Although NMR studies indicate that the hydration shell of hexamine cobalt (III) [CoHex(III)] does not appear to be altered on binding to DNA (46), there does appear to be at least three different binding classes for this cation (47). It is emphasized that the NMR methods cannot detect those ions "trapped" in the ion cloud, and thus these ions are not counted as being in the "bound" state by the NMR technique. Granot and Kearns (45) state, for example,

those ions which are only held in an ion atmosphere around the polyelectrolyte by long-range, through space, electrostatic interactions, would not be considered bound and are not detected by the PMR method.

This definition of "condensed" counterions is not universally applied to all techniques used to study counterion condensation. Electrophoretic mobilities, however, are sensitive to electroviscous effects whose origins are associated with the thickness of the surrounding ion cloud of the polyion. Electrophoretic light scattering (ELS) methods therefore cannot distinguish between counterions tightly bound to the surface of the macroion and those that are trapped in the ion cloud. Nonetheless ELS methods are also interpreted in terms of counterion condensation (48, 49). In the study of Klein and Ware (49) on 6,6-ionene, for example, a sharp change in the electrophoretic mobility occurs at  $\xi_{OM} = 1$  over the range  $0.82 < \xi_{OM} < 1.82$  in accordance with the Oosawa-Manning prediction.

Of direct bearing to the question of the condensation volume are the results of Le Bret and Zimm (50). The computational model used by these authors is a composite of the Alexandrowicz and Katchalsky (18) and Russel (19) models for the Poisson-Boltzmann equation. In these calculations the "salt free" expressions are used

in the vicinity of the charged cylindrical surface while the "excess salt" expressions are used far from the surface but with the constraint that the screening parameter is the same in both regions. The "Manning distance"  $R_M$  is thus defined as that distance from the charged surface such that the inscribed volume contains the number of electrolyte ions predicted by the Manning condensation expression. From this analysis they conclude that  $R_M$  is proportional to  $\kappa^{-1/2}$ , and thus increases as the electrolyte concentration decreases in value. Hence the Le Bret-Zimm calculations are more consistent with the idea that "condensed" counterions are those trapped in the vicinity of the polyion, including those in the distal regions of the ion cloud as well as the tightly bound as detected by NMR.

**Comments on the Concept of Counterion Condensation.** There is ample experimental evidence that supports the concept of counterion condensation. The "two-state" models introduced by Oosawa and by Manning provide a very good quantitative picture of counterion condensation for very long polyions whose linear charge density is accurately represented as a line charge. Conspicuously missing in the Manning theory is any reference to the electrostatic interactions of the electrolyte ions. For example, there is no term that reflects the association energy of the electrolyte ion with the charged line. Trapping a counterion within the volume  $v_c$  serves only to uniformly reduce the repulsive interactions between the lattice sites. Likewise there is no term for the pairwise interaction between "bound" counterions within the "condensation" volume,  $v_c$ . The latter contribution does not appear for point charges that are "absorbed" into the lattice charge, i.e., the coincidence of the centers of positive and negative charge. Ions of finite size, however, do not result in complete neutralization of the site charges but rather give rise to "dipole" lattices (51). The apparent success of the Manning formulation of counterion condensation to large DNA fragments may be due to the observation that ion binding to DNA is largely entropy driven (see the paper by Bloomfield, Ma, and Arscott in this volume) or that experimental data is over a relatively narrow concentration range of the ligand (51). Further tests on the counterion condensation models should be carried out on systems of very flexible polyions and/or enthalpy driven associations of the ions.

### Gibbs Versus Helmholtz Free Energy in Describing Macroion Systems

Both the Oosawa and Manning models employ the somewhat ill-defined quantity of the "condensation volume" that contains "thermodynamically bound" counterions. That is, the "bound" counterions act to reduce both the net charge of the macroion and the effective concentration of counterions in the bulk solution. If the "condensation volume" depends upon the ionic strength of the solution as indicated from the Le Bret-Zimm calculations (50), then it necessarily follows that the "free volume" is likewise a variable quantity. Thus the question is now raised as to whether the Helmholtz or the Gibbs free energy is the appropriate function to describe the thermodynamics of macroionic solutions and suspensions.

Matsumoto and Kataoka (52) point out that the volume of the solution accessible to the small ions ( $V_{f,s}$ ) differs from that of the polyions ( $V_{f,1}$ ). To illustrate this concept we note that both the Oosawa and the Manning models partition the solution that is accessible to the small ions into two volumes; the condensation volume about the polyion containing the thermodynamically "bound" counterions ( $v_c$ ), and the remainder of the solution containing the thermodynamically "free" electrolyte ions ( $V_{f,s}$ ). These two quantities are related to the total volume of the solution,  $V$ , by the expression,

$$V_{f,s} = V - N_1 v_c \quad (22)$$

where  $N_1$  is the number of macroions present in the volume  $V$ . This equation is similar to that employed by Oosawa, Imai, and Kagawa (23), except that now  $v_c$  can vary with both the charge of the macroion and the concentration of charged molecules in accordance with the Le Bret-Zimm calculations of  $R_M$  (50). The net effect is that the free volume accessible to the electrolyte ions is a variable quantity. In contrast the total volume accessible to the polyion is dependent upon the physical volume  $v_1$  of the polyion,

$$V_{f,1} = V - N_1 v_1 \quad (23)$$

Note that  $v_1$  does not in general vary with the charge or the ionic strength of the solution.

The question of whether the Gibbs or the Helmholtz free energy should be used thus becomes one of whether one should use for the total volume  $V$  or  $V_{f,s}$  to describe the properties of the "thermodynamically free" electrolyte ions.

### Electrolyte Ions and Attraction Between Identical Macroions

As mentioned in the introductory paragraph, Langmuir (1) concluded that there is a net attractive electrostatic interaction when the counterions in a non uniform distribution (i.e., between the micelles) were included in the calculation. Kirkwood and Schumaker (53) showed that fluctuations in the net charge of spheres resulted in an attraction between the macroions. Oosawa (54) showed that an attraction occurs between two parallel rods at distances on the order of the Bjerrum length if the fluctuations in the axial distribution of counterions are correlated. Along similar lines Fulton (55, 56) pointed out that fluctuations in the dipole moment of polyions resulted in long range correlations between the charged spheres. Along these lines it was suggested that *distortions* in the electrolyte atmosphere about nearby polyions (57, 58), or the *sharing* of electrolyte ions in overlapping ion clouds of neighboring polyions (59) are responsible for the occurrence of the very slow relaxation mode reported in dynamic light scattering data. Yoshino (60) attempted to explain the "two state" observations of PLSL with no added salt in terms of a distortion from spherical symmetry of the Debye cloud about a charged sphere. Yoshino proposed that these distortions could be represented in terms of multipole contributions as described by spherical harmonics. Recall also that both the Sogami and the Sogami-Ise potentials (equations 12 and 16, respectively) differ from the standard DLVO potential (equation 1) solely on the assumptions regarding the distribution of the electrolyte ions. If the electrolyte ions are uniformly distributed in the medium then equations 1, 12, and 16 become identical in form. In his lecture at this mini symposium, Manning (61) presented preliminary results on the interaction between parallel line charges. As the parallel line charges were brought closer together, it was found that the condensation volumes  $v_c$  became distorted such that there was an increase in the volume between the line charges. Under certain conditions the free energy associated with the distortions in  $v_c$  overcame the repulsive Coulombic contributions with the result of a net attraction between the line charges. Sánchez-Sánchez and Lozada-Cassou (62) reported three-point hypernetted chain/mean spherical results for the interaction between two charged spheres. They found that for the higher surface charge densities the counterion distribution between the two spheres was greatly enhanced over that of the bulk solvent. The force between the two spheres was reduced due to the accumulation of intermittent counterions, but no attraction between the two spheres was reported.

**Comments on the Role of Electrolyte Ions and Polyion Attraction.** A common theme of the studies reviewed in the previous paragraph is the increase in the

concentration of counterions between the two charge macroions. These studies differ, however, in the mathematical models employed to describe the interacting systems. The quantitative expression of the Sogami-Ise and Sogami potentials predict a minimum in the potential located 1000-2000Å from the central macroion. Manning reported that a minimum in the net attraction curve appears at 50-60Å separation when distortion in the condensation volume dominates the electrostatic interactions.. The calculations of Sánchez-Sánchez and Lozada-Cassou do not indicate any attraction between the spheres. The absence of attraction may be due to the close proximity of the two spheres, being on the order of 5 sphere diameters. Thus the apparent attraction between the macroions results from the distortion of some characteristic property of the model as compared to that quantity for the isolated macroion. Hence it may be of value to treat the collective effect of small ion-polyion interactions within the vocabulary associated with electrons and atoms.

### Electrostatic Persistence Length: Stiff Versus Flexible Polyelectrolytes

Odijk (63) and, independently, Skolnick and Fixman (64) presented a theory for the electrostatic component to the persistence length for an infinitely long polymer based on slight deviations from the rigid rod configuration. This model was corrected for finite chain of length L by Odijk and Houwaart (65), with the result,

$$L_{\text{elec}}(\kappa L) = \frac{\lambda_B}{4\langle b \rangle^2 \kappa^2} h(\kappa L) \quad (24)$$

where  $\langle b \rangle$  is the average charge spacing (to account for Oosawa-Manning condensation) and the finite chain length correction factor is,

$$h(\kappa L) = 1 - \frac{8}{3\kappa L} + \frac{e^{-\kappa L}}{3} \left( \kappa L + 5 + \frac{8}{\kappa L} \right) \quad (25)$$

Hence the prediction for this model is that  $L_{\text{elec}}$  is proportional to the reciprocal of the salt concentration,  $1/C_s$ .

The dependence of  $L_{\text{elec}}$  on  $C_s$  does now always exhibit the -1 power law as given by equation 24. Le Bret (66) solved the Poisson-Boltzmann equation numerically for a toroid both with and without a conducting surface. The power law for a conducting surface tended to follow the -1 power law, but for a non conducting surface it varied from -1 for very low ionic strength solvents to -1/4 for  $C_s$  on the order of 1 M. Similar results were found by Fixman (67).

In the case of flexible polyelectrolytes, Tricot (68) pointed out that the experimental data supported a power law of -1/2. Barrat and Joanny (69) took into consideration the effect of fluctuations in the chain configuration on the calculation of the electrostatic component to the persistence length. It was found that the Odijk/Skolnick-Fixman equations are correct in the limit of stiff chains ( $L_p/L > 1$ ) but breaks down for very flexible chains ( $L_p/L \ll 1$ ). Their results indicated that for very flexible chains  $L_{\text{elec}}$  was proportional to  $1/\kappa$ , or  $C_s^{-1/2}$ , as experimentally observed for several polyion systems.

### Comments on the Electrostatic Component to the Persistence Length.

Exact numerical calculations of the electrostatic persistence length were performed for a continuously bent rod using a screened Coulomb pairwise interaction (21). These calculations indicated that equations 24 and 25 gave very good values for bending angles much larger than those considered in the original derivation, i.e., in

excess of a bending angle of  $180^\circ$ . It was further shown that if these various degrees of bending were averaged over a Boltzmann distribution then the power law of  $\langle L_{elec} \rangle$  was considerably less than -1 even though each contributing configuration obeyed the Odijk/Skolnick-Fixman power law, and that  $\langle L_{elec} \rangle$  appeared to become independent of  $C_s$  at sufficiently small values of  $\kappa L$ .

When trying to interpret the experimental observation that  $L_{elec}$  is proportional to  $C_s^{-1/2}$  because of fluctuations, one must consider two types of averages. In case 1 there is a single molecular weight species and the average is carried out over all possible configurations of these chains, including the continuous, smooth bending polyion as in the Odijk and Skolnick-Fixman models. In case 2 the sample that is polydisperse in regard to the molecular weight, or chain length, distribution but all of the polyions undergo a continuous, smooth bend as in the Odijk and Skolnick-Fixman models (case 2). Apparently both of these cases give rise to an average value of the electrostatic persistent length that is proportional to  $C_s^{-n}$ , where  $n$  is less than 1.

### Slow Modes in the Dynamic Light Scattering Correlation Function

Lin, Lee, and Schurr (70) reported rather bizarre behavior of the [NaBr] profile of the apparent diffusion coefficient,  $D_{app}$ , of poly(L-lysine) with a degree of polymerization of 955, denoted by (PLL)955. The value of  $D_{app}$  increased as [NaBr] decreased from 0.5 M, in accordance with the Einstein expression for the mutual diffusion coefficient,  $D_m$ .

$$D_m = \frac{1}{f_m} \left( \frac{\partial \pi}{\partial C_1} \right) \alpha \frac{kT}{f_m I_{tjls}} \quad (26)$$

where  $f_m$  is the mutual friction factor that contains indirect hydrodynamic interactions,  $(\partial \pi / \partial C_1)$  is the osmotic susceptibility that measures the direct interaction between the polyions and is proportional to the reciprocal of the total intensity,  $I_{tjls}$ , and  $C_1$  is the polyion concentration. Hence in this region of the salt profile  $D_{app} = D_m$ , and the polyion is said to exhibit "ordinary" behavior.

At a well-defined value of [NaBr] that was dependent only on the weight concentration of PLL955,  $D_{app}$  underwent an unexpected catastrophic drop in value that could not be explained in terms of current polyelectrolyte theory (70). For the solution that was 1 mg/mL in PLL,  $D_{app}$  changed from a value of  $\approx 8 \times 10^{-7} \text{ cm}^2/\text{s}$  at  $[\text{NaBr}] \approx 1.1 \times 10^{-3} \text{ M}$  to a value of  $\approx 4 \times 10^{-8} \text{ cm}^2/\text{s}$  at  $[\text{NaBr}] \approx 9.1 \times 10^{-4} \text{ M}$ , where the latter value of  $D_{app}$  was much smaller than that calculated for PLL955 modeled as a cylinder. Furthermore, they searched with no avail for two relaxation modes on either side of the transition. In their search in the ordinary regime they stated (70),

There seemed to be virtually no sign of the very slow relaxation characteristic of the extraordinary solutions, however.

They also reported that  $I_{tjls}$  also changed sharply in value over this range (70),

the 1 mg/mL solution exhibited at  $\theta = 60^\circ$  a 2.5 fold increase in intensity between  $9.1 \times 10^{-4}$  and  $1.1 \times 10^{-3} \text{ M}$  NaBr.

The concomitant decrease in  $D_{app}$  and decrease in  $I_{tjls}$  was therefore contrary to the relationship given by equation 26. Thus  $D_{app}$  for  $[\text{NaBr}] < 10^{-3} \text{ M}$  was not associated

with the mutual diffusion coefficient, but rather is a manifestation of an extraordinary behavior of the dynamics of the PLL955 solution. This *very sharp* drop in the value of  $D_{app}$  for a 1 mg/mL solution of PLL at  $10^{-3}$  M univalent salt for a has been verified for PLL406 (71), PLL946 (71), PLL2273 (71), PLL616 (72), PLL2500 (73), PLL3800 (74), and PLL952-PLL1380 (75). Representative data are shown in Figure 1, where the location of the ordinary-extraordinary (o-e) transition is indicated by the solid line. The sharpness of the o-e transition for both the PLL and poly(styrene sulfonate) (PSS) is further reflected in the empirical expression of Drifford and Dalbiez (76). Let us define the ratio  $\rho_{DD}$  as

$$\rho_{DD} = \frac{C_m \langle b \rangle}{Z_s \lambda_B \sum_j C_j Z_j^2} \quad (27)$$

where  $C_m$  is the concentration of monomer units of the polyion. The empirical relationship for the location of the o-e transition is when  $\rho_{DD} = 1$ . Hence for a fixed electrolyte concentration this condition obtains when the polyion concentration is,

$$C_m^{o-e} = \frac{Z_s \lambda_B \sum_j C_j Z_j^2}{\langle b \rangle} \quad (28)$$

Equation 28 is referred to as the Drifford-Dalbiez ratio. Although not as dramatic as in  $D_{app}$ , small changes in the relative viscosity (77), conductivity (78), and electrophoretic mobility (71, 72) were reported to occur at  $C_m^{o-e}$ . In contrast the tracer diffusion coefficient obtained by fluorescence recovery after photobleaching methods did not show any unusual behavior through the o-e transition region (72).

**Classification of  $D_{app}$  Versus  $C_s$  Profiles.** Since the original studies on PLL and PSS that defined the characteristics of the o-e transition, there have been several references to the "extraordinary" properties of other polyion systems in which a "splitting" of values in  $D_{app}$  occurred as a function of added salt or polyion concentration if salt was not added to the system. The "anomalously slow" relaxation mode has been referred to as the "extraordinary behavior" of the system, and reference was made to the work on PLL and PSS. Not all of the  $D_{app}$  versus  $C_s$  profiles, however, exhibit the characteristics of the o-e transition as originally defined for the PLL system. It has been suggested that the profiles can be separated into three distinct classes (79). Both Class 1 and Class 2 profiles are defined by a "gradual" splitting, i.e., over several decades of  $C_s$ , of  $D_{app}$  from a common origin as  $C_s$  is lowered into  $D_{fast}$  (increasing in value) and  $D_{slow}$  (decreasing in value). Class 1 profiles are defined by the constraint that  $(D_{fast}/D_{slow})_{max} < 5$ , whereas the ratio  $D_{fast}/D_{slow}$  is unconstrained for Class 2 profiles. The separation of these two classes was based on the possible interpretation of the data. Class 1 profiles can be explained as a slight polydispersity in the molecular weight of the sample, where the behavior of  $D_{fast}$  and  $D_{slow}$  may reflect the relative responses of the flexible polyions to chain expansion and osmotic susceptibility changes. Class 2 profiles may result from strongly coupled modes of the macroions of the polydisperse system, where the magnitude of the splitting reflects the off-diagonal coupling constant in the diffusion tensor. Class 3 profiles exhibit a sudden appearance of  $D_{slow}$  as  $C_s$  is decreased, with  $D_{fast}/D_{slow} > 10$ . The primary example of the Class 3 profile is the o-e transition in

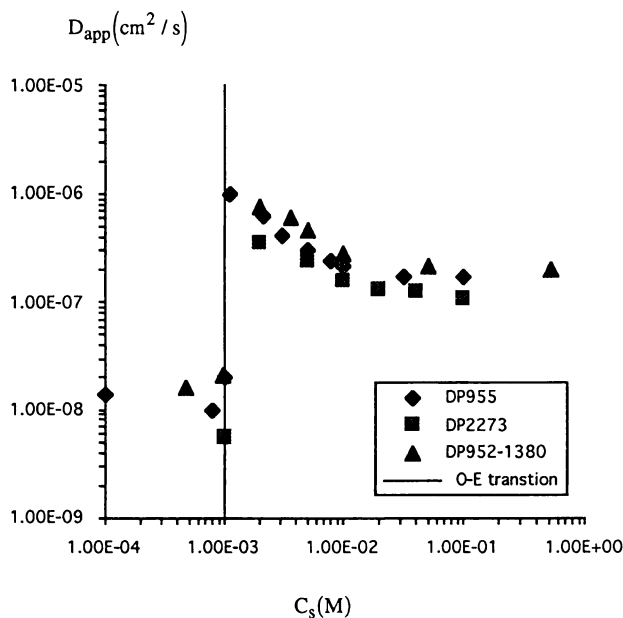


**Figure 1. The o-e transition in Poly(L-lysine).** The apparent diffusion coefficient  $D_{app}$  is plotted as a function of the electrolyte concentration  $C_s$  for poly(L-lysine) with various degrees of polymerization (DP). The location of the o-e transition is indicated by a vertical line. [▲ from Figure 1 of Ghosh, Peitzsch, and Reed (75); ◆ from Table I of Lin, Lee, and Schurr (70); ■ from Table I of Wilcoxon and Schurr (71).]

the PLL system. In the Class 3 profiles  $D_{fast}$  may be described as a continuous function of  $C_s$  whereas  $D_{slow}$  exhibits an apparent discontinuity at a well-defined value of  $C_s$  that is dependent upon  $C_m$ . The  $D_{app}$  versus  $C_s$  profiles for copolymers of acrylamide/sodium acrylate (PAmA) (80) (Class 1), proteoglycan monomers (PG) (81) (Class 2), and quaternized poly(2-vinylpyridine) (P2VP) (82) (Class 3) are given in Figure 2.

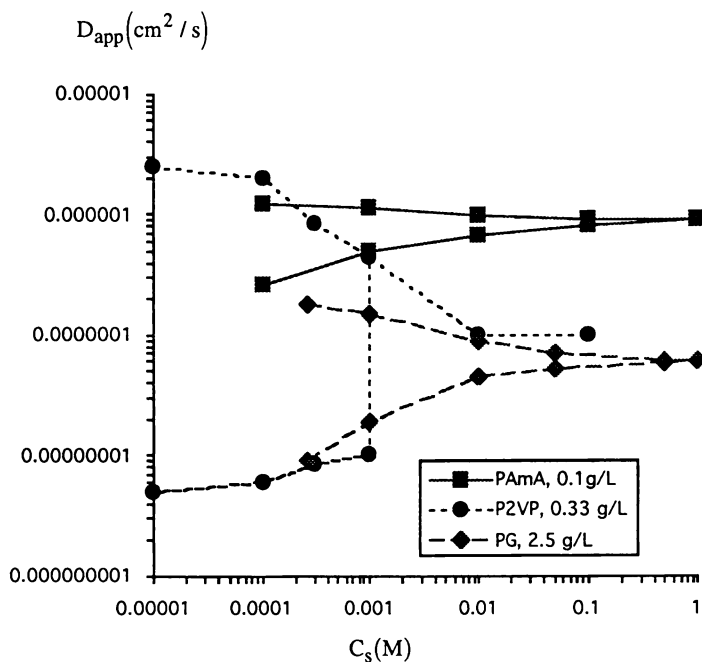


**Figure 2. Three Classifications of the  $D_{app}$  Versus  $C_s$  Profiles.**

■ Class 1, represented by poly(acrylamide/acrylate) data from Figure 2 of Reed, Ghosh, Medjahdi, and François (80).

◆ Class 2, represented by proteoglycan monomer data from Figure 9 of Li and Reed (81).

● Class 3, represented by quaterized poly(2-vinylpyridine) data from Figure 15 of Förster, Schmidt, and Antonietti (82).



**Interpretation of the Class 3 Profiles.** Both Class 1 and Class 2 profiles exhibit a continuous change in both  $D_{fast}$  and  $D_{slow}$  as  $C_S$  is lowered. Hence these profiles can be interpreted by a clever researcher in terms of continuous functions related to the osmotic susceptibility, relative scattering powers of the constituent macromolecules, and/or differential expansion properties of the polyions. What is difficult to comprehend within the context of the current polyelectrolyte paradigm is both the sharpness and the magnitude of the  $D_{app}$  versus  $C_S$  profile exhibited by Class 3 systems, in particular the o-e transition of PLL and PSS. Indeed the explanation of the o-e transition is currently a controversial topic in the literature, including some of the papers in this symposium-based volume. It is neither the intent to review the many studies in the literature on the o-e transition, nor to examine in detail the attributes any one interpretation of this phenomenon. Attention is thus directed to the salient features of three models of the o-e transition that have been advanced in the literature: "filterable aggregates", "temporal aggregates", and "cluster domains."

**The Filterable Aggregate Interpretation.** Ghosh, Peitzsch, and Reed (75) summarized most of their work on several polyelectrolyte systems and described in detail a "filterable aggregate" (FA) interpretation to explain all of the anomalous slow modes in Classes 1-3 described above. The basic assumption is that a relatively small population of filterable aggregates exist in most polymer preparations. As the ionic strength is lowered the increase in the osmotic susceptibility suppresses only the light scattered by the "monomer" units, thus revealing the aggregated material to the point that it dominates in the low ionic strength region. It has previously been pointed out that the FA model is inconsistent with some of the experimental observations related to the o-e transition of PLL (83). For example, Bruno and Mattice (84) reported Förster energy transfer studies on PLL with the intent to determine the optimal distance between the donor-acceptor pair. The o-e transition was identified by a sharp increase in the intensity ratio  $I_{585}/I_{515}$  at  $[NaCl] = 10^{-3}$  M. It was concluded from this study that the optimal distance was in the range 60-100 Å, which was noted to be comparable to the average interparticle spacing deduced from X-ray scattering data.

Even though data exist that are inconsistent with the FA model, it is nonetheless important to examine the virtues of this model in regard to the o-e transition of PLL. The colorful metaphor for this model is that of "stars" (the aggregates, denoted by EP for "extraordinary phase") and the "sun" (the monomer particles, denoted by OP for "ordinary phase"). These authors thus envision the o-e transition as follows (75),

The weak EP scattering from the aggregates (the "stars") is detectable against the dark (extremely weakly scattering) background of the ordinary polyelectrolyte populations at low ionic strength. As  $C_a$  increases, the scattering from the ordinary polyelectrolytes rises dramatically (the sun comes up and the atmosphere scatters brightly), and overwhelms the feeble scattering from the aggregates of the EP phase.

Reed and co-workers state that the aggregated material can always be filtered from the solution if one uses a membrane of sufficiently small pore size.

In the context of the "star-sun" metaphor  $D_{app}$  is an amplitude weighted value,

$$D_{app} = \frac{A_{EP}D_{EP} + A_{OP}D_{OP}}{A_{EP} + A_{OP}} \quad (29)$$

where the scattering amplitude  $A_{OP}$  is suppressed as the osmotic susceptibility is increased. To be consistent with the *apparent discontinuity* in the profiles in Figure

1, it follows that  $A_{EP} \ll A_{OP}$  for  $[NaBr] > 1.1 \times 10^{-3}$  M and  $A_{EP} \gg A_{OP}$  for  $[NaBr] < 9.1 \times 10^{-4}$  M. The sharpness of the variation in the relative amplitudes of the two components is an experimental fact that must be explained by any model for the o-e transition. It is thus necessary to verify the relative magnitudes of the change for the FA model before pursuing the task of explaining the sharpness of the transition.

The relative magnitudes of the scattered light intensity attributed to the OP and EP particles in the extraordinary regime can be estimated from the data of Ghosh *et al* (75) on PLL. The measured intensities of the sample filtered through 0.22  $\mu$ m membrane filters (EP and OP particles are present) at added salt concentrations 0 and  $C_{add}$  are defined as  $I_{tils}(0)$  and  $I_{tils}(C_{add})$ . According to these authors filtration through the 0.05  $\mu$ m. membrane filters removes the EP particles. Hence  $I_{OP}(0)$  is the measured intensity of the EP-free solution at  $C_{add} = 0$ . They then represented their measurements in terms of a "normalized" intensity,  $I'_e(C_{add})$ ,

$$I'_e(C_{add}) = \frac{I_{tils}(C_{add}) - I_{OP}(0)}{I_{tils}(0) - I_{OP}(0)} \quad (30)$$

The relative intensity of light scattered by the EP particles to the OP particles in zero added electrolyte solvent,  $I_{EP}(0)$  and  $I_{OP}(0)$ , respectively, can be calculated from equation 30 using the Ghosh *et al.* (75) measured values  $I_{tils}(\text{high salt}) = 8I_{tils}(0)$  and calculated values  $I'_e(\text{high salt}) = 40I'_e(0) = 40$ . Such a calculation gives (79),

$$I_{EP}(0) = \frac{7}{32} I_{OP}(0) \quad (31)$$

In other words, the "sun" scatters approximately 5 times more light than the "stars" in the zero added electrolyte solution where the filterable aggregate model requires that only the "stars" be visible.

Aggregation is a potential problem in the interpretation of light scattering data, as emphasized by Reed and co-workers. The discussion above does not diminish the importance of taking steps to remove aggregated material, but rather that the filterable aggregates model is not consistent with the experimental data on the o-e transition.

**"Temporal Aggregate" and "Cluster Domain" Interpretations.** The descriptions of the "temporal aggregate" (TA) (85) and "cluster domain" (86) models are quite similar, hence it may not be possible to experimentally distinguish between them. [The original phrase used by Sedláč *et al.* (86) is "interchain domains (clusters)" which was altered to be "cluster domain" (79).]. Both the TA and CD models interpret the fast mode in terms of small ion-polyion coupled mode theory. It is noted, however, that Förster *et al.* (82) interpret the fast mode as a "gel mode" due to intertwining chains.

The slow mode in the TA model is envisioned to reflect the dynamics of polyions that are coupled due to the "sharing" of the common electrolyte ions in their overlapping ion clouds. The TA model reinterprets the Drifford/Dalbiez ratio (cf. equation 27) in terms of the volume ratio of the Debye-Hückel cloud per unit charge,  $V_{DH}$ , to the volume of the monomer unit,  $V_m$ , i.e. (87),

$$\rho_{DD} = 4 \frac{\pi \langle b \rangle \lambda_{DH}^2 C_m^{0-e} N_A}{Z_s 1000} = 4 \frac{V_{DH}}{V_m} \quad (32)$$

The nature of the dynamics of the system for  $\rho_{DD} > 1$  is statistically different than solutions for which  $\rho_{DD} < 1$  because of the more active role of the electrolyte ions. The temporal aggregates are therefore *metastable*. The anomalously slow relaxation time may reflect translation of the TA, the kinetics of dissolution of the temporal structure, or a combination of both.

The CD model envisions the slow mode as the translational diffusion of an "interchain domain" whose dimensions can be obtained from the angle dependence of either static or dynamic light scattering (86). These domains are formed in the semidilute solution regime, i. e., when the polyion chains physically overlap. These "clusters" of polyions, however, are not "hard aggregates" and the dimensions can be altered, for example, by filtration (88).

The importance of the polyion charge in establishing the slow mode is brought out by recent experiments by Sedláč (88) on partially ionized poly(methacrylic acid) (PMA) in salt free solutions. In these experiments the neutral PAM ( $\alpha=0$ ) was first filtered through 0.1 $\mu\text{m}$  Nucleopore filter. CONTIN analysis of the correlation function showed a large amplitude "fast" peak with a small amplitude "slow" peak. The sample was then titrated while in the scattering cell by likewise filtering through 0.1 $\mu\text{m}$  Nucleopore filters appropriate aliquots of a standard NaOH solution to  $\alpha=0.4$ . The CONTIN analysis now showed a tremendous increase in the relative amplitude of the "slow" peak. The charged PAM was then removed from the scattered cell and re-filtered through a 0.1 $\mu\text{m}$  membrane back into the scattering cell. The CONTIN profile for the re filtered sample was similar to that of the previous run. Hence the presence of the slow mode is strongly dependent upon the charged state of the polyion and is not a permanent "filterable aggregate" caused by entanglements.

**Comments on the o-e transition.** It is not intuitively obvious that the "splitting" phenomenon observed for polyions in "salt-free" solutions is the same as the o-e transition reported for polyions at a fixed concentration as the electrolyte concentration is varied. Förster *et al.* (82) reported both types of studies on P2VP. The apparent discontinuity in the  $D_{app}$  versus  $C_s$  profile was present (cf. Figure 2) whereas the  $D_{app}$  versus  $C_1$  profile exhibited a "continuous" splitting reminiscent of the Class 2 systems. In order to better understand the relationship between these two profiles it seems imperative that both kinds of studies be carried out simultaneously on the same sample. It is likewise important to take into consideration the overlap concentration of the polyions, in going from dilute to semidilute solution conditions.

### Concluding Comments

We have briefly examined only six topics in the field of polyelectrolytes that have been applied with varying degrees of consistency in the literature. To some, the chosen examples may not be as interesting as the more complex systems such as mixed polyion solutions, adsorption on polyions onto heterogeneous surfaces, the effect of the gel stiffness and charge on the movement of a macroion through the matrix in the presence of an electric field, or the rate of chemical reactions involving polyions, to name only a few. The interpretation of data for these systems also contain some aspects of ambiguity. Nonetheless progress towards the understanding of the fundamental nature of these complex systems has been made, even though precise quantitative agreement with theory may not be achieved. If I may paraphrase a memorable comment made by Dirk Stigter during his talk at this conference,

There was such good agreement between theory and experiment that we looked for compensating errors.

## References

1. Langmuir, I. *J. Chem. Phys.* **1938**, *6*, 873-896.
2. Verwey, E. J. W.; Overbeek, J. Th. G., *Theory of the Stability of Lyophobic Colloids*, Elsevier: Amsterdam, 1948, 135-185.
3. Ise, N.; Okubo, T., *J. Phys. Chem.*, **1966**, *70*, 2400-2405.
4. Sugimura, M.; Okubo, T.; Ise, N.; Yokoyama, S., *J. Am. Chem. Soc.*, **1984**, *106*, 5069-5072.
5. Ise, N.; Okubo, T.; Ito, K.; Dosho, S.; Sogami, I., *Langmuir*, **1985**, *1*, 176-177.
6. Matsuoka, H.; Murai, H.; Ise, N., *Phys. Rev. B*, **1988**, *37*, 1368-1375.
7. Ito, K.; Okumura, H.; Yoshida, H.; Ueno, Y.; Ise, N., *Phys. Rev. B*, **1988**, *37*, 10852-10859.
8. Ito, K.; Nakamura, H.; Yoshida, H.; Ise, N., *J. Am. Chem. Soc.*, **1988**, *110*, 6955-6963.
9. Ise, N.; Matsuoka, H.; Ito, K.; Yoshida, H., *Faraday Discuss. Chem. Soc.*, **1990**, *90*, 153-162.
10. Ise, N.; Matsuoka, H.; Ito, K.; Yoshida, H.; Yamanaka, J., *Langmuir*, **1990**, *6*, 296-302.
11. Sogami, I.; Ise, N. *J. Chem. Phys.* **1984**, *81*, 6320-6332.
12. Overbeek, J. Th. G., *J. Chem. Phys.*, **1987**, *87*, 4406-4408.
13. Smalley, M. *Molec. Phys.*, **1990**, *71*, 1251-1267.
14. Medin a-Noyola, M.; McQuarrie, D. A. *J. Chem. Phys.*, **1980**, *73*, 6279-6283.
15. Lin, S.-C.; Lee, W. I., Schurr, J. M. *Biopolymers* **1978**, *17*, 1041-1064.
16. Beresford-Smith, B.; Chan, D. Y. C.; Mitchell, D. J. *J. Colloid and Interf. Sci.* **1985** *105*, 216-234.
17. Belloni, L. *J. Chem. Phys.* **1986**, *85*, 519-526.
18. Alexandrowicz, Z.; Katchalsky, A. *J. Polym. Sci. Part A*, **1963**, *1*, 3231-3260.
19. Russel, W. B. *J. Polym. Sci.* **1982** *29*, 1233-1247.
20. Sogami, I. In *Ordering and Organisation in Ionic Solutions*, Editors, Ise, N.; Sogami, I., Eds.; World Scientific Publ.: Teaneck, N. J., 624-634.
21. Schmitz, K. S. *Polym.* **1990**, *31*, 1823-1830.
22. Fowler, R. H. *Trans. Faraday Soc.* **1927**, *23*, 434-443.
23. Oosawa, F.; Imai, N. *J. Chem. Phys.* **1954**, *22*, 2084-2085.
24. Oosawa, F.; Imai, N.; Kagawa, I. *J. Polym. Sci.* **1954**, *13*, 93-111.
25. Oosawa, F. *J. Polym. Sci.* **1957**, *23*, 421-430.
26. Ohnishi, T.; Imai, N.; Oosawa, F. *J. Phys. Soc. Jpn.* **1960**, *15*, 896-905.
27. Oosawa, F. *Polyelectrolytes*, Marcel Dekker, New York, New York, 1971.
28. Manning, G. S. *J. Chem. Phys.* **1965**, *43*, 4260-4267.
29. Manning, G. S. *J. Chem. Phys.* **1969**, *51*, 924-933.
30. Manning, G. S. *J. Chem. Phys.* **1969**, *51*, 934-938.
31. Manning, G. S. *Biophys. Chem.* **1977**, *7*, 95-102.
32. Manning, G. S. *Biophys. Chem.* **1978**, *8*, 65-70.
33. Manning, G. S. *Quart. Rev. Biophys.* **1978**, *11*, 179-246.
34. Manning, G. S. *Acc. Chem. Res.* **1979**, *12*, 443-449.
35. MacGillivray, A. D. *J. Chem. Phys.* **1972**, *56*, 80-82.
36. MacGillivray, A. D. *J. Chem. Phys.* **1972**, *56*, 83-85.
37. Lampert, M. A.; Crandall, R. S. *Chem. Phys. Lett.* **1980**, *72*, 481-485.
38. Skolnick, J.; Grimmelmann, E. K. *Macromolecules* **1980**, *15*, 335-338.
39. Woodbury, Jr., C. P.; Ramanathn, G. V. *Macromolecules* **1982**, *15*, 82-86.
40. Skolnick, J.; Fixman, M. *Macromolecules* **1978**, *11*, 867-871.
41. Dewey, T. G. *Biopolymers* **1990**, *29*, 1793-1799.
42. Anderson, C. F.; Record, Jr., M. T.; Hart, P. A. *Biophys. Chem.* **1978**, *7*, 301-316.
43. Bleam, M. L.; Anderson, C. F.; Record, M. T., Jr. *Proc. Natl. Acad. Sci. USA* **1980**, *77*, 3085-3089.

44. Rose, D. M.; Bleam, M. L.; Record, M. T., Jr.; Bryant, R. G. *Proc. Natl. Acad. Sci. USA* **1980**, *77*, 6289-6292.
45. Granot, J.; Kearns, D. R. *Biopolymers* **1982**, *21*, 219-232.
46. Braunlin, W. H.; Anderson, C. F.; Record, M. T., Jr. *Biochemistry*, **1987**, *26*, 7724-7731.
47. Braunlin, W. H.; Xu, Q. *Biopolymers*, **1992**, *32*, 1703-1711.
48. Rhee, K. W.; Ware, B. R. *J. Chem. Phys.* **1983**, *78*, 3349-3353.
49. Klein, J. W.; Ware, B. R. *J. Chem. Phys.* **1984**, *80*, 1334-1339.
50. Le Bret, M.; Zimm, B. H. *Biopolymers* **1984**, *23*, 287-312.
51. Schmitz, K. S. *Macroions in Solution and Colloidal Suspension* VCH Publishers: New York, NY, **1993**, 243-251.
52. Matsumoto, M.; Kataoka, Y. In *Ordering and Organisation in Ionic Solutions*, Editors, Ise, N.; Sogami, I., Eds.; World Scientific Publ.: Teaneck, N. J., 574-582.
53. Kirkwood, J. G.; Schumaker, J. B. *Proc. Natl. Acad. Sci. USA* **1952**, *38*, 863-871.
54. Oosawa, F. *Biopolymers* **1968** *6*, 1633-1647.
55. Fulton, R. L. *J. Chem. Phys.* **1978**, *68*, 3089-3094.
56. Fulton, R. L. *J. Chem. Phys.* **1978**, *68*, 3095-3098.
57. Schmitz, K. S.; Parthasarathy, N.; Vottler, E. *Chem. Phys.* **1982**, *66*, 187-196.
58. Schmitz, K. S.; Parthasarathy, N.; Kent, J. C.; Gauntt, J. *Biopolymers* **1982**, *21*, 1365-1382.
59. Schmitz, K. S.; Lu, M.; Gauntt, J. *J. Chem. Phys.* **1983**, *78*, 5059-5066.
60. Yoshino, S. In *Ordering and Organisation in Ionic Solutions*, Editors, Ise, N.; Sogami, I., Eds.; World Scientific Publ.: Teaneck, N. J., 449-459.
61. Manning, G. S. Invited lecture at the 205th National Am. Chem. Soc. Meeting, Denver, CO, 1993.
62. Sánchez-Sánchez, J. E.; Lozada-Cassou, M. *Chem. Phys. Letts.* **1992**, *190*, 202-208.
63. Odijk, T. *J. Polym. Sci. Polym. Phys. Ed.* **1977** *15*, 477-483.
64. Skolnick, J.; Fixman, M. *Macromolecules*, **1977** *10*, 944-948.
65. Odijk, T.; Houwaart, A. C. *J. Polym. Sci. Polym. Phys. Ed.* **1978** *16*, 627-639.
66. Le Bret, M. *J. Chem. Phys.* **1982** *76*, 6243-6255.
67. Fixman, M. *J. Chem. Phys.* **1982** *76*, 6346-6353.
68. Tricot, M. *Macromolecules* **1984** *17*, 1698-1704.
69. Barrat, J.-L.; Joanny, J.-F. (submitted to *Europhysics Lett.*).
70. Lin, S.-C.; Lee, W. I.; Schurr, J. M. *Biopolymers* **1978**, *17*, 1041-1064.
71. Wilcoxon, J. P.; Schurr, J. M. *J. Chem. Phys.* **1983**, *78*, 3354-3364.
72. Zero, K.; Ware, B. R. *J. Chem. Phys.* **1984**, *80*, 1610-1616.
73. Schmitz, K. S.; Lu, M.; Singh, N.; Ramsay, D. J. *Biopolymers* **1985**, *23*, 1637-1646.
74. Ramsay, D. J.; Schmitz, K. S. *Macromolecules* **1985**, *18*, 2422-2429.
75. Ghosh, S.; Peitzsch, R. M.; Reed, W. F. *Biopolymers* **1992**, *32*, 1105-1122.
76. Drifford, M.; Dalbiez, J.-P. *Biopolymers* **1985**, *24*, 1501-1514.
77. Martin, N. B.; Tripp, J. B.; Shibata, J. H.; Schurr, J. M. *Biopolymers* **1979**, *18*, 2127-2133.
78. Shibata, J. B.; Schurr, J. M. *Biopolymers* **1979**, *18*, 1831-1833.
79. Schmitz, K. S. *Biopolymers* **1993** *33*, 953-959.
80. Reed, W. F.; Ghosh, S.; Medjahdi, G.; Francois, J. *Macromolecules* **1991**, *24*, 6189-6198.
81. Li, X.; Reed, W. F. *J. Chem. Phys.* **1991**, *94*, 4568-4580.
82. Förster, S.; Schmidt, M.; Antonietti, M. *Polymer* **1990**, *31*, 781-792.
83. Schmitz, K. S. *Macroions in Solution and Colloidal Suspension* VCH Publishers: New York, NY, **1993**, 340-348.
84. Bruno, K.; Mattice, W. L. *Macromolecules* **1992**, *30*, 310-330.

85. Schmitz, K. S.; Lu, M.; Singh, N.; Ramsay, D. J. *Biopolymers* **1984** *23*, 1637-1646.
86. Sedlák, M.; Konák, C.; Stepánek, P.; Jakes, J. *Polymer*, **1987**, *28*, 873-880.
87. Schmitz, K. S.; Ramsay, D. J. *J. Colloid and Interf. Sci.* **1985**, *105*, 388-398.
88. Sedlák, M. *Macromolecules* **1993**, *26*, 1158-1162.

RECEIVED August 6, 1993

## Chapter 2

# Ion–Ion Correlations in the Electrical Double Layer around a Cylindrical Polyion

J. Reščič<sup>1</sup> and V. Vlachy<sup>1</sup>

Department of Chemistry, University of Ljubljana, 61000 Ljubljana, Slovenia

Ion-ion correlations in the electrical double-layer around a cylindrical polyion are studied using the grand canonical Monte Carlo technique. The results for the ion-ion distribution functions are used to examine the effect of DNA on bimolecular chemical reaction rates. The comparison with experimental data for the energy transfer in DNA-electrolyte mixtures indicates, that the theory significantly overestimates the effects of DNA on the counterion-counterion collision frequency.

The clustering of counterions around linear polyelectrolytes in the solution has long been theoretically predicted (1-3). This phenomenon has important consequences for thermodynamic and transport properties of polyelectrolyte solutions. Theoretical studies, published so far, are primarily concerned with the distribution of ions around polyion (1) (singlet distribution function) and little attention is paid to the ion-ion distributions (two-particle distribution functions) in the cylindrical double-layer. Two-particle distribution functions are rarely studied even for a simpler, planar, geometry (4). The study of ion-ion correlations in the cylindrical double-layer presented here, is motivated by the experimental work of Wensel and co-workers (5), who measured the effect of DNA on rates of bimolecular energy transfer between small ions. These measurements provide a direct indication of how the ions are distributed in the electrical double-layer around the polyion. The measured effect of DNA on ion-ion collision frequencies has been used to test various polyelectrolyte theories, like counterion-condensation theory (2) and the Poisson-Boltzmann cell theory (1,5). The conclusion is that both, in general quite successful polyelectrolyte theories, grossly overestimate the effect of DNA on rates of energy transfer. The analysis of experimental data presented in Reference (5) is based on the equation of Morawetz (6), where the observed rate constants for energy transfer in the presence

<sup>1</sup>Corresponding author

of a polyelectrolyte  $k$  and its absence,  $k_0$ , are related as:

$$\frac{k}{k_0} = \frac{V^{-1} \int n_i(r) n_j(r) dV}{\left[ V^{-1} \int n_i(r) dV \right] \left[ V^{-1} \int n_j(r) dV \right]} \quad (1)$$

The local number concentrations of small ions,  $n_i(r)$ , are evaluated by the Poisson-Boltzmann equation. The domain of integration extends over all volume accessible to small ions. The shortcomings of the Poisson-Boltzmann theory have been analyzed in many papers, most recently perhaps in References (7-9). In short, the Poisson-Boltzmann approximation treats the small ions as pointlike charges, ignoring their mutual correlations (10). It should be noted that equation 1 contains similar mean-field type of approximations, as inherent to the Poisson-Boltzmann theory.

In the present paper we suggest an alternative approach to analyze the effect of polyelectrolyte upon reaction rates. The grand canonical Monte Carlo method is used to study the correlations between small ions in the double-layer around the DNA polyion. If DNA is added to an electrolyte solution, the counterions concentrate in the vicinity of DNA molecules. The effect of DNA on ion-ion correlations is assumed to be a measure of the increase of bimolecular energy transfer rate in the DNA-electrolyte mixtures (5). During the Monte Carlo simulation, the spherically symmetric ion-ion correlation functions  $g_{ij}(r)$ , not studied in previous calculations, are monitored. The ratio  $k / k_0$  is approximated by (11)

$$\frac{k}{k_0} = \frac{\langle g_{AB}(a) \rangle}{g_{AB}^0(a)} \quad (2)$$

where  $a$  is the distance of collision of the two ions and  $\langle \dots \rangle$  denotes the volume average. The Monte Carlo results for equation 2 are compared with the results of the Morawetz equation (with local concentrations calculated from the Poisson-Boltzmann theory) and with experimental data of Reference (5).

## Models and Methods

**Cell Model.** The model of DNA-electrolyte mixture used in this study treats the polyion as an impenetrable, infinitely long cylinder. Each polyion is placed along the long axis of a cylindrical cell. A collection of such, identical and independent cells, is taken to represent as solution. The radius  $R$  of the cell is related to the concentration of the solution  $C_m$ , expressed in moles of the monomer units.

$$C_m = \frac{l}{\pi (R^2 - \sigma^2) b N_A} \quad (3)$$



where  $b$  is the length of the monomer unit,  $\sigma$  is the distance of closest approach between ion and polyion and  $N_A$  is Avogadro's number. The fixed charge, one per length  $b$ , is assumed to be smeared uniformly over the polyion surface. The counterions and co-ions, in Monte Carlo calculation they are modeled as charged hard spheres of diameter  $a$ , move in a dielectric continuum. Moreover, the relative permittivity  $\epsilon_r$  is assumed to be uniform through the system.

**Poisson-Boltzmann Equation.** The Poisson-Boltzmann equation for the cylindrical symmetry reads

$$\frac{1}{r} \frac{d}{dr} \left( r \frac{d\psi(r)}{dr} \right) = - \frac{e_0}{\epsilon_0 \epsilon_r} \sum_i z_i n_i(r) \quad (4)$$

$$n_i(r) = n_i(R) \exp[-z_i e_0 \psi(r)]$$

where  $\psi(r)$  is the mean electrostatic potential at a distance  $r$  and  $n_i(0)$  is the number concentration of ionic species  $i$  at  $r = R$ . As usual  $\beta = (k_B T)^{-1}$ , where  $k_B$  is the Boltzmann's constant and  $T$  absolute temperature. The appropriate boundary conditions, given by the Gauss Law, are

$$\left( \frac{d\psi(r)}{dr} \right)_R = 0, \quad \left( \frac{d\psi(r)}{dr} \right)_0 = \frac{e_0}{2\pi \epsilon_0 \epsilon_r \sigma b} \quad (5)$$

The Poisson-Boltzmann equation has been solved subject to the boundary conditions using the so-called "shooting method" (12). Once the mean electrostatic potential is known, the volume averages needed in equation 1 can readily be calculated.

**Grand Canonical Monte Carlo Calculation.** The grand canonical Monte Carlo method has been introduced in the electrical double-layer studies by Valleeau and co-workers (13,14). The mixture of electrolyte and DNA is assumed to be separated from "bath" of pure electrolyte (bulk) by a semipermeable membrane. In equilibrium, the distribution of small ions (polyions cannot cross the membrane) between DNA-electrolyte mixture and bulk electrolyte solution is given by equality of the chemical potential on each side. The advantage of the method is that by sampling at constant chemical potential, the relevant bulk phase is defined unambiguously. The method has been used and described in detail in several papers (9,13-16).

The simulation procedure consists of two steps. The first step is canonical: a randomly chosen ion is moved into a new random position in the Monte Carlo cell. The attempted move is accepted with probability  $f_{ij}$  (equation 6), where  $U_i$  ( $U_j$ ) is the configurational energy of state  $i$  ( $j$ ), and  $Y = 1$ . In the next step, a random decision is made to either attempt the insertion or deletion of a neutral combination of ions. The transition probability from the state  $i$  ( $N_i, N^+$ ) to state  $j$  ( $N_j, N^+$ ) is given by

combination of equations 6 and 7:

$$f_{ij} = \min \{ 1, Y \exp[-\beta (U_j - U_i)] \} \quad (6)$$

$$Y = \frac{N^+ N^- \gamma_{\pm,s}}{N_j^+ N_j^-} \quad (\text{addition}) \quad ; \quad Y = \frac{N_i^+ N_i^-}{N^+ N^- \gamma_{\pm,s}} \quad (\text{deletion}) \quad (7)$$

$\gamma_{\pm}$  is the mean activity coefficient of bulk electrolyte with ionic concentrations  $N_+/V$  and  $N_-/V$ . The corrections due to the finite size of the Monte Carlo cell, which may be important for anisotropic systems, have been evaluated using the procedure developed by Rosky and co-workers (17). In this calculation the number of monomer units  $b$  included in the Monte Carlo cell is from 90 to 180 depending on the polyelectrolyte concentration.

## Results

In this section we present numerical results for the model system described above. Counterions and co-ions are of equal size, diameter  $a = 0.8$  nm and  $\sigma = 1.38$  nm. All calculations apply to water-like solutions at  $T = 298$  K. The central parameter of the Poisson-Boltzmann cell theory,  $\lambda = \beta e^2 / (4\pi\epsilon_0\epsilon_b) = 4.2$ . The grand canonical simulation requires as input the mean activity coefficient of the pure (bulk) electrolyte solution. The results for  $\gamma_{\pm}$  at various concentrations are obtained separately and they are given in Table I.

Table I. Numerical Results for the Model System

$C_s \cdot 10^3 / (\text{mol}/\text{dm}^3)$	1.24	1.99	2.47	3.60	5.00
$\gamma_{\pm}$	0.966	0.957	0.955	0.949	0.943
$C_s \cdot 10^3 / (\text{mol}/\text{dm}^3)$	6.32	10.18	28.05	49.92	100.1
$\gamma_{\pm}$	0.940	0.931	0.935	0.960	1.051

The two-particle distribution function  $g_{ij}(\mathbf{r}_i, \mathbf{r}_j) = g_{ij}(\mathbf{r}_i, \mathbf{r}_{ij})$  depends on the positions  $\mathbf{r}_i$  and  $\mathbf{r}_j = \mathbf{r}_i + \mathbf{r}_{ij}$ , of the two ions in the cylindrical cell. We are interested in the correlation function  $g_{ij}(r_{ij}) = g_{ij}(|\mathbf{r}_i - \mathbf{r}_j|)$ , which measures the probability for two ions to be within the distance  $r, r + dr$  from each other. During the computer simulation,  $g_{ij}(\mathbf{r}_i, \mathbf{r}_{ij})$  is averaged over the position  $\mathbf{r}_i$  to obtain  $g_{ij}(r_{ij})$ . In order to accumulate good statistics very long Monte Carlo runs are needed. The distribution functions are collected on the grid of 0.1 nm and averaged over 3000 or more configurations per particle.

In Figure 1 we present the correlation function  $g_{++}(r)$  for counterions in the DNA-electrolyte mixture with  $C_m = 0.01$  monomol/dm<sup>3</sup> and  $C_s = 0.002$  mol/dm<sup>3</sup>. Small enhancement in  $g_{++}(r)$  is due to the clustering of counterions around the DNA

molecule. The same effect has been observed in solutions of highly asymmetric electrolytes (18-20). The equivalent correlation function for bulk electrolyte of concentration  $C_s$  is shown in the same figure. The addition of polyelectrolyte dramatically changes the counterion-counterion correlations and it is expected to have a strong effect on the chemical reaction rate. The similar holds true for the counterion-coion pair (+,-) as presented in Figure 2, while the equivalent function for co-ions (not shown here),  $g_{-}(r)$ , is almost unaffected by the presence of polyelectrolyte. The results for electrolyte-polyelectrolyte mixture with  $C_m = 0.002$  monomol/dm<sup>3</sup> and  $C_s = 0.002$  mol/dm<sup>3</sup> are shown in Figures 3 and 4. Finally, the results for the case where simple electrolyte is added in an excess, i.e.  $C_m = 0.0004$  monomol/dm<sup>3</sup> and  $C_s = 0.002$  mol/dm<sup>3</sup>, are presented Figures 5 and 6. In this case the correlation function for +,- pair,  $g_{\pm}(r)$ , shows almost no change upon addition of polyelectrolyte in the system.

The theory of chemical reactions suggests that reaction rates may be related to the static structure of the solution. Under certain approximations the rate for bimolecular reaction is proportional to  $g_{ij}(a)$ , where  $a$  is a distance of closest approach of two ions (11). The ratio of the energy-transfer rates between counterions, calculated by equation 2 at several DNA concentrations, is shown in Figure 7. In the same figure we show the results obtained from equation 1 and the solution of the Poisson-Boltzmann equation (line) and the experimental data compiled from Figure 3 of Reference (5). It is quite clear from this comparison that equation 2 (and Monte Carlo simulation) yields a slightly better agreement with the experiment, but the agreement is far from being quantitative. Both theories, based either on equation 1 or 2, greatly overestimate the effects of DNA on collision frequencies at low DNA concentrations. For example, at  $C_m = 0.0004$  mole/dm<sup>3</sup> and  $C_s = 0.002$  mole/dm<sup>3</sup> equation 1 (Poisson-Boltzmann theory) and equation 2 (Monte Carlo simulation) give  $k/k_0 = 35$  and 22, respectively, while the experimentally obtained value for these concentrations is much lower, around 3. Finally we need to mention, that evaluation of  $g_{ij}(a)$  requires an extrapolation of the correlation function, what is associated with a measurable uncertainty, as shown in Figures 1-6.

## Conclusions

In 1988 Wensel and coworkers (5) presented an interesting experimental study of DNA-electrolyte mixtures. Initial theoretical analysis, based on the Poisson-Boltzmann theory (5) is only qualitatively correct; the effects of DNA on the rate of energy transfer between counterions is much smaller than theoretically predicted. The similar conclusion seems to apply to the condensation theory of Manning, though the possibilities of this theory have not been fully explored yet. The third calculation used in analysis of the energy transfer data is a semiempirical theory suggested by Matthew (5). This approach, which uses the molecular structure of B-DNA, yields better agreement with measured data than other two theories, but it also contains more parameters.

In this paper we have explored an alternative approach, where the ion-ion correlations between small ions in the cylindrical double-layer are studied by the computer simulation method. No such data are taken in previous Monte Carlo studies of polyelectrolyte solutions. The correlation function between counterions is

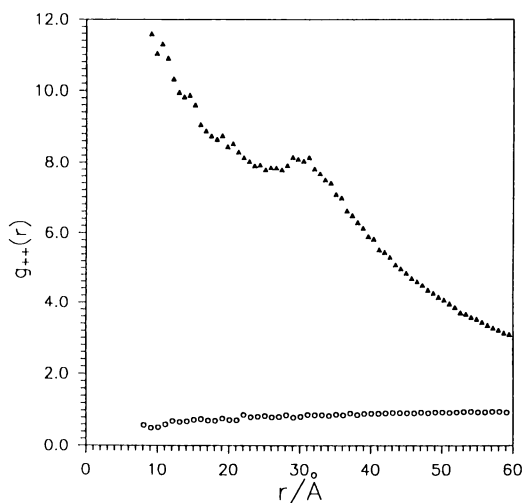


Figure 1. Counterion-counterion correlation function,  $g_{++}(r)$ , for DNA-electrolyte mixture (▲), and for pure electrolyte solution (○). The concentrations are:  $C_m = 0.01$  monomol/dm<sup>3</sup> and  $C_s = 0.002$  mol/dm<sup>3</sup>.

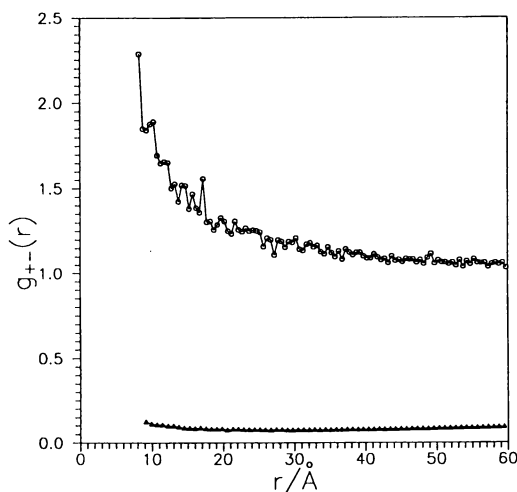


Figure 2. Counterion-coion correlation function,  $g_{+-}(r)$ , for DNA-electrolyte mixture (▲) and for pure electrolyte solution (○). The concentrations are:  $C_m = 0.01$  monomol/dm<sup>3</sup> and  $C_s = 0.002$  mol/dm<sup>3</sup>.

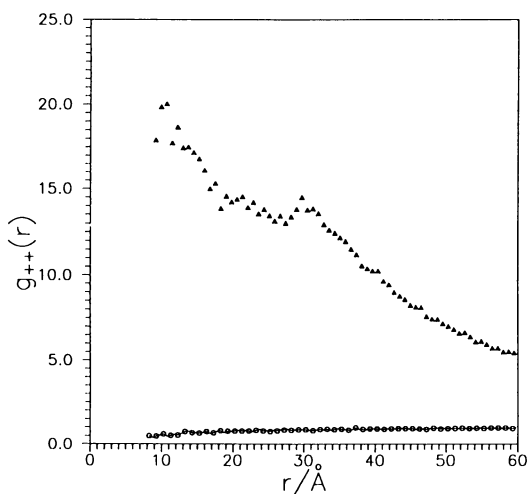


Figure 3. The same as for Figure 1. The concentrations are:  $C_m = 0.002$  monomol/dm<sup>3</sup> and  $C_s = 0.002$  mol/dm<sup>3</sup>.

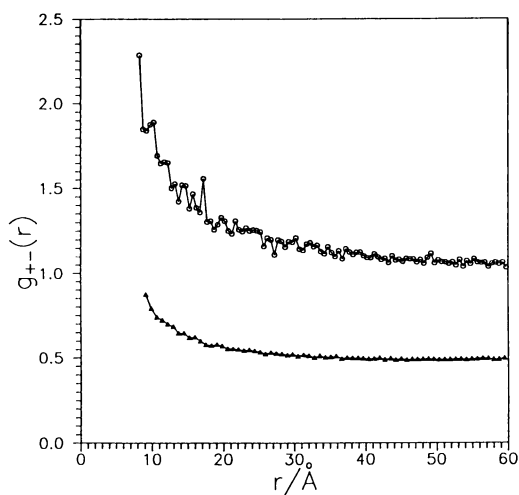


Figure 4. The same as for Figure 2. The concentrations are:  $C_m = 0.002$  monomol/dm<sup>3</sup> and  $C_s = 0.002$  mol/dm<sup>3</sup>.

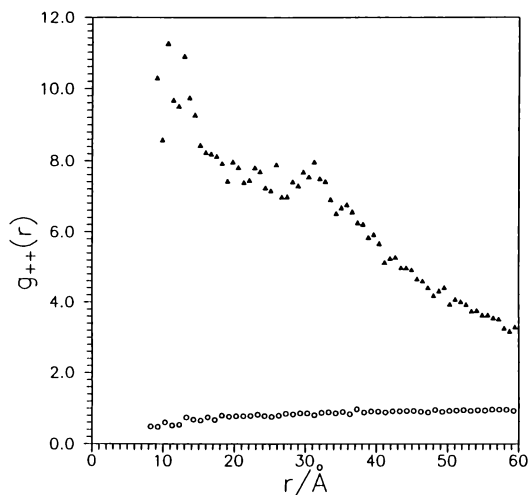


Figure 5. The same as for Figure 1. The concentrations are:  $C_m = 0.0004$  monomol/dm<sup>3</sup> and  $C_s = 0.002$  mol/dm<sup>3</sup>.

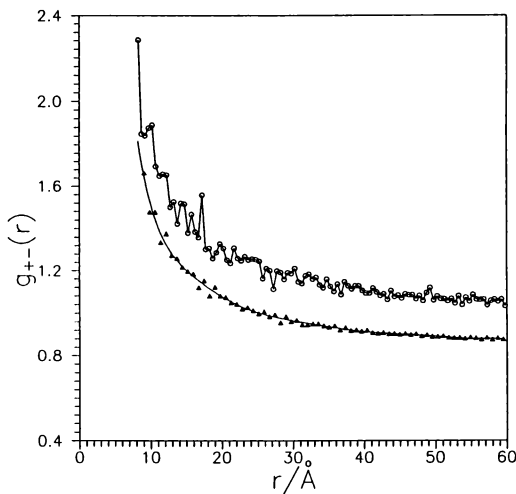


Figure 6. The same as for Figure 2. The concentrations are:  $C_m = 0.0004$  monomol/dm<sup>3</sup> and  $C_s = 0.002$  mol/dm<sup>3</sup>.

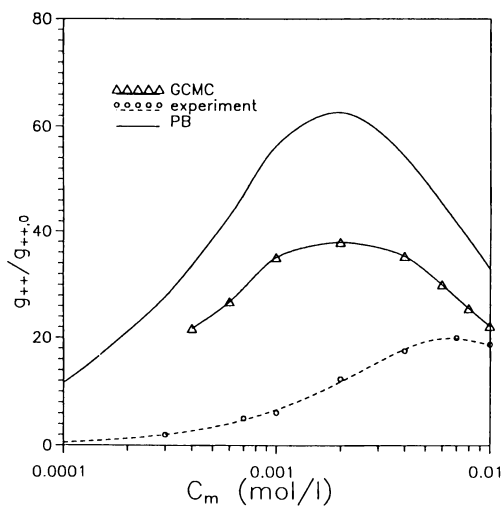


Figure 7. Rate constant ratio  $k/k_0$  for energy transfer between monovalent cations as a function of DNA concentration. Experimental data (broken line) from Reference (5). The uncertainty in the Monte Carlo results is from 5% to 10%.

via equation 2 related to the energy-transfer rate in DNA-electrolyte mixtures. The results are disappointing. The new approach seems to work slightly better than a combination of equation 1 and the Poisson-Boltzmann theory, but there is no quantitative agreement with the experimental data. Particularly poor agreement is obtained for low concentrations of DNA in mixture. The fact that various, very different theories, fail to describe the experimental results seems to suggest that the (rod-like) model used here is a poor representation for the DNA polyanion.

### Literature Cited

- 1) Katchalsky, A. *Pure. Appl. Chem.* **1971**, *26*, 327.
- 2) Manning, G. S. *Acc. Chem. Res.* **1976**, *12*, 443.
- 3) Anderson, C. T.; Record Jr., M. T. *Annu. Rev. Phys. Chem.* **1982**, *33*, 191.
- 4) Henderson, D.; Plischke, M. *J. Phys. Chem.* **1988**, *92*, 7177.
- 5) Wensel, T. G.; Meares, C. F.; Vlachy, V.; Matthew, J. B. *Proc. Natl. Acad. Sci. U. S.* **1986**, *83*, 3267.
- 6) Morawetz, H. *Acc. Chem. Res.* **1970**, *3*, 354.
- 7) Valleau, J. P.; Ivkov R.; Torrie, G. M. *J. Chem. Phys.* **1991**, *95*, 520.
- 8) Torrie, G. M. *J. Chem. Phys.* **1992**, *96*, 3772.
- 9) Jamnik B.; Vlachy, V. *J. Am. Chem. Soc.* **1993**, *115*, 660.
- 10) Fixman, M.; *J. Chem. Phys.* **1979**, *70*, 4995.
- 11) Keizer, J. *Acc. Chem. Res.* **1985**, *18*, 235.
- 12) Carnahan, B.; Luther, H. A.; Wilkes, J. O. *Applied Numerical Methods*; Wiley: New York, U.S., 1969.
- 13) Torrie, G. M.; Valleau, J. P. *J. Chem. Phys.* **1980**, *73*, 5807.
- 14) Torrie, G. M.; Valleau, J. P. *J. Phys. Chem.* **1982**, *86*, 3251.
- 15) Vlachy, V.; Haymet, A. D. J. *J. Chem. Phys.* **1986**, *84*, 5874.
- 16) Mills, P.; Anderson, C. F.; Record, M. T. *J. Phys. Chem.* **1986**, *90*, 6541.
- 17) Murthy, C. S.; Bacquet R. J.; Rossky, J. P. *J. Phys. Chem.* **1985**, *89*, 701.
- 18) Vlachy, V.; Marshall, C.; Haymet, A. D. J. *J. Am. Chem. Soc.* **1989**, *111*, 4160.
- 19) Reščič, J.; Vlachy, V.; Haymet, A. D. J. *J. Am. Chem. Soc.* **1990**, *112*, 3398.
- 20) Linse, P. *J. Chem. Phys.* **1990**, *93*, 1376.

RECEIVED August 6, 1993



## Chapter 3

# A Perturbative Approach to Polyelectrolyte Configuration

D. Bratko<sup>1</sup> and K. A. Dawson<sup>2</sup>

Department of Chemistry, University of California, Berkeley, CA 94720

A simple self-consistent perturbative approach is applied to study the configuration of an isolated ringlike polyion. The calculation is based on the application of Edwards Hamiltonian for a self avoiding macromolecule, supplemented by screened electrostatic interactions among ionized units of the chain. The structure is described in terms of mean square distances between the beads, calculated using the probability distribution of a reference Hamiltonian with purely harmonic interactions. The method provides analytic scaling relations for mean square distances among distant units and lends itself in a form, suitable for numerical solution. The swelling of a strongly ionized polyion is studied as a function of its length  $L$  and the ionic strength of the supporting solution. Extension of the method to systems with attractive intramolecular forces between nonadjacent units is considered and numerical results for a helix-forming polymer are presented.

The configuration of an ionized macromolecule in solution is determined by an interplay of chain elasticity, steric effects and long-ranged electrostatic repulsion. These interactions have been the subject of a variety of theoretical (1-21) and simulation (8,22-30) studies of polyelectrolyte solutions. In view of the complexity of real systems, different simplifications were introduced to facilitate the theoretical analysis. A conventional model of polymer theory describes the bonds among monomer units as harmonic springs and treats the excluded volume forces in terms of the Dirac  $\delta$  function

<sup>1</sup>Also affiliated with J. Stefan Institute, University of Ljubljana, Ljubljana, Slovenia

<sup>2</sup>Current address: Department of Chemistry, University College Dublin, Belfield, Dublin 4, Ireland

0097-6156/94/0548-0034\$06.00/0

© 1994 American Chemical Society

(31). Electrostatic effects may be introduced as an additional term in the polymer Hamiltonian, in the simplest case represented by a sum of pairwise additive Yukawa interactions among the charged groups on the chain. In the case of long neutral macromolecules, valuable insights are known to be obtained by studying polymer rings which behave in a similar way as linear chains and, in the case of the above Hamiltonian, lend themselves to a useful analytic solution (32-34). In the preceding works (21,35), a generalization of the ringlike polymer model to charged systems has been suggested and a numerical scheme based on the variational method for the polyelectrolyte structure has been proposed (21,35,36). In the present paper, the variational treatment of these works is shown to be equivalent to a special case of a more general perturbative approach (37). For the particular type of the Hamiltonian, used in our system, the first order perturbation approximation is equivalent to the application of the Gibbs-Bogoliubov bound for the free energy of the polymer. In either approach, the polymer configuration is determined by averaging with respect to an approximate probability distribution of a reference system with a Gaussian Hamiltonian of a collection of Harmonic oscillators. The true Hamiltonian of our system and the perturbative analysis will be described in the following Section. The results will be used to establish scaling relations for mean square distance between distant beads in a number of characteristic situations. In the last Section, we describe the numerical solution of the system of nonlinear equations for reference Hamiltonian couplings and present numerical results for a set of strongly charged dilute polyelectrolytes in a good solvent and at varying degree of polymerization and concentration of the simple electrolyte. Finally, we consider extensions to anisotropic systems and polymers with specific attractive intramolecular interactions.

### Model and Method

The cyclic polyelectrolyte molecule is pictured as a necklace comprising  $L$  monomer units. The unit length in the absence of steric and electrostatic forces is  $l$ . The total charge of the polyion is uniformly spread over all beads, each carrying an average charge  $q$ . The bonds between neighbouring units are treated as harmonic springs and we describe the excluded volume interactions in terms of a virial expansion for the Dirac  $\delta$  function form of the potential between the particles. The electrostatic effects are approximated by the Debye-Huckel screened potential among the beads of the polyion. The solution is sufficiently diluted that there are no significant intermolecular interactions. The configuration dependent part of the Hamiltonian is

$$\begin{aligned}
 H = & \frac{3}{2l^2} \sum_{s=1}^{L-1} (\mathbf{r}_{s+1} - \mathbf{r}_s)^2 + \frac{u_2}{2} \sum_{s,s'} \delta(\mathbf{r}_s - \mathbf{r}_{s'}) \\
 & + \frac{u_3}{3!} \sum_{s,s',s''} \delta(\mathbf{r}_s - \mathbf{r}_{s'}) \delta(\mathbf{r}_s - \mathbf{r}_{s''}) + \dots + V \sum_{s,s'} \frac{e^{-\kappa l |\mathbf{r}_s - \mathbf{r}_{s'}|}}{|\mathbf{r}_s - \mathbf{r}_{s'}|} \quad (1)
 \end{aligned}$$

where the energy is given in units  $kT$ ,  $k$  is the Boltzmann constant and  $T$  the temperature,  $\kappa$  is the Debye screening parameter,  $V=q^2/8\pi\epsilon kT$  is one half of the Bjerrum length,  $\epsilon$  the permittivity,  $s$  the relative position on the chain and the summations are carried out over all  $L$  units of the polyion. At nonzero values of the two particle excluded volume parameter  $u_2$ , the three body term can usually be omitted but will become important (35) at theta conditions where it represents the dominant short ranged interaction. The structure of the polyion is described in terms of mean square distances  $\langle |\mathbf{r}(s) - \mathbf{r}(s')|^2 \rangle$  for all separations  $|s - s'|$  in the range from 0 to  $L/2$ . The averages will be calculated by considering the probability distribution over possible configurations for a reference system with a Gaussian Hamiltonian  $H_0$

$$H_0 = \sum_{s < s'} \Gamma(s - s') |\mathbf{r}_s - \mathbf{r}_{s'}|^2 \quad (2)$$

where the couplings  $\Gamma(s - s')$  have yet to be determined. We proceed to this end by employing a self-consistent perturbative approach, investigated some time ago (37) in a study of a neutral polymer. We begin by writing the canonical average of an observable  $O(\{\mathbf{r}_s\})$

$$\langle O \rangle_H = \frac{\text{Tr}[e^{-(H - H_0)} e^{-H_0} O]}{\text{Tr}[e^{-(H - H_0)} e^{-H_0}]} \quad (3)$$

Expansion in cumulant series gives

$$\langle O \rangle_H = \langle O \rangle_{H_0} - \langle O(H - H_0) \rangle_{H_0} + \langle O \rangle_{H_0} \langle (H - H_0) \rangle_{H_0} + O[(H - H_0)^2] \quad (4)$$

and we can choose the reference Hamiltonian in such a way that

$$\langle O(H - H_0) \rangle_{H_0} = \langle O \rangle_{H_0} \langle (H - H_0) \rangle_{H_0} \quad (5)$$

which amounts to the first order perturbation theory, the difference between the averages of the observable  $O$  in the true and the reference ensemble being of the order  $(H - H_0)^2$ . Within this level of approximation, equation 5 can, therefore, be used to determine the couplings  $\Gamma(s - s')$  of equation 2. The procedure is simplified (32,33) by using the Fourier components (38)

$$\hat{\mathbf{r}}(q) = \frac{1}{\sqrt{L}} \sum_s \mathbf{r}(s) e^{iqs}, \quad \mathbf{r}(s) = \frac{1}{\sqrt{L}} \sum_q \hat{\mathbf{r}}(q) e^{iqs} \quad (6)$$

with  $q=2\pi i/L$ ,  $i=0,1,2\dots L-1$ ,

$$\sum_{s<s'} \Gamma(s-s') |\mathbf{r}_s - \mathbf{r}_{s'}|^2 = \sum_q g(q) |\hat{\mathbf{r}}(q)|^2 \quad (7)$$

and

$$\frac{3}{2l^2} \sum_{s=1}^{L-1} (\mathbf{r}_{s+1} - \mathbf{r}_s)^2 = \sum_q j(q) |\hat{\mathbf{r}}(q)|^2 \quad (8)$$

where

$$g(q) = \sum_s \Gamma(s)[1 - \cos qs] \quad \text{and} \quad j(q) = \frac{3}{l^2}(1 - \cos q) \quad (9)$$

The difference  $\langle H - H_0 \rangle$  is obtained by expanding the  $\delta$  functions in plane waves and then averaging with respect to the reference Hamiltonian

$$\begin{aligned} \langle H - H_0 \rangle &= \sum_q [j(q) - g(q)] \langle |\hat{\mathbf{r}}(q)|^2 \rangle + \frac{\hat{u}_2}{2} \sum_{s,s'} \langle |\mathbf{r}(s) - \mathbf{r}(s')|^2 \rangle - \frac{3}{2} + \\ &\frac{\hat{u}_3}{3!} \sum_{s,s',s''} \int d\mathbf{k} \int d\mathbf{k}' e^{-\frac{k^2}{6} \langle |\mathbf{r}(s) - \mathbf{r}(s')|^2 \rangle - \frac{k'^2}{6} \langle |\mathbf{r}(s) - \mathbf{r}(s'')|^2 \rangle} \\ &e^{-\frac{\mathbf{k}\mathbf{k}'}{4} [\langle |\mathbf{r}(s) - \mathbf{r}(s')|^2 \rangle + \langle |\mathbf{r}(s) - \mathbf{r}(s'')|^2 \rangle - \langle |\mathbf{r}(s') - \mathbf{r}(s'')|^2 \rangle]} \\ &\frac{2}{\pi} v \sum_{s,s'} \int_0^{\infty} e^{-\frac{k^2}{6} \langle |\mathbf{r}(s) - \mathbf{r}(s')|^2 \rangle} \frac{k^2 dk}{k^2 + \kappa^2} \quad (10) \end{aligned}$$

where  $\hat{u}_2 = (3/2\pi)^{3/2} u_2$ , and  $\langle |\mathbf{r}(s) - \mathbf{r}(s')|^2 \rangle$  is the mean squared distance between the units  $s$  and  $s'$ .

$$\langle |\mathbf{r}(s) - \mathbf{r}(s')|^2 \rangle = \frac{3}{L} \sum_q \frac{1 - \cos q(s-s')}{g(q)} \quad (11)$$

Applying equation 5 to the observables  $O = |\hat{\mathbf{r}}(q)|^2$  at  $L/2$  discrete values  $q_i = 2\pi i/L$ ,

$i=1,2..L/2$ , and neglecting the three body or higher terms, we obtain the first order approximation for the unknown coupling coefficients  $g(q)$ :

$$g(q) - j(q) + \frac{3\hat{u}}{2L} \sum_{s,s'} \langle |\mathbf{r}(s) - \mathbf{r}(s')|^2 \rangle^{-\frac{5}{2}} [1 - \cos q(s-s')] +$$

$$\frac{2V}{3\pi L} \sum_{s,s'} \int_0^\infty e^{-\frac{k^2}{6} \langle |\mathbf{r}(s) - \mathbf{r}(s')|^2 \rangle} \frac{-\frac{k^2}{6} \langle |\mathbf{r}(s) - \mathbf{r}(s')|^2 \rangle}{k^2 + \kappa^2} k^4 dk [1 - \cos q(s-s')] + \dots = 0 \quad (12)$$

Identical result has previously been derived by minimizing the Gibbs-Bogoliubov bound of the free energy of the system (21,35). Applying direct iteration along with the analytic solution to the integral in the electrostatic term, equation 12 can readily be solved at arbitrary conditions (35). In the limits of either very strong or vanishingly weak screening, expansions in terms of  $k^2/\kappa^2$  can be used to simplify the electrostatic term of equation 12 thus making possible a direct scaling analysis at some extreme conditions. The knowledge of the long distance (large  $|s-s'|$ ) behavior requires the small  $q$  dependence of  $g(q)$  which may be shown to vanish as

$$g(q) \underset{q \rightarrow 0}{\sim} \frac{1}{D} q^{2\beta} \quad (13)$$

Equations 11 and 13 give

$$\langle |\mathbf{r}(s) - \mathbf{r}(s')|^2 \rangle \approx D |s - s'|^{2\alpha}, \quad 2\alpha = 2\beta - 1 \quad (14)$$

In view of equations 11-14, equation 12 at large  $\kappa$  simplifies to

$$g(q) - \frac{3}{2l^2} q^2 + \left( a_1 \frac{V}{\kappa^2} + \frac{3}{2} \hat{u} \right) \frac{1}{L} \sum_{s,s'} [1 - \cos q(s-s')] \langle |\mathbf{r}(s) - \mathbf{r}(s')|^2 \rangle^{-\frac{5}{2}}$$

$$- \frac{b_1 V}{L \kappa^4} \sum_{s,s'} [1 - \cos q(s-s')] \langle |\mathbf{r}(s) - \mathbf{r}(s')|^2 \rangle^{-\frac{7}{2}} + \dots = 0 \quad (15)$$

with  $a_1 = 9\sqrt{\frac{6}{\pi}}$  and  $b_1 = 15a_1$ . For small  $q$  ( $q \ll \kappa$ ) and large  $L$ , the leading behavior of equation 15 is

$$\frac{1}{D} q^{2\beta} - \frac{3}{2l^2} q^2 + \frac{I_1}{D^{\frac{5}{2}}} \left( a_1 \frac{V}{\kappa^2} + \frac{3}{2} \hat{u}_2 \right) q^{5\alpha-1} - \frac{b_1 I_2}{D^2} \frac{V}{\kappa^4} q^{7\alpha-1} + \dots = 0 \quad (16)$$

where  $I_1$  and  $I_2$  are pure constants obtained by integration over  $|s-s'|$ . Applying the method of dominant balance (39) at small  $q$  we find the solution

$$5\alpha - 1 = 2, \quad \alpha = \frac{3}{5}, \quad D = \left[ \frac{2I_1 l^2}{3} \left( a_1 \frac{V}{\kappa^2} + \frac{3}{2} \hat{u}_2 \right) \right]^{\frac{2}{5}} \quad (17)$$

Over long distances  $|s-s'| \gg 1$  a well screened polymer resembles a self-avoiding ring with a modified second virial coefficient. A more careful analysis (35) avoiding the approximations of the preceding paragraph yields similar results but with Reiss exponent  $2\alpha=4/3$  replacing the Flory result. At shorter distances or in the absence of simple electrolyte, when we may ignore the screening of Coulombic interactions, an alternative expansion of equation 12 gives

$$\begin{aligned} g(q) - \frac{3}{2l^2} q^2 + \frac{3\hat{u}_2}{2L} \sum_{s,s'} \langle |\mathbf{r}(s) - \mathbf{r}(s')|^2 \rangle > -\frac{5}{2} [1 - \cos q(s-s')] + \\ \frac{a_2 V}{L} \sum_{s,s'} \langle |\mathbf{r}(s) - \mathbf{r}(s')|^2 \rangle > -\frac{3}{2} [1 - \cos q(s-s')] + \\ -\frac{b_2 V \kappa^2}{L} \sum_{s,s'} \langle |\mathbf{r}(s) - \mathbf{r}(s')|^2 \rangle > -\frac{1}{2} [1 - \cos q(s-s')] + \dots = 0 \end{aligned} \quad (18)$$

with  $a_2 = \sqrt{\frac{6}{\pi}}$  and  $b_2 = \frac{a_2}{3}$ . The leading terms of equation 18 are

$$\frac{1}{D} q^{2\beta} - \frac{3}{2l^2} q^2 + \frac{I_1}{D^{\frac{5}{2}}} \frac{3}{2} \hat{u}_2 q^{5\alpha-1} + \frac{I_3 V}{D^2} q^{3\alpha-1} - \frac{I_4 V \kappa^2}{D^{\frac{1}{2}}} q^{\alpha-1} + \dots = 0 \quad (19)$$

At  $\kappa \rightarrow 0$ , the dominant balance for small  $q$  (big  $|s-s'|$ ) gives

$$3\alpha - 1 = 2, \quad D = \left( \frac{2}{3} l^2 V I_3 \right)^{\frac{2}{3}} \quad (20)$$

or  $\alpha=1$ . In the absence of screening, a full extension of the polyion segment is predicted. A moderately screened polyion can be viewed as a self-avoiding chain over distances considerably exceeding the screening length  $1/\kappa$  while its segments behave as rigid rods over the range short in comparison with  $1/\kappa$ . In poor solvents, the three-particle term of equation 2 represents an important short-ranged repulsive contribution. In the absence of the screening, analogous considerations as applied above reveal a fully stretched long-distance configuration,  $\alpha\sim 1$ . For smaller separations  $|s-s'|$ , a rather different scaling may be observed. Here, the dominant balance has to be applied to the large  $q$  regime. Depending on the sign and the magnitude of the short-ranged coupling  $u_2$ , this may yield the scaling exponent  $\alpha=1/2$  or  $\alpha=3/5$ . A globally extended segment can comprise smaller blobs (2,11,17) with internal scaling of a gaussian or a self avoiding coil. In poor solvents, characterized by negative values of the parameter  $u_2$ , attractive forces between the units would lead to the formation of collapsed blobs with  $\alpha=1/3$ . A detailed analysis along these lines will be reported (35).

## Numerical Results

The system of  $L/2$  nonlinear equations 12 for coefficients  $g(q)$  is solved by direct iteration. The procedure is initiated by assuming an ideal Gaussian behavior of the ring and using the corresponding mean square distances  $\langle |\mathbf{r}(s) - \mathbf{r}(s')|^2 \rangle$  in calculation of corrected  $g(q)$ . From those, improved distances  $\langle |\mathbf{r}(s) - \mathbf{r}(s')|^2 \rangle$  are determined and the procedure is repeated until a self consistent solution of a sufficient accuracy is obtained. The use of mixing parameter of rather low value between  $10^{-3}$  and  $10^{-1}$  is needed to ascertain the convergence of the iteration. The number of iterations needed depends on the length of the chain  $L$ , the charge  $q$  and the screening parameter  $\kappa$ . About  $10^2$ - $10^3$  cycles were usually sufficient to obtain the accuracy better than 0.01% in calculated mean square distances  $\langle |\mathbf{r}(s) - \mathbf{r}(s')|^2 \rangle$ . In the following paragraph, we present numerical results for polyion expansion obtained from equations 12-14 at various conditions. The model parameters in these calculations correspond to aqueous solutions of vinylic polyions of monomer length  $l=2.52$  Å and the degree of ionization determined by Manning's limiting charge density of the polyion (40-42). According to the concept of ion condensation (40-42), seen to conform with the results of computer simulation (43), these results should be approximately valid for all ionizations above the critical value. The monomer units are treated as hard spheres of diameter  $l$ . In Table I, the mean square distances  $\langle |\mathbf{r}(s) - \mathbf{r}(s')|^2 \rangle$  and the scaling exponents  $2\alpha = d \ln \langle |\mathbf{r}(s) - \mathbf{r}(s')|^2 \rangle / d \ln L$  for various degrees of polymerization  $L$  and the ionic strengths are collected. At very strong screening, numerical data approach the results for self avoiding cyclic polymers (32,33). As pointed out by des Cloizeaux (32-34), the self-avoiding rings under present approximations are characterized by the Reiss exponent  $2\alpha=4/3$  and this is confirmed by the present results. The nonscreened polyions, on the other hand, behave as fully extended rings. In a few extreme cases,  $\alpha$  slightly exceeds unity reflecting not

only the full expansion but also the extension of individual links due to the increase of the electrostatic repulsion with growing  $L$ . The problem is not seen in studies of intramolecular exponent measured at constant  $L$ . Figure 1 illustrates the dependence of the renormalized intramolecular scaling exponent  $2\alpha' = \{d\ln\langle|\mathbf{r}(s) - \mathbf{r}(s')|^2\rangle/d\ln|s-s'|\} / \{(\pi|s-s'|/L)\cotg(\pi|s-s'|/L)\}$  on the relative distance  $|s-s'|$ . These results are corrected in order to eliminate the effect of the mean curvature present in finite-sized polymer rings.

**Table I** Scaling exponents  $2\alpha = d\ln\langle|\mathbf{r}(s) - \mathbf{r}(s')|^2\rangle/d\ln L$ , renormalized exponents  $2\alpha'(L/2)$ , and mean square distances  $\Delta R^2 = \langle|\mathbf{r}(s) - \mathbf{r}(s')|^2\rangle$  in units  $l$  for various degrees of polymerization  $L$  and ionic strengths  $I$  [ $\text{mol dm}^{-3}$ ]

$I$	0.001	0.01	0.1	1.0
N=100	2.08	1.94	1.69	1.46
	1.84	1.79	1.65	1.42
	27.6	25.8	21.4	16.3
200	2.04	1.87	1.64	1.43
	1.90	1.83	1.64	1.40
	56.4	49.8	38.0	26.9
500	1.96	1.77	1.56	1.40
	1.93	1.83	1.59	1.37
	141	115.2	79.1	51.4
2000	1.88	1.67	1.47	1.38
	1.91	1.73	1.48	1.32
	531	384	226	134.7

Weakly screened polyion is globally extended over large distances, the scaling exponent decaying with the increase in the ionic strength of the solution. Decreasing distance  $|s-s'|$  and concomitant weakening of the screening of Coulombic forces lead to a slow increase in  $\alpha'$  until the curves pass the maxima located at relatively small values  $|s-s'| \ll L$ . A rapid drop in  $\alpha'$  seen at even smaller  $|s-s'|$  reveals the existence of electrostatic blobs predicted in earlier analysis. A full discussion of these issues can be found in a related report (35).

The methods of the present work are not restricted to the particular polymer Hamiltonian and can be used in cases with quite arbitrary distribution of interacting groups along the chain. This invites studies of complex macromolecules and phenomena like helix-coil transition, folding or collapse of the polymer in solution. For illustration, we present the results of an analogous calculation for a cyclic polymer with excluded volume interactions and attractive forces that impose the formation of a helix-like configuration. Apart from the steric term of equation 1, the Hamiltonian includes the attractive contribution of the form  $u_a(s,s') = (1/3) \langle|\mathbf{r}(s) - \mathbf{r}(s')|^2\rangle \delta_{|s-s'|,6}$ . Figure 2



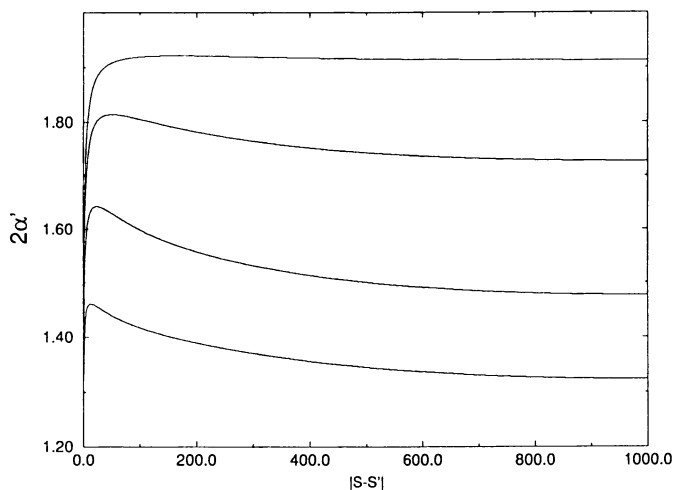


**Figure 1** The renormalized intramolecular scaling exponent  $2\alpha'$  as a function of the separation  $|s-s'|$  at  $L=2000$  and at ionic strengths (top to bottom):  $I=10^{-3}$ ,  $10^{-2}$ ,  $10^{-1}$  or  $1.0 \text{ mol dm}^{-3}$ .

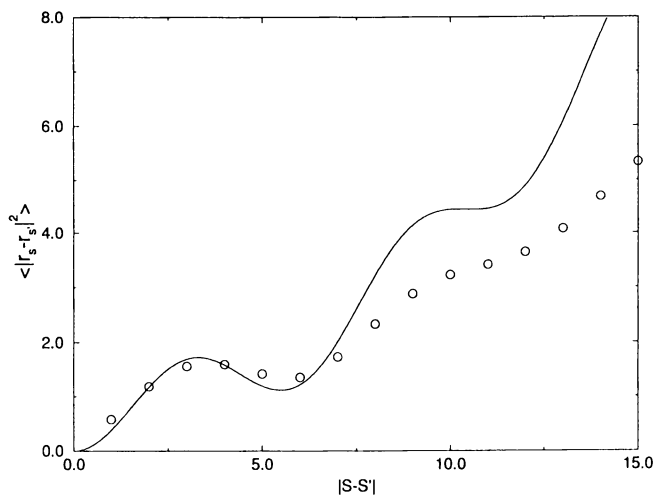


**Figure 2** The mean square distance  $\langle |\mathbf{r}(s) - \mathbf{r}(s')|^2 \rangle$  in a flexible polymer with helix-imposing intramolecular forces at  $L=192$  (O) compared to a rigid helical configuration (—).

compares preliminary results for a flexible chain with above short-ranged interactions to those predicted by assuming a rigid helical configuration. Other examples and a generalization of present perturbative theory to nonisotropic situations such as the macromolecule in external field or under tension (44) will be described at a later date.

### Literature Cited

1. Kuhn, W.; Kunzle, O.; Katchalsky, A. *Helv. Chim. Acta* **1948**, *31*, 1994-2037.
2. DeGennes, P. G.; Pincus, P.; Velasco, R. M.; Brochard, F. *J. Phys.* **1976**, *18*, 1461-1473.
3. Skolnick, J.; Fixman, M. *Macromolecules* **1977**, *10*, 944-948.
4. Bailey, M. *Macromolecules* **1977**, *10*, 725-730.
5. Odijk, T. *J. Polym. Sci., Polym. Phys. Ed.* **1977**, *15*, 477-483.
6. Odijk, T.; Houwart, A. C. *J. Polym. Sci., Polym. Phys. Ed.* **1978**, *16*, 627-639.
7. Fixman, M.; Skolnick, J. *Macromolecules* **1978**, *11*, 863-867.
8. Woodward, C. E.; Jonsson, B. *Chem. Phys.* **1991**, *155*, 207-219.
9. Granfeldt, M.; Jonsson, B.; Woodward, C. E. *J. Phys. Chem.* **1992**, *96*, 10080-10086.
10. Fixman, M. *J. Chem. Phys.* **1982**, *76*, 6346-6353.
11. Khoklov, A. R.; Khachaturian, K. A. *Polymer* **1982**, *23*, 1742-1750.
12. Kholodenko, A. L.; Freed, K. F. *J. Chem. Phys.* **1983**, *78*, 7412-7428.
13. Bawendi, M. L.; Freed, K. F. *J. Chem. Phys.* **1986**, *48*, 449-464.
14. Muthukumar, M. *J. Chem. Phys.* **1987**, *86*, 7230-7235.
15. Qian, C.; Kholodenko, A. L. *J. Chem. Phys.* **1988**, *89*, 2301-2311.
16. Qian, C.; Kholodenko, A. L. *J. Chem. Phys.* **1988**, *89*, 5273-5279.
17. Higgs, P. E.; Raphael, E. *J. Phys. I* **1991**, *1*, 1-7.
18. Podgornik, R. *J. Phys. Chem.* **1991**, *95*, 5249-5255.
19. Podgornik, R. *J. Phys. Chem.* **1992**, *96*, 884-896.
20. Victor, J. M. *J. Chem. Phys.* **1991**, *95*, 600-605.
21. Bratko, D.; Dawson, K. A. *Polym. Prepr.* **1993**, *34*, 936-937.
22. Brender, C.; Lax, M. *J. Chem. Phys.* **1977**, *67*, 1785-1787.
23. Brender, C.; Lax, M. *J. Chem. Phys.* **1981**, *74*, 2659-2660.
24. Brender, C. *J. Chem. Phys.* **1990**, *92*, 4468-4472.
25. Carnie, S. L.; Christos, G. A.; Creamer, T. P. *J. Chem. Phys.* **1988**, *89*, 6484-6496.
26. Christos, G. A.; Carnie, S. L. *J. Chem. Phys.* **1989**, *91*, 439-453.
27. Christos, G. A.; Carnie, S. L. *J. Chem. Phys.* **1990**, *92*, 7661-7677.
28. Reed, C. E.; Reed, W. F. *J. Chem. Phys.* **1991**, *94*, 8479-8486.
29. Reed, C. E.; Reed, W. F. *J. Chem. Phys.* **1992**, *96*, 1609-1620.
30. Valleau, J. P. *Chem. Phys.* **1989**, *129*, 163-175.
31. Doi, M.; Edwards, S. F. *The Theory of Polymer Dynamics*, Oxford Science Publishers, New York, NY, 1992.
32. des Cloizeaux, J. *J. Phys. Soc. Japan* **1969**, *26*, 42-45.

33. des Cloizeaux, J. *J. Phys* **1970**, *31*, 715-736.
34. des Cloizeaux, J.; Jannink, G. *Polymers in Solution. Their Modelling and Structure*, Clarendon Press, Oxford, 1990.
35. Bratko, D.; Dawson, K. A., submitted.
36. Barrat, J. L.; Boyer, D., submitted.
37. Edwards, S. F.; Singh, P. *J. Chem. Soc., Faraday II* **1979**, *75*, 1001-1029.
38. Arfken, G. *Mathematical Methods for Physicists*, Academic Press, San Diego, CA, 1985.
39. Bender, C. M.; Orszag, S. A. *Advanced Mathematical Methods for Scientists and Engineers*, McGraw-Hill, New York, NY, 1978.
40. Manning, G. S. *J. Chem. Phys.* **1969**, *51*, 924-933.
41. Manning, G. S. *Q. Rev. Biophys.* **1978**, *11*, 179-246.
42. Manning, G. S. *Acc. Chem. Res.* **1979**, *12*, 443-449.
43. Bratko, D.; Vlachy, V. *Chem. Phys. Lett.* **1985**, *115*, 294-298.
44. Dawson, K. A.; Bratko, D. In *Condensed Matter Theories*, Vol. 8, Blum, L.; Malik, F. B., Eds.; Plenum, New York, NY, 1993.

RECEIVED August 6, 1993

## Chapter 4

# Branched Polyelectrolytes

M. Daoud

Laboratoire Léon Brillouin, Centre d'Etude de Saclay, 91191 Gif-sur-Yvette,  
Cédex France

We discuss the conformation of randomly branched polyelectrolytes. Because these are synthesized in the neutral state, and then charged electrically, the distribution of molecular weights is the same as for the neutral polymers, and is assumed to be given by percolation. We review the various regimes that might be found when concentration is changed, in the absence of salt. We find the possible existence of two dilute regimes. In the first one electrostatic interactions are present, and the polymers are swollen. In the second one, the Debye-Hückel length is smaller than the radius of the largest macromolecules, and screening is present, leading to a neutral behavior for large distances. In the various regimes, we consider the structure of the polymers and the effects of polydispersity.

Randomly branched polymers have been studied recently both theoretically (1-5) and experimentally (6-11). Polydispersity is very important (12), and effective exponents (12-14) may be observed in the averaged quantities that are measured experimentally. The latter exponents are different from those of a single macromolecule, and are also related to the distribution of masses. All these studies were performed on electrically neutral systems. Polyelectrolytes were somewhat discarded, even though they constitute an important class of materials. Some experimental results (15-17) have recently appeared, but very few theoretical work was made (18-19). This is especially true for the finite branched polymers constituting the sol part. It is however possible to consider these polymers within a simplified Flory approximation. The reason for this is that they are usually synthesized in the neutral state and then charged electrically. Because of this procedure, the distribution of masses should be very similar to the one that was observed in the neutral case. Therefore, the polydispersity effects that were observed in the latter case should also be present in this case. Moreover, because of the presence of the counterions, we know that screening effects are present in these electrically charged systems. In order to characterize them, one usually introduces a Debye-Hückel length  $\lambda_D$ . The latter depends only on the density of free charges in the solution. As we will see, except for very dilute solutions, this screening length becomes smaller than the radius of the largest polymers, and therefore screening effects for the charges are present even in the dilute regime, that is below the overlap concentration  $C^*$ . This leads us to introduce a second concentration,  $C_S$ , smaller than

0097-6156/94/0548-0045\$06.00/0  
© 1994 American Chemical Society

$C^*$ , and corresponding to the appearance of these screening effects. We are mainly interested in this effect. We stress that the following is a first approach to this problem. Many approximations are made in order to focus on the possibility of having two dilute regimes instead of only one usually. As far as we can see, the main approximations concern the value of the exponents, which are assumed here to have the Flory values. We also assume that the counterions are free. This is obviously a rough approximation, as the attractive potential by larger and larger polymers will bring the counterions back to the polymer. Thus we assume that the various macromolecule have a constant fraction  $f$  of their monomers that is charged. Finally, for small  $f$ , we also neglect the possibility that uncharged parts may phase separate because the solvent is not good for them.

In the following, we will first recall briefly the properties of the distribution of molecular weights. We will assume that the percolation distribution is valid, and that there is a power law decay for increasing masses. We will then turn to the swelling properties of a single branched polyelectrolyte and to the effects of the polydispersity in the case of very dilute solutions. Section 4 deals with the eventual existence of screening of the electrostatic interactions above a concentration  $C_S$ . Section 5 is devoted to the concentration effects. We will introduce the screening and overlap concentrations  $C_S$  and  $C^*$ , and discuss the conformation of the polymers in the various regimes that will be defined. All the following will be in the Flory approximation. Such approximation usually gives values for the exponents that are very close to the best known ones calculated by computer simulations or renormalization group, but one has to be very cautious about it because we do not really control the validity of this approximation. Nevertheless, what is important in our opinion is the eventual existence of a dilute regime where power law dependences with concentration may be observed for many quantities. As we will see, the existence of such regime does not depend crucially on the exact values of the exponents.

### The distribution of masses.

We consider multifunctional units that react with each other to form randomly branched polymers. We assume that in the reaction bath there is no solvent, and that the monomers are not ionized. The ionization process is assumed to take place after the polymers are formed, and the synthesis has been quenched. Because we assume that we are dealing with systems at equilibrium, the case when solvent and some ionization of the monomers are present is in principle equivalent to a solution that has been synthesized without any solvent, and then add the solvent and /or adjust the pH of the solution. There results a semi-dilute solution, to be studied below. Thus we consider the synthesis only in the neutral case. The latter was studied carefully these last few years, and it seems that percolation provides a good description for the sol-gel transition (20-21) for a wide variety of cross-linking procedures (22-24). In what follows, we will consider only this case, and assume that it describes the formation of branched polymers. The main result is that there is a very wide distribution of masses, characterized by the probability  $P(N,\epsilon)$  of finding a macromolecule made of  $N$  segments at a distance  $\epsilon = p - p_c$  from the gelation threshold. Here  $p$  is the extent of reaction for instance. This function decreases (25) as a power law, with a cut-off at large masses that also depends on  $\epsilon$ .

$$P(N,\epsilon) \sim N^{-\tau} p(N/N_2) \quad (1)$$

where  $\tau$  is an exponent that is related to the fractal dimension of the polymers in the reaction bath. The second moment of the distribution is the weight average molecular

weight, and also diverges at the gelation threshold. It was shown that it may be related to the largest mass  $N_z$

$$N_w \sim N_z^{(2D-3)/D} \approx N_z^{4/5} \quad (2)$$

where  $D$  is the fractal dimension of every macromolecule in the reaction bath, and 3 is the dimension of space. The exponent in the right hand side is given within the Flory approximation for  $D$ . The radius  $R_z$  of the largest cluster may be related to its mass via the fractal dimension

$$N_z \sim R_z^D \quad (3)$$

We assume that equation 3 is not valid only for the largest macromolecule, but relates the radius to the mass whatever the polymer in the distribution.

Finally, the exponent  $\tau$  of the distribution  $P(N, \epsilon)$  was also related to  $D$ . It was found

$$\tau = 1 + 3/D \quad (4)$$

The latter equation was interpreted (26) as a generalized  $C^*$  situation. It implies that if one defines classes of polymers with given mass, each of these classes is at  $C^*$ , that is there is a filling of space by the macromolecules of similar sizes. Because they are fractal however, there is space left, which is filled by smaller polymers, with the prescription that every class is space filling. When all classes have been considered, no space is left. Let us note that as the gelation threshold is approached, the characteristic masses diverge in different ways, so that polydispersity also diverges. This has to be opposed to other models where there is only one characteristic diverging mass (27). In what follows, we will assume that this distribution of masses is given and fixed. The various manipulations that are subsequently done on the polymers, such as dilution or adding salt, etc..., are made with a fixed distribution, and only the conformation of the polymers changes, but their proportions remains constant.

#### Very dilute solutions. Neutral blobs.

Once the synthesis is made, we add solvent in excess, so that the resulting solution is dilute. We assume that during this dilution the charges appear on the macromolecules, or are created, by changing the pH of the solution for instance, so that the result is a dilute solution of polyelectrolytes. We also assume that a constant fraction  $f$  of the monomers of all polymers is charged. It is clear that because both the swelling and the electrostatic screening effects are closely related to the density of charges, the effect of the latter is important. We consider first the case of a single polyelectrolytes, within a Flory approximation. Following Isaacson and Lubensky (28), The free energy may be written as

$$F = \frac{R^2}{N^{1/2} a^2} + f^2 N^2 \left\{ \frac{\lambda_B}{R} \right\}^{d-2} \quad (5)$$

where the first term is an elastic contribution, the second one the electrostatic one,  $\lambda_B$  is the Bjerrum length (35), and is assumed to be of the same order than the step length  $a$ ,  $d$  is the dimension of space, and we assumed the Zimm-Stockmayer (29) result for an ideal branched polymer:

American Chemical  
Society Library  
1155 16th St., N.W.  
Washington, D.C. 20036

$$R_O \sim N^{1/4} a \quad (6)$$

Minimizing equation 5 with respect to R gives

$$R \sim N^{5/2d} \left[ \frac{af}{\lambda_B} \right]^{2/d} \lambda_B \quad (7)$$

and a fractal dimension  $D_O$

$$N \sim R^{D_O} \quad (8a)$$

with

$$D_O = 2d/5 \quad (8b)$$

In our case, we get  $D_O = 6/5$ . Note that one recovers the ideal Zimm Stockmayer value for  $d = 10$ , so that large deviations are expected for the three dimensional case we are considering. Note also that in order to get equation 7, we neglected the excluded volume interactions in the free energy, equation 5. As a result, there is a condition that we have to set on the resulting radius, namely that it has to be larger than that of a neutral branched polymer with equivalent mass. From previous studies, we know the latter is

$$R_n(N) \sim N^{D_a} a \quad (9a)$$

with

$$D_a \sim 2(d+2)/5 \quad (9b)$$

This leads us to compare these estimates. For  $d=3$ , we find that the electrostatic effects are important if the polymer is sufficiently large or charged. Equation 8 is valid only if  $N > N^*$  for given  $f$  (or  $f > f^*$  for given  $N$ ) such that

$$N^* \sim f^{-2} \frac{a}{\lambda_B} \quad (10a)$$

This in turn allows us to introduce local blobs, with neutral behavior. These are made of  $N^*$  units and have a radius  $R^*$  related to  $N^*$  by equation 9:

$$R^* \sim N^{*1/2} a \quad (10b)$$

For larger distances, the behavior of the polymer is governed by equation 8 if one takes the blob as a statistical unit. Thus for  $d=3$ , we have:

$$R \sim \left[ \frac{N}{N^*} \right]^{5/6} R^* \quad (10)$$

Using equations 9 and 10, one recovers equation 8. We finally observe that in the above analysis, we assumed that the polymer is in a good solvent. This might be questioned because the solvent may be a poor solvent for the uncharged parts of the

polymer. In the following, we will not consider this local structure, and rather focus on the mass dependence of the radius.

The latter result may be observed only if one has a single molecular weight. This implies a fractionation of the distribution. If the whole distribution is kept, averages have to be made. These lead to effective fractal dimension as we will see now. The average radius that is measured by light or neutron scattering is

$$R_z^2 = \frac{1}{N_w} \int dN N^2 P(N, \epsilon) R^2(N) \quad (11)$$

Using equations (1),(4), (7) and (8), and eliminating  $\epsilon$  with equation(3), we get

$$R_z^2 \sim N_w^{25/12} \left[ \frac{af}{\lambda_B} \right]^{4/3} \lambda_B^2 \quad (12)$$

Another measurable quantity, namely the intrinsic viscosity may also be measured. For one mass, this would be

$$[\eta(N)] \sim N^{-1+3/D_0} \approx N^{3/2} [af] \lambda_B^2 \quad (13)$$

where we used equation 8. The measured quantity however is an average over the whole distribution. It was shown (30) that this is

$$\langle [\eta(N)] \rangle = \int dN N P(N) [\eta(N)] \quad (14)$$

Performing the integration and eliminating  $N_z$  with equation 2, we get

$$\langle [\eta(N)] \rangle \sim N_w^{1-\tau+3/D_0} \approx N_w^{13/8} [af]^2 \lambda_B^2 \quad (15)$$

One might also calculate the overlap concentration  $C^*$  where the various macromolecules start overlapping each other. However, an important concentration effect appears even below  $C^*$ . This is related to the screening of the electrostatic interactions.

### Screening of the electrostatic interactions.

The previous results are valid for very dilute solutions. However, even in this regime, when the monomer concentration  $C$  is increased, some screening of the electrostatic interactions appears, because of the presence of the free counterions in the solution. These effects are not important as long as the concentration of the solution is small. However, because of the polydispersity and the compactness of the polymers, they become important sooner for the branched polymers than for the linear ones. Whereas they become important in the semi-dilute regime for linear polyelectrolyte, we will see that they are already even in a dilute range for the branched case. Screening effects are usually described by a Debye-Hückel screening length  $\lambda_D$ , related to the presence of free counterions in the solution. This length depends on concentration. As mentioned in the introduction, we assume that all counterions are free. Therefore their concentration is  $fC$ , where  $C$  is the monomer concentration. The Debye length is thus



$$\lambda_D \sim (fC\lambda_B)^{-1/2} \quad (16)$$

and is smaller than the radius of the polymers as long as the concentration is low enough. There is a special concentration  $C_S$  where the screening length becomes of the order of the radius of the largest polymers, with size  $N_Z$ . Using equations 7 and 16, we get

$$C_S a^3 \sim N_W^{-25/12} f^{-7/3} \left[ \frac{\lambda_B}{a} \right]^{-5/3} \quad (17)$$

Therefore, for concentrations smaller than  $C_S$ , screening effects may be considered as perturbations to the laws derived in the previous section. For concentrations larger than  $C_S$  however, these effects are no longer corrections, but become predominant. For any concentration  $C$  larger than  $C_S$ , the largest clusters are screened, and one has to partition the distribution of masses into two parts, and to introduce a cross-over mass  $g_S$  between two behaviors. The larger masses are screened whereas the smaller ones are still interacting with long range electrostatic interactions. Generalizing equation 17, we get the cross-over mass

$$g_S \sim (C a^3)^{-3/5} f^{-7/5} \left[ \frac{a}{\lambda_B} \right] \quad (18)$$

Note that this is the largest unscreened mass, and that, for the lower mass part of the distribution, the corresponding weight average molecular weight  $g_{SW}$  is  $g_{SW} \sim g_S^{4/5}$ . Using equation 18 together with 12 gives the size  $\lambda_D$  of the screening length, equation 16, as expected. Thus above  $C_S$ , the conformation of the polymers with mass smaller than  $g_S$  is the same as discussed above. The structure of the larger polymers is obtained by introducing blobs made of  $g_S$  monomers, with size  $\lambda_D$ . Using such blobs as statistical units, one may neglect the electrostatic interactions between blobs as a first approximation. Therefore, the conformation of the largest masses in the distribution is the same as in the neutral case. This was studied previously and, for dilute solution, one gets a fractal dimension  $D_a$ , which, in a Flory approximation, is given by equation 9b. Therefore the radius of a large polymer is, for  $d=3$ :

$$R(N) \sim \left\{ \frac{N}{g_S} \right\}^{1/2} \lambda_D \quad (19a)$$

Using equations 8, 16 and 18, we get, in the three dimensional case

$$R(N) \sim N^{1/2} (C a^3)^{-1/5} f^{1/5} a \quad (N \gg g_S) \quad (19b)$$

As in the neutral case, the observed (average) radius is

$$R_Z^2 = \frac{1}{N_W} \int_{g_S}^{N_Z} N^2 R(N)^2 P(N) dN \quad (20)$$

Neglecting the lower limit of the integral for  $C \gg C_s$ , and using equation 2 to eliminate  $N_z$  in favor of the measurable  $N_w$ , we get

$$R_z \sim N_w^{5/8} (C a^3)^{-1/5} f^{1/5} a \quad (21)$$

Note that in both equations 19b and 21, the Bjerrum length has disappeared, so that there is no longer any explicit reference to the electrostatic interactions. It is interesting to consider the reduced viscosity  $\eta_r = (\eta - \eta_s)/C \eta_s$  in this concentration regime. Here  $\eta$  and  $\eta_s$  are respectively the viscosities of the solution and the solvent. The contribution of each mass is

$$\begin{aligned} \eta_r(N) &\sim R(N)^3 / N \\ &\sim N^{1/2} [Ca^3]^{-3/5} f^{3/5} a^3 \end{aligned} \quad (22)$$

Therefore the average relative viscosity is

$$\langle \eta_r \rangle \sim \int dN N P(N) \eta_r(N) \quad (23)$$

leading to

$$\langle \eta_r \rangle \sim N_w^{3/8} [Ca^3]^{-3/5} f^{3/5} a^3 \quad (24)$$

Thus we find that the relative viscosity of a dilute solution of branched polyelectrolytes decreases as concentration increases. Such result is in agreement with the Fuoss law, valid for linear polyelectrolytes. The latter was recently discussed by Witten and Pincus (31) who found a very different reason for this behavior in the case of linear charged chains.

We conclude this section by noting that the existence of this unusual dilute regime,  $C_s \ll C \ll C^*$ , that has concentration dependences that are not perturbations is related to the branched nature of the polymers. At the overlap concentration  $C^*$ , the largest polymers are therefore screened and behave as neutral branched macromolecules. The latter concentration corresponds to space filling by the polymers. This may be written in the following form:

$$\{C^* a^3\}^{-1} \sim \int^{N_z} R(N)^3 P(N, \epsilon) dN \quad (25)$$

In principle, this should be split into two parts, corresponding to the unscreened and screened portions of the distribution of masses. In the following, we will neglect the contribution of the smallest polymers, and consider only the largest ones. Using equations 1, 2, and 21, we get

$$C^* a^3 \sim N_w^{-15/16} f^{-3/2} \quad (26)$$

Note that although this concentration is small, it is not as small as for linear polyelectrolytes because of these screening effects.

For higher concentrations,  $C \gg C^*$ , the polymers start interpenetrating each other. This is studied in next section.

### The semi-dilute regime.

The overlap concentration  $C^*$  is the highest concentration where the polymers do not overlap and where one may assume that they behave independently of each other. We turn now to more concentrated solutions, well above  $C^*$ , where scaling may be applied. In this concentration range, two lengths are present, namely the Debye length  $\lambda_D$ , equation 16, and a screening length  $\xi$  corresponding to the interpenetration of the large polymers by the smaller ones. Before we calculate this length, we describe briefly the conformation of the polymers. This is identical to what was found for neutral branched macromolecules (32). One has to split again the distribution of masses into two parts. The smaller part, for masses less than  $g$ , corresponds to swollen state, equation 21. These polymers behave as in a dilute solution. The polymers with size larger than  $g$  are penetrated by the smaller polymers and are screened. Their overall behavior is therefore the same as in the reaction bath, that is they have the same fractal dimension as in a melt. We know that the latter is the fractal dimension  $D$  of percolation. We define the blob  $\xi$  as the size of the cross-over mass  $g$ . As for neutral polymers, it is a local property that has to be independent of the size  $N_Z$  of the largest polymers, and should depend on concentration only. One may estimate it with a scaling argument. The characteristic distance has the scaled form

$$L \sim N_w^{5/8} [Ca]^3^{-1/5} f^{1/5} a g(C/C^*) \quad (27)$$

Assuming that  $f(x)$  behaves as a power law for  $x \gg 1$ , and using equation 29 and the condition that  $\xi$  is independent of  $N_w$ , we get

$$\xi \sim [Ca]^3^{-13/15} f^{-4/5} a \quad (28)$$

Note that  $\xi \gg \lambda_D$ , and that both lengths become of the same order for large concentrations. This may also be seen by comparing the number of monomers  $g_s$  in a Debye length and  $g$  in the screening length. The latter may be obtained by scaling arguments, with the limit that  $g \approx N_Z$  for  $C \approx C^*$ . One finds

$$g \sim [Ca]^3^{-3/4} \quad (29a)$$

Note that this is the largest mass in the distribution of small clusters, and that it corresponds to a weight average mass  $g_w$

$$g_w \sim [Ca]^3^{-16/15} \quad (29b)$$

Finally, the average radius of gyration in the semi-dilute regime may also be obtained by scaling arguments similar to those we just used for the screening length  $\xi$ . The constraint now is that the fractal dimension of each macromolecule is the one of percolation. Therefore, the average radius has a mass dependence that is proportional to  $N_w^{1/2}$ . We find

$$R_z \sim N_w^{1/2} [Ca^3]^{-1/3} a \quad (30)$$

Note that this corresponds to an overall behavior for each of the polymers

$$R(N) \sim N^{2/5} [Ca^3]^{-1/3} a \quad (31)$$

The concentration dependence both in equations 29 and 30 is indicative of a local behavior that is different from the overall behavior. Indeed, as discussed above, one may introduce blobs made of  $g$  monomers, and size  $\xi$  such that for instance

$$R(N) \sim \{N/g\}^{2/5} \xi \quad (32)$$

Using equation 29a and generalizing equation 19b to the blob, one recovers equation 31. A similar treatment is also valid for the average radius. In both cases, this amounts to say that the behavior of large polymers is the same as that of the percolation clusters, if one takes the blob as a statistical unit. These laws may be checked by light or neutron scattering experiments. As for linear polyelectrolytes however, these are not straightforward to interpret. The reason for this is that the scattered intensity at very low scattering vectors is related to the osmotic compressibility. The latter is itself related to the fact that the osmotic pressure does not depend on the polymer-polymer contacts, but rather to the concentration in counterions. Therefore, we expect, as in the linear case, that the intensity is very low for  $q$  going to zero, and exhibits a maximum.

### The concentrated regime.

As monomer concentration is still increased, a last cross-over occurs, to a "dense" regime where the electrostatic interactions are screened at all distances, and the behavior of the polymers is the same as that of neutral ones. In the semi-dilute regime, we had three different distance scales. For small distances, because electrostatic interaction is not strong enough, there is a neutral a neutral blob with size  $R^*$ . For larger distances the electrostatic interactions come into play, for distances smaller than the Debye screening length  $\lambda_D$ . Finally, for distances larger than  $\lambda_D$ , the long range forces are screened, and the behavior of neutral branched polymers is recovered, although the size of the concentration blobs  $\xi$  is different from what was obtained in the neutral case. All these distances depend on monomer concentration. The cross-over from the semi-dilute regime to the concentrated one corresponds to the special concentration  $C^{**}$  when the sizes of neutral blob  $R^*$  and the screening length  $\lambda_D$  become equal. Using equations 10b and 16, we get:

$$C^{**} a^3 \sim f \quad (33)$$

For concentrations larger than  $C^{**}$ , or for a given value of  $C$ , for small values of the fraction  $f$  of charged monomers, the electrostatic interactions are no longer playing any role in the problem. Thus we fully recover the neutral case. This implies that the correlation length  $\xi$ , equation 28, corresponding to the concentration blob should no longer depend on the  $f$  or  $\lambda_B$ . This is obtained by using the scaling equation for  $\xi$ : In order to describe the cross-over from semi-dilute to dense regimes, we assume that

$$\xi \sim [\text{Ca}^3]^{-13/15} f^{-4/5} a g(C/C^{**}) \quad (34)$$

Assuming that  $g(x)$  behaves as a power law for large  $x$ , in the dense region and insisting that  $\xi$  should be independent on  $f$ , we get

$$\xi \sim [\text{Ca}^3]^{-5/3} a \quad (C \gg C^{**}) \quad (35)$$

Equation 35 is identical to what was obtained in the semi-dilute regime in the case of neutral polymers. Note also that it may be obtained directly from equations 9 and 10: we saw in the first section that small polymers have neutral behavior. The overlap concentration  $C^*$  between dilute and semi-dilute regimes is evaluated directly in this case using equations 9 and 25. As for neutral polymers, we find

$$C^* \sim N_z^{-3/10} \sim N_w^{-3/8} \quad (36)$$

This corresponds to the cross-over line between regions DN and SDN in figure 1. Finally, note that we gave the analysis with neutral blobs only when screening was not present, region I in figure 1. It is clear that such analysis may be extended to the case when screening is present. The cross-over from the regime where screened electrostatic interactions are present, region II in figure 1, to the neutral one is then obtained by comparing the screening length with the size of the neutral blob. As this is precisely what we did when we considered the cross-over from the semi-dilute to the dense regimes, such comparison leads us to the  $C^{**}$  line that we considered above. The resulting diagram shown in figure 1, summarizes the various regimes that we considered.

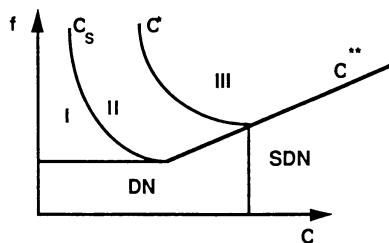


Figure 1. Crossovers between regions with increasing concentration.

## Conclusion

We considered the conformation of randomly branched polyelectrolytes within a Flory approximation. It is well-known that the validity of such approach has to be checked. It is important to note at this level that de Gennes (33) very recently made a conjecture contradicting the Isaacson-Lubensky results, equation 8. His argument is that in the ideal case, the radius of the polymer is as if we had a linear chain made of  $N^{1/2}$  monomers. This would imply that the conformation would already be stretched in the excluded volume case, because the radius is already proportional to  $N^{1/2}$ . Therefore, a

variation faster than this is not to be expected, and one gets for the branched polyelectrolyte the same behavior instead of equation 8. This of course would change completely our results, and very few would survive such a criticism. The idea that another concentration is present would be among these. Indeed, because the Debye

length  $\lambda_D$  varies as  $[Cf\lambda_B]^{-1/2}$ , there is a concentration  $C_S'$  such that the radius of the largest polymers is of the order of  $\lambda_D$ . We would then find

$$[C_S' f \lambda_B] \sim N_Z^{-1} \sim N_W^{-5/4} \quad (37)$$

Because the difference in the radii of the polymers between the regimes above and below  $C_S'$  is merely in constants however, it is not clear to us at this point what the differences are between these concentration ranges as long as the conformation of the macromolecules is concerned. It would certainly be interesting to check this point, for instance with computer simulations, and to look experimentally at the effect of the density of charges on the structure of branched polymers (34, 35).

If we accept the validity of the Flory approximation, equation 8, however, charge effects would be important, and the conformation of the polymers would much more expanded below  $C_S$  than above. The screening effects would be present in the dilute

regime, because  $C_S \sim N_W^{-25/12}$  is smaller than  $C^*$ , and lead to important changes between these two concentration regimes. More precisely, we found that explicit concentration dependences would be present for all measurable quantities in the dilute and screened regime II of figure 1. Among others, we found that the relative viscosity would decrease as concentration increases between  $C_S$  and  $C^*$ . An important result is that the dilute regimes should be easier to reach in the case of branched polymers

whereas they were much too dilute for linear chains (37). We found  $C^* a^3 \sim N_Z^{-3/4} \sim N_W^{-15/16}$ , instead of  $C^* a^3 \sim N_Z^{-2}$  in the linear case. This would allow for instance a search for an eventual regime where ordering of the polymers would be present. The latter question was not addressed here. Another interesting concept that we found is the eventual presence of neutral blobs when the fraction  $f$  of charged monomers is low. In this paper, we considered the simplest possibility for these blobs, namely that they behave as neutral branched polymers in a good solvent. This assumption has obviously to be studied more carefully by including the option that there might be locally a poor solvent (37).

## References.

1. Stockmayer, W. H., *J. Chem.Phys.* **1943**, *11*, 45.
2. De Gennes, P. G., *Scaling Concepts in Polymer Physics*, Cornell University Press, Ithaca, **1979**.
3. Flory, P. J., *Principles of Polymer Chemistry*, Cornell University press, Ithaca **1953**.
4. Benedek, G. B., "*The Theory of the Sol-Gel Transition*," lecture at E.T.H. Zurich **1980**.
5. Daoud, M., Martin, J.E., in *The fractal approach to Heterogeneous Chemistry*, D. Avnir Ed., J. Wiley, **1990**.
6. Candau, S. J., Ankrim, M., Munch, J. P., Rempp, P., Hild, G., Osaka, R., in *Physical Optics of Dynamical Phenomena in Macromolecular Systems*, W. De Gruyter, Berlin, **1985**, 145.
7. Adam, M., Delsanti, M., Munch, J. P., Durand, D, *J. Physique* **1987**, *48*, 1809.

8. Allain, C., Salome, L., *Macromolecules* **1987**, *20*, 2957.
9. Burchard, W., *Adv. Pol. Sci.* **1983**, *48*, 1.
10. Schosseler, F., Leibler, L., *Macromolecules* **1985**, *18*, 398.
11. Patton, E. V., Wesson, J.A., Rubinstein, M., Wilson, J. C., Oppenheimer, L. E. *Macromolecules* **1989**, *22*, 1946.
12. Bouchaud, E., Delsanti, M., Adam, M., Daoud, M., Durand, D., *J. Physique Lett.* **1986**, *47*, 1273.
13. Martin, J. E., Ackerson, B. J., *Phys. Rev.* **1985**, *A31*, 1180.
14. Daoud, M., Family, F., Jannink, G., *J. de Phys. Lett.* **1984**, *45*, 119.
15. Moussaid, A., Munch, J.P., Schosseler, F., Candau, S.J., *J. Physique II* **1991**, *1*, 637.
16. Schosseler, F., Moussaid, A., Munch, J.P., Candau, S.J., *J. Physique II* **1991**, *1*, 1197.
17. Schosseler, F., Ilmain, F., Candau, S.J., *Macromolecules* **1991**, *24*, 225.
18. Borue, V., Erukhimovich, I., *Macromolecules* **1988**, *21*, 3240.
19. Joanny, J.F., Leibler, L., *J. Physique* **1990**, *51*, 545.
20. De Gennes, P. G., *J. Physique Lett.* **1976**, *37*, 1.
21. Stauffer, D., *J. Chem. Soc. Faraday Trans. II* **1976**, *72*, 1354.
22. Leibler, L., Schosseler, F., in *Physics of Finely Divided Matter*, Springer Proc. Phys. 5,135, N. Boccaro and M. Daoud eds., Springer Verlag, Berlin **1985**.
23. Adam, M., Delsanti, M., Durand, D., *Macromolecules* **1985**, *18*, 2285.
24. Lapp, A., Leibler, L., Schosseler, F., Strazielle, C., *Macromolecules* **1989**, *22*, 2871.
25. Stauffer, D., Introduction to percolation theory, Taylor and Francis **1985**.
26. Cates, M. E., *J. de Phys. Lett.* **1985**, *38*, 2957.
27. Meakin, P., in *The fractal approach to Heterogeneous Chemistry*, D. Avnir Ed. J. Wiley **1990**.
28. Isaacson, J., Lubensky, T. C., *J. Physique* **1981**, *42*, 175.
29. Zimm, B. H., Stockmayer, W. H., *J. Chem. Phys.* **1949**, *17*, 1301.
30. Sievers, D., *J. Physique* **1980**, *41*, L 535.
31. Witten, T.A., Pincus, F.Y., *Europhys. Lett* **1987**, *3*, 315
32. Daoud, M., Leibler, L., *Macromolecules* **1988**, *41*, 1497.
33. De Gennes, P.G., *Comptes Rendus Ac. Sci. (Paris) II* **1988**, *307*, 1497.
34. Odijk, T., *J. Pol. Sci. (Phys.)* **1977**, *15*, 477
35. Manning, G., *Quart. Rev. Biophys.* **1978**, *11*, 179.
36. De Gennes, P.G., Pincus, P., Velasco, R.M., Brochard, F., *J. de Physique* **1976**, *37*, 1461.
37. Khokhlov, A.R., *J. Phys.* **1980**, *A13*, 979.

RECEIVED September 7, 1993

## Chapter 5

# Molecular Dynamics Simulations of Charged Polymer Chains from Dilute to Semidilute Concentrations

Mark J. Stevens<sup>1</sup> and Kurt Kremer

Institut für Festkörperforschung, Forschungszentrum Jülich, Postfach  
1913, D-5170 Jülich, Germany

We have performed molecular dynamics simulations on multichain systems of flexible charged polymers in which full Coulomb interactions of the monomers and counterions are treated explicitly. This model produces osmotic pressure and structure factor data that agrees excellently with experimental measurements. As expected we find the chain conformation changes from stretched to coiled as the density increases from dilute to semidilute values. However, the nature of the stretched conformations is different from theoretical predictions.

Polyelectrolytes remain one of the most mysterious states of condensed matter (1-3). This is in great contrast to the well developed theory of neutral polymer solutions (4). Experimentally bulk properties like the osmotic pressure (2) and the viscosity (5) are well known, but an understanding of the microscopic origin is lacking. This ignorance is especially critical since, for example, one of the prototypical polyelectrolytes is DNA which is of fundamental importance to biology. The lack of progress is in part due to unfortunate situation in which theory is best done in one regime (dilute) and experiment is best done in another regime (semidilute). We present results of simulations which bridge this gap and handle the inherent theoretical difficulties.

Polyelectrolytes pose difficulties not encountered in the theory of neutral polymers. The main difficulty is the long range nature of the Coulomb interaction which can only be handled theoretically by severe approximations. The usual approach is the Debye-Hückel approximation which treats the Coulomb pair interactions between monomers as strongly screened and thus short ranged. This approach should be valid at low concentrations. But, the experimentally relevant regime is at semidilute concentrations. Furthermore, the counterions enter only as a part of the screening, and any effect of the discrete nature of the counterions is neglected. Further theoretical complications arise because not only is a new length scale due to the Coulomb interaction introduced, but also other length scales occur due to the presence of extra species (counterions and any added salt). Attempts at scaling theories of polyelectrolytes are thus more speculative as one must choose the most relevant subset of the length scales.

The above difficulties suggest that simulations of polyelectrolytes are especially warranted. While several simulation studies have been done, they only considered a

<sup>1</sup>Current address: Corporate Research Science Laboratories, Exxon Research and Engineering Company, Annandale, NJ 08801



single chain (6). Yet, as noted above the experimentally relevant regime is at semidilute concentrations. Thus, it is essential to simulate a system of *several* chains with counterions explicitly treated. Here, we describe results of such molecular dynamics simulations on salt-free systems of polyelectrolytes that cover the concentration range from dilute to semidilute.

The rest of the paper is organized as follows. The simulation method and parameters are described. Then a brief discussion of relevant polyelectrolyte theory is given. Our simulation data is compared with experimental measurements of the osmotic pressure and the structure factor to verify accuracy. The chain structure is examined through a combination of the end-to-end distance,  $\langle R \rangle$ , and the radius of gyration,  $\langle S^2 \rangle$ . Finally, we discuss our calculated form factors.

## Simulation Method

We use the freely-jointed bead-spring model of a polymer which has been very successful in simulations of neutral polymers (7,8). Each polymer chain consists of  $N_b$  monomers of mass  $m$  connected by a nonlinear bond potential. The bond potential is given by

$$U_{bond}(r) = -\frac{1}{2}kR_0^2 \ln(1 - r^2/R_0^2), \quad (1)$$

with  $k = 7\epsilon/\sigma^2$  used for the spring constant, and with  $R_0 = 2\sigma$  used for the maximum extent (8). Here, as throughout this paper Lennard-Jones units are used. Excluded volume between the monomers is included via a repulsive Lennard-Jones (RLJ) potential with the cutoff,  $r_c$ , at  $2^{1/6}\sigma$ :

$$U_{LJ}(r) = \begin{cases} 4\epsilon \left[ \left(\frac{\sigma}{r}\right)^{12} - \left(\frac{\sigma}{r}\right)^6 - \left(\frac{\sigma}{r_c}\right)^{12} + \left(\frac{\sigma}{r_c}\right)^6 \right]; & r \leq r_c \\ 0; & r > r_c \end{cases} \quad (2)$$

The counterions are given a repulsive core by using the same repulsive Lennard-Jones potential. Since simulations on neutral polymers give good results starting at 16 bead chains (7), the polyelectrolyte simulations were done with 16, 32 and 64 bead chains, and in some cases we extended the runs to  $N_b = 128$  beads to test chain length dependence. The number of chains was either 8 or 16. The average bond length,  $\langle b \rangle$ , is  $1.1\sigma$ .

Coulomb interactions pose special difficulties for simulations as well as theory (9). The long range interaction usually requires the Ewald summation method in order to include interactions of the periodic images. In our simulations the Coulomb interactions are evaluated by a spherical approximation to the Ewald sum given by Adams and Dubey (9). This approximation is better by an order of magnitude in the calculation of the energy than the minimum image evaluation which is the best used to date for polyelectrolytes (6). This approximation is good if the Coulomb interaction are not much stronger than the thermal interactions. The Coulomb strength is given by the Bjerrum length,  $\lambda_B = e^2/\epsilon k_B T$  which for this work is taken to be  $1\sigma$  as many experiments and theoretical works have been done in this critical regime (1,3,10). For this value of  $\lambda_B$  the Coulomb pair interactions are generally less than  $k_B T$ .

The dynamics of the system is done at constant temperature,  $T = 1.2\epsilon$ , using the Langevin thermostat with damping constant  $\Gamma = 1\tau^{-1}$ , and timestep  $0.015\tau$ , where  $\tau = \sigma(m/\epsilon)^{1/2}$  (7). Besides the necessary temperature control, the Langevin thermostat also stabilizes the trajectories making possible the long runs necessary. The length of the simulation is such that the chains move at least 10 times the contour length. For 64 bead chains this required about a million timesteps.

## Theoretical Models

Polyelectrolytes are stretched in comparison to neutral polymers due to the Coulomb repulsion between charges on the polymer chain. Flory type arguments (10–12) give  $R \sim N_b$  which corresponds to a rodlike conformation for the chain. Much theoretical work has been done calculating the effect of increasing the polymer concentration or adding salt on rigid rod state (13–17). These works describe the polymer as a wormlike chain with a persistence length,  $L_p = L_e + L_o$ , where  $L_o$  is the intrinsic persistence length of the uncharged polymer, and  $L_e$  is the electrostatic persistence length. The electrostatic contribution to the persistence length has been calculated to be asymptotically (13,14)

$$L_e = \lambda_{DH}^2 \lambda_B / 4(b)^2, \quad (3)$$

where  $\lambda_{DH} = \kappa^{-1} = (4\pi\lambda_B\rho_m)^{-1/2}$  is the Debye length and  $\rho_m$  is the monomer (=counterion) density.

The polymer structure in the transition between dilute and semidilute concentrations is speculative (1,3,10,18,19). Odijk (18) and Hayter *et al.* (1) have proposed similar pictures of polyelectrolyte structure albeit for different physical reasons. The chain structure is that of an ideal chain of ‘batonnets’, where the ‘batonnets’ are straight segments of length,  $L_p$ . Using this picture Odijk has proposed a scaling theory and picture of polyelectrolyte conformation as a function of concentration (18). At dilute concentrations the chains are rodlike. With increasing concentration the chains remain rodlike until  $L_e \approx L$  at monomer concentration  $c_1^* = 1/16\pi(b)^2L$  ( $\kappa L \gg 1$ ) where the chains begin to bend. A second threshold sets in when the strand-strand distance,  $\xi > L_e$ . This occurs at  $c_2^* = 0.04/4\pi\lambda_B^3 = 0.003\sigma^{-3}$  which is independent of chain length. De Gennes *et al.* (10) have described an alternative picture in the semidilute regime. In their picture, the length of the straight segments is pinned at the average strand-strand distance.

## Comparison of Simulation Results to Experiment

One quantity which is relatively easily measured and thus a good test of the simulations is the osmotic pressure,  $\Pi$ . The osmotic pressure has been measured on several systems and two scaling regimes are exhibited (2). At low densities  $\Pi \sim \rho_m^{9/8}$ . This dependence is predicted by Odijk’s scaling theory (18). In the high concentration regime the scaling exponent changes to 9/4 which is the scaling for semidilute neutral polymers (4). These results suggest that the polyelectrolyte chains are stretched at dilute concentrations and are coiled at semidilute concentrations.

Our simulation results shown in Figure 1 give two scaling regimes. In the high density regime we find the same scaling exponent 9/4. For densities two orders of magnitude lower than the crossover density,  $\rho_m^{(\Pi)} = 0.07 \pm 0.04$ , our data is consistent with the 9/8 value. Our simulation extend the experimental results to lower densities where the noninteracting limit,  $\Pi = k_B T \rho_m (1 + 1/N_b)$ , is reached. At these lowest concentrations, the chain length dependence decreases.

One striking aspect of the osmotic pressure data is the chain length independence of the crossover density,  $\rho_m^{(\Pi)}$ . Since for  $\rho_m > \rho_m^{(\Pi)}$  the  $\Pi$ -dependence is that of neutral polymers, the Coulomb interactions must be completely screened at  $\rho_m^{(\Pi)}$ . For complete screening, the Debye screening length should be less than all interparticle distances. The bond length is the shortest particle separation distance. We find  $\lambda_{DH} = (b)$  at  $\rho_m = 1/(4\pi\lambda_B(b)^2) = 0.066\sigma^{-3}$  for our set of parameters. This value agrees with our simulation data.

Experimentally, the polymer structure can be probed through measurements of the structure factor. The interpolymer structure factor has been measured and exhibits a peak whose position,  $q_m$ , varies with concentration,  $c$ , in a rather intriguing fashion

(20). At low concentrations, the peak position scales as  $c^{-1/3}$  which corresponds to the variation of an average interpolymer separation. At high concentrations, the peak position scales as  $c^{-1/2}$  which corresponds to a correlation length that scales as the Debye length. The crossover density depends on the particular polyelectrolyte.

In Figure 2, we show our calculated  $q_m$  for  $N_b = 32$ . Our data exhibits the same two scaling regimes seen in experiments. The crossover density is not well resolved, but it occurs at about  $\rho_m^{(q)} = 0.01\sigma^{-3}$ . The overlap density,  $\rho_m^* \equiv 1/(\pi\langle R^2 \rangle^{3/2}/6)$  is about  $0.05\sigma^{-3}$ . As will be shown below, the chain begins to significantly contract above  $\rho_m^{(q)}$ . Beyond this density the intrachain peak is no longer solely dependent on the average chain separation distance. The contraction of the chain is also important. The results on the osmotic pressure and the structure factor peak position show that our simulations model the experimental systems quite well.

## Discussion

We can use our calculated structure factors to examine the question of chain length dependence of the individual chain. The form factor is directly related to the individual chain structure. We define the chain form factor as

$$P(\mathbf{q}) = \frac{1}{N_b} \left| \sum_{j=1}^{N_b} \exp(i\mathbf{q} \cdot \mathbf{r}_j) \right|^2, \quad (4)$$

where the normalization is  $P(0) = N_b$ , and we calculate the spherically averaged quantity,  $P(q)$ . Figure 3 shows  $P(q)$  for  $N_b = 16, 32, 64$  and  $128$  at  $\rho_m = 5 \cdot 10^{-7}\sigma^{-3}$  which is well below the overlap density for all the chain lengths. The plot exhibits the chain length *independence* that holds for all densities. Namely, for  $q \gtrsim q_{min} \equiv 2\pi/\langle R^2 \rangle^{1/2}$ , no chain length dependence exists. This result is a very important since our chains are short in comparison to experiment. Using it we can describe the structure of a chain with  $N_b > 64$  on length scales shorter than  $\langle R^2(N_b = 64) \rangle^{1/2}$  using the  $N_b = 64$  simulations.

Before presenting quantitative results, we graphically display the single chain structure. In Figure 4 (a) and (b) we show typical conformations for  $N_b = 32$  at  $\rho_m = 1 \cdot 10^{-4}\sigma^{-3}$  and  $0.3\sigma^{-3}$ , respectively. Configuration (a) is at a very dilute density which is three orders of magnitude below the overlap density, and (b) is well above the overlap density. The configurations are oriented by plotting in the plane of the eigenvectors of the inertia tensor with the two largest eigenvalues. The figure clearly shows a transition from stretched to coiled with increasing density. The dilute example is quite stretched but not rodlike. The structure exhibits kinks at short length scales and is bent at long length scales. From such pictures we know that horseshoe shaped fluctuations exist even for longer chains and lower densities. Such structure is not expected at those dilute densities which a persistence length calculation predicts should be fully stretched. The dense case exhibits the coiling reminiscent of neutral good solvent chains.

A convenient quantity to see the transition from stretched to coiled conformation is the ratio of the end-to-end distance and the radius of gyration,  $r \equiv \langle R^2 \rangle / \langle S^2 \rangle$ . For ideal chains,  $r = 6$ ; for good solvent chains,  $r = 6.3$ ; for rigid rods,  $r = 12$ . The plot of  $r$  versus  $\rho_m$  in Figure 5 shows that the transition from stretched to coiled is present. At the highest densities  $r$  approaches the ideal chain value. With decreasing density  $r$  rises independent of chain length. In the dilute limit the rigid rod value is not reached for any of the chain lengths. Instead, there is a chain length dependent saturation. This agrees with the expectation that longer chains which have more charges and experience a stronger Coulomb repulsion are straighter. For charged or neutral polymers, the chain ends are always more flexible than the centers.

The saturation of  $r$  occurs at  $\rho_m \simeq 1 \cdot 10^{-4}\sigma^{-3}$ ,  $2 \cdot 10^{-5}\sigma^{-3}$  and  $1 \cdot 10^{-6}\sigma^{-3}$  for  $N_b = 16, 32$ , and  $64$  respectively. One might expect this saturation to occur at  $c_1^*$ , where chain stiffness is maximal. For these chain length,  $c_1^*$  is not defined as the condition  $\kappa L > 1$  is not satisfied. However, for  $N_b = 128$  using the full Odijk form (14)  $c_1^* = 2.8 \cdot$

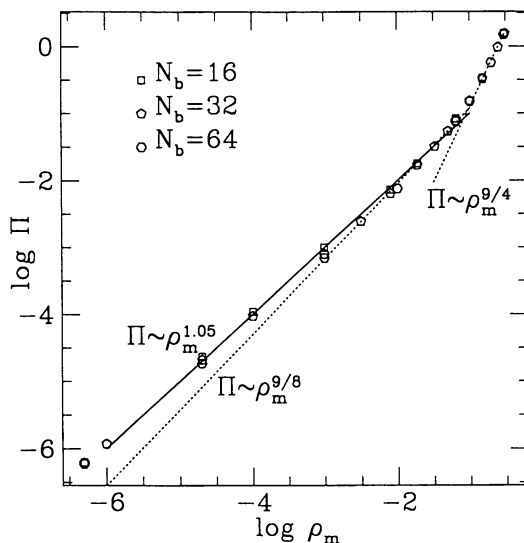


Figure 1. The osmotic pressure is plotted as a function of the monomer density on a log-log scale for various chain lengths. The 16, 32 and 64 bead chains are represented by squares, pentagons and hexagons, respectively. For low densities our relatively small chains tend to have values above the Odijk prediction. This is consistent with the molecular weight dependence found in experiments. At high densities the exponent is  $9/4$  which is that of neutral chains. (Reproduced with permission from ref. 22. Copyright 1993 APS.)

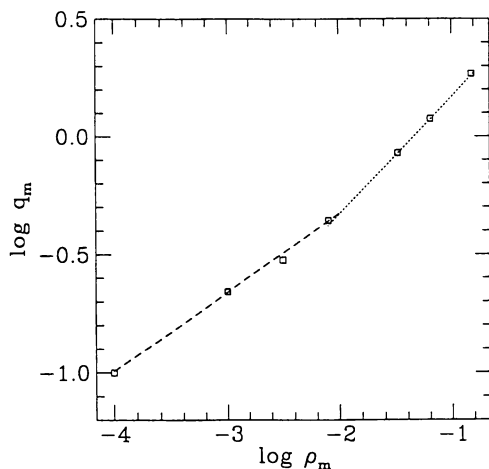


Figure 2. The position of the maximum of the inter-polymer structure factor,  $q_m$ , is plotted as a function of monomer density. The same scaling dependence as found in experiments is exhibited. At low densities  $q_m$  scales as  $\rho_m^{1/3}$  (dashed line) and at high densities  $q_m$  scales as  $\rho_m^{1/2}$  (dotted line).

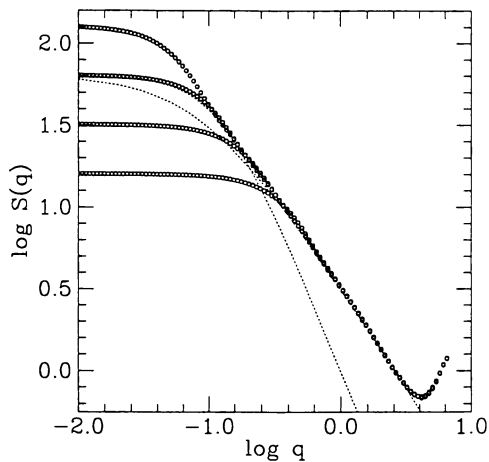


Figure 3. The form factor at  $\rho_m = 5 \cdot 10^{-7} \sigma^{-3}$  for  $N_b = 16, 32, 64$  and  $128$ . The form factors are chain length independent for  $q > 2\pi / \langle R^2 \rangle^{1/2}$ . This condition holds for all densities. We are thus able to determine the structure of very long chains on length scales up to the end-to-end distance of our longest chains.

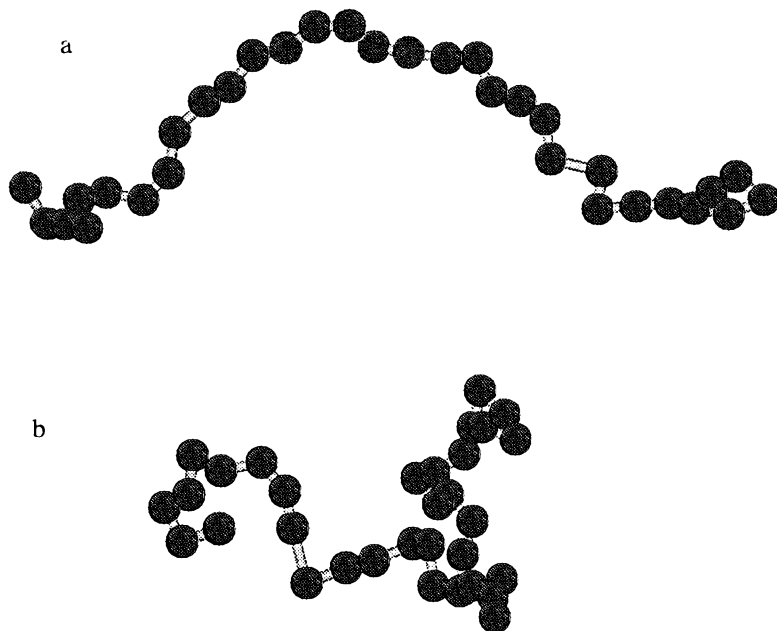


Figure 4. Two typical polymer configurations for  $N_b = 32$  at (a)  $\rho_m = 1 \cdot 10^{-4} \sigma^{-3}$  and (b)  $\rho_m = 0.3 \sigma^{-3}$  are shown. At dilute densities the chains are quite stretched (a) and at high densities the chains are coiled (b) like neutral chains.

$10^{-5}\sigma^{-3}$ . This value is much too high. One reasonable value of the saturation density,  $\rho_m^{(s)}$ , is the density at which there is one counterion per polymer volume. For densities below this value, the counterion screening of the intrachain interactions is negligible and one expects  $r$  to be constant. For  $N_b = 16, 32$  and  $64$ ,  $\rho_m^{(s)} \equiv 1/(\pi R^2)^{3/2}/6 = 2.3 \cdot 10^{-3}\sigma^{-3}$ ,  $2.3 \cdot 10^{-4}\sigma^{-3}$  and  $2.3 \cdot 10^{-5}\sigma^{-3}$ , respectively. Especially the ratios of these values agree much better with our data.

To compare to scaling predictions, we show the end-to-end distance as a function of monomer density for the same three chain lengths as above in Figure 6. At high densities where  $L_e \ll L_i$ ,  $R \sim \rho_m^{-3/16}$  according to Odijk's scaling theory. Our results do not clearly show any scaling regime. However, the solid lines represent the  $\rho_m^{-3/16}$  dependence and show that the  $-3/16$  exponent is in agreement with our data. This agreement occurs even though the above criterion is not valid for our simulations. deGennes *et al.* (10) have predicted an exponent of  $-1/8$  which is close to Odijk's value and which also fits our data, though not as well as Odijk's value. At lower densities, our results disagree with Odijk's predictions. When  $L_e \gg L_i$  at low densities, Odijk predicts  $R \sim \rho_m^{-5/16}$ , but our curves are flatter than at high densities instead of steeper as Odijk predicts.

Scaling predictions for  $P(q)$  have been based on the picture that the polyelectrolyte's structure is composed of straight segments which together form an ideal chain (1,10,18). For wavevectors greater than the inverse rodlength, or persistence length,  $L_p$ , the form factor should scale as  $1/q$ . In terms of the exponent  $\nu$  of the general form,  $P(q) \sim 1/q^{1/\nu}$ ,  $\nu = 1$  for the rod. For  $q < 2\pi/L_p$ , the ideal chain would yield  $\nu = 1/2$ . However, we have good solvent chains and should see  $\nu = 3/5$  at dilute densities.

We show our calculated  $P(q)$  spanning dilute and semidilute ranges for the 32 bead chains in Figure 7. Two  $q$ -regimes are evident in  $P(q)$ . A density and chain length independent regime occurs at relatively high wavevector ( $1 < q\sigma < 2\pi/2$ ) which corresponds to short length scales up to six bond lengths. At low wavevectors the form factor changes continuously as a function of the monomer density.

The high  $q$ -regime dependence is not as expected from present theory. The slope of form factor here is *not*  $-1$ . From examination of  $q^{1/\nu}P(q)$ , we find that for  $1 < q\sigma < 2\pi/3$ ,  $\nu = 0.80$  gives the best scaling. This corresponds to chains which are stretched beyond the neutral good solvent value, but well below the rod value. On short length scales, one expects thermal fluctuations to yield values of  $\nu$  less than one. However, the  $\nu = 0.80$  scaling extends to a rather long  $6\langle b \rangle$ . Furthermore, the chain structure does not become more stretched with increasing length as expected (10). This chain length independence is quite surprising, because it implies that the Coulomb interaction can stretch a chain only to a limited extent at least on short length scales. The density independence suggests the existence of a fundamental structural building block of length  $6\langle b \rangle$ .

The lines in Figure 7 show that at low  $q$  the slope varies from about  $-1$  to beyond  $-5/3$ , but not quite to  $-2$ . Presumably, at higher densities a slope of  $-2$  would be reached. The variation in  $\nu$  contrasts with the picture of just two values of  $\nu$ . Evidently, not only the length over which the Coulomb interaction stretches the chain, but also the degree of stretching depends on the screening. At the lowest densities where the form factor has saturated, the value of  $\nu$  is  $0.9$ . Thus, the chain at very dilute concentrations is stretched more at long length scales than at short length scales, but the chain is not rodlike. The value of  $\nu$  is the same on short and long length scales at the the overlap density. In the semidilute regime the chain is more contracted at long length scales than at short length scales.

## Conclusions

Our results imply a new picture of the chain structure (Figure 8). On short length scales the chain is stretched, but not rodlike. Figure 8 shows tubelets of length  $6\langle b \rangle$  which combine to form the complete chain. The tubes have been drawn for simplicity as cylinders. The cylinder radius gives some idea of the curvature of the enveloped monomers. The

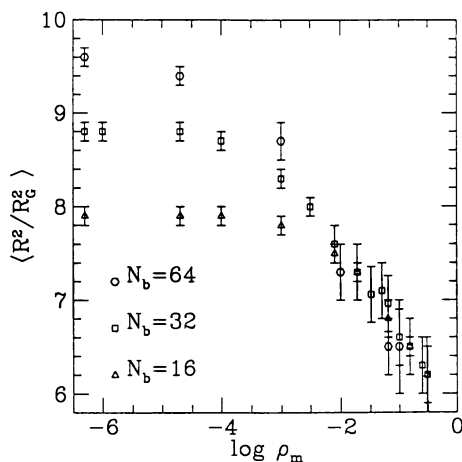


Figure 5. The ratio,  $r$ , of the end-to-end distance and the radius of gyration is plotted versus the log of the monomer density. A value of 12 corresponds to a rigid rod and a value of 6 corresponds to a gaussian coil. (Reproduced with permission from ref. 22. Copyright 1993 APS.)

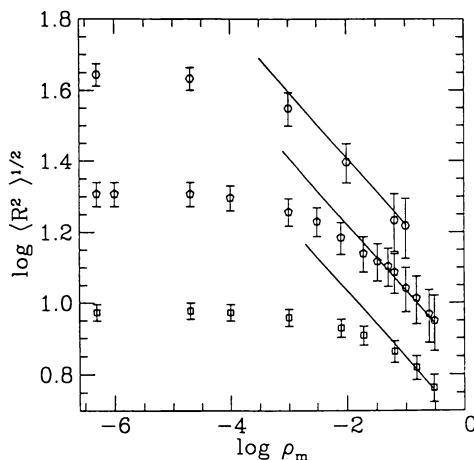


Figure 6. The concentration dependence of the average end-to-end distance agrees with Odiijk's scaling prediction which gives an exponent of  $-3/16$ . The solid lines show this dependence. The prediction of  $-1/8$  by deGennes *et al.* also is consistent with the data. At low concentrations the curve becomes flatter instead of steeper as predicted by Odiijk.

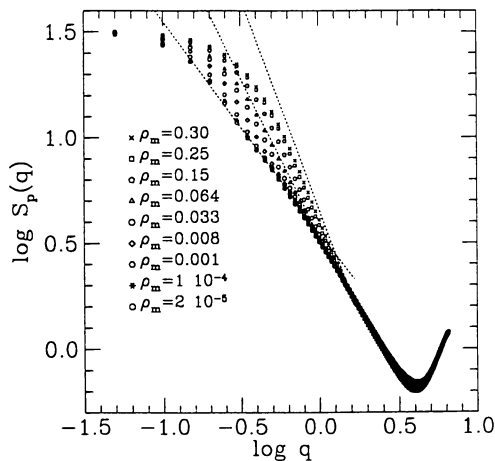


Figure 7. The form factor for 32 bead chains gradually changes from apparent rodlike to coiled form with increasing monomer density. This contradicts the theoretically expected form which is a combination of rigid rod, good solvent chain and ideal chain forms. The dotted lines give slopes of  $-1$ ,  $-5/3$  and  $-2$  which correspond to the  $q$ -dependence of a rigid rod, good solvent chain and ideal chain, respectively. For  $0 < \log q < 0.2$  the slope is steeper than  $-1$ , implying the chains are not fully stretched in this regime.

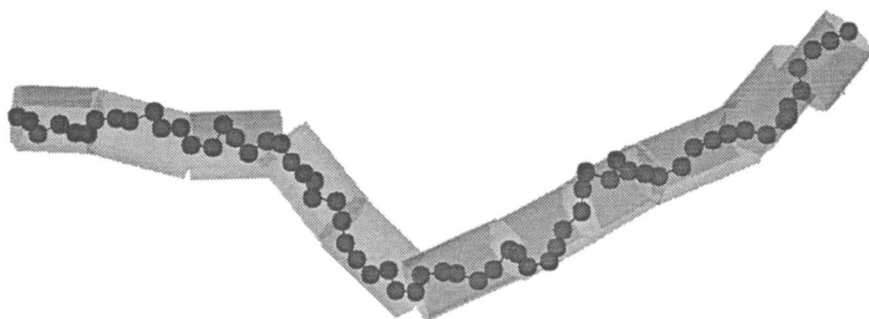


Figure 8. A schematic of our picture of polyelectrolyte structure is shown for a 64 bead chain. The chain is wrapped by a tube composed of tubelets made of length  $6(b)$ . For this length scale, the polymer structure is concentration independent. On longer length scales the chain structure is density dependent.



chain of these tubelets depends on the density or, equivalently, on the degree of screening. At low densities the chain of tubelets is highly stretched but not rodlike. As the density increases the chain become gradually more coiled on long length scales, but the tubelet structure is unchanged. In the semidilute regime the structure is similar to a neutral chains composed of the tubelets. When the strand-strand distance becomes shorter than the tubelet length, the tubelet structure does change.

We would like to acknowledge fruitful discussions with P.A. Pincus and a large grant of computer time from the Höchstleistungsrechenzentrum, Germany within the Disordered Polymers Project. A NATO Travel Grant is gratefully acknowledged.

## Literature Cited

- (1) Hayter, J.; Janninck, G.; Brochard-Wyart, F.; and de Gennes, P.; *J. Physique Lett.* **1980**, *41*, 451.
- (2) Wang, L.; and Bloomfield, V.; *Macromolecules* **1990**, *23*, 804.
- (3) Witten, T.; and Pincus, P.; *Europhys. Lett.* **1987**, *3*, 315.
- (4) de Gennes, P.; *Scaling Concepts in Polymer Physics*; Cornell University Press: Ithaca, New York, 1979.
- (5) Kim, M.; and Pfeiffer, D.; *Euro. Phys. Lett.* **1988**, *5*, 321.
- (6) Christos G. A.; Carnie, S. L. *J. Chem. Phys.* **1989**, *91*, 439. Reed, C.; Reed, W *J. Chem. Phys.* **1990**, *92*, 6916. Brender, C; Danino, M *J. Chem. Phys.* **1992**, *97*, 2119. Barrat, J. L.; Boyer, D. *J. Phys. II France* **1993**, *3*, 343. See also references therein.
- (7) Kremer, K.; and Grest, G.; *J. Chem. Phys.* **1990**, *92*, 5057.
- (8) Dünweg, B.; and Kremer, K.; *Phys. Rev. Lett* **1982**, *66*, 2996.
- (9) Adams, D.; and Dubey, G.; *J. Comp. Phys.* **1987**, *72*, 156.
- (10) de Gennes, P.; Pincus, P.; and Velasco, R.; *J. Physique* **1976**, *37*, 1461.
- (11) Kuhn, W.; Kunzle, D.; and Katchalsky, A.; *Helv. Chim. Acta* **1948**, *31*, 1994.
- (12) Hermans, J.; and Overbeek, J.; *Recents Travaux Chimiques* **1968**, *67*, 761.
- (13) Skolnick, J.; and Fixman, M.; *Macromolecules* **1977**, *10*, 944.
- (14) Odijk, T.; *J. Polym. Scil, Polym. Phys. Ed.* **1977**, *15*, 477.
- (15) Odijk, T.; *Polymer* **1978**, *19*, 989.
- (16) Fixman, M.; *J. Chem. Phys.* **1982**, *76*, 6346.
- (17) Bret, M. L.; *J. Chem. Phys.* **1982**, *76*, 6242.
- (18) Odijk, T.; *Macromolecules* **1979**, *12*, 688.
- (19) Cates, M.; *J. Phys. II France* **1992**, *2*, 1109.
- (20) Wang, L.; and Bloomfield, V.; *Macromolecules* **1991**, *24*, 5791.
- (21) Stevens, M.; and Kremer, K.; *Macromolecules* **1993**, *26*, 4717.
- (22) Stevens, M.; and Kremer, K.; to be published in *Phys. Rev. Lett.*

RECEIVED August 6, 1993

## Chapter 6

# Electrophoresis of Nonuniformly Charged Chains

John L. Anderson and Yuri Solomentsev

Department of Chemical Engineering, Carnegie Mellon University,  
Pittsburgh, PA 15213

A hydrodynamic analysis of the electrophoretic motion of chain-like particles is presented. The key feature is that the charge is nonuniformly distributed on the particle. Three particle geometries are considered: (1) a polymer-colloid complex, which might arise when a polyelectrolyte attaches itself to several colloidal particles; (2) straight filaments, which could be a model for the coagulation of colloidal spheres or the bundling of charged fibers; and (3) a toroidal ring, which might be a model for DNA plasmids. The theory is based on balancing hydrodynamic and electrophoretic driving forces that operate unevenly on different parts of the heterogeneous particle. The zeta potential, defined as the ion potential at the plane of shear between the suspending liquid (water) and the particle, is allowed to be a function of position along the chain. Although the theory is more general, here we consider for simplicity the case where the Debye screening length is smaller than the radius of the chain. Two interesting results emerge. First, the mobility of a particle is not proportional to its mean charge (or, zeta potential), and hence neutral particles can have significant electrophoretic mobilities given certain distributions of the charge. The second interesting result is that the electrophoretic mobility of a chain of spheres of equal size but different charge depends on the relative placement of the spheres. An example is presented to show that a chain of spheres that is neutral overall could have a zero, positive or negative mobility depending on the relative positions of the spheres of different charge.

Electrophoresis is used to characterize, transport and separate charged macromolecules and colloidal particles in electric fields. The electrophoretic mobility, defined as the velocity of charged particles per unit electric field, is related to the charged state of the particles ( $I$ ). Two extreme cases are defined in terms of the size of the particle ( $a$ ) compared to the Debye screening length of the solution ( $\kappa^{-1}$ ). If  $a \ll \kappa^{-1}$  then the particle looks like a point charge and the counterion cloud has a negligible screening effect; for a sphere of charge  $q$  the electrophoretic velocity is given by

0097-6156/94/0548-0067\$06.00/0

© 1994 American Chemical Society

In Macro-ion Characterization; Schmitz, K.;

ACS Symposium Series; American Chemical Society: Washington, DC, 1993.

$$U = \frac{q}{6\pi\eta a} E_{\infty} \quad (1)$$

where  $\eta$  is the coefficient of viscosity of the fluid and  $E_{\infty}$  is the applied electric field.

At the other extreme,  $a \gg \kappa^{-1}$ , the charge on the surface is highly screened; Smoluchowski's equation gives the electrophoretic velocity:

$$U = \frac{D\zeta}{4\pi\eta} E_{\infty} \quad (2)$$

where  $\zeta$  is the "zeta potential" of the particle's surface, which is taken to be the plane of shear between the particle and the surrounding liquid. Note that electrostatic units of charge (e.s.u.) are used here, and  $D$  is the dielectric constant of the liquid ( $\approx 78$  for water). The classical Gouy-Chapman theory of the electrical double layer gives the following relation between charge/area on the surface ( $\sigma$ ) versus zeta potential:

$$\sigma = \frac{DkT}{2\pi ze} \kappa \sinh\left(\frac{ze\zeta}{2kT}\right) \approx \frac{Dk\zeta}{4\pi} \quad (3)$$

where the approximation holds when  $|ze\zeta/kT|$  is order unity or less. ( $z$  is the valence of the ions of the electrolyte.) Combining equations 2 and 3 we have the following for the highly screened case when  $|z\zeta| \lesssim kT/ze$ :

$$U = \frac{q}{6\pi\eta a} \frac{3}{2} \frac{1}{\kappa a} E_{\infty} \quad (4)$$

where  $q$  is the total charge on the particle ( $q = 4\pi a^2 \sigma$ ).

Equation 2 applies to particles of any shape as long as (i)  $\zeta$  is uniform over the surface of the particle, and (ii)  $(\kappa a)^{-1} \exp(|ze\zeta/2kT|) \ll 1$  where "a" is the characteristic size of the particle (e.g., radius of a sphere). General results are available for arbitrary  $\kappa a$  and  $\zeta$  for uniformly charged spheres (2,3,4). For particles satisfying constraint (ii), models are available to account for arbitrary distributions of  $\zeta$  on the surface of ellipsoids (5). These particles can translate and *rotate* depending on the distribution of charge; Smoluchowski's equation predicts no rotation. A theory is also available for chains composed of two (6) and three (7) spheres each differing in zeta potential. Experiments (8) with colloidal doublets are consistent with the theory.

In this paper we are concerned with chain-like particles for which the charge (or zeta potential) varies along the chain. Three basic geometries are considered, as shown in Figure 1. The next section deals with a model for the polymer-colloid complex. When hydrodynamic interactions among the various subunits are neglected, an analytic expression for the electrophoretic velocity of the complex is obtained. The analysis of electrophoresis of straight chains is based on the hydrodynamic theory of "slender bodies". Results for long prolate spheroids and right circular cylinders are presented. The results for the circular cylinder are used to model a straight chain of equal spheres attached to each other. Finally, the hydrodynamic analysis by Johnson and Wu (9) is used to model the electrophoresis

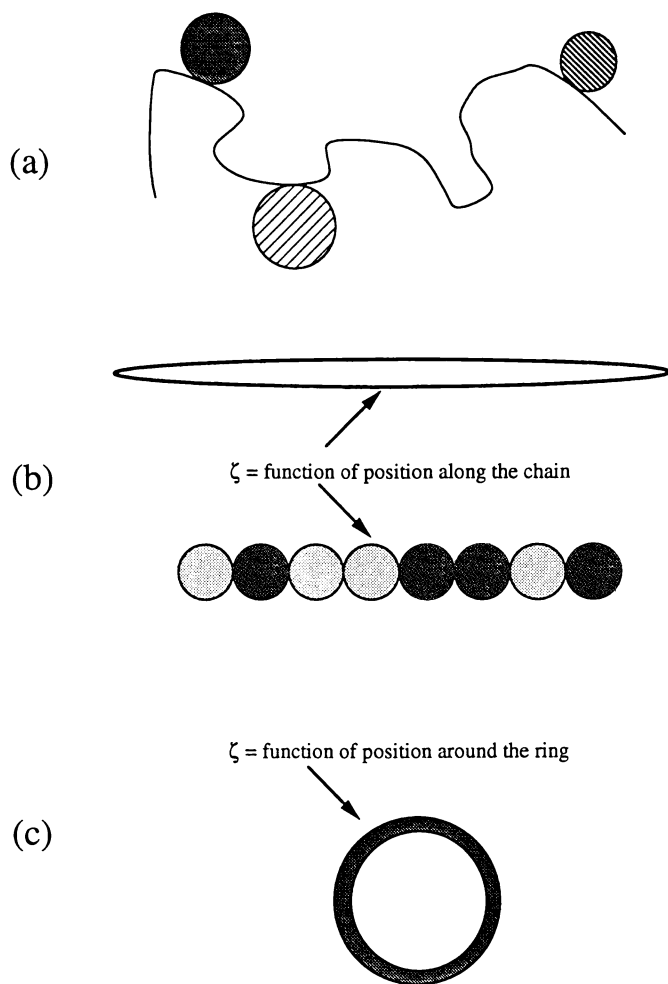


Figure 1. Examples of nonuniformly charged colloidal chains. (a) Polymer-colloid complex; (b) straight chains having a slender shape; (c) toroidal ring. In all cases the charge density varies with position along the chain.

of a toroidal ring having a variable charge along its contour. For all three geometries shown in Figure 1, our theory predicts that neutral chains will move in electric fields if the distribution of the charge along the chain has certain properties.

## POLYMER-COLLOID COMPLEXES

Consider  $N$  spherical colloids connected through their attachment to a polymer chain, as shown in Figure 1a. If particle "i" were not constrained by its attachment to the polymer, then its velocity in the applied electric field ( $\mathbf{E}_\infty$ ) would be simply  $\mu_i \mathbf{E}_\infty$  where  $\mu_i$  is the electrophoretic mobility; for the highly screened case the mobility is given by the coefficient of  $\mathbf{E}_\infty$  in equation 2 or 4. Likewise, the polymer would move at velocity  $\mu^{(p)} \mathbf{E}_\infty$  in the absence of the attached colloids. If the complex is a rigid body, then the polymer and attached colloids must all move at the same velocity  $\mathbf{U}$  in the field. The total hydrodynamic force is found by summing up the friction on each element, which is proportional to the difference between  $\mathbf{U}$  and the unconstrained electrophoretic velocity of the element:

$$\mathbf{F} = - \sum_{i=1}^N f_i [\mathbf{U} - \mu_i \mathbf{E}_\infty] - f^{(p)} [\mathbf{U} - \mu^{(p)} \mathbf{E}_\infty] = \mathbf{0} \quad (5)$$

The  $f_i$  and  $f^{(p)}$  are orientation-averaged friction coefficients of the colloids and the polymer, respectively. Rotation of the complex is neglected; this is justified if the ensemble-averaged angular velocity is zero, either because of strong Brownian motion or by alignment of the dipole of the complex with the electric field. If dipole alignment is a factor, the electrophoretic mobility ( $U/E_\infty$ ) would be a function of the applied field.

$\mathbf{F}$  must equal zero because in the screened case the electric field exerts no force on the elements if their double layers are included (10). Thus, the velocity of the complex is given by

$$\mathbf{U} = \frac{f^{(p)} \mu^{(p)} + \sum_{i=1}^N f_i \mu_i}{f^{(p)} + \sum_{i=1}^N f_i} \mathbf{E}_\infty \quad (6)$$

If we neglect all hydrodynamic interactions in the complex and consider only spherical colloids, then  $f_i = 6\pi\eta a_i$ . If we further assume that the polymer's structure is not significantly perturbed by the attached colloids, we have  $f^{(p)} = 6\pi\eta R_H$  where  $R_H$  is the Stokes-Einstein (hydrodynamic) radius which is calculated from the diffusion coefficient of the polymer. Combining these expressions into equation 6 produces

$$\mathbf{U} = \frac{R_H \mu^{(p)} + \sum_{i=1}^N a_i \mu_i}{R_H + \sum_{i=1}^N a_i} \mathbf{E}_\infty \quad (7)$$

The above is the "free draining" result for the complex because colloid-colloid and colloid-polymer hydrodynamic interactions are neglected; however, hydrodynamic interactions among elements of the polymer chain are included in  $f^{(p)}$ , or

equivalently  $R_H$ . Because hydrodynamic and electrostatic interactions among the colloids are neglected, the velocity of the complex is independent of the relative spacing and orientation of the colloids on the polymer chain.

As an example, assume all  $N$  colloids are identical with radius "a" and electrophoretic mobility in free solution equal to  $\mu_0$ . The dimensionless electrophoretic mobility of the complex,  $U/\mu_0 E_\infty$ , is given by

$$\frac{U}{\mu_0 E_\infty} = \frac{\frac{\mu^{(p)}}{\mu_0} + \left(\frac{a}{R_H}\right) N}{1 + \left(\frac{a}{R_H}\right) N} \quad (8)$$

This expression is plotted in Figure 2 for the case  $a/R_H = 0.5$ . (Note that  $a/R_H$  equals the ratio of polymer-to-colloid diffusion coefficients, each of which is a measurable property before the complex is formed.) For the case  $\mu^{(p)} = \mu_0$  the velocity of the complex is independent of  $N$  and  $U = \mu_0 E_\infty$ ; this is expected because all the elements of the complex ( $N$  colloids plus the polymer chain) move at  $\mu_0 E_\infty$ . For the case where  $\mu^{(p)}$  and  $\mu_0$  have opposite signs, the direction of electrophoresis changes as  $N$  increases.

Experiments have been performed with silica particles bound to polyelectrolyte chains (11). One objective of such measurements is to relate the number of adsorbed colloids ( $N$ ) to the electrophoretic mobility of the complexes. Equation 8, though approximate because of the free-draining model, indicates that  $N$  can be deduced from the electrophoretic mobility if the mobilities of the polyelectrolyte ( $\mu^{(p)}$ ) and micelles ( $\mu_0$ ) are known *a priori*.

Another interesting question is how the mobility of the complex is related to the total charge. To investigate this using the free-draining model, we must assume a model relating the mobility of each subunit to the charge. If we assume modest zeta potentials ( $|\zeta|$  comparable to  $kT/ze$ ) and highly screened double layers for the colloids ( $\kappa a \gg 1$ ), we have the following from equation 4:

$$\mu_0 = \frac{q_0}{4\pi\eta\kappa a^2} \quad (9)$$

where  $q_0$  is the charge on each colloid. The relationship between mobility and charge for the polymer chain is more ambiguous, depending on the configurational model for the chain (12,13). Here, for illustration purposes only, we consider a general linear model:

$$\mu^{(p)} = W \frac{q^{(p)}}{2\pi\eta l \kappa b} \quad (10)$$

where  $b$  is the radius and  $l$  the length of the chain. The coefficient  $W$  is a function of  $\kappa b$  and the contour of the chain; here we take it to be unity, which would be the case for a highly screened ( $\kappa b \gg 1$ ), extended chain. In Figure 3 we re-plot the calculations for  $\mu^{(p)}/\mu_0 = -2$  shown in Figure 2. These graphs show that neutral complexes will move and zero-mobility does not imply charge neutralization. This result would not significantly change had we chosen a different value for  $W$ .

Another example of the motion of neutral complexes is given by two colloids of equal but opposite charge ( $q_1 = -q_2$ ) connected by a neutral polymer ( $\mu^{(p)} = 0$ ) having a negligible hydrodynamic resistance ( $R_H \ll a_1$  or  $a_2$ ). For cases when the mobility of the colloids is given by equation 4, the velocity of the complex is

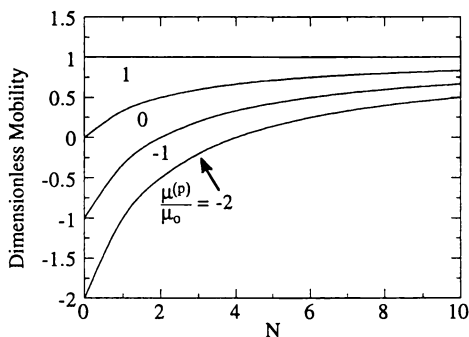


Figure 2. Dimensionless mobility of a polymer-colloid complex (mobility of the complex,  $U/E_{\infty}$ , divided by the mobility of the colloids,  $\mu_0$ ) as a function of the number of colloids attached to the polymer. The curves are from equation 8 with  $a/R_H = 0.5$ .

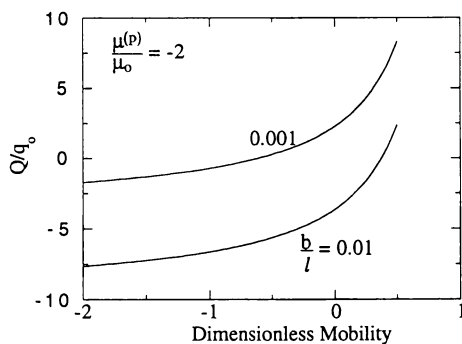


Figure 3. The total charge ( $Q$ ) of the complex versus the dimensionless mobility (defined in Figure 2) of a polymer-colloid complex.  $q_0$  is the charge on each colloid attached to the polymer. The curves were computed from equations 8-10 with  $a/R_H = 0.5$  and  $\mu^{(p)}/\mu_0 = -2$ . The hydrodynamic radius of the polymer chain was determined from the theory for a rod of length  $l$  and radius  $b$ :  $R_H = l/[3 \ln(l/b)]$ .

$$\mathbf{U} = \frac{q_1}{\epsilon \kappa a_1^2} \left[ \frac{1 - \frac{a_1}{a_2}}{1 + \frac{a_2}{a_1}} \right] \mathbf{E}_\infty \quad (11)$$

Clearly the complex moves in the field if the radii of the two colloids differ, even though the *net charge on the entire complex is zero*. An interesting prediction of equation 11 is that the direction of electrophoresis is determined by the *smaller* colloid. Hydrodynamic analysis of nonuniformly charged spheroidal particles also shows that such particles can have a significant electrophoretic mobility even when they are neutral (5).

A more quantitatively accurate model for complexes would allow for hydrodynamic interactions among the colloidal subunits. If the hydrodynamic effects of the connecting polymer chain are negligible ( $R_H \ll a$ ), the force on each colloidal subunit can be written in terms of general friction tensor ( $\xi_j$ ) which is a function of the size ( $a_j$ ) and relative position ( $\{\mathbf{r}_j\}$ ,  $j = 1 \rightarrow N$ ) of all the spherical particles in the complex:

$$\mathbf{F}_i = -\xi_i \cdot [\mathbf{U} - \mu_i \mathbf{E}_\infty] \quad (12)$$

where  $\xi(\{\mathbf{r}_j\})$  accounts for hydrodynamic interactions among the particles; in the absence of these interactions  $\xi_j$  equals  $(6\pi\eta a_j)\mathbf{I}$  where  $\mathbf{I}$  is the unit tensor. Calculations based on the Oseen approximation for hydrodynamic interactions have been used to model the hydrodynamic resistance of particles of different geometry (14,15). The velocity of the complex is found by equating the sum all the forces on the  $N$  subunits to zero:

$$\mathbf{U} = (\sum \xi_j)^{-1} \cdot \sum \mu_j \xi_j \cdot \mathbf{E}_\infty \quad (13)$$

This formula is valid if rotational effects are negligible, that is,  $\langle \boldsymbol{\Omega} \rangle = \mathbf{0}$ . Because the velocity is a function of the relative configuration of the particles,  $\{\mathbf{r}_j\}$ , the measurable velocity is the ensemble average of equation 13. Note that if all the subunits have the same electrophoretic mobility,  $\mu_i = \mu_0$ , then the velocity of the complex is simply  $\mu_0 \mathbf{E}_\infty$  no matter what the relative configuration of the subunits.

Equations 12 and 13 do not allow for interactions among the subunits in the electrophoresis terms; that is,  $\mu_i$  is assumed independent of  $\{\mathbf{r}_j\}$ . In principle the electrophoretic mobilities  $\mu_i$  are also tensors that are functions of the relative configuration of the particles. However, interactions among spheres undergoing electrophoresis are extremely weak (10,16) and neglect of these interactions is probably justified given the simplicity of the model itself.

## ELECTROPHORESIS OF SLENDER PARTICLES

Figure 4 shows the general model of a "slender particle" which may possess a distribution of charge along its contour. The contour length equals  $2L$  and "s" is the dimensionless position measured along the contour ( $s = -1$  and  $+1$  at the ends). The cross section at any contour position is a circle of radius  $b$  which varies with  $s$ , and  $\lambda(s)$  is defined as  $b(s)/b_{\max}$ . The three length scales of the system have the



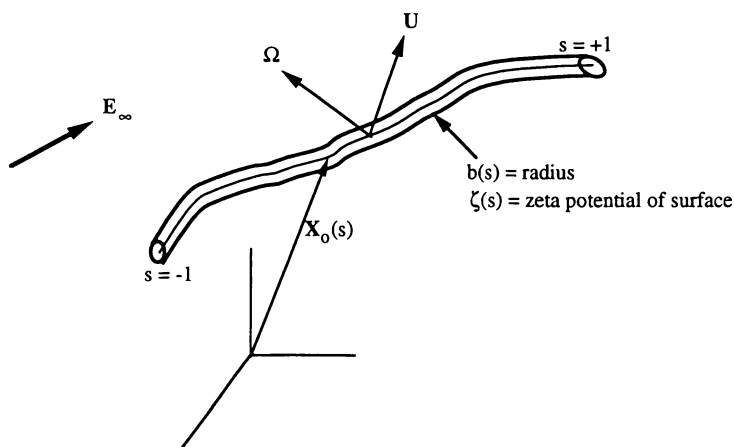


Figure 4. Geometry of a slender particle.  $L$  is the half-length of the contour, and  $s$  is the distance along the contour from the center divided by  $L$ . The cross-section of the particle is a circle whose radius ( $b$ ) varies with  $s$ . The contour of the particle is defined by the function  $\mathbf{X}_0(s)$ . The particle is assumed to be a rigid body with the velocity of the center equal to  $\mathbf{U}$  and the angular velocity equal to  $\mathbf{\Omega}$ .

following scaling:  $\kappa^{-1} \leq b_{\max} \ll L$ . The slenderness parameter ( $\epsilon$ ) is defined as  $b_{\max}/L$ . The locus of points along the axis of the contour is defined by the vector function  $\mathbf{X}_0(s)$ , and the position vector is defined as  $\mathbf{r} = \mathbf{X}_0(s) - \mathbf{X}_0(0)$ . The contour can be curved as long as its radius of curvature is much greater than  $b_{\max}$ .

A continuous representation of the "subunit model" introduced in the previous section is the basis of the model for slender particles. A subunit of dimensionless length  $ds$  would have an electrophoretic velocity equal to  $\boldsymbol{\mu}(s) \cdot \mathbf{E}(s)$  where  $\mathbf{E}$  is the local electric field and the tensor  $\boldsymbol{\mu}$  depends on the zeta potential at  $s$ . Because the particle is locally a cylinder,  $\boldsymbol{\mu}$  has two principle values, one for the field parallel to the axis (i.e., parallel to the local tangent of  $\mathbf{X}_0(s)$ ) and the other for the field perpendicular to the axis (17). If  $\kappa^{-1} \ll b(s)$  then  $\boldsymbol{\mu}(s) = (D/4\pi\eta) \zeta(s) \mathbf{I}$ ; we make this assumption here.

The slender particle is assumed to be a rigid body.  $\mathbf{U}$  is the translational velocity of the center ( $s = 0$ ) and  $\boldsymbol{\Omega}$  is the angular velocity. The force per unit length,  $\boldsymbol{\Gamma}(s)$ , is given by

$$\boldsymbol{\Gamma}(s) = -\boldsymbol{\xi}(s) \cdot [\mathbf{U} + \boldsymbol{\Omega} \times \mathbf{r}(s) - \boldsymbol{\mu}(s)\mathbf{E}] \quad (14)$$

where the hydrodynamic resistance tensor,  $\boldsymbol{\xi}(s)$ , allows for hydrodynamic interactions along the contour of the particle. The determination of the local electric field involves solution of Laplace's equation for the electrical potential outside the double layer. Cole (18) showed that to  $O(\epsilon^2 \ln \epsilon)$ ,  $\mathbf{E}$  equals the applied field ( $\mathbf{E}_\infty$ ) which is a constant.  $\mathbf{U}$  and  $\boldsymbol{\Omega}$  are determined by setting the total force and torque on the particle equal to zero:

$$\int_{-1}^{+1} \boldsymbol{\Gamma}(s) ds = \mathbf{0} \quad (15a)$$

$$\int_{-1}^{+1} \mathbf{r}(s) \times \boldsymbol{\Gamma}(s) ds = \mathbf{0} \quad (15b)$$

The remaining problem, then, is to determine  $\boldsymbol{\xi}(s)$  for translation and rotation given the geometry of the particle,  $\mathbf{X}_0(s)$  and  $\lambda(s)$ . Note that if the particle has certain symmetry, for example is straight and symmetric ( $\lambda(s) = \lambda(-s)$ ), then translation and rotation are uncoupled; in this case equation 15a yields  $\mathbf{U}$  and equation 15b yields  $\boldsymbol{\Omega}$ .

Theories for the hydrodynamics of slender particles are based on determining the distribution of "Stokeslets" along the contour of the chain. The Stokeslet distribution  $\boldsymbol{\alpha}(s)$  is defined such that for a given motion of the particle the force per unit length exerted by the fluid on the particle is given by  $-8\pi\eta\boldsymbol{\alpha}$ . In terms of the resistance tensor  $\boldsymbol{\xi}$  we have

$$\boldsymbol{\alpha}(s) = \frac{1}{8\pi\eta} \boldsymbol{\xi}(s) \cdot \mathbf{V}(s) \quad (16)$$

where  $\mathbf{V}(s)$  is the velocity of position  $s$  of the particle. From equation 14 we have

$$\mathbf{V}(s) = \mathbf{U} + \boldsymbol{\Omega} \times \mathbf{r}(s) - \boldsymbol{\mu}(s)\mathbf{E}_\infty \quad (17)$$

The velocity of the particle is determined by substituting equations 16 and 17 into equation 15. The Stokeslet functions for translation ( $\mathbf{U}$ ) and rotation ( $\mathbf{\Omega}$ ) are evaluated using the theory of Cox (19), which is correct to  $O(1/\ln \epsilon)^2$ . By using the Lorentz reciprocal theorem (5) we avoid the calculation of the Stokeslet distribution for electroosmotic flow ( $\mathbf{V} = -\mu(s)\mathbf{E}_\infty$ ). Below are some results for the shapes shown in Figure 1. Details of the hydrodynamic analysis are presented elsewhere (20).

*LONG SPHEROID* ( $\lambda(s) = \sqrt{1-s^2}$ )

For this particular shape the Stokeslet distribution can be determined to an error of  $O(\epsilon^2 \ln \epsilon)$ . The three Stokeslet functions are:

$$\alpha_{\parallel} = \frac{1}{2[2 \ln(2/\epsilon) - 1]} \quad (18a)$$

$$\alpha_{\perp} = \frac{1}{2 \ln(2/\epsilon) + 1} \quad (18b)$$

$$\alpha_r = \frac{s}{2 \ln(2/\epsilon) - 1} \quad (18c)$$

where  $\alpha_{\parallel}$  and  $\alpha_{\perp}$  are for translation at unit velocity parallel and perpendicular to the axis of rotational symmetry of the spheroid, respectively, and  $\alpha_r$  is the Stokeslet for rotation perpendicular to the axis. Equations 14-16 then give the following for any distribution of mobilities along the chain:

$$\mu_{\parallel} \equiv \frac{U_{\parallel}}{E_{\parallel}} = \langle \mu \rangle \quad (19a)$$

$$\mu_{\perp} \equiv \frac{U_{\perp}}{E_{\perp}} = \langle \mu \rangle \quad (19b)$$

$$\mu_r \equiv \frac{\Omega L}{E_{\perp}} = 3 \langle s\mu \rangle \quad (19c)$$

where the brackets define an average over the contour length:

$$\langle f \rangle = \frac{1}{2} \int_{-1}^{+1} f \, ds \quad (20)$$

For the highly screened case,  $\kappa b(s) \gg 1$ , we can substitute the following for the local mobility:

$$\mu(s) = \frac{D}{4\pi\eta} \zeta(s) \quad (21)$$

For zeta potentials of order  $kT/e$  or less, the charge per unit length of the particle is proportional to  $\zeta(s)$ . At first glance it might appear that the mobilities in equations 19 are proportional to the average potential, or charge, on the chain, but this is not the case. If we let  $\zeta_{\text{ave}}$  denote the average of  $\zeta$  over the surface area of the particle, then the translational mobilities in equations 19 are re-expressed as

$$\mu_{\parallel} = \mu_{\perp} = \frac{D}{4\pi\eta} \left\{ \zeta_{\text{ave}} + \frac{2}{\pi} \int_{-1}^{+1} \left[ \frac{\pi}{4} - (1-s^2)^{1/2} \right] \zeta(s) ds \right\} \quad (22)$$

Thus, for distributions of  $\zeta$  that depend on even powers of  $s$ , the electrophoretic mobility of the chain is not zero even if  $\zeta_{\text{ave}}$  equals zero; that is, neutral chains will move in an electric field if the distribution of the zeta potential is an even function of  $s$ . For the distribution  $\zeta = \zeta_0 + \zeta_1 s + \zeta_2(3s^2-1)$ , where the  $\zeta_i$  are constant, equation 22 yields

$$\mu_{\parallel} = \mu_{\perp} = \frac{D}{4\pi\eta} \left[ \zeta_{\text{ave}} + \frac{1}{4} \zeta_2 \right] \quad (23a)$$

$$\mu_r = \frac{D}{4\pi\eta} \zeta_1 \quad (23b)$$

#### STRAIGHT CIRCULAR CYLINDER ( $\lambda(s) = 1$ )

Using Cox's model (19) we obtain the following Stokeslet distributions:

$$\alpha_{\parallel} = \frac{1 - 2 \ln(2\epsilon \sqrt{1-s^2})}{8 \ln^2 \epsilon} \quad (24a)$$

$$\alpha_{\perp} = - \frac{1 + 2 \ln(2\epsilon \sqrt{1-s^2})}{4 \ln^2 \epsilon} \quad (24b)$$

$$\alpha_r = \frac{-s(1 + 2 \ln(2\epsilon \sqrt{1-s^2}))}{4 \ln^2 \epsilon} \quad (24c)$$

The largest errors in these expressions occur at the ends  $s = \pm 1$ . Because these results have an error of order  $(1/\ln\epsilon)^3$  they are probably only valid for  $\epsilon \leq 0.1$ . Using equations 14-16 we have

$$\mu_{\parallel} = \frac{D}{4\pi\eta} \frac{\langle \zeta(s) [1 - 2 \ln(2\epsilon \sqrt{1-s^2})] \rangle}{3 - 2 \ln(4\epsilon)} \quad (25a)$$

$$\mu_{\perp} = -\frac{D}{4\pi\eta} \frac{\langle \zeta(s) [1 + 2 \ln(2\epsilon \sqrt{1-s^2})] \rangle}{1 - 2 \ln(4\epsilon)} \quad (25b)$$

$$\mu_r = -9 \frac{D}{4\pi\eta} \frac{\langle s \zeta(s) [1 + 2 \ln(2\epsilon \sqrt{1-s^2})] \rangle}{5 - 6 \ln(4\epsilon)} \quad (25c)$$

For a cylinder the area-average zeta potential ( $\zeta_{ave}$ ) equals  $\langle \zeta \rangle$ , so it is apparent from equation 25 that if  $\zeta(s)$  is an even function then the particle will move even if it is neutral. Given the distribution  $\zeta = \zeta_0 + \zeta_1 s + \zeta_2 (3s^2 - 1)$ , where  $\zeta_{ave} = \zeta_0$ , equations 25 give

$$\mu_{\parallel} = \frac{D}{4\pi\eta} \left[ \zeta_0 + \frac{2}{3(3 - 2 \ln(4\epsilon))} \zeta_2 \right] \quad (26a)$$

$$\mu_{\perp} = \frac{D}{4\pi\eta} \left[ \zeta_0 + \frac{2}{3(1 - 2 \ln(4\epsilon))} \zeta_2 \right] \quad (26b)$$

$$\mu_r = \frac{D}{4\pi\eta} \zeta_1 \quad (26c)$$

The parallel and perpendicular mobilities are different; in fact, the mobility perpendicular to the cylinder's axis is slightly *greater* than for parallel to the axis if  $\zeta_2$  and  $\zeta_0$  have the same sign.

#### CHAIN OF EQUAL SIZE SPHERES

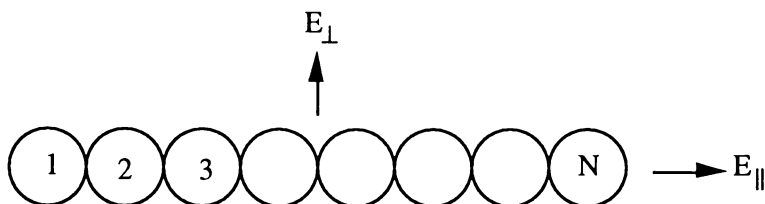
The results for a straight cylinder can be used to estimate the electrophoretic mobility of a straight chain of touching spheres all of which are the same size but could have different zeta potentials. For the highly screened case ( $\kappa a \gg 1$ ) we have the general formula

$$\mu = \frac{D}{4\pi\eta} \sum_{i=1}^N A_i \zeta_i \quad (27)$$

where  $\zeta_i$  is the zeta potential of sphere  $i$  and  $N$  is the number of spheres in the chain. Three possible motions are possible: translation parallel to the chain ( $\mu_{\parallel} = U_{\parallel}/E_{\parallel}$ ), translation perpendicular to the chain ( $\mu_{\perp} = U_{\perp}/E_{\perp}$ ) and rotation about an axis perpendicular to the chain ( $\mu_r = Na\Omega/E_{\perp}$ ). The chain is approximated by a straight cylinder with  $\epsilon = N^{-1}$ ; there are  $N$  equal sections of potential  $\zeta_i$ . The mobilities, and hence  $A_i$ , are calculated from equations 25 with  $\mu = \epsilon\zeta/4\pi\eta$ . Table I gives the formulas for calculating the  $A_i$ , and a plot of  $A_i$  for  $N = 10$  is made in Figure 5. From symmetry considerations we know the following

$$\mu_{\parallel} \text{ and } \mu_{\perp} : \sum_{i=1}^N A_i = 1 ; A_{N+1-i} = A_i \quad (28a)$$

**TABLE I.** Mobility of a chain of  $N$  particles of the same size but different zeta potential. The coefficients  $A_i$  appear in equation 27.  $\epsilon = N^{-1}$  where  $\epsilon$  is the diameter/length of the equivalent cylinder



$$\mu_{\parallel} = U_{\parallel}/E_{\parallel} : \quad A_i = \left\{ 2 \left[ (1-i\epsilon) \ln(1-i\epsilon) - \ln[1-(i-1)\epsilon] \right. \right. \\ \left. \left. - i\epsilon \ln(4i\epsilon) \right] + \epsilon \left[ 6 - 4 \ln(2\epsilon) - 2(1-i) \ln[4\epsilon(i-1)] \right. \right. \\ \left. \left. (1 - (i-1)\epsilon) \right] \right\} [6 - 4 \ln(4\epsilon)]^{-1} \quad (1.1)$$

$$\mu_{\perp} = U_{\perp}/E_{\perp} : \quad A_i = \left\{ 2 \left[ (1-i\epsilon) \ln(1-i\epsilon) - \ln[1-(i-1)\epsilon] \right. \right. \\ \left. \left. - i\epsilon \ln(4i\epsilon) \right] + \epsilon \left[ 6 - 4 \ln(2\epsilon) - 2(1-i) \ln[4\epsilon(i-1)] \right. \right. \\ \left. \left. (1 - (i-1)\epsilon) \right] - 4 \right\} [2 - 4 \ln(4\epsilon)]^{-1} \quad (1.2)$$

$$\mu_r = Na\Omega/E_{\perp} : \quad A_i = \frac{C}{2} \left[ (2\epsilon i - 1)^2 - (2\epsilon(i-1) - 1)^2 \right] \\ + \frac{D}{4} \left\{ -2(\epsilon i - 1)^2 + (2\epsilon(i-1) - 1)^2 + ((2\epsilon i - 1)^2 - 1) \right. \\ \left. \ln[4\epsilon i(1-\epsilon i)] - [(2\epsilon(i-1) - 1)^2 - 1] \ln[4\epsilon(i-1)(1-\epsilon(i-1))] \right\} \\ (1.3)$$

where

$$C = \frac{9}{2} \frac{1 + 2 \ln(2\epsilon)}{-5 + 6 \ln(4\epsilon)}$$

$$D = \frac{9}{2} \frac{1}{-5 + 6 \ln(4\epsilon)}$$

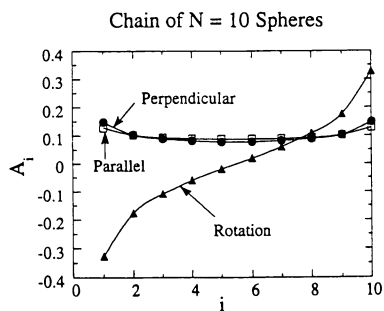


Figure 5. The coefficient  $A_i$  versus  $i$  for a chain of 10 spheres (see equation 27). The symbols have the following meanings:  $\parallel \rightarrow \mu_{\parallel}$ ;  $\perp \rightarrow \mu_{\perp}$ ;  $r \rightarrow \mu_r$ .

$$\mu_r : \sum_{i=1}^N A_i = 0 ; \quad A_{N+1-i} = -A_i \quad (28b)$$

The spheres at either end of the chain have the greatest influence on the electrophoretic mobility. As an example of the importance of the location of the charges, consider a chain of 10 spheres only two of which are charged. In Table II the mobility of the chain is shown as a function of the positioning of the two charged spheres for a) the same  $\zeta$  for both spheres and b) the same  $|\zeta|$  for both spheres but the signs are opposite. Note that in case b) the chain is *neutral*.

For an ensemble of chains with a *random* positioning of the spheres, the average mobilities are given by the following:

$$\langle \mu_{\parallel} \rangle = \langle \mu_{\perp} \rangle = \frac{D}{4\pi\eta} \langle \zeta \rangle \quad (29a)$$

$$\langle \mu_r \rangle = 0 \quad (29b)$$

where  $\langle \zeta \rangle$  is the statistical-mean zeta potential which is the same for all  $i$ . This is the result expected from intuition. In example (a) of Table II,  $\langle \zeta \rangle = 0.2 \zeta_0$ ; in example (b),  $\langle \zeta \rangle = 0$ . If, however, the relative positioning of the different types of spheres is *not random*, then equations 29 are invalid.

#### TORUS ( $\lambda(s) = 1$ )

A torus is a circular cylinder whose contour is a circle. The Stokeslet distribution for the torus was derived by Johnson and Wu (9) to order  $\epsilon^2 \ln \epsilon$ ; these functions of  $s$  are listed in the Table III. The electrophoretic motion is described by defining two mobilities:

$$\mathbf{U} = \mathbf{M}_T \cdot \mathbf{E}_{\infty} ; \quad \mathbf{\Omega} = \mathbf{M}_R \cdot \mathbf{E}_{\infty} \quad (30)$$

We consider the distribution  $\zeta = \zeta_0 + \zeta_1 s + \zeta_2 (3s^2 - 1)$ . The two mobilities defined above can be expressed as

$$\mathbf{M}_T = \zeta_0 \mathbf{I} + \zeta_1 \mathbf{M}_T^{(1)} + \zeta_2 \mathbf{M}_T^{(2)} \quad (31a)$$

$$\mathbf{M}_R = \zeta_1 \mathbf{M}_R^{(1)} + \zeta_2 \mathbf{M}_R^{(2)} \quad (31b)$$




Expressions for the dipole ( $\sim \zeta_1$ ) and quadrupole ( $\sim \zeta_2$ ) mobilities are shown in Table IV.

The area-averaged zeta potential of the torus equals  $\zeta_0$ ; thus, for modest potentials the charge on the torus is proportional to  $\zeta_0$ . Equations 31 clearly show that even if the torus is *neutral* there is rotation and translation proportional to the dipole and quadrupole moments, respectively. As an example consider  $\zeta_0 = \zeta_1 = 0$ . A torus with  $\epsilon = 0.1$  will experience the following velocities for different orientations of the electric field.








**TABLE II.** Mobility of a chain of 10 spheres only two of which are charged. The dimensionless mobility is defined as  $U_{||}/\mu_0 E_{||}$  where  $\mu_0$  ( $=\epsilon\zeta_0/4\pi\eta$ ) is the mobility of sphere  $\bullet$ .  $A_1 = 0.1280$ ,  $A_2 = 0.1016$ ,  $A_3 = 0.0934$ ,  $A_4 = 0.0894$ ,  $A_5 = 0.0876$ .  $A_{11-i} = A_i$

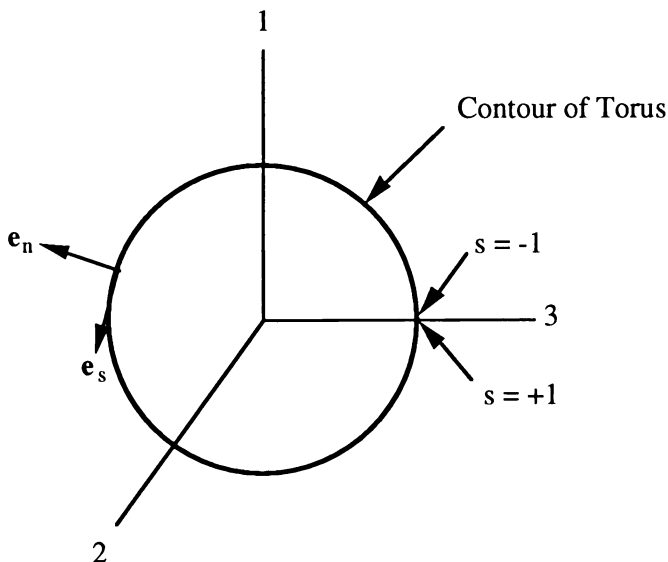
a) The two charged spheres have the same zeta potential

<u>Configuration</u>	<u>Dimensionless Mobility</u>
$\rightarrow E_{  }$ 	0.256
	0.175
	0.216

b) The two spheres have zeta potentials of equal magnitude but opposite sign (i.e., the chain is *neutral*)

<u>Configuration</u>	<u>Dimensionless Mobility</u>
$\rightarrow E_{  }$ 	+0.040
	-0.040
	+0.035
	-0.035
	0.000

**TABLE III.** Torus of contour length  $2L$  and cross-sectional radius  $b_0$ .  $\epsilon = b_0/L$  and  $\gamma = \pi\epsilon$ . The Stokeslet distributions are from reference (9). The orthonormal set  $(\mathbf{e}_n, \mathbf{e}_s, \mathbf{e}_b)$  is defined such that  $\mathbf{e}_s$  is tangent to the contour at each position  $s$ ,  $\mathbf{e}_n$  is in the plane of the ring and  $\mathbf{e}_b$  points in the direction "2"



Translation (subscript denotes direction)

$$\alpha_1 = \frac{-3 + \ln(8/\gamma)}{-2 - 5 \ln(8/\gamma) + 2 \ln^2(8/\gamma)} \sin[\pi(1+s)] \mathbf{e}_n + \frac{-5 + 2 \ln(8/\gamma)}{-8 - 20 \ln(8/\gamma) + 8 \ln^2(8/\gamma)} \cos[\pi(1+s)] \mathbf{e}_s$$

$$\alpha_2 = \frac{1}{1 + 2 \ln(8/\gamma)} \mathbf{e}_b$$

Rotation (subscript denotes rotation axis)

$$\alpha_1 = \frac{1}{3 - 2 \ln(8/\gamma)} \cos[\pi(1+s)] \mathbf{e}_b$$

$$\alpha_2 = \frac{1}{-8 + 4 \ln(8/\gamma)} \mathbf{e}_s$$

**TABLE IV.** Mobility tensors for the torus as defined by equations 31. See Table 3 for the definitions of the Cartesian axes ( $X_1, X_2, X_3$ ).  $\gamma = \pi \epsilon$ . For the tensors  $M(i, j)$ ,  $j$  is the direction of the field and  $i$  is the direction of the velocity

$$M_T^{(1)}(1,3) = M_T^{(1)}(3,1) = \frac{17-6 \ln(8/\gamma)}{2\pi[-7+2 \ln(8/\gamma)]}$$

All other  $M_T^{(1)}(i,j) = 0$

$$M_T^{(2)}(1,1) = -M_T^{(2)}(3,3) = \frac{3[17-6 \ln(8/\gamma)]}{2\pi^2[-7+2 \ln(8/\gamma)]}$$

All other  $M_T^{(2)}(i,j) = 0$

$$M_R^{(1)}(2,3) = -\frac{1}{2} M_R^{(1)}(3,2) = \frac{1}{\pi}$$

All other  $M_R^{(1)}(i,j) = 0$

$$M_R^{(2)}(1,2) = -2M_R^{(2)}(2,1) = -\frac{12}{\pi^2}$$

All other  $M_R^{(2)}(i,j) = 0$

Field oriented toward direction "3":  $U_3/E_\infty = 0.8 D\zeta_2/4\pi\eta$

Field oriented toward direction "1":  $U_1/E_\infty = -0.8 D\zeta_2/4\pi\eta$ ,  
 $\Omega_2 L/E_\infty = 0.61 D\zeta_2/4\pi\eta$

Field oriented toward direction "2":  $\Omega_1 L/E_\infty = -1.22 D\zeta_2/4\pi\eta$

This simple example illustrates the interesting electrophoretic dynamics possible when the charge is nonuniformly distributed on a ring.

### ACKNOWLEDGMENT

Support for this work came from the National Aeronautics and Space Administration (Grant NANAG8-964) and the Westvaco Corporation.

### LITERATURE CITED

1. Hunter, R.J. *Zeta Potential In Colloid Science*; Academic Press: New York, 1981.
2. Derjaguin, B.V.; Dukhin, S.S. Nonequilibrium Double Layer and Electrokinetic Phenomena. In *Surface and Colloid Science*, Matijevic, E., Ed.; John Wiley & Sons: New York, 1974; Vol. 7, Chapter 3.
3. O'Brien, R.W.; White, L.R. *J. Chem. Soc., Faraday Trans. 2*, **1978**, *74*, 1607.
4. O'Brien, R.W. *J. Colloid Interface Sci.* **1983**, *92*, 204.
5. Fair, M.C.; Anderson, J.L. *J. Colloid Interface Sci.* **1989**, *127*, 388.
6. Fair, M.C.; Anderson, J.L. *Int. J. Multiphase Flow* **1990**, *16*, 663.
7. Keh, H.J.; Yang, F.R. *J. Colloid Interface Sci.* **1991**, *145*, 362.
8. Fair, M.C.; Anderson, J.L. *Langmuir*, **1992**, *8*, 2850.
9. Johnson, R.E.; Wu, T.Y. *J. Fluid Mech.* **1979**, *95*, 263.
10. Anderson, J.L. *Annu. Rev. Fluid Mech.* **1989**, *21*, 61.
11. Cabane, B.; Wong K.; Wang, T.K.; Lafuma, F.; Duplessix, R. *Colloid and Polymer Sci.* **1988**, *266*, 101.
12. Stütger, D. *Phys. Chem.* **1978**, *82*, 1417.
13. Stütger, D. *Phys. Chem.* **1978**, *82*, 1424.
14. Bloomfield, V.; Dalton, W.O.; Van Holde, K.E. *Biopolymers*, **1967**, *5*, 135.
15. De La Torre, J.G.; Bloomfield, V. *Biopolymers* **1978**, *17*, 1605.
16. Keh, H.J.; Chen, S.B. *J. Colloid Interface Sci.* **1989**, *130*, 542, 556.
17. Henry, D.C. *Proc. R. Soc. London*, **1932**, *133*, 106.
18. Cole, J.D. *Perturbation Methods in Applied Mathematics*. Waltham, MA: Blaisdel, 1968.
19. Cox, R.G. *J. Fluid Mech.* **1970**, *44*, 791.
20. Solomentsev, Y.; Anderson, J.L. "Electrophoresis of Slender Bodies," submitted for publication, **1993**.

RECEIVED September 1, 1993

## Chapter 7

# Undulation-Enhanced Forces in Hexagonal Gels of Semiflexible Polyelectrolytes

Theo Odijk

Faculty of Chemical Engineering and Materials Science, Delft University of Technology, P.O. Box 5045, 2600 GA Delft, Netherlands

A theoretical analysis is given of undulation-enhanced forces in solutions of semiflexible polyelectrolytes. Undulation enhancement is fairly weak when the system is isotropic, nematic or cholesteric. Electrostatic repulsion can easily be enhanced by an order of magnitude in hexagonal gels. Van der Waals forces are perturbed mildly by configurational fluctuations although their enhancement does affect the free energy function near the secondary minimum. A stability analysis of enhanced electrostatic versus Van der Waals forces is presented in order to discuss experiments on gels of tobacco mosaic virus.

Semiflexible polyelectrolytes are here defined as having a persistence segment of large aspect ratio i.e. the persistence length  $L_p$  is much greater than the effective diameter. At high ionic strength, the latter reduces to a geometric diameter  $D$ ; at low salt, it is approximately proportional to the Debye screening length  $\kappa^{-1}$ . Several important biopolymers are semiflexible polyelectrolytes exhibiting intriguing phase behavior. For instance, aqueous DNA forms a variety of lyotropic liquid crystals. Upon increasing the concentration, the following sequence of phases is seen ( $I$ ): isotropic to cholesteric to two dimensional columnar hexagonal to three dimensional columnar hexagonal and finally to orthorhombic crystalline. There is a possibly optimistic tendency to believe that these phases ought to be understood in fairly simple statistical physical terms. It may be argued that the chemical detail of the polyion backbone is not critically important for long-range electrostatics swamps any other interactions, except possibly those of dispersion type. Furthermore, our qualitative insight in the condensed matter physics of complex systems is increasing each decade, slowly yet steadily.

The purpose of this paper is to show that the electrostatic interaction may be greatly enhanced by undulations or chain fluctuations in the hexagonal phase of positionally ordered polyions. In nonadhesive states, Van der Waals forces are influenced to a much lesser degree at least within the Gaussian approximation adopted here. Nonetheless, undulation enhancement of dispersion forces cannot be neglected when trying to locate the secondary minimum for a gel stabilized by these interactions. Undulation enhancement is of minor import in solutions where positional order is weak or absent as I now show.

0097-6156/94/0548-0086\$06.00/0

© 1994 American Chemical Society

### Isotropic, Nematic and Cholesteric Phases

Undulation enhancement of the electric potential exerted by a polyion was first considered by Odijk and Mandel (2) who developed a perturbation scheme in terms of the large parameter  $L_p\kappa$ . A similar procedure can be used to evaluate the average interaction between two nearby undulating polyions. However, I here present only a qualitative analysis for wormlike polyelectrolytes of zero diameter, for simplicity. The case  $D > 0$  leads to similar conclusions.

A contour point of a wormlike polyion is chosen to be the origin  $O$  of our Cartesian coordinate system. The contour distance from  $O$  is specified by  $s_1$ . The vector tangential to the chain at  $O$  is constrained to point in the  $z$  direction (see Figure 1). The first chain interacts with a second, one contour point of which is fixed at  $(R, 0, 0)$  with the associated tangent vector pointing along the  $Z_2$  axis. The contour distance  $s_2$  is defined with respect to this contour point. The  $Z_2$  axis is skewed at an angle  $\gamma$  with respect to the  $Z_1$  axis. I wish to investigate the average interaction between two nearby sections of the two chains ( $-\ell \leq s_1 \leq \ell$ ,  $-\ell \leq s_2 \leq \ell$ ;  $\ell$  is specified below). They are statistically close to the rod limit, so that they are uniquely specified by the vectors  $\epsilon_1(s_1)$  and  $\epsilon_2(s_2)$  perpendicular to the  $Z_1$  and  $Z_2$  axes respectively. Of course, two long chains may have many domains of nearby interaction like the one shown in Figure 1, but in each case a similar analysis holds.

For the moment it suffices to use the Debye-Hückel approximation. In the continuum limit the average interaction between the two sections can be written as

$$V_{12}/kT = \lambda_b b^{-2} \ll \int_{-1}^1 ds_1 \int_{-1}^1 ds_2 \frac{e^{-\kappa r_{12}}}{r_{12}} \gg \quad (1)$$

where  $\langle \langle \rangle \rangle$  denotes the average over the undulations of both sections,  $b$  is the linear charge spacing,  $\lambda_b$  the Bjerrum length,  $T$  the temperature,  $k$  Boltzmann's constant and  $r_{12}$  the distance between points  $s_1$  and  $s_2$ . To a first approximation, the two sections fluctuate independently, so we have (2)

$$\langle \epsilon_i^2 \rangle = O\left(\frac{s_i^3}{L_p}\right) \quad i = 1, 2 \quad (2)$$

This can be understood in simple terms: the angular fluctuation of a worm near the rod limit obeys the central limit theorem  $\langle \theta_i^2 \rangle \simeq s_i/L_p$  and furthermore  $\langle \epsilon_i^2 \rangle \simeq s_i^2 \langle \theta_i^2 \rangle$  by a geometrical argument. Pythagoras' theorem yields

$$r_{12}^2 = r_{12,0}^2 + O(\epsilon_1^2) + O(\epsilon_2^2) \quad (3)$$

$$r_{12,0}^2 = R^2 + (Z_1(s_1) - Z_2(s_2)\cos\gamma)^2 + Z_2^2(s_2)\sin^2\gamma \quad (4)$$

where  $r_{12,0}$  refers to the interaction between charges projected on the respective  $Z_1$  and  $Z_2$  axes, the reference configuration if the polyions were infinitely stiff. We next gauge the impact of the undulatory  $O(\epsilon_i^2)$  terms in equation 3.

Relevant configurations for a system without positional order are those for which  $V_{12} = O(kT)$  since the Boltzmann factor associated with equation 1 approaches zero rapidly for  $V_{12} > > kT$ . Owing to the screening factor, we have

$R = O(\kappa^{-1})$  to within logarithmic order. Furthermore, the leading contribution to equation 1 stems from the region  $s_1 = O(s_2)$ . Since the segments are close to the rod limit, we have to account mainly for separations of the following type in an explicit evaluation of equation 1.

$$r_{12}^2 = O(\kappa^{-2}) + O(s_1^2 \sin^2 \gamma) + O\left(\frac{s_1^3}{L_p}\right) \quad (5)$$

There are then two extreme cases:

i)  $s_1 = O(\kappa^{-1})$ ; the relevant contribution from the undulation is  $O(1/L_p \kappa)$ .  
 ii)  $s_1 = O(\ell)$ ; the relative undulatory contribution  $= O(\ell L_p^{-1} \sin^2 \gamma)$  and depends on  $\ell$ . In the isotropic phase, we have  $\sin \gamma = O(1)$  and the persistence length  $L_p$  is the relevant scale i.e.  $\ell = O(L_p)$ . In the nematic, the deflection length  $\lambda = L_p \gamma^2$  is the important characteristic scale (3), i.e.  $\ell = O(\lambda)$ . Therefore, in both cases the relative magnitude of the last two terms in equation 5 is at most of order unity. I conclude that undulations merely perturb the interaction between two polyions at close separations for solutions without long range positional order. Although a cholesteric solution is positionally ordered, the director undergoes only a gradual twist for the pitch is predicted to be a large mesoscopic scale (4). Hence, cholesteric organization should have virtually no influence on the local interaction displayed in Figure 1.

Current polyelectrolyte theories of the nematic phase (3,5,6) disregard local undulations which appears to be a reasonable zero-order approximation in view of the above arguments. They agree quite well with experiments on DNA and Xanthan (7-9).

### Hexagonal phase

The hexagonal phase has long-range positional order defined by the spacing  $R$  of the reference configuration, the hexagonal array of perfectly rigid rods (Figure 2). The spacing is fixed by some external constraint (volume of the sample, imposed osmotic stress, Van der Waals forces, etc.), and is often substantially greater than the Debye radius  $\kappa^{-1}$ . In addition, the undulation amplitude  $d$  of the wormlike polyions may also be larger than  $\kappa^{-1}$ , thus modulating the electrostatic screening considerably. On average, the result is an undulation-enhanced interaction. In the previous section, the distance  $R = O(\kappa^{-1})$  was determined by a balance of electrostatic forces and thermal motion so an entirely different scenario prevails. A summary of the simple theory developed in reference 10 is given here, with greater emphasis on its limitations.

In Figure 2 thermal excitations cause the polyions to fluctuate away from the reference configuration which is obviously opposed by their repulsive interaction. An effective way to approach this problem is to posit a spatial distribution function  $G$  depending on some variational parameter (the amplitude  $d$  in this case), calculate the total Helmholtz free energy  $A_{\text{tot}}$  self-consistently, and minimize  $A_{\text{tot}}$  with respect to  $d$  keeping the spacing  $R$  constrained. We bear in mind that the system is translationally invariant along the long hexagonal axis, the distribution and its derivative are continuous, and  $G$  must be sharply peaked at the lattice points otherwise the notion of a hexagonal phase would not be meaningful. In the limit  $d \ll R$  we may suppose the Gaussian distribution (10)

$$G \sim (\pi d^2)^{-1} e^{-r^2/d^2} \quad (6)$$

to be correct to the leading order, at least for screened or "soft" confinement. In effect,  $G$  may be regarded as a Boltzmann factor  $\exp(-V_{\text{eff}}/\kappa T)$  where the

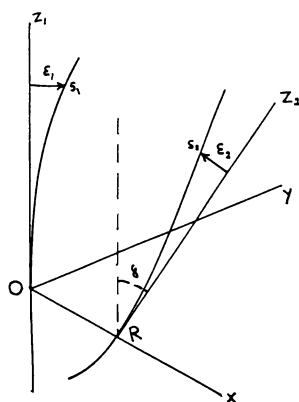


Figure 1. Two nearby sections of two interacting polyions.

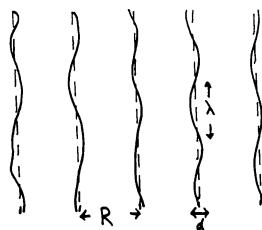


Figure 2. Two dimensional representation of a hexagonal lattice of wormlike polyions.



effective self-consistent potential  $V_{\text{eff}}$  exerted on an infinitesimal segment of a test polyion is expanded to second order in  $r$ , the distance from the segment to its respective position in the reference configuration.

Equation 6 asserts that a test polyion is trapped in a fuzzy cylindrical tube. The configurational or undulatory free energy  $F_{\text{conf}}$  is calculated approximately via a second moment condition implied by equation 6

$$\langle r^2 \rangle = d^2 \quad (7)$$

Helfrich and Harbich (11) presented a fluctuation theory for a worm restricted in such a fashion only

$$A_{\text{conf}} = 2^{-2/3} kT \lambda^{-1} \quad (8)$$

In essence, this agrees with a scaling analysis (12) proposed earlier in terms of the deflection length  $\lambda \equiv d^{3/2} L_p^{1/2}$  (In order to avoid confusion, it is well to stress that equation 8 applies to soft confinement as expressed by equation 6. In ref. (12) I considered the statistics of a worm trapped in a hard cylindrical pore. In ref. (11)  $A_{\text{conf}}$  is derived within a second moment restriction and then rescaled geometrically to account for confinement within a hard tube. The predictions of refs. (11) and (12) have been borne out by extensive Monte Carlo simulations (32). A scaling law analogous to equation 8 is verified but of course the numerical coefficient depends on the type of confinement. Note that there is an important difference between soft and hard confinement: in the latter case there is a depletion entropy because the chain cannot cross the cylindrical boundary).

A test polyion can be viewed as an sequence of deflection segments. Each behaves more or less like a cylindrical rod exerting an electrostatic potential  $\phi(s)$  at  $s$ , the vector distance from the rod axis. In the outer double layer, Debye-Hückel superposition holds so we have a renormalized potential  $\phi_R$  which is the bare  $\phi$  smeared out by the distribution given by equation 6

$$\phi_R(\mathbf{t}) = \langle \phi \rangle = \int d\mathbf{r} G(\mathbf{r}) \phi(\mathbf{t}-\mathbf{r}) \quad (9)$$

The vector  $\mathbf{t}$  is defined with respect to the reference axis. Next, the test polyion interacts with six neighbors i.e. there are three pair interactions per test chain. Since the neighboring chains are smeared charge distributions themselves, the electrostatic free energy of interaction per unit length of polyion becomes

$$A_{\text{el}}/kT = 3 \nu_{\text{eff}} \int dt G(\mathbf{t}) \phi_R(\mathbf{R}-\mathbf{t}) \quad (10)$$

At large distances the polyion may be regarded as a line charge of spacing  $1/\nu_{\text{eff}}$  (10). An asymptotic evaluation of equations 9 and 10 is fairly straightforward (10)

$$A_{\text{el}}/kT = \frac{3(2\pi)^{1/2} \xi_{\text{eff}}^2 \exp(-\kappa R + 1/2 \kappa^2 d^2)}{Q(\kappa R)^{1/2} (1 + 1/2 \kappa d^2 R^{-1})} \quad (11)$$

with  $\xi_{\text{eff}} \equiv \lambda_B \nu_{\text{eff}}$ . The effect of undulations is marked when the undulatory amplitude  $d$  is of the order of the Debye radius.

Minimization of the total free energy  $A_{\text{tot}} = A_{\text{conf}} + A_{\text{el}}$  yields a nonlinear expression for  $d$

$$\frac{d^{8/3} e^{1/2} \kappa^2 d^2}{1 + 1/2 \kappa d^2 R^{-1}} = \frac{2^{1/3} \lambda_B R^{1/2} e^{\kappa R}}{9(2\pi)^{1/2} \xi_{\text{eff}}^2 L_p^{1/3} \kappa^{3/2}} \quad (12)$$

and an osmotic pressure (10)

$$\pi_{\text{os}} = \frac{2^{1/3} kT}{3^{3/2} \kappa R d^{8/3} L_p^{1/3}} \quad (13)$$

At this stage it is important to list the considerable number of physical approximations implicit in the derivation of equations 12 and 13.

- a)  $R\kappa \gg \gg d$ . An excess of salt is present.
- b)  $L_p \gg \gg d$ . This ensures that the hexagonal lattice exists. There is virtually no folding of the chains. Furthermore, a deflection segment of length  $\lambda = L_p^{1/3} d^{2/3} \gg d$  has a large aspect ratio so that the orientational fluctuations of order  $d/\lambda$  are small.
- c)  $\kappa d^3 R^{-2} \ll 1$ . This ensures that the asymptotic analysis of equations 9 and 10 is viable.
- d) i)  $d \ll R$ ; ii)  $1/2 \kappa^2 d^2 + 3\kappa d + \kappa D \leq \kappa R$  ( $D =$  bare diameter of the polyion). The first inequality may seem adequate enough to guarantee the validity of the Gaussian ansatz. Yet, the tail of the Gaussian is weighted heavily in the average interaction. If we take due care of a cut-off at  $R$ , we derive the second more restrictive condition. Then, a self-consistent theory neglecting certain correlations is reasonable. In a similar vein, the neglect of hexagonal symmetry in the isotropic distribution  $G$  is justified.
- e)  $\kappa \lambda \gg 1$ . The deflection segment has the electric properties of a charged rigid rod.
- f)  $(D^{1/2} + \kappa^{-1/2})/\kappa^{1/2} \lambda > d/\lambda$ . Electrostatic twist is negligible (3). The polyions are basically parallel. Orientation-translation coupling can be disregarded. Still, though very weak, undulations play an important role.
- g)  $R \geq D + 2d + 2\kappa^{-1}$ . Counterion fluctuations do not couple to undulations.
- h)  $\lambda F_{\text{el}}/kT \leq 1$  for  $\kappa d \geq 1$ . The electrostatic interaction of an independently fluctuating deflection segment is small enough to circumvent a virial expansion (13).

Equations 12 and 13 have the following features.

- 1) For  $\kappa d \ll 1$ , the osmotic pressure tends to a previous result (14) for an hexagonal array of rigid cylindrical polyions i.e. our reference configuration

$$\pi_{\text{os},0} = \left( \frac{(6\pi)^{1/2} \xi_{\text{eff}}^2 \kappa^{1/2}}{\lambda_B} \right) \frac{e^{-\kappa R}}{R^{3/2}} \quad (14)$$

- 2) For  $\kappa d \ll 1$ , the first-order correction to equation 14 reads

$$\pi_{\text{os}} = \pi_{\text{os},0} + \pi_{\text{os},1} \quad (15)$$

where  $\pi_{\text{os},1} \ll \pi_{\text{os},0}$  and  $\pi_{\text{os},1} \sim \exp(-\kappa R/4)$ . This gradual decay agrees with a qualitative sketch given by Selinger and Bruinsma (13), provided we neglect their nematic interaction in accordance with condition f. An enhanced decay length was first proposed by Podgornik and Parsegian (15) but for a Gaussian random coil enclosed in a tube. This calculation is valid when the step length is smaller than the tube diameter which is the reverse of the case focused on here

( $L_p \gg R$ ). Note that an enhanced decay length shows up within a perturbation that is weak.

3) The case of experimental interest is  $\kappa d = O(1)$  for which no simple power or decay law can be derived. Recall that in view of restrictions c and d, we cannot take the limit of dominating exponentials in equation 12 which would lead to  $d^2 \approx 2R/\kappa$ .

4) Similarly, we cannot address the approach to the uncharged hexagonal phase which is strongly fluctuating. In that case,  $d = O(R-D)$  and  $\pi_{os} \approx kT L_p^{-1/3} (R-D)^{-8/3}$  as discussed at length by Selinger and Bruinsma (13).

5) The list of restrictions (a-h) looks awesome. Still, as a rule, the hexagonal gels formed in osmotic stress experiments (DNA (16), tobacco mosaic virus (TMV, 14, 17), muscle filament (14,18) satisfy these requirements for the polyions are relatively thick, stiff and highly charged. For a detailed comparison of theory with experiment, the reader should consult ref. (10). A Lindemann melting rule has also been formulated with the help of equation (12) (T. Odijk, *Europhysics Lett.*, in press). It appears to explain the stability of the hexagonal phase of DNA (16).

### Van der Waals forces

Stability theories of the DLVO type have been developed for hexagonal lattices of rigid polyelectrolytes by various authors (19-21). The work of Parsegian and Brenner (21) inspired Millmann et al (17) to reinvestigate the classic experiments of Bernal and Fankuchen (22) on gels of TMV. How do undulations influence the interpretation of these measurements? To begin with, we must keep in mind that requirements a-h of the previous section are rather restrictive when attractive forces are taken into consideration. In particular, I disregard entirely configurations like those shown in Figure 3 in which chains adhere. If adhesion does occur, the Gaussian distribution evidently becomes a poor approximation. Given these limitations, the first problem to be faced is the possible effect of undulations on the Van der Waals interaction itself.

The bare Van der Waals interaction per unit length between two parallel rigid cylinders is known in terms of a hypergeometric function (23) but physical insight is afforded by studying the expansions at small and large separations (24,25). For an hexagonal lattice we have

$$A_w/kT = -\frac{HD^{1/2}}{8.2^{1/2}(R-D)^{3/2}} \left[ 1 - \frac{2(R-D)}{D} + \dots \right] \quad R-D \ll D \quad (16)$$

$$A_w/kT = -\frac{9\pi H}{128D} \left( \frac{D}{R} \right)^5 \left[ 1 + \frac{25 D^2}{16 R^2} + \frac{31.9 D^4}{16 R^4} + \frac{150.7 D^6}{64 R^6} + \dots \right] \quad (17)$$

$$R \geq 3/2D$$

where H is the Hamaker constant scaled by kT. I now approximate the undulatory average of the lead term of equation 16 by noting that those fluctuations can be neglected in a zero-order analysis, that are transverse to the vector connecting the two axes of the deflection segments in the reference configurations. It is convenient to introduce the relative change J in  $A_w$

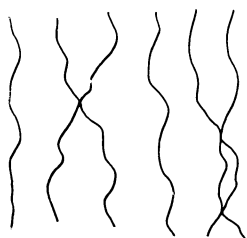


Figure 3. Forbidden adhesive states.

$$J \equiv E^{3/2} \ll (E + X_1 + X_2)^{-3/2} \gg$$

$$\approx \pi^{-1} d^{-2} E^{3/2} \int_{-C}^C \int dX_1 dX_2 e^{-(X_1^2 + X_2^2)/d^2} (E + X_1 + X_2)^{-3/2} \quad (18)$$

with  $E \equiv R - D$ , and  $X_1$  and  $X_2$  the longitudinal positions of the two segments. Here and below,  $C$  denotes a formal cut-off which temporarily avoids a divergence at contact. It is assumed that the chains never enter their primary minimum so the real distribution is zero at zero separation. On introducing polar coordinates  $X_1 = r \cos \phi$ ,  $X_2 = r \sin \phi$ ,  $W \equiv r^2$ , and the Legendre function  $P_{1/2}(z)$ , we obtain (31)

$$J = d^{-2} \int_0^C dW e^{-W/d^2} P_{1/2} \left[ \left[ \frac{E^2}{E^2 - 2W} \right]^{1/2} \right] \left( 1 - \frac{2W}{E^2} \right)^{-3/4} \quad (19)$$

For  $z \geq 1$ , the Legendre function is approximated quite well by  $z^{1/2}$ .

$$J \approx d^{-2} \int_0^C dW e^{-W/d^2} \left( 1 - \frac{2W}{E^2} \right)^{-1} \quad (20)$$

$$\approx -\frac{1}{4} E^2 d^{-2} \log \left( 1 - \frac{4d^2}{E^2} \right) \quad (2d < E) \quad (21)$$

The second form is chosen because it has the correct Taylor expansion for small  $d/E$  and a logarithmic divergence is expected at close packing when  $d = O(E)$  and the Gaussian approximation ultimately breaks down. For  $d < 6E = 6(R - D)$ ,  $J$  deviates from unity by six percent at most. Similar considerations apply to equation 17, an undulatory correction being negligible since  $d^2 \ll R^2$ .

In the application to TMV gels, the analysis proceeds by investigating the total free energy  $A_{\text{tot}}(d, R) = A_{\text{conf}} + A_{\text{el}} + JA_w$  numerically as a function of  $R$ . The variational amplitude  $d$  is determined by minimizing  $A_{\text{tot}}$  for each spacing  $R$ . There are two solutions, the one for higher  $d$  being unstable. For  $R \geq (3/2) D$ , the factor  $J$  is set equal to unity. Since the function  $A_{\text{tot}}(R)$  is very sensitive to the values of  $H$  and  $L_p$  which are not known precisely, the scaled Hamaker constant  $H$  is adjusted so as to let the spacing  $R$  corresponding to the *secondary* minimum, conform to the experimental spacing  $R_{\text{exp}}$ . The latter were measured for hexagonal TMV gels as a function of the electrolyte concentration by Millman et al (17) after long equilibration under zero external stress. Representative values of the microscopic parameters are (17): TMV diameter  $D = 18$  nm, length  $L = 300$  nm, real charge density  $b^1 = 14$  nm<sup>-1</sup>, Bjerrum length  $\lambda_B = 0.71$  nm. The scaled Hamaker constant  $H$  is estimated to range from about unity to two for proteins at room temperature (21,25). The quantity  $\xi_{\text{eff}}$  is calculated using the Philip-Wooding solution (26) to the Poisson-Boltzmann

equation. In electron micrographs, fluctuations of TMV from the straight rod configuration typically amount to 5 nm so the persistence length  $L_p$  should be of order  $10^4$  nm from equation 2.

A comparison with experiments (17) is given for three ionic strengths.

i)  $C=0.87$  M. The spacing  $R_{exp}$  is about 20 nm or a bit higher (17). The existence of a feasible secondary minimum for the free energy  $F_p \equiv LF_{tot}/kT$  of a TMV polyion is established for a plausible range of values of  $L_p$ . Several combinations of parameters at the minimum are compiled in Table I. Only a very narrow range of  $H$  is allowed for each value of  $L_p$ , both here and below.

Table I. Combinations of Parameters at the Minimum  $F_p$  at  $C = 0.87$  M

$L_p(\text{nm})$	$3.10^4$		$10^4$		$3.10^3$
H	0.6	0.5	0.7	0.6	0.8
R(nm)	19.8	20	19.6	19.9	19.6
$F_p$	-1.3	-1.44	-4.91	-0.59	-2.4
$\kappa d$	1.42	1.26	1.20	1.45	1.34

From a theoretical point of view undulations cannot be dismissed for stable gels of TMV ( $\kappa d = O(1)$ ). The influence of undulations on the Van der Waals interaction is significant ( $J=1.1-1.2$ ) because confinement entropy, and electrostatic and dispersion forces, are delicately balanced at the secondary minimum. The  $H$  values are compatible with independent estimates (21,25).

ii)  $C=0.096$  M. The spacing  $R_{exp}$  is about 28 nm with a fairly large variance. Stability analysis results in Table II.

Table II. Combinations of Parameters at Spacing  $R_{exp}$  of 28 nm and  $C = 0.096$  M

$L_p(\text{nm})$	$3.10^4$	$10^4$	$3.10^3$
H	6	7	10
R(nm)	26	25.5	25
$F_p$	-1.43	-0.70	-2.23
$\kappa d$	1.29	1.24	1.22

The values of  $H$  are an order of magnitude greater than those in case (i) and too large to be realistic. If the present Gaussian approximation is taken seriously, an additional attractive force needs to be postulated.

iii)  $C=0.01$  M;  $R_{exp} \approx 35$  nm. The scaled Hamaker constant  $H$  needs to be of order  $10^2$ , independent of  $L_p$ . The existence of another attractive interaction is unambiguous. I remark that the existence of adhesive states (Figure 3) is extremely unlikely in view of the relatively small undulations ( $d/R=0.05$  although  $\kappa d = O(1)$ ).

I conclude that undulation theory explains the stability of TMV gels solely at high ionic strength. At low ionic strength, we can state that adhesive states should not occur because the undulations would have to surmount a huge electrostatic barrier. It is now thought that hydration forces may be attractive under the right conditions (27,28). In fact, if TMV were to have a long range hydrophobic attraction, decaying exponentially and similar to the one displayed in Figure 3 of ref. (28), it would overwhelm the usual Van der Waals force at low ionic strength, but not at 1 M. For the moment, this is mere speculation. Doubtless, further investigation is needed on the following topics: a) a rigorous self-consistent theory incorporating dispersion forces, possibly of the Lifshitz type; b) in several of the calculations for TMV,  $A_{tot}$  becomes *positive* beyond the

secondary minimum because undulation enhancement is powerful; this raises the possibility of a tertiary minimum in the strongly fluctuating limit ( $d = O(R^{1/2}\kappa^{-1/2})$  to  $O(R)$ ); for the theory of uncharged adhering polymers, see refs. (11), (29) and (30)); c) the quantitative analysis of newly postulated forces; d) dynamic stability.

### Literature Cited

1. Durand, D.; Doucet, J.; Livolant, F. *J. Phys. II France* 1992, 2, 1769.
2. Odijk, T.; Mandel, M. *Physica* 1978, 93A, 298.
3. Odijk, T. *Macromolecules* 1986, 19, 2313.
4. Odijk, T. *J. Phys. Chem.* 1987, 91, 6060.
5. Vroege, G.J. *J. Chem. Phys.* 1989, 90, 4560.
6. Khokhlov, A.R. in "Liquid Crystallinity in Polymers", ed. A. Ciferri, VCH, New York, 1991.
7. Strzelecka, T.; Rill, R.L. *Macromolecules* 1991, 24, 5124.
8. Inatomi, S.; Jinbo, Y.; Sato, T.; Teramoto, A. *Macromolecules* 1992, 25, 5013.
9. Vroege, G.J.; Lekkerkerker, H.N.W. *Rep. Prog. Phys.* 1992, 55, 1241.
10. Odijk, T. *Biophys. Chem.* 1993, 46, 69.
11. Helfrich, W.; Harbich, W. *Chemica Scripta* 1985, 25, 32.
12. Odijk, T. *Macromolecules* 1983, 16, 1340.
13. Selinger, J.V.; Bruinsma, R.F. *Phys. Rev. A* 1991, 43, 2910, 2922.
14. Millman, B.M.; Nickel, B.G. *Biophys. J.* 1980, 32, 49.
15. Podgornik, R.; Parsegian, V.A. *Macromolecules* 1990, 23, 2265.
16. Podgornik, R.; Rau, D.C.; Parsegian, V.A. *Macromolecules* 1989, 22, 1780.
17. Millman, B.M.; Irving, T.C.; Nickel, B.G.; Loosley-Millman, M.E. *Biophys. J.* 1984, 45, 551.
18. Millman, B.M.; Wakabayashi, K.; Racey, T.J. *Biophys. J.* 1983, 41, 259.
19. Elliott, G.F. *J. Theor. Biol.* 1968, 21, 71.
20. Brenner, S.L.; McQuarrie, D.A. *Biophys. J.* 1973, 13, 301.
21. Parsegian, V.A.; Brenner, S.L. *Nature* 1976, 259, 632.
22. Bernal, J.D.; Fankuchen, I. *J. Gen. Physiol.* 1941, 25, 111.
23. Bouwkamp, C.J. *Kon. Ned. Akad. Wetenschap* 1947, 50, 1071.
24. Sparnaay, M.J. *Rec. Trav. Chim. Pays-Bas* 1959, 78, 680.
25. Mahanty, J.; Ninham, B.W. "Dispersion Forces", Academic, New York, 1976.
26. Philip, J.R.; Wooding, R.A. *J. Chem. Phys.* 1970, 52, 953.
27. Rau, D.C.; Parsegian, V.A. *Biophys. J.* 1992, 61, 24.6
28. Christenson, H.K.; Claesson, P.M.; Parker, J.L. *J. Phys. Chem.* 1992, 96, 6725.
29. Maggs, A.C.; Huse, D.A.; Leibler, S. *Europhys. Lett.* 1989, 8, 615.

30. Lipowsky, R. *Phys. Scripta* 1989, T29, 259.
31. Gradshteyn, I.S.; Ryzhik, I.M. *"Table of Integrals, Series and Products"*, Academic, London, 1980.
32. Dijkstra, M.; Frenkel, D; Lekkerkerker, H.N.W. *Physica A* 1993, 193, 374.

RECEIVED August 6, 1993



## Chapter 8

# Quasi-elastic Light Scattering by Polyelectrolytes in Buffers of Low Ionic Strength

Narinder Singh<sup>1</sup>, Kenneth S. Schmitz, and Yueying Y. Gao<sup>2</sup>

Department of Chemistry, University of Missouri—Kansas City,  
Kansas City, MO 64110

The  $q$ -dependent apparent diffusion coefficient,  $D_{app}(q)$ , for translational diffusion of hard spheres in the *weak interaction limit* is discussed in detail. In this theory the small ion-polyion coupled mode equation is solved exactly for added electrolyte and salt-free solutions of a monodispersed solution of charged spheres. Electrolyte dissipation and hydrodynamic interactions are included in an *ad hoc* manner. The model is applied to the systems of bovine serum albumin (BSA) obtained in our laboratory and polystyrene latex spheres (PLS) reported in the literature. It is concluded that the  $q = 0$  theories are valid for the BSA data but not for the PLS data.

Interparticle interactions greatly influence the dynamics of macromolecules in solution and colloidal suspensions. Perturbation methods can provide information regarding the nature of these interactions, but only in their relaxation from a sometimes highly disruptive state to the so-called equilibrium state of the system. It is well-known that the viscosity of charged macroions is shear-rate dependent. Giordano *et al.* (1), for example, reported that the viscosity of bovine serum albumin (BSA) determined with a low shear rotating cylinder viscometer was about 10 times larger than those obtained from the capillary flow method. The more subtle weak interparticle interactions may, therefore, go entirely undetected unless one can somehow examine these systems with a sensitive, non perturbation method. Quasi-elastic light scattering (QELS) is such a non perturbative method for studying the solution dynamics of macromolecules. In the QELS technique, temporal fluctuations in the scattered light intensity are monitored, from which molecular information is deduced from the autocorrelation function of the scattered light intensity.

The focus of this communication is on the "ordinary" polyion behavior that results from the weak electrostatic coupling between the various charged species present in the solution. Attention is given to the  $q$ -dependence of the apparent diffusion coefficient,  $D_{app}(q)$ , for the small ion-polyion coupled mode (CM) system.

<sup>1</sup>Current address: Department of Biochemistry, University of Kansas Medical Center at the VA Medical Center, 4801 Linwood Boulevard, Kansas City, MO 64128

<sup>2</sup>Current address: Department of Chemistry, Peking University, Beijing 100871, People's Republic of China

**Generalized Diffusion Equation for Interacting Hard Sphere Systems**

Consider an electrically neutral volume element in the solution located at  $\mathbf{r}$  with a uniform particle concentration for the  $j$ th component represented as  $\langle n_j \rangle_u$  (particles/mL). The combined Fick's first and second laws of diffusion for the temporal evolution of a *concentration fluctuation* for the  $j$ th component from the *uniform distribution*  $\langle n_j \rangle_u$ , i. e.,  $\Delta n_j(\mathbf{r}, t) = n_j(\mathbf{r}, t) - \langle n_j \rangle_u$ , is given by,

$$\left\langle \frac{\partial \Delta n_j(\mathbf{r}, t)}{\partial t} \right\rangle = -\nabla \cdot \langle \mathbf{j}_j \rangle = \nabla \cdot \left\langle \underline{\mathbf{D}}_j \cdot \left[ \nabla \Delta n_j(\mathbf{r}, t) + \beta \nabla \phi(\mathbf{r}, t) \right] \right\rangle \quad (1)$$

where  $\langle \mathbf{j}_j \rangle$  is the average particle flux of the  $j$ th component,  $\underline{\mathbf{D}}_j$  is the diffusion tensor that couples the  $j$ th component with the other particles in the complex fluid through *kinetics related* interparticle interactions (viz., dissipation forces),  $\beta = 1/k_B T$  where  $k_B$  is Boltzmann's constant and  $T$  is the absolute temperature, and  $\phi(\mathbf{r}, t)$  is the *direct interaction potential*. Before proceeding to the generalized expression for small ion-polyion coupled modes, it is necessary to review the approximations usually employed to simplify equation 1 that provides tractable expressions for interpreting experimental data.

The solution to equation 1 is generally converted to an expression for the average quantities, with the approximation,

$$\nabla \cdot \left\langle \underline{\mathbf{D}}_j \cdot \nabla \right\rangle = \left\langle \underline{\mathbf{D}}_j \right\rangle \nabla^2 \quad (2)$$

Substitution of equation 2 into equation 1 may limit the range of concentrations to which the expression can be applied. For example, the hydrodynamic interaction between two spheres of radius  $R_S$  separated by a distance  $r_{ij}$  is expressed in terms of power laws in the relative parameter  $R_S/r_{ij}$ , viz.  $(R_S/r_{ij})^n$ . Carter and Phillies (2) have shown that using the right hand side of equation 2 is restricted to  $n < 7$  since the divergence of higher powers is not zero.

The average of the second term in equation 1 is expressed as,

$$\beta \nabla \cdot \left\langle \underline{\mathbf{D}}_j \cdot \nabla \phi(\mathbf{r}, t) \right\rangle = \nabla \cdot \left\langle \frac{\nabla \phi(\mathbf{r}, t)}{f_m} \right\rangle \equiv \left\langle \frac{1}{f_m} \right\rangle \nabla \cdot \langle \nabla \phi(\mathbf{r}, t) \rangle \quad (3)$$

where the inverse friction tensor for the  $j$ th particle is represented by the mutual friction factor  $f_m$ . Anderson and Reed (3) examined the consequences of the right-most approximation in equation 3 for a one-dimensional system. Using only the hard sphere and long range hydrodynamic interaction potentials, they reported that, as the two spheres approached each other, the right-most average defined in equation 3 led to an increased viscous force such as to prevent the spheres from touching. Hence in their analysis there is no direct hard sphere repulsion interaction term in the evaluation of the second virial coefficient.

**Generalized Diffusion Equation for Small Ion-Polyion Coupled Modes: Weak Electrostatic Interaction Limit**

Lin, Lee, and Schurr (4) considered  $j$ th component of charge  $Z_{je}$  ( $Z_j$  includes both magnitude and sign, and  $e$  is the magnitude of the electron charge) diffusing under the influence of an electrical potential  $\phi_{elec}(\mathbf{r}, t)$  in accordance with the equation,

$$\frac{\partial \Delta n_j(\mathbf{r}, t)}{\partial t} = D_j^0 \nabla^2 \Delta n_j(\mathbf{r}, t) + Z_j e \beta \langle n_j \rangle_u D_j^0 \nabla^2 \phi_{elec}(\mathbf{r}, t) \quad (4)$$

where  $D_j^0$  is in their theory the infinite dilution limit of the diffusion coefficient of the  $j$ th species in the absence of electrostatic coupling with the other particles. They assumed that the electrical potential obeyed the Poisson equation, which generalized to a system of  $N$  types of ionic species is,

$$\beta \nabla^2 \phi_{elec}(\mathbf{r}, t) = -4\pi \lambda_B \sum_{i=1}^N Z_i \Delta n_i(\mathbf{r}, t) \quad (5)$$

where  $\lambda_B = e^2 / \epsilon k_B T$  is the Bjerrum length and  $\epsilon$  is the dielectric constant of the medium. Note that  $\phi_{elec}(\mathbf{r}, t)$  arises from particle fluctuations away from the uniform concentration distribution. Quasi-elastic light scattering measurements do not monitor concentrations in real space, but in momentum space, hence one substitutes  $\Delta n_j(\mathbf{r}, t) \rightarrow \Delta n_j(\mathbf{q}, t)$  and  $\nabla^2 \Delta n_j(\mathbf{q}, t) \rightarrow -q^2 \Delta n_j(\mathbf{q}, t)$  into equation 4, where the scattering vector  $q$  is defined as  $q = (4\pi \bar{n} / \lambda_0) \sin(\theta/2)$  for the scattering angle  $\theta$ , wavelength of incident light  $\lambda_0$ , and index of refraction  $\bar{n}$ . The resulting equation in  $q$ -space in matrix form is,

$$\frac{\partial \underline{\Delta n}(\mathbf{q}, t)}{\partial t} = -\underline{\Omega}(\mathbf{q}) \bullet \underline{\Delta n}(\mathbf{q}, t) \quad (6)$$

where  $\underline{\Omega}(\mathbf{q})$  is the frequency matrix whose elements are given by,

$$[\underline{\Omega}(\mathbf{q})]_{ij} = D_j \left[ q^2 \delta_{ij} + \frac{Z_i}{Z_j} \kappa_j^2 \right] \quad (7)$$

where  $\delta_{ij}$  is the Dirac delta function and the *partial* screening parameter  $\kappa_j$  is defined by  $\kappa_j^2 = 4\pi \lambda_B Z_j^2 \langle n_j \rangle_u$ . Note that  $D_j$  occurs in equation 7 rather than  $D_j^0$ , in anticipation of later inclusion of hydrodynamic and electrolyte dissipation effects.

**$D_{app}(\mathbf{q})$  for Polyions in the Presence of Added Electrolyte.** It is assumed that there are three species present in the solution: the polyions (component 1); the counterions (component 2) and the coions (component 3). The frequency matrix for this system is therefore a 3x3 matrix whose secular cubic equation has been solved exactly using the Cardan solution. The coefficients of the  $n$ th power term,  $c_n$ , in the secular equation are:  $c_1 = - (D_1 + D_2 + D_3)q^2 - (D_1 \kappa_1^2 + D_2 \kappa_2^2 + D_3 \kappa_3^2)$ ;  $c_2 = (D_1 D_2 + D_2 D_3 + D_3 D_1)q^4 + [D_1 D_2 (\kappa_1^2 + \kappa_2^2 + D_2 D_3 (\kappa_2^2 + \kappa_3^2)) + D_3 D_1 (\kappa_3^2 + \kappa_1^2)]q^2$ ; and  $C_3 = - D_1 D_2 D_3 q^6 - D_1 D_2 D_3 \kappa_{tot}^2 q^4$ , where  $\kappa_{tot}^2 = \kappa_1^2 + \kappa_2^2 + \kappa_3^2$  is the total screening parameter. The apparent diffusion coefficient for the  $k+1$  root is (5),

$$D_{k+1}(q) = \frac{1}{q^2} \left[ 2 \left( \frac{-a^3}{27} \right)^{1/6} \cos \left( \frac{\psi + 2\pi k}{3} \right) - \frac{c_1}{3} \right] \quad (k = 0, 1, \text{ or } 2) \quad (8)$$

where  $a = c_2 - (c_1^2/3)$ ,  $b = (2c_1^3/27) - (c_1c_2/3) + c_3$ , and  $\cos(\psi) = -b/[2(-a/3)^{1/2}]$ . The polyion diffusion mode is the root for which  $k = 1$ . Representative calculations for this model are given in Table I.

**$D_{app}(q)$  for Mixed Polyion System with No Added Salt.** The development in the previous section can be directly applied to a system of mixed polyions with no added salt, where components 1 and 2 represent the polyions and component 3 represents the counterions of concentration,  $C_3 = -(Z_1C_1 + Z_2C_2)/Z_3$  (24). Representative results are given in Table II. The roots to the cubic equation that are associated with the polyion diffusion modes ( $k = 1$  and 2, or roots  $R_2$  and  $R_3$ , respectively) were determined from the apparent diffusion coefficient obtained under high salt-low charge conditions (top row in Table II).

**Single Polyion Species with No Added Salt.** The frequency matrix for a single macroionic species with no added electrolyte is a  $2 \times 2$  matrix. From the charge neutrality condition one has the relationship  $\kappa_2^2 = -Z_2\kappa_1^2/Z_1$ .  $D_{app}(q)$  for the polyion is obtained from the quadratic expression, where the "+" root corresponds to the polyion as determined from the high salt-low charge conditions.

### Series Expansion Representation of $D_{app}(q)$

Petsev and Denkov (7) represented their  $D_{app}(q)$  versus  $q$  plots for PLS as a power series expansion to the 4th power in  $q$ ,

$$D_{app}(q) = D_m + Aq^2 + Bq^4 \quad (9)$$

As might be the case for premature truncation of the series expansion, the numerical values of  $D_m$ ,  $A$ , and  $B$  can adequately fit the data profile but may not have physical significance in regard to the values of molecular parameters calculated from an appropriate theory. Equation 8 has previously been expanded to the  $q^6$  term (5, 8). Hence model dependent expressions for  $D_m$  (see next section),  $A$ , and  $B$  are available to assess the "curve fitted" values for these coefficients. Such a comparison is delayed to the discussion section. Unfortunately the mathematical expressions are too long to be reproduced in this short communication, so the interested reader is directed to the literature for the mathematical forms of  $A$  and  $B$ .

### Linearized Form of $D_{app}(q = 0)$

For the special case  $Z_2 = -Z_3$  and  $D_s = D_2 = D_3$ , where  $D_s$  is the small ion diffusion coefficient, the  $q = 0$  limit for the expression in equation 8 is the Lin *et al.* (4) result,

$$D_{app}(q = 0) = \frac{1}{2} \left[ D_1 + D_s + \frac{1 - x(1 + y)}{1 + x(1 + y)} (D_1 - D_s) \right] \quad (10)$$

where  $x = D_s/D_1Z_1$ , and  $y = 2C_s/Z_1C_1$ . We distinguish between added electrolyte,  $C_{add}$ , and the counterions in our definition of  $2C_s$ , viz.,  $2C_s = 2C_{add} + |Z_1|C_1$ .

**Table I.  $D_{app}(q)^a$  for Selected Values of  $q$  for a Spherical Macroion in the Presence of Added Electrolyte**

$C_1 \times 10^6$ (M)	$Z_1$	$D_1 \times 10^8$ ( $\text{cm}^2/\text{s}$ )	$C_3 \times 10^4$ (M)	$q$ ( $10^5 \text{ cm}^{-1}$ )			
				1.0	1.5	2.0	2.5
50.0	500	2.0	0.0001	668.0	668.0	667.0	667.0
50.0	500	2.0	1.0	664.0	664.0	664.0	664.0
0.01	50	2.0	1.0	2.2	2.2	2.2	2.2
0.01	50	60.0	0.0001	138.0	95.4	80.1	72.9
0.01	50	60.0	1.0	66.6	66.0	65.3	64.6
0.01	150	20.0	0.0001	242.0	124.0	79.3	58.3
0.01	150	20.0	1.0	83.0	77.4	71.0	64.6
0.10	150	20.0	1.0	195.0	182.0	166.0	149.0

a - units of  $10^{-8} \text{ cm}^2/\text{s}$

**Table II.  $D_{app}(q)^a$  for Selected Values of  $q$  for Mixed Macroions in Salt-free Solutions**

$D_1^a$	$Z_1$	$C_1^b$	$D_2^a$	$Z_2$	$C_2^b$	$R_2/q^2$	$R_3/q^2$
1.0	1	0.01	10.0	1	0.01	1.0	10.0
2.0	500	0.01	20.0	150	0.01	11.3	369.0
2.0	500	0.01	20.0	150	1.0	2.2	1170.0
2.0	500	1.0	20.0	150	0.01	19.8	660.0
2.0	150	0.01	20.0	500	0.01	2.16	1340.0
2.0	150	0.01	20.0	500	1.0	2.00	1670.0
2.0	150	1.0	20.0	500	0.001	10.4	447.0

a - units of  $10^{-8} \text{ cm}^2/\text{s}$  at a scattering vector  $q = 1 \times 10^5 \text{ cm}^{-1}$ ; b - units of  $10^{-6} \text{ M}$

Many experiments are carried out under relatively dilute solution conditions such that  $D_{\text{app}}(q = 0)$  appears to be a linear function of the polyion volume fraction  $\phi_1$ . Equation 10 in the limit  $y \gg 1$  yields the desired linearized expression,

$$D_{\text{app}}(q = 0) \cong D_1^0 \left( 1 + A_d \frac{Z_1^2 C_1}{2C_s} \right) = D_1^0 \left[ 1 + \left( A_d \frac{Z_1^2}{2C_s} \frac{3}{4\pi R_S^3} \frac{1000}{N_A} \right) \phi_1 \right] \quad (11)$$

where  $N_A$  is Avogadro's constant,  $A_d = (D_S - D_1)/D_S$  is the dynamic attenuation term due to the finite response time of the small ions to the movement of the polyion.

### The Cell Model and the Composite Diffusion Coefficient.

Macroionic solutions and suspensions are multicomponent systems that involve complex interparticle interactions between the solute and solvent particles. No theory exists, therefore, that takes all of these effects into consideration under arbitrary experimental conditions. We therefore resort to an *ad hoc* construction of a composite diffusion coefficient based on the assumption that in the linearized approximation these additional effects are additive.

**Hydrodynamic Interaction.** Hydrodynamic interactions differ from other types of interparticle interactions in the sense that they can be *reflected* off of the other particles in the solution. A hydrodynamic wake originating from the "test" particle can therefore be reflected off of other particles and thereby affect its own motion. Hydrodynamic interactions, therefore, are *indirect* interparticle interactions. These interactions are expressed as a multiplicative factor in the diffusion coefficient, i.e.,  $D_1(q) = D_1^0 H_{11}(q)$ , where  $D_1^0$  is the infinite dilution value of  $D_1$  (9, 10).

**Electrolyte Dissipation.** Electrolyte dissipation refers to the retardation effect on the polyion motion due to the instantaneous distortion of the surrounding ion atmosphere as the macroion moves through the medium. If hydrodynamic and electrolyte dissipation contributions are not coupled, then the infinite dilution expression for the polyion diffusion coefficient is  $D_1^0 = k_B T / (f_{SE} + f_{elec})$  where  $f_{SE} = 6\pi\eta R_S$  is the usual Stokes-Einstein friction factor for hard spheres and  $f_{elec}$  accounts for electrostatic dissipation effects. Expressions have been obtained for  $f_{elec}$  for a charged sphere without (11-14) and with (15) hydrodynamic interaction between the small ions and the polyion.

**Direct Macroion-Macroion Interactions in Strong Interaction Limit.** It is well-known that  $D_1$  for a system of strongly interacting macroions exhibits a  $q$ -dependence due to the highly ordered nature of the macroions in solution or colloidal suspension. The  $q$ -dependence is manifested in the macroion-macroion partial structure factor  $S_{11}(q)$ . The inclusion of both the indirect hydrodynamic and direct interactions between the macroions yields the following form for  $D_1(q)$  (9, 10)

$$D_1(q) = \frac{D_1^0 H_{11}(q)}{S_{11}(q)} \quad (12)$$

In the  $q = 0$  limit the osmotic susceptibility and the solution structure factor are related through the pairwise direct interaction potential, where it is easily shown through the second virial coefficient that,

$$\frac{1}{RT} \left( \frac{\partial \pi}{\partial C_1} \right)_{\mu, T} = \frac{1}{S_{11}(q=0)} \quad (13)$$

If the interparticle interaction between the macroions is composed of a hard sphere and weak screened Coulombic interaction, then to the first power in the concentration,

$$\frac{1}{S_{11}(q=0)} \cong 1 + \left( 8 + \frac{Z_1^2}{2C_s} \frac{3}{4\pi R_S^3} \frac{1000}{N_A} \right) \phi_1 \quad (14)$$

The first term in the parentheses of equation 14 results from the hard sphere potential and the second term from the screened Coulombic interaction in which the exponential form of the long range pair distribution function is expanded to only the first two terms.

**Dilemma of the Electrostatic Interactions.** In comparison of equations 11, 13, and 14 one might conclude that the two electrolyte dependent terms are the same if  $A_d = 1$ . These two terms, however, result from two mutually exclusive model assumptions regarding the role of the electrolyte ions. In equation 11 the electrolyte ions play an *active role* in the dynamics of the macroions through the coupled terms in the Poisson equation, whereas in equation 14 the electrolyte ions act in a *passive manner* by simply screening the interaction between the dynamically coupled macroions. It is our opinion that these two terms, although numerically identical if  $A_d = 1$ , have two distinct origins in the scheme of interparticle interactions of macroionic solutions and suspensions. The manner in which the separate origins of active and passive contributions of the small ions affects the expression of the mutual diffusion coefficient is discussed in the following section.

### The Cell Model and the Modified Form of $D_{app}(q=0)$

Partial support for the supposition of separate contributions of polyion-polyion and polyion-small ion to  $D_{app}(q=0)$  is found in the cell model of Imai and Mandel (18) and of Penfold and co-workers (19). In this approach the cell is assumed to contain one polyion and a sufficient number of electrolyte ions to be electrically neutral. Penfold and co-workers (19) explicitly considered three types of electrostatic interactions: 1) the macroion interactions with the counterions inside the cell; 2) the interaction between macroions in neighboring cells, and 3) the interactions between electrolyte ions of neighboring cells. They found that the latter interactions are negligible in comparison with the first two types of interactions. Hence  $D_1$  in equation 7 is assumed to be the same form as in equation 12, viz.,

$D_1 \rightarrow D_1(q) = D_1^0 H_{11}(q) / S_{11}(q)$ . Within the context of the Penfold *et al.* study, we interpret this substitution in terms of polyion-polyion interactions in different cells and equation 7 as the frequency matrix for macroion-electrolyte coupled dynamics within the cell. If these contributions are additive as supposed, then the mutual diffusion coefficient,  $D_m = D_{app}(q=0)$ , for the cell model is,

$$D_m = D_1^0 \left[ \frac{1}{RT} \left( \frac{\partial \pi}{\partial C_1} \right)_{\mu, T} + A_d \frac{Z_1^2 C_1}{2C_s} \right] H_{11} \cong D_1^0 (1 + \lambda \phi_1) \quad (15)$$

where  $D_1^0$  includes electrolyte dissipation effects. This form for  $D_m$  is precisely the same as that of Imai and Mandel (18) for the cell model if one sets  $A_d = 1$ . In view of the above development the generalized form of the coefficient  $\lambda$  is,

$$\lambda = 8\delta_{hs} + (\delta_{11} + A_d) \frac{Z_1^2}{2C_s} \frac{3000}{4\pi R_S^3 N_A} - k_h \quad (16)$$

where  $\delta_{hs} = 1$  if hard sphere interactions are important or  $\delta_{hs} = 0$  if there are no hard sphere contributions (such as in the Anderson-Reed model),  $\delta_{11} = 1$  if the concentration coefficients in equations 11 and 14 have different origins (cell model) or  $\delta_{11} = 0$  if these equations have a common origin, and  $k_h$  accounts for the hydrodynamic interactions *between the macroions*. The numerical value of  $k_h$  is model dependent. For example, Carter and Phillies (17) obtained the value  $k_h = 8.898$  for uncharged hard spheres where divergent terms (cf. equation 2) and the effect of solvent back flow are included.

## Experimental

Many QELS studies in the literature rely on data obtained in other laboratories on similar samples for the interpretation of QELS data. In order to better assess the relative importance of the various contributions to the diffusion coefficient it is important to perform several complementary experiments on the same preparation of the sample. We summarize, therefore, the studies of Singh (20) on well-defined BSA preparations and the complementary measurements of QELS, total intensity ( $I_{tjls}$ ), osmotic susceptibility, and viscosity.

**Preparation and characterization of BSA monomers.** The BSA was purchased from Sigma Chemical Company in St. Louis (Lot No. A-6003, Fraction V, essentially fatty acid free). Gel permeation chromatography (12 in long column, Bio-Gel P-200, Tris-HCl buffer, pH 7.2, 5 °C) separated the monomers from the dimers and trimers as monitored by absorbance of the elution and later verified by mini-slab gel electrophoresis. The running gel was 30% (w/v) acrylamide with 0.8% (w/v) bis-acrylamide in Tris-HCl pH 8.8 buffer with 1% (w/v) SDS. The electrophoresis was performed initially with 60 volts until the dye reached the running gel, after which 100 volts was applied for 8-12 hours. The gels were stained with coomassie blue for 8-10 hours and then destained with a mixture of 2-propanol and acetic acid. The gels were then photographed with a Polaroid MP-4 Land camera for future reference.

**Preparation of the dialysis bags.** The BSA samples used in the osmometry and light scattering experiments were exhaustively dialyzed against the appropriate solvent. Pre treatment of the dialysis tubing was to first boil for 15 minutes in 5%  $\text{NaHCO}_3$  and 0.01M EDTA, and then rinse with distilled water to remove diffusible salts and UV absorbing material (21). The dialysis tubing was stored under refrigeration (5 °C) in 50% ethanol-water until needed, and then rinsed with copious amounts of distilled water prior to use.

**Characterization of the BSA solutions.** Several complementary methods were employed in the characterization of the BSA solutions. Listed below are only those methods that have a direct bearing on the interpretation of the data.



**Osmometry.** Osmotic pressure ( $\pi$ , in atmospheres) measurements were made with a Knauer Membrane Osmometer Type 01.00 connected to a Kipp and Zonen (Holland) type B D 40/04/05 recorder. The temperature was monitored with a telethermometer model 4310 (Yellow Springs Instrument Co., Inc.) to an accuracy of  $\pm 1$  °C. The osmometer was equilibrated with pH adjusted KCl solutions overnight at 25 °C. The membranes used in these experiments were B-19 S&S deacetylated acetyl membranes (Catalog number 2001-5, suitable for molecular weights greater than 20,000). The plotting scale was calibrated to 10 cm of water. After attaining a constant baseline 0.4 mL aliquots of a given BSA solution was injected very carefully into the inlet tube of the osmometer and the osmotic pressure was recorded in units of cubic centimeters of water. The solutions at a given pH and ionic strength were studied in order of increasing concentration of BSA. Data for which drifts in the baseline of greater than 1% were not retained. The cell was thoroughly rinsed with the pH adjusted KCl solution after each set of measurements. The osmotic pressure was fitted to the cubic equation,

$$\pi = \frac{RT}{M_{BSA}} c_{BSA} + b_{\pi} c_{BSA}^2 + c_{\pi} c_{BSA}^3 \quad (16)$$

where  $M_{BSA}$  is the molecular weight of the BSA,  $c_{BSA}$  is the weight concentration (g/L) of the BSA solutions, and  $b_{\pi}$  and  $c_{\pi}$  are least-square fitting parameters to the data. Representative results are summarized in Table III.

**Viscometry.** A Cannon 100 A 45 capillary-flow viscometer (Cannon Instrument, Box 16, State College, PA.) with a flow time of 60 seconds for water was used in these experiments. The viscometer was submerged in a water bath with a temperature control to  $\pm 0.1$  °C using a Haake E 12 thermostatic control. The time flow between the two marks was measured by an electronic digital stopwatch (catalog number 14-648, Fisher Scientific Co.). Between each run the viscometer was cleaned and washed with distilled water, followed by lab-grade acetone and dried at 120 °C. The relative viscosity of the BSA solutions was calculated from the ratio of the flow times  $t_{BSA}$  and  $t_{KCl}$ , for the BSA and KCl solutions, respectively. The relative viscosity obtained in these studies did not deviate substantially from unity.

**Light scattering measurements.** Both quasi-elastic and total intensity ( $I_{tjls}$ ) light scattering measurements were carried out on the same instrument. The cylindrical cells, which had an inlet and outlet tube, were cleaned with hot nitric acid (50% v/v) and then thoroughly rinsed with distilled water prior to use in the light scattering experiments. In preparation for the experiment the cell was placed in a specially designed "dust box" with a gravity-flow filtration system. In this arrangement the solutions to be filtered were placed in a reservoir outside of the dust box, where the unsupported Millipore filter was located at the bottom of the reservoir.

Tygon tubing connected to the inlet arm of the cell and filter reservoir assured that air was eliminated in the filtration process. To extract the liquid from the cell in the rinsing process a movable tapered glass tube was inserted in the other arm of the cell and connected to tygon tubing that led into a three-way valve, where one of the two outlets was connected to an aspirator and the other to the outside air. We found that this somewhat elaborate method eliminated the introduction of unfiltered air into the scattering cell. The filters used in these experiments were 0.45  $\mu\text{m}$  Millipore filters. The cells were first rinsed several times with filtered distilled water, followed by two (or more) rinses with the desired KCl solution, and then one rinse with the BSA solution. This rinsing protocol was then followed by filtration of the BSA solution to be used in the light scattering experiments. The  $I_{tjls}$  measurements were

made at 5° intervals over the range 30° < θ < 120° using a digital multimeter. The absolute excess intensities were obtained using spectroscopic grade benzene as a standard, and correcting for the solvent contribution. The q-independent "solution structure factor" was then calculated from the expression,

$$S_{11} = \frac{I_{BSA}([KCl]) - I_0([KCl])}{I_{3.80}(0.1M) - I_0(0.1M)} \quad (17)$$

where  $I_{BSA}([KCl])$  is the intensity of scattered light normalized to the benzene reference and BSA concentration that was measured for the dimensionless BSA concentration  $[BSA] \times (10^5 \text{ M}^{-1})$  (the numerical value is the subscript) at the specified KCl concentration and  $I_0([KCl])$  is the *intercept* of the  $I_{BSA}([KCl])$  versus  $[BSA]$  profile corresponding to the solvent scattering. These measurements of the excess scattering intensity were then normalized to the scattering of a  $3.80 \times 10^{-5} \text{ M}$  solution of BSA in 0.1 M KCl.

QELS measurements were carried out on the same BSA samples as the  $I_{tills}$  measurements. The autocorrelation functions were obtained with a Langley-Ford autocorrelator. These functions were characterized as a single exponential decay function with a baseline. Data were obtained at several delay times and extrapolation of these values to zero delay time provided the value of  $D_{app}(q)$ . In all  $[KCl]$  solutions no angle dependence was observed for  $D_{app}(q)$ , hence the equivalence  $D_{app}(q) = D_{app}(q=0) = D_m$ . were assumed. Linear regression analysis of the data obtained at pH 5.0 (near the isoelectric point) at 25 °C in 0.1 M KCl was found to be  $D_m(25 \text{ }^\circ\text{C}) = 6.58 \times 10^{-7} (1 - 0.023c_{BSA}') \text{ cm}^2 / \text{s}$  where  $c_{BSA}'$  is the concentration in g/mL (20). This expression is comparable to the 20 °C study of Oh and Johnson (22) for their highly purified BSA at pH 4.7 in 0.12 M NaCl/acetic acid, where the concentration coefficient was reported to be - 0.0166 mL/g. The difference may be attributed to the slight differences in pH, T, and electrolyte concentration. Plots of  $D_{app}$  versus  $1/2C_{add}$  for BSA concentrations in the range 1-3 g/L and at four values of the pH are shown in Figure 1.

## Discussion

In order to understand the complex diffusion process of macroions in moderate to low ionic strength solvents, it is necessary to examine the theoretical predictions of over simplified mathematical models. According to the results given in Table I for the added electrolyte - single macroion system, the CM model predicts that  $D_{app}(q)$  decreases as q increases, and that this dependence is strongest for moderately charged macroions in extremely low ionic strength solvents. In the case of *highly charged* macroions the apparent q dependence is suppressed because  $D_{app}(q)$  is near its low salt *plateau value*. The situation is somewhat more complex in the two macroion - no added electrolyte system. We hesitate to ascribe a specific motion to these eigenvalues and the resulting values of  $D_{app}(q)$  given in Table II. Our caution is based on the study of Pusey, Fijnaut, and Vrij (23) in which they examined a system of two interacting (neutral) polymers. Based on the relative changes of the eigenvectors they interpreted the faster "+" mode in terms of a "collective mode" and the slower "-" mode in terms of an "exchange mode" for these dissimilar polymers. These assignments are consistent with the labels given, without proof, to the observed fast and slow relaxation modes in QELS studies. However, the fact that the two polymers move in opposite directions for the "-" mode does not necessarily mean that the motion is *towards* each other, as implied by an "exchange" of particles, since they could also be moving *away* from each other.

Our reluctance to associate eigenvalues with specific molecular motions is further supported by the behavior of these eigenvalues. From the low charge, low concentration limit in Table II, root 2 is identified with polyion 1 and root 3 with polyion 2. It is evident from the data in Table II that the eigenvalue identified with smaller of the two macroions is more affected by the electrical properties of the solution. In the case of polyions of equal size but different charge, the polyion with the smaller charge is more affected by concentration changes than the higher charged polyion which appears to retain its neutral charge value of  $D_1$ . It is not obvious to us at this time what type of coupled motion gives rise to these behavioral patterns.

Attention is now directed to the summary of the BSA results given in Figure 2 and Table IV for KCl solutions at pH 7.4. As shown in Figure 2, a decrease in  $2C_{add}$  results in an increase in  $D_{app}$  and the functional dependence is stronger for the larger charge (higher pH). This behavior is consistent with equations 15 and 16. It is concluded from the data in Table IV that  $D_{app}$  obtained in 0.1 M KCl contains no interparticle interactions since the ratio  $R_A$  (cf. Table IV caption) is independent of [BSA], where  $D_{1,h}^0$  is defined as  $D_1^0$  at this salt concentration.

The mutual diffusion coefficient is related to the osmotic susceptibility by,

$$D_m = \frac{1}{f_m} \left( \frac{\partial \pi}{\partial C_1} \right)_{\mu, T} \quad (18)$$

The ratio  $R_B/R_A$  in Table IV is therefore a measure of the ratio  $f_m / f_{1,h}^0$ . The trend evident in Table IV is that  $R_B/R_A$  decreases as [BSA] increases, which is opposite to what one would expect if hydrodynamic interactions alone were operative in this system. However, this trend is in the correct direction for electroviscous effects since there is an increase in the counterion concentration concomitant with an increase in [BSA]. The ratio  $R_C/R_A$  is equation to  $H_{11}(q)$  in accordance with equation 12. Since hydrodynamic interactions effectively appear as an attractive interaction the observation that  $H_{11}(q)$  is greater than unity for 0.001 M KCl indicates that electrical rather than hydrodynamic interparticle interactions affect the magnitude of the apparent friction factor.

Direct rather than dissipation interparticle interactions are dominant for [KCl] = 0.001M since  $R_A$  increases with an increase in [BSA]. It is noted, however, that the inequality  $(1/RT)(\partial \pi / \partial C_1) < 1/S_{11}$ . ( $R_B < R_C$ , where  $R_B$  was computed from equation 16 using a molecular weight  $M_{BSA} = 68,000$ ) prevails for the 0.001M KCl solvent. Failure of the generally accepted equality of equation 13 can be explained in terms of the reduced intrinsic scattering power of the polyions in the low ionic strength solvent. Stigter (24) and Vrij and Overbeek (25) showed that the scattered light intensity for the multicomponent polyion system is decreased when compared with the expected two-component system result. This is because the index of refraction increment at constant chemical potential must be used instead of at constant concentration. Vrij and Overbeek (25) obtained the following ratio,

$$\left[ \frac{(\partial \bar{n} / \partial c_1)_{\mu}}{(\partial \bar{n} / \partial c_1)_{c'}} \right]^2 = \left[ 1 - \frac{Z_1 \alpha M_2 (\partial \bar{n} / \partial c_2)_{c'}}{2 M_1 (\partial \bar{n} / \partial c_1)_{c'}} \right]^2 \quad (19)$$

where the subscript 1 (2) denotes the polyion (electrolyte), the subscript  $c'$  denotes constant concentrations of all other components, and the factor  $0 < \alpha < 0.5$  is the

**Table III. Least-Squares Fit of the Osmotic Pressure for BSA**

pH	[KCl] (M)	$b_{\pi} \times 10^5$ (atm L <sup>2</sup> g <sup>-2</sup> )	$c_{\pi} \times 10^7$ (atm L <sup>3</sup> g <sup>-3</sup> )	$\sigma^{1/2} \times 10^4$ a
5.00	0.100	-0.0342	0.290	5.45
5.00	0.005	-0.277	0.847	3.21
6.50	0.100	-0.193	1.90	1.34
6.50	0.001	2.01	8.88	10.1
7.40	0.100	2.68	-15.3	2.64
7.40	0.010	2.68	3.59	1.08
7.40	0.0001	6.56	-14.2	1.80
8.50	0.100	-0.0129	2.86	2.06
8.50	0.005	3.72	-2.74	4.48
8.50	0.001	7.05	-6.43	4.64

$$a - \sigma^{1/2} = \left[ \sum_{i=1}^n (x_{\text{calculated}} - x_{\text{experimental}})^2 / n \right]^{1/2}$$

**Table IV. Characterization of BSA in KCl at pH 7.4 and 25 °C**

[KCl] (M)	$c_{\text{BSA}}$ (g/L)	$R_A$	$R_B$	$R_C$	$R_B/R_A$	$R_C/R_A$
0.100	3.80	1.01	1.31	1.00	1.30	0.99
0.100	16.4	1.06	1.06	0.88	1.00	0.83
0.100	18.0	0.99	0.88	0.85	0.83	0.86
0.001	7.56	1.56	2.76	3.75	1.77	2.40
0.001	12.7	2.07	3.31	3.81	1.60	1.84
0.001	14.9	2.56	3.53	5.42	1.38	2.12

$$R_A = \frac{D_m}{D_{i,h}^0}; \quad R_B = \frac{1}{RT} \left( \frac{\partial \pi}{\partial [\text{BSA}]} \right)_{\mu,T}; \quad R_C = \frac{I_{3.80}(0.1M) - I_0(0.1M)}{I_{\text{BSA}}([\text{KCl}]) - I_0([\text{KCl}])}$$

deficit of coions, where the upper limit of 0.5 results for low potentials. Vrij and Overbeek (25) reported in their Table II the index of refraction increments of poly(methacrylic acid) at constant  $\mu$  and constant  $c'$  in different salt solutions. Using their values one has  $[(\partial \bar{n}/\partial c_1)_\mu / (\partial \bar{n}/\partial c_1)_c]^2 = (0.209/0.234)^2 = 0.80$  in 0.1 M NaCl and  $(0.169/0.227)^2 = 0.55$  in 0.01 M  $(\text{NH}_4)_6\text{Mo}_7\text{O}_{24}$ . Hence it is important to correct for the intrinsic scattering power of the macroions in the lower ionic strength solvents when using equation 13. An alternative explanation, however, is found by comparison of equations 12 and 15. Given that hydrodynamic interaction are negligible in comparison to the electrical effects, one has from equations 12 and 15 the difference  $R_C - R_B = A_d Z_1^2 C_1 / 2C_s$ . Using the two extreme BSA concentrations one obtains  $(R_C - R_B)/c_{\text{BSA}} = A_d Z_1^2 / 2C_s M_{\text{BSA}} \approx 0.13$ , from which one obtains for  $A_d = 1$  the approximate value  $Z_1 \approx -4$ . In view of the approximations employed in the calculation, this value is in reasonable agreement with the value of  $Z_1 = -9$  reported by Tanford *et al.* (26) for BSA in pH 7.4 buffer in  $10^{-3}$  M electrolyte.

We now turn to the data of Petsev and Denkov (7) of PLS over the ranges  $1 \times 10^{-4} < \phi_1 < 6 \times 10^{-4}$  and  $10^{-4} \text{ M} < [\text{NaCl}] < 10^{-2} \text{ M}$ . A detailed analysis of these data will be presented elsewhere. Of relevance to the present communication is that  $D_m$  (cf. equation 9) is a linear function of  $\phi_1$ . The reported slopes,  $\lambda$ , are plotted as a function of  $1/2C_{\text{add}}$  in Figure 2. The counterions from the macroions are not included since [PLS] is on the order of  $5 \times 10^{-8}$  M. Although there are only four points, these data indicate two linear regions. The solid line in Figure 2 is the equation

$$\lambda = \frac{0.173}{2C_{\text{add}}} + 135 \quad (20)$$

To estimate the charge from equation 20 we use the reported micrograph value of  $R_S = 95 \times 10^{-8}$  cm (7) and assume  $\delta_{11} + A_d = 2$ , with the result  $Z_1 \approx 14$ . This is an extremely low estimate but is consistent with the very low results obtained for polyions using conventional polyelectrolyte models. The intercept, however, is much larger than the *maximum* prediction of the neutral hard sphere, viz.,  $8 - k_h$ . It is tempting to suggest that this provides support for the existence of an "effective" hard sphere with a radius determined by the screening length  $1/\kappa$ , as proposed recently by Okubo (27). We do not, however, ascribe to this interpretation since it leads to unphysical results such as an erroneous value of Avogadro's constant (28).

## Conclusions

The reciprocal intensity of scattered light first normalized to theta conditions (high salt for polyions) is sometimes employed for the osmotic susceptibility. It is concluded from the BSA studies that this equivalence is valid only if the intensity is measured under low electrolyte concentration is first corrected for multicomponent solution effects. A second interpretation that deserves consideration is the "cell model" that explicitly separates small ion-macroion and macroion-macroion contributions. Although to be discussed in detail elsewhere, the "composite" diffusion coefficient appears to be adequate in the interpretation of the PLS data of Petsev and Denkov (7). It is quite clear that many effects must be taken into consideration when attempting to make sense of polyelectrolyte data in solutions with very low electrolyte concentrations.

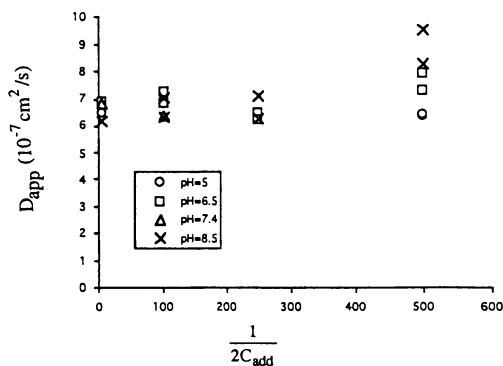


**Figure 1. Electrolyte Concentration Dependence of  $D_{app}$  for BSA at Varying pH values.** The BSA concentrations are in the range 1-3 g/L.

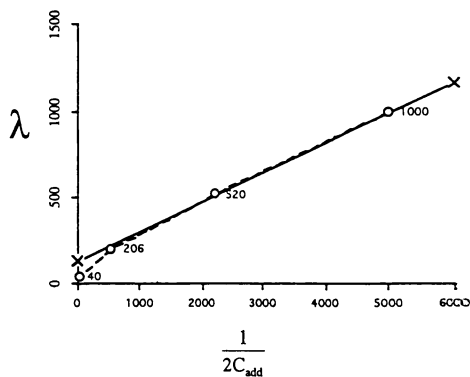


**Figure 2. Electrolyte Concentration Dependence of Volume Fraction Coefficient.** The data shown above were obtained from Petsev and Denkov (7). The solid line was computed from equation 20.

## References

1. Giordano, R.; Maisano, G.; Mallamace, F.; Micali, N.; Wanderlingh, F. *J. Chem. Phys.* **1981**, *74*, 2011-2015.
2. Carter, J. M.; Phillies, G. D. J. *J. Phys. Chem.* **1985**, *89*, 5118-5124.
3. Anderson, J. L.; Reed, C. C. *J. Chem. Phys.* **1976**, *64*, 3240-3250.
4. Lin, S.-C.; Lee, W. I.; Schurr, J. M. *Biopolymers* **1978**, *17*, 1041-1064.
5. Schmitz, K. S. *An Introduction to Dynamic Light Scattering by Macromolecules*; Academic Press, Boston, MA., **1990** pp 207-210.
6. Tivant, P.; Turq, P.; Drifford, M.; Magdelenat, H.; Menez, R. *Biopolymers* **1983**, *22*, 643-662.
7. Petsev, D. N.; Denkov, N. D. *J. Colloid and Interf. Sci.* **1992**, *149*, 329-344
8. Schmitz, K. S. *Macroions in Solution and Colloidal Suspension*, VCH Publishers, New York., N.Y., **1993** pp 140-145.
9. Belloni, L.; Drifford, M.; Turq, P. *J. Physique Lett.*, **1985**, *46*, L207-L215
10. Schurr, J. M. *Chem. Physics*, **1987**, *111*, 55-86.
11. Schurr, J. M., *Chem. Physics*, **1980**, *45*, 119-132.
12. Medina-Noyola, M.; Vizcarra-Rendón, A. *Phys. Rev. A* **1985**, *32*, 3596-3605.
13. Ruín-Estrada, H.; Vizcarra-Rendón, A.; Medina-Noyola, M.; Klein, R. *Phys. Rev. A* **1986**, *34*, 3446-3451.
14. Vizcarra-Rendón, A.; Ruín-Estrada, H.; Medina-Noyola, M.; Klein, R. *J. Chem. Phys.*, **1987**, *86*, 2976-2985.
15. Booth, F. *J. Chem. Phys.* **1954**, *22*, 1956-1968.
16. Geigenmüller, U. *Chem. Phys. Lett.* **1984**, *110*, 666-667.
17. Carter, J. M.; Phillies, G. D. J. *J. Phys. Chem.* **1985**, *89*, 5118-5124.
18. Imai, N.; Mandel, M. *Macromolecules* **1982**, *15*, 1562-1566.
19. Penfold, R.; Nordholm, S.; Jönsson, B. *J. Chem. Phys.* **1990**, *92*, 1915-1922.
20. Singh, N. *On the Possible Role of Small Ions in the Dynamics of Polyelectrolytes* **1986**, University of Missouri Ph. D. Dissertation.
21. Fu, J. C. C.; Gruenwedel, D. W. *Biopolymers* **1976**, *15*, 265-282.
22. Oh, Y. S.; Johnson, C. S. *J. Chem. Phys.* **1981**, *74*, 2717-2720.
23. Pusey, P. N.; Fijnaut, H. M.; Vrij, A. *J. Chem. Phys.* **1982**, *77*, 4270-4281.
24. Stigter, D. *J. Chem. Phys.* **1960**, *64*, 842-846.
25. Vrij, A.; Overbeek, J. Th. G. *J. Colloid Sci.* **1962**, *17*, 570-588.
26. Tanford, C.; Swanson, S. A.; Shore, W. S., *J. Am. Chem. Soc.* **1955**, *77*, 6414-6421.
27. Okubo, T. *Acc. Chem. Res.* **1988**, *21*, 281-286.
28. Ito, K.; Ieki, T.; Ise, N. *Langmuir*, **1992**, *8*, 2952-2956.

RECEIVED August 6, 1993

## Chapter 9

### Reactive Polymers

#### Water-Soluble Vinyl-Terminated Oligomeric Poly( $\beta$ -alanine)

Sun-Yi Huang and M. M. Fisher<sup>1</sup>

Stamford Laboratory, Cytec Industries, 1937 West Main Street,  
Stamford, CT 06904-0060

Low molecular weight water soluble vinyl terminated oligomeric poly ( $\beta$ -alanine) was synthesized using organolithium initiators. Vinyl terminated poly ( $\beta$ -alanine) consists of N-2-carboxyamidoethylacrylamide and oligomers which were fully characterized by analytical methods. The results show that one vinyl terminated group per chain was produced. Reaction time and temperature were the main variables used to control the N-2-carboxyamidoethylacrylamide content, molecular weight, and molecular weight distribution. N-2-carboxyamidoethylacrylamide was homopolymerized in aqueous medium by redox initiation. Poly (N-2-carboxyamidoethylacrylamide) was converted to a Mannich derivative and was quaternized. This new cationic water soluble polymer is an effective organic flocculant for bentonite clarification.

Block and graft copolymers represent an important class of materials which are achieving ever increasing commercial success. Examples are Shell's Kraton, Phillips' Salprene, DuPont's Hytrel, B. F. Goodrich's Estines and Cyanamid's XT polymers. The field of block and graft copolymers has been extensively reviewed in a number of recent monographs (1-3). A significant development in the area of graft copolymer synthesis is the concept of copolymerizing conventional monomers with vinyl terminated prepolymers (4-6). The principal advantage of this approach is the avoidance of a homopolymer which is always obtained when conventional free radical grafting techniques are used. The potential application of vinyl terminated prepolymers, in a number of areas of commercial significance to industries has served as the basis for the development of a novel graft copolymer useful as paper additives, flocculants, fibers, and thermoplastic elastomers. The general purpose was to improve the properties of these materials by incorporating graft segments capable of strong side chain interactions. It was

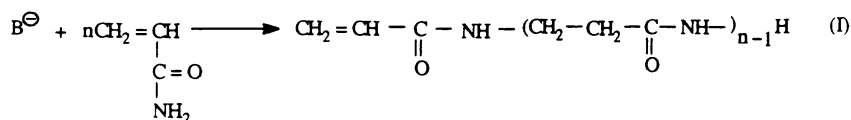
<sup>1</sup>Current address: American Plastic Council, 1275 K Street, NW, Washington, DC 20005

NOTE: This chapter is Part III in a series of articles.

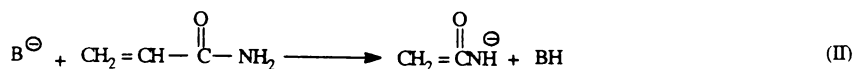
0097-6156/94/0548-0114\$06.00/0  
© 1994 American Chemical Society



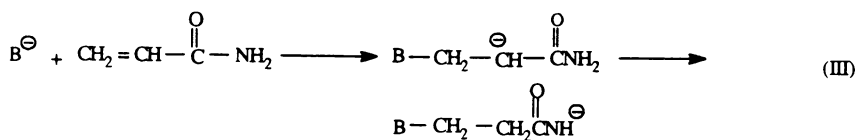
envisioned that a macromonomer with desired properties could be synthesized through the base initiated hydrogen transfer polymerization of acrylamide (7):



In 1954, a patent by Matlack (7), and papers by Breslow, et al. (8,9) described the anionic polymerization of acrylamide to high molecular weight poly (beta-alanine). Breslow, et al. suggested two possible mechanisms for the base initiated polymerization of acrylamide. One is a proton abstraction from the amide group by the base in reaction (II).



The second is the Michael addition of the initiator to the carbon carbon double bond of acrylamide in reaction (III).



They concluded that the predominant initiation reaction is (II) because a solid material from a reaction mixture of potassium tert-butoxide and acrylamide was a dimer or an oligomer containing a vinyl group. Ogata (10) concluded that nucleophilic addition to the vinyl group must be the initiation step for the polymerization of acrylamide using sodium methoxide by infrared spectroscopy. Tani, et al. (11) studied the products of the reaction of acrylamide with sodium methoxide and sodium tert-butoxide. They found that the tert-butoxide anion abstracts a proton from amide groups and adds to the carbon-carbon double bond, but the methoxide anion only adds to the carbon-carbon double bond. Trossarelli, et al. (12) found that the amounts of tert-butanol in the reaction products agreed with those calculated from the quantity of sodium tert-butoxide employed. Leoni, et al. (13) isolated dimeric and trimeric products from alkyl lithium initiated polymerization of acrylamide. Both groups supported the initiation mechanism in equation (II). Kobayashi, et al. (14) observed that acrylamide was readily polymerized to poly (beta-alanine) by sodium celluloseate and sodium polyvinyl alcohol initiators. No block and graft copolymers were found. However, the reaction led to carbamoylethylation of the polymer backbones which supported the

initiation mechanism of equation (II). Moore, et al. (15,16) found that in-situ polymerization of acrylamide initiated by poly (phenylene terephthalamide) anion in solution in vacuo at 80-115°C gave molecular composites of a poly (beta-alanine)-graft copolymer and poly (beta-alanine) homopolymer. The result supported the reactions (II) and (III). It is very difficult to draw conclusions based on the conflicting evidence reviewed above. Initiation of the hydrogen transfer polymerization of acrylamide appears to be dependent on the nature of the bases. Many other factors such as reaction temperature and medium are also expected to influence the reaction. It was also found that the basicity of the initiator and steric effects influence the mode of initiation and the ultimate degree of unsaturation of the poly (beta-alanine) (17). Tarvin (18) successfully copolymerized a high vinyl content of poly (beta-alanine) with acrylonitrile and methyl methacrylate. The terpolymers have wet fusion points at 175°C.

In this paper, we have focused on the synthesis and characterization of low molecular weight vinyl terminated poly (beta-alanine) (VTN-3). To obtain a better understanding of the polymerization process, acrylamide was converted to the low molecular weight VTN-3 and N-2-carboxyamidoethylacrylamide (AMD dimer) in various solvents and the rate of formation was measured. We report and discuss the molecular weight determination obtained by gel-permeation chromatographic separation of oligomer and AMD dimer, vapor phase osmometry, NMR, and bromine-bromate titration for unsaturation. AMD dimer was successfully isolated from oligomeric mixtures. Homopolymerization of this monomer produced a high molecular weight water soluble polymer using an aqueous redox system. The preparation of Mannich derivatives and subsequent quaternization with dimethylsulfate was investigated for the cationic derivatives of poly (acrylamide dimer) covering a wide range of molecular weight. This new cationic water soluble polymer has been studied as an effective organic flocculant for bentonite water clarification.

## Experimental

**VTN-3 Oligomer Preparation.** Ten g of sublimed acrylamide and 100 ml of p-dioxane distilled from CaH<sub>2</sub> are placed in a 250 ml, 4-neck, round-bottom flask equipped with a stirrer, N<sub>2</sub> inlet, thermometer, condenser, and rubber septum. The mixture is stirred in a N<sub>2</sub> atmosphere at ambient temperature for 30 mins. until all of the acrylamide is dissolved. The acrylamide solution is thermostated at 25°C, vigorously stirred, and 4.3 ml (1.58 M) of n-butyl lithium solution slowly added through the rubber septum by a syringe. The reaction between acrylamide and n-butyl lithium is exothermic and the addition is carried out slowly over a few mins. to maintain at 25°C. After 24 hrs. 1 ml of water is added to terminate the reaction. The white dispersed solid is separated from p-dioxane by centrifugation. The solid phase is dried under vacuum at 60°C for 24 hrs. The yield is 9 g of oligomer.

**Synthesis of Acrylamide Dimer [N-2-Carboxyamidoethylamide].** AMD dimer was obtained in 75% yield by triple ultrafiltration of a crude VTN-3 reaction mixture prepared in p-dioxane at ambient temperature. A 2-3% aqueous solution

of the initial reaction product was pressurized through an Amicon Model 402 stirred ultrafiltration cell equipped with a UM-5 membrane. The filtrate purity was 98-100% of AMD dimer. An alternative procedure for obtaining pure dimer in 40% yield was to heat the same crude VTN-3 product in p-dioxane to reflux. The slurry was quickly filtered to separate the insoluble oligomer. The dimer recrystallized from the filtrate on cooling.

**Homopolymerization of AMD Dimer.** Polymerization of AMD dimer was carried out in a 250 ml 3-neck flask containing 4 g of AMD dimer and 96 g deionized water at pH=6.0. The initiation temperature was 40°C. Sodium metabisulfite concentration was varied between 38-5000 ppm based on monomer while the ammonium persulfate concentration was 1500-30000 ppm based on monomer. The polymerization was complete in six hrs. In some runs, 4,4'-azobis (4-cyanovaleric acid) was used as the initiator.

**Mannich and Quaterization on Poly(acrylamide dimer).** The preparation of Mannich derivatives of poly (acrylamide dimer) using formaldehyde and dimethylamine and subsequent quaternization with dimethyl sulfate were carried out as follows: A solution of freeze-dried polymer, 0.5 g in 10.22 g of water was prepared. 0.91 g of 35%  $(\text{CH}_3)_2\text{NH}$  solution was added followed by 0.48 g of 44% HCHO solution. The reaction was carried out at ambient temperature at pH=11 for 6 hrs. and then 0.89 g of  $(\text{CH}_3)_2\text{SO}_4$  was slowly added. After 12 hrs. the Mannich quaternary polymer solution was analyzed (19) and cationic equivalent (CEQ) was found to be 5.14 meq/g. The degree of substitution is defined as  $[\text{CEQ}/3.08 - 1] \times 100\%$  where 3.08 is the theoretical CEQ of 100% quaternization. A 67% quaternization was achieved. The quaternary polymer was dialyzed for 2 days in Spectrapor membrane (m.wt. cut off 2,000) and freeze-dried. The CEQ on the dialyzed product was 2.15.

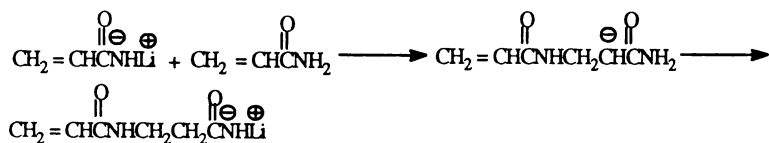
**Kinetic Measurement.** Aliquots of the reaction mixture were removed at various times and analyzed for the residual AMD monomer using a Hewlett Packard 7620 Research Gas Chromatograph. The column was packed with 8'x20 mm 20% Carbowax 20M WA-N-DMCS 60/80 mesh and helium was used as the carrier gas.

**Characterization.** Number average molecular weights were determined by a Knauer Dampf-Druck vapor phase osmometer. GPC analyses were performed using a Perkin-Elmer M601 equipped with  $10^6$ ,  $10^5$ ,  $10^4$ ,  $10^3$  Å styragel columns. Columns were standardized by purified standard VTN-3 samples,  $M_w = 141$ , 13,800, 19,200, 20,200, 28,200;  $\ln M_i = a + bV_i$ , where  $a = 1.545 \cdot 10^8$ , and  $b = 36.2$ . Samples concentrations were 0.1 - 0.5% by weight in hexafluoroisopropanol (0.01 M KOAC). GPC analyses were also performed using Sephadex G-10 and G-25. G-10 and G-25 were packed with cross-linked polysaccharide swollen in 0.1M  $\text{NaNO}_3$  solution.

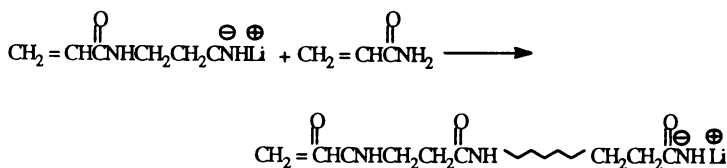
**Flocculation of Bentonite Suspensions.** Bentonite flocculation results for the cationic poly (AMD dimer) samples and commercial cationic polyamine and poly (diallyldimethylammonium chloride) were compared. The standard practice (20)



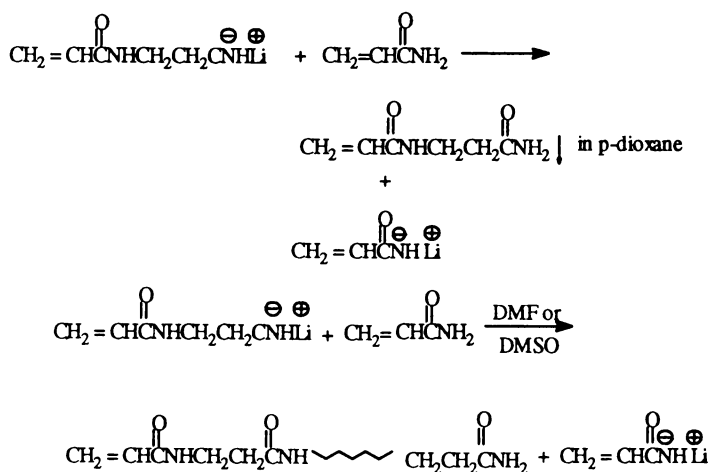
INITIATION.



PROPAGATION



TERMINATION.



CHAIN TRANSFER.

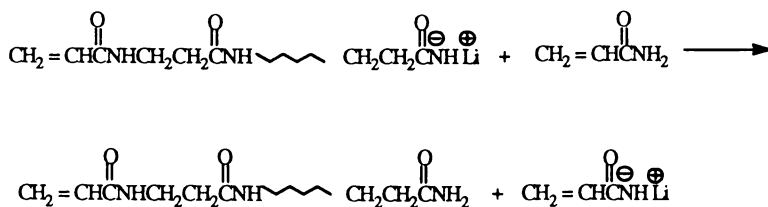


Table I. Synthesis of Vinyl Terminated Poly (beta-alanine) Oligomer

Sample No.	Monomer		Temp. (°C)	Time (hr)	Conversion (%)	$\eta_{inh}^a$	$\bar{M}_n$ by Unsaturation	$\bar{M}_n^c$	$\bar{M}_n$ by NMR	Unsaturation %
	Initiator	Initiator (mole/mole)								
118-2	n-Butyl	21.3	25	24	75	0.040	286		270	106
118-1	sec-Butyl Li	20.9	25	24	75	0.039	289	290	256	113
119-1	t-Butyl Li	20.4	25	22	90	0.032	260	270	231	112
119-3	t-Butyl Li	25.5	25	24	79	----	---		256	---
119-2	t-Butyl Li	20.1	25	40	85	0.046	252		276	91
117-C	Vinyl Li	25.2	25	24	83	0.030	---		234	---
117-B	Vinyl Li	25.2	25	24	90	0.039	430	430	490	88

<sup>a</sup> Inherent viscosities were measured for 1% polymer in IN aqueous NaCl.

<sup>b</sup> Unsaturation was determined by bromine-bromate titration.

<sup>c</sup>  $\bar{M}_n$  was determined by vapor phase osmometry.

**Effect of Temperature on the Conversion of Acrylamide to AMD Dimer and Oligomer.** For organolithium initiated oligomerization of acrylamide in p-dioxane, the relative yield of dimer and oligomer was found to depend strongly on the reaction temperature. Results are shown in (Table II). A large amount of acrylamide dimer is produced in the early stages of the polymerization especially when the lowest polymerization temperatures were used. Therefore, pure dimer is isolated essentially free from oligomer contamination. The concentration of dimer linearly decreased from 80% to 20% as the polymerization temperature was increased from 16°C to 50°C. Correspondingly, the concentration of oligomer linearly increased from 15% to 70%. The overall conversion was ~90%. The reason that dimer can readily be isolated is that acrylamide dimer has a very low solubility in p-dioxane (13). The formation of oligomer occurs predominantly after dimer has precipitated. The molecular weight distribution of oligomer was also found to depend on reaction temperature.  $\bar{M}_w/\bar{M}_n$  increases as the reaction temperature increases. For reaction temperatures between 15°C and 25°C,  $\bar{M}_w/\bar{M}_n$  is about 2 - 3 in an agreement with a step-growth mechanism. However, when the reaction temperature is the range of 30 - 50°C,  $\bar{M}_w/\bar{M}_n > 3$  which may indicate chain branching is occurring. The formation of acrylamide dimer was also shown to depend on the nature of the solvent. DMF or DMSO are solvents for AMD dimer and oligomerization past the dimer stage occurs readily as shown in (Figure 1). (Figures 2 and 3) are typical GPC curves of VTN-3.

**Solvent Effect.** Both the rate of reaction and formation of oligomers strongly depend on solvent. Comparable reactions were carried out in DMSO, DMF, and p-dioxane. t-Butyl Li was used as the initiator under identical reaction conditions in three different solvents. (Figure 4) shows that 80% of the acrylamide monomer has disappeared in 30 minutes in DMSO. In the same experiment, 65% of the monomer has disappeared in DMF. Only 50% of the monomer is converted to oligomer in p-dioxane. After ~1 hour of reaction time, acrylamide dimer starts to precipitate in p-dioxane but remains in solution in DMF and DMSO. A homogeneous phase is obtained throughout the reaction in DMF and DMSO solvents and a heterogeneous phase in p-dioxane.

**Poly (acrylamide dimer).** Homopolymerization of acrylamide dimer produced a relatively low molecular weight polymer. Since higher molecular weights were desired for paper additives and water treating applications, an effort was made to upgrade the yield and molecular weight of this polymer. Initiator types, initiator concentration, temperature, and the reaction time were varied for a series of acrylamide dimer polymerizations in aqueous medium, and the results are summarized in (Table III). Initiator levels of ~15,000 ppm persulfate and 35-75 ppm of metabisulfite resulted in high conversion and acceptable viscosity. Yields dropped off rapidly below 15,000 ppm persulfate and high conversion but low viscosities were obtained when the metabisulfite concentration was increased in contrast to acrylamide. Acrylamide (sample no. 101-4) could be polymerized to a very high molecular weight polymer under similar conditions. This bulk viscosity is about the weight-average molecular weight of greater than  $10^6$  of polyacrylamide (21).

Table II. The effect of Temperature on the Acrylamide Dimer Content and the Molecular Weight<sup>a</sup>

Sample No.	Initiator	Temp. °C	Time (hrs.)	Conv. (%)	AM Dimer <sup>b</sup> Content (%)	Oligomer <sup>c</sup> Content (%)	$\bar{M}_w$	$\bar{M}_n$	$\bar{M}_w/\bar{M}_n$	$\eta_{inh}^d$
58-1	n-BuLi	10	16	98	80	18	-----	-----	-----	0.02
5-1		15	24	85	57	28	7,910	2,900	2.73	0.04
5-5		20	2	50	50	1	-----	-----	-----	-----
5-4		20	24	92	55	37	11,000	3,600	2.99	0.03
5-2		31	24	85	33	52	14,000	4,100	3.39	0.06
5-3		41	24	90	13	76	29,400	5,880	4.49	0.08
6-3	n-BuLi	15	24	85	57	28	6,200	2,600	2.38	0.04
6-1		18	24	83	51	32	3,750	11,000	2.64	0.05
6-4		35	83	83	17	66	22,000	5,600	3.96	0.06
6-2		50	24	85	13	72	21,000	5,970	3.51	0.08
6-5	n-BuLi	16	24	85	71	14	-----	-----	-----	0.03
6-6		25	24	90	52	38	-----	-----	-----	0.05
6-7		35	24	85	36	49	-----	-----	-----	0.06
6-8		45	24	90	21	69	-----	-----	-----	0.07

<sup>a</sup> Reaction conditions: 1). 20g acrylamide, 200 ml p-dioxane, 8.8 ml (1.58M) n-BuLi. 2). 20g acrylamide, 200 ml p-dioxane, 9.5 ml (1.5M) s-BuLi. 3). 20g acrylamide, 200 ml p-dioxane, 6.3 ml (2.30M) t-BuLi.

<sup>b</sup> Acrylamide dimer and oligomer contents calculated from GPC data.

<sup>c</sup> Oligomer molecular weight distribution was calculated from integrated GPC chromatograms.

<sup>d</sup> Inherent viscosities were determined for 1% polymer in 1N NaCl aqueous solution.



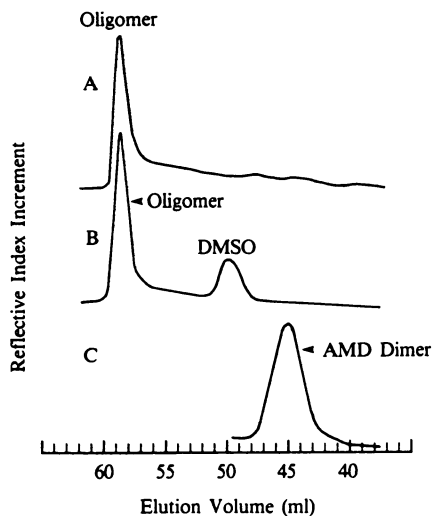


Figure 1. GPC chromatogram of vinyl terminated poly (beta-alanine) oligomer prepared in DMF and DMSO. A. 20 g acrylamide, 200 ml DMF, 6.4 ml t-BuLi (1.8 M). B. 20 g acrylamide, 200 ml DMSO, 6.4 ml t-BuLi (1.8 M). C. acrylamide dimer.

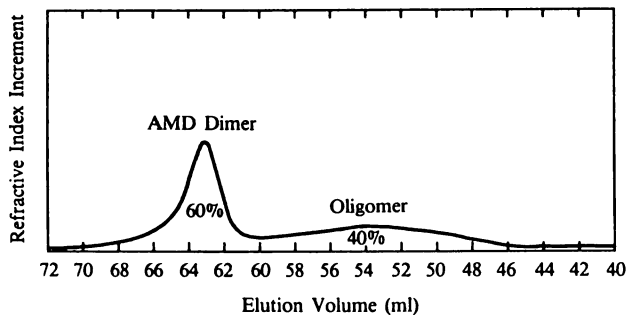


Figure 2. GPC chromatogram of vinyl terminated poly (beta-alanine) oligomer (Perkin-Elmer Styragel Column).

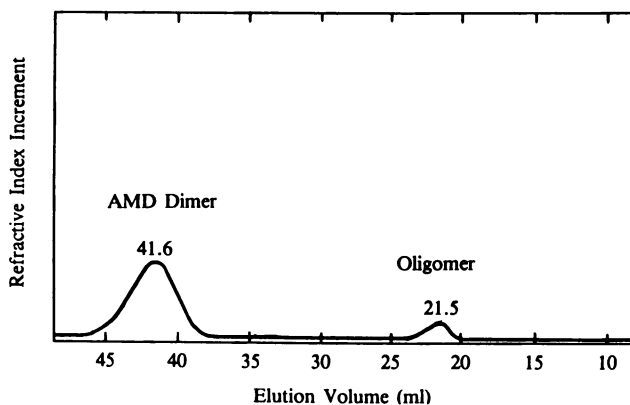


Figure 3. GPC chromatogram of vinyl terminated poly (beta-alanine) oligomer (Sephadex G-10 Column).

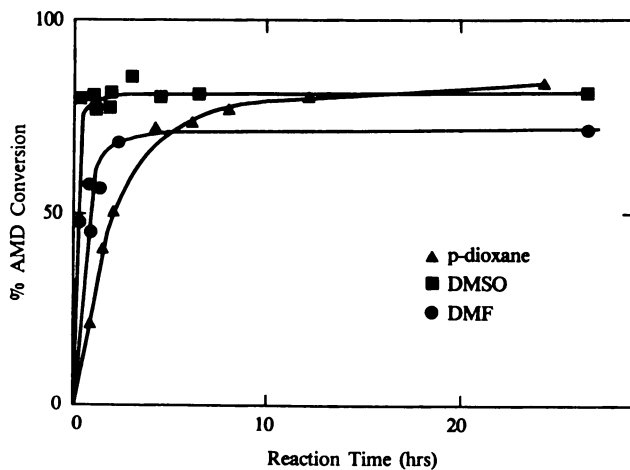


Figure 4. Percent acrylamide conversion to poly (beta-alanine) oligomer as function of time using t-Buli as initiator in different solvents: ■ DMSO ● DMF ▲ p-dioxane.

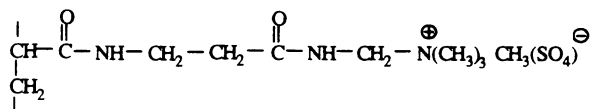
Table III. Homopolymerization of N-2-Carboxyamidoethylacrylamide in Aqueous Solution at pH 6.5-7

Sample No.	(NH <sub>4</sub> ) <sub>2</sub> S <sub>2</sub> O <sub>8</sub> ppm <sup>a</sup>	Na <sub>2</sub> S <sub>2</sub> O <sub>5</sub> ppm <sup>a</sup>	ADVA <sup>b</sup> ppm <sup>a</sup>	Monomer Conc., %	Temp. °C	Time Hrs.	Residual AM Dimer, %	BV <sup>d</sup> (cps)
82-2A	30,000	5,000	---	4	40	6	T <sup>e</sup>	2.25
82-2B	20,000	5,000	---	4	40	6	T	2.10
83-2B	20,000	5,000	---	4	50	6	T	2.10
83-2C	15,000	1,000	---	4	40	6	11	----
84-1A	10,000	175	---	4	40	6	45	----
100-1	15,000	37.5	---	4	40	6	T	620 <sup>e</sup>
100-2	15,000	75	---	4	40	6	T	575
101-1	1,500	37.5	---	4	40	6	L <sup>e</sup>	----
101-4	15,000	37.5	---	4	40	1	10	10,000
55-4	-----	-----	6,300	(acrylamide)	50	6	(acrylamide)	high <sup>f</sup>
97-1	-----	-----	6,000		60	4.5		medium
101-3	-----	-----	1,000		50	6		180

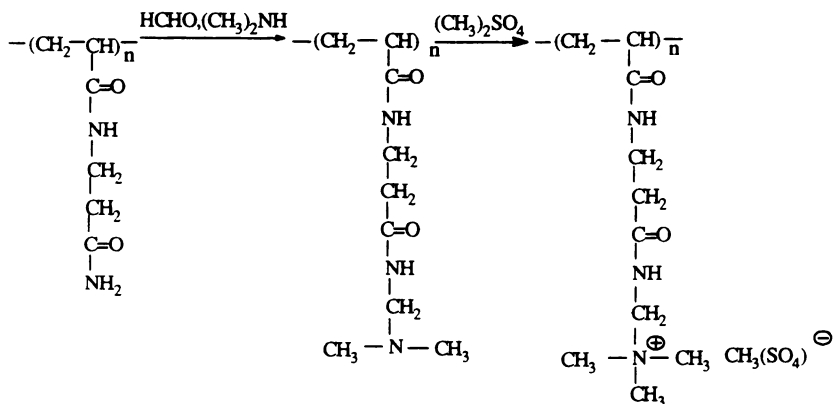
<sup>a</sup> ppm are based on monomer weight.<sup>b</sup> ADVA is 4,4'-azobis(4-cyanovaleric acid).<sup>c</sup> T(trace), L(large). Residual AM dimer determined using GPC.<sup>d</sup> Bulk viscosity.<sup>e</sup>  $\eta_{inh}$  (0.1% polymer in 1M NaCl) = 3.82 after dialyzing and freeze drying.<sup>f</sup>  $\eta_{inh}$  = 5.0.

A water soluble azo initiator, 4,4'-azobis (4-cyanovaleric acid) (ADVA) was also used in some experiments. Molecular weight decreased with decreasing ADVA concentration. Additional experiments confirmed that higher molecular weights could be achieved with ADVA than with the aqueous redox system.

**Mannich Quaternary of Poly (acrylamide dimer).** Poly (acrylamide dimer) after conversion to the Mannich derivative and quaternization, contained cationic functions separated from the polymer backbone by an 8-atom spacer group:



The preparation of Mannich derivatives and subsequent quaternization with dimethyl sulfate was investigated for poly (acrylamide dimer) covering a range of molecular weights.



Reaction conditions and cationic equivalent data are shown in (Table IV). Mole ratios of polymer, formaldehyde, dimethylamine and dimethylsulfate were 1:1:1:1, 1:1:2:2 and 1:2:2:2. The degree of quaternization increased with an increase in the formaldehyde/polymer ratio, but increasing the DMA:HCHO ratio had little effect. Cationic equivalent data per unit weight of cationic poly (AMD dimer) (non-isolated samples) and per unit weight of cationic poly (AMD dimer) (isolated after dialysis) indicated that a cationicity of at least 70% was achieved.

**Flocculation of Bentonite Suspensions Using Cationic Poly (acrylamide dimer).** Bentonite flocculation results for the poly (AMD dimer) samples and commercial cationic polyamine and poly (diallyldimethylammonium chloride) are

Table IV. Preparation of Cationic Poly (Acrylamide Dimer)

Sample No.	Polymer (g)	$\eta_{inh}^a$	H <sub>2</sub> O (g)	HCHO (g)	(CH <sub>3</sub> ) <sub>2</sub> NH (g)	(CH <sub>3</sub> ) <sub>2</sub> SO <sub>4</sub> (g)	CEQ <sup>b</sup>	CEQ <sup>c</sup>	DQ <sup>d</sup>
98-1	0.93	2.23	19.42	0.20	0.59	1.68	3.48		13
98-2	0.96	2.50	20.13	0.20	0.61	1.71	3.36		9
103-1	0.50	3.83	12.00	0.10	0.16	0.44	4.20		36
103-2	0.50	3.78	12.00	0.10	0.16	0.44	4.48		45
103-3	0.50	4.41	12.00	0.10	0.16	0.44	2.98		--
106-2	0.50	0.95	10.22	0.21	0.32	0.89	5.39		75
106-3	0.50	0.95	10.47	0.21	0.32	0.89	5.24		70
106-4	0.50	0.95	10.22	0.21	0.32	0.89	5.41	0.90	76
107-1	0.50	3.78	12.00	0.10	0.16	0.44	4.46	2.50	45
107-2	0.50	3.78	10.22	0.21	0.32	0.89	5.00	2.60	62
107-3	0.50	2.50	10.22	0.21	0.32	0.89	5.29	2.15	72
107-4	0.50	4.41	10.22	0.21	0.32	0.89	5.14		67

<sup>a</sup>: 0.1% polymer in aqueous 1M NaCl.

<sup>b</sup>: Cationic equivalent per gram of backbone polymer.

<sup>c</sup>: Cationic equivalent per gram of quaternary poly (acrylamide dimer).

<sup>d</sup>: Quaternary polymers were isolated and freeze-dried after dialysis.

<sup>e</sup>: Degree of quaternization was defined as  $[\text{CEQ}/(3.08 - 1)] \times 100\%$  where 3.08 is the theoretical CEQ assuming 100% quaternization.

reported in (Table V). Standard practice uses the dosage in ppm of polymer solution required to reduce the slurry transmittance to 20% of its initial value,  $T_{20}$ , as a measure of the relative efficiency. Because the true weight percent of cationic poly (AMD dimer) could not readily be determined for each of the experimental polymers,  $T_{20}$  dosages could not be used to consistently evaluate relative efficiency. Since one of the objectives of this work was to determine flocculation efficiency inherent to the poly dimer structure,  $T_{20}$  and cationic equivalent data were combined in order to evaluate relative efficiency at constant cationicity. The results of this calculation are shown in column 5 in Table V. All of the experimental polymers were superior to polyamine on a molar charge basis. Efficiency tended to increase with decreasing molecular weight and increasing charge density. Lowest molecular weight samples 106-3, 106-4, 161-3 were superior to polyDADM. Limited stability tests showed that performance of cationic poly (AMD dimer) begins to decrease after two weeks at room temperature. However, the results of Series II demonstrate that cationic poly (AMD dimer) is generally less effective than the commercial polymers on an equivalent weight basis. An exception is the lowest molecular weight sample 161-3 which was found to be much more effective than any of the commercial polymers on a molar charge and equivalent weight basis.

The adsorbed charge distribution over the substrate surface by the low molecular weight cationic polymers should be more even than the charge distribution by high molecular weight chains. Therefore, loop dimensions of the adsorbed chain must be very small in comparison to the substrate hydrodynamic size. Consequently, the cationic polymer has folded down closer to the substrate particle surface. Such contacts will be prevented by the electrical repulsion between the substrate particles, thus flocculation would take place.

The flocculation of suspensions containing either bentonite clay or model polystyrene substrate, using commercially available cationic polyelectrolytes (22), showed that in most cases the dose of the flocculant was independent of its molecular weight. The charge density was the predominant factor in correlating with the optimum dose. However, the size and strength of a floc is dependent on the molecular weight of the polymer.

The effect of charge spacing between the quaternary nitrogens along the polymer chain on flocculation has not yet been studied. A wide range of molecular weights, and especially the very low molecular weight cationic polyelectrolytes on flocculation has not yet fully investigated. These will be explored as a future research direction.

## Conclusions

Water soluble vinyl terminated oligomeric poly (beta-alanine) was synthesized with one vinyl group per chain. The reaction time and temperature were varied to control the molecular weight, molecular weight distribution, and AMD dimer content. AMD dimer and the oligomeric the VTN-3 were fully characterized by NMR, GPC, viscosity, vapor phase osmometry, and unsaturation determination. AMD dimer was homopolymerized in aqueous medium. Poly (AMD dimer) was successfully converted to the Mannich derivative and quaternary product. This

Table V. Flocculation of Bentonite Suspensions Using Cationic Poly (acrylamide Dimer)

Ref. No.	Dosage at $T_{20}$ (ppm)	CEQ <sup>a</sup> (meq/g)	$\eta_{inh}$ <sup>b</sup>	Efficiency (%) <sup>c</sup>
<b>Series I</b>				
98-1	2.25	3.48	2.23	141
98-2	2.83	3.36	2.50	116
103-1	2.05	4.20	3.83	128
103-3	3.00	2.98	4.41	126
Polyamine	1.75	6.30		100
<b>Series II</b>				
107-1-D	6.60	0.90	3.78	141
107-2-D	2.50	0.50	3.78	135
107-3-D	2.10	2.60	2.50	154
107-4-D	3.35	2.15	4.41	117
Polyamine	1.35	6.25		100
<b>Series III</b>				
161-3	0.50	5.40	0.50	296
106-2	0.82	5.39	0.95	180
107-1	1.30	4.46	3.78	138
107-2	0.95	5.00	3.78	168
107-4	1.22	5.14	4.41	128
Polyamine	1.28	6.25		100
<b>Series IV</b>				
106-3	0.90	5.24	0.94	167
106-4	0.90	5.40	0.95	159
Polyamine	1.24	6.21		100
Poly(DADM)	1.12	4.68		147

<sup>a</sup> CEQ values are based on unit weight of backbone polymer except for dialyzed samples in Series II.

<sup>b</sup> 1% polymer in aqueous 1M NaCl.

<sup>c</sup> Efficiency =  $[\text{Dosage}(T_{20}) \times \text{CEQ}] \times 100\% / [\text{Dosage}(T_{20}) \times \text{CEQ}_r]$ ; r is polyamine.

new cationic water soluble polyelectrolyte has been shown to be an effective organic flocculant for the clarification of bentonite.

### Acknowledgments

The authors would like to thank Dr. J. Miller for viscosity, GPC and molecular weight measurements, Mr. Ray H. Anderson for unsaturation determination, Dr. J. Lancaster and Ms. M. Yao for NMR analysis, Dr. Fred Halverson and Ms. Marybeth Gutafason for flocculation studies, also Ms. Inez Minor and Ms. Valerie D. McNeil for the manuscript typing.

### Literature Cited

1. Noshay, A.; McGrath, J. E. *Block Copolymers*; Academic Press: New York, 1977.
2. *Cationic Graft Copolymerization*; Kennedy, J. P. Ed.; *J. Appl. Polym. Symp.* No. 30; John Wiley & Sons: New York, 1977.
3. Mark, H. F.; Overberger, C. G. *Encyclopedia of Polym. Sci. and Eng.*; John Wiley & Sons: New York, 1985; Vol. 2, p.324; 1986; Vol. 5, p.416.
4. *Macromer, Monomer Presentation*; GPC International Inc.: Englewood Cliffs, NJ, 1979.
5. Entelis, S. G.; Evreinov, V. V.; Gorshkov, A. V. *Adv. Polym. Sci.* 1985, Vol. 76, 129.
6. Kennedy, J. P.; Huang, Sun-Yi; Smith, R. R. *J. Macromol. Sci.* 1980, A14(7), 1085.
7. Matlack, A. S. U. S. Pat. 2,672,480, 1954.
8. Breslow, D. S.; Hulse, G. E.; Matlack, A. S. *J. Am. Chem. Soc.* 1957, 79, 3760.
9. Bush, L. W.; Breslow, D. S. *Macromolecules* 1968, 1, 189.
10. Ogata, N., *Makromol. Chem.* 1960, 40, 55.
11. Tani, H.; Oguni, N.; Akiraki, I.; *Makromol. Chem.* 1964, 76, 82.
12. Trosarrelli, L.; Guaita, M.; Camino, G. *J. Polym. Sci., C* 1969, 22, 721.
13. Leoni, A.; Franco, S.; Polla, G. *J. Polym. Sci.* 1968, A-1, 6, 3187.
14. Kobayashi, Y. *J. Polym. Sci., Polym. Lett. Ed.* 1976, 14, 299.
15. Moore, D. R.; Mathias, L. J. *J. Polym. Mater. Sci. Eng.* 1985, 53, 693.
16. Moore, D. R.; Mathias, L. J. *J. Appl. Polym. Sci.* 1986, 32 (8), 6299.
17. Huang, Sun-Yi, *Polym. Prepr.* 1983, Vol. 24, No. 2, 60.
18. Tarvin, R. F, Cytec Industries, personal communication.
19. Ueno, K.; Kina, Ken'yu, *J. Chem. Ed.* 1985, 62 (7), 627.
20. Huang, Sun-Yi; Fisher, M. M. U. S. Pat. 4,247,432, 1981.
21. *Polyacrylamide, New Product Bull. Collective Vol. III*, No. 34; Am. Cyanamid Co.: Stamford, Ct., 1955.
22. Dentel, S. K. *Crit. Rev. Environ. Control* 1991, 21 (1), 41.

RECEIVED August 6, 1993



## Chapter 10

# Molecular-Weight Distributions of Water-Soluble Polyelectrolytes

## Gel Permeation Chromatography Spectrophotometry—Low-Angle Laser Light Scattering

Ellen M. Meyer and Stephen R. Vasconcellos

Betz Industrial, 4636 Somerton Road, Trevose, PA 19053-6783

Recent developments in the use of gel permeation chromatography (GPC) for the determination of the molecular weight distributions of water soluble cationic polyelectrolytes are discussed. Absolute molecular weight measurements were made using a low-angle laser light scattering (LALLS) spectrophotometer. The polymers studied included five samples of an epichlorohydrin dimethylamine (epi/dma) copolymer with weight average molecular weights ranging from  $10^3$  to  $10^5$ , and four samples of polymeric diallyldimethylammonium chloride (dadmac) with weight average molecular weights ranging from  $10^4$  to  $10^5$ . These polymers are typically used for water clarification in waste treatment applications.

A correlation exists between the molecular weight and activity of polymers in wastewater treatment applications, but there is insufficient data to determine the effect of the molecular weight distribution on performance. Although the techniques used to determine the molecular weight distribution of polymers have been established for some time, the majority of the research has been conducted on non-aqueous polymers. Since most of the polymers used for wastewater treatment are water soluble, and often contain anionic or cationic functionalities, this research was an attempt to improve the database of molecular weight distribution information available for this important class of polymers.

The cationic polymers, epichlorohydrin/dimethylamine (epi/dma) and diallyldimethylammonium chloride (dadmac), are well known for their ability to clarify wastewater (1). Previous work with these polymers has been performed with gel permeation chromatography (GPC) using calibration standards chemically different from the polymers being characterized (Bauer, D.S., Betz Chromatography Services, unpublished data.). In the present study, GPC was performed in

0097-6156/94/0548-0131\$06.00/0  
© 1994 American Chemical Society

conjunction with low angle laser light scattering (LALLS) to obtain absolute molecular weight distributions.

## Experimental

Differential refractive indices ( $dn/dc$ ) were measured with the LDC/Milton Roy Chromatix KMX-16 differential refractometer in the same solvent system as that used for the LALLS experiments. Four different concentrations of polymer were used and the differential refractive index values were averaged. If the  $dn/dc$  values changed with concentration, the y-intercept of a plot of  $dn/dc$  vs concentration was used in the molecular weight calculations.

Preliminary to running the GPC/LALLS experiments, the weight average molecular weights of the polymers were measured by using static LALLS in 1 M NaCl. These experiments were conducted using the Chromatix KMX-6 instrument from LDC/Milton Roy. The system parameters are contained in Table I. Two of the polymer samples were also measured in the 0.2 M LiNO<sub>3</sub>/0.1% TFA solvent system used for the GPC/LALLS experiment.

The GPC/LALLS instrumentation configuration consisted of an LDC Analytical ConstaMetric 3200 Bio Solvent Delivery System, Rheodyne Model 7125 Syringe Loading Sample Injector, LDC/Milton Roy Chromatix KMX-6 Low Angle Light Scattering Photometer, and LDC Analytical RefractoMonitor IV Refractive Index Detector. Data were collected and processed with the use of the LDC Analytical PCLALLS software package. Synchropak CATSEC columns were used in the following series: CATSEC 300 A (50 mm x 7.8 mm) guard column, CATSEC 4000 A (300 mm x 7.8 mm) column, CATSEC 300 A (30 mm x 7.8 mm) column.

The injector sample loop volume was calibrated by injecting a known concentration of sodium benzoate into a volumetric flask, filling to the mark, and measuring the UV-VIS absorbance. The absorbance was compared to a calibration curve to obtain the volume of injected sodium benzoate. The interdetector volume was calibrated by measuring the time difference between the LALLS and RI detector responses for an unfractionated polymer. The pump was calibrated daily by measuring the time required to fill a volumetric flask.

In order to avoid complications from impurities in the sample, the dadmac samples were dialyzed to remove any residual synthesis process salts. The solvent systems were prepared using doubly distilled water. For the GPC/LALLS experiments, a mobile phase of 0.1% trifluoroacetic acid (TFA) and 0.2 M LiNO<sub>3</sub> was chosen (Bauer, D.S., Betz Chromatography Services, unpublished data.). D. J. Nagy et al. have shown universal calibration behavior with cationic polymers in a similar solvent system (0.1% TFA/0.20 N NaNO<sub>3</sub>) using CATSEC columns (2).

The intrinsic viscosities were measured by the Chromatography Services Group at Betz using the Schott-Gerate Automatic Viscometer.

## Results

**Epi/dma Polymers.** Table II summarizes the numerical results for the epi/dma polymers. From Table II, it is evident that the Mw values obtained from the GPC/LALLS experiments with 0.2 M LiNO<sub>3</sub>/0.1% TFA, are consistently lower than

**Table I. LALLS System Parameters**

	Static LALLS	GPC/LALLS
Attenuator Constant	1.7703e-8	1.7703e-8
Fieldstop	0.15	0.15
Annulus	6-7 degrees	6-7 degrees
Cell Length	15 mm	4.93 mm
Solvent	1.0 M NaCl	0.2 M LiNO <sub>3</sub> /0.1% TFA
Refractive Index	1.343	1.335
Scattering Angle	4.835	4.865
1/(sigma <sup>l</sup> )	881.33	877.36
Interdetector Volume		57 microliters
Flow	~0.2 mL/min	~0.6 mL/min
Loop Volume		60.5 microliters

**Table II. Epi/dma Results**

Polymer Sample	Intrinsic Viscosity	Static LALLS Mw	GPC LALLS Mw	Mz	Mn
A	0.22	324,000(+/-4,000)	235,000(+/-20,000)	1,810,000(+/-280,000)	15,300(+/-980)
B	0.16	43,800(+/-500)	36,100(+/-3,200)	131,000(+/-17,000)	10,800(+/-950)
C	0.13	30,100(+/-400)	19,700(+/-2,200)	41,100(+/-8,200)	6,900(+/-2,600)
D	0.05	8,800(+/-600)	4,180(+/-420)	15,000(+/-2,200)	1,880(+/-220)
E	0.03	3,510(+/-20)	2,350(+/-590)	3,280(+/-650)	1,450(+/-520)

the values obtained using static LALLS with 1 M NaCl. Since the hydrodynamic volume of a polymer may be influenced by the ionic strength of the solvent (3,4), it is not surprising that the values obtained from these two experiments should differ. Subsequent static LALLS measurements using 0.2 M LiNO<sub>3</sub>/0.1% TFA indicate that lower weight average molecular weight values are obtained with this solvent system compared to the NaCl solvent system (Table III). With the same solvent system, the GPC/LALLS and static LALLS values are within experimental error.

Figures 1-5 show the unusual curve shapes seen for some of these polymers. The LALLS curve of Polymer A seems to indicate that the polymer is being excluded from the column pores, but the sharp rise in the LALLS peak is not duplicated in the RI peak. Polymers D and E appear to be mixtures of different low molecular weight batches. Polymer D has three distinct peaks in the LALLS curve and a shoulder on the RI curve. The LALLS data of Polymer E show one large peak and another small peak with a much higher molecular weight. The RI data does not show this extra peak, possibly because the concentration is too low. Both Polymers D and E are difficult to measure using this method because the LALLS technique is not very sensitive to low molecular weight polymers. Polymers B and C have nearly gaussian curve shapes.

**Dadmac Polymers.** Table IV summarizes the results for the dadmac polymers. Figures 6-9 show typical chromatograms for these samples. As with the epi/dma polymers, the weight average molecular weight values from the LiNO<sub>3</sub> solvent system are lower than the values obtained using NaCl (Table III). Except for the very low molecular weight sample, E, the reproducibility of the epi/dma polymers was fairly good (+/- 10%) from run to run, and from day to day. The dadmac polymer data showed greater variation and concentration dependence. M<sub>z</sub> and M<sub>w</sub> increased with increasing concentration, while M<sub>n</sub> decreased. The solvent system for this particular polymer may not be optimized. Future work will include the use of different solvent systems to obtain more consistent, reproducible results.

**Intrinsic Viscosities.** Figure 10 shows the correlation between intrinsic viscosity and weight average molecular weight. A greater increase in intrinsic viscosity is seen with increasing molecular weight for the dadmac polymers, compared to the epi/dma polymers. This Figure also shows the trend toward higher molecular weight values measured in 1 M NaCl (solid symbols) compared to 0.2 M LiNO<sub>3</sub>/0.1% TFA (hollow symbols). For both the epi/dma and dadmac polymers, the log of molecular weight is nearly linear with the log of intrinsic viscosity, but the data show some curvature. This curvature may be due to changes in the polymer conformation with increasing molecular weight. The linear correlation coefficients and the Mark Houwink constants are summarized in Table V. The Mark Houwink constants for the two solvent systems are within experimental error of each other and of the theoretical range predicted by Flory (5).

Table III. Comparison of Different Solvent Systems

Polymer Sample	1 M NaCl	0.2 M LiNO <sub>3</sub> /0.1% TFA	0.2 M LiNO <sub>3</sub> /0.1% TFA
	Static LALLS	Static LALLS	GPC/LALLS
C	30,100 (+/-400)	20,400 (+/-400)	19,700 (+/-2,200)
X	337,000 (+/-14,000)	213,000 (+/-18,000)	234,000 (+/-19,000)

Table IV. Dadmac Results

Polymer Sample	Intrinsic Viscosity	Static LALLS	GPC LALLS	Mz Mn
		Mw	Mw	
W	0.99	703,000(+/-7,000)	418,000(+/-148,000)	952,000(+/-476,000)
X	0.90	337,000(+/-14,000)	234,000(+/-19,000)	716,000(+/-66,000)
Y	0.52	191,000(+/-1,000)	73,500(+/-9,000)	132,000(+/-18,000)
Z	0.15	15,700(+/-800)	11,900(+/-3,400)	19,800(+/-9,000)

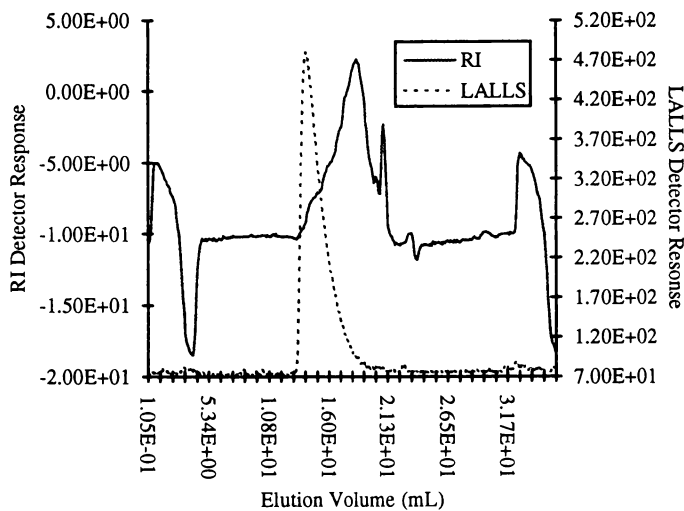


Figure 1. 1% A

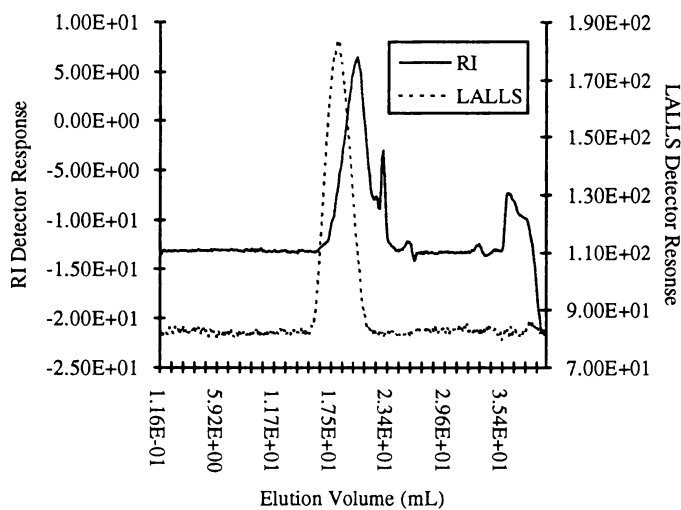


Figure 2. 1% B

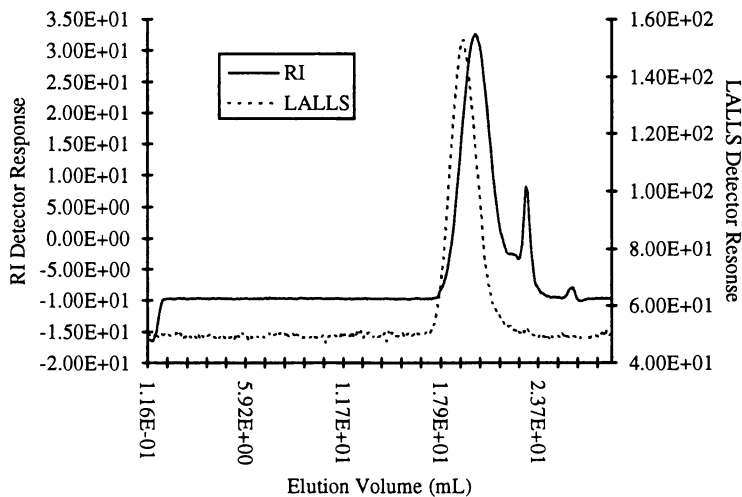


Figure 3. 2% C

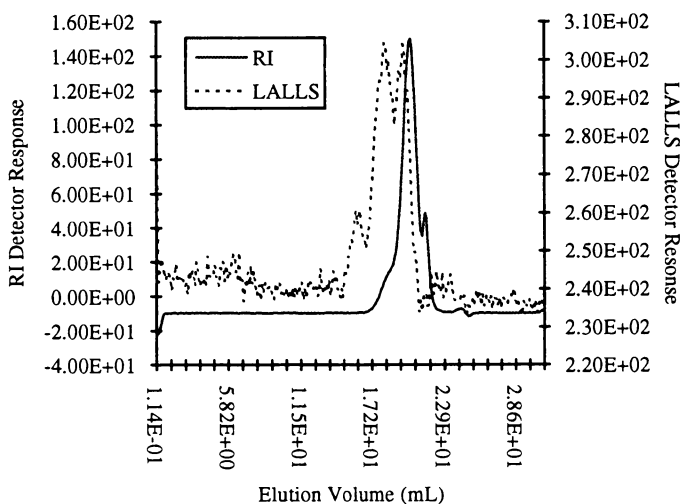


Figure 4. 4% D

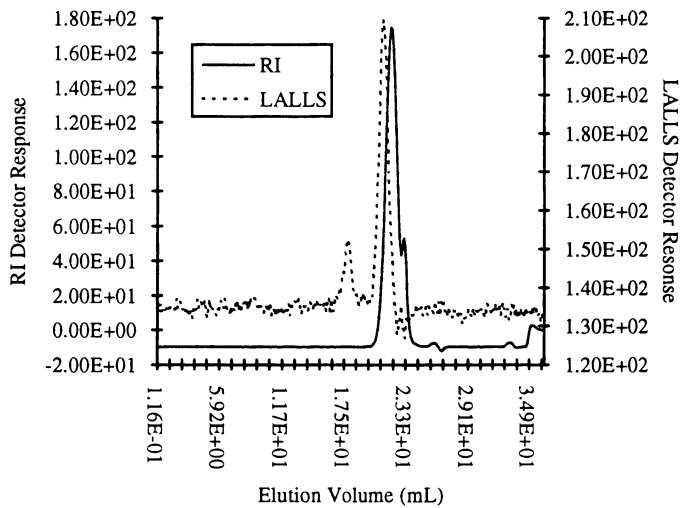


Figure 5. 4% E

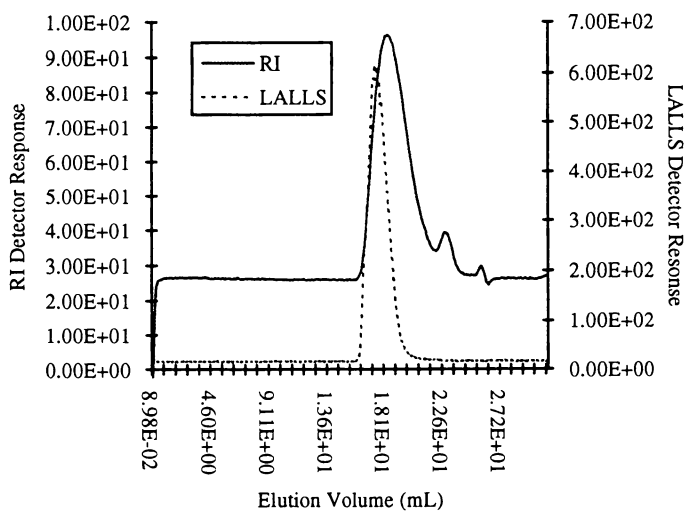


Figure 6. 1.5% W



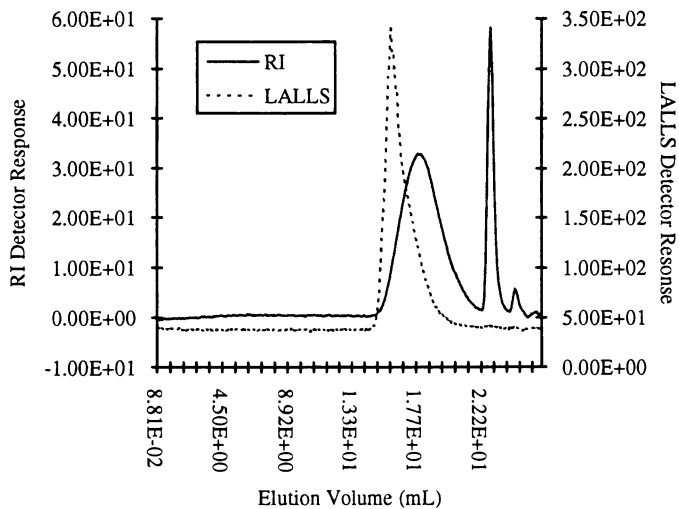


Figure 7. 1% X

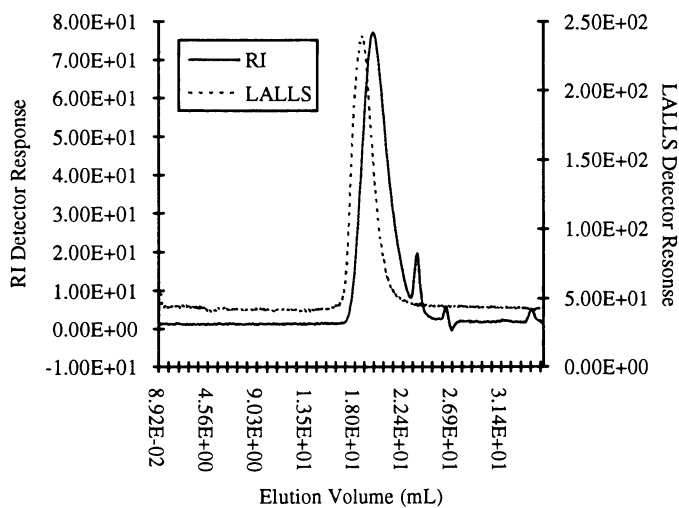


Figure 8. 1.5% Y

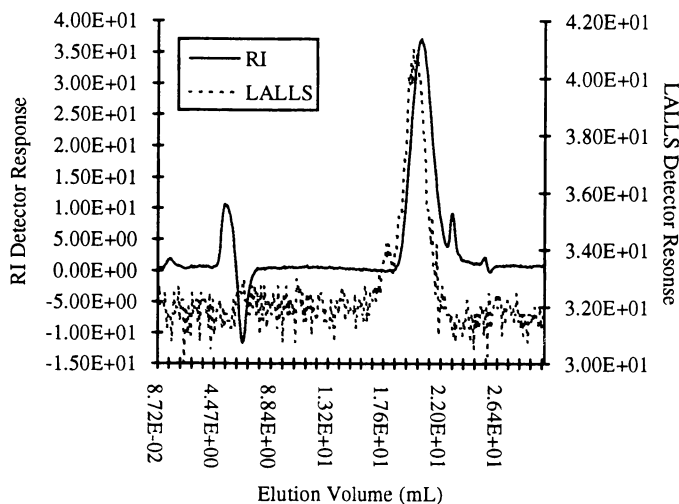


Figure 9. 3.5% Z

Table V. Least Squares Analysis of Log  $[\eta]$  vs Log Mw

Polymer	Static LALLS	GPC/LALLS	Static LALLS	GPC/LALLS
	1 M NaCl EPI/DMA	0.2 M LiNO <sub>3</sub> EPI/DMA	1 M NaCl DADMAC	0.2 M LiNO <sub>3</sub> DADMAC
a	0.459 (+/-0.093)	0.434 (+/-0.082)	0.521 (+/-0.055)	0.548 (+/-0.063)
Log (K)	-3.06 (+/-0.42)	-2.87 (+/-0.35)	-3.01 (+/-0.29)	-3.02 (+/-0.32)
corr. coeff.	0.94	0.95	0.99	0.99

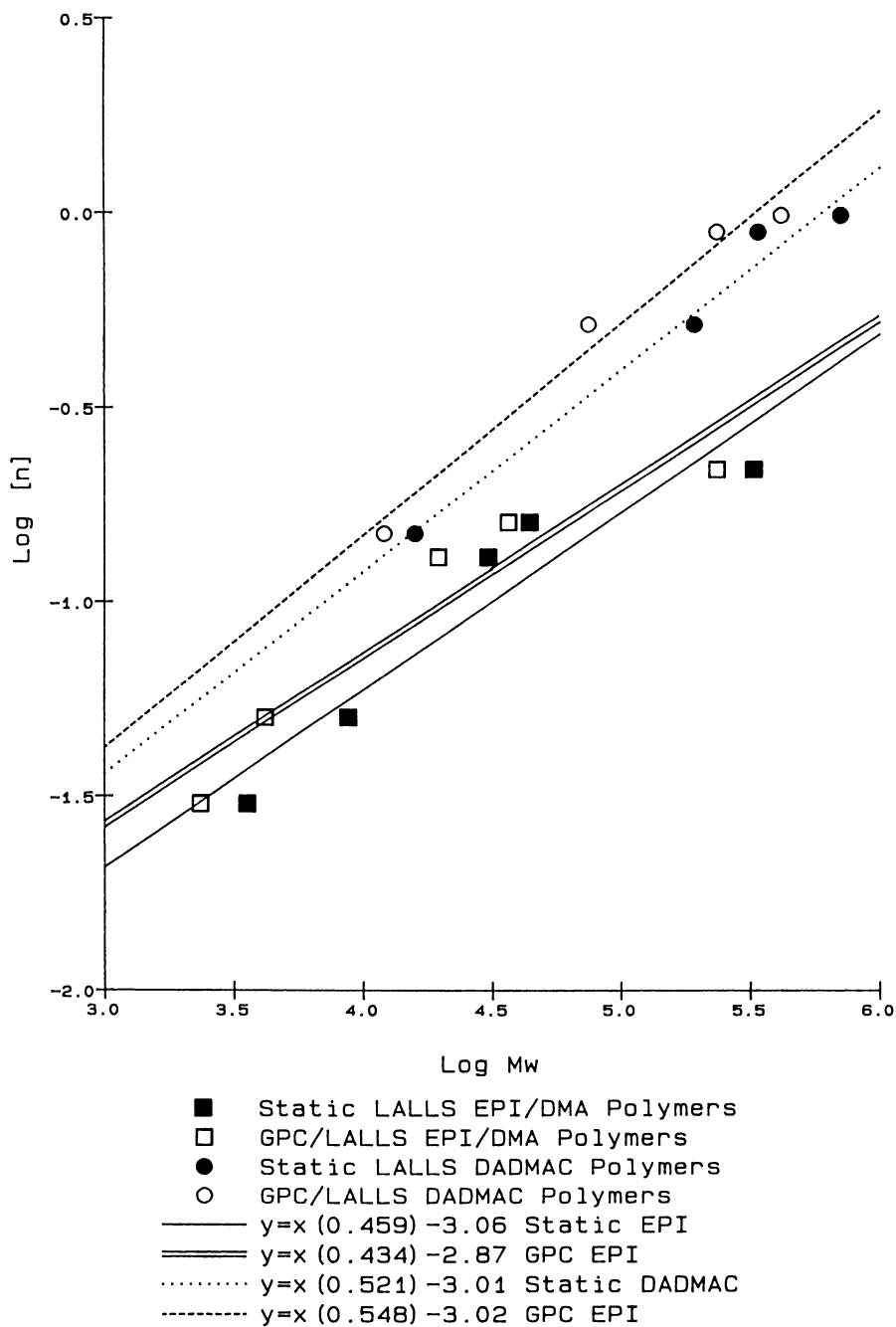


Figure 10. Intrinsic viscosity as a function of molecular weight, EPI/DMA and DADMAC polymers

## Discussion

For static LALLS, 1.0 M NaCl was chosen as the solvent for two reasons: consistency with historical data generated on intrinsic viscosity measurements, and to minimize polymer extension. It is well established that in the presence of sufficient electrolyte polyelectrolytes will behave as neutral macromolecules. The solvent system chosen for GPC/LALLS was based on two criteria as well: the elimination of ion exclusion effects and the minimization of column corrosive effects caused by the presence of chloride ions (6).

The static LALLS  $M_w$  values measured in 1 M NaCl are higher than those generated by static LALLS in 0.2 M  $\text{LiNO}_3/\text{TFA}$  or GPC/LALLS in 0.2 M  $\text{LiNO}_3/\text{TFA}$  (the latter two are in agreement), but comparison of the 'a' constants for the Mark Houwink equation do not indicate any coil expansion as might be expected. A possible explanation may involve comparison of both the concentration and the nature of the solvent system.

When a salt is added to a polyelectrolyte solution, the counterions in the coils screen the cationic sites and the electrostatic interactions cause a reduction of the hydrodynamic dimension of the polymer. Based on these effects, the more highly concentrated 1 M NaCl solution is expected to exhibit a lower  $M_w$  than that measured in 0.2 M  $\text{LiNO}_3$ . It has also been shown by Boussouira et al. (7) that for cationic ammonium copolymers, increased shielding of the polyion occurs when  $\text{NO}_3^-$  is used relative to  $\text{Cl}^-$ . This behavior was in agreement with the affinity order for an ammonium type anion exchanger. The increased shielding would result in a more tightly coiled polymer, which would manifest itself as lower  $M_w$ . Coupled with the effects the TFA and lower pH, the increased shielding ability of  $\text{NO}_3^-$  may account for the lower  $M_w$  measured in this solvent system. The competing effects of the concentration and the nature of the solvent system may then explain why the Mark Houwink constants for these two solvent systems are nearly identical. The influence of the solvent choice on the  $M_w$  will be explored in a future publication.

## Conclusions

The technique of GPC/LALLS can be used to measure the molecular weight distribution of water soluble cationic polyelectrolytes typically used for industrial water treatment processes. Weight average molecular weights calculated from the GPC elution curves for epi/dma and dadmac polymers in 0.2 M  $\text{LiNO}_3/0.1\%$  TFA are consistently lower than those measured using 1 M NaCl. The different salts used in these two experiments are postulated to contribute to this effect.

## Acknowledgments

The authors would like to acknowledge Dean S. Bauer of the Betz Chromatography Services Group for developing the buffer system used in these experiments, and thank him for his invaluable assistance throughout this project.

**Literature Cited**

- (1) *Betz Handbook of Industrial Water Conditioning*; Moore, B. C., et al., Eds.; Ninth Edition; Betz Laboratories, Inc.: Treose, PA, 1992; pp 24-25.
- (2) Nagy, D. J.; Terwillinger, D. A.; Lawrey, B. D.; Tiedge, W. F. *In International GPC Symposium 1989 Proceedings*; Waters/Millipore Corporation: Milford, MA, 1989; pp 637-662.
- (3) Potschka, M. J. *Chromatography* **1988**, *441*, pp 239-260.
- (4) Herold, M. *American Laboratory* **1993**, *March*, pp 35-38.
- (5) Flory, P. J. *Principles of Polymer Chemistry*; Cornell University Press: Ithaca, NY, 1953; pp. 280, 606.
- (6) Gooding, D. L.; Schmuck M. N.; Gooding, K. M. *J. Liq. Chromatogr.* **1982**, *5*, 2259.
- (7) Boussouira, B.; Ricard, A.; Audebert, R. *J. Poly. Sci.: Part B* **1988**, *26*, 649-661.

RECEIVED August 6, 1993

## Chapter 11

# Chromatographic Characterization of Acrylic Polyampholytes

C. S. Patrickios, S. D. Gadam, S. M. Cramer, W. R. Hertler, and  
T. A. Hatton

Department of Chemical Engineering, Massachusetts Institute  
of Technology, Cambridge, MA 02139

The adsorption properties of synthetic polyampholytes based on methacrylic acid were investigated by gradient and frontal techniques on a strong anion-exchange column. These polyampholytes are of well-defined size (4,000 Da) and composition, contain low levels of impurities, and include random, diblock and triblock copolymers. While the random copolymers show no retention in the gradient elution and low adsorption in the frontal experiments, the block copolymers are strongly retained and adsorbed at large amounts. The diblock polyampholyte, which does not form micelles, exhibits similar adsorption properties as the triblock polyampholytes which form micelles. This suggests that the micellar character of the triblocks does not inhibit or reduce adsorption; on the contrary, the higher (than the single chain) micellar charge may provide a greater driving force for polymer adsorption.

Ion-exchange displacement chromatography of proteins is a separation technique in which a mixture of proteins is adsorbed on the column and subsequently displaced by a polyelectrolyte of higher column affinity, the displacer. This technique results in concentrated protein fractions and is therefore particularly suitable for separations of mixtures in which the desired proteins occur in very low concentrations. As displacement chromatography is gaining popularity, the quest for more efficient displacers is becoming necessary (*1*). We recently synthesized low-molecular-weight block polyampholytes based on methacrylic acid (Patrickios et al., MIT, submitted for publication). Initial experiments showed that these polymers can successfully displace and separate protein mixtures in ion-exchange columns. Most importantly these polymers possess two novel features: the column regeneration can be accomplished either by pH change or salinity increase, and any polymer contaminating the last protein fraction can be precipitated at the isoelectric point of the polymer.

These polyampholytes contain up to four different methacrylic residues presented in Figure 1: methacrylic acid (Ac) which can be negatively charged and has a pK of 5.4 (*2*), dimethylaminoethyl methacrylate (B) which can be positively charged and has a pK of 8.0 (*2*), methyl methacrylate (M) which is neutral and hydrophobic, and phenylethyl methacrylate (P) which is neutral and more hydrophobic than methyl methacrylate. The Group Transfer Polymerization (GTP) technique used for the

0097-6156/94/0548-0144\$06.00/0  
© 1994 American Chemical Society

synthesis resulted in polymers with polydispersities as low as 1.3 and high composition homogeneity. The molecular weight of the polyampholytes is approximately 4,000 Da, with the exception of one polymer which is 15,000 Da. One neutral and one base-rich random polyampholytes were also synthesized. One polyampholyte is a neutral diblock (MW = 2,500 Da) and the rest are ABC triblocks with different acid/base ratio, hydrophobicity, and block sequence. Table I, in the Results and Discussion section, gives the composition and sequence of most of our copolymers. Both the diblock and the triblock copolymers precipitate around the isoelectric point. Light scattering studies revealed that at intermediate pH (=3-10) the triblocks, not the diblock, form micelles with hydrodynamic size larger than 10 nm. A steady-state pyrene fluorescence study on Polymer 6 (Table I) at pH 4.5 indicated a very low critical micellar concentration (below 0.1mg/mL) suggesting that, at the polymer concentrations employed in this study, typically 10 mg/mL, the triblock polyampholytes occur as micellar aggregates rather than free chains.

The aim of this study is to investigate the chromatographic behavior of these novel polyampholytic displacers in the absence of proteins. Most of the experiments were performed at pH 8.5 at which all of the polymers are soluble. The polymer parameters determined are the adsorptive capacity, the characteristic charge, and the steric factor ( $\beta$ -6). The characteristic charge is determined as the number of ionic bonds that a polymer forms with the stationary phase. The steric factor is the number of inaccessible column sites per polymer molecule at maximum (lowest salt concentration) column saturation.

## Experimental

An analytical Waters Ion Exchange column of internal diameter 5 mm was packed to a length of 39 mm with 8  $\mu$ m strong anion exchange (quaternary methylamine) beads of 100 nm average pore size. The same column was used for both the gradient elution and the frontal experiments. The equilibration buffer was Tris, typically at pH 8.5 and containing 50 mM Cl<sup>-</sup>. A Waters Maxima 820 workstation was used for data acquisition.

**Gradient Elution.** A linear 10 min-gradient from 0.2 to 1.0M NaCl was applied at a flow rate of 0.5 mL/min using a Waters 600 Multisolvant Delivery System. The gradient delay was 9 min (due to the volume of the mixing chamber) and the dead volume of the column was 0.6 mL. A Waters 481 Lamda-Max LC Spectrophotometer was used to monitor the column effluent at 240 nm. It was not convenient to employ the wavelength of 310 nm used in the frontal experiments because the signal-to-noise ratio was very low. 20  $\mu$ L of 10 mg/mL polymer samples prepared in Tris of pH 8.5 and 50 mM Cl<sup>-</sup> were injected using a Rheodyne manual injector.

**Frontal Experiments.** Five frontal experiments (five steps) were performed for the characterization of each polymer at column saturation (5). An LKB 2150 HPLC pump was used for solvent delivery and a Spectroflow 757 detector was used to measure the absorbance of the effluent at 310 nm. A ten-port Valco manual injector with a 10 mL loop was used to inject the polymer, the nitrate, and the regenerant solutions. In the first frontal experiment (step 1), the column capacity in small anions was calculated by passing a front of 100 mM sodium nitrate at 0.5 mL/min through the equilibrated column and determining the nitrate breakthrough time. Second, after reequilibrating the column with buffer, a front of 10 mg/mL (2.5 mM) polyampholyte solution was passed at 0.2 mL/min, the polymer breakthrough time was determined and the amount of adsorbed polymer was calculated (step 2). The lower flow rate in step 2 secures low levels of pressure drop and adequate time for polymer adsorption. The non-adsorbed polymer in the dead volume was washed with buffer for 10 column volumes. Third, with the polymer adsorbed, a 30 mM sodium nitrate front was

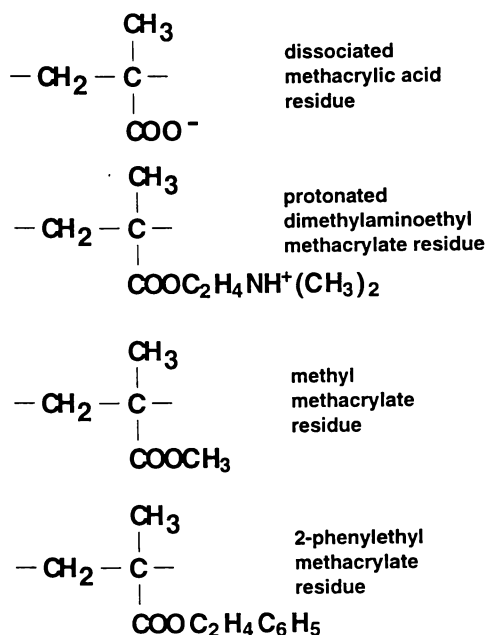


Figure 1. Chemical formulas of the polyampholyte residues.

Table I. Salt concentration required for polymer elution at pH=8.5

Polymer	Sequence	Composition	[NaCl] <sup>1</sup> (mM)	# negative charges
1 <sup>2</sup>	B-M-Ac	16-12-8	< 200	8
2 <sup>2</sup>	B-M-Ac	12-12-12	< 200	12
3	M/Ac/B	12/12/12	247	12
4	B/Ac	10/10	298	10
5 <sup>3</sup>	M/Ac/B	36/36/36	376	36
6	B/M/Ac	12/12/12	432	12
7	B/M/Ac	8/12/16	470	16
8	B/M/P/M/Ac	12/6/1/6/12	490	12
9	P/B/M/Ac	1/12/12/12	498	12
10	B/M/Ac	16/12/8	500	8
11	B/M/Ac	10/20/10	525	10
12	B/P/Ac	10/10/10	550	10

<sup>1</sup>salt concentration at peak maximum.<sup>2</sup>random copolymers<sup>3</sup>MW = 15,000Da



introduced at 0.2 mL/min, the nitrate breakthrough time was determined and the number of column sites not occupied by the polymer was calculated (step 3). The low sodium nitrate concentration was chosen so that the nitrate not displace any polymer. In the case of the one experiment at which the buffer used was only 5 mM  $\text{Cl}^-$ , a 5 mM sodium nitrate concentration was used. Fourth, a 1M NaCl in 100 mM phosphate solution at pH 7.5 or 3.0 was introduced at 0.2 mL/min to desorb the displacer and regenerate the column (step 4). Fifth, after regeneration, the column was equilibrated with the buffer and a 100 mM sodium nitrate front was passed at 0.5 mL/min to test the regeneration efficiency by determining the nitrate breakthrough time and calculating the column capacity in nitrate (step 5).

In steps 2 and 3, the effluent between the column dead volume and the breakthrough volume was collected and analyzed for polyampholyte by gradient elution, and for chloride ions according to the ASTM assay (7). For calibration, 1 mL chloride standards in Tris buffers of different pH as well as in deionized water were transferred to 50 mL deionized water and titrated against 0.01 M silver nitrate using potassium chromate indicator solution. It was found that while standards in 50 mM  $\text{Cl}^-$  Tris buffers at pH 7.2 and 7.5 gave the same slope ( $\mu\text{moles of Cl}^-/\text{mL of titrant}$ ) as standards in deionized water, standards in 50 mM  $\text{Cl}^-$  Tris buffers at pH 8.5 gave approximately twice the slope probably due to the increased concentration of Tris Amine at this pH which competes with silver ions for chloride. We also observed that the presence of the polycationic impurities in the polyampholytes caused sometimes different color changes in the assay.

## Results and Discussion

Both the gradient elution and the frontal experiments were performed at concentrations of 10 mg/mL that belong to the non-linear part of the polymer isotherm (with the exception perhaps of the random copolymers). The non-linearity at 10 mg/mL was established in preliminary frontal experiments with triblock copolymers and showed that an increase in the feed polymer concentration from 10 to 50 mg/mL had no effect on the amount of polymer adsorbed. Polyelectrolytes of high charge density, such as DEAE-dextran or dextran sulphate, typically exhibit square isotherms with the linear part lying at concentrations below 1 mg/mL (5).

**Gradient Elution.** Figure 2 is the gradient elution chromatogram of the acid-rich triblock polyampholyte (Polymer 7 in Table I). Similar chromatograms were obtained for the other polymers listed in Table I. Polymer 7 comes out of the column after 14 min which corresponds to a salt concentration of 470 mM. The sharpness of this peak suggests that the polymer is homogeneous in composition. Besides the major peak, three small unretained peaks appear that add up to less than 5% of the area of the major peak. This means that the polymer is very pure. The peak at 1 min corresponds to the dead volume of the column and is probably a polycationic impurity (terminated first block and diblock). The other two peaks are probably polymer with a small number of negative charges (early terminated triblock).

The estimation of 95% purity of Polymer 7 is based on the assumption that the impurities and the pure polymer have similar extinction coefficients. If the extinction coefficient of the impurities is much smaller than that of the polymer, the purity is much lower than 95%. For this reason it was necessary to estimate the purity by a second method. Polymer was dissolved in acid solution and precipitated at the isoelectric point by addition of the appropriate volume of potassium hydroxide solution. This procedure results in the purification of the polymer because the impurities do not precipitate. The dissolution-precipitation cycle was repeated five times and, finally, the polymer was dried. A solution of the purified polymer was subjected to gradient elution analysis and the obtained chromatogram was compared to that of the unpurified polymer. The major peak of the unpurified polymer was 15%

smaller than that of the purified polymer both in terms of area and height. This suggests that the original sample contains 15% impurities which can still be considered a small contamination. These results are in agreement with the findings of Möller and coworkers who determined impurity levels around 10% for their copolymers synthesized by GTP.

Table I summarizes the results of the gradient elution experiments. The retention time at the peak maximum was determined and converted to the corresponding salt concentration. The number of negative charges per polymer molecule (taken from the experimental titration curves) at the pH of the experiment also appears in Table I. By examining the Table, we can make four important observations.

First, the random copolymers (Polymers 1 and 2) are not retained, in spite of the fact that they have the same composition with block copolymers that are retained (Polymers 10, 3 and 6). This can be attributed to the random distribution of the adsorbing residues of the random copolymers which results in a lower local charge density. By comparing, for example, Polymers 2 and 3, we can estimate that the linear density in negative charges of the former is the one third of that of the latter.

Second, although the diblock copolymer (Polymer 4) and the random copolymers do not form micelles (Patrickios et al., MIT, submitted for publication), the diblock is retained. More specifically, it can be observed that it is retained more strongly than triblock Polymer 3 that does form micelles.

Third, although all the block polyampholytes are retained, there is no correlation between the retention and the length of the negative block. There is also no correlation between the retention and the net charge (not shown in the Table). There is, however, a strong effect of the hydrophobic block on retention. Focusing on Polymers 4, 6, and 11, which have similar lengths of negative and positive blocks but different lengths of the methyl methacrylate block in the middle, we can see that retention increases with the length of the methyl methacrylate block. This can be attributed to two effects: first, the middle block spaces away from the adsorbing surface the repelling amine block and, second, lateral middle block interpolymer hydrophobic interactions enhance retention. The comparison of the retentions of Polymers 11 and 12 points towards the greater importance of the hydrophobic interactions as the retention of Polymer 12, which bears the very hydrophobic phenylethyl methacrylate residues, is stronger, in spite of the shorter spacer length. Since the hydrophobic interactions are of short range and since the hydrophobic blocks of the adsorbed molecules are probably not in direct contact, one would dispute the two-dimensional hydrophobic interaction scheme. A different explanation can be given by considering the hydrophobic interactions in three dimensions, i.e. the micellization of the triblocks in solution. The polymer migrates down the column probably not as single chains but as micelles with a charge which is several times that of the chain monomer. It is likely that a more hydrophobic block will result in micelles with larger aggregation numbers and, therefore, higher micellar charge. It might be expected that retention would correlate well with the micellar charge.

Fourth, by examining Polymers 3 and 5, the significance of the position of the adsorbing block can be realized. These polymers show decreased retention because the adsorbing block lies in the middle of the molecule which leads to steric hindrance and decreased flexibility of the adsorbing block. Another negative factor is the close proximity of the repelling block to the adsorbing surface. Polymer 5 is retained more than Polymer 3 because it is three times larger.

The above interpretations on the order of elution are qualitative and are not based on any model. A more complete analysis is in progress and is based on isocratic elution of polymer samples at different salt concentrations which will result in the determination of the characteristic charge and the equilibrium constant (5). These two quantities define the affinity of the solute for the stationary phase according to the model of Brooks and Cramer (6). It is therefore likely that the block copolymers with similar adsorbing blocks (and probably similar characteristic charge) exhibited

different elution times because of different equilibrium constants. The equilibrium constant is expected to incorporate the effects of the length of the neutral block (hydrophobic interactions and spacing out of oppositely charged blocks) and of the block sequence, in addition to those of the lengths of the adsorbing and repelling blocks (electrostatic interactions). It is worth pointing out that the saturation capacities determined by the frontal analysis in the following section, performed mainly at a single set of conditions, are not expected to be influenced by the equilibrium constant but they should be dictated only by the characteristic charge and the steric factor (6). Consequently, it should not be surprising if hydrophobic interactions appear to play no role in these results.

**Frontal Experiments.** Figure 3 shows two typical polymer fronts at pH 8.5 and 50 mM Cl<sup>-</sup> as monitored at 310 nm. The midpoint of the polymer breakthrough is very clear and can be used to calculate the amount of polymer adsorbed. The shallow breakthrough from 2.5 min (dead volume of the column) to the polymer breakthrough is due to displaced salt and unretained impurities. Samples collected from this volume and analyzed by gradient elution showed the absence polymer and the presence of unretained impurities. Also chloride analysis demonstrated the presence of chlorides at concentrations higher than that of the buffer. The exact amount of chlorides displaced by the polymer was determined from the chloride analysis. Assuming a stoichiometric model for polymer adsorption, this amount of chlorides corresponds to the number of bonds between the polymer and the column.

As already mentioned, after polymer adsorption and washing with buffer, the number of sites inaccessible to the polymer are calculated by passing sodium nitrate and determining the breakthrough volume of the front. Sodium nitrate was chosen as the nitrate ion has a high absorbance. Samples collected from this step and analyzed by gradient elution showed absence of polymer. This analysis confirmed that the nitrate does not displace any polymer, which was expected because the nitrate concentration was lower than that of the chloride in the buffer. As the nitrate front goes through the column, it displaces the chloride ions which are bound to the column sites which are inaccessible to the polymer. Samples collected from this step and analyzed for chloride resulted in the determination of a number of inaccessible column sites very similar to that determined by the nitrate breakthrough volume. The number of sites occupied by the polymer can be calculated by subtracting the number of inaccessible sites from the total small-ion column capacity which was approximately 132  $\mu$ moles.

One can argue that the nitrate front will also displace the chloride counterions of the positively charged residues of the adsorbed polyampholyte as well. This will result in an overestimation of the number of inaccessible sites and an underestimation of the number of occupied sites. We checked the extent of this error by comparing the number of occupied sites calculated in step 3 from the nitrate front with the number of occupied sites determined in step 2 from the chloride analysis. The difference was less than 5% which is within experimental error. This should have been expected because at the pH of most of the experiments (= 8.5), 40% of the amine residues are uncharged.

Regeneration in step 4 was always successful and it took place in less than two column volumes. At the beginning of regeneration the pressure drop rose up to 20 atm for 2-3 min due to the high concentration of the polymer that was released. The nitrate frontal experiment in step 5 showed that the ion capacity of the column was fully recovered.

**Effect of Polymer Type.** Table II summarizes the results obtained for different polymers at pH 8.5 and 50 mM Cl<sup>-</sup> and includes the adsorptive capacity, the number of occupied sites as determined from the nitrate front of step 2, and the characteristic charge calculated as the number of occupied sites per adsorbed polymer molecule.

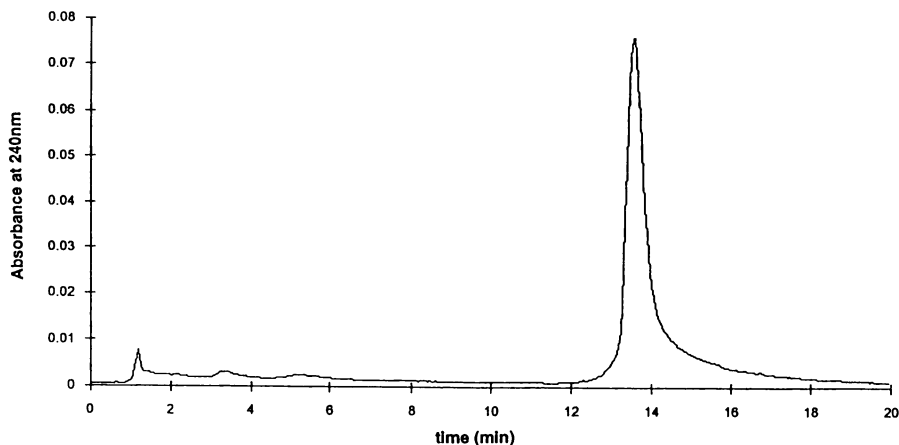


Figure 2. Elution of the acid-rich triblock polyampholyte by a linear 0.2-1.0M NaCl gradient at pH 8.5 and flow rate of 0.5 mL/min.

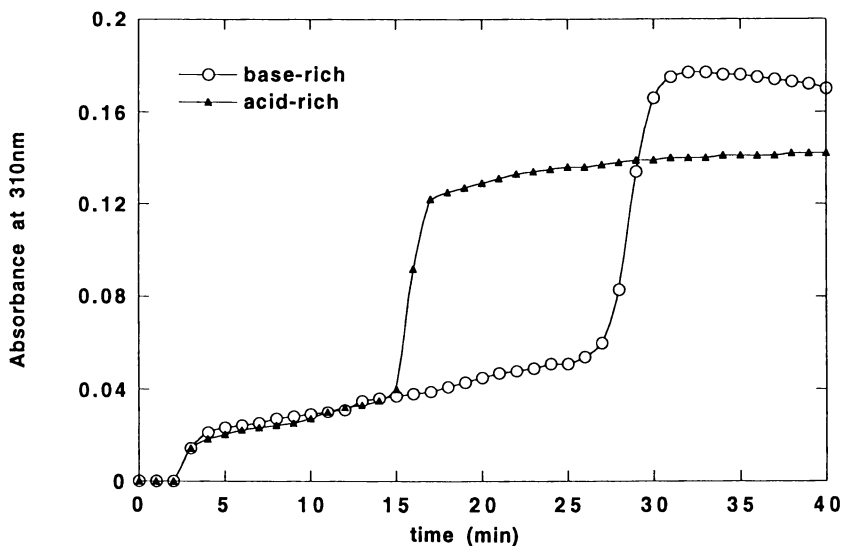


Figure 3. Fronts of the acid-rich and the base-rich triblock polyampholytes at polymer concentration 10 mg/mL, pH 8.5 and flow rate 0.2 mL/min.

Table II. Adsorptive capacity and characteristic charge for synthetic polyampholytes at pH = 8.5

Pol	MW	ads. (mg)	ads. ( $\mu\text{mol}$ )	unoc. sites ( $\mu\text{mol}$ )	occ. sites ( $\mu\text{mol}$ )	char. charge	# neg. charges	fraction of groups bound
7	3832	24.5	6.39	78.2	53.8	8.4	16	0.53
6	4116	31.0	7.52	78.9	53.1	7.1	12	0.59
4	2430	16.1	6.63	81.9	50.1	7.6	10	0.76
2	4116	12.0	2.91	104.9	27.1	9.3	12	0.78
10	4400	49.9	11.3	82.1	49.9	4.4	8	0.55

By examining the fourth column of the Table it can be observed that, with the exception of random Polymer 2, the number of polymer molecules adsorbed increases as the number of negative charges per molecule decreases. By examining now the sixth column we can see that, again with the exception of the random polymer, the number of occupied sites is always the same, independent of polymer composition. This can be understood because all the polymers have the same adsorbing block, poly(methacrylic acid), located at the end of the molecule. The number of occupied column sites does not appear to be affected by the different lengths of the positive block or the absence of hydrophobic block in Polymer 4. A recent frontal experiment with poly(methacrylic acid) (an oligomer of 12 units) showed that the homopolymer occupied the same number of column sites as the block copolymers. This confirmed that, at this pH, the non-adsorbing blocks do not affect the adsorption and probably extent vertically to the adsorbing surface as shown in Figure 4. The calculated characteristic charge of the block copolymers follows the same trend as the number of negative charges obtained from the experimental titration curves. The random copolymer has the negative charges randomly distributed and "mixed" with the positive ones. This results in a weak driving force for adsorption and in a flat adsorption conformation. These lead finally to the small amount of polymer adsorbed and the smaller number of column sites occupied per molecule.

**Effect of pH.** Table III shows the results for the adsorption of the acid-rich polymer at pH from 7.2 to 8.5. It was not possible to go to lower pH because the polymer precipitates. We can see that more polymer molecules are adsorbed as the pH is lowered. For the pH range studied the number of occupied sites does not appreciably change and the experimental hydrogen-ion titration curve suggests that the number of negative charges of the polymer is almost constant. On the other hand, by decreasing the pH from 8.5 to 7.2, the hydrogen-ion titration curve suggests that the number of positive charges per molecule increases from 5 to 8. It seems, therefore, that the stronger repulsion between the matrix and the amine block at lower pH allows only to a smaller number of negative residues per molecule to interact with the adsorbing surface. Since the number of occupied sites is constant, more polymer molecules per column area will adsorb.

**Effect of salt concentration.** We performed one experiment with Polymer 6 at the very low chloride concentration of 5 mM at pH 8.5 in order to test whether the 50 mM chloride concentration, used in all the previous experiments, was low enough to lead to maximum column occupancy. The results, listed in Table IV, indicate that, at the lower ionic strength, more polymer is adsorbed and more column sites are covered. This can be attributed to the weaker screening of the electrostatic interactions between the matrix and the polymer at the lower salt concentration. The constant value of the characteristic charge at the two chloride concentrations suggests that the adsorption conformation remains the same. Assuming now that the column occupancy will not increase further by going to even lower chloride concentrations, we calculate the steric factor for the polymer as the number of inaccessible sites per adsorbed polymer molecule at 5 mM chloride. The steric factor equals 7.3 and the ratio of the steric factor to the characteristic charge equals  $7.3/7.2 = 1.01$  which is very similar to that of dextran sulphate (5). A similar result was obtained in the frontal experiment with the oligo(methacrylic acid) giving again a steric factor to characteristic charge ratio close to one. This is in agreement with the very low (5%) isotacticity of polymethacrylates synthesized by GTP at room temperature (9) which implies that only 50% of the carboxylates can be oriented towards the adsorbing surface.

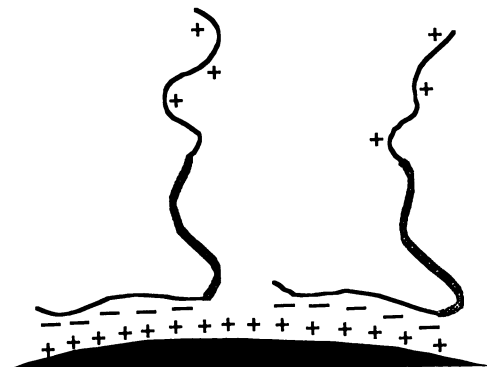


Figure 4. Adsorption conformation of a triblock polyampholyte at pH 8.5.

Table III. Effect of pH on the adsorptive capacity and characteristic charge of the acid-rich triblock polyampholyte (Pol 7)

pH	ads. (mg)	ads. ( $\mu\text{mol}$ )	unoc. sites ( $\mu\text{mol}$ )	occ. sites ( $\mu\text{mol}$ )	char. charge	# neg. charges	fraction of groups bound
7.2	41.5	10.8	75.0	57.0	5.3	15	0.35
7.5	38.5	10.0	68.1	63.9	6.4	16	0.40
8.5	24.5	6.4	78.2	53.8	8.4	16	0.53

Table IV. Effect of salt concentration on the adsorptive capacity and characteristic charge of the neutral triblock polyampholyte (Pol 6) at pH = 8.5

[Cl <sup>-</sup> ] (mM)	ads. (mg)	ads. ( $\mu\text{mol}$ )	unoc. sites ( $\mu\text{mol}$ )	occ. sites ( $\mu\text{mol}$ )	char. charge	steric factor
5	37.5	9.1	66.2	65.8	7.2	7.3
50	31.0	7.5	78.9	53.1	7.1	—

## Conclusion

The chromatographic techniques of this investigation are powerful tools for providing an understanding of the complicated behavior of our block polyampholytes in two dimensions. At low loading, the polymer affinity to the column is enhanced by the hydrophobic interactions. At column saturation and pH 8.5, the adsorptive capacity is dictated by the size of the adsorbing methacrylic acid block and not by the amine block which is only partially charged (Figure 4). At column saturation and at lower pH, the adsorptive capacity is also influenced by the amine (repelling) block which gets fully charged. Further studies will result in a more complete understanding of the adsorption behavior of these polymers and provide the ability to predict their protein displacing characteristics.

## Literature Cited

1. Cramer, S. M. *Nature* **1991**, *351*, 251.
2. Merle Y. J. *Phys. Chem.* **1987**, *91*, 3092.
3. Kopaciewicz, W.; Rounds, M. A.; Fausnaugh, J.; Regnier, F. E. *J. Chromatogr.* **1983**, *266*, 3.
4. Jen, S. C. D.; Pinto, N. G. *J. Chromatogr. Sci.* **1991**, *29*, 478.
5. Gadam, S. D.; Jayaraman, G.; Cramer S. M. *J. Chromatogr.* **1993**, *630*, 37.
6. Brooks, C. A.; Cramer, S. M. *AIChE J.* **1992**, *38*, 1969.
7. *ASTM Annual Book of ASTM Standards* Philadelphia, PA, 1991; 11.01.
8. Möller, M. A.; Augenstein, M.; Dumont, E.; Pennewiss, H. *New Polymeric Mater.* **1991**, *2*, 315.
9. Sogah, D. Y.; Hertler, W. R.; Webster, O. W.; Cohen, G. M. *Macromolecules*, **1987**, *20*, 1473.

RECEIVED August 30, 1993

## Chapter 12

# Determination of Microdomain Size of Hydrophobic Polyelectrolytes by Luminescence Quenching

Ulrich P. Strauss, Vincent S. Zdanowicz, and Yuanzhen Zhong<sup>1</sup>

Department of Chemistry, Rutgers, The State University of New Jersey,  
New Brunswick, NJ 08903

The luminescence decay kinetics of a ruthenium complex solubilized by a hydrolyzed copolymer of maleic anhydride and n-hexyl vinyl ether (DP 1100) were measured at different pHs as a function of the concentration of quencher, 9-methyl anthracene, in order to determine the size of the intramolecular micelles formed by the copolymer. The solubilization of quencher was used to determine the degree of micellization of the copolymer at various pHs. A time-resolved, single photon counting technique was employed for the luminescence decay measurements. Results indicated that an average of 42 repeat units comprised a micelle, indicating that one copolymer chain can form many intramolecular micelles. The micelle size was independent of pH and quencher concentration.

The hydrolyzed alternating copolymers of maleic anhydride and alkyl vinyl ethers have been useful for exploring the effects of hydrophobicity on the behavior of polyelectrolytes (*1-4*). With these copolymers the hydrophobicity is determined by the size of the alkyl group, while the charge density may be controlled by varying the pH. When the alkyl group contains less than four carbon atoms, the copolymers behave as normal polyacids; when the alkyl group contains twelve or more carbon atoms, the copolymers behave as typical polysoaps, showing the characteristic hypercoiled compact structures brought about by hydrophobic interactions between the alkyl groups. Perhaps the most interesting behavior is exhibited by the copolymers with alkyl group sizes in the range between four and ten carbon atoms: here we observe typical polysoap behavior at low pH and normal polyelectrolyte behavior at high pH, connected by a conformational transition reminiscent of denaturation phenomena exhibited in the realm of biological macromolecules (*1*).

One of the questions that arose in the course of these investigations was

<sup>1</sup>Current address: International Specialty Products, 1361 Alps Road, Wayne, NJ 07470

0097-6156/94/0548-0154\$06.00/0  
© 1994 American Chemical Society



whether the hypercoiled state was characterized by one large compact cluster or by several smaller intramolecular micelles. The rather small cooperative unit size deduced from the pH dependence of the conformational transition (5) suggested the latter. This conclusion was later confirmed by aggregation number determinations employing luminescence quenching (2). The basis for this technique is to deduce the number of micelles from the probability of a quenching event: if both probe and quencher are solubilized by the micelles, the probability of probe and quencher molecules being located simultaneously in the same micelle will decrease with increasing number of micelles (6). This method is especially useful for intramolecular micelles for which more conventional techniques, such as light scattering or hydrodynamic procedures requiring that the micelles occur as independent units, are not applicable (2,4,7).

The system investigated previously in this laboratory consisted of a hydrolyzed copolymer of maleic anhydride and n-hexyl vinyl ether (hexyl copolymer) with degree of polymerization 1700, tris(2,2'-bipyridyl)ruthenium(II) ion,  $[\text{Ru}(\text{bpy})_3^{2+}]$ , as the probe, 9-methylanthracene (9-MeA) as the quencher, and an aqueous 0.1 M LiCl solution as the solvent (2). The microdomains were found to encompass approximately 24 repeat units, unaffected by the concentration or by the extent of micellization of the polyacid. Neither did varying the probe concentration have any effect on this number. However, the previous investigation suffered from the disadvantage that the light source of the pulse sampling apparatus used had a 14 ns pulse width, too large to allow a direct determination of the initial luminescence intensity, necessary for the complete determination of all the physically significant parameters. Consequently, the dynamic method had to be supplemented with data obtained with a steady state luminescence instrument. The lack of perfect matching of the light sources and some of the assumptions needed in combining the data from the two instruments may have resulted in errors of unknown magnitude.

When a more satisfactory, time-resolved, single photon counting instrument became available to us, we resumed the measurements on similar systems, involving a hexyl copolymer with the same probe, quencher and solvent used previously. With this instrument, the pulse width of the light source was narrow enough ( $< 2$  ns) to allow acquisition of all necessary decay parameters. In this new investigation we also used an improved method for measuring the solubilization limit of the quencher by the polyacid. This quantity is needed for the determinations of both the fraction of polymer in micellar form and the distribution of quencher between the polymer molecules and the solvent medium. Previously the solubilization was obtained by monitoring the increase in the turbidity caused by increasing amounts of quencher beyond its solubility limit; in the new study, that method was replaced by measurements of the optical density originating from the solubilized quencher at its solubility limit. The results of this new investigation will be presented below.

## Experimental

**Materials.** The copolymer of maleic anhydride and hexyl vinyl ether was our sample BRB #2. Its degree of polymerization was estimated from viscosity measurements to be 1100. Its concentration,  $C_p$ , is expressed in moles of repeat units per liter. 9-Methylanthracene was recrystallized from ethyl alcohol. It was brought to the

desired concentrations in the polymer solutions from alcoholic stock solutions as described previously (2). Tris(2,2'-bipyridyl)ruthenium(II) chloride hexahydrate was used as received.

**Methods.** Luminescence lifetime measurements were conducted using a Photochemical Research Associates (PRA) Model 3000 Fluorescence Lifetime Instrument (FLI), configured for single photon counting. The configuration and operation were similar to those described by Snyder et al (8). Luminescence decay data were analyzed using software obtained from Photon Technologies International (PTI), which utilizes an iterative reconvolution procedure employing a weighted, non-linear, least squares curve fitting method. The decay function used was

$$I(t) = A_1 \exp [- A_2 t - A_3 (1 - \exp (- A_4 t)) ] \quad (1)$$

where  $I(t)$  is the luminescence intensity (9). The criteria used to judge the goodness of fit were the reduced Chi-squared value, the Durbin-Watson parameter, the Runs Test statistic and plots of weighted residuals and the autocorrelation function.

The solubility limit of 9-MeA in polymer solutions was determined from a plot of the absorbance at 333 nm against the concentration of 9-MeA. Up to the solubility limit, the data follow Beer's Law. Beyond the solubility limit, the points lie on a horizontal line, if sufficient time is allowed for the excess 9-MeA to precipitate out of solution. The intersection between the two lines gives the limit of solubility. The absorbance measurements were performed with a Hewlett Packard 8450 Diode Array Spectrophotometer.

## Results and Discussion

**Solubilization of Quencher.** Values of the solubilization,  $S$ , expressed in moles of 9-MeA solubilized per mole of polymer repeat unit, are shown in Table I as a function of pH. The values of  $S$  were obtained from the measured solubilities in polymer solutions, corrected for the solubility in the 0.1 M LiCl solvent, which we determined to be  $3.0 \times 10^{-6}$  M. As had been observed previously, the values of  $S$  decrease with increasing pH, reflecting a corresponding decrease in the extent of micellization of the polyacid (10). Since we found that the solubilization does not increase further as the pH is decreased below 4.2, we assume that micellization has reached its maximum at this point and that  $\Theta_m$ , defined as the fraction of repeat units in micellized form, is equal to unity at pH 4.2 and below. By taking  $\Theta_m$  proportional to  $S$ , we obtain the values given in the last column of Table I.

It has been shown experimentally that the distribution of solubilized molecules, in this case the quencher molecules, among micelles is given by a mass action law of the form

$$K' = \frac{[Q_m]}{[Q_a] \Theta_m C_p} \quad (2)$$

Table 1. Solubilization of 9-Methylantracene as Function of pH

pH	S ( $\times 10^3$ ) <sup>a</sup>	$\Theta_m$
4.2	8.62	1.000
4.5	8.34	0.967
4.8	7.54	0.875
5.1	6.75	0.783
5.4	5.61	0.651
5.7	5.17	0.600

a. Moles of 9-MeA per mole of polyacid repeat unit.

where  $[Q_m]$  and  $[Q_a]$  are the molar concentrations of solubilized and free quencher, respectively (11). This law can be derived with the assumption that the presence of solubilized guest molecules in a micelle does not affect the entry rate of further guest molecules (4). Since the equation is valid below, as well as at, the solubility limit, we can make use of the fact that in the latter case  $[Q_m] / \Theta_m C_p = S$  and  $[Q_a]$  is the solubility of the quencher in the solvent. We then find that  $K' = 2870 \text{ M}^{-1}$ . This value, together with the known total concentration of quencher, allows the calculation of  $[Q_m]$  and  $[Q_a]$  by means of equation 2.

**Luminescence Quenching.** The time dependence of the luminescence of a probe in a micellar environment containing mobile quenchers is given by equation 1 above. The coefficients of this equation are related to the molecular parameters of interest by the relations (9)

$$A_2 = k_0 + \frac{k_Q k_-}{k_Q + k_-} \frac{[Q_m]}{[M]} \quad (3)$$

$$A_3 = \left( \frac{k_Q}{k_Q + k_-} \right)^2 \frac{[Q_m]}{[M]} \quad (4)$$

$$A_4 = k_Q + k_- \quad (5)$$

where  $k_0$  is the first-order rate constant for the luminescence decay of the probe in the absence of quencher,  $k_Q$  is the first-order rate constant for quenching inside a micelle,  $k_-$  is the exit rate constant for a quencher from a micelle, and  $[M]$  is the concentration of micelles expressed in moles per liter.

The procedure used for obtaining the desired molecular parameters by means of equations 3 - 5 is illustrated with a sample run involving five solutions differing only in their quencher concentrations. The relevant data are given in Table II. First, the derivatives of  $A_2$  and  $A_3$ , with respect to  $[Q_m]$  are determined by linear, least squares fitting. If the ratio of these derivatives is denoted by  $D$ ,  $k_+$  is obtained by the relation

$$k_+ = \frac{D}{1 + (D/A_4)} \quad (6)$$

which, together with the average value of  $A_4$ , leads to  $k_Q$  via equation 5. Next, the micelle concentration,  $[M]$ , is determined from  $dA_3/d[Q_m]$  by means of equation 4. Finally, the micelle size,  $n$ , defined as the average number of hexyl groups per micelle, is obtained from the expression

$$n = \Theta_m C_p / [M] \quad (7)$$

Results obtained under different experimental conditions and calculated in the manner illustrated above are compared in Table III. We have also included values of the equilibrium constant,  $K$ , for the distribution between micelles and solvent, given by the relation

$$K = \frac{[Q_m]}{[Q_a] [M]} \quad (8)$$

and calculated more efficiently by the equation  $K = nK'$ .

The values of  $n$  are substantially larger and the values of  $k_Q$  and  $k_+$  substantially smaller than those found in our previous investigation. We ascribe these differences to the improvements in the experimental methods discussed above. The new values of  $k_Q$  are also smaller than those found with micelles of simple surfactants, such as sodium dodecyl sulfate, but are of the same magnitude as those observed by others for intramolecular micelles attached to macromolecules. This effect has been attributed to an enhancement of the intramicellar viscosity caused by the attachment of the hydrocarbon groups to the polymeric backbone (4, 12). It has been shown previously that the values of  $k_+$  cannot be solely attributed to the transfer of quencher from micelles into the aqueous phase (2). The argument previously made to reach this conclusion is also supported by the present data in that they show that the hypothetical value of the second order rate constant for a quencher entering a micelle from the aqueous phase,  $k_+$ , given by the product of  $K$  and  $k_+$ , is too large to be theoretically feasible. The new data, however, are quite compatible with the hypothesis of a direct exchange of quencher between micelles, for which several mechanisms have been proposed (13), and which should be facilitated by the close proximity of micelles belonging to the same macromolecule.

Table II. Parameters of Sample Run <sup>a</sup>

[Q]	A <sub>2</sub>	A <sub>3</sub>	A <sub>4</sub>	dA <sub>2</sub> /d[Q <sub>m</sub> ]	dA <sub>3</sub> /d[Q <sub>m</sub> ]	k	[M]	n
x10 <sup>4</sup>	x10 <sup>-6</sup> (s <sup>-1</sup> )		x10 <sup>-6</sup> (s <sup>-1</sup> )	x10 <sup>-8</sup> (M <sup>-1</sup> s <sup>-1</sup> )	(M <sup>-1</sup> )	x10 <sup>-5</sup> (s <sup>-1</sup> )	x10 <sup>4</sup>	
0.00	1.196							
0.69	1.230	0.068	4.66					
1.37	1.259	0.145	3.98					
2.05	1.271	0.229	3.16					
2.73	1.290	0.307	3.03					
			3.93 <sup>b</sup>	2.85	1190	2.3	7.45	44

a. C<sub>p</sub> = 0.0538 M; pH = 5.7; Θ<sub>m</sub> = 0.600; [Ru(byp)<sub>3</sub>Cl<sub>2</sub>] = 1.08x10<sup>-5</sup> M; [Q<sub>m</sub>] / [Q] = 0.989.

b. Average A<sub>4</sub>.

It is worth noting that the calculation of *n* is based on the assumption that the probe is completely solubilized in the micelles. Any probe molecules located elsewhere would, for all practical purposes, not be subject to quenching by the 9-methylanthracene, which is known to be 99% solubilized in the micelles. The resulting decrease in quenching would produce an apparent increase in the calculated micelle concentration, [M], and, hence, an apparent decrease in the micelle size, *n*. However, it has been shown previously by fluorescence experiments that the probe, even though cationic, is solubilized almost exclusively in the micellar regions (2), thus validating the procedure used here. Further validation of the approach taken here was obtained by the use of a different probe-quencher combination with the same polymer-solvent system (14). With pyrene as the probe and nonyl phenyl ketone as the quencher, both of which were shown to be solubilized exclusively in the micelles, the value of *n* obtained was 45 ± 1, which is within the upper range of the data given in Table III.

Published accounts of polymer-based micelles are scarce, and difficult to compare with our results. Chu and Thomas reported that the micelle sizes of two maleic acid-octadecene copolymers, one of DP 24 (12) and one of DP 17 (15), were equal to their respective degrees of polymerization. In contrast to our copolymer, their whole polymer molecules were smaller than one of our micelles. Binana-Limbelé and Zana (4) studied a high molecular weight copolymer of maleic acid and

Table III. Micelle Size and Related Parameters

pH	$C_p$	$[\text{Ru}(\text{byp})_3^{2+}]$	$\Theta_m$	$k_0$	$k_Q$	$k_c$	$K$	$n$
	$\times 10^2$	$\times 10^6$		$\times 10^{-6}$ ( $\text{s}^{-1}$ )	$\times 10^{-6}$ ( $\text{s}^{-1}$ )	$\times 10^{-5}$ ( $\text{s}^{-1}$ )	$\times 10^{-4}$	
4.5	5.21	9.83	0.967	1.21	3.77	3.4	12.3	43
4.8	4.90	9.02	0.874	1.11	1.67	5.4	13.5	47
5.1	4.79	9.02	0.782	1.13	1.76	3.9	10.9	38
5.7	4.53	9.02	0.600	1.17	4.34	3.1	10.3	36
5.7	5.38	10.8	0.600	1.20	3.70	2.3	12.6	44
Ave:				1.16	3.05	3.6	11.9	42

decyl vinyl ether and reported a decrease in the micelle size from 79 to 15 with increasing degree of ionization, in contrast to our results which showed no such change. However, their calculations contained the implicit assumption that their quencher, dodecyl pyridinium chloride, was bound to the polymer exclusively in its micellar regions. It is likely that the cationic dodecyl pyridinium ions are also bound to non-micellar anionic polymer groups. Knowledge of the actual quencher distribution would strongly affect the calculated micelle size and its dependence on the degree of ionization. Resolution of this question requires experimental determination before a quantitative comparison between our results and theirs can be made. Nevertheless, whatever the outcome of such a determination, their conclusion, in agreement with our findings, that a large polysoap molecule contains a great number of small micellar microdomains, will retain its validity.

## References

1. Dubin, P.; Strauss, U. P. *J. Phys. Chem.* **1970**, *74*, 2842.
2. Hsu, J.-L.; Strauss, U. P. *J. Phys. Chem.* **1987**, *91*, 6238.
3. Ito, K.; Ono, H.; Yamashita, Y. *J. Colloid Sci.* **1964**, *19*, 28.
4. Binana-Limbele, W.; Zana, R. *Macromolecules.* **1990**, *23*, 2731.
5. Barbieri, B. W.; Strauss, U. P. *Macromolecules.* **1985**, *18*, 411.
6. Turro, N. J.; Yekta, A. *J. Am. Chem. Soc.* **1978**, *100*, 5951.
7. Olea, A. F.; Thomas, J. K. *Macromolecules.* **1989**, *22*, 1165.
8. Snyder, S. W.; Demas, J. N.; DeGraff, B. A. *Anal. Chem.* **1989**, *61*, 2704.

9. Tachiya, M. *Chem. Phys. Lett.* **1975**, *33*, 289.
10. Strauss, U. P.; Schlesinger, M.S. *J. Phys. Chem.* **1978**, *82*, 1627.
11. Almgren, M.; Grieser, F.; Thomas, J. K. *J. Am. Chem. Soc.* **1979**, *101*, 279.
12. Chu, D.-Y.; Thomas, J. K. *Macromolecules.* **1987**, *20*, 2133.
13. Malliaris, A.; Lang, J.; Zana, R. *J. Phys. Chem.* **1986**, *90*, 655.
14. Zdanowicz, V. S.; Strauss, U. P. *Macromolecules.* In press.
15. Chu, D.-Y.; Thomas, J. K. In *Polymers in Aqueous Media: Performance through Association*; Glass, J. E., Ed.; Advances in Chemistry Series 233; American Chemical Society: Washington, DC, **1989**, pp 325-341.

RECEIVED August 6, 1993

## Chapter 13

# Characterization of Polyacrylamide-co-Sodium Acrylate

D. Hunkeler<sup>1</sup>, X. Y. Wu<sup>2</sup>, A. E. Hamielec<sup>2</sup>, R. H. Pelton<sup>2</sup>, and D. R. Woods<sup>2</sup>

<sup>1</sup>Department of Chemical Engineering, Vanderbilt University,  
Nashville, TN 37235

<sup>2</sup>Institute of Polymer Production Technology, Department of Chemical  
Engineering, McMaster University, Hamilton, Ontario L8N 3Z5, Canada

A series of polyacrylamide-co-sodium acrylates were prepared through alkaline hydrolysis of well fractionated polyacrylamides. The polymers were subsequently analyzed by light scattering, viscometry and size exclusion chromatography in aqueous Na<sub>2</sub>SO<sub>4</sub> solutions. The dilute solution properties such as the specific refractive index increment, intrinsic viscosity, Mark-Houwink parameters and elution volume were found to systematically depend on the ionic content of the copolymer. These relationships were used to develop quantitative techniques for the molecular weight characterization of polyelectrolytes, including the use of the universal calibration method.

The molecular weight characterization of polyelectrolytes is relatively difficult since variations in copolymer composition alter the electrostatic environment and hence the size and structure of the polymer chain. Hydrolyzed polyacrylamide is therefore often used for methods development since it has a random distribution of charged groups along the backbone, and the molecular weights of the parent polyacrylamide can be estimated accurately by conventional techniques.

Copolymers of acrylamide and sodium acrylate can be prepared by direct copolymerization or derivatization from polyacrylamides. When the ionogenic monomer is introduced through a free radical addition mechanism, long acrylate and amide sequences form, with the microstructure conforming to Bernoullian statistics (1,2). By comparison, polymers produced through alkaline saponification of the amide side chain are atactic (3) and have a relatively uniform charge density distribution which maximizes the viscosity increase for a given molecular weight and improves the polymer's performance (4).

The purpose of this research is to develop valid characterization methods for copolymers of acrylamide and sodium acrylate. Initially a series of polyacrylamides will be synthesized and fractionated to yield narrow molecular weight distributions. The fractions will first be measured in their nonionic form where light scattering, viscometry and size exclusion chromatography (SEC) are more reliable and accurate than for ion containing polymers. The polyacrylamides will then be hydrolyzed

0097-6156/94/0548-0162\$06.00/0  
© 1994 American Chemical Society



to various degrees and analyzed in their ionic form. The measured weight average chain lengths will be used to evaluate the absolute accuracy of the polyelectrolyte characterization methods. The results of these studies will also be applied to SEC calibration. Therefore we have employed aqueous Na<sub>2</sub>SO<sub>4</sub> solution as a solvent and chosen to fractionate over a Mw range between 1.4 x10<sup>4</sup> to 1.2 x10<sup>6</sup> daltons. A second objective of this work is to investigate the validity of the universal calibration for polyacrylamide-co-sodium acrylate (PAM-co-NaAc) and nonionic polyacrylamides. Since the PAM-co-NaAc's which were prepared had narrow molecular weight distributions and relatively homogeneous composition distribution, the heterogeneity in composition and molecular weight is not expected to be an important factor in assessing the validity of the universal calibration.

### Theoretical Considerations

The universal calibration method is based on Einstein's viscosity theory for spherical particles:

$$[\eta] = 2.5 N_A (V_h/M) \quad (1)$$

where  $[\eta]$  is the intrinsic viscosity,  $V_h$  the hydrodynamic volume of the particles,  $M$  the particle molecular weight and  $N_A$  Avogadro's number. From equation (1) it is obvious that the product  $[\eta]M$  is proportional to the hydrodynamic volume. Since SEC separates polymer molecules on the basis of their hydrodynamic volume, one would expect that the product  $[\eta]M$  is a function of the elution volume ( $V_e$ ). The universal calibration is often expressed in logarithmic form:

$$\log[\eta]M = f(V_e) \quad (2)$$

Accordingly, all polymer molecules with the same hydrodynamic volume elute at the same time. For example, if we designate a nonionic polyacrylamide with the subscript 'o' and a PAM-co-NaAc with a sodium acrylate composition of x% with the subscript 'x' then the following identity holds:

$$[\eta]_o M_o = [\eta]_x M_x \quad (3)$$

The calibration curve for a single polymer can often be represented by the following equation, over a considerable range in elution volumes by(5):

$$M(V_e) = D_1 \exp(-D_2 V_e) \quad D_1, D_2 > 0 \quad (4)$$

This can be expressed in a linear form:

$$\log_{10} M = D_1' - D_2' V_e \quad (5)$$

### Experimental Methods and Procedures

**Polymer Preparation.** Polyacrylamides (PAMs) were synthesized by aqueous free radical polymerizations using potassium persulfate (BDH Chemicals, 99% purity) as an initiator and ethanol mercapton (BDH Chemicals) as a chain transfer agent. The polymers were heterodisperse in

molecular weight, with polydispersities between 2.0 and 2.5 as determined by Size Exclusion Chromatography.

The synthesis conditions did not lead to preliminary hydrolysis as was determined by the  $^{13}\text{C}$  NMR spectra. The spectra were recorded for a 10 wt%  $\text{D}_2\text{O}$  solution at 125.76 MHz and 70.9°C in the Fourier transform mode with inverse gate decoupling. The pulse width was 6.8 ms with an acquisition time of 0.557s.

**Size Exclusion Chromatography.** SEC chromatograms were measured with a Varian 5000 liquid chromatograph, using Toya Soda columns (TSK 3000,5000,6000 PW) each of which had dimensions of 7.5 mm x 30 cm and were connected in series. These columns contained polyether gel packing with hydrophilic OH groups on the surface (6). One of the advantages of this gel was that the surface groups were neither charged nor highly polar, therefore the adsorption and electrostatic interactions were greatly reduced (7). An aqueous mobile phase of 0.2 M  $\text{Na}_2\text{SO}_4$  (BDH Chemicals; ionic strength 0.6 M) was used at a flow rate of 1.0 mL/min. Polymer solutions, 0.1% w/v, were prepared from dry polymer and the mobile phase. 100  $\mu\text{L}$  of polymer solution was injected in each analysis. sodium azide (0.1 wt%, Aldrich) and Tergitol NPX (0.01% wt%, Union Carbide Corp.) were also added to the mobile phase to protect the column from microorganisms and reduce adsorption. The chromatograms were recorded on a Varian CDS 401 Data Station. Peak broadening correction was performed using standard methods (5,8).

**Fractionation, Hydrolysis and Copolymer Characterization.** A complete discussion of the fractionation conditions, the saponification reaction and the characterization of polyacrylamide-co-sodium acrylate has been presented in two previous publications (9,10).

**Polymer Viscometry.** The intrinsic viscosities of polymers in 0.2  $\text{Na}_2\text{SO}_4$  were obtained from the quadratic form as well as the conventional form of Huggins equation by the least squares technique (11,12). The efflux time was measured with a No.75 Cannon-Ubbelohde semi-micro dilution viscometer at  $25 \pm 0.05^\circ\text{C}$ .

**Dialysis.** A cellulose dialysis membrane (Spectra/Por 6) with a molecular weight cutoff of 1000 was purchased from Spectrum Medical Industries, Inc. (Los Angeles, CA). A small pore size was selected to prevent oligomers from diffusing into the dialysate. Prior to use the membranes were conditioned in the dialyzing buffer (0.2 M  $\text{Na}_2\text{SO}_4$ ) for one hour, and rinsed with distilled deionized water.

Polymer solutions were prepared at a concentration suitable for light scattering (13). One hundred mL of these solutions were pipetted into the membrane which was sealed at one end with a dialysis tubing enclosure. After the second end of the membrane was secured, it was submersed in three liters of saline solution. This solution was housed in a four liter polyethylene container, isolated from the atmosphere.

After chemical potential equilibrium was obtained (120 h), the vessel was opened and the membrane removed. Several concentrations of the polymer were prepared by diluting the dialyzed solution with the dialysate. The samples were immediately analyzed by light scattering or differential refractometry.

**Light Scattering.** The molecular weight of each fraction was measured using a Chromatix KMX-6 LALLS photometer, with a cell length of 15 mm and a field stop of 0.2. These parameters corresponded to an average scattering angle of  $4.8^\circ$ . A  $0.45 \mu\text{m}$  cellulose-acetate-nitrate filter (Millipore) was used for the polymer solutions. A  $0.22 \mu\text{m}$  filter of the same type was used to clarify the solvent. Distilled deionized water with  $0.02 \text{ Na}_2\text{SO}_4$  (BDH Chemicals, analytical grade) was used as the solvent.

For characterization of dilute solution properties of polyacrylamide-co-sodium acrylate, Wu (9) has determined that polyelectrolyte interactions are suppressed for  $\text{Na}_2\text{SO}_4$  concentrations of  $0.2 \text{ mol/L}$ . This salt concentration was consequently selected as a solvent for the light scattering and SEC characterizations performed in this investigation.

The refractive index increment of the polymer in solution was determined using a Chromatix KMX-16 laser differential refractometer at  $25^\circ\text{C}$ , and a wavelength of  $632.8 \text{ nm}$ . The  $dn/dc$  was found to be  $0.1869$  for acrylamide homopolymers.

## Results and Discussion

**I. Characterization of Polyacrylamide.** Eight PAM fractions with polydispersity indices  $1.2 - 2.0$  were obtained by fractionation. The homopolymers were subsequently analyzed by viscometry and light scattering with the intrinsic viscosities and weight-average molecular weights summarized in Table I.

The Mark-Houwink constants,  $K$  and  $a$ , were estimated with the Error-In-Variables method (14,15). The variances in molecular weight were evaluated from Hunkeler and Hamielec's data (13), while those in intrinsic viscosity were calculated from the present data using Chee's equation (11). The variance in concentration was assumed to be negligible. The following equation has been established for PAM in  $0.2 \text{ M Na}_2\text{SO}_4$  at  $25 \pm 0.05^\circ\text{C}$ :

$$[\eta] = 2.43 \times 10^{-4} M_w^{0.69} \quad (6)$$

The 95% confidence intervals for parameters  $K$  and  $a$  are:

$$K = 2.43 \times 10^{-4} \pm 0.36 \times 10^{-4}$$
$$a = 0.69 \pm 0.014$$

The 'a' value is consistent with that obtained by Kulicke (16) in  $0.1 \text{ M Na}_2\text{SO}_4$  (0.7).

## II. Light Scattering Characterization of Polyacrylamide-co-Sodium-Acrylate

**Determination of the Refractive Index Increment at Constant Chemical Potential.** The refractive index increment at constant chemical potential was determined as a function of the extent of hydrolysis (10). The observed decrease in  $(dn/dc)_\mu$  with acrylate content, a manifestation of the negative selective sorption of sodium sulphate, has been reported previously (17-19). None of these authors have used the

same solvent as in this work, and therefore direct comparison of the magnitude of  $dn/dc$  is not possible. Nonetheless, the validity of these measurements will be confirmed in the next section.

The equation:

$$dn/dc)_{\mu, \text{PAM-NaAc}} = 0.1869 (F_{\text{NaAc}})^{-0.076} \quad (7)$$

has been fit from this data so that the refractive index may be computed at any specific copolymer composition (F) between zero and thirty three percent sodium acrylate (NaAc).

**Evaluation of the Molecular Weight Method for Polyacrylamide-co-Sodium Acrylate.** Light scattering measurements were made for each of the five narrow polymer standards. The molecular weight data were normalized with respect to composition, with the corresponding chain lengths summarized in Table II. The polyelectrolyte chain lengths deviate on average by 7.68% from the original polyacrylamide homopolymer. Such an agreement is well within the random errors of aqueous light scattering ( $\pm 10\%$ )(12). We can conclude, therefore, that the measured molecular sizes of the ionic and nonionic polymers agree. It is worthwhile to note that without the correct refractive index increment, the estimation of the molecular weight of a thirty percent hydrolyzed polyacrylamide is 62% underpredicted. Therefore, the polyelectrolyte method, and the specific refractive index increments at constant chemical potential are accurate and reliable. Furthermore, it is sufficient to correct the optical constant for  $dn/dc)_{\mu}$  in order to obtain accurate molecular weights of polyelectrolytes.

Table III lists the weight average molecular weight data directly obtained from preceding measurements of polyacrylamide-co-sodium acrylate as well as calculated from a the following stoichiometric conversion of light scattering data from nonionic polyacrylamides.

$$M_{ws} = M_{w\text{PAM}}/71.08(94.04x + 71.08(1-x)) \quad (8)$$

The values calculated from equation (8) will subsequently be used for the generation of calibration curves. Table III also lists the intrinsic viscosity and exclusion volume data for the polyacrylamide-co-sodium acrylates at each molecular weight and copolymer composition.

### III. Viscometric Characterization of Polyacrylamide-co-Sodium Acrylate.

**Mark-Houwink Equations for PAM-co-NaAc.** In the Mark-Houwink equation the parameters 'K' and 'a' are constant only if the polymer composition, solvent and temperature are unchanged. For PAM-co-NaAc under the given conditions, 'K' and 'a' are functions of the hydrolysis degree. Klein et al. (20) observed a maximum value of exponent 'a' at about 40% sodium acrylate and a minimum value of 'K' at about 20% sodium acrylate. McCarthy et al. (21) showed some changes in the values of 'K' and 'a' with sodium acrylate but did not show definite trends. In the data presented herein 'K' is a decreasing function of the hydrolysis degree (HD) and 'a' an increasing function. This data is shown in Figure 1. In order to allow for interpolation of the Mark-Houwink equation for

**Table I: Weight Average Molecular Weight (Mw), Polydispersity (PDI), and Intrinsic Viscosities  $[\eta]$  of the Polyacrylamide Fractions**

Sample	F1	F2	F3	F4	F5	F6	F7	F8
Mw (daltons)	1.244E6	9,90E5	4.01E5	2.01E5	9.90E4	3.60E4	2.69E4	1.39E4
PDI	1.8	2.0	1.8	1.7	1.6	1.5	1.3	1.2
$[\eta]$ dl/g	3.804	3.555	1.733	1.096	0.6502	0.3220	0.2741	0.1754

**Table II: A Comparison of the Polyelectrolyte and Nonionic Molecular Weight Characterization Procedures**

Weight Average Chain Length ( $r_w$ ) of Polyacrylamide measured by the Nonionic Method	Weight Average Chain Length ( $r_w$ ) of Polyacrylamide-co-Sodium Acrylate measured by the Polyelectrolyte Method		Percentage deviation from the Nonionic Characterization Method	
$r_w$ (Nonionic Polyacrylamide)	$r_w$ (10% hydrolysis)	$r_w$ (30% hydrolysis)	(10% Hydrolysis)	(30% Hydrolysis)
379	482	402	21.4	5.7
1,676	1,633	1,702	2.6	1.5
3,282	3,413	3,39	3.8	4.6
6,563	6,412	5,959	2.4	10.1
13,859	13,845	10,466	0.1	24.6
			Average Deviation 7.68%	

**Table III: Molecular Weight, Intrinsic Viscosity and Elution Volume of Polyacrylamide-co-Sodium Acrylates as a function of the copolymer composition**

Sample Identification	Copolymer Composition (mol % sodium acrylate)	Weight Average Molecular Weight (Light Scattering) (daltons)	Weight Average Molecular Weight (Stoichiometric) (daltons)	Intrinsic Viscosity (dl/g)	Elution Volume (mL)
F7HY	10.77	35,800	27,800	0.3524	24.89
	36.00	31,700	30,000	0.4692	/
F5HY	36.08	/	30,000	0.4872	24.09
	10.30	119,600	102,300	0.8468	22.27
	16.70	/	104,300	1.049	22.83
	34.42	/	110,000	1.303	21.84
F4HY	39.20	135,500	111,500	1.342	21.66
	9.68	247,000	207,300	1.353	21.50
	31.90	/	221,700	2.200	21.09
F3HY	34.90	268,000	223,700	2.127	21.19
	6.40	/	409,300	1.961	20.30
	9.95	468,000	413,300	2.075	20.214
	14.90	/	420,300	2.640	20.02
	23.20	/	431,100	3.242	/
HY5*	26.00	/	434,700	3.470	19.73
	33.10	467,000	443,900	3.372	19.73
	9.46	/	1,061,500	3.979	18.33
	11.50	/	1,068,300	4.228	18.23
	20.15	/	1,097,000	5.329	17.81
F2HY	36.60	/	1,132,500	6.893	/
	10.30	1,014,000	1,029,000	4.354	18.38
	32.30	/	1,093,000	6.709	17.72
	33.40	822,000	1,096,000	7.067	17.72

\* HY5 is an unfractionated polyacrylamide with a PDI of 2.5.

copolymer compositions not measured in this work the following polynomial expressions were regressed to the data:

$$a = C_0 + C_1HD + C_2(HD^2) + C_3(HD^3) \quad (9)$$

where

$$C_0 = 0.625 \pm 0.007$$

$$C_1 = 8.86 \times 10^{-3} \pm 1.27 \times 10^{-3}$$

$$C_2 = -2.405 \times 10^{-4} \pm 0.617 \times 10^{-4}$$

$$C_3 = 2.48 \times 10^{-6} \pm 0.89 \times 10^{-6}$$

$$\log K = d_0 + d_1HD + d_2(HD^2) + d_3(HD^3) \quad (10)$$

where

$$d_0 = -3.36 \pm 0.024$$

$$d_1 = -2.39 \times 10^{-2} \pm 0.42 \times 10^{-2}$$

$$d_2 = 6.96 \times 10^{-4} \pm 2.05 \times 10^{-4}$$

$$d_3 = -7.37 \times 10^{-6} \pm 2.95 \times 10^{-6}$$

The regressed equations (9 and 10) show a good fit with the Mark-Houwink parameters (Figure 1). Therefore, one can accurately calculate the values of  $K$  and  $a$  at any polymer composition of interest over the range 6 - 40% acrylate from these polynomials. In the absence of intrinsic viscosity data, equations (9 and 10) are useful for the construction of a universal calibration curve, particularly if on-line intrinsic viscosity detectors are not available. It is interesting to note that the sum ( $1000 K + a$ ) is essentially constant (0.97-0.98) for copolymers of all compositions, and has a value of approximately unity.

#### IV. Size Exclusion Chromatography of Polyacrylamide-co-Sodium Acrylate.

**Elution Volume and Molecular Weight of Polyacrylamide.** Figure 2 is a plot of the logarithm of the molecular weight of nine nonionic polyacrylamide samples versus elution volume. A linear relationship is observed and the following equation has been regressed to the data ( $\rho=0.998$ ):

$$\log_{10}M = 10.78 - 0.2505V_e \quad (11)$$

In equation (11),  $M$  is the geometric mean molecular weight ( $M=(M_n \times M_w)^{1/2}$ ).

**Hydrodynamic Volume and Elution Volume of Polyacrylamide and Polyacrylamide-co-Sodium Acrylate.** The hydrodynamic volume is plotted against the elution volume on a semi-log scale in Figure 3. The data for both ionic and nonionic polymers show no systematic deviation and the same correlation can be observed for all samples. Therefore, the universal calibration curve based on nonionic polyacrylamide seems to be a reasonable way to determine the molecular weights of polyacrylamide-co-sodium acrylate. The universal calibration has been linearly regressed to the data. A correlation coefficient of 0.995 was determined along with the following parameter values:

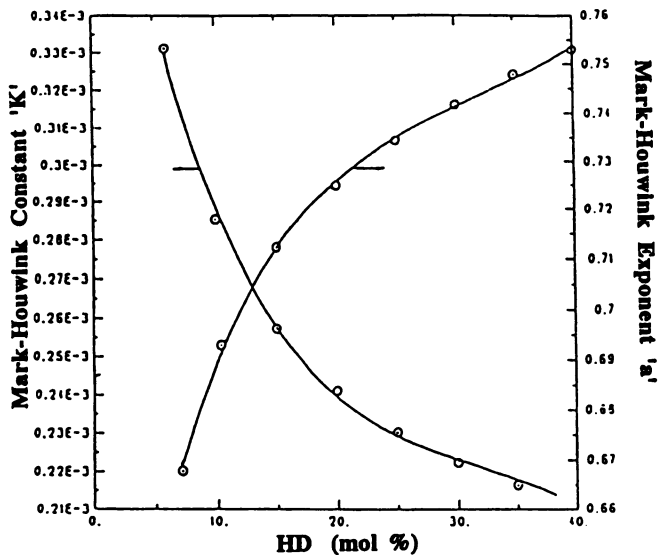


Figure 1: Mark-Houwink constants 'K' and 'a' for polyacrylamide-co-sodium acrylate at various hydrolysis degrees. (—): from correlated polynomials, (O): experimentally measured data point.

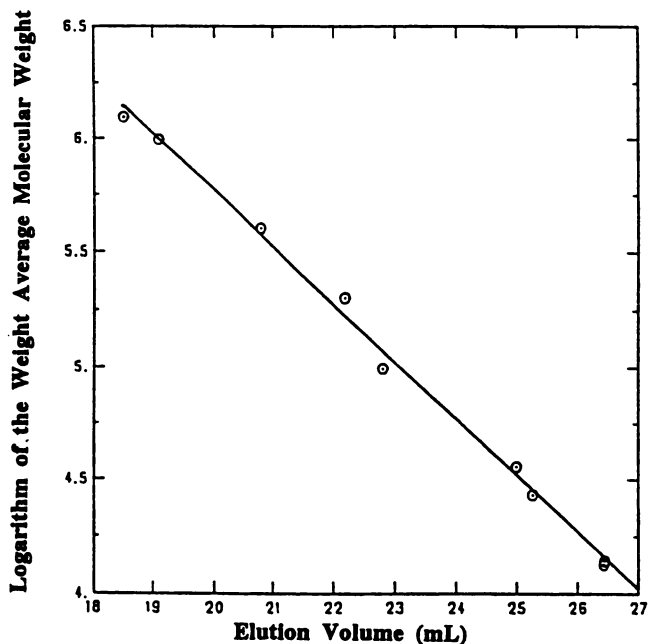
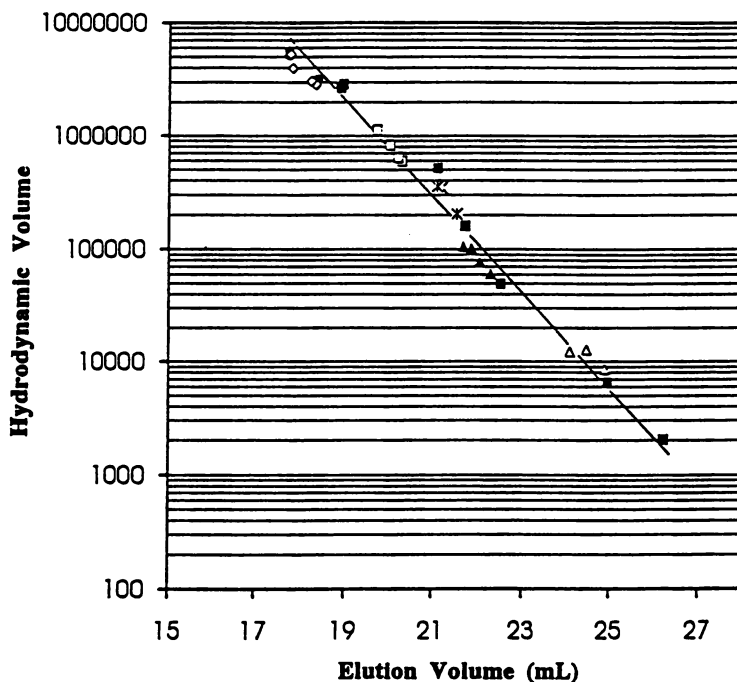


Figure 2: The logarithm of the weight average molecular weight ( $M_w$ ) of nine nonionic polyacrylamide samples versus elution volume.





**Figure 3:** The hydrodynamic volume,  $[\eta]M$ , is plotted as a function of the elution volume ( $V_e$ ) on a semi-log scale. (■): polyacrylamide homopolymer, (▲): F5HY, (□): F3HY, (Δ): F7HY, (●): F2HY, (◇): HY5, (\*): F4HY

$$\log_{10}M[\eta] = 14.50 - 0.4248V_e \quad (12)$$

**Effect of Charge Density on the Elution Volume.** Figure 4 shows SEC chromatograms for polyacrylamide and polyacrylamide-co-sodium acrylate at various hydrolysis degrees. When the hydrolysis degree, or charge density, is increased the chromatogram shifts to lower elution volumes indicating a larger hydrodynamic volume. This is to be expected since an expansion of the polymer coil occurs when the electrostatic repulsion is increased.

**Relationship between the Molecular Weight and the Elution Volume for Polyacrylamide-co-Sodium Acrylate.** Figure 5 shows a plot of the logarithm of the molecular weight as a function of retention volume for various hydrolysis degrees. The parameters  $D_1'$  and  $D_2'$  have been regressed and are found to decrease linearly with the logarithm of the hydrolysis degree:

$$D_1' = 11.22 - 0.5055 \log HD \quad (\rho=0.9985) \quad (13)$$

$$D_2' = 0.2650 - 0.0148 \log HD \quad (\rho=0.9994) \quad (14)$$

The above correlations hold provided the hydrolysis degree exceeds 9%. For sodium acrylate levels less than 9% the  $D_1'$  and  $D_2'$  values for the nonionic polyacrylamide exceed those for the polyelectrolyte. This is a similar observation as reported in a prior publication (9) for the behavior of the Mark-Houwink exponent 'a' at low hydrolysis degrees. The above dependence can be explained through a combination of hydrogen bonding and electrostatic forces. For nonionic chains intramolecular hydrogen bonds between the C=O and NH<sub>2</sub> groups result in extended segments with an oriented structure (23). At low charge concentrations the oriented structure of the polyacrylamide is partly reduced due to a lower concentration of NH<sub>2</sub> groups. At the same time the concentration of COO<sup>-</sup> groups is insufficient to generate sufficient electrostatic expansion to compensate for the lost expansion due to hydrogen bonding. Therefore, for sodium acrylate levels below 9% the chain expansion is less than for pure polyacrylamide.

**Comparison of SEC Measurement with Light Scattering Data.** Table IV shows the measured elution volumes and calculated weight average molecular weights for polyacrylamide-co-sodium acrylate over a range of copolymer compositions and molecular weights. The molecular weights were regressed with the use of the universal calibration (equation 12), as well as the 'linear' calibration curve (equation 5) where the parameters  $D_1'$  and  $D_2'$  are slight function of the copolymer composition (equations 13 and 14). Also tabulated are the weight average molecular weights measured by light scattering (equation 8). The linear calibration curve provided an average accuracy ( $1-M_{w,SEC}/M_{w,LS}$ ) of  $\pm 11.5\%$ , whereas the universal calibration had an average accuracy of  $\pm 19.8\%$ . With neither calibration curve are the molecular weights systematically over or underpredicted. The superior data obtained with the linear calibration is not surprising since it is regressed to both molecular weight and copolymer composition data. The universal calibration has larger errors due to the

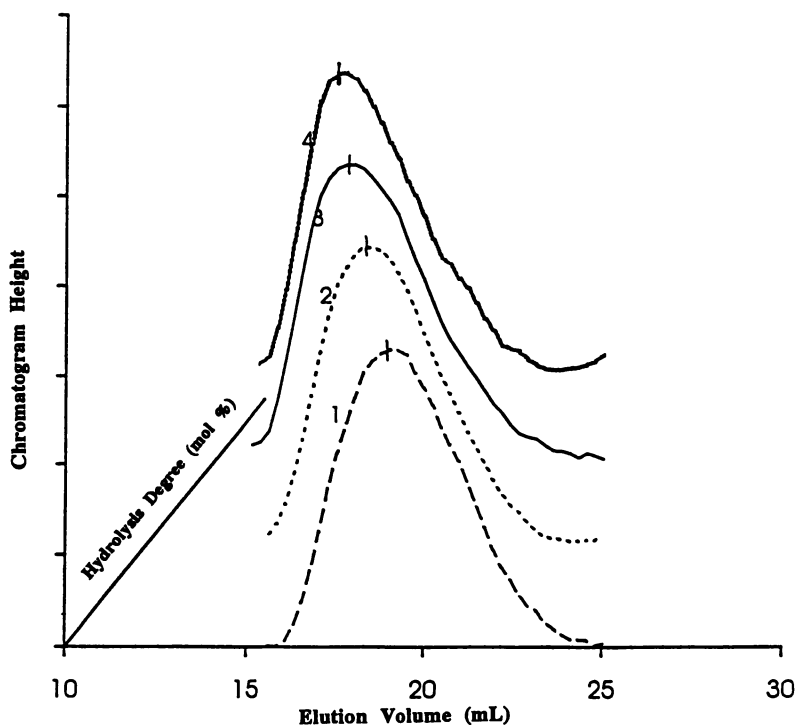


**Figure 4:** SEC chromatograms for polyacrylamide (HY5) and polyacrylamide-co-sodium acrylate at various hydrolysis degrees. When the hydrolysis degree, or charge density, is increased the chromatogram shifts to lower elution volumes indicating a larger hydrodynamic volume. Curve 1: polyacrylamide homopolymer, curve 2: 11.5 mol% sodium acrylate, curve 3: 19.8 mol % sodium acrylate, curve 4: 30.8 mol % sodium acrylate.

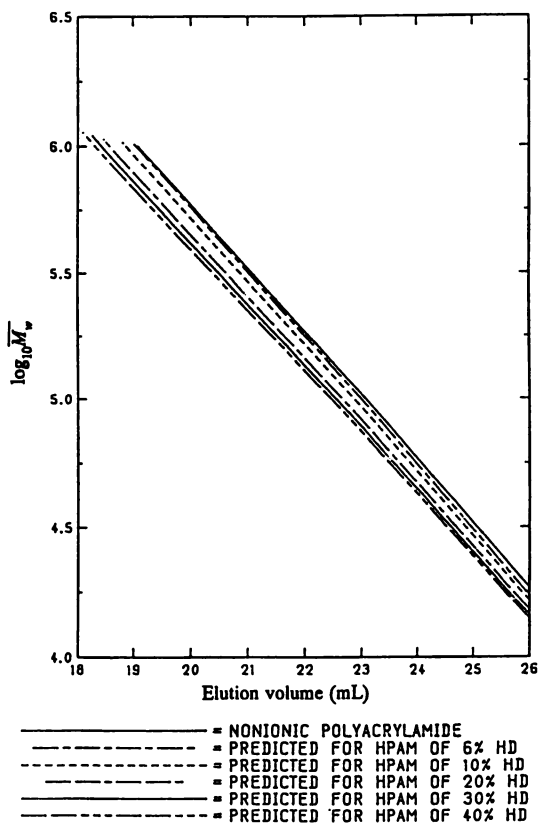


**Figure 5:** Logarithm of the molecular weight as a function of retention volume for various hydrolysis degrees. The calibration for polyacrylamide homopolymer is based on experimental data. The calibration curves for various hydrolysis degrees (HD) were calculated from equations (5,13,14).

**Table IV: A Comparison of the Weight Average Molecular Weights as measured by Light Scattering with those estimated by Size Exclusion Chromatography**

Sample Identification	Copolymer Composition (mol % sodium acrylate)	Weight Average Molecular Weight (Light Scattering) (Stoichiometric) (daltons)	Weight Average Molecular Weight (SEC, daltons) (Linear Calibration, Eqs. 5,13,14)	Weight Average Molecular Weight (SEC, daltons) (Universal Calibration, Eq. 12)
F7HY	10.77	27,800	27,300	23,970
	36.00	30,000	/	/
F5HY	36.08	30,000	34,210	38,330
	10.30	102,300	124,370	129,400
	16.70	104,300	128,110	132,090
F4HY	34.42	110,000	121,100	128,060
	39.20	111,500	129,940	148,280
	9.68	207,300	196,560	171,990
F3HY	31.90	221,700	187,370	157,960
	34.90	223,700	178,350	148,160
	6.40	409,300	435,410	383,780
HY5*	9.95	413,300	414,200	394,530
	14.90	420,300	413,500	374,890
	23.20	431,100	/	/
	26.00	434,700	422,460	378,760
	33.10	443,900	396,900	389,770
F2HY	9.46	1,061,500	1,230,500	1,299,100
	11.50	1,068,300	1,234,000	1,348,200
	20.15	1,097,000	/	/
F2HY	36.60	1,132,500	/	/
	10.30	1,022,900	1,167,500	1,130,500
	32.30	1,093,000	1,229,100	1,399,200
	33.40	1,096,000	1,216,200	1,328,300

\* HY5 is an unfractionated polyacrylamide with a PDI of 2.5.

variance introduced to the calculation from the intrinsic viscosity measurements, which lowered the correlation coefficient. Improved accuracy can be obtained with the universal calibration curve if the Mark-Houwink equation is employed with the constants 'K' and 'a' determined from the polynomials given in equations (9 and 10). Figure 6 provides visual verification of the agreement between the calculated molecular weights from the linear SEC calibration and those measured by light scattering

## Conclusions

The universal calibration method is valid for the estimation of molecular weights of ionic polyacrylamide-co-sodium acrylates and nonionic polyacrylamides and can be based on a calibration from polyacrylamide homopolymers.

The molecular weights of ionogenic copolymers can be calculated from either the application of the universal calibration or the correlation  $\log_{10}M = D_1' - D_2' V_e$ , where  $D_1'$  and  $D_2'$  are functions of the hydrolysis degree (copolymer composition). The latter provides superior agreement with light scattering data.

The polyelectrolyte effects commonly observed in aqueous measurements of water soluble polymers are suppressed for polyacrylamide-co-sodium acrylate in 0.2 M  $\text{Na}_2\text{SO}_4$ .

Light scattering characterization of PAM-co-NaAc is valid provided the polymer solution and solvent are at chemical potential equilibrium. The equilibrium condition is primarily manifested in the specific refractive index increment, which must be estimated on well dialyzed samples to avoid introducing large systematic errors into the molecular weight estimation.

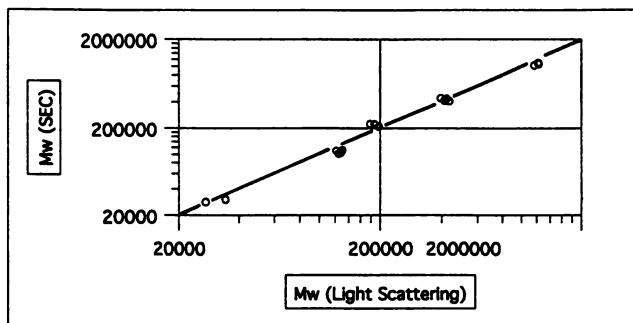


Figure 6: The weight average molecular weight determined by SEC ( $M_{w,SEC}$ ) is compared with the weight average molecular weight determined by light scattering ( $M_{w,LS}$ ). The molecular weights calculated from the SEC chromatograms and the universal calibration are in reasonable agreement with the absolute measurements as is evidenced by the proximity of the data to the  $45^\circ$  line. (O): Calculated from the universal calibration (equation 12).

**Literature Cited**

1. Troung, N.D., Galin, J.C., Francois, J., Pham, Q.T., *Polymer*. 1986, 27, 459.
2. Candou, F., Zekhini, Z., Heatley, F., *Macromolecules*. 1986, 19, 1895.
3. Troung, N.D., Galin, J.C., Francois, J., Pham, Q.T., *Polymer*. 1986, 27, 467.
4. Ellwanger, T.E., Jaeger, D.A., Barden, E., *Polymer Bulletin*. 1980, 3, 369.
5. Hamielec, A.E., Ray, W.H., *J. Appl. Poly. Sci.* 1969, 13, 1317.
6. Hashimoto, T., Sasaki, H., Aiura, M., Kato, Y., *J. Polym. Sci. Polym. Phys. Ed.* 1978, 16, 1789.
7. Hamielec, A.E., Syring, M., *Pure & Appl. Chem.* 1985, 57(7), 955.
8. Balke, S.T., Hamielec, A.E., *J. Appl. Poly. Sci.* 1969, 13, 1381.
9. Wu, X.Y., Hunkeler, D., Pelton, R.H., Hamielec, A.E., Woods, D.R., *J. Appl. Polym. Sci.*, 1991, 42, 2081.
10. Hunkeler, D., Wu, X.Y., Hamielec, A.E., *J. Appl. Polym. Sci.* 1992, 46, 649.
11. Chee, K.K., *J. Appl. Polym. Sci.* 1985, 30, 2607.
12. Fanood, M.H.R., George, M.H., *Polymer*. 1987, 28, 2241.
13. Hunkeler, D., Hamielec, A.E., *J. Appl. Polym. Sci.* 1988, 35, 1603.
14. Sutton, T.L., MacGregor, J.F., *Canadian J. Chem. Eng.* 1977, 55, 609.
15. Reilly, P.M., Patino-Leal, H., *Technometrics*. 1981, 23(3), 221.
16. Kulicke, W.-M., Bose, N., *Polymer Bulletin*. 1982, 7, 205.
17. Kulicke, W.-M., Hori, H.H., *Colloid and Polymer Sci.* 1985, 263, 530.
18. Gunari, A.A., Gundiah, S., *Makromol. Chem.* 1981, 182, 1.
19. Kulicke, W.-M., Siesler, H.W., *J. Polym. Sci. Polym. Phys.* 1982, 20, 557.
20. Klein, J., Conrad, K.-D., *Makromol. Chem.* 1978, 179, 1635.
21. McCarthy, K.J., Burkhardt, C.W., Parazak, D.P. *J. Appl. Polym. Sci.* 1987, 33, 1699.
22. Brandup, J., Immergut, E.H., *Polymer Handbook*, 2nd Ed., John Wiley & Sons: New York, NY, 1975.
23. Kulicke, W.-M., Kniewske, R., Klein, *J. Prog. Poly. Sci.* 1982, 403.

RECEIVED August 6, 1993

## Chapter 14

# Electric Transport of Polyelectrolytes in Aqueous Salt-Free Solutions

Amer H. Shaaban, Kerrie Behilo, and Paul Ander<sup>1</sup>

Department of Chemistry, Seton Hall University, South Orange, NJ 07079

The counterion condensation theory of Manning has influenced polyelectrolyte research since its inception. Principally, the charge density parameter,  $\xi$ , governs the solution properties of polyelectrolyte solutions. The theory proposes that counterion condensation occurs when  $\xi=1$  for monovalent counterions. It was desirable to investigate the critical point for the poly(acrylates), namely aqueous solutions of sodium poly-(acrylic) acid and sodium poly(methacrylic) acid at several charge densities. The conductance, electric mobility of the polyion and the counterion, sodium, were measured along with the reduced viscosities of these solutions to elucidate any configurational changes as  $\xi_c=1$  is approached. The degree of dissociation of the polyions were calculated and compared to the theory.

The counterion condensation (CC) theory of Manning (1-5) is still being scrutinized. Nevertheless, the CC theory is thought of widely when rationalizing experimental results for a wide variety of properties and it is not difficult to apply. Principally, this two state theory for the counterion has the infinite line charge polyelectrolyte dissociating its counterions completely if  $\xi < \xi_c$ , with the charge density parameter (reduced charge density, stoichiometric charge density parameter)

$$\xi = e^2/(\epsilon k T b) \quad (1)$$

with  $e$  the elementary charge,  $\epsilon$  the bulk dielectric constant,  $k$  is the Boltzmann constant,  $T$  the absolute temperature, and  $b$  the average axial distance between charges and  $\xi_c = |Z_c|^{-1}$ , where  $Z_c$  is the counterion valence. When  $\xi > \xi_c$ , an instability exists requiring counterions to condense so that the effective value of  $\xi$  is reduced to  $\xi_c$ , with the remaining ions dissociated in the ion atmosphere. Experimental findings have shown

<sup>1</sup>Corresponding author

0097-6156/94/0548-0180\$06.00/0  
© 1994 American Chemical Society



monovalent counterions do indicate a critical charge density of unity for monovalent counterions. More recently, Ware and Klein (6), have shown using a 6-6 ionene bromide and varying the dielectric constant of the medium that the electrophoretic mobility of the polyelectrolyte had a discontinuity at  $\xi_c = 1$  and had a constant value for the mobility for  $\xi > 1$ . Also, Ander et al. (7) found that the sodium counterion diffusion coefficient in poly(acrylic) acid solutions at several degrees of neutralization was linear when the sodium ion diffusion coefficient was plotted against  $\xi^{-1}$  for  $0 < \xi^{-1} < 1$ , and constant for  $\xi^{-1} > 1$ , i.e., at reduced charge densities below the critical charge density. The precipitous drop found at  $\xi_c = 1$  was profound! Similar findings were reported for the sodium ion diffusion coefficient in aqueous solutions of sodium salts of poly(acrylamide) and carboxymethylcellulose for a range of  $\xi$  values (8). It was suggested (7,8) that the critical point could be a critical point of stability for not only the condensation of the counterion, but also for the conformation of the polyion as well. When the stoichiometric charge density is lower than the critical charge density, i.e.  $\xi < \xi_c$ , the potential of the polyelectrolyte remains constant by adjusting its local conformation. Manning rationalized this theoretically (5). Because of this phenomena, one of several problems to be investigated is the determination of the degree of dissociation of a polyelectrolyte over a range of  $\xi$  values across  $\xi_c$ . Here we report the results of such a study using the sodium salts of poly(acrylic) acid (NaPA) and sodium poly(methacrylic) acid (NaPMA) aqueous solutions at several degrees of neutralization. Conductance and electric mobility measurements were made on aqueous solutions of these polyelectrolytes to evaluate the degree of dissociation of the polyelectrolyte solutions and both the electric mobility of polyion and of the counterion were determined, unlike the previous assumptions of Wall et al. (9), where the counterion mobility was assumed to be equivalent to its value in salt solutions. Two concentrations of 0.0010N and 0.010N NaPA and NaPMA over the range  $0.50 < \xi < 2.85$  were studied. From the electric transport measurements, degrees of dissociation of these polyelectrolytes were evaluated.

### Experimental

**Isotachopheresis.** The electrophoretic mobilities were obtained using a Shimadzu IP-2A Isotachopheretic Analyzer (Shimadzu Scientific Instruments, Inc., Columbia, MD, USA) equipped with a 60 mm  $\times$  1.0 mm I.D. polytetrafluoroethylene first stage capillary coupled to a 100 mm  $\times$  0.5 mm I.D. fluorinated ethylenepropylene second stage capillary. The potential-gradient detector was fixed at 25°C. The stage one current ran for 8 to 12 minutes at 200  $\mu$ A, and stage two current continued for about 12 minutes longer at a current of 100  $\mu$ A.

The leading electrolyte used was 0.010N HCl solution, buffered to a pH of 3.0 with  $\beta$ -Alanine (Sigma Chemical Co., No. A-7752). A 12M HCl stock solution was diluted with distilled water to make the 0.010N HCl solution.  $\beta$ -Alanine was then added until the pH was determined to be between 2.99 and 3.03. The solution was stirred under vacuum for approximately 30 minutes to eliminate excess chlorine gas that could produce bubbles in the capillary tubes of the analyzer. The surfactant, Triton X-100 (Sigma) was also used to eliminate electroosmotic flow in the capillaries. The terminal electrolyte used was a 0.010M n-caproic acid (Aldrich Chemical Co., Cat. # 15, 374-5) solution with pH between 3.4 and 3.5. The 99.5% solution was diluted with distilled water without additional buffers added to it. Isotachopheresis was

used in determining the mobilities of the sodium poly(acrylate) solutions with minimal error. The average relative deviation is 0.55% provided that the counterions are fully dissociated or fully bound to the polymer; it is especially useful since microliter volumes can be used with good results, as was indicated in past publications. The solutions were injected into the port where it mixes with the leading and terminal electrolyte solutions. The applied current then separate the three solutions according to their charge densities. The higher the net charge of the molecule, the quicker it will migrate in the separation tubes. The detector cell at the end of the migration tube measures the potential gradients of the separated ion zones and potential is graphed as step heights against time of migration. From the isotachopherograms, the effective mobility  $U_p$  can be measured. The ratio in millimeters of the step heights of the polymer sample  $h_p$  to that of the leading electrolyte  $h_L$ , is related to the mobility in the following manner

$$U_p = U_L(h_L/h_p) \quad (2)$$

where the mobility of the chloride ion ( $Cl^-$ ) in water is  $7.91 \times 10^{-4} \text{ cm}^2/V \text{ s}$  at  $25^\circ\text{C}$ .

**Conductivity.** Conductivity measurements were made in a thermostated bath at  $25.00 \pm 0.01^\circ\text{C}$  using a Pyrex conductivity cell of the modified Shedlovsky design. The electrodes had been lightly platinized with platinum black. A Beckman model RC-18A conductivity bridge which utilizes a precision a.c. Wheatstone bridge was employed using a frequency of 3000 Hz. The resistance of polyelectrolyte is not frequency dependent in the audio range and therefore, no attempt was made to correct for frequency dependence. The cell constant was obtained from measurements of the conductivity of aqueous solutions of KCl. The resulting value of  $1.2509 \pm 0.0007 \text{ cm}^{-1}$  was verified throughout the study.

**Preparation of Polyelectrolytes.** Stock solutions of poly(acrylic) acid and poly(methacrylic) acid were prepared by dissolving a known weight of the hydrogen form of the polymer in a 500 mL volumetric flask and diluting to the mark with doubly distilled water. After complete dissolution of the polymer sample, the stock solution was dialyzed against distilled water for three days and then titrated with standard sodium hydroxide to a phenolphthalein end point. The equivalent weight was calculated and found to be 72 g/eq for poly(acrylic) acid (HPA). For HPA and HPMA solutions, 0.010M NaOH was then used to alter the degree of neutralization of the polyions, HPA and HPMA. For a pH of 9.8, the HPA solution is known to be fully neutralized and hence the degree of neutralization ( $\alpha_N$ ) is unity, and the relationship between charge density ( $\xi$ ) and the degree of neutralization is

$$\alpha_N = \xi/2.85 \quad (3)$$

and the volumetric ratio is  $V_u = (V_t \xi / 2.85)$ , where  $V_u$  is the volume of NaOH needed to obtain a specific  $\xi$  value, and  $V_t$  is the volume of NaOH used to obtain the phenolphthalein end point in mL. All solutions were then stored in poly(ethylene) containers and filtered prior to any measurement. The relationship between charge density and pH can be therefore found to be directly proportional, i.e. an increase in pH, or the degree of neutralization causes an increase in the charge density of the polyelectrolyte solution, where equation 3 above clearly states it. The measured pH for NaPA solutions as a function of  $\xi$  is given in Table I.

## Results and Discussion

The equivalent conductance of the polyelectrolyte solutions is

$$\Lambda = 10^3(\kappa - \kappa^0)/C \quad (4)$$

where  $\kappa$  and  $\kappa^0$  are the specific conductances of the solution and solvent, respectively, and  $C$  is the equivalent concentration of the solution. For a polyelectrolyte in water,  $\kappa$  is much greater than  $\kappa^0$  and  $\kappa^0$  can be neglected. The concentration dependence of the equivalent conductance of fully neutralized NaPA ( $\xi = 2.85$ ) and for HPA in aqueous solutions at 25°C are shown in Figure 1. It is well known that HPA is almost completely undissociated in water and hence, its  $\Lambda$  values are low (10). With a crude approximation, Okubo (10) showed that the fraction of dissociated charges of HPA increased slightly as its concentration decreased; then the rise in  $\Lambda$  as dilution proceeds is readily understood. Since NaPA is partially dissociated, the CC theory of Manning is a possible source for the interpretation of the experimental points in Figure 1 (11). The curves in all graphs were apparent average values of the points. The line charge model for the polyelectrolyte contains both electrophoretic and relaxation effects and the equivalent conductance of the polyion is

$$\lambda_p = (279A|Z_c|^{-1}|\ln \lambda_{Da}|)/(1 + 43.2A(|Z_c|\lambda_c^0)^{-1}|\ln \lambda_{Da}|) \quad (5)$$

where  $A = \epsilon kT/(3\pi\eta e)$ , and  $\eta$  is the solvent viscosity in poise (0.00803P),  $\lambda_D$  is the Debye screening parameter and is defined as

$$\lambda_D^2 = 4\pi e^2 \xi^{-1} N_A C / (1000 \epsilon kT) \quad (6)$$

and  $N_A$  is Avogadro's number and  $C$  is the equivalent concentration of the polyion. In equation 5,  $a$  is the polyion radius, and for poly(acrylic) acid,  $a$  has a value of 2.5Å. The dashed lines in Figure 1 indicate that the Manning theory accounts for the decrease in  $\Lambda$  with an increase in  $C$ ; however, the values chosen for the radius of the polyion in equation 5 appear to fit the experimental values for the lowest concentration when  $2.5 < a < 6.0$  Å, which are realistic values. To achieve accord between theory and experiment for the higher concentrations between 0.0021N and 0.0090N, higher, unrealistic values of the polyion radius are required of the theory. It should be recalled that the theory should be most validly applied at the lowest concentration.

To further analyze the data, the method of Vink (12-14) was applied. Equation 4 could be written as

$$\Lambda = 10^3(\kappa - \kappa^0)/C = \Lambda^0 + \Phi(C) \quad (7)$$

where  $\Lambda^0$  is the equivalent conductance at infinite dilution and  $\Phi(C)$  represents the effect of interionic conductivity on  $\Lambda$ . Equation 7 could be written as

Table I : Measured pH as a Function of Charge Density,  $\xi$ , for Sodium Poly(acrylic) Acid Aqueous Solutions, at 25°C

$\xi$	pH
0.50	5.90
0.70	6.41
0.90	6.65
1.00	6.67
1.30	6.98
1.50	7.21
2.00	7.78
2.50	8.59
2.85	9.17

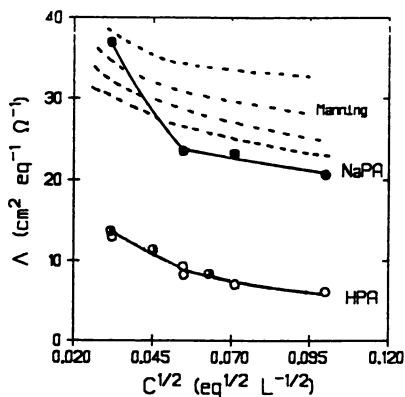


Figure 1. Equivalent conductance of NaPA/HPA aqueous solutions as a function of concentration at 25 °C. Half-open circles: Data of Okubo (10) for HPA. Broken lines: Manning's theoretical lines for NaPA using equation 3 for several polyion radii  $a$  from top to bottom in angstrom units: 2.5, 6.0, 10.0, and 15.0.

$$\kappa = \kappa^0 + 10^{-3}\Lambda^0 C + 10^{-3}C\phi(C) \quad (8)$$

where  $\Lambda^0$  could be obtained from the slope of the linear portion of the  $\kappa$  versus  $C$  plot if the derivatives of  $\kappa^0$  and  $C\phi(C)$  terms with respect to  $C$  are small and can be neglected when compared to  $\Lambda^0$ , and  $\kappa^0$  is the intercept at  $C = 0$ . Figure 2 indicates a linear relation is obtained for HPA and fully neutralized NaPA, with the slopes of 5.04 and 19.0  $\text{cm}^2/\text{eq } \Omega$  for HPA and NaPA, respectively. Vink obtained  $\Lambda^0 = 22.1 \text{ cm}^2/\text{eq } \Omega$  for NaPA, in close agreement with our findings. The value obtained from Figure 2 and equation 8 of  $1.02 \times 10^{-5} \text{ cm}^{-1} \Omega^{-1}$  for HPA was in agreement with the value obtained from the data of Okubo (10) of  $0.85 \times 10^{-5} \text{ cm}^{-1} \Omega^{-1}$  for HPA. The experimentally determined mobility,  $U_p$ , of the polyion of HPA is shown in Figure 3 and Table II, where  $U_p$  is in units of  $\text{cm}^2/\text{V s}$ . The profile of the curve in Figure 3 is similar to those obtained for typical macroions of higher charge densities, such as NaPA, which will be discussed later. At low concentrations, the rise in  $U_p$  will be attributed to the expansion of the polyion.

The limiting equivalent conductivity  $\Lambda^0$  is related to those of the individual ion equivalent conductances  $\lambda_c^0$  and  $\lambda_p^0$  by

$$\Lambda^0 = f(\lambda_c^0 + \lambda_p^0) \quad (9)$$

where  $f$  is an interaction parameter which includes electrostatic interactions between counterions and the polyion in addition to the degree of ionization. For finite concentrations equation 9 is usually written

$$\Lambda = f(\lambda_c^0 + \lambda_p) \quad (10)$$

To determine  $f$ , conductance and mobility experiments are determined. To obtain  $\lambda_p^0$  an equation analogous to equation 8 is assumed for the polyion

$$\kappa_p = \kappa_p^0 + \lambda_p^0 C + C\phi(C) \quad (11)$$

The electrophoretic mobility of the polyion  $U_p$  was determined and used to calculate  $\kappa_p$  from  $U_p = \lambda_p/F = 10^3 \kappa_p/CF$ , where  $F$  is Faraday's constant. The mobility values are shown in Figure 3, the profile of the curve to be discussed later. The plot of  $\kappa_p$  versus  $C$  for HPA solutions, shown in Figure 4, proved to be linear and the slope and intercept are  $\lambda_p^0 = 40.9 \text{ cm}^2/\text{eq } \Omega$  and  $\kappa_p^0 = 1.02 \times 10^{-5} \text{ cm}^{-1} \Omega^{-1}$ , respectively. It is interesting that Okubo (10) found a  $\lambda_p^0$  value of  $42.0 \text{ cm}^2/\text{eq } \Omega$  for the acrylate ion, a value close to that found here for the polyacrylate ion. Now  $f$  can be approximated from  $f = \Lambda/(\lambda_c^0 + \lambda_p^0)$ . The average value for  $f$  was found to be  $0.020 \pm 0.003$  in very close agreement with the results of Okubo who found a very slight increase of  $f$  with dilution over the same concentration range. With a knowledge of  $\Lambda$ ,  $U_p$  and  $U_{\text{Na}^+}$ , the interaction parameter,  $f$ , can be determined from

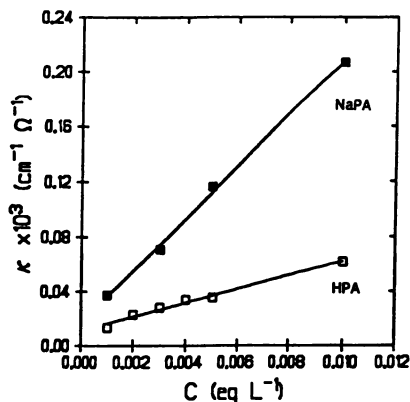


Figure 2. Specific conductance of HPA (open squares) and NaPA (solid squares) ( $\xi=2.85$ ) aqueous solutions as a function of concentration at 25 °C.

Table II : Measured Specific Conductance,  $\kappa$ , and Mobility,  $U_p$ , for HPA as a Function of Concentration at 25° C

$C \times 10^3$ (eq/L)	$U_p \times 10^4$ (cm <sup>2</sup> /V s)	$\kappa_p^* \times 10^5$ (cm <sup>-1</sup> Ω <sup>-1</sup> )	$\Lambda$ (cm <sup>2</sup> /eq Ω)
5.04	3.95	19.2	7.04
10.0	4.51	43.5	6.14
30.0	4.36	126	8.97
50.0	4.22	204	7.98

\*  $\kappa_p$  was computed from  $\kappa_p = FCU_p/10^3$

$$\Lambda = f(\lambda_p + \lambda_{\text{Na}^+}) = fF(U_p + U_{\text{Na}^+}) \quad (12)$$

For two concentrations, 0.0010N and 0.010N polyelectrolyte, the quantities in equation 12 were determined experimentally over the range  $0.50 < \xi < 2.85$ . The conductance results are represented in Figures 5 and 6 for NaPA and NaPMA, respectively. It is noted from Figure 5 for NaPA that there is a slight rise in  $\Lambda$  below the critical  $\xi$  value of unity; at  $\xi$  values close to  $\xi_c$  there is a break in the curve followed by a steeper rise in the  $\Lambda$  values, then  $\Lambda$  levels off as  $\xi$  increases for  $\xi > \xi_c$ . This is more pronounced for the more dilute solution. The break at  $\xi_c$  is more clearly accentuated for the NaPMA in Figure 6. One would expect similar trends for the mobility of the polyion. These results are shown in Figure 7 and 8 for NaPA and NaPMA, respectively. To account for the rise in  $U_p$  as  $\xi$  increases, it is useful to look at the change in the configuration of the polyelectrolyte as  $\xi$  increases initially. For both polyelectrolyte concentrations, 0.010N and 0.0010N, there is a pronounced rise in the reduced viscosity ( $\eta_{sp}/C$ ) as  $\xi$  increases to unity shown in Figures 9 and 10 for NaPA and NaPMA, respectively, a definite break at  $\xi_c = 1$ , followed by a general leveling off of the reduced viscosity for  $\xi > \xi_c$ . This trend is interpreted in reference (10) where the large increase in  $\eta_{sp}$  occurs at approximately  $\xi_c$  with a small change in the degree of neutralization, followed by a leveling off. It is interpreted from Okubo's plot that a clear break occurs close to  $\alpha_N$  of 0.30, which is close to the critical  $\xi$  value of unity. At low charge densities, it is plausible that the ion atmosphere is not tight about the polyion and so the polyion can expand as the low values of  $\xi$  increase. At  $\xi_c = 1$ , Manning has shown theoretically that a slight conformation change is possible to keep the effective  $\xi$  value at critical value, even though the stoichiometric charge density is increased. This can account for the constant values of  $\eta_{sp}/C$  for  $\xi > \xi_c$ , as it has for the constant values of the counterion diffusion constant for  $\xi > \xi_c$  (7,8).

Use is usually made of equation 12 to evaluate the interaction parameter,  $f$ . However, it was possible to determine experimentally the value of  $\lambda_c$  at each  $\xi$  value and not rely on the assumption that  $\lambda_c \approx \lambda_c^0$ . To accomplish this, the electrophoretic mobility of the sodium counterion  $U_{\text{Na}^+}$  was determined for each  $\xi$  value. The results for NaPA and NaPMA are shown in Figures 11 and 12, respectively. For NaPA,  $U_{\text{Na}^+}$  increases as  $\xi$  increases at low  $\xi$  values, reaches a maximum  $U_{\text{Na}^+}$  at approximately  $\xi=1$  and then levels off for 0.0010N and decreases for 0.010N solutions. It is again interesting that the break in the curve occurs close to the critical charge density of unity, where Manning predicts changes in counterion condensation occurs, as well as a conformation change. For NaPMA solutions, shown in Figure 12, there is no initial rise in  $U_{\text{Na}^+}$  at low  $\xi$  values, but a continuous decrease with a break at approximately  $\xi_c$ , followed by either a leveling off or a decrease in  $U_{\text{Na}^+}$ . At low  $\xi$  values for NaPMA, below  $\xi = 0.5$ , it should be recalled that a unique conformation change was found to occur and to indicate an anomalous behavior for this polyelectrolyte at low  $\xi$  values.

The experimental results for both NaPA and NaPMA will be used to calculate the interaction parameter,  $f$ , using equation 12. The results are

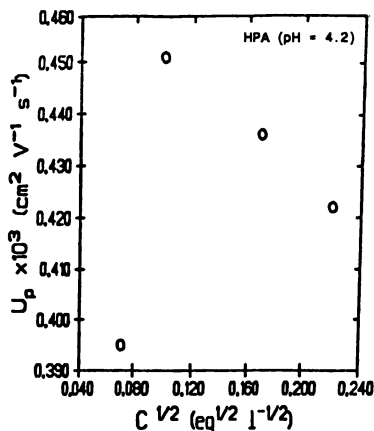


Figure 3. Electric mobility of the polyion HPA as a function of concentration at 25 °C.

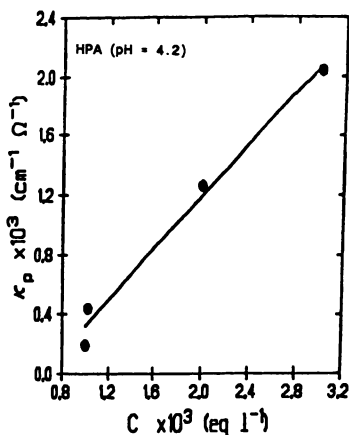


Figure 4. Polyion specific conductance of HPA aqueous solutions as a function of polymer concentration at 25 °C.

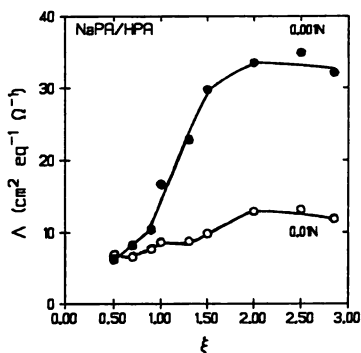


Figure 5. Equivalent conductance of NaPA aqueous solutions as a function of charge density at 25 °C.



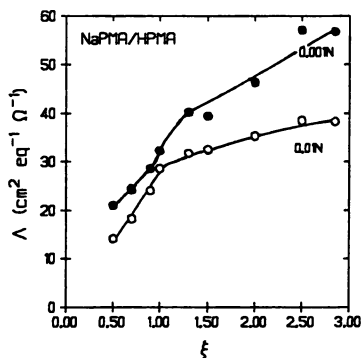


Figure 6. Equivalent conductance of NaPMA aqueous solutions as a function of charge density at 25 °C.

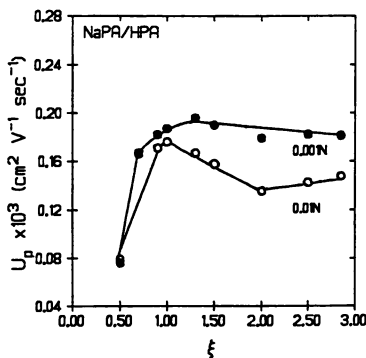


Figure 7. Electric mobility of NaPA aqueous solutions as a function of charge density at 25 °C.

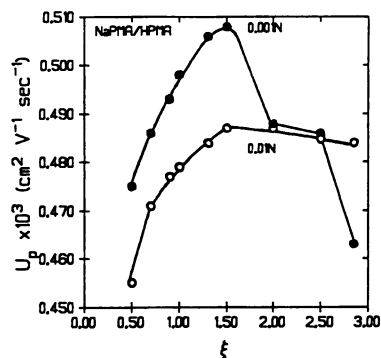


Figure 8. The electric mobility of NaPMA aqueous solutions as a function of charge density at 25 °C.

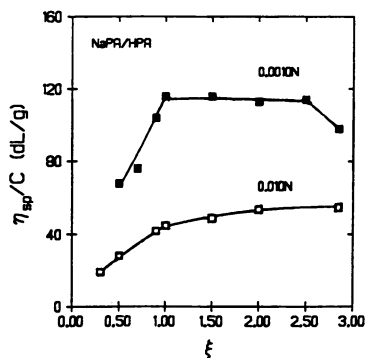


Figure 9. The reduced viscosity of NaPA aqueous solutions as a function of charge density at 25 °C.

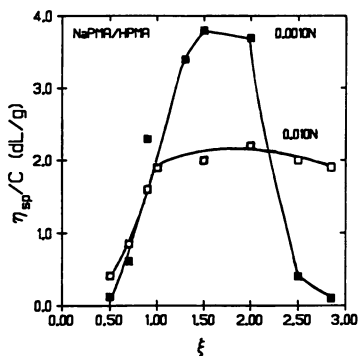


Figure 10. The reduced viscosity of NaPMA aqueous solutions as a function of charge density at 25 °C.

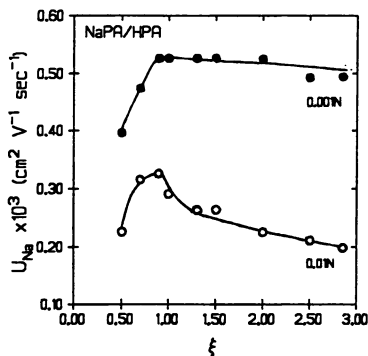


Figure 11. Electric mobility of the  $\text{Na}^+$  counterion in NaPA aqueous solutions as a function of charge density at 25 °C.

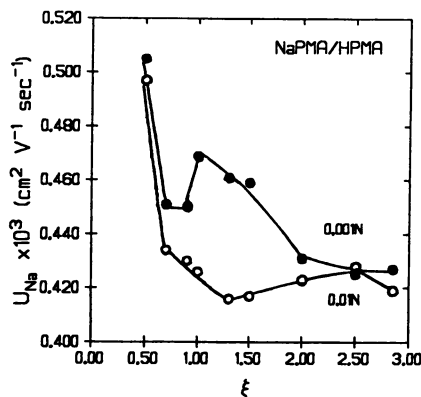


Figure 12. The counterion mobility of NaPMA aqueous solutions as a function of charge density at 25 °C.

illustrated in Figures 13 and 14 for NaPA and NaPMA, respectively. The data for 0.0010N NaPA appears to be close to the values obtained from counterion diffusion studies (7,8), while the  $f$  values obtained for 0.010N NaPA seem to be closer to the Manning theoretical curve for  $\xi > 2$ . Figure 14 shows that the theoretical curve underestimates the dissociation of counterions, especially for  $\xi > 1$ . More of the counterions might be conducting than is accounted for by the theory. However, the "break" observed near  $\xi_c = 1$  gives some justification of the theoretical predictions of the critical point. It was of interest to obtain  $f$  using the method of Shavit (15), who considered  $f$  to be the degree of dissociation of the polyelectrolyte. For fully neutralized NaPA/HPA ( $\xi = 2.85$ ), the equivalent conductances of LiPA, NaPA and KPA were determined as a function of the concentration (16). The data is shown in Figure 15, where it is evident that the three polyelectrolytes show the same independence of concentration from 0.10N to 0.0050N followed by a rise in  $\Lambda$  as further dilution proceeds. At any given concentration, the  $\Lambda$  values are in the order LiPA < NaPA < KPA. This is the order of binding to polycarboxylates found by Strauss (17) using dialysis studies. If these counterions interact with the polyion in the same manner,  $f$  can be defined

$$f = (\Lambda_{MP} - \Lambda_{NP}) / (\lambda_M^0 - \lambda_N^0) \quad (13)$$

where the subscripts M and N refer to different counterions. From Figure 16, it is seen that for a fully neutralized polyacrylate,  $f$  or the degree of dissociation is independent of concentration over most of the concentration range studied, with a slight difference at the most dilute solutions. The value of  $f = 0.43$  appears to be independent of the pair of counterions used. It is gratifying that this method yielded a value for  $f$  in close agreement with those obtained for  $\xi = 2.85$  in Figure 13 ( $f = 0.35$ ), and not too far from the

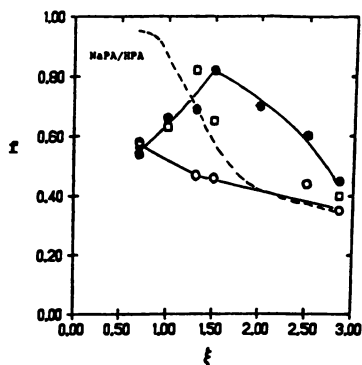


Figure 13. The interaction parameter,  $f$ , as a function of charge density for aqueous solutions of NaPA at 25 °C. Solid circles: 0.0010N NaPA. Open circles: 0.010N NaPA. Squares: Diffusion data of reference 7 for 0.0010N NaPA. Dashed line: Manning prediction.

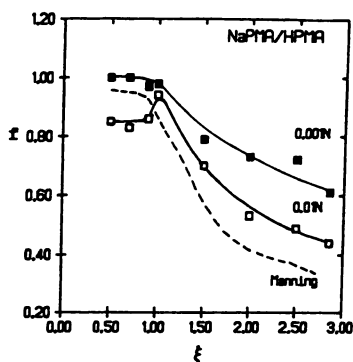


Figure 14. The interaction parameter,  $f$ , as a function of the charge density for aqueous solutions of NaPMA at 25 °C.

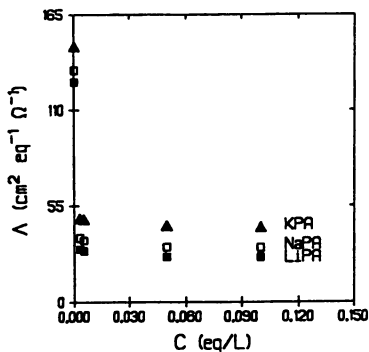


Figure 15. Equivalent conductance of LiPA, NaPA, and KPA aqueous solutions as function of concentration at 25 °C.

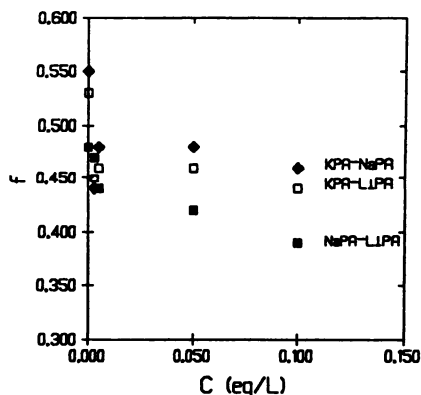


Figure 16. Interaction parameter,  $f$ , for LiPA, NaPA, and KPA aqueous solutions calculated using the method of Shavit (17).

theoretical value of Manning of  $f = 0.866(|Z_c|\xi)^{-1} = 0.31$ . It may be that the condensation theory overestimates the electrostatic interactions.

It should be understood from this work that the critical charge density parameter is a real representation of the solution at a transition state. The nature of the transition at  $\xi_c$  need further experimentation. The discontinuity of a solution property at this particular point has been shown from different experiments (8,18-23) and can be interpreted from several others. Thorough discussions of the counterion condensation theory is found in two recent excellent monographs (24-26).

## References

1. Manning, G.S. *J.Chem.Phys.* **1967**, *46*, 2624.
2. Manning, G.S. *J.Chem.Phys.* **1969**, *51*, 924, 934.
3. Manning, G.S. *Annual Rev. Phys. Chem.* **1972**, *117*.
4. Manning, G.S. *Acct. Chem. Res.* **1979**, *12*, 443.
5. Manning, G.S. *J. Chem. Phys.* **1988**, *89*, 3772.
6. Klein, J.W.; Ware, B.R. *J. Chem. Phys.* **1983**, *80*, 1334.
7. Ander, P.; Kardan, M. *Macromol.* **1984**, *17*, 2431.
8. Henningson, C.; Karluk, D.; Ander, P. *Macromol.* **1987**, *20*, 1286.
9. Huizenga, J.R.; Grieger, P.F.; Wall, F.T. *J.Amer.Chem.Soc.* **1950**, *72*, 2636.
10. Okubo, T. *Macromol.* **1989**, *22*, 3651.
11. Manning, G.S. *J. Phys. Chem.* **1975**, *79*, 262.
12. Vink, H. *J. Chem. Soc. Far. Trans. 1.* **1989**, *85*, 699.
13. Vink, H. *J. Chem. Soc. Far. Trans. 1.* **1981**, *77*, 2439.
14. Vink, H. *Makromol. Chem.* **1982**, *183*, 2273.
15. Shavit, N. *Isr. J. Chem.* **1973**, *11*, 235.
16. Behilo, K., B.S. Thesis, Seton Hall University, **1993**.
17. Strauss, U.P.; Leung, Y.P. *J.Amer.Chem.Soc.* **1965**, *87*, 1476.
18. Penafiel, L.M.; Litovitz, T.A. *J. Chem. Phys.* **1992**, *96* (4), 3033.
19. Cesàro, A.; Paoletti, S.; Benegas, J.C. *Biophysical Chem.* **1991**, *39*, 1.
20. Kaji, K. Private Communications.

21. Okamoto, H.; Wada, Y. *J. Polymer. Sci.: Poly. Phys.* **1974**, *12*, 2413.
22. Sedlak, M.; Konak, C.; Stepanek, P.; Jakes, J. *Polymer* **1987**, *28*, 873.
23. Hirasawa, E.; Yamamoto, Y.; Tadano, K.; Yano, S. *J. Applied Poly. Sci.* **1991**, *42*, 351.
24. Mandel, M. In *Polyelectrolytes*, Hara, M. Ed., Marcel Dekker, Inc., New York, **1992**, Chapter 1.
25. Hodgson, D.F.; Amis, E. In *Polyelectrolytes*, Hara, M. Ed. Marcel Dekker, Inc., New York, **1992**, Chapter 3.
26. Schmitz, K.S. *Macroions In Solution and Colloidal Suspension*, VCH Publishers, Inc., New York, **1993**.

RECEIVED September 3, 1993

## Chapter 15

# Role of Multivalent Cations in Condensation of DNA

Victor A. Bloomfield, Chenglie Ma, and Patricia G. Arscott

Department of Biochemistry, University of Minnesota, St. Paul, MN 55108

We critically survey the ways in which multivalent cations may induce the condensation of DNA, and describe results using alcohol-water mixtures which shed some light on the relative roles of electrostatics and solvent structure in the condensation process. DNA condensation arises from the interplay of several forces, including stiffness, electrostatic repulsion and counterion fluctuation attraction, hydration structure, crossbridging by condensing ligands, and interhelical binding between bases whose normal intra-duplex pairing and stacking have been disrupted by interactions with solvent or ligand.

DNA is often studied by physical techniques in dilute solution, where it is a wormlike or random coil with a very low segment density (e.g.  $4 \times 10^{-5}$  for T4 DNA). However, in biological systems such as cells and viruses, DNA is typically very tightly packaged, with a fractional occupancy of its domain that may approach 0.5. This enormous decrease in volume of the molecular coil is termed condensation. A fundamental problem in molecular biology, and in polymer physical chemistry, is to understand how DNA condensation is established and maintained. Model systems that can produce condensation in solution are of great interest for understanding DNA behavior inside cells and viruses. A general review of polymer condensation has been written by Frisch et al (1), and there are several recent overviews of DNA condensation mechanisms (2-5). Our purpose in this paper is to critically survey the ways in which multivalent cations may induce the condensation of DNA, and to describe our results using alcohol-water mixtures which shed some light on the relative roles of electrostatics and solvent structure in the condensation process.

Many different types of substances cause condensation of DNA. In aqueous solutions, condensation is caused by multivalent cations: the naturally occurring polyamines spermidine<sup>3+</sup> and spermine<sup>4+</sup> (6-8), the inorganic cation hexaammine cobalt (III),  $\text{Co}(\text{NH}_3)_6^{3+}$  (9, 10), which we shall henceforth abbreviate as CoHex(III), cationic polypeptides such as polylysine (11) and histone H1 (12). Divalent metal cations do not provoke condensation in water at room temperatures, but they will do so at somewhat elevated temperatures (13) or in water-methanol mixtures (14, 15). Ethanol at high concentrations is widely used as a precipitant in the purification of DNA, but under properly controlled conditions it can produce particles of defined morphology (16, 17). Even neutral polymers, such as polyethylene glycol, at high concentrations and in the presence of adequate concentrations of salt, can provoke

0097-6156/94/0548-0195\$06.00/0  
© 1994 American Chemical Society

DNA condensation (18). The resulting structure has been termed psi-DNA, or  $\Psi$ -DNA, the acronym for *Polymer-and-Salt-Induced* which describes the condensation process.  $\Psi$ -DNA is also produced by anionic polymers, such as polyaspartate, polyglutamate, and the anionic peptides found in the capsid of bacteriophage T4 (19).

In addition to the basic fact of condensation, the size and shape of the condensed particles is characteristic and presumably holds clues to underlying mechanisms. DNA condensation by multivalent cations leads to ordered particles. They are usually toroidal or rod-shaped in aqueous solutions, and rather uniform in size distribution regardless of DNA length (4), though closed circular DNA produces somewhat smaller particles (20). The size and shape of the condensates produced in nonaqueous solutions, or at high temperature, is more highly varied. Toroids and rods are produced as well as lateral aggregation of DNA into multistranded, fibrous structures (17). Permethylated spermidine produces a higher proportion of rods (21). Even when extensively aggregated networks are formed after long times, as predicted by statistical thermodynamic equilibrium theory (3), the initially formed ordered particles maintain their compact, discrete morphologies.

Comprehension of the fundamental mechanisms of DNA condensation is needed to understand packaging of DNA (and RNA) in viruses (22, 23), and the functional arrangement of DNA in eukaryotic nucleic and prokaryotic nucleoids (24, 25). DNA functions in compact environments stabilized by multivalent cations. In vitro, such environments can be produced by multivalent cations. They are probably a major factor in stabilizing compaction in vivo, as are proteins, RNA crosslinks (24), and crowding/excluded volume effects (18). Viral DNA packaging usually, though not always, requires polyamines (26). DNA condensation is required for efficient catenation and recombination (27), and changes in intracellular DNA compaction produced by varying polyamine levels affect susceptibility to radiation damage (28). Excluded volume and higher local concentration in condensed DNA may lead to a speedup of several orders of magnitude in renaturation of single stranded to double helical DNA (29). In biotechnology, DNA packaging is important for genetic transfer using viral vectors and liposomes.

The obvious importance of coulombic interactions in a polyion as highly charged as DNA might lead to the assumption that electrostatics is the dominant factor in regulating condensation. In the presence of divalent and higher valence cations, however, DNA behavior is not governed just by simple electrostatics. Most obviously, the very fact that condensation implies attractive forces means that other forces must overcome the coulombic repulsion between DNA phosphate charges. Hydration, counterion fluctuations, bridging by condensing ligands, and distortion of DNA secondary structure by binding interactions are also involved in condensation and other functionally significant changes of DNA behavior. Our purpose in this paper is to examine critically these various factors, to move closer to a balanced assessment of their relative importance.

### Interaction of multivalent cations with DNA

Many of the fundamental features of counterion interaction with DNA appear to be well understood. Polyelectrolyte theories, ranging from counterion condensation to Poisson-Boltzmann and beyond (30, 31) agree pretty well on the thermodynamic consequences of the strong field of the DNA charges for the behavior of the counterions, and on the localization of a relatively constant number of counterions near the DNA regardless of bulk ionic concentration (territorial binding in counterion condensation terms). Equilibrium dialysis measurements of the salt dependence of polyamine binding (32) shows that the predictions of counterion condensation theory are very well obeyed for cations of charge +2, +3, and +4. A study of CoHex(III) binding (33) showed that over the range from 52 to 159 mM Na<sup>+</sup>, the binding constants of CoHex(III) and spermidine<sup>3+</sup> to double stranded DNA are essentially the



same and have the salt dependence predicted by polyelectrolyte theory. The 5-6 fold greater efficiency of CoHex(III) in producing DNA condensation (9) must therefore be due to some specific factor not reflected in binding constants.

The predominantly coulombic interaction of polycations with DNA is buttressed by calorimetric measurements (34). For binding of spermine<sup>4+</sup> to salmon sperm DNA,  $\Delta H = 0$ . For poly (L-lysine) binding,  $\Delta H = -300$  cal/mol DNA-P; and for Mg<sup>2+</sup> binding,  $\Delta H = +350$  cal/mol DNA-P. All of these enthalpies are very small, indicating that association of cations with DNA is entropy-driven.

NMR studies of cation interaction with DNA have confirmed some of the basic ideas of territorial binding, but have also demonstrated some ion- and base sequence-specific tight binding. Wemmer et al (35) used NMR to study polyamine binding to a defined DNA sequence. They found no broadening of the spermine linewidth when most of it is bound to DNA, and weak positive NOEs. (Negative NOEs would be expected if spermine tumbled with the DNA relaxation time.) Similar results were obtained for spermidine. Polyamine mobility thus appears to be independent of its binding to DNA. This is true even in spermine-induced aggregates of DNA.

Pulsed field gradient NMR measurement (36) of the self-diffusion coefficient *D* of permethylated spermidine (PMS) fits best to a two-state model, in which the PMS is either free, or bound to DNA (of a range of lengths) where it has a diffusion coefficient equal to that of the DNA. The extent of binding is computed from the Poisson-Boltzmann cell model. This implies a considerable diminution of *D* when bound ( $\approx 3-5\%$  of *D*<sub>0</sub>) in contrast to the territorial binding model, which predicts *D*<sub>bound</sub>  $\approx 1/3$  *D*<sub>0</sub>. This could arise either because of high localization, or by trapping along the finite length of a DNA molecule. The latter appears more plausible in light of the results of Wemmer et al (35).

<sup>59</sup>Co and <sup>23</sup>Na NMR measurement of competitive interactions of CoHex(III) and Na<sup>+</sup> with helical B-DNA showed relatively minor changes in chemical shift and relaxation time, indicating that the octahedral coordination shell of CoHex(III) remains intact (37). More recent <sup>59</sup>Co NMR measurements (38) of CoHex(III) in the presence of DNA of varying GC content show evidence for at least three classes of bound CoHex(III): a small, transiently localized class; a larger, highly mobile class; and a very small, tightly bound class observed only with *M. lysodeikticus* DNA, which contains 72% G+C.

Crytallography shows a different side of oligocation-nucleic acid interactions. Since only those ligands which are stably bound to reproducible sites appear in crystal structures, ions which are territorially bound will not be seen. Indeed, the results surveyed previously in this section would suggest that no ions should ever be seen bound to DNA. But this is not the case, and the contradiction is instructive.

Early ideas on the interaction of polyamines with DNA came from the x-ray crystal structure of spermine-HCl (39). The polyamine was supposed to bind in the minor groove of the DNA, with its NH's making H-bonds with the DNA phosphates. The first two polyamine charges neutralize phosphates on one chain, and the other two bridge across the minor groove and neutralize phosphates on the opposing chain. Seemingly consistent with this picture, x-ray fiber photographs of the spermine-DNA complex showed the B-form of DNA at high humidity (40). Calculation of intensities was consistent with the minor groove-binding model. However, the interhelix distance increased with hydration, and reached an upper limit. This implied interhelical crosslinking, which was also compatible with computed fiber patterns.

Actual crystal structures (as opposed to fiber diffraction and model building) show a very different story. Spermine is a common component of crystallization buffers for nucleic acids. The first B-DNA structure, of a dodecamer (41), showed that spermine was bound in the major groove, and was associated with a bend at the GC-rich end of the duplex. This behavior is also found by computer simulation (42).

This association of bound spermine with loops or distortions of regular double helix structure was first noted in tRNA crystal structures (43). In a review (44) of

crystallographic evidence about metal and spermine binding to tRNA, two types of electronegative binding sites for cations were identified: pockets and clefts. "Pockets are formed by high concentrations of negative charge at a point produced by a sharp bend or loop in the negatively charged phosphate backbone or by the juxtaposition of accessible N and O atoms on adjacent bases. Clefts ... are formed when rows of backbone atoms approach each other closely." Metals prefer pockets, polyamines prefer clefts. Spermine is in the major (not minor) groove of the RNA double helix. It is in a slightly coiled conformation, rather than in the extended, all-trans form expected from the crystal structure of spermine-HCl. There is a strong contrast of these crystallographic studies of spermine binding, which show only two binding sites to tRNA, with equilibrium dialysis (45) which shows that there are 13-15 strong binding sites of spermidine to various tRNAs, and that binding is governed predominantly by electrostatic forces. It is probably generally true that there is much delocalized binding in addition to a few localized sites for most multivalent cations.

Returning to complexes of spermine with B-DNA, the highest resolution crystal structures are those of Williams et al (46). Spermine binds in the major groove of complexes of d(CGATCG) with the anthracycline drug 4'-epiadriamycin. A "continuous hydrophobic zone" is formed by the 5-methyl and C6 of thymidine, C5 and C6 of cytidine, and the chromophore of the anthracycline. Spermine, through its methylene residues, makes extensive van der Waals contacts with this hydrophobic zone. Different drug complexes have different geometries, but the flexibility of the spermine allows hydrophobic contacts to be made in all cases. About 5-7 water molecules are displaced by a spermine, indicating strong hydrophobic stabilization. Spermine binds near the floor of the major groove in these complexes, where the calculated electrostatic potential is highly negative. Therefore, favorable coulombic interactions are important in stabilizing the complexes. The amino groups of spermine make H-bonds to the DNA bases, phosphates, and sugars in some but not all cases; some of these are water-mediated. Thus, electrostatics, H-bonding, and hydrophobic interactions are all important in polyamine-DNA binding.

When the base sequence of the DNA permits (alternating purine-pyrimidine), binding of polyamines or CoHex(III) may provoke a transition from the right-handed B form to the left-handed Z form (47). In this initially solved structure, it was found that the spermine does not bind in the grooves, because they are very narrow. Instead, it binds between the molecules in the crystal. A very recently determined structure of the pure-spermine form of Z-DNA (magnesium free) at 1-Å resolution showed some striking features (48). Crystals of the DNA hexamer d(CGCGCG)<sub>2</sub> in the Z-conformation, when crystallized with Spm as the only multivalent cation, have structural features quite different from those of other Z-DNA crystals which had generally been crystallized from Mg-spermine solutions. The relative orientations and positions of the DNA molecules in the crystal are changed, and the DNA structure itself is different: The helix axis is compressed, the base pairs are shifted into the major groove, and the minor groove is narrower. Most important for a potential understanding of the role of polyamines in DNA condensation, each spermine interacts with three DNAs (and each DNA oligomer with three spermines). Thus crosslinking could stabilize the condensed form of DNA. This interhelical bridging has been found to be generally true for Z-DNA, but not for B-DNA. The spermine is quite long (15.4 Å from N1 to N14 in the pure-spermine form) but is not always completely stretched out. Its flexibility, as well as the dispersion of various sorts of interactions - electrostatic, H-bonding, and hydrophobic - along its length, allows for a wide variety of possible interactions with different DNA molecules.

When CoHex(III) and Mg<sup>2+</sup> are the crystallizing agents instead of spermine, crosslinks between molecules are not observed, but the structural basis for stabilization of the Z-form is clear (49). CoHex(III) stabilizes the Z-form of DNA at concentrations four orders of magnitude lower than does Mg<sup>2+</sup>. X-ray crystallography shows that the CoHex(III) ion forms five H-bonds to groups on the surface of

d(CGCGCG)<sub>2</sub>, binding to O6 and N7 of G as well as to a phosphate group in the Z<sub>II</sub> conformation. In contrast, Mg<sup>2+</sup> forms only three H-bonds through its hydration shell, to N7 and O6 of G. The greater number of H-bonds, specific steric fit, and higher charge all contribute to the greater stability of the CoHex complex.

These x-ray results (and similar hints from NMR) show that, in addition to the delocalized binding predicted by polyelectrolyte theory, specific complexes of polyamines and CoHex(III) with DNA and RNA can form. These may have distorted geometries and crosslinking between helices. The relevance of these observations for the mechanism of DNA condensation by multivalent cations is obvious.

### How multivalent cations may cause DNA condensation

There is strong evidence that electrostatic forces are important in condensation. The laws of physics require that something must be done to neutralize the strong repulsive interactions as negatively charged DNA segments approach closely; this is the most obvious reason that high salt is required in Ψ-condensation (18). Numerous studies (9, 10, 14, 50) make quantitative the requirement for reduction of coulombic interactions: approximately 90% of the DNA charge must be neutralized by counterion condensation before DNA collapse can occur. As reported later in this paper, this result holds for alcohol-water mixtures as well as for pure aqueous solvent.

However, there are some subtleties in this conclusion. Co(NH<sub>3</sub>)<sub>6</sub><sup>3+</sup> is a 5-6 fold more effective condensing agent than spermidine<sup>3+</sup> (9, 50) despite equal binding of these isoivalent compounds (33). Therefore, factors other than valence are important. Further, as Benbasat (50) showed, equal percentage charge neutralization does not necessarily mean equal residual linear charge densities for all types of DNA. She studied wild-type and mutant forms of ϕW14 phage DNA, in which some of the thymidines are derivatized to give average charges per phosphate ranging from -0.76 to -1.24 (compared to -1 for normal DNA). In all cases except the lowest charge density, condensation with spermidine occurred when 89% of the DNA charge was neutralized. Thus the key factor seems not to be the effective linear charge density, but rather the neutralization of each fixed unit phosphate charge.

A further subtlety is that the electrostatic repulsion determined by osmotic stress measurements cannot be explained simply by screened coulombic interactions between parallel rods (51). At large interhelical distances, greater than 30 Å, the force-distance curve depends on ionic strength with a decay length about half that predicted by Debye-Hückel theory. This is due to fluctuations of the flexible DNA helices, maximizing configurational entropy and bringing charged groups closer together than expected for an orderly array of parallel cylinders.

Substantial reduction of the repulsive electrostatic interaction between DNA helices does not in itself account for the attractive interaction stabilizing the condensed form. Induced dipole interactions between the polarizable ion atmospheres surrounding the polyions can lead to a net attraction, as first proposed by Oosawa (52). As estimated by Marquet and Houssier (5), this attraction should be sufficient to stabilize condensed DNA with trivalent cations in water or divalent cations in water-methanol mixtures. Analytical calculations in our laboratory (Rouzina & Bloomfield, in preparation) show that similar results can be obtained from a model based on fluctuating interactions between closely apposed surface charge lattices. Rather elaborate grand canonical Monte Carlo calculations show a net attraction between hexagonally packed DNA cylinders in the presence of divalent counterions (53, 54).

These theoretical results seem to show that coulombic interactions have the strength to account for both the repulsive and attractive aspects of DNA condensation. But that does not mean that they are the whole story. Not only can hydration forces (see below) apparently give an equally good account of the phenomena. But our results with water-alcohol mixtures clearly show that while the solvent dielectric constant is a controlling variable, other factors are also at work.

Despite the intuition that electrostatics should dominate, the reality is more complicated. Force-distance measurements of DNA parallel helices as a function of salt concentration and valence, with monovalent and divalent cations, show a surprising result: all ionic influences nearly disappear when the separation between DNA surfaces is 5-15 Å. The repulsive pressure decays exponentially, with a characteristic length of 2.5 - 3.5 Å, behavior which has also been observed for forces between phospholipid bilayers and muscle fibers. This was interpreted by Rau et al (55) to demonstrate the overwhelming importance of hydration structure forces as the DNA surfaces approach. These forces are presumed to be due to water structure imposed not by hydrophobic groups, as in the familiar hydrophobic bonding, but rather by the water-soluble, polar and charged groups at the DNA surface. At interaxial distances of 26-30 Å typical of DNA packing in bacteriophage, the packing energy per base is 0.1 - 0.4 kcal/mol, corresponding to a DNA pressure of  $1.2 - 5.5 \times 10^7$  dyne/cm<sup>2</sup>. This is about one order of magnitude less than the electrostatic repulsion estimated by Riemer and Bloomfield (56), but greater than the conformational energies estimated in that work.

These hydration structure forces can under suitable conditions be attractive as well as repulsive. Rau and coworkers (57, 58) found that condensing agents such as CoHex(III), spermidine, spermine and chromium exert an attractive force that brings DNA molecules only to an 8 - 10 Å separation. If the molecules are pushed further together by osmotic stress, an exponential repulsion with a 1.3 to 1.5 Å decay length - half the normal value - is observed. This type of behavior is explained by a theory that postulates the rearrangement of surface-bound water by condensing ligands, to create regions of hydration attraction, or water bridging, between helices. Thermodynamic analysis shows that a significant amount of extra CoHex(III) is bound upon condensation.

The collapse transition is largely entropy-driven (58). A chaotropic anion, perchlorate, favors the collapse of Mn-DNA because the accompanying displacement of bound water into the bulk has a more favorable  $\Delta S$ . In contrast to CoHex(III), there is no net binding of Mn<sup>2+</sup> when condensation occurs, implying that a subtle rearrangement of cations causes water restructuring and a switch to net attraction.

In view of these observations, Rau and Parsegian (57) give reasons why they feel that forces between DNA helices cannot be characterized by balance of repulsive double-layer and attractive van der Waals interactions. (1) At distances of 10-15 Å, the repulsive force decreases exponentially with a 3 Å decay length which is independent of ionic strength or ion type. The coefficient of the force differs for different counterions, but magnitudes are similar. (2) At distances shorter than the collapse minima, the decay length is 1.3 to 1.5 Å, independent of ionic strength and valence or chemical nature of the condensing ion. (3) Added NaCl should screen repulsions and enhance net attraction according to double-layer theory. Instead, it causes the condensate to dissociate. (4) The same decay lengths are seen in other systems: e.g. phospholipid bilayers and collagen.

These arguments are cogent, but perhaps not definitive. For example, while mean-field Poisson-Boltzmann theory cannot explain the exponential decay and the independence on counterion concentration and valence, the situation is not so clear for a polyelectrolyte theory that takes fluctuations and correlations into account. And objection (3) is explicable even in terms of counterion condensation theory, since addition of NaCl displaces multivalent counterions, thereby lowering the fractional neutralization of DNA backbone charge.

Perhaps the most obvious cause of DNA condensation is crosslinking by the condensing ligand. There are several pieces of evidence favoring this idea. Suwalsky et al (40) used X-ray diffraction to measure the distance between DNA fibers in DNA-spermine complexes, as a function of relative humidity. The distance increased with hydration, but reached an upper limit consistent with spermine crosslinking. Allison et al (59) condensed DNA with homologs of spermidine, in which the butyl

moiety was replaced by longer pentyl through octyl groups. Aggregation became a more prevalent occurrence relative to condensation as the length of the end chain increased, suggesting an important role for crosslinking. Schellman and Parthasarathy (60) used spermidine analogs of the structure  $\text{NH}_3^+-(\text{CH}_2)_3-\text{NH}_2^+- (\text{CH}_2)_n-\text{NH}_3^+$  with  $n = 3, 4, 5$ , and 8 and aliphatic diamines  $\text{NH}_3^+-(\text{CH}_2)_n-\text{NH}_3^+$  with  $n = 2, 3, 4$ , and 6 to collapse DNA. They found that the interhelical spacing varied systematically with the length of the methylene bridge, and that the ionic strength of the solution had no effect on the spacing. This suggests that the arrangement of DNA in the complexes is determined by the structure of the polycation, not by long-range electrostatic repulsive and attractive forces.

However, the crosslinking mechanism is challenged by results with  $\text{Mg}^{2+}$  in water-methanol, where the spacing is as much as  $32\text{\AA}$ , much greater than the diameter of a hydrated  $\text{Mg}^{2+}$  ion (57). It must also be emphasized that in B-DNA crystals where spermine or  $\text{Co}(\text{NH}_3)_6^{3+}$  has been localized, it has never been found in a crossbridging location. Instead, as noted above, it is generally associated with some loop or distortion of a double helix. However, linking by spermine between molecules of a Z-DNA hexamer has been observed (48, 61).

There is increasing evidence that at least part of the glue that holds condensed DNA together comes from distorted secondary structure induced by the ligands. This idea is supported by numerous observations that condensing cations induce conformational changes in DNA. The chemical specificity of  $2^\circ$  and  $3^\circ$  structural changes contrasts with the nonspecificity predicted by polyelectrolyte theories based solely on cation size and radius.

It is by now widely accepted that DNA is quite a plastic molecule, able to adopt a wide range of conformations both within the B family and in other helical families (A, C, D, Z, etc) (62) depending on sequence, humidity, superhelical stress and other factors. Raman spectroscopy and crystallography of oligonucleotides show that a rather large number of sequences [not just the canonical  $(\text{dCdG})_n$  or  $(\text{dCdA})_n$ ] are either strongly or weakly susceptible to being in the Z conformation under high salt conditions (63, 64). Using chemical probes, Johnston (65) has shown that with increasing negative supercoiling, Z-DNA sequences can extend from an initial 14 bp region that is mainly alternating purine-pyrimidine, to flanking regions that have less alternating character.

Polyelectrolyte theories have been remarkably successful in explaining and predicting thermodynamic properties of DNA and its complexes. Perhaps because of this success, it is not widely appreciated that, in those cases where structures have been determined, multivalent cations seem to be generally associated with distortions of the double helix. An early demonstration of this was by Eichhorn and Shin (66), who showed that a wide variety of divalent cations, especially transition metals that bind to bases in preference to phosphates, cause apparent optical melting of DNA at temperatures well below those expected on the basis of ionic strength. The rapid reversibility of the hyperchromicity upon addition of EDTA suggests that bases were locally unpaired or unstacked, without extensive unwinding of the backbones. Under low ionic strength conditions,  $\text{Mg}^{2+}$  provokes the B-Z transition in poly[d(G-me<sup>5</sup>C)] (67). IR and CD studies of DNA in the presence of  $\text{Ni}^{2+}$  show helical distortion (68); the  $\text{Ni}^{2+}$  appears to form a strong inner-sphere complex with N7 of adenine (69). Extrusion of cruciforms by an S-type pathway depends on ionic size in a series of divalent cations, suggesting that specific ion-binding cavities are formed by the geometry of the four-way junction (70). The formation of extreme bends in kinetoplast minicircles is also induced by binding of  $\text{Zn}^{2+}$ ,  $\text{Co}^{2+}$ ,  $\text{Ba}^{2+}$ , and  $\text{Mn}^{2+}$  (71). The distortions induced by spermine<sup>4+</sup> have been noted earlier.

We have reviewed the evidence that DNA is structurally plastic, and that structural variations are induced by the same multivalent cations that cause condensation or aggregation. An intriguing possibility is thus suggested, that condensed DNA structures are stabilized to a significant extent by interaction

between helical segments that have been perturbed from the normal B conformation. There is a range of circumstantial evidence supporting this hypothesis. Cytosine residues of S<sub>d</sub> phage DNA which has been condensed by poly-lysine are reactive to HSO<sub>3</sub>, indicating perturbed 2° structure (72). Much data comes from Z-forming polymers, particularly poly[d(G-C)] and poly[d(G-me<sup>5</sup>C)]. Van de Sande and Jovin (73) showed that the left-handed form of poly[d(G-C)] (designated Z\* DNA) produced by 0.4 mM MgCl<sub>2</sub> and 20% ethanol, or 4 mM MgCl<sub>2</sub> and 10% ethanol, sedimented readily out of solution at low speed, indicative of extensive aggregation. Kinetic turbidity studies indicate that Z\* DNA is formed by a nucleated condensation mechanism (74). Detailed studies from our lab and elsewhere (75-78) have shown that collapse/aggregation and B-Z transition generally occur together for poly[d(G-C)] and poly[d(G-me<sup>5</sup>C)] in a wide variety of conditions. Chaires and Sturtevant (79) have shown by differential scanning calorimetry and spectroscopy that the B-Z transition in poly[d(G-C)] is followed by a transition with the characteristics of an aggregation reaction; both are reversible at low Mg<sup>2+</sup> and well below T<sub>m</sub>. Electron microscopy often shows close parallel association of DNA strands under condensing conditions. Some helical modifications observed with poly[d(G-C)], such as four-stranded hairpins and loops built up by the sticking together of two segments of DNA, have also been seen with natural sequence plasmid DNAs (75).

Further insight into the mechanism of aggregation comes from use of transition metal ions which prefer to bind to the bases, in contrast to Mg<sup>2+</sup> which preferentially binds to phosphate. An aggregating, left-handed form of poly[d(G-C)] can be produced in the absence of EtOH by Mn<sup>2+</sup>, Ni<sup>2+</sup> and Co<sup>2+</sup> (80). The ability of transition metals to aggregate natural sequence calf thymus DNA at elevated temperatures has been extensively studied in our lab (13). There is a strong correlation between the effectiveness of the divalent cations in producing aggregation, their effectiveness in producing apparent thermal melting of DNA (66) (although without extensive unwinding of the strands of the double helix), and their strength of binding to the bases, particularly N7 of guanine. Raman spectroscopy of 5% DNA solutions with equivalent amounts of transition metal chlorides (Duguid et al, submitted for publication) shows many spectral changes which are characteristic of DNA melting (base unpairing and unstacking, and backbone disorder) both at room temperature and at elevated temperatures.

A similar picture is presented by the unusual P-form of DNA, formed in low water/high alcohol solutions, which is condensed and whose bases are neither paired nor stacked (81, 82). The P-form is produced in a cooperative transition when the temperature or EtOH concentration of a 95% methanol solution is increased. Collapse occurs when about 90% of the DNA charge is neutralized by counterion condensation. The B->P transition is not reversed on cooling or adding MeOH, but is instantaneously reversed when water is added, indicating no extensive strand separation in the P-form. Similar unstacked but rapidly renatured DNA is observed at lower MeOH in the presence of divalent ions (15).

### Effects of alcohol on DNA condensation

If electrostatic interactions are important in condensation, then solutions with lower  $\epsilon$  should need less, or lower valence, condensing agent because electrostatic interactions leading to counterion condensation are stronger (14). To test this, we varied  $\epsilon$  from 80 to 50 by adding various amounts of alcohols (methanol, ethanol, and isopropanol) to water. We used laser light scattering and electron microscopy (EM) to study effects of dielectric constant on changes in aggregation number, hydrodynamic radius, and morphology of plasmid pUC 18 DNA condensed with Co(NH<sub>3</sub>)<sub>6</sub><sup>3+</sup>. We determined the relation between  $\epsilon$  and the critical Co(NH<sub>3</sub>)<sub>6</sub><sup>3+</sup> concentration required to induce condensation. The fraction of DNA phosphate charge neutralized by both Na<sup>+</sup> (held constant at 1 mM) and Co(NH<sub>3</sub>)<sub>6</sub><sup>3+</sup> was calculated using a modification of

the two-variable theory of counterion condensation. EM allowed estimation of the number of DNA molecules per particle, and the detection of a trend in particle morphology from toroidal through rodlike to fibrous states as  $\epsilon$  decreases.

The closed circular plasmid pUC 18 DNA (2686 base pairs) was isolated and purified by standard procedures, and analyzed by agarose gel electrophoresis and restriction endonuclease. The plasmid DNA was stored at 4 °C as a concentrated stock solution, 50  $\mu\text{g}/\text{ml}$  in 10 mM Tris Cl + 10 mM Na cacodylate, pH 7.0, 1 mM EDTA. All static and dynamic light scattering studies were done with 10-fold dilutions of this stock solution (5  $\mu\text{g}/\text{ml}$  DNA, 1 mM NaCl, 1 mM Na cacodylate) into alcohol-water mixtures of the desired composition. Highly purified  $\text{Co}(\text{NH}_3)_6\text{Cl}_3$  was purchased from Kodak and used without further purification. All buffers were filtered through 0.22  $\mu\text{m}$  GS Millipore filters before mixing.

The weight percentages of alcohols used to obtain a specific  $\epsilon$  are

$\epsilon$	80	75	70	65	60	55	50
MeOH	0.0	11.7	22.0	32.1	42.6	53.1	63.0
EtOH	0.0	8.2	17.0	25.9	34.7	43.6	52.4
i-PrOH	0.0	7.4	14.2	21.1	28.0	34.8	41.7

To compute the extent of counterion condensation and DNA charge neutralization in a solution with two cation species 1 and 2 of different valences, we solved numerically the coupled equations (14)

$$1 + \ln \left( \frac{1000 \theta_1}{C_1 V_{p1}} \right) = -2Z_1 \xi (1 - Z_1 \theta_1 - Z_2 \theta_2) e^{-\kappa b} \quad (1)$$

$$\ln \left( \frac{\theta_2}{C_2} \right) = \ln \left( \frac{V_{p2}}{1000 \epsilon} \right) + \frac{Z_2}{Z_1} \ln \left( \frac{1000 \theta_1 \epsilon}{C_1 V_{p1}} \right) \quad (2)$$

$\theta_i$  is the number of associated counterions of species  $i$  per DNA phosphate charge,  $C_i$  and  $Z_i$  are the molar concentration and valence of ion  $i$ ,  $e$  is the base of natural logarithms,  $\kappa$  is the Debye-Hückel screening parameter,  $b$  is the linear charge spacing of the DNA in the absence of condensed counterions.  $\xi$  is the familiar counterion condensation parameter,  $q^2/\epsilon\kappa_B T b$ . For DNA in aqueous solution,  $b = 1.7 \text{ \AA}$  and  $\xi = 4.2$  at 25°C.  $V_{pi}$  is the volume per mole of phosphate in which the condensed counterions are territorially bound,

$$V_{pi} = 4\pi N_A (1 + Z_i) (\xi - Z_i^{-1}) b^3 \quad (3)$$

where  $N_A$  is Avogadro's number. Once  $\theta_1$  and  $\theta_2$  are known, the fractional charge neutralization of the DNA is given by

$$r = Z_1 \theta_1 + Z_2 \theta_2. \quad (4)$$

Dynamic light scattering autocorrelation functions were analyzed by second order cumulant analysis to obtain the  $z$ -average diffusion coefficient, from which the hydrodynamic radius  $R_H$  was derived by Stokes' law. All scattering measurements were made at a scattering angle of 90° with an Ar<sup>+</sup> laser operating at 488 nm.

For electron microscopy, a drop of sample was deposited on a carbon coated 200 mesh copper specimen grid and allowed to stand for 1.5 minutes. The grids were previously glow-discharged for 1.5 minutes to render them hydrophilic and thereby facilitate staining. Each grid was stained by a drop of 1% uranyl acetate solution and blotted with filter paper after 30 seconds. The grid was then allowed to dry in air for at least 10 minutes. EMs were taken at a magnification of 50,000 with an Hitachi H-6010 microscope operating at 75 kV. Negatives were optically projected at 6x

enlargement, and the images of individual particles were traced on paper. These traces were scanned and digitized. For each toroid, inner and outer radii were the average of four perpendicular measurements.

The random coil conformation of DNA in buffered aqueous or low to moderate concentrations of alcoholic solution has little scattering power compared to condensed DNA. When DNA molecules condense to a smaller structure, or when the average number of DNA molecules in a scattering particle is increased by aggregation, the intensity of scattered light greatly increases. Figure 1 shows the scattering intensity two hours after addition of  $\text{Co}(\text{NH}_3)_6^{3+}$ , plotted against  $\epsilon$  of EtOH-water mixtures. The intensity increases as  $\epsilon$  decreases, reaching a maximum at  $\epsilon = 70$ . It then decreases to a plateau as  $\epsilon$  further decreases. The increase in scattering intensity as the concentration of  $\text{Co}(\text{NH}_3)_6^{3+}$  increases indicates that the DNA molecules get more compact and/or the aggregates get larger as larger amounts of condensing reagent are added. Similar behavior is seen with MeOH and PrOH.

$R_H$ , measured two hours after addition of the condensing reagent, decreases moderately as  $\epsilon$  decreases from 80 to 70, and then increases as  $\epsilon$  is further lowered. At  $\epsilon = 70$  and above,  $R_H$  is independent of the species of alcohol. These results indicate chain compaction (along with multimolecular association) down to  $\epsilon = 70$ , then further growth of the particles at lower dielectric constant. We were unable to monitor reliably the dynamic scattering behavior of condensed DNA molecules at  $\epsilon$  less than 65. This is due to the low scattering intensity, partial precipitation, and polydispersity of the remaining soluble DNA particles in the presence of multivalent cations and large amounts of alcohol. Under these circumstances, EM shows that the molecules are crosslinked and may produce a gel-like structure.

When increasing amounts of the condensing cation are added, an abrupt increase in the light-scattering intensity is noted at a critical concentration. The critical concentrations  $C_{\text{crit}}$  of  $\text{Co}(\text{NH}_3)_6^{3+}$  needed for collapse in water and alcohol solutions with  $\epsilon \geq 70$  are

	$\epsilon: 80$		75		70	
	$C_{\text{crit}}$	$r_{\text{calc}}$	$C_{\text{crit}}$	$r_{\text{calc}}$	$C_{\text{crit}}$	$r_{\text{calc}}$
MeOH	$30 \pm 2$	.894	$28 \pm 2$	.900	$25 \pm 2$	.905
EtOH	$30 \pm 2$	.894	$27 \pm 2$	.899	$23 \pm 2$	.905
PrOH	$30 \pm 2$	.894	$24 \pm 2$	.898	$18 \pm 1$	.902

As expected,  $C_{\text{crit}}$  generally decreases with decreasing  $\epsilon$ , but  $C_{\text{crit}}$  is not the same for different alcohols at a given  $\epsilon$ . The values of  $r$  at  $C_{\text{crit}}$ , calculated according to equations 1-4, all confirm the empirical rule that DNA condensation occurs at about 89-90% DNA phosphate charge neutralization.

Light scattering kinetic measurements were made with the first point measured 15 seconds after addition of  $\text{Co}(\text{NH}_3)_6^{3+}$ . Decreasing  $\epsilon$  by increasing the alcohol concentration speeds up DNA condensation and produces more strongly scattering particles. There are two phases: an initial very rapid rise, followed by a slower increase over a couple of hours. The initial phase is greater in magnitude and rate, the longer the hydrocarbon side-chain of the alcohol. However, kinetic measurements at equivalent  $r$  values show that the concentration of condensing agent is an even more important factor than the dielectric constant or hydrophobicity of the alcohol.

The EM morphology of condensed DNA particles was found to be dependent on  $\epsilon$ , but not on the species of alcohol. In the range of alcohol concentrations used, secondary structural transitions should not occur in the absence of condensing reagent (15). The proportion of rods increases sharply from 4.9% to 85% as  $\epsilon$  decreases from 80 to 65. At  $\epsilon = 60$  or below, multistrand fibers are dominant. The observation of toroids in aqueous solution is commonplace by now, but the high fraction of rods has not previously been observed in plasmid DNAs condensed in low concentration of alcohol solutions. Rods had been observed in very high EtOH solutions (95% v/v) or in solutions containing poly-(lysine) or PMS as condensing agents (11, 17, 21).



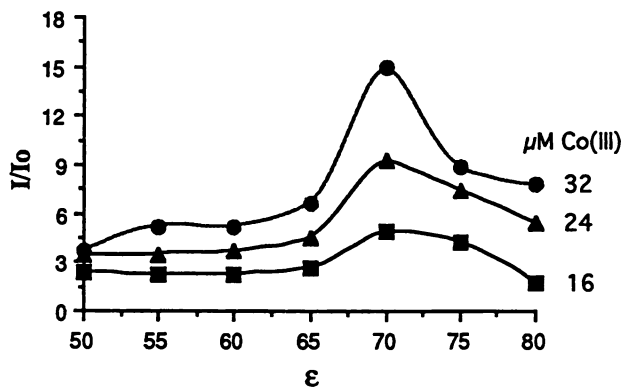


Figure 1. Scattering intensity two hours after addition of  $\text{Co}(\text{NH}_3)_6^{3+}$ , plotted against  $\epsilon$  of EtOH-water mixtures.

From the interhelical spacing of  $27.5\text{\AA}$  determined for  $\text{Co}(\text{NH}_3)_6^{3+}$ -condensed DNA (60), an assumption of hexagonal packing, and the measured dimensions of toroids, we can estimate the number of plasmid molecules per condensed particle. In aqueous solutions this number is fairly stable, remaining about 5.5 for up to a month. The molecularity in alcohol solutions with  $\epsilon = 75$  is less reproducible and changes more with time. The average, however, is 5.2 molecules/toroid, not significantly different from the value in aqueous solutions.

## Discussion

DNA, in the presence of  $\text{Co}(\text{NH}_3)_6^{3+}$ , collapses into different types of compact structures when subjected to different degrees of alcohol dehydration. Electrostatic, hydration, and kinetic factors are probably all involved in determination of morphology (4, 5).

The mechanism of formation of condensed particles, and the factors leading to different relative amounts of toroid or rod even in aqueous solution, are still matters of debate. Marx and Ruben (83) have shown that DNA in toroidal condensates is circumferential wrapped; each DNA molecule winds several times around the toroid. Formation of toroids requires continuous bending of the DNA double helix with a positive free energy related to the persistence length and radius of curvature. Plum et al. (21) suggested that morphological differentiation of condensates is controlled by a kinetic process. They presented data to show that PMS induces condensation at a slower rate and produces many more rods than either  $\text{Co}(\text{NH}_3)_6^{3+}$  or unmodified spermidine. Formation of rods requires sharp bending or kinking of the DNA helix at the ends of the rod. These deformations require more energy locally than constant circumferential bending. Thus they might require more activation energy and therefore be slower than smooth wrapping of the DNA. However, bending occurs continuously and kinking occurs only at the ends of rods. They are therefore expected to have similar total energies.

Matters become even more complicated when alcohol is added to the mix. When the concentration of alcohol is low, the water structure around the DNA helix remains unchanged, but the dielectric constant decreases. This leads to a higher degree of charge neutralization, causing both reduced electrostatic repulsion and also a lower persistence length or greater flexibility. This should permit compact, strongly curved toroidal or rodlike particles to form more readily.

Further increasing the alcohol concentration leads to progressive dehydration of the DNA. This has been shown to elicit extensive changes in the hydrodynamic properties of the DNA helix and can lead to the formation of compact structures. Multivalent cations could modulate this dehydration, particularly by augmenting the associated distortion of helix geometry. Alcohol at higher concentration also decreases DNA solubility due to the hydrophobicity of alcohol molecules and shielding the negatively charged backbones of interacting helical segments, thus facilitating the contact of DNA molecules. It is interesting that ethanol and water have maximal enthalpy of mixing in the concentration range from 35 to 60% (84). This is just the range where the transition from rods to multi-strand fibers occurs, suggesting that some thermodynamic or structural property of the mixed solvent system must be important in determining morphology.

Kinetic factors may also be important in these morphological differences. It seems likely that DNA in solutions containing multivalent cations at low dielectric constant may be subjected to such strong condensing forces that there is insufficient time for bending or kinking. Widom and Baldwin (9) showed that condensation by  $\text{Co}(\text{NH}_3)_6^{3+}$  in aqueous solutions to yield toroidal particles took about 1/2 hour. Thus DNA molecules may pack together more rapidly by aligning side by side.

**Summary**

An overview of all these results indicates that DNA condensation arises from the interplay of several forces. Stiffness sets limits on tight curvature. Electrostatic repulsions must be overcome by high salt concentrations or binding of multivalent cations. While mean field polyelectrolyte theories of the Poisson-Boltzmann type may not account for net attraction, counterion fluctuation mechanisms cannot be ruled out. Hydration must be adjusted to allow a cooperative accommodation of the water structure surrounding surface groups on the DNA helices as they approach. Unfortunately, hydration forces cannot be convincingly computed from first principles for comparison with experiment at the present time. Repulsive excluded volume interactions with other polymers in the solution can force the DNA segments closer together. Additional attractive free energy may be provided by bridging through condensing ligands (but there are at least some instances where necessary bridging distances are too large), and/or by interhelical binding between bases whose normal intra-duplex pairing and stacking have been disrupted by interactions with solvent or ligand. In cation-induced condensation of random sequence DNA, only a small fraction of the base pairs can be disrupted since the CD spectrum is very similar to that of B-form DNA. However, the evidence in favor of the involvement of such disrupted helices is sufficiently great, and suggests such novel possibilities, that it deserves serious consideration.

**Acknowledgments**

This research was supported by NIH Grant GM28093.

**Literature Cited**

- (1) Frisch, H. L.; Fesciyan, S. *J. Polym. Sci., Polym. Lett. Ed.* **1979**, *17*, 1-7.
- (2) Post, C. B.; Zimm, B. H. *Biopolymers* **1979**, *18*, 1487-1501.
- (3) Post, C. B.; Zimm, B. H. *Biopolymers* **1982**, *21*, 2123-2137.
- (4) Bloomfield, V. A. *Biopolymers* **1991**, *31*, 1471-1481.
- (5) Marquet, R.; Houssier, C. *J. Biomol. Struct. Dynam.* **1991**, *9*, 159-167.
- (6) Gosule, L. C.; Schellman, J. A. *Nature* **1976**, *259*, 333-335.
- (7) Gosule, L. C.; Schellman, J. A. *J. Mol. Biol.* **1978**, *121*, 311-326.
- (8) Chatteraj, D. K.; Gosule, L. C.; Schellman, J. A. *J. Mol. Biol.* **1978**, *121*, 327-337.
- (9) Widom, J.; Baldwin, R. L. *J. Mol. Biol.* **1980**, *144*, 431-453.
- (10) Widom, J.; Baldwin, R. L. *Biopolymers* **1983**, *22*, 1595-1620.
- (11) Laemmli, U. K. *Proc. Natl. Acad. Sci. USA* **1975**, *72*, 4288-4292.
- (12) Hsiang, M. W.; Cole, R. D. *Proc. Natl. Acad. Sci. USA* **1977**, *74*, 4852-4856.
- (13) Knoll, D. A.; Fried, M. G.; Bloomfield, V. A., in *Structure & Expression: DNA and Its Drug Complexes*, ed. Sarma, R.H. & Sarma, M.H., Adenine Press, Albany, NY, 1988, 123-145.
- (14) Wilson, R. W.; Bloomfield, V. A. *Biochemistry* **1979**, *18*, 2192-2196.
- (15) Votavová, H.; Kucerová, D.; Felsberg, J.; Sponar, J. *J. Biomolec. Struct. Dynam.* **1986**, *4*, 477-489.
- (16) Lang, D. *J. Mol. Biol.* **1973**, *78*, 247-254.
- (17) Eickbush, T. H.; Moudrianakis, E. N. *Cell* **1976**, *13*, 295-306.
- (18) Lerman, L. S. *Proc. Natl. Acad. Sci. USA* **1971**, *68*, 1886-1890.
- (19) Laemmli, U. K.; Paulson, J. R.; Hitchins, V. *J. Supramol. Struc.* **1974**, *2*, 276-301.
- (20) Arscott, P. G.; Li, A.-Z.; Bloomfield, V. A. *Biopolymers* **1990**, *30*, 619-630.
- (21) Plum, G. E.; Arscott, P. G.; Bloomfield, V. A. *Biopolymers* **1990**, *30*, 631-643.

- (22) Earnshaw, W. C.; Casjens, S. R. *Cell* **1980**, *21*, 319-331.
- (23) Casjens, S.; Hendrix, R., in *The Bacteriophages*, ed. Calendar, R., Plenum Press, New York, 1988, 1-75.
- (24) Sinden, R. R.; Pettijohn, D. E. *Proc. Natl. Acad. Sci. USA* **1981**, *78*, 224-228.
- (25) Kellenberger, E. *Trends in Biochem. Sci.* **1987**, *12*, 3-3.
- (26) Bode, V. C.; Harrison, D. P. *Biochemistry* **1973**, *12*, 3193-3196.
- (27) Krasnow, M. A.; Cozzarelli, N. R. *J. Biol. Chem.* **1982**, *257*, 2687-2693.
- (28) Hung, D. T.; Marton, L. J.; Deen, D. F.; Shafer, R. H. *Science* **1983**, *221*, 368-370.
- (29) Sikorav, J.-L.; Church, G. M. *J. Mol. Biol.* **1991**, *222*, 1085-1108.
- (30) Manning, G. S. *Q. Rev. Biophys.* **1978**, *11*, 179-246.
- (31) Anderson, C. F.; Record, M. T., Jr. *Annu. Rev. Biophys. Biophys. Chem.* **1990**, *19*, 423-465.
- (32) Braunlin, W. H.; Strick, T. J.; Record, M. T., Jr. *Biopolymers* **1982**, *21*, 1301-1314.
- (33) Plum, G. E.; Bloomfield, V. A. *Biopolymers* **1988**, *27*, 1045-1051.
- (34) Ross, P. D.; Shapiro, J. T. *Biopolymers* **1974**, *13*, 415-416.
- (35) Wemmer, D. E.; Srivenugopal, K. S.; Reid, B. R.; Morris, D. R. *J. Mol. Biol.* **1985**, *185*, 457-459.
- (36) Andreasson, B.; Nordenskiöld, L.; Braunlin, W.; Schultz, J.; Stilbs, P. *Biochemistry* **1993**, *32(3)*, 961-967.
- (37) Braunlin, W. H.; Anderson, C. F.; Record, M. T., Jr. *Biochemistry* **1987**, *26*, 7724-7731.
- (38) Braunlin, W.; Xu, Q. *Biopolymers* **1992**, *32(12)*, 1703-1711.
- (39) Liquori, A. M.; Constantino, L.; Crescenzi, V.; Elia, V.; Giglio, E.; Puliti, R.; Savino, M. D.; Vitagliano, V. *J. Mol. Biol.* **1967**, *24*, 113-122.
- (40) Suwalsky, M.; Traub, W.; Shmueli, U.; Subirana, J. A. *J. Mol. Biol.* **1969**, *42*, 363-373.
- (41) Drew, H. R.; Dickerson, R. E. *J. Mol. Biol.* **1981**, *151*, 535-556.
- (42) Feuerstein, B. G.; Pattabiraman, N.; Marton, L. J. *Proc. Natl. Acad. Sci. USA* **1986**, *83*, 5948-5952.
- (43) Quigley, G. J.; Teeter, M. M.; Rich, A. *Proc. Natl. Acad. Sci. USA* **1978**, *75*, 64-68.
- (44) Teeter, M. M.; Quigley, G. J.; Rich, A. *Adv. Inorg. Biochem.* **1981**, *3*, 233-272.
- (45) McMahon, M. E.; Erdmann, V. A. *Biochemistry* **1982**, *21*, 5280-5288.
- (46) Williams, L. D.; Frederick, C. A.; Ughetto, G.; Rich, A. *Nucleic Acids Res.* **1990**, *18*, 5533-5541.
- (47) Wang, A. H.-J.; Quigley, G. J.; Kolpak, F. J.; Crawford, J. L.; van Boom, J. H.; van der Marel, G.; Rich, A. *Nature* **1979**, *282*, 680-686.
- (48) Egli, M.; Williams, L. D.; Gao, Q.; Rich, A. *Biochemistry* **1991**, *30*, 11388-11402.
- (49) Gessner, R. V.; Quigley, G. J.; Wang, A. H.-J.; van der Marel, G. A.; van Boom, J. H.; Rich, A. *Biochemistry* **1985**, *24*, 237-240.
- (50) Benbasat, J. A. *Biochemistry* **1984**, *23*, 3609-3619.
- (51) Podgornik, R.; Rau, D. C.; Parsegian, V. A. *Macromolecules* **1989**, *22*, 1780-1786.
- (52) Oosawa, F., *Polyelectrolytes*, Marcel Dekker, New York, 1971.
- (53) Guldbbrand, L.; Nilsson, L. G.; Nordenskiöld, L. *J. Chem. Phys.* **1986**, *85*, 6686-6698.
- (54) Nilsson, L. G.; Guldbbrand, L.; Nordenskiöld, L. *Mol. Phys.* **1991**, *72*, 177-192.
- (55) Rau, D. C.; Lee, B. K.; Parsegian, V. A. *Proc. Natl. Acad. Sci. USA* **1984**, *81*, 2621-2625.
- (56) Riemer, S. C.; Bloomfield, V. A. *Biopolymers* **1978**, *17*, 785-794.
- (57) Rau, D. C.; Parsegian, V. A. *Biophys. J.* **1992**, *61*, 246-259.
- (58) Rau, D. C.; Parsegian, V. A. *Biophys. J.* **1992**, *61*, 260-271.

- (59) Allison, S. A.; Herr, J. C.; Schurr, J. M. *Biopolymers* 1981, 20, 469-488.
- (60) Schellman, J. A.; Parthasarathy, N. *J. Mol. Biol.* 1984, 175, 313-329.
- (61) Gessner, R. V.; Frederick, C. A.; Quigley, G. J.; Rich, A.; Wang, A. H.-J. *J. Biol. Chem.* 1989, 264, 7921-7935.
- (62) Wells, R. D.; Harvey, S. C., "Unusual DNA Structures", Springer-Verlag, New York, 1987.
- (63) Rich, A.; Nordheim, A.; Wang, A. H.-J. *Annu. Rev. Biochem.* 1984, 53, 791-846.
- (64) Peticolas, W. L.; Wang, Y.; Thomas, G. A. *Proc. Natl. Acad. Sci. USA* 1988, 85, 2579-2583.
- (65) Johnston, B. H. *J. Biomol. Struct. Dynam.* 1988, 6, 153-166.
- (66) Eichhorn, G. L.; Shin, Y. A. *J. Amer. Chem. Soc.* 1968, 90, 7323-7328.
- (67) Devarajan, S.; Shafer, R. H. *Nucleic Acids Res.* 1986, 14, 5099-5109.
- (68) Ridoux, J.-P.; Liquier, J.; Taillandier, E. *Nucleic Acids Res.* 1987, 15, 5813-5822.
- (69) Sigel, H., in *Metal-DNA Chemistry*, ed. Tullius, T.D., Amer. Chem. Soc., Washington, DC, 1989, 159-204.
- (70) Sullivan, K. M.; Lilley, D. M. *J. Mol. Biol.* 1987, 193, 397-404.
- (71) Laundon, C. H.; Griffith, J. D. *Biochemistry* 1987, 26, 3759-3762.
- (72) Sklyadneva, V. B.; Shie, M.; Tikchonenko, T. I. *FEBS Lett.* 1979, 107, 129-133.
- (73) Van de Sande, J. H.; Jovin, T. M. *EMBO J.* 1982, 1, 115-120.
- (74) Chaires, J. B.; Norcum, M. T. *J. Biomolec. Struct. Dynam.* 1988, 5, 1187-1207.
- (75) Revet, B.; Delain, E.; Dante, R.; Niveleau, A. *J. Biomolec. Struct. Dynam.* 1983, 1, 857-871.
- (76) Castleman, H.; Erlanger, B. F. *Cold Spring Harbor Sym. Quant. Biol.* 1983, 47, 133-142.
- (77) Castleman, H.; Specthrie, L.; Makowski, L.; Erlanger, B. F. *J. Biomolec. Struct. Dynam.* 1984, 2, 271-283.
- (78) Thomas, T. J.; Bloomfield, V. A. *Biochemistry* 1985, 24, 713-719.
- (79) Chaires, J. B.; Sturtevant, J. M. *Biopolymers* 1988, 27, 1375-1387.
- (80) Van de Sande, J. H.; McIntosh, L. P.; Jovin, T. M. *EMBO J.* 1982, 1, 777-782.
- (81) Zehfus, M. H.; Johnson, W. C., Jr. *Biopolymers* 1981, 20, 1589-1603.
- (82) Zehfus, M. H.; Johnson, W. C., Jr. *Biopolymers* 1984, 23, 1269-1281.
- (83) Marx, K. A.; Ruben, G. C. *J. Biomolec. Struct. Dynam.* 1986, 4, 23-39.
- (84) Franks, F.; Ives, D. J. G. *Quart. Rev. (London)* 1966, 20, 1-44.

RECEIVED September 2, 1993

## Chapter 16

# Light-Scattering Studies of Polyelectrolyte Complex Formation

## Effect of Polymer Concentration

H. Dautzenberg, G. Rother, and J. Hartmann

Max-Planck-Institute of Colloid and Interface Research, 14513 Teltow-Seehof, Germany

Polyelectrolyte complex formation in diluted aqueous solutions was studied on the system Na-poly(styrenesulfonate)/poly(diallyl-dimethylammonium chloride), using static and dynamic light scattering. By variation of the polymer concentration of the component solutions the level of aggregation could be changed and polyelectrolyte complex homologues could be prepared, offering the possibility of a comprehensive structural characterization. The polyelectrolyte complex investigated exists as a highly polydisperse system of compact and nearly spherical particles.

Polyelectrolyte complex (PEC) formation represents an interesting principle of structure formation with extremely high variability, due to the great variety of polyelectrolyte components and the influence of the solvent and the external preparation conditions. In practice polyelectrolyte complexes are used, e.g. as membranes with special separation properties, coatings, flocculants or for microencapsulation (1), in more or less concentrated systems. Under such conditions it is difficult to assess the influence of the different parameters which control the structure of PEC. The investigation of PEC formation in highly diluted aqueous solutions offers the possibility to study these effects by methods, normally used in polymer characterization (1-5). While the characteristics of the polyelectrolyte components (molecular weight, nature of ionic groups, charge density, branching) and the solvent (ionic strength, pH-value) primarily determine the internal structure of the PEC particles, the level of aggregation is dominantly controlled by the polymer concentration of the component solutions (1).

Especially scattering methods seem to be a powerful tool to obtain comprehensive information about the structure of PEC particles. Since the PEC particles in highly diluted solutions are stable for some hours, but change their structure in long times

0097-6156/94/0548-0210\$06.00/0  
© 1994 American Chemical Society

(6), small-angle X-ray and neutron scattering experiments are difficult to realize. Therefore, light scattering should be the appropriate method, particularly the combination of static and dynamic light scattering. However, light scattering data suffer from the disadvantage that only a limited section of the scattering curves can be measured, leading to a loss of structural information for small particles and problems in a reliable extrapolation to the scattering angle zero for large ones (7). The handicap may be overcome, if we are successful in preparation of PEC homologues, which would additionally allow to determine the mass-size relation. Main objectives of this paper are the preparation of such PEC homologues and the determination of the structure type, structural parameters of the particles as well as the polydispersity of the systems investigated by light scattering experiments. The effectiveness of such investigations is demonstrated on the system Na-poly(styrenesulfonate) (NaPSS)/poly (diallyl-dimethyl-ammonium chloride) (PDADMAC).

### Experimental

**Materials.** The samples employed were prepared under laboratory conditions, carefully purified by repeated dialysis, freeze-dried and characterized by osmometry and light scattering. The molecular weight  $M_w$ , polydispersity  $M_w/M_n$  and the refractive index increment  $dn/dc$  in water as well as the molecular weights  $m_0$  of the monomer units are given in Table I.

All investigations were carried out in pure water, highly clarified by ion exchange and filtration.

Table I: Characteristics of samples employed in complex formation

Polymer	$M_w$ g/mol	$M_w/M_n$	$dn/dc$ $cm^3/g^{-1}$	$m_0$
Na-PSS	60 000	1.1	0.192	206
PDADMAC	140 000	2.0	0.193	161.5
Solvent saltfree water, purified by repeated ion exchange and filtration				

**Static light scattering.** For static light scattering a Sofica 42 000 (Wippler and Scheibling, Strasbourg, France) was used, which was equipped with a 5mW He-Ne-laser as light source and a PC for data record. The accuracy of measurements was better than 1%. PEC formations were carried out directly in the scattering cell by mixing the polyelectrolyte component solutions under gentle stirring.

8 mL of the polycation solutions were put into the scattering cell and the polyanion solutions of twice of the concentration of the polycation solutions were added slowly via an immersed capillary. The scattering intensity at fixed angle ( $\theta=45^\circ$ ) was continuously registered. Solutions were made dust-free by filtration through 0.2  $\mu m$  membrane filters. The success of filtration must be checked carefully, because

extremely low amounts of remaining aggregates or gel particles may influence the PEC formation to a great extent, leading to bad reproducibility. To include a large size range of the PEC particles we studied the complex formation in a concentration range of the polycation solutions  $c_C$  between  $1 \cdot 10^{-5}$  and  $1 \cdot 10^{-3}$  g mL<sup>-1</sup> in seven steps:

1 -  $c_C = 1 \cdot 10^{-5}$ , 2 -  $2 \cdot 10^{-5}$ , 3 -  $5 \cdot 10^{-5}$ , 4 -  $1 \cdot 10^{-4}$ , 5 -  $2 \cdot 10^{-4}$ ,  
6 -  $5 \cdot 10^{-4}$ , 7 -  $1 \cdot 10^{-3}$  g mL<sup>-1</sup>.

In all systems a clearly pronounced flocculation occurred at a composition, corresponding to a 1:1 charge stoichiometry. For the concentration  $c_C = 1 \cdot 10^{-4}$  g mL<sup>-1</sup> the dosage was interrupted in steps of ten percent of conversion X and the complete angular dependence of the scattering intensity was measured. From all PEC solutions of different concentrations, given above, a sample was taken at a conversion of 50% and studied by static and dynamic light scattering. For higher concentrations the scattering intensity is very large, suggesting effects of multiple scattering. However, it could be proved that the systems can be diluted without disturbances of the PEC particles. Therefore the scattering intensity could be adjusted by subsequent dilution to an appropriate level.

**Dynamic light scattering.** Dynamic light scattering measurements were carried out with the instrument SIMULTAN (ALV, Langen; Germany), equipped with the correlator 3 000. As light source a 140 mW YAG Laser DPY 325c (Adlas GmbH, Luebeck, Germany),  $\lambda_0 = 532$  nm, was used. All measurements were performed in linear sampling time mode. The correlation functions were measured in steps of 10° in the range between 30° and 150°.

## Data Analysis

**Static light scattering.** For quantitative analysis of static light scattering the concentration and the refractive index increment of the PEC particles must be known. We calculated the concentration of the PEC under the assumption of a 1:1 stoichiometry, neglecting the contribution of the low molecular counterions. As refractive index increment the identical value of the two components was used.

For particle radii smaller than 50 nm the scattering curves can be analyzed by a Guinier plot, which allows a reliable extrapolation to the scattering angle zero and yields the weight average molecular mass  $M_w$  and the z-average of the square of the radius of gyration  $\langle S^2 \rangle_z$ . However, no conclusions can be drawn from the scattering curves about the polydispersity of the particle systems and also no information about the structure type, the average polymer packing density and an unadulterated mass-size relation can be obtained. With increasing particle size the scattering curves become more instructive, but reveal a stronger curvature in the small-angle range, impeding a reliable extrapolation to the scattering angle zero and the determination of the correct structural parameters. Therefore, we used an algorithm based on a comparison of the experimental scattering curves with theoretically calculated ones for various basic structure types (7,8).

For highly diluted particle systems the Rayleigh ratio of the scattering intensity  $R(q)$  is given by the simple expression (9):



$$R(q) = M_w K c P(q) \quad (1)$$

where  $M_w$  is the weight average molecular mass of the scattering particle,  $K$  - a contrast factor, containing the optical parameters of the system,  $c$  - the mass concentration in  $\text{g mL}^{-1}$  and  $P(q)$  is the intraparticle scattering function,  $q = 4\pi/\lambda \sin^2(\theta/2)$ ,  $\lambda$  - wavelength in the medium,  $\theta$  - scattering angle between the incident and the scattered beam.

Describing the polydispersity of the system by a continuous normalized mass distribution function  $p_w(M)$ , we obtain:

$$M_w = \int_0^{\infty} M p_w(M) dM \quad (2)$$

and

$$P(q) = \frac{1}{M_w} \int_0^{\infty} P(q, M) M p_w(M) dM \quad (3)$$

In the framework of the Rayleigh-Debye-approximation (RDA) the relation

$$P(q) = 1 - \frac{1}{3} \langle S^2 \rangle_z q^2 + \dots \quad (4)$$

was derived, whatever the shape and structure of the particles.

However,  $P(q)$  is known for a variety of structure types and in the RDA the argument of the scattering function is the product of the size parameter and  $q$ . Therefore, a double logarithmic plot  $\log R(q)/(Kc)$  versus  $\log q$  yields a scaled representation, where a change of  $M_w$  corresponds to a shift along the ordinate and a change of the size parameter to a shift along the abscissa. Model calculations were carried out for spheres, Gaussian coils, branched chains and rods (8), assuming a logarithmic as well as a Schulz-Zimm distribution for  $p_w(M)$ . Results obtained show that the influence of the type of distribution function on the shape of the scattering function may be neglected, but the structure type can be discussed, if an appropriate section of the scattering curve is known. In the following we restrict the considerations to the model of polydisperse systems of homogeneous spheres, which has been proved quite well in describing the scattering curves of the PEC solutions investigated. As distribution function we used the special logarithmic distribution of radii:

$$p_w(a) = \frac{a^{-5/2} \exp[-(\ln a - \ln a_m)^2 / 2 \sigma^2]}{\sqrt{2\pi} \sigma a_m^{-3/2} \exp[9 \sigma^2/8]} \quad (5)$$

For the distribution function (equation 5) the following integration rule is valid:

$$\int_0^{\infty} a^i p_w(a) da = a_m^i \exp[(-5i + i^2 + 2i) \sigma^2/2] \quad (6)$$

The parameter  $a_m$  is then related to  $M_w$  by the expression

$$M_w = \frac{4\pi}{3} \rho N_A a_m^3 \quad (7)$$

$\langle S^2 \rangle_z^{1/2}$  is given by:

$$\langle S^2 \rangle_z^{1/2} = \left(\frac{3}{5}\right)^{1/2} a_m e^{\frac{5}{2}\sigma^2} \quad (8)$$

where  $N_A$  is the Avogadro's number and  $\rho$  is the average polymer density in the particles. The parameter  $\sigma$  corresponds for low polydispersities to the relative standard deviation. For the scattering function of spheres following equation was derived:

$$P(q) = \left[ 3 \frac{\sin aq - aq \cos aq}{a^3 q^3} \right]^2 \quad (9)$$

The scattering curves of polydisperse systems of spheres are given in Figure 1a. With increasing polydispersity the curves become more flat, so that the polydispersity may be estimated by the assignment of an experimental scattering curve to the appropriate theoretical one, if a sufficient section is known. The dashed lines in Figure 1 mark the available range of typical light scattering experiments ( $30^\circ \leq \theta \leq 150^\circ$ ,  $\lambda = 633$  nm,  $n = 1.333$ ) for  $a_m = 200$  nm. However, it must be emphasized that the interpretation can not be unambiguous, because deviations from the spherical shape and internal density gradients are largely equivalent to an additional polydispersity.

**Dynamic light scattering.** Dynamic light scattering measurements yield the electric field correlation function  $g(q,t)$ , which corresponds to the Fourier transform of the fluctuating number density of scattering particles. Considering the center of mass motion of a monodisperse system of particles, the simple expression is valid:

$$g(q,t) = \exp[-\Gamma t] \quad (10)$$

where  $\Gamma = D q^2$ ,  $\Gamma$  is the decay constant or line width (reciprocal of decay time  $\tau$ ) and  $D$  is the translational diffusion constant (for details see (10,11)). For a polydisperse system  $g(q,t)$  is given by an integral equation

$$g(q,t) = \int_0^{\infty} G(q,\Gamma) e^{-\Gamma t} d\Gamma \quad (11)$$

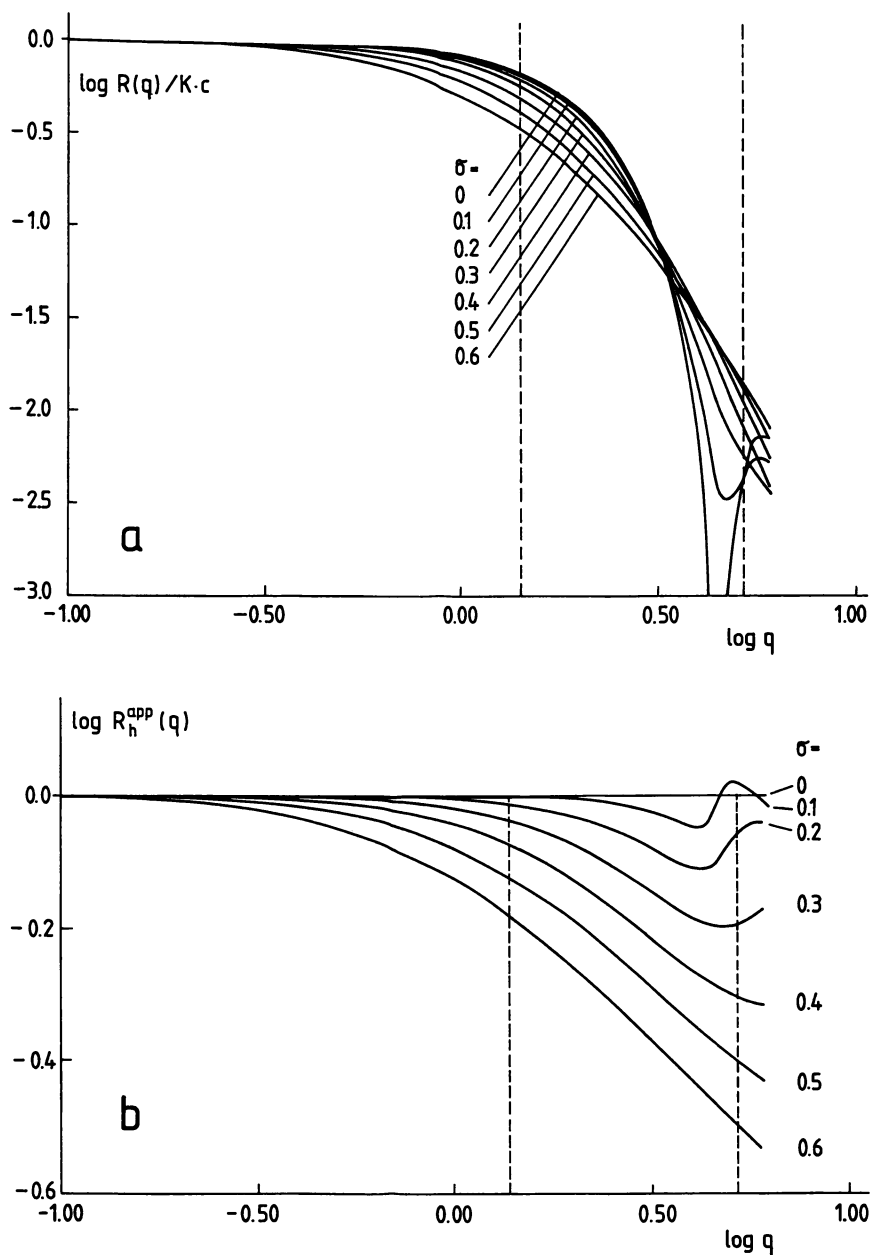


Figure 1. Scaled representation of the  $q$ -dependence of the static particle scattering factor  $P(q)$  (a) and the apparent hydrodynamic radius  $R_h(q)$  (b) in a double logarithmic plot ( $a_m = 1 \mu\text{m}$ ,  $q$  in  $\mu\text{m}^{-1}$ )

where  $G(q, \Gamma)$  is the normalized characteristic line width distribution. In principle  $G(q, \Gamma)$  can be calculated from equation (11) by an inverse Laplace transform, but the mathematical problem is ill-conditioned. A corresponding procedure was derived by Provencher (12), yielding  $G(q, \Gamma)$  and the moments  $m_i$  up to  $m_3$  of  $G(q, \Gamma)$ , where

$$m_i = \int_0^{\infty} \Gamma^i G(q, \Gamma) d\Gamma \quad (12)$$

To obtain the polydispersity in molecular weight of a particle system from  $G(q, \Gamma)$ , the contribution of a particle must be weighted by its scattering intensity, leading to

$$m_i = \frac{1}{M_w P(q)} \int_0^{\infty} M P(q, M) (q^2 D)^i p_w(M) dM \quad (13)$$

For  $q \rightarrow 0$  the first moment yields the  $z$ -average of the diffusion coefficient.

From each  $D$  value the hydrodynamic radius  $R_h$  can be calculated by the Einstein-Stokes-equation

$$R_h = \frac{kT}{6\pi\eta D} \quad (14)$$

where  $k$  is Boltzmann's constant,  $T$  is the absolute temperature and  $\eta$  is the viscosity of the solvent. For spheres the hydrodynamic radius is equal to the radius  $a$ . Changing from the mass distribution function  $p_w(M)$  to the distribution of radii (equation 5), also the parameter of polydispersity  $\sigma$  can be calculated from the ratio of different moments.

We used for the inverse Laplace transform a version of the Provencher program, installed by ALV (Langen, Germany).

However, all correlation functions were also analyzed by a third order cumulant fit, corresponding to the expression:

$$\ln g(q, t) = -\bar{\Gamma} t + \frac{\mu_2}{2} t^2 - \dots \quad (15)$$

where  $\bar{\Gamma} = m_1$ ,  $\mu_2 = m_2 - m_1^2$ .

For systems of large particles ( $> 50$  nm) and higher polydispersity the angular dependence of the apparent diffusion coefficient must be taken into account and an extrapolation to the scattering angle zero is necessary to determine  $D_z$  and the hydrodynamic radius  $R_h$ . Assuming that no interparticular interactions and internal motions contribute to the angular dependence of the apparent diffusion coefficient,  $D_{app}(q)$  may be calculated by the equation:

$$D_{app}(q) = \frac{\int_0^{\infty} D(M) P(q,M) M p_w(M) dM}{\int_0^{\infty} P(q,M) M p_w(M) dM} \quad (16)$$

or expressed in radii:

$$R_h^{app}(q) = \frac{\int_0^{\infty} a^3 P(aq) p_w(a) da}{\int_0^{\infty} a^2 P(aq) p_w(a) da} \quad (17)$$

Using the logarithmic distribution (equation 5), we obtain:

$$R_h(0) = a_m e^{\sigma^2} \quad (18)$$

Corresponding to  $P(q)$  also  $R_h(q)$  can be calculated. The results obtained are given in Figure 1b in the scaled double logarithmic representation, showing the inverse behavior in comparison to the particle scattering function. While for monodisperse systems no angular dependence occurs, the curves decrease steeper with increasing polydispersity. Therefore, the combination of static and dynamic light scattering should provide a reliable information about the polydispersity of the systems investigated. Additionally, the polydispersity can be calculated by the inverse Laplace transform, if the structural model is known.

## Results and Discussion

**Degree of conversion.** First we checked our previous findings (1) that for strong and highly charged polyelectrolytes the size and structure of PEC particles depend only slightly on the degree of conversion. The scattering curves of PEC solutions at a polycation concentration of  $c_c = 1 \cdot 10^{-4} \text{ g mL}^{-1}$  are given in Figure 2 for a degree of conversion from 10 to nearly 100 % in steps of 10 %. All scattering curves are very similar and could be fitted quite well by polydisperse systems of spheres with  $\sigma = 0.6$ . The polydispersity obtained is very high and corresponds to a  $M_w/M_n$  - ratio of 25. Therefore it must be absolutely taken into account in the estimation of the average polymer density of the particles. The structural parameters, obtained by a quantitative analysis of the scattering curves are represented in Figure 3. With increasing conversion we find a decrease of the particle mass  $M_w$  and the size parameter  $a_m$ , while the polymer density  $\rho$  increases slightly. The results confirm our previous findings (1) that the generation of new particles is the dominating process with increasing conversion and no further particle growth

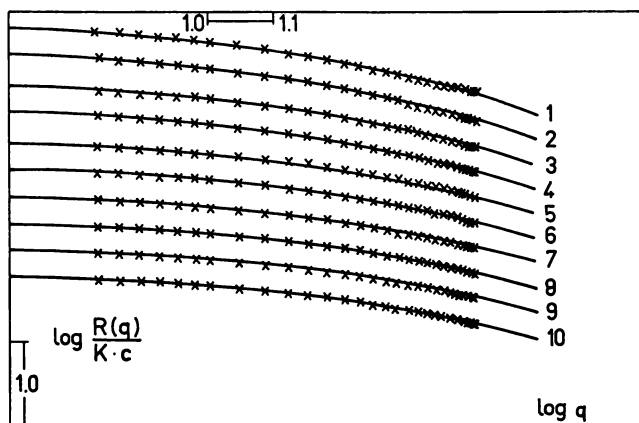


Figure 2. Scattering curves of the PEC NaPSS/PDADMAC in dependence on the degree of conversion ( $c_c = 1 \cdot 10^{-4} \text{ g cm}^{-3}$ )

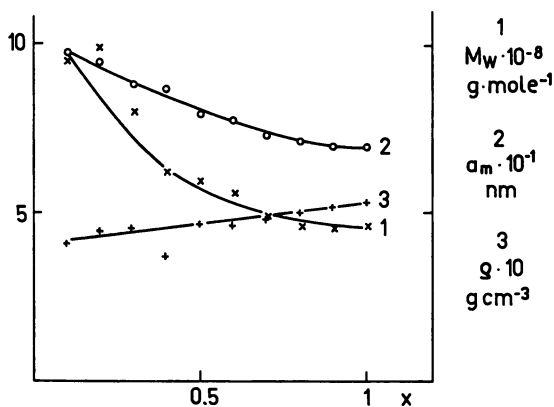


Figure 3. Structural parameters of the PEC NaPSS/PDADMAC in dependence on the degree of conversion ( $c_c = 1 \cdot 10^{-4} \text{ g cm}^{-3}$ )

occurs. The decrease of the aggregation level may be explained by the diminishing concentration of free polycations in the system with increasing conversion.

**Concentration dependence.** Very interesting findings result from the investigation of the influence of polymer concentration on PEC formation. Figure 4 depicts the scattering curves obtained at different concentrations in a range of two orders of magnitude at a degree of conversion of 50 %. Again all curves could be fitted quite well by the scattering functions of polydisperse systems of spheres with the  $\sigma$ -values given in Figure 4. It must be noticed here that no conclusions about the polydispersity could be drawn from the slight angular dependence of the curves 1 and 2. Therefore we analyzed these curves with  $\sigma$  suggested from the other curves. Figure 4 shows that the scattering curves become steeper with increasing polymer concentration, indicating the increase of the level of aggregation. This effect may be understood by the existence of two competitive processes of charge compensation, by conformational changes of the chains and by incorporation of other polyelectrolyte molecules, where the latter is favored in more concentrated systems. Figure 5 demonstrates that simple power laws were found for the concentration dependence of the particle mass and size, resulting in a mass-size-relation  $a_m \sim M^{1/3}$  and confirming the compact structure of the PEC particles (Figure 6). In the whole range of concentration we found a polymer density in the particles of  $\rho = 0.43 \pm 0.03 \text{ g mL}^{-1}$ .

Since all scattering curves could be fitted by the same structural model, it should be expected that the superposition of the normalized experimental curves yield a common scattering curve in a wide range of the argument  $a_m q$ . This is illustrated in an excellent manner by Figure 7. The composed scattering curve extends from the initial range up to the asymptotic one, which gives the expected  $q^{-4}$  dependence of spheres.

The findings confirm that for the PEC NaPSS/PDADMAC the objective to prepare PEC homologues could be realized, offering the possibility of reliable assessing of the structure type and determination of the structural parameters. The PEC solutions of different concentration levels were additionally studied by dynamic light scattering. Figure 8 shows the angular dependence of the apparent hydrodynamic radius, determined from the third order cumulant fit.

Therefore, an extrapolation to the scattering angle zero is absolutely necessary when conclusions about the structure type should be drawn via the ratio of the radius of gyration to the hydrodynamic one and again the polydispersity must be taken into account. Using the structural parameters, obtained by static light scattering, we calculated the angular dependence of  $R_g(q)$  corresponding to equation 17. The results are given as full lines in Figure 8. While for the curves 1 to 5 a sufficient agreement could be observed, remarkable deviations occur for the last two systems with the largest particles. The reason for this is not quite clear, but the calculations contain a lot of assumptions (structure type, distribution function, monomodality, no interparticular interactions). Moreover, the cumulant method is correct only for low polydispersities (10) and gives in our case reliable results with respect to the first cumulant, while the second cumulant reveals too low polydispersities.

Despite of the deviating shape of the experimental and theoretical  $R_g(q)$  curves,

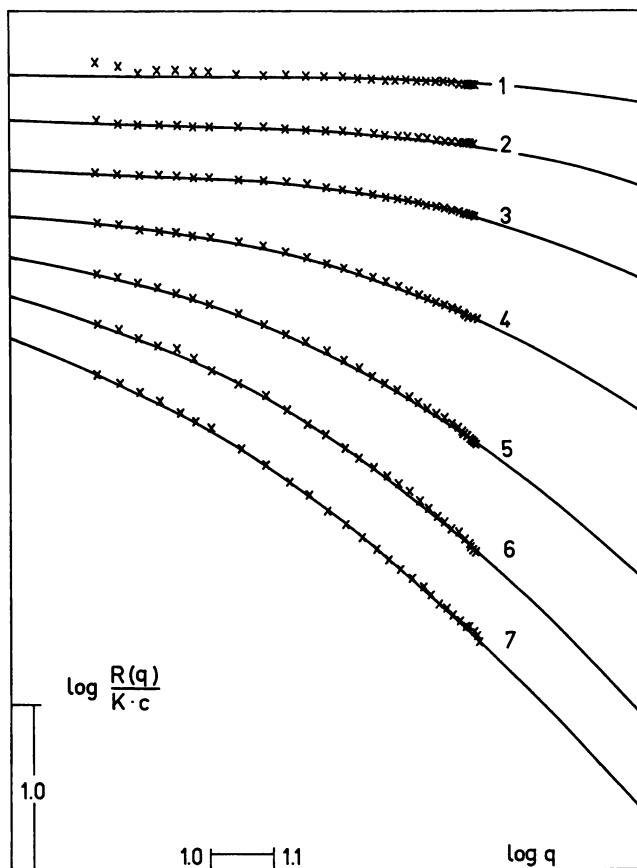


Figure 4. Scattering curves of PEC systems NaPSS/PDADMAC at different polymer concentrations ( $X = 50\%$ )



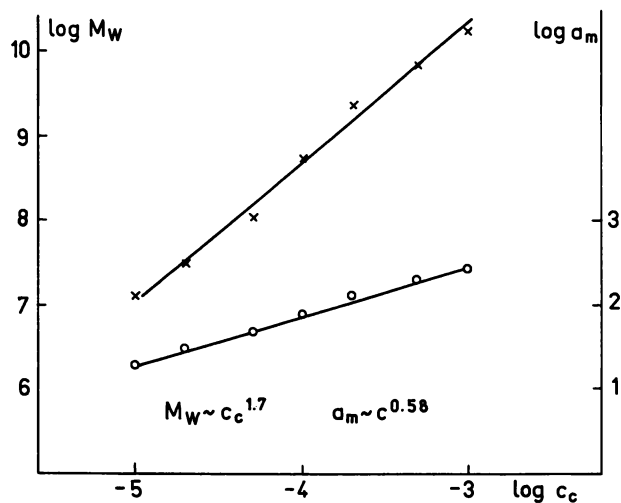


Figure 5. Structural parameters  $M_w$  and  $a_m$  of PEC systems NaPSS/PDADMAC in dependence on the polycation concentration

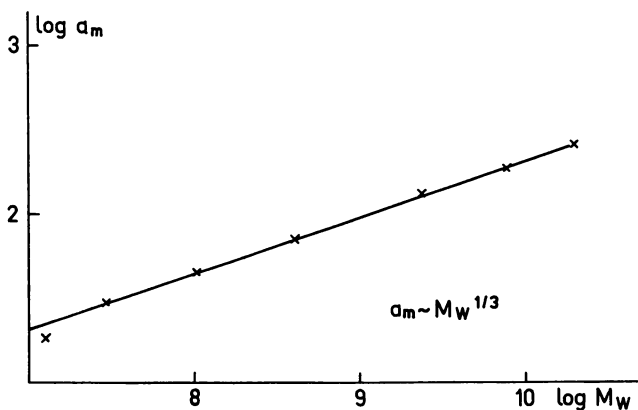


Figure 6.  $a_m - M_w$  - relation of NaPSS/PDADMAC - PEC "homologues"

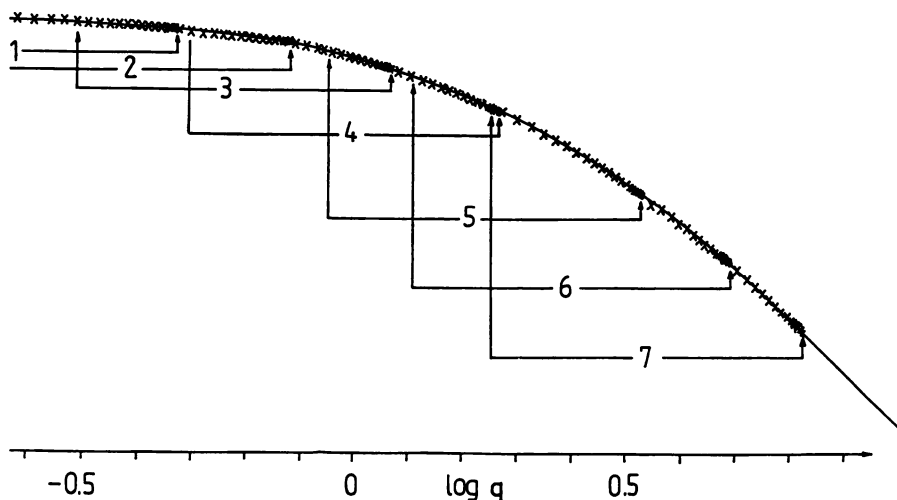


Figure 7. Superposition of the normalized scattering curves of the NaPSS/PDADMAC - PEC solutions of different polymer concentrations x - experimental points, full line - scattering curve of polydisperse systems of spheres ( $\sigma = 0.6$ )

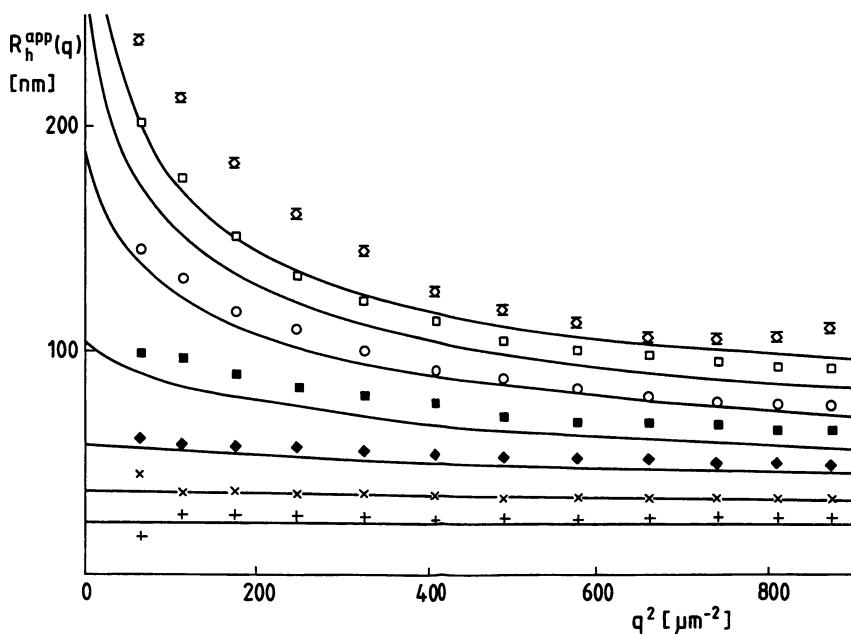


Figure 8. Angular dependence of the apparent hydrodynamic radius of NaPSS/PDADMAC - PEC solutions of different polymer concentrations symbols - experimental points, full lines - theoretical curves

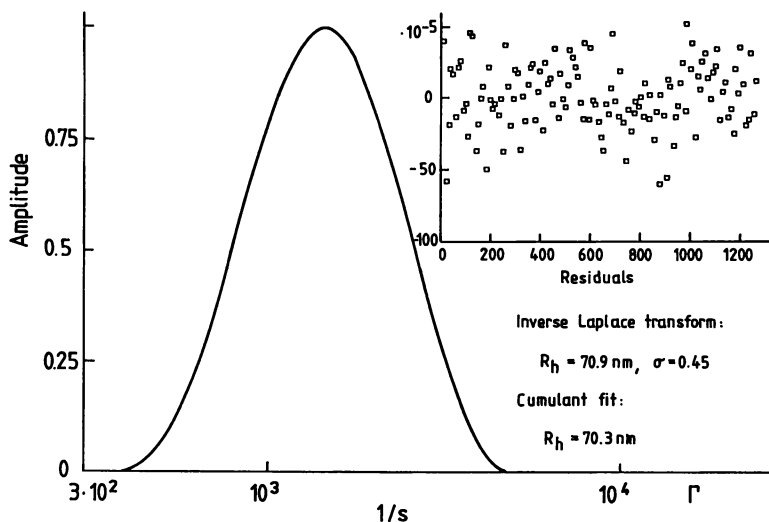


Figure 9. Inverse Laplace transform of the correlation function of the PEC NaPSS/PDADMAC ( $c_c = 1 \cdot 10^{-4} \text{ g cm}^{-3}$ ) at 50% conversion, scattering angle  $\theta = 90^\circ$

they yield nearly the same  $R_h(0)$ -values, which correspond for all systems to a ratio of the radius of gyration to the hydrodynamic one of about 0.78, when the polydispersity is taken into account. This value is characteristic for spheres (13).

The correlation functions were partly analyzed by inverse Laplace transform too. A typical result is given in Figure 9, showing a broad distribution of the decay constant  $\Gamma$  and also confirming that the logarithmic distribution function is a good approximation for the systems investigated. From the different moments of the distribution function  $R_h(q)$  and  $\sigma$  were calculated.  $R_h(q)$  is in good agreement with the value obtained by the cumulant fit and also the polydispersity parameter  $\sigma$  is nearly the same as it was determined by static light scattering. Normally, the  $\sigma$ -values must be extrapolated to the scattering angle zero, but this can be neglected due to the slight angular dependence for the given example.

## Conclusions

Static and dynamic light scattering investigations on PEC solutions of NaPSS / PDADMAC, prepared at different polymer concentrations of the component solutions, show that for this system PEC homologues could be obtained. This makes it possible to study the structure type in detail and to determine the structural parameters of the PEC particles in a reliable way. All results obtained are consistent and lead to the following picture:

The NaPSS/PDADMAC complex exists in diluted solutions as a highly polydisperse system of compact and nearly spherical particles.

The level of aggregation increases proportional to  $c'$ , where  $c$  is the polymer concentration of the component solutions. The exponent  $\nu$  was found to be 1.7 and the size parameter  $a_m$  is proportional to  $M_w^{1/3}$  in the whole concentration range. The average polymer density of the PEC particles does not change with the level of aggregation.

The consideration of the high polydispersity is a necessary precondition to get correct structural information.

Although the experimental work was consciously restricted to one system, the methodical progress achieved by the combination of SLS and DLS opens the way for systematic and comprehensive studies of the influence of the molecular and solvent parameters as well as of the preparation conditions, on the structure of PECs.

### Literature cited

1. Philipp, B.; Dautzenberg, H.; Linow, K.J.; Koetz, J.; Dawydoff, W. *Prog. Polym.Sci.* **1989**,*14*,91
2. Bekturov, E.A.; Bimendinna, L.A. *Adv. Polym. Sci.* **1981**,*41*,100
3. Tsuchida, E.; Abe, K. *Adv. Poly. Sci.* **1982**,*45*,1
4. Smid, J.; Fish, D. *Encycl. Polym. Sci. and Engin.* **1988**,*11*,720
5. Kabanov, V.A.; Zezin, A.B. *Pure Appl. Chem.* **1984**,*56*,343
6. Dautzenberg, H.; Linow, K.J.; Philipp, B. *Plaste und Kautschuk* **1982**,*29*,631
7. Dautzenberg, H.; Rother, G. *J. Polym. Sci., Polym. Phys. Ed., Part B* **1988**,*26*,353
8. Dautzenberg, H.; Rother, G. *Makromol. Chem., Macromol. Symp.* **1992**,*61*,94
9. Kerker, M. *The Scattering of Light and other Electromagnetic Radiation*, Academic Press, New York 1969
10. Chu, B. *Laser Light Scattering*, Second Edition, Academic Press 1991
11. Pecora, R.; Berne, B.J. *Dynamic Light Scattering*, Wiley, New York 1976
12. Provencher, S.W. *Comp. Phys. Comm.* **1982**,*27*,213
13. Burchard, W. *Adv. Polym. Sci.* **1983**,*48*,75

RECEIVED August 6, 1993

## Chapter 17

# Stoichiometric and Nonstoichiometric Complex Formation of Bovine Serum Albumin—Poly(dimethyldiallyl ammonium chloride)

Jiulin Xia<sup>1</sup>, Paul L. Dubin<sup>1,3</sup>, Lasker S. Ahmed<sup>1</sup>, and Etsuo Kokufuta<sup>2</sup>

<sup>1</sup>Department of Chemistry, Indiana University—Purdue University  
at Indianapolis, Indianapolis, IN 46202

<sup>2</sup>Institute of Applied Biochemistry, University of Tsukuba, Tsukuba, Ibaraki  
305, Japan

Complexation between bovine serum albumin (BSA) and Poly(dimethyldiallyl-ammonium chloride) (PDMDAAC) was studied by static and quasi-elastic light scattering (QELS), electrophoretic light scattering and turbidimetric titration in dilute electrolyte solution. Both QELS and turbidimetric titration show that complexation occurs at  $\text{pH} \geq 4.6$  for the ionic strength of 0.01 M. The results obtained support the following mechanism. Upon addition of PDMDAAC to BSA, at  $I = 0.01$  M, a stoichiometric complex is initially formed. Subsequent addition of polymer causes this complex to form a coacervate with concomitant charge neutralization. The stoichiometric complex was found by static light scattering to have 120 BSA bound per polymer chain. At higher ionic strengths (0.05 and 0.10 M), the initial complex is nonstoichiometric, and coacervates are formed by the aggregation of the complex. These coacervates are observed as *ca* 700 nm droplets by optical microscopy.

Proteins interact strongly with natural and synthetic polyelectrolytes mainly through electrostatic forces. These forces may lead to the formation of soluble complexes,<sup>(1-2)</sup> complex coacervates<sup>(3-6)</sup> and amorphous precipitates<sup>(7-9)</sup>. The practical consequences of these phase changes may include (a) the use of polyelectrolytes for protein separation (10-12), (b) immobilization or stabilization of enzymes in polyelectrolyte complexes (13), and (c) the modification of protein-substrate affinity (14). Related phenomena are also undoubtedly significant in the cell, as in, for example, the Coulombic association of DNA with basic histones which leads to the collapse of the nucleic acid; and the effects of basic polypeptides such as polylysine on DNA behavior. Electrostatic interactions between proteins and nucleic acid are also likely to play a role in the transcription process (15).

<sup>3</sup>Corresponding author

0097-6156/94/0548-0225\$06.00/0

© 1994 American Chemical Society

We have been investigating the interaction between synthetic polyelectrolytes and proteins (16-19). One motive is the possible use of protein phase separation by polyelectrolytes for protein purification and recovery. In this process the target proteins are obtained first through selective protein-polyelectrolyte phase separation, then recovered by adjusting pH or ionic strength (10,20). The efficiency of final protein purification and recovery depends largely on the phase separation step.

The phase separation of proteins by polyelectrolytes, commonly called precipitation, may in fact be more frequently coacervation. In coacervation, the concentrated phase is a second liquid phase, while precipitation corresponds to formation of a solid (21). The distinction between coacervation and precipitation becomes apparent upon centrifugation. It appears likely that precipitation is characteristic of oppositely charged polyelectrolytes with symmetric charge spacing at low ionic strength (22), while coacervation is typical of weakly charged and/or asymmetric polyelectrolyte systems.

Macromolecular complex coacervation, of which protein-polyelectrolyte coacervation is a special case, usually occurs when mixing two oppositely charged polyelectrolytes. This phenomenon was first studied by Bungenberg de Jong (21). It was found that the coacervate represents a kind of aggregate colloidal particle in aqueous solution. These particles appear as floating microscopic droplets, which may fuse with each other but do not mix with the solvent. An important question is the relationship between complex formation and phase separation.

Even though protein-polyelectrolyte complexes have been examined for more than two decades, few studies have dealt with the mechanism of complex formation. In the purification of lysozyme from egg white by precipitation with polyelectrolytes, Glatz et al (11) first suggested that the protein-polyelectrolyte flocs or coacervates are formed by aggregation of so called "primary particles". Recently, Berg et al (23) reported a mechanism for floc formation of lysozyme-polyacrylic acid. It was concluded that coacervation is due to polymer bridging at high polymer MW (over one million), and to charge neutralization at low polymer MW (several thousand). In studies of both Glatz and Berg, the initial formation of the "primary particle" was not fully discussed; in particular, they did not elucidate mechanism of formation of the primary particle or its structure.

Other studies (7, 13, 24) dealing with protein-polyelectrolyte complex composition and properties have provided more focus on the molecular level. For the complexation of bovine serum albumin (BSA), ribonuclease and lysozyme with both polycations and polyanions, Dubin et al (16, 19) proposed formation of soluble complexes prior to phase separation. Kokufuta (25) employed colloidal titration to study complexation between human serum albumin (HSA) and poly(dimethyldiallylammonium chloride) (PDMDAAC) and potassium poly(vinyl alcohol sulfate) (KPVS) in pure water. Titrating the protein with the polyelectrolytes, he found turbidity maxima (referred to as "end points") corresponding to conditions under which the mole numbers of quaternary ammonium groups in PDMDAAC and sulfate groups in KPVS were approximately identical to the contents of the acidic and basic groups in HSA. Therefore, it was concluded that the complexation between HSA and PDMDAAC and KPVS involves "stoichiometric" binding.

Stoichiometric polyelectrolyte complexes have been thoroughly studied since the 1970s. The mechanism of complex formation is believed to be a result of charge neutralization, i.e. the ratio between the oppositely charged groups in the complexes is 1:1 (22, 26). One of the most important properties of the complex is insolubility in both water and organic solvents (22,26).

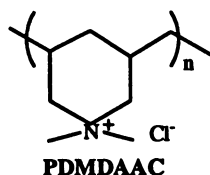
There are also reports of non-stoichiometric polyelectrolyte complexes. Kabanov (22) first reported that non-stoichiometric water-soluble polyelectrolyte complexes are formed by poly(*N,N*-dimethylaminoethylmethacrylate hydrochloride) and sodium polyphosphate. It was found that the complexes in aqueous salt media undergo considerable conformational change prior to phase separation. Conformational change was also found for some other non-stoichiometric protein-polyelectrolyte complexes in salt solution (18, 27-28).

Consideration of the foregoing results suggests that stoichiometry may be related to salt concentration, but further understanding is needed. In particular, it is not clear how stoichiometric and non-stoichiometric binding are controlled, and how the two different binding processes lead to phase separation. In the present paper, we investigate complexation between BSA and PDMDAAC, focusing in particular on complex structure, and on the effect of ionic strength on binding stoichiometry and coacervate formation.

## Experimental

### Materials:

Poly(dimethyldiallylammonium chloride) with the following chemical structure,



a commercial sample "Merquat 100" from Calgon Corporation (Pittsburgh, PA) possessing a nominal molecular weight of  $2 \times 10^5$  and  $M_w/M_n = 10$ , was dialyzed and freeze-dried before use. Bovine serum albumin ( $pI = 4.9$ ) was obtained from Sigma as 95-99% pure. Monobasic and dibasic sodium phosphate salts and sodium chloride with AR grades were obtained from Mallinckrodt Inc. Distilled and deionized water was used in all experiments.

### Sample Preparation

Solutions for "type I" titration were made in 0.01 M NaCl to maintain constant ionic strength ( $I$ ). For "type III" titration, solutions were prepared in ionic strength  $I = 0.01$  M pH 7.88 phosphate buffer. All solutions were made dust-free by filtering through Gelman 0.2  $\mu$ m syringe filters.

### Methods

**Turbidimetric Titration.** Turbidimetric titrations were carried out at 22°C in solutions of the desired ionic strength. A 2 ml microburet was used to deliver titrant and the turbidity was followed with a Brinkmann PC600 probe colorimeter (420 nm, 2 cm pathlength). Solutions were always stirred, and turbidity values were obtained after several minutes of stabilization in all cases. Two types of titration were

involved in the study. In "type I" titrations NaOH was added to an initial solution of PDMDAAC, BSA and NaCl at a pH around 4. A pH electrode connected to Beckmann  $\Phi$  34 pH meter was used to monitor pH change during the titration. The turbidity was monitored as a function of pH. In the other type of titration, referred as "type III", BSA in phosphate buffer solution was titrated with PDMDAAC. The turbidity was recorded as a function of the concentration ratio of [PDMDAAC]/[BSA] =  $W$  (=  $1/r$ ).

**Quasi-Elastic Light Scattering (QELS).** QELS measurements were made at scattering angles from  $30^\circ$  to  $150^\circ$  with a Brookhaven (Holtsville, NY) 72 channel BI-2030 AT digital Correlator and using a Jodon 15 mW He-Ne laser (Ann Arbor, MI). A  $200 \mu\text{m}$  pinhole aperture was used for the EMI photomultiplier tube, and decahydronaphthalene (decalin) was used as the refractive index matching fluid to reduce stray light. We obtain the homodyne intensity-intensity correlation function  $G(q,t)$ , with  $q$ , the amplitude of the scattering vector, given by  $q=(4\pi n/\lambda)\sin(\theta/2)$ , where  $n$  is the refractive index of the medium,  $\lambda$  is the wavelength of the excitation light in a vacuum, and  $\theta$  is the scattering angle. For a Gaussian distribution of intensity profile of the scattered light,  $G(q,t)$  is related to the electric field correlation function  $g(q,t)$  by:

$$G(q,t) = A(1 + b g(q,t)^2) \quad (1)$$

where  $A$  is the experimental baseline and  $b$  is a constant, which depends on the number of coherence areas that generates the signal ( $0 < b < 1$ ). The quality of the measurements were verified by determining that the difference between the measured value of  $A$  and the calculated one was less than 1%. The electric field correlation function depends on the Fourier transform of the fluctuating number density of particles or molecules. For the center of mass diffusion of identical particles the following simple relation holds:

$$g(q,t) = e^{-t/\tau} \quad (2)$$

$$\frac{1}{\tau} = Dq^2$$

where  $\tau$  is decay time and  $D$  is diffusion coefficient. More detailed discussions of QELS data analysis may be found in refs. (29) and (30).

For polydisperse systems the correlation function  $g(q,t)$  can be expressed as an integral of the exponential decays weighted over the distribution of relaxation times  $\rho(\tau)$ :

$$g(t) = \int_0^{\infty} e^{-t/\tau} \rho(\tau) d\tau \quad (3)$$

In principle, it is possible to obtain the distribution  $\rho(\tau)$  by integral transformation of the experimental  $[G(t)/A-1]^{1/2}$ , but in practice this presents a formidable problem for numerical analysis, since taking the inverse Laplace transform is numerically an ill-posed problem. Several numerical methods developed so far are devoted to calculating  $\rho(\tau)$ . In the present work, we analyze the autocorrelation functions by



using the CONTIN program, which employs the constrained regularization method (31).

From equation (3), the mean relaxation time,  $\langle \tau \rangle$ , defined as the area of  $g(t)$ , is given by

$$\begin{aligned} \langle \tau \rangle &= \int_0^{\infty} g(t) dt \\ &= \int_0^{\infty} \tau \rho(\tau) d\tau / \int_0^{\infty} \rho(\tau) d\tau \end{aligned} \quad (4)$$

This  $\langle \tau \rangle$  value can be resolved from each of the distribution modes of  $\rho(\tau)$ , as the first moment of the normalized relaxation spectrum. Therefore, the diffusion coefficient, which corresponds to each value of  $\langle \tau \rangle$ , can be calculated using

$$D = \frac{\lambda^2}{16\pi^2 \sin^2(\theta/2) \langle \tau \rangle} \quad (5)$$

From each  $D$  value we obtain Stokes' radius,  $R_s$ , by the Einstein equation

$$R_s = \frac{kT}{6\pi\eta D} \quad (6)$$

where  $k$  is Boltzmann's constant,  $T$  is the absolute temperature and  $\eta$  is the viscosity of the solvent. In the present study the experimental uncertainty in  $R_s$  is less than 10%.

**Static Light Scattering (SLS).** SLS measurements were made with the same Brookhaven system described above. Intensity measurements were calibrated by pure (>99.5%) toluene and optical alignment was ensured by less than 3% deviation from linearity in the  $I \cdot \sin\theta$  vs  $\theta$  plot. Each measurement was carried out for 5 seconds. The average of 10 such measurements was reported as  $I_s$ . These values were used to calculate Rayleigh ratio,  $R_\theta$ . In this  $R_\theta$  measurement we use as the reference solvent pure BSA solution with the same ionic strength and pH as complex-containing solution.

For PDMDAAC, we used the refractive index increment,  $dn/dc = 0.186$ , determined by Burkhardt (32) with a differential refractometer. Attempts to measure  $dn/dc$  of the complex failed because of scattering effects. Since the complex is comprised of polymer and protein, we calculated  $(dn/dc)_x$  of the complex by using

$$\left( \frac{dn}{dc} \right)_x = \frac{1}{1+\beta} \left( \frac{dn}{dc} \right)_p + \frac{\beta}{1+\beta} \left( \frac{dn}{dc} \right)_{pr} \quad (7)$$

where the subscripts  $x$ ,  $p$ , and  $pr$  represent complex, polymer and protein, respectively.  $\beta$  represents the mass ratio of bound protein to polymer, and  $(dn/dc)_{pr} = 0.185$  for BSA (33).

Static light scattering results are usually plotted as Zimm-diagrams corresponding to the equation:

$$\frac{Kc}{R_\theta} = \frac{1}{M_w} \left( 1 + \frac{16\pi^2}{3\lambda^2} R_g^2 \sin^2 \frac{\theta}{2} \right) + 2A_2c \quad (8)$$

where  $c$  is the mass concentration of polymer,  $K$  is a constant which contains the optical parameters of the system;  $M_w$  and  $R_g$  are the weight average molecular weight and the root mean square radius of gyration of the macromolecule, respectively; and  $A_2$  is the second virial coefficient.

**Electrophoretic Light Scattering (ELS).** ELS measurements were made at four scattering angles ( $8.6^\circ$ ,  $17.1^\circ$ ,  $25.6^\circ$  and  $34.2^\circ$ ), using a Coulter (Hiialeah, Florida) DELSA 440 apparatus. The electric field was applied at a constant current of 5 mA. The temperature of the thermostated chamber was maintained at  $25^\circ\text{C}$ .

In ELS, the photon-counting heterodyne correlation function for a solution with an electrophoretically monodisperse solute can be written as (34):

$$C(\tau) = \beta_0 \delta(\tau) + \alpha_0 + \alpha_1 \exp(-2Dq^2 \tau) + \alpha_2 \exp(-Dq^2 \tau) \cos(\Delta\omega\tau) \quad (9)$$

where  $\beta_0$ ,  $\alpha_0$ ,  $\alpha_1$ , and  $\alpha_2$  are constants independent of correlation time,  $\tau$ , and  $\delta(\tau)$  is the delta function.  $D$  and  $\theta$  have the same definitions as in QELS. The cosine term is due to simultaneous electrophoresis and diffusion.

The Fourier transform of equation (9) with respect to time, as stipulated by the Wiener-Khinchine theorem (35), gives the power spectrum:

$$S(\omega) = \beta_0 + \alpha_0 \delta(\omega) + \frac{2(\alpha_1 / \pi) Dq^2}{\omega^2 + (2Dq^2)^2} + \frac{\alpha_2 Dq^2}{2\pi} \left[ \frac{1}{(\omega + \Delta\omega)^2 + (Dq^2)^2} + \frac{1}{(\omega - \Delta\omega)^2 + (Dq^2)^2} \right] \quad (10)$$

where  $\alpha$  is a constant independent of  $\omega$ .

In both equations (9) and (10),  $\Delta\omega$  is the difference between the angular frequency of the scattered light,  $\omega_s$ , and that of the reference beam,  $\omega_r$ , which is the same as that of the incident beam. Since the frequency of the incident beam is modulated in the scattered light by the amount of the so called Doppler shift frequency,  $\Delta\omega$  is given by:

$$\Delta\omega = \frac{2\pi n}{\lambda} E u \sin\theta \quad (11)$$

where  $E$  (volts/cm) and  $u$  ( $(\mu\text{m s}^{-1})/(\text{V cm}^{-1})$ ) are the applied electric field strength and electrophoretic mobility, respectively. Therefore,  $u$  can be directly evaluated from frequencies of the power spectrum. The  $u$  values obtained in this work are repeatable within less than 6%. Detailed discussion on ELS measurements can be found in refs. (29) and (34).

**Optical Microscopy.** Microscopic observation of BSA-PDMDAAC coacervates was carried out using a WILD MPS 51S compound microscope. Coacervates were prepared by mixing BSA and PDMDAAC in 0.10 M NaCl solution with NaOH to adjust pH to 7.9. The coacervate solution was placed on a slide, and then covered by a cover slip for microscopic observation. The size of coacervates were estimated from a calibration scale.

## Results and Discussions:

**BSA-PDMDAAC Complexation at Varying pH, Mass Ratio and Constant Ionic Strength.** Figure 1 shows Type 1 turbidimetric titrations curves of PDMDAAC at various polymer concentrations in 0.60 g/L BSA solution, at ionic strength ( $I$ ) of 0.01 M NaCl. All of the curves display an abrupt increase in turbidity at pH 5.1, about 0.2 pH unit above the isoelectric point of BSA, corresponding to colloidal complex formation. Prior to colloid formation, we observe a ~2% turbidity increase at pH 4.6 for all polymer concentrations. This small turbidity increase is due to the initial formation of the soluble complex: particles with a size larger than either BSA or PDMDAAC are detected at this pH by QELS, as shown in Figure 2. All solutions exhibit turbidity maxima at *ca* pH 6.4. These turbidity maxima can be understood from the simultaneous effects of increasing complex size and solubility. It is well known that protein-polyelectrolyte complexation is a result of electrostatic interactions (16-19). Therefore, increasing the net negative charge of BSA via increase in pH will enhance its binding to polymer, leading initially to a loss of solubility. After the polymer is saturated with bound BSA, the solubility of the complex may increase with pH because the whole polymer chain is covered by the highly charged proteins. The competition of these size and solubility effects causes the maxima in turbidity. The fact that the position of these turbidity maxima is relatively independent of the mass ratio and pH suggests that the turbidity maximum reveals a certain stoichiometric character. Since all the systems correspond to the excess protein, the stoichiometric reaction product formed at the turbidity maxima should be an intrapolymer complex saturated with bound BSA.

Figure 2 shows the diameters obtained by QELS for the BSA-PDMDAAC complex as a function of pH for complexes formed at 300. Clearly, size increases with pH after initial binding and reaches to a constant diameter of *ca* 270 nm at pH > 5.80. This constant diameter of the complex supports the hypothesis of a stoichiometric intrapolymer complex.

**BSA-PDMDAAC Complexation at Various Ionic Strength, Mass Ratio and Constant pH.** Figures 3-5 show Type III turbidimetric titrations of various concentrations of BSA with PDMDAAC in pH 7.88 sodium phosphate buffer, at ionic strengths of 0.01, 0.05 and 0.10 M, respectively. The value of pH 7.88 was chosen to ensure coacervate formation on the basis of the type I titrations in Figure 1. All solutions probably exhibit turbidity maxima. In the case of the high BSA concentration (0.6g/L), the plateau is not meaningful, because the sensitivity of the photodetector is not sufficient to record accurate transmittances for such turbid solutions. For the lowest ionic strength, the position of this turbidity maximum is relatively independent of protein concentrations, i.e. the turbidity maximum reveals a certain stoichiometric character. For higher ionic strengths, the position of the maximum shifts to larger relative polymer concentrations with decreasing protein concentration.

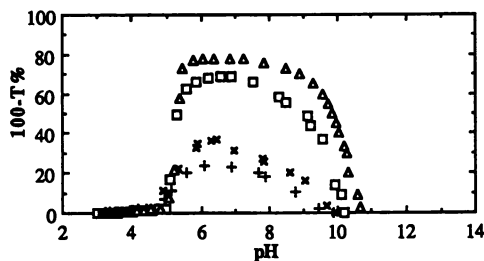


Figure 1. Type I titrations of various PDMDAAC concentration in 0.60 g/L BSA and 0.01 M NaCl.  $r$ : 50 ( $\Delta$ ); 100 ( $\square$ ); 300 ( $\times$ ) and 500 ( $+$ ).

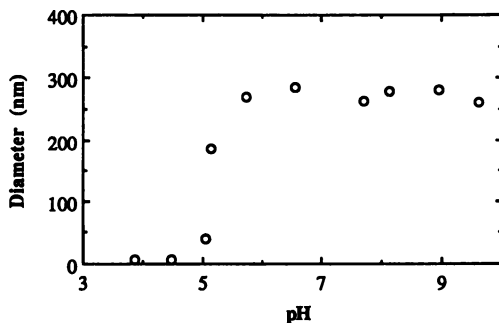


Figure 2. The complex size obtained by QELS as a function of pH for PDMDAAC in 0.60 g/L BSA and 0.01 M NaCl with  $r = 300$ .

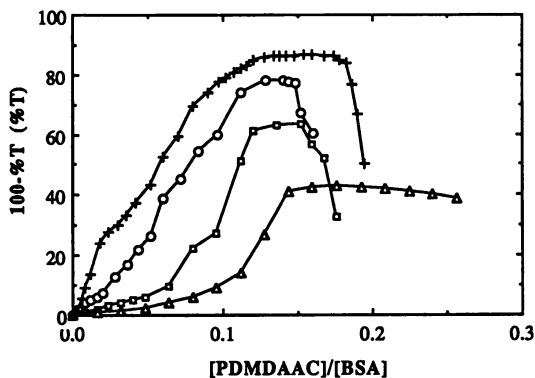


Figure 3. Type III turbidimetric titrations of various concentrations of BSA with PDMDAAC at ionic strength 0.01 M and pH 7.88 phosphate buffer solutions. BSA concentrations (g/L): 0.6 ( $\times$ ); 0.12 ( $\circ$ ); 0.06 ( $\square$ ); and 0.03 ( $\Delta$ ).

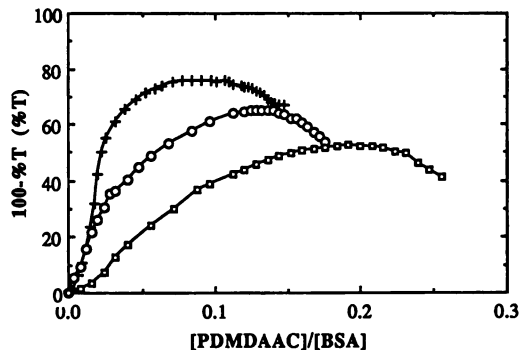


Figure 4. Type III turbidimetric titrations of various concentrations of BSA with PDMDAAC at ionic strength 0.05 M and pH 7.88 phosphate buffer solutions. BSA concentrations (g/L): 0.36 (+); 0.12 (O); and 0.06 (□).

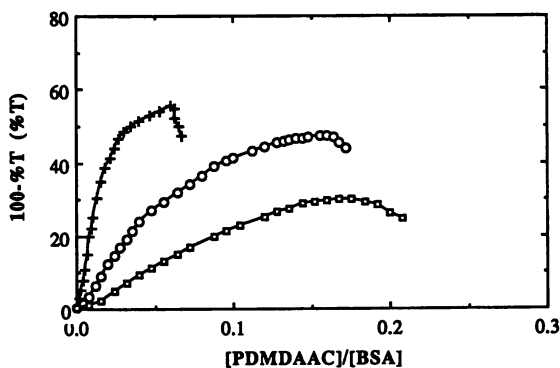


Figure 5. Type III turbidimetric titrations of various concentrations of BSA with PDMDAAC at ionic strength 0.10 M and pH 7.88 phosphate buffer solutions. BSA concentrations (g/L): 0.36 (+); 0.12 (O); and 0.06 (□).

August 10, 2012 | http://pubs.acs.org  
 Publication Date: December 13, 1993 | doi: 10.1021/bk-1994-0548.ch017

In order to understand the distinction between the behavior at high and low ionic strength, measurements of the apparent size of the scattering species were conducted by QELS, at a protein concentration of 0.60 g/L, and at both low ( $I=0.01M$ ) and high ( $I=0.10M$ ) salt concentrations. Figure 6a and Figure 7 are the QELS results obtained at low and high ionic strengths, respectively. A dramatic difference between the two ionic strengths is obvious. Under the former condition, a remarkably stable species with  $R_s \approx 100$  nm is observed to form at very low added polymer concentration, and persists as the sole scattering species until a polymer concentration close to the turbidity maximum is attained. The same concentration of polymer corresponds to the onset of a plateau in the electrophoretic mobility, as shown in Figure 6b. Below this concentration, the mobility exhibits a sign change after displaying a constant value of  $u = -1.3 \mu\text{m}\cdot\text{cm}/V\cdot\text{s}$ . In contrast, QELS measurements at  $I = 0.10$  show that the size of the scattering particle increases rapidly with added polymer even at very low polymer concentration.

**Static Light Scattering of BSA-PDMAAC Complex.** Prior to static light scattering, the degree of protein binding was first estimated by the following procedure. An equilibrium solution of BSA and PDMAAC at pH 7.88 and ionic strength 0.01, with  $r = 300$ , was centrifuged and filtered through a 20 nm filter (Alltech, Deerfield, IL). The filtrate was found to be complex-free by QELS. The concentration of free BSA in this solution was then determined by optical density measurement at 280 nm using the reported extinction coefficient of  $4.36 \times 10^4$  (36). From the free BSA concentration, we obtained  $\beta = 39$ , which corresponds to 120 BSA bound per PDMAAC chain.

Static light scattering was carried out for the complex in 0.01 M phosphate buffer at pH 7.88 and varying  $C_p$  and  $r$ . The refractive index increment of the complex was calculated from equation (7) with  $\beta = 40$ . To analyze the SLS results, we ignore the particle interaction term, i.e. the second virial coefficient in equation (8). The error caused by this approximation is less than 5% (37, 38) because of the very low polymer concentration (37). Therefore, equation (8) can be simplified to

$$\frac{KC_x}{R_\theta} \cong \frac{1}{M_x} \left( 1 + \frac{16\pi^2}{3\lambda^2} R_g^2 \sin^2 \frac{\theta}{2} \right) \quad (12)$$

where  $c_x$  and  $M_x$  are the concentration and molecular weight of the complex, respectively.  $c_x$  and  $M_x$  are related to the polymer concentration and polymer molecular weight by

$$c_x = c_p (1 + \beta) \quad (13)$$

$$M_x = \alpha M_p (1 + \beta) \quad (14)$$

where  $\alpha$  is the degree of aggregation, i.e. number of polymer chains within one complex. Substitution of equations (13) and (14) into (12) yields

$$\frac{KC_p}{R_\theta} \cong \frac{1}{\alpha M_p (1 + \beta)^2} \left( 1 + \frac{16\pi^2}{3\lambda^2} R_g^2 \sin^2 \frac{\theta}{2} \right) \quad (15)$$

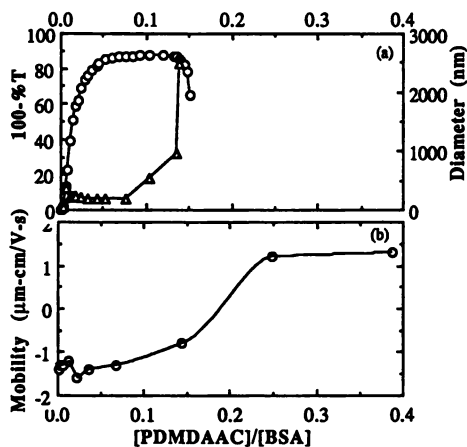


Figure 6. (a) Diameter of BSA-PDMAAC complex as a function of polymer concentration in 0.60 g/L BSA and 0.01 M, pH 7.88 phosphate buffer. ( $\Delta$ ) is QELS results, and ( $\circ$ ) represents the corresponding turbidity. (b). Mobility of BSA-PDMAAC complex at the same conditions as those in (a).

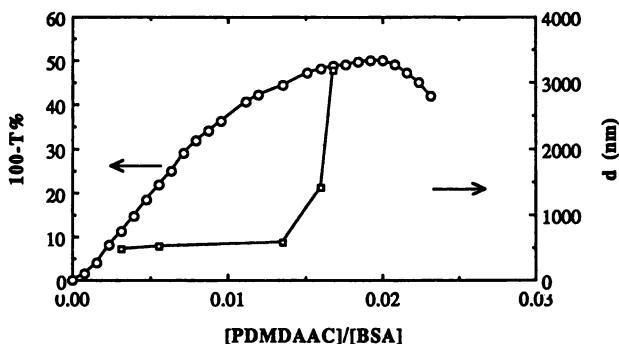


Figure 7. Diameter of BSA-PDMAAC complex as a function of polymer concentration in 0.60 g/L BSA and 0.1 M, pH 7.88 phosphate buffer. ( $\square$ ) is QELS results, and ( $\circ$ ) represents the corresponding turbidity.

Therefore, we may use the known polymer concentration  $C_p$  to evaluate the molecular weight of the complex, by plotting the angular dependence of the scattered light as  $KC_p/R_\theta$  vs  $\sin^2(\theta/2)$ . Assuming  $\alpha = 1$  in the limit of low  $C_p$ , the intercept yields  $\beta$ , and hence  $M_x$ , and the slope leads to a value for  $R_g$ . The linearity of the plots, as shown for example in Figure 8, indicates the validity of the low concentration approximation. Values of  $M_x$  for different  $C_p$  are calculated from the intercepts of  $KC_p/R_\theta$  vs  $\sin^2(\theta/2)$  plots using  $\alpha = 1$ . Such results are plotted in Figure 9 as  $M_x$  vs  $C_p$ . The constant molecular weight at low polymer concentration of  $M_x = 8.1 \times 10^6$  corresponds to a  $\beta$  value of  $40 \pm 2$ , which is consistent with the value obtained by filtration. This initial constant molecular weight is consistent with the  $\alpha = 1$  assumption, which corresponds to an intrapolymer complex structure.

The radius of gyration of the complex may be obtained from the slope of Figure 8. For different amounts of added polymer, values of  $R_g$  and corresponding hydrodynamic radii, obtained from QELS, as well as  $\rho = R_g/R_h$ , are given in Table I. Hydrodynamic theory (39) shows that  $\rho$  changes from infinity to 0.775 when the polymer structure changes from a long rod to a sphere. The random coil structure is believed to occupy an intermediate position between long rod and sphere. For random coils,  $\rho$  assumes values from 1.3 to 1.5 (39). In a previous study (40), we found through a similar analysis that the complex formed from PEO and SDS micelles behaves like a random coil polymer; and similar results were obtained for the complex of ribonuclease A and sodium polystyrene sulfonate (41). However, the values for  $\rho$  in Table I are intermediate between those of random coil and long rod. These values suggest a extended structure of BSA-PDMDAAC complexes. The extended structure could be the result of the inter-protein repulsive forces which prevail at low ionic strength and pH well above pI.

**Table I. Hydrodynamic Radius and Radius of Gyration of the BSA-PDMDAAC Complex<sup>(a)</sup>**

$C_p$ (g/L)	$R_h$ (nm)	$R_g$ (nm)	$r (=R_g/R_h)$
$1.2 \times 10^{-3}$	110	250	2.3
$2.1 \times 10^{-3}$	115	230	2.0
$2.4 \times 10^{-3}$	95	240	2.5
$3.7 \times 10^{-3}$	90	245	2.7
$5.1 \times 10^{-3}$	110	235	2.2
$6.6 \times 10^{-3}$	120	290	2.4
$8.3 \times 10^{-3}$	110	420	3.8

(a) Protein concentration 0.60 g/L, pH=7.88, ionic strength 0.01M.

**Electrophoretic Light Scattering of BSA-PDMDAAC Complex.** Figure 10 shows the electrophoretic mobility  $u$  of the complex formed at  $r = 300$ ,  $C_{BSA} = 0.60$  g/L, in 0.01 M NaCl as function of pH. The decrease in mobility is due to the simultaneous increase in BSA negative net charge and the number of BSA bound per polymer chain. One may note that the mobility changes sign between pH 4.8 and 5.9. The positive value for  $u$  at pH 5 suggests that the complex initially formed in  $pH \leq 5$  is not saturated by BSA.

Upon further increase in pH above 5.9, the mobility changes linearly with pH. As discussed below, this may be explained on the basis of an intrapolymer complex saturated with BSA, the presence of which in this pH range is supported by



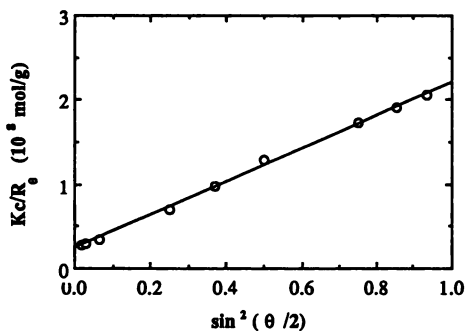


Figure 8.  $Kc_p/R_\theta$  vs  $\sin^2(\theta/2)$  plot obtained for BSA-PDMDAAC complex at  $C_p = 0.002 \text{ g/L}$  in  $C_{BSA} = 0.60 \text{ g/L}$  ( $r = 300$ ) and  $0.01 \text{ M}$  phosphate buffer solution of  $\text{pH } 7.88$ .

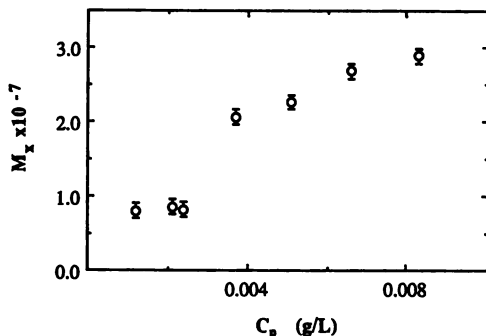


Figure 9.  $M_x$  vs  $C_p$  for BSA-PDMDAAC complex in  $0.01 \text{ M}$   $\text{pH } 7.88$  phosphate buffer with  $C_{BSA} = 0.60 \text{ g/L}$ .

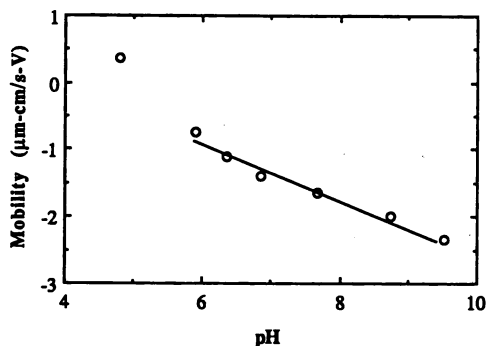


Figure 10. Mobility of BSA-PDMDAAC complex as a function of  $\text{pH}$ :  $r = 300$ ,  $C_{BSA} = 0.60 \text{ g/L}$  and  $I = 0.01 \text{ M NaCl}$ .

the observation from QELS of constant diameter above pH 5.8. The mobility of the intrapolymer complex,  $u$ , can be written as

$$u = \frac{q_p + nq_{pro}}{f_p + nf_{pro}} = \frac{q_p + nq_{pro}}{f_x} \quad (16)$$

where  $q_p$  and  $q_{pro}$  are the charges of polymer and protein, respectively;  $n$  is the number of proteins bound per polymer chain; and  $f_p$ ,  $f_{pro}$  and  $f_x$  are friction coefficients of polymer, protein and complex, respectively. Published pH titration curves (42) show that the net charge of BSA ( $q_{pro}$ ) varies approximately linearly with pH in the range of 6 to 10:

$$q_{pro} \cong 26.4 - 6.0\text{pH} \quad (17)$$

Since  $q_p$  is independent of pH, eqs. (16) and (17) suggest that the mobility will be linear with pH at  $6 < \text{pH} < 10$ , if the friction coefficient of complex  $f_x$  is independent of pH. This result which we observe is consistent with a saturated state of the complex (i.e.  $n$  is constant). Substituting eq.(17) and  $n=120$  obtained by SLS into eq.(16), we obtain  $f_x=3.2 \times 10^{-5}$  Poise-cm, which is much larger than that obtained by the Einstein equation:  $f=6\text{pH}R=2.4 \times 10^{-6}$  Poise-cm. The Einstein relationship is not expected to hold in the present case because of hydrodynamic and electrostatic interactions. Even though some errors exist in the estimation of  $f_x$  due to ignoring counterion condensation, the linear dependence of  $u$  vs pH is qualitatively satisfied by both calculation and experimental results.

In Figure 10 we observe a negative mobility at pH 6.4, which is corresponding to the turbidity maximum in Type I titration. This suggests that the turbidity maximum is not the point of charge neutralization. For neutrality of charge we have

$$Z_T = Z_p + n Z_{pr} = 0 \quad (18)$$

where  $Z_p$  is the formal charge of the polyion (i.e., for homopolymers, the degree of polymerization),  $n$  is the average number of protein molecules bound per polyion chain, and  $Z_{pr}$  is the net charge of a bound protein molecule. At pH 6.4, BSA has a negative net charge of  $Z_{pr} = -12$  (42), and therefore  $n = 110$  is obtained from equation (18). This  $n$  value is close to but smaller than the binding capacity i.e., 120 BSA per PDMDAAC chain obtained by SLS. Substitution of  $n = 120$  into eq. (18) we obtain the net charge  $Z_T = -228$  for the complex. This net charge is consistent with the observed negative mobility. Therefore, the turbidity maximum in "type I" titration may correspond to the position of BSA saturation.

**Mechanism of BSA-PDMDAAC Complex Formation and Complex Coacervation.** Results of the present study are consistent with the following model for complexation and phase separation. At low ionic strength and at pH 7.88, the binding of BSA to PDMDAAC is quite strong, and in the limit of  $r \rightarrow \infty$  each polymer chain binds a full complement of protein molecules, i.e. on the order of 120 proteins per polymer chain. Because the proteins are highly charged at this pH,  $Z = -21$  (42), strong repulsion among neighboring bound proteins causes the chain

to adopt an extended configuration, with a hydrodynamic radius approximately four times larger than the value of the protein-free polymer ( $R_h = 24$  nm). The net negative charge of this complex precludes its further association. Therefore, the turbidity increases only because of an increase in the number of such species. Because of the large binding constant, there is essentially no free polymer in these systems, only the primary complex and free protein. When a sufficient amount of polymer has been added to bind all the free protein, further addition of polycation leads to the coacervation of the primary complexes. The instability of the coacervate and the very large related particle sizes produce the ultimate decrease in turbidity. The maxima observed at low ionic strength therefore display a stoichiometric character, in the sense that a doubling of the protein concentration produces an approximate doubling of the amount of polymer added at the point where the turbidity no longer increases.

In contrast to stoichiometric protein-polyelectrolyte complexes formed in pure water (24,25), and stoichiometric polycation-polyanion complexes (22) which are neutral particles, the BSA-PDMDAAC stoichiometric complex has a negative charge. This negative charge prevents the complex from forming coacervates through simple aggregation. Addition of polymer neutralizes this charge and overcomes the Coulombic resistance to coacervation. This model is consistent with the experimental results in Figure 5b, which show a constant negative mobility at low polymer concentration, and then an increase from negative to positive values. The initial constant mobility corresponds to the stable stoichiometric complex; the mobility change with polymer concentration corresponds to the coacervation of the complex upon additional polymer.

As seen in Figure 7, the size of the complex formed at higher ionic strength always increases with addition of polymer. Thus, the complexation is not stoichiometric because there is no well-defined product. Furthermore, the lowest value for  $R_s$  seen, *ca* 250 nm, is very much larger than the dimensions of the protein-free polymer at this ionic strength. This result indicates that "primary" complexes are not particularly stable, but instead strongly tend to associate to form higher-order aggregates. Phase separation occurs when these aggregates become very large. We suggest that the size of the aggregates is not a function of the bulk solution stoichiometry alone, but instead increases strongly with total solute concentration. Thus, in two solutions that have the same polymer:protein stoichiometry, the one with the higher protein concentration will form larger aggregates. The turbidity is thus observed to increase more rapidly with the concentration ratio of the polymer to the protein ( $W$ ) when the protein concentration is higher, as seen in Figures 4 and 5. Also the size required for bulk phase separation is attained at lower  $W$  in this case.

There are two reasons why complexes may tend to aggregate more readily at higher ionic strength. First, the intrinsic polymer-protein binding constant may be expected to be smaller at larger  $I$ . Therefore, the number of proteins bound per polymer chain may be less and the charge of the "primary complex" closer to electrical neutrality. Second, the Debye length decreases from 30 Å to 10 Å as the ionic strength increases from 0.01 to 0.10 M. In the low  $I$  condition, two primary complexes can interact with each other in their entirety, and the net charge of the entire complex determines association or coacervation. In the high  $I$  case, two primary complexes may interact with specific regions within each other's domain. Thus, a protein-rich portion of one complex (negatively charged) could interact with a protein-poor region (positively charged) in another complex. The "polarizability"

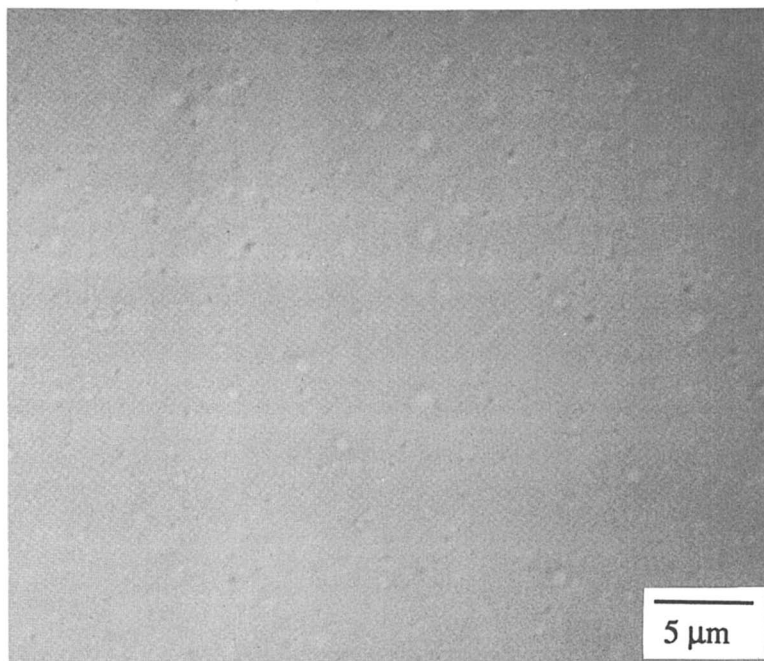


Figure 11. Optical photomicrograph of BSA-PDMAAC coacervate.

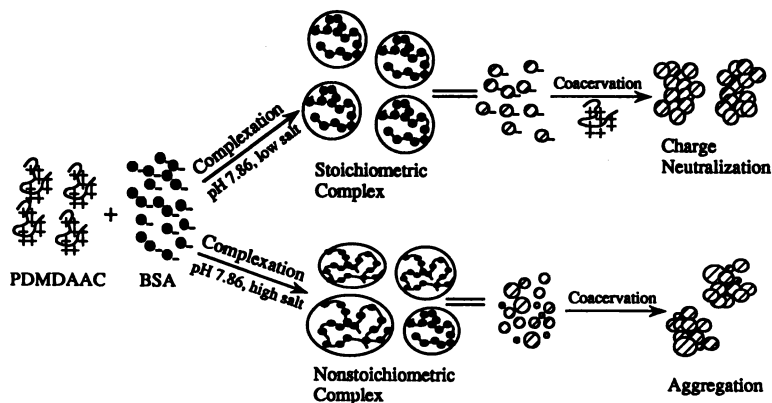


Figure 12. Schematic diagram of complex formation in protein separation by polyelectrolytes.

of the primary complex may therefore promote higher-order aggregation. In all the cases the higher aggregates or coacervates have a size about 700 nm (Figure 11) as observed by microscope.

In summary, the mechanism we propose for BSA-PDMAAC complex formation and complex coacervation is shown schematically in Figure 12. At low ionic strength, e.g.  $I=0.01$  M, BSA and PDMAAC first form a negatively charged stoichiometric complex with a diameter of *ca.* 200 nm. The 200 nm particles then coacervate, through charge neutralization, upon further addition of the polycation. In the case of higher ionic strength, the initial formed complexes are nonstoichiometric with a size of *ca.* 500 nm in diameter. The nonstoichiometric complexes bear less charge and may exhibit charge polarization. The polarized particles then aggregate to form coacervates.

## Conclusions

The structure of the BSA-PDMAAC complex in solutions of  $C_{pr} = 0.6$ ,  $I = 0.01$  M and pH 7.88 depends on the polymer concentration. At low polymer concentration, a stoichiometric intrapolymer complex is saturated with BSA. The mass ratio of the bound BSA to polymer in the saturation limit is about 40. This intrapolymer complex aggregates upon increase in the polymer concentration. In the case of higher ionic strength  $I = 0.1$  M, the initial formed complexes have nonstoichiometric interpolymer structure with a size of *ca.* 500 nm in diameter.

**Acknowledgments.** This research was supported by grants from the National Science Foundation (DMR 9014945); American Chemical Society (ACS-PRF#25532-AC7B); Eli Lilly Company, Reilly Industries, and the Exxon Education Fund.

## Literature Cited

1. Sacco, D.; Bonneaux, F.; Dellacherie, E. *Int. J. Biol. Macromol.* **1988**, *10*, 305.
2. Dellacherie, E. *Am. Chem. Soc., Div. Polym. Chem. Prepr.* **1991**, *32* (1), 602 and references therein.
3. Lenk, T.; Thies, C. In *Coulombic Interactions in Macromolecular Systems*; Eisenberg, A., Bailey, F. E., Eds.; American Chemical Society: Washington, DC, 1987; Chapter 8.
4. Dubin, P.; Ross, T. D.; Sharma, I.; Yegerlehner, B. In *Ordered Media in Chemical Separations*; Hinz, W. L., Armstrong, D. W., Eds.; American Chemical Society: Washington, DC, 1987; Chapter 8.
5. Veis, A. *Am. Chem. Soc., Div. Polym. Chem. Prepr.* **1991**, *32* (1), 596, and references therein.
6. Burgess, D. J.; Carless, J. E. *J. Colloid Interface Sci.* **1984**, *98*, 1.
7. Nguyen, T. Q. *Makromol. Chem.* **1986**, *187*, 2567.
8. Sternberg, M.; Hershberger, C. *Biochim. Biophys. Acta* **1974**, *342*, 195.
9. Kokufuta, E.; Shimizu, H.; Nakamura, I. *Macromolecules* **1981**, *14*, 1178.
10. Bozzano, A. G.; Andrea, G.; Glatz, C. E. *J. Membr. Sci.* **1991**, *55*, 181.
11. Clark, K. M.; Glatz, C. E. *Biotechnol. Prog.* **1987**, *3*, 241.
12. Fisher, R. R.; Glatz, C. E. *Biotechnol. Bioeng.* **1988**, *32*, 777.

13. Margolin, A.; Sheratyuk, S. F.; Izumrudov, V. A.; Zezin, A. B.; Kabanov, V. A. *Eur. J. Biochem.* **1985**, *146*, 625.
14. Ruckpoul, K.; Rein, H.; Janig, G. R.; Pfeil, W.; Ristau, O.; Damaschun, B.; Damaschun, H.; Muller, J. J.; Purschel, H. V.; Bleke, J.; Scheler, W. *Stud. Biophys.* **1972**, *34*, 81.
15. Shaner, S. L.; Melancon, P.; Lee, K. S.; Burgess, R. R.; Record, M. T., Jr. *Cold Spring Harbor Symp. Quant. Biol.* **1983**, *47*, 463.
16. Park, J. M.; Muhoberac, B. B.; Dubin, P. L.; Xia, J. *Macromolecules* **1992**, *25*, 290.
17. Strege, M. A.; Dubin, P. L.; West, J. S.; Daniel Flinta, C. D. In *Protein Purification: from Molecular Mechanisms to Large-Scale Processes*; Ladisch, M., Willson, R. C., Panton, C. C., Builder, S. E., Eds.; American Chemical Society: Washington, DC, 1990; Chapter 5.
18. Dubin, P. L.; Murrell, J. M. *Macromolecules* **1988**, *21*, 2291.
19. Xia, J.; Dubin, P.; Muhoberac, B. B.; Kim, Y. S.; Klimkowski, V. J. *J. Phys. Chem.*, accepted for publication.
20. Sternberg, M. *Process Biochemistry* **1976**, *11*, 11.
21. B.de Jong, H. *Protoplasma* **1932**, *15*, 110.
22. Kabanov, V. A.; Zezin, A. B. *Makromol. Chem. Suppl.* **1984**, *6*, 259.
23. Chen, W.; Walker, S.; Berg, J. C. *Chemical Engineering Science* **1992**, *47*, 1039.
24. Kokufuta, E.; Takahashi, K. *Polymer* **1990**, *31*, 1177.
25. Kokufuta, E.; Shimizu, H.; Nakamura, I. *Macromolecules* **1982**, *15*, 1618.
26. Kabanov, V. A. *Pure Appl. Chem. (Macromol. Chem.)* **1973**, *8*, 121.
27. Morawetz, H.; Hughes, W. L. *J. Phys. Chem.* **1952**, *56*, 64.
28. Kabanov, V. A.; Evdakov, V. P.; Mustafaev, M. I.; Antipina, A. D. *Molekularnaya Biologiya* **1977**, *11*, 582.
29. Pecora, R.; Berne, B. J. *Dynamic Light Scattering*; Wiley: New York, 1976.
30. Stock, R. S.; Ray, W. H. *J. Polym. Sci. Polym. Phys. Ed.* **1985**, *23*, 1393.
31. Provencher, S. W. *Comput. Phys. Commun.* **1982**, *27*, 229.
32. Burkhardt, C. W.; McCarthy, K. J.; Parazak, D. P. *J. Polym. Sci., Polym. Let.* **1987**, *25*, 209.
33. Doty, P. *Adv. Protein Chem.* **1951**, *6*, 35.
34. Ware, B. R.; Haas, D. D. in *Fast Methods in Physical Biochemistry and Cell Biology*; Shaafi, R. I.; Fernandez, S. M., Ed.; Elsevier: Amsterdam, 1983.
35. McQuarrie, D. A. *Statistical Mechanics*; Harper and Row: New York, 1976, page 553.
36. Gerald, D. F. in *Practical Handbook of Biochemistry and Molecular Biology*, CRC:Boca Raton, 1989.
37. Dautzenberg, H.; Rother, G. *J. Appl. Polym. Sci. Appl. Polym. Symp.* **1991**, *48*, 351.
38. Murphy, R. M.; Slayter, H.; Schurtenberger, P.; Chamberlin, R. A.; Colton, C. K.; Yarmush, M. L. *Biophys. J.* **1988**, *54*, 45.
39. Konishi, T.; Yoshizaki, T.; Yamakawa, H. *Macromolecules* **1991**, *24*, 5614.
40. Xia, J.; Dubin, P.; Kim, Y. S. *J. Phys. Chem.* **1992**, *96*, 6805.
41. Xia, J.; Dubin, P., unpublished results.
42. Tanford, C. *J. Am. Chem. Soc.* **1950**, *72*, 441.

RECEIVED September 21, 1993

## Chapter 18

# Amphiphilic Polyelectrolytes and Their Coulombic Complexes with Surfactants as Novel Photochemical Systems

Y. Morishima, M. Seki, S. Nomura, and M. Kamachi

Department of Macromolecular Science, Faculty of Science, Osaka University, Toyonaka, Osaka 560, Japan

Amphiphilic polyelectrolytes bearing bulky hydrophobic pendant groups form "unimolecular" micelles in dilute aqueous solution due to intramolecular self-organization of the hydrophobic groups. Coulombic complexes of the polyelectrolyte micelles with didodecyldimethylammonium bromide were prepared in dilute aqueous solution. The complexes were soluble in common organic solvents with a range of polarities. Light scattering, GPC, NMR relaxation, 2D-NOESY, ESR spin probe, and fluorescence studies showed that the micellar structure was retained in the complexes in organic solution, particularly so in benzene. Pyrene encapsulated in the core of the complexes exhibited fluorescence and photochemical properties typical of those of a "compartmentalized" chromophore.

In recent years, complexes between water-soluble polymers and surfactant molecules have been extensively studied from theoretical and experimental points of view (1-5). These complexes are of interest because they provide self-organized molecular assemblies which may serve as vehicles for chemical reactions relevant to biological phenomena. Because of considerable scientific and technological interests, a number of studies have focused on the complex formation of polyelectrolytes with oppositely charged surfactants below (6) and above (7-11) the critical micelle concentration (cmc).

Amphiphilic polyelectrolytes bearing bulky hydrophobic substituents adopt micellar structures in aqueous solution due to self-organization of the hydrophobic groups (12-17). A remarkable feature for such micelles, as compared with conventional surfactant micelles, is that the clusters of the hydrophobic groups in the amphiphilic polyelectrolyte micelles are *rigid* and *static* in the sense that local motions of the hydrophobic groups are highly restricted (13, 15, 16).

When a small mole fraction of a hydrophobic photoactive chromophore is covalently incorporated into such amphiphilic polyelectrolytes, it becomes encapsulated in the cluster of the hydrophobic groups. Thus, a photoactive chromophore can be confined to the nonpolar microenvironment in which the chromophore is "protected" from the aqueous phase. Furthermore, the molecular motions of the chromophore are restricted due to the rigidity of the hydrophobic cluster. Unlike chromophores solubilized in conventional surfactant micelle, the chromophore "compartmentalized" in the cluster of amphiphilic polyelectrolytes shows unique behavior in fluorescence and phosphorescence (18), in energy transfer and migration (16), in photoinduced electron transfer

0097-6156/94/0548-0243\$06.00/0

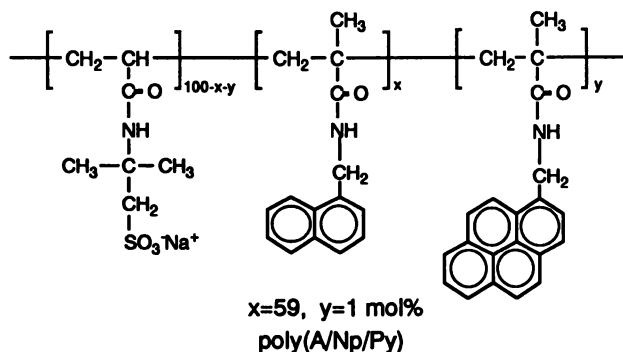
© 1994 American Chemical Society

(19-21), and in photoisomerization (22). Therefore, the compartmentalization of a photoactive group seems to be an interesting approach to the design of photosystems including photon-harvesting, photoinduced charge separation, and photochromic systems.

Coulombic complexes of such amphiphilic polyelectrolyte micelles with oppositely charged surfactants below the cmc provide new types of molecular assemblies which may have a variety of interesting features worth studying. The complexes can be dissolved in a variety of organic solvents. Therefore, they may act as novel vehicles for photochemical reactions (23,24) in organic solution. However, a question is whether or not the micellar structure of the parent amphiphilic polyelectrolytes remains as such in the Coulombic complexes in organic solution. To answer this question, we prepared Coulombic complexes of amphiphilic polysulfonic acid and cationic double-chain surfactants, and characterized their structures and dynamic properties in organic solution by dynamic light scattering (DLS), GPC,  $^1\text{H-NMR}$  relaxation, 2D-NOESY, ESR spin probe, and fluorescence techniques.

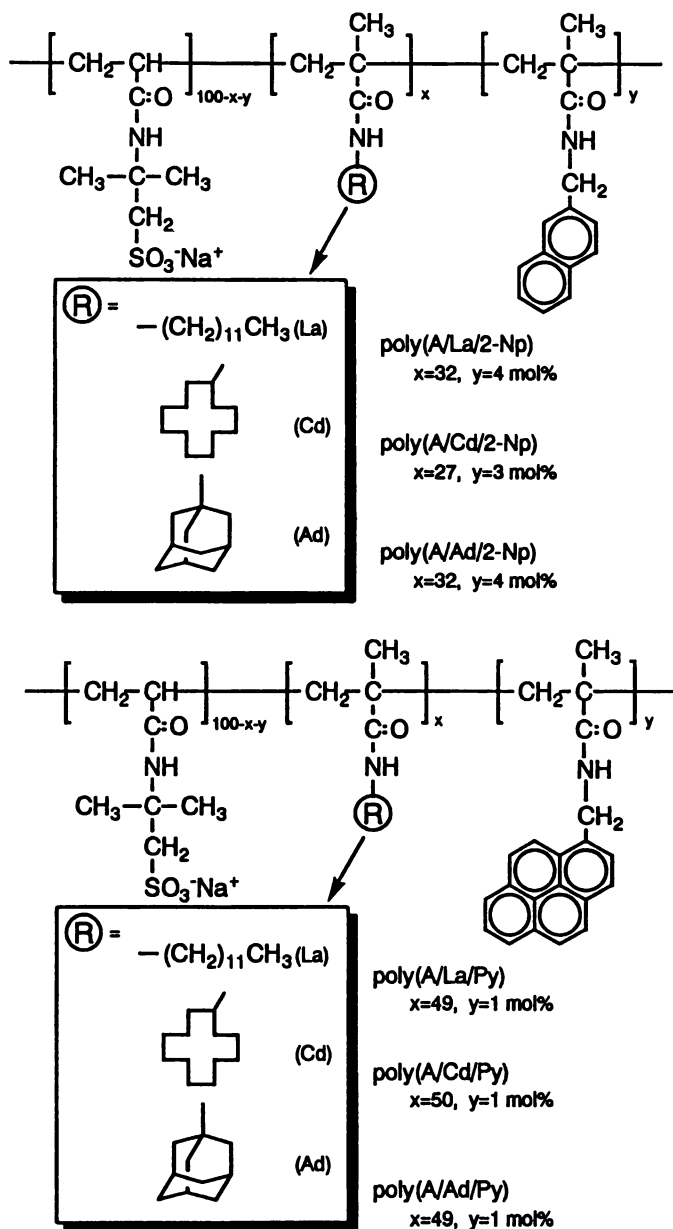
### Hydrophobic Self-Organization in Amphiphilic Polyelectrolytes in Aqueous Solution

Amphiphilic polyelectrolytes with bulky hydrophobic groups were prepared by free-radical terpolymerization of sodium 2-(acrylamido)-2-methylpropanesulfonate (AMPS), methacrylamides bearing bulky hydrophobic substituents, and small mole fractions of methacrylamides bearing spectroscopic probes (16, 18, 21, 22, 25). The lauryl (La), cyclododecyl (Cd), 1-adamantyl (Ad), and 1-naphthylmethyl (Np) groups were employed as the bulky hydrophobic substituents. The 1-pyrenyl (Py) and 2,2,6,6-tetramethylpiperidine-N-oxide (NO) groups were employed as fluorescence and spin labels, respectively. The terpolymerizations were performed in *N,N*-dimethylformamide (DMF) at 60 °C in the presence of 2,2'-azobis(isobutyronitrile). The compositions of the terpolymers were found to be virtually the same as the monomer feed compositions. In the text, the terpolymers are abbreviated as poly(A/R/P), where A, R, and P represent the AMPS, hydrophobic, and probe units, respectively.



The amphiphilic terpolymers are soluble in water to give transparent solutions in which "unimolecular" micelles are formed owing to intramolecular self-organization of the hydrophobic groups (13-16).  $^1\text{H-NMR}$  spectroscopy provides information about the hydrophobic self-organization. Considerable line broadening of the resonance peaks due to protons of the hydrophobic groups occurs when they form a hydrophobic cluster in water (13,15,24,25). In 2D-NOESY spectra of the terpolymer poly(A/Np/Py) in  $\text{D}_2\text{O}$  at room temperature, cross peaks were observed due to dipolar





Scheme I

interactions between the naphthyl and methyl and/or methylene protons (see Figure 3a).

NMR relaxation techniques are useful tools to study local segment motions in polymers. Spin-spin relaxation time ( $T_2$ ) for the naphthyl resonance in poly(A/Np/Py) in  $D_2O$  was found to be very short, being one order of magnitude shorter than that observed in DMF- $d_7$  (see Table I). This is in agreement with the fact that the naphthyl protons in poly(A/Np/Py) show much broader resonance lines in  $D_2O$  than in DMF- $d_7$ . These findings are indicative of strongly restricted motions of the naphthyl groups due to their cluster formation in aqueous solution. The spin-lattice relaxation occurs most efficiently through molecular motion whose frequency is comparable to the NMR frequency. Therefore, spin-lattice relaxation time ( $T_1$ ) decreases with a decrease in molecular motion, reaches a minimum, and then increases with a further decrease in the molecular motion. The long  $T_1$  observed for the naphthyl resonance in poly(A/Np/Py) in  $D_2O$ , in spite of the very short  $T_2$ , is attributable to a longitudinal relaxation in a highly restricted motion.

### Evidence for Unimolecular Micelle

A question may be asked as to whether the hydrophobic self-organization is an intramolecular or intermolecular event. A study of intermolecular energy transfer from a naphthalene-labeled polymer to a pyrene-labeled polymer may give an answer to this question.

Amphiphilic polyelectrolytes labeled with 2-Np [poly(A/R/2-Np)] and with Py [poly(A/R/Py)], where R is La, Cd, or Ad, were employed for this experiment (Scheme I). In these polymers in aqueous solution, 2-Np and Py are encapsulated in the hydrophobic clusters of La, Cd, and Ad. If the hydrophobic self-organization occurs intramolecularly, 2-Np and Py should be isolated from each other in each separate polymer and no energy transfer from photoexcited 2-Np to Py should be observed. On the other hand, if an intermolecular association takes place, there should be a chance for Py to come close to 2-Np within the Förster radius ( $R_0=2.86$  nm for transfer from 1-methylnaphthalene to pyrene (26)).

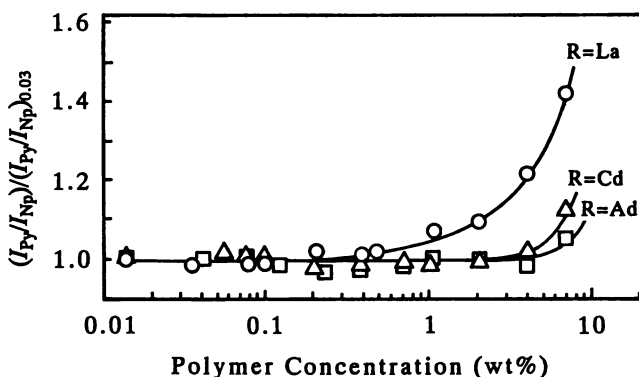
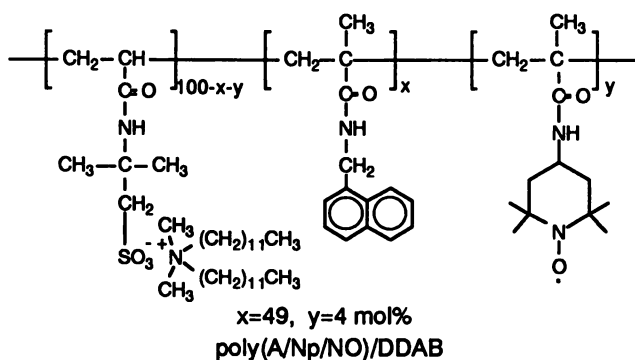
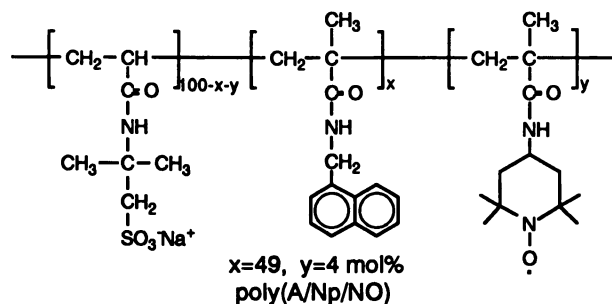
A mixture of poly(A/R/2-Np) and poly(A/R/Py) in aqueous solution was irradiated at 290 nm, at which virtually 2-Np can be excited selectively. Fluorescence emissions from 2-Np and Py were monitored at 340 and 395 nm, respectively. Figure 1 shows the ratios of the intensities of Py fluorescence and 2-Np fluorescence as a function of the total polymer concentration. The ratios were normalized by dividing by the ratios at the lowest polymer concentration (0.03 wt %) for ease of comparison. In the case of Ad as the hydrophobic group, practically no Py fluorescence was observed at polymer concentrations below ca. 4 wt%. This implies that a "unimolecular" micelle is formed as a result of intramolecular self-organization of Ad, when the polymer concentration is lower than ca. 4 wt%. For the amphiphilic terpolymers with Cd, the formation of the unimolecular micelle was also implied, when the polymer concentration was below ca. 2 wt%. On the other hand, amphiphilic polyelectrolytes with La showed a much stronger tendency for intermolecular association. A unimolecular micelle was suggested to be formed at polymer concentrations lower than ca. 0.5 wt%, being one order of magnitude lower than the Ad and Cd cases.

### Preparation of Coulombic Complexes of Amphiphilic Polyelectrolytes and Double-Chain Surfactants

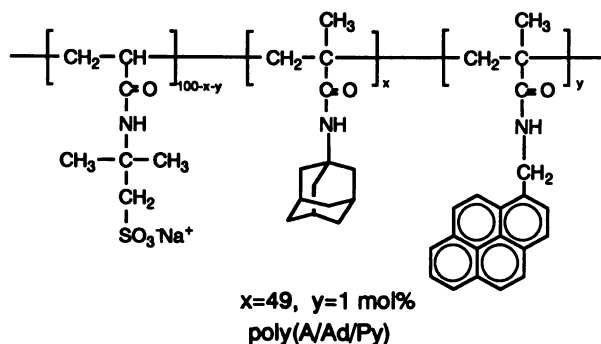
Figure 2a shows a histogram for the size distribution of the unimolecular micelle of poly(A/Ad/Py) in aqueous solution measured by DLS. At the polymer concentration of 0.32 wt% employed for the DLS measurement, the possibility of intermolecular association can be excluded as discussed in the previous section. The particle size distribution of the poly(A/Ad/Py) micelle in water was found to be rather narrow, ranging from ca. 6 to 13 nm in diameter.

**Table I.  $T_1$  and  $T_2$  for naphthyl protons and for methylene protons in the DDAB residues**

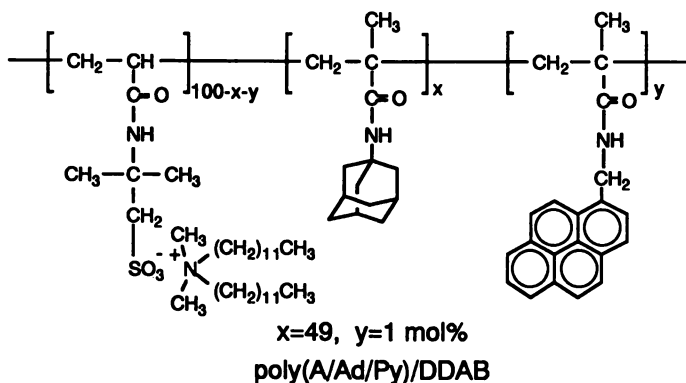
sample	solvent	$T_1$ (ms)		$T_2$ (ms)	
		naphthyl	DDAB	naphthyl	DDAB
poly(A/Np/Py)	D <sub>2</sub> O	726		4	
poly(A/Np/Py)	DMF- <i>d</i> <sub>7</sub>	854		45	
poly(A/Np/Py)/DDAB	benzene- <i>d</i> <sub>6</sub>	598	655	11	137
poly(A/Np/Py)/DDAB	DMF- <i>d</i> <sub>7</sub>	712	792	26	737

**Figure 1.** Ratio of the fluorescence intensities for the Py and 2-Np probes as a function of the total concentration of the mixture of poly(A/R/Py) and poly(A/R/2-Np) in aqueous solution, where R is La, Cd, or Ad.

When an aqueous solution of didodecyldimethylammonium bromide (DDAB) was added to an aqueous solution of poly(A/Ad/Py), the solution became turbid because of phase separation of the resulting Coulombic complexes. The complexes, which were collected by centrifugation, were purified by dialysis in a water suspension and recovered by freeze-drying. The complexes are abbreviated in the text as poly(A/R/Py)/DDAB, where R represents the hydrophobic groups.



In Figure 2b is shown the particle size distribution of the as-prepared complex poly(A/Ad/Py)/DDAB. The size of the complex in water was distributed from 60 to 250 nm in diameter. The particles of the complex were stable in water for a long period of time. No coagulation of the particles occurred, and the size of the as-prepared complex remained unchanged for more than 12 days in water. The complexes thus prepared were soluble in common organic solvents with a range of polarities including benzene, toluene, tetrahydrofuran (THF), chloroform, methanol, acetonitrile (ACN), and DMF.



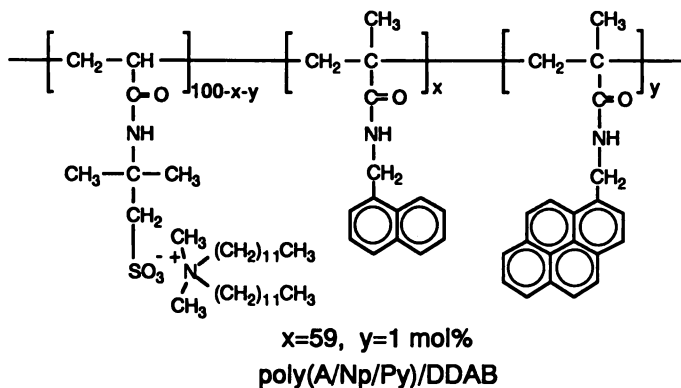
A reason for the use of a double-chain surfactant, instead of a conventional single-chain surfactant, was that the solubility of the former complex in organic solvents was much higher than that of the latter complex. In fact, complexes of poly(A/Ad/Py) and poly(A/Np/Py) with cetyltrimethylammonium bromide (CTAB) were soluble in DMF but insoluble in benzene, THF, methanol, and ACN.

The particle size of poly(A/Ad/Py)/DDAB in THF solution was estimated by DLS. The size distribution was found to be quite narrow, ranging from 6 to 15 nm, which is similar to that of the parent terpolymer in water. From a GPC elution curve for

poly(A/Ad/Py)/DDAB in THF, the number-average molecular weight was estimated to be  $\langle M \rangle_n = 3.9 \times 10^4$  with standard polystyrenes. The radius of gyration of the complex was calculated to be ca. 6 nm (ca. 12 nm in diameter) from the polystyrene equivalent molecular weight, which is in fair agreement with the size estimated by DLS.

### Characterization of the Complexes in Organic Solution

Because the complexes were prepared in aqueous solution, the micellar structure of the parent terpolymers should be retained at least in the as-prepared complexes. A main purpose for the characterization of the complexes is to examine whether the micellar structure can be retained even after the complexes are dissolved in organic solvents.



In the  $^1\text{H-NMR}$  spectra of poly(A/Np/Py)/DDAB in  $\text{DMF-}d_7$ , the integrated peak intensities for the naphthyl and DDAB protons were such that almost quantitative numbers of DDAB were ionically bound with the  $\text{SO}_3^-$  groups in poly(A/Np/Py). The resonance peaks due to the naphthyl protons were much broader than those due to the aliphatic protons in the DDAB residues. It is important, however, to note that the resonance line widths were different for different solvents used. In benzene- $d_6$ , the resonance lines were markedly broader than those in  $\text{DMF-}d_7$ . The peaks due to the naphthyl protons in poly(A/Np/Py)/DDAB in benzene- $d_6$  were as broad as those of the parent terpolymer in  $\text{D}_2\text{O}$ . These findings suggest that, in the complex in benzene solution, the naphthyl groups are still densely packed as reminiscent of the hydrophobic cluster of the parent terpolymer in aqueous solution. Furthermore, the quaternary ammonium cation of DDAB and the sulfonate anion form a contact ion pair in nonpolar solvents such as benzene, giving rise also to a compact conformation.

Figure 3 compares 2D-NOESY spectra of the parent terpolymer poly(A/Np/Py) in  $\text{D}_2\text{O}$  and the complex poly(A/Np/Py)/DDAB in benzene- $d_6$ . The complex in benzene- $d_6$  showed NOESY spectra very similar to those of the parent terpolymer in  $\text{D}_2\text{O}$ . Strong cross peaks occurred between the resonances of the naphthyl and aliphatic protons in the complex in benzene- $d_6$ . This suggests that the cross peaks observed for the complex in benzene- $d_6$  is attributed to the same type of cross interactions existing in the parent terpolymer in  $\text{D}_2\text{O}$ . In other words, the complex in benzene may retain the cluster of the naphthyl groups formed in aqueous solution. Considering that hydrogen bonding is strengthened in nonpolar media, hydrogen bonding between the spacer amide bonds existing in the unimolecular micelle of the parent terpolymer in aqueous solution may still be retained in the complex in benzene. It may be reasonable to consider that the hydrogen bonding is responsible for retaining the naphthyl clusters even in the complexes in organic solution.

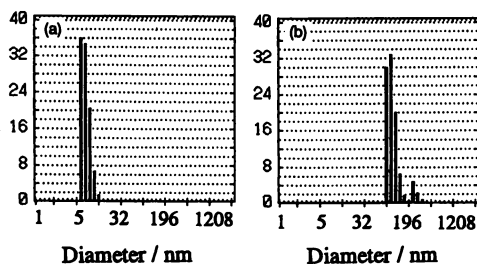


**Figure 2.** Histograms for the size distributions (number) for the parent terpolymer poly(A/Ad/Py) in aqueous solution (0.32 wt%) (a) and as-prepared complex poly(A/Ad/Py)/DDAB in aqueous media (b).

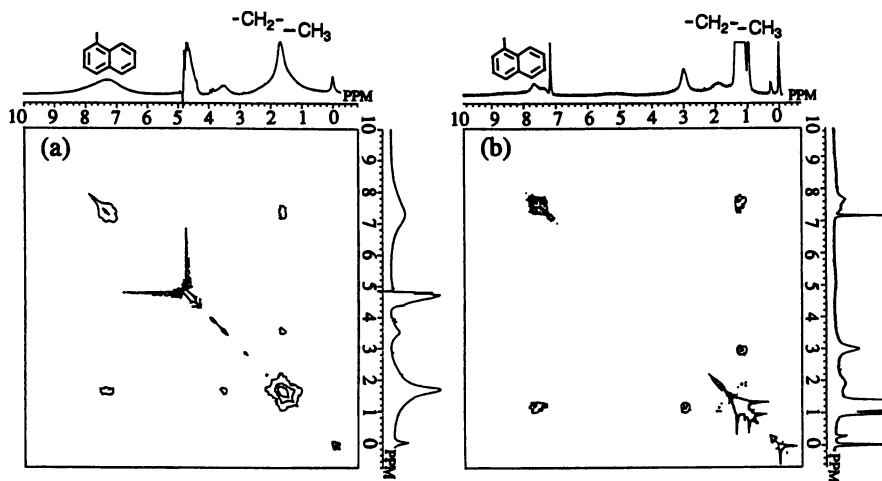


**Figure 3.** 2D-NOESY contour plots for the terpolymer poly(A/Np/Py) in D<sub>2</sub>O (a) and the complex poly(A/Np/Py)/DDAB in benzene-*d*<sub>6</sub> (b) at room temperature. (Reproduced with permission from reference 25. Copyright 1992 American Chemical Society.)

To estimate the mobility of the hydrophobic groups in poly(A/Np/Py)/DDAB,  $T_1$  and  $T_2$  in  $^1\text{H-NMR}$  were measured in benzene- $d_6$  and DMF- $d_7$ . Figure 4 shows  $^1\text{H-NMR}$  stack plots for the measurements of the relaxation times for poly(A/Np/Py)/DDAB in benzene- $d_6$  at room temperature.  $T_1$  and  $T_2$  are listed in Table I in comparison with the relaxation times for the parent terpolymer.  $T_2$  for the naphthyl protons in the complex poly(A/Np/Py)/DDAB were shorter than  $T_2$  for the parent polymer poly(A/Np/Py) in DMF- $d_7$ . This suggests that the motions of the naphthyl groups in the complex in organic solution is still restricted as reminiscent of the parent terpolymer in aqueous solution. A very short  $T_2$  of 11 ms for the naphthyl resonance for poly(A/Np/Py)/DDAB in benzene is indicative of considerably restrained naphthyl motions, similar to those in the parent polymer in  $\text{D}_2\text{O}$ . Much longer  $T_2$  for the aliphatic protons of the DDAB residues in poly(A/Np/Py)/DDAB indicate that the motions of the aliphatic double-chains in DDAB are much less restrained in the complex. It should be noted that both  $T_1$  and  $T_2$  for the complex in benzene- $d_6$  were shorter than those in DMF- $d_7$ , indicating that the conformation was more compact in benzene than in DMF.

Information about mobility of a local segment in the complex can be obtained from a nitroxide (NO) spin probe covalently attached to the parent amphiphilic polyelectrolyte. Figure 5 shows ESR spectra of the parent terpolymer poly(A/Np/NO) in aqueous solution and the complex poly(A/Np/NO)/DDAB in various solvents at room temperature. The spectra were analyzed by simulation using the procedure reported by Schneider and Freed (27). Brownian rotational diffusion was used as a model of rotational motion of the spin probe. The  $g$  and  $A$  tensor components were determined by the simulation of rigid-limit ESR spectra observed at 77 K. The rotational correlation times ( $\tau_R$ ) which gave the best simulated spectra at room temperature are indicated in the figure.  $\tau_R$  of the NO probes in the complex depended on the solvent, indicating that the motions of the NO probes were restricted in the order of MeOH < DMF < benzene as solvent. In benzene, the motions of the NO probes in the complex were slowest, and even slower than those of the parent terpolymer in water. These results imply that, in benzene, the complex retains the micellar structure of the parent polymer.

A conceptual drawing of a speculated structure of the Coulombic complex is shown in Figure 6.

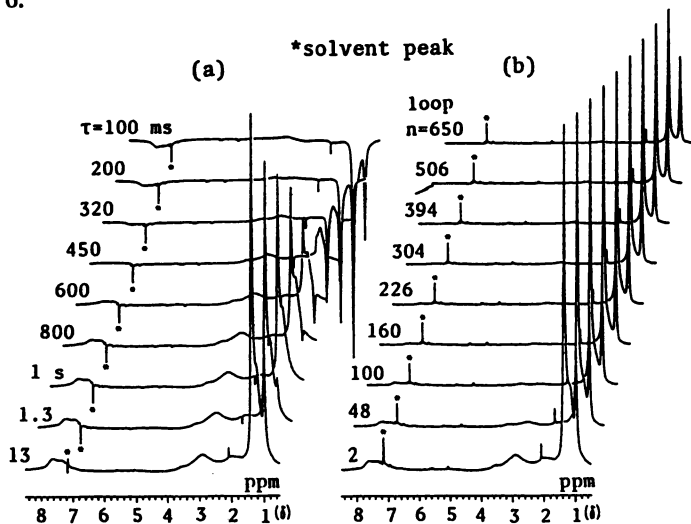
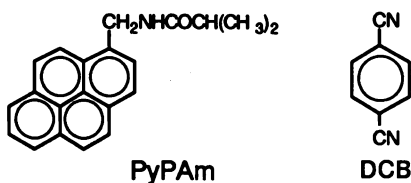


**Figure 4.**  $^1\text{H-NMR}$  Stack plots for the complex poly(A/Np/Py)/DDAB in benzene- $d_6$ , from which  $T_1$  (a) and  $T_2$  (b) were determined.

## Fluorescence from Pyrene Labels

Fluorescence emitted by the pyrene label gives information about the nature of their local environments, because the ratio of the third to first vibrational fine structure,  $I_3/I_1$ , of the pyrene fluorescence is sensitive to local environmental polarity, the  $I_3/I_1$  ratio being larger in less polar media (28). In fact, fluorescence spectra of a small molecular weight model compound PyPAm showed  $I_3/I_1$  ratios of 0.67 and 0.43 in benzene and in DMF, respectively, clearly reflecting solvent polarities. Figure 7 compares the spectra emitted by Py labels in poly(A/Ad/Py)/DDAB in benzene and in DMF. The values of  $I_3/I_1$  for poly(A/Ad/Py)/DDAB in benzene and in DMF were found to be very similar although the solvent polarities are different. This indicates that the Py labels in the complex experience micropolarities which are different from the solvent polarities and that they are confined to microenvironments which are separated from the solvent phase. In poly(A/Ad/Py)/DDAB, Py is surrounded by Ad and also by ion pair groups. Therefore, Py may not be exposed to the solvent phase but may experience a polar microenvironment owing to the surrounding ion pairs in the complex even though the complex is in benzene solution.



Singlet-excited pyrene forms an exciplex with 4,4'-dicyanobenzene (DCB) which shows a characteristic structure-less emission at about 450 nm in nonpolar solvents (29). Figure 8 compares fluorescence spectra of poly(A/Ad/Py)/DDAB and PyPAm in benzene in the presence of varying concentrations of DCB. The fluorescence of PyPAm was quenched by DCB and was replaced with an exciplex emission band peaking at about 460 nm. The intensity of the exciplex increased progressively with increasing concentration of DCB. By contrast, the exciplex emission was strongly suppressed in poly(A/Ad/Py)/DDAB, although the fluorescence was quenched by DCB. These observations may be attributed in part to the polar microenvironment around Py as discussed above and in part to a hindered approach of DCB to Py in poly(A/Ad/Py)/DDAB due to the retained compartmentalization of Py.

It should be noted, however, that electron transfer (ET) quenching of singlet-excited Py by DCB can occur despite the compartmentalization of Py. The geometrical requirements such as distance and orientation for exciplex formation should be more rigorous than those for photoinduced ET. Therefore, a long-range or collisionless ET can occur, even though the exciplex formation is sterically prohibited.

Stern-Volmer constants ( $K_{SV}$ ) for the fluorescence quenching of PyPAm and poly(A/Ad/Py)/DDAB by DCB in benzene were determined to be 166 and 90  $M^{-1}$ , respectively. In benzene, the fluorescence quenching for Py in poly(A/Ad/Py)/DDAB was less effective than that for PyPAm because of a hindered approach of DCB to Py.

## Photoinduced Electron Transfer

Photoinduced ET from Py in the complex poly(A/Ad/Py)/DDAB to pyromellitic dianhydride (PMDA) in ACN solution was investigated by laser photolysis at room temperature in comparison with the PyPAm model system (23). Transient absorption



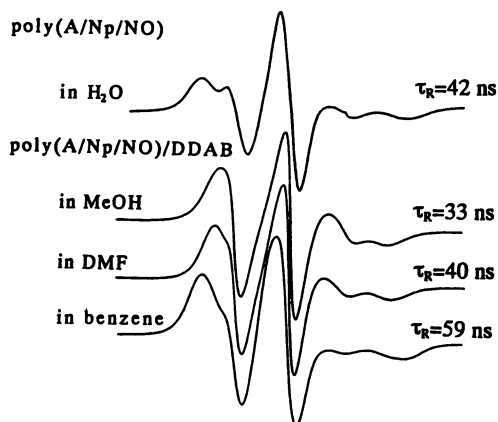


**Figure 5.** ESR signals for poly(A/Np/NO) in water and poly(A/Np/NO)/DDAB in various organic solvents.

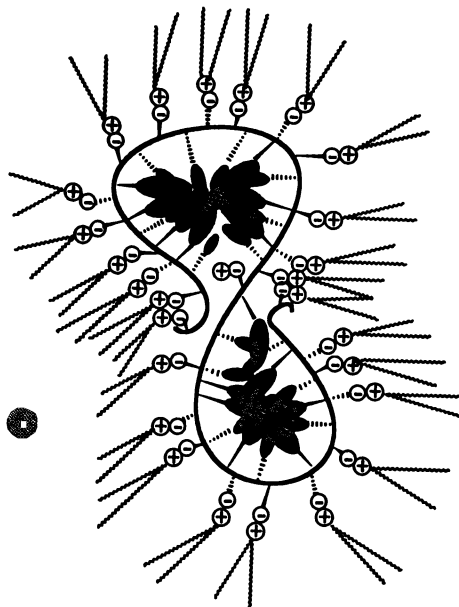


**Figure 6.** Conceptual illustration of a local structure of the complex.

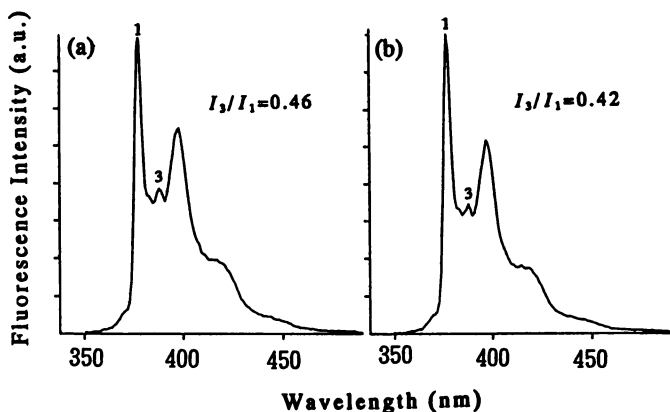


**Figure 7.** Fluorescence spectra of the complex poly(A/Ad/Py)/DDAB in benzene (a) and in DMF (b); excitation wavelength, 347 nm. The  $I_3/I_1$  ratios are indicated in the figure. (Reproduced with permission from reference 25. Copyright 1992 American Chemical Society.)

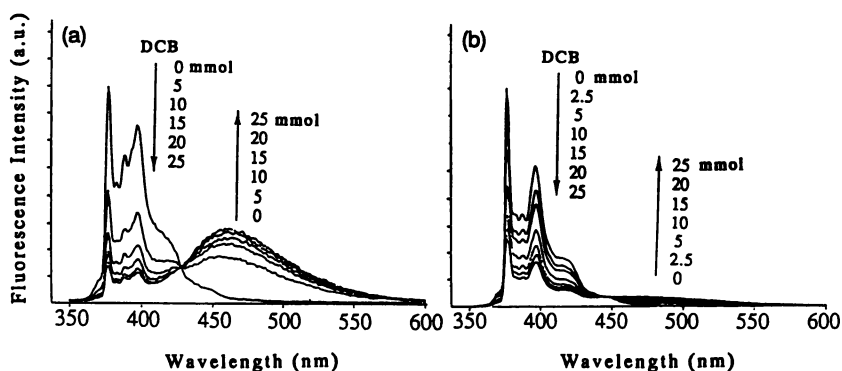
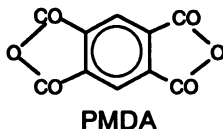


**Figure 8.** Fluorescence spectra of the model compound PyPAm (a) and the complex poly(A/Ad/Py)/DDAB (b) in benzene in the presence of varying concentrations of DCB at room temperature; excitation wavelength, 347 nm. (Reproduced with permission from reference 23. Copyright 1992 John Wiley & Sons.)

peaks were observed at 460 and 660 nm due to the cation radical of Py ( $\text{Py}^{\cdot+}$ ) (21) and the anion radical of PMDA ( $\text{PMDA}^{\cdot-}$ ) (30), respectively. In the model system, these transient species decayed almost completely 30  $\mu\text{s}$  after the laser pulse. However, these transient species in the complex system were found to be much longer-lived than those in the model system.  $\text{PMDA}^{\cdot-}$  in the complex system persisted for tens of milliseconds. In the model system,  $\text{PMDA}^{\cdot-}$  decayed via a second order process with a rate constant of  $1.1 \times 10^{10} \text{ M}^{-1} \text{ s}^{-1}$  in the microsecond region, indicating that the decays are due to diffusion-controlled back ET from  $\text{PMDA}^{\cdot-}$  to  $\text{Py}^{\cdot+}$ . The decay of  $\text{PMDA}^{\cdot-}$

in the complex system, on the other hand, approximately followed first-order kinetics with an apparent rate constant of  $2.5 \times 10^3 \text{ s}^{-1}$ . Such a slow back ET rate observed for the complex system is attributable to a collisionless, long-range ET between the compartmentalized  $\text{Py}^+ \cdot$  and  $\text{PMDA}^- \cdot$ :



In conclusion, the unimolecular micelles of parent amphiphilic polyelectrolytes formed in aqueous solution are maintained, if not in the exact form, in the Coulombic complexes dissolved in organic solvents, particularly so in benzene. Since the complexes are soluble in vinyl monomers such as methyl methacrylate and styrene, they can be incorporated in polymer matrices by polymerizing the monomer solutions containing the complexes to give optically transparent polymer films, sheets, or blocks which give an opportunity to study unique photochemistry of compartmentalized photoactive chromophores in the state of polymer solid.

### Literature Cited

- (1) Zana, R.; Lianos, P.; Lang, J. J. *Phys. Chem.* 1985, 89, 41.
- (2) Chu, D.-Y.; Thomas, J. K. *J. Am. Chem. Soc.* 1986, 108, 6270.
- (3) Turro, N. J.; Kuo, P.-L. *Langmuir* 1986, 2, 438.
- (4) Winnik, F. M.; Winnik, M. A.; Tazuke, S. *J. Phys. Chem.* 1987, 91, 594.
- (5) Chandar, P.; Somasundaran, P.; Turro, N. J. *Macromolecules* 1988, 21, 950.
- (6) Goddard, E. D. *Colloids Surf.* 1986, 19, 301.
- (7) Dubin, P. L.; Oteri, R. J. *Colloid Interface Sci.* 1983, 95, 453.
- (8) Dubin, P. L.; Davis, D. D. *Macromolecules* 1984, 17, 1294.
- (9) Dubin, P. L.; Rigsbee, D. R.; McQuigg, D. W. *J. Colloid. Interface Sci.* 1985, 105, 509.
- (10) Dubin, P. L.; Rigsbee, D. R.; Fallon, M. A.; Gan, L. M. *Macromolecules* 1988, 21, 2555.
- (11) Dubin, P. L.; The, S. S.; Gan, L. M.; Chew, C. H. *Macromolecules* 1990, 23, 2500.
- (12) Dubin, P. L.; Strauss, U. P. *J. Am. Chem. Soc.* 1970, 74, 2842.
- (13) Morishima, Y.; Itoh, Y.; Nozakura, S. *Makromol. Chem.* 1981, 182, 3135.
- (14) Morishima, Y.; Kobayashi, T.; Nozakura, S. *J. Phys. Chem.* 1985, 89, 4081.
- (15) Morishima, Y.; Kobayashi, T.; Nozakura, S. *Polym. J.*, 1989, 21, 267.
- (16) Morishima, Y.; Tominaga, Y.; Nomura, S.; Kamachi, M.; Okada, T. *J. Phys. Chem.* 1992, 96, 1990.
- (17) Guillet, J. E.; Rendall, W. A. *Macromolecules* 1986, 19, 224.
- (18) Aota, H.; Morishima, Y.; Kamachi, K. *Photochem. Photobiol.* 1993, 57, 989.
- (19) Morishima, Y.; Kobayashi, T.; Furui, T.; Nozakura, S. *Macromolecules* 1987, 20, 1707.
- (20) Morishima, Y.; Furui, T.; Nozakura, S.; Okada, T.; Mataga, N. *J. Phys. Chem.* 1989, 93, 1643.
- (21) Morishima, Y.; Tominaga, Y.; Kamachi, M.; Okada, T.; Hirata, Y.; Mataga, N. *J. Phys. Chem.* 1991, 95, 6027.
- (22) Morishima, Y.; Tsuji, M.; Kamachi, M.; Hatada, K. *Macromolecules* 1992, 25, 4406.
- (23) Morishima, Y.; Seki, M.; Tominaga, Y.; Kamachi, M. *J. Polym. Sci., Polym. Chem. Ed.* 1992, 30, 2099.

- (24) Seki, M.; Morishima, Y.; Kamachi, M. *Macromolecules* **1992**, *25*, 6540.
- (25) Morishima, Y.; Tominaga, Y.; Nomura, S.; Kamachi, M. *Macromolecules* **1992**, *25*, 861.
- (26) Berlman, I. B. *Energy Transfer Parameters of Aromatic Compounds*; Academic Press: New York, 1973; pp 312.
- (27) Schneider, D. J.; Freed, J. H. In *Biological Magnetic Resonance*; Berliner, L. J.; Teuben, J., Eds.; Plenum Press: New York, 1989, Vol.8; pp 1-76.
- (28) Kalyanasundaram, K.; Thomas, J. K. *J. Am. Chem. Soc.* **1977**, *99*, 2039.
- (29) Beens, H.; Knibble, H.; Weller, A. J. *Chem. Phys.*, **1967**, *47*, 1183.
- (30) Mataga, N.; Shioyama, H.; Kanda, Y. *J. Phys. Chem.* **1987**, *91*, 314.

RECEIVED August 6, 1993

## Chapter 19

# Interaction of Proteins with Acrylic Polyampholytes

C. S. Patrickios, C. J. Jang, W. R. Hertler, and T. A. Hatton

Department of Chemical Engineering, Massachusetts Institute of Technology, Cambridge, MA 02139

The interaction of dilute solutions of synthetic polyampholytes with proteins was investigated by turbidimetric titration. As in the homopolyelectrolyte-protein system, the onset of interaction in the polyampholyte-protein system is manifested by a large increase in turbidity at a certain pH, the critical pH. An interesting complication of our system is the self-aggregation of the polyampholyte near its isoelectric point. The critical pH of the polyampholyte-protein system lies in between the polyampholyte's self-aggregation pH and the protein's isoelectric point. Increasing salt concentration suppresses the protein - polyampholyte and polyampholyte - polyampholyte interactions. The determining role of the pH both in the protein-polyampholyte and polyampholyte-polyampholyte interactions as well as the suppression by the salt suggest that these phenomena are mainly driven by electrostatic forces. We studied mixtures of one protein and one synthetic polyampholyte and we investigated the effect of salt concentration, protein concentration, protein and polymer type.

Synthetic polyelectrolytes are known to interact strongly with proteins of opposite charge and form soluble or insoluble complexes (1). When the complexation products are insoluble, this interaction may be employed for protein separation (2-6). The important contribution of the electrostatic forces in these interactions is manifested by the strong dependence of the complexation on pH, salt concentration and the polymer-protein ratio (2-6). Other determining factors can be the existence of charge patches (1,7) or charged blocks (8) on the protein as well as polymer-protein hydrophobic interactions (9).

While a wide variety of polyelectrolytes has been tested, very few reports involve the utilization of polyampholytes, polymers with both positive and negative charges (10). In this study we utilize low-molecular-weight block polyampholytes based on methacrylic acid (Ac), dimethylaminoethyl methacrylate (B) and methyl methacrylate (M) and prove that these polymers interact strongly with proteins of opposite net charge. The block acrylic polyampholytes were synthesized by a living polymerization technique and are of a well-defined composition and size, with polydispersity indices less than 1.3. Contrary to previous studies in which the polyelectrolyte polydispersity indices varied from 2 to 10 (2,6) the data interpretation

0097-6156/94/0548-0257\$06.00/0  
© 1994 American Chemical Society

with our polymers is free of size inhomogeneity effects. Another advantage of these polyampholytes related to the protein separation process is their property to precipitate around their isoelectric point, which could facilitate polymer recycling after protein separation. In the previous polyampholyte-protein study (10), a random copolymer was used that did not precipitate at the isoelectric point.

## Experimental

Table I lists the synthetic polyampholytes utilized in this study along with the number of residues per molecule and the isoelectric point. All the polymers have a molecular weight of approximately 4,000 Da. The first three are triblock copolymers with block sequence B/M/AC and the fourth is a random terpolymer. The proteins used are soybean trypsin inhibitor (STI,  $pI = 4.5$ ), ovalbumin ( $pI = 4.7$ ), ribonuclease ( $pI = 8.8$ ) and lysozyme ( $pI = 11.0$ ).

Most of the experiments were turbidimetric titrations of pure polymer, pure protein or polymer-protein binary mixtures. Fresh stock solutions of 0.01% w/w polymer and 0.05% w/w protein in 0.01M McIlvane's buffer (citrate and phosphate) were prepared before the titrations. 1 mL of polymer solution or 1 mL of protein solution was taken for the titration of the pure species. Binary solutions of protein and polymer were prepared by mixing 0.5 mL of a 0.05% w/w protein solution with 0.5 mL of a 0.01% w/w polymer solution. The salt concentration was adjusted by adding the appropriate volume of 3M KCl solution. The pH was gradually changed by adding one or two drops of KOH (in most of the experiments) or HCl (in one experiment) of the appropriate concentration. The pH was varied between 4 and 10, and at each pH, the optical density at 420 nm was measured. The experiments were designed so that the pH at which the optical density increases abruptly, the critical pH, was reached within the addition of a small number of drops of reagent in order to keep the extent of protein and polymer dilution as well as the decrease in ionic strength at negligible levels. All the experiments were completed by extensive addition of reagent in order to show the redissolution of the complex after crossing the isoelectric point of the polymer or the protein. The resulting dilution of the mixture allows only qualitative interpretation of the optical density signal, particularly after the critical pH. Another limitation for the interpretation of the data after the critical pH arises from the time dependence of the optical density. However, it was observed in the kinetic study that the optical density increases very quickly within the first two minutes and subsequently it increases very slowly. Therefore, since the pH change and measurement of the optical density took place less frequently than every two minutes, it can be considered that we were in the regime of a quasi-steady state.

The time-dependence of aggregation was followed using solutions of Polymer N at concentrations 0.004, 0.01, 0.02, and 0.04% w/w prepared at the non-aggregating pH of 4.4. Each sample was transferred to the cuvette and a precalculated amount of KOH solution was added to change the pH to the aggregating value of 6.1. The cuvette compartment of the spectrophotometer was immediately closed and the optical density was measured as a function of time on a chart recorder.

To study the extent of polymer-protein complexation quantitatively, mixtures of Polymer B and STI were prepared at different pH and protein concentrations. Equal volumes of 0.01% polymer and 0.02, 0.05, 0.10, and 0.2% protein were mixed and adjusted to two pH levels, 4.8 and 5.1. After centrifugation for 30 min at 4,000 rpm a two-phase system, composed of an optically clear supernatant and a solid precipitate, resulted. The supernatant was analyzed for protein by measuring the absorbance at 280 nm and the amount of precipitated protein was calculated by mass balance.

## Results and Discussion

Figure 1 depicts the time dependence of aggregation of Polymer N at different polymer concentrations. With increasing polymer concentration the turbidity increases. For the most concentrated solution the optical density exceeds the value of one very quickly. The curves, however, have similar shape and can be divided into two time regimes borderlined at two minutes from the beginning of the experiment. In the early regime the curves are very steep indicating a high rate of aggregation. After two minutes, however, the rate of increase in the optical density is noticeably slowing down approaching a constant value.

All but one of the turbidimetric titrations that will be presented below were performed by changing the pH from low to high values and will be referred to as forward titrations. The only backward titration (pH changed from high to low values) is the one presented in Figure 4(b). The direction of titration is indicated in the Figures by an arrow.

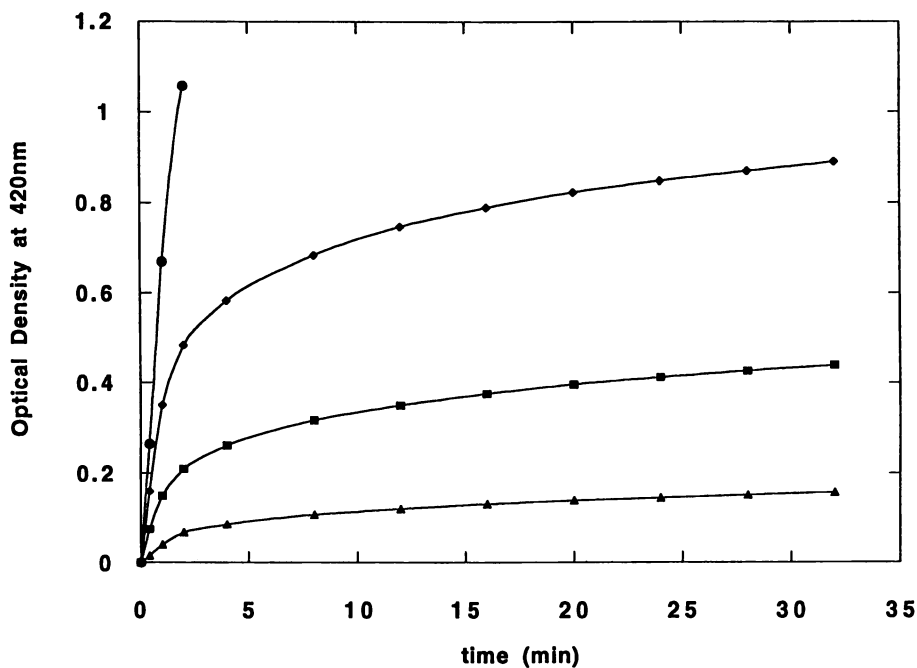
Figures 2(a) and (b) are the turbidimetric titrations of Polymer N and illustrate the effect of polymer concentration and salt concentration, respectively. Figure 2(a) shows that the polymer precipitates at pH 5.5 and goes back to solution at pH 8.0. This is a direct result of the pH-dependence of the solubility of the polyampholyte which is very low around the isoelectric point and increases sharply 1-2 pH units away from the isoelectric point. Although the curves of higher polymer concentration display a higher optical density, the critical pH is the same for all polymer concentrations and its value is 5.5. The independence of the critical pH on polymer concentration is a consequence of the fact that the critical pH is determined by a critical net charge which does not depend on polymer concentration. It is well known that polymer concentration does not influence the titration curve of a polymer. Figure 2(b) shows that increasing salt concentration suppresses polyampholyte precipitation. As the concentration of KCl was increased from 0.0 to 0.1, 0.35 and 0.75M, the values of the optical density decreased, and at the same time the critical pH increased approaching the value of the isoelectric pH at the highest salt concentration. The salt weakens the attractive Coulombic interactions and a better balance between positive and negative charges is required for phase separation. This drives the critical pH closer to the isoelectric point of the polymer.

Figure 3(a) presents the optical densities of pure Polymer N, pure STI and a mixture of the two. While pure protein solution does not precipitate, pure polymer solution does at pH 5.3 and redissolves close to pH 8. The polymer-protein mixture exhibits a critical pH of 4.6 which is lower than that of pure polymer and close to the isoelectric point of the protein; the mixture also exhibits an optical density higher than that of the pure polymer. Both of the above manifest a strong polymer-protein interaction. Figure 3(b) illustrates the effect of salt concentration on Polymer N-STI interaction. The trends are similar to those of Figure 2(b). Salt suppresses the interaction as manifested by the decrease in optical density. The critical pH is shifted towards the isoelectric point of the polymer rather than that of the protein because the former has a higher charge density than the latter and, therefore, controls the interaction.

Figure 4(a) illustrates the interaction between Polymer B and STI. The trends are identical to those of Figure 3(a). The critical pH of the more basic Polymer B is 5.6, slightly higher than that of Polymer N. The critical pH of the mixture, on the other hand, is almost the same for the two polymers and has a value of 4.6. Similar results were obtained for the Polymer B-ovalbumin system. The difference, however, between the critical pH's of pure polymer and the protein-polymer mixture, as well as the difference between the maximum optical densities of pure polymer and the mixture were less pronounced in the ovalbumin case as compared to the STI case, in spite of the higher molecular weight of ovalbumin. This can be attributed either to extensive charge patches on STI or to the greater hydrophobicity of STI. Figure 4(b)

**Table I. Properties of the polyampholytes**

Polymer	B/M/Ac	pI
A (acidic)	8/12/16	5.4
N (neutral)	12/12/12	6.6
B (basic)	16/12/8	8.0
R (random)	12/12/12	6.6



**Figure 1.** Time dependence in self-aggregation of Polymer N at different polymer concentrations without added salt. From top to bottom: 0.040, 0.020, 0.010 and 0.004% w/w polymer.



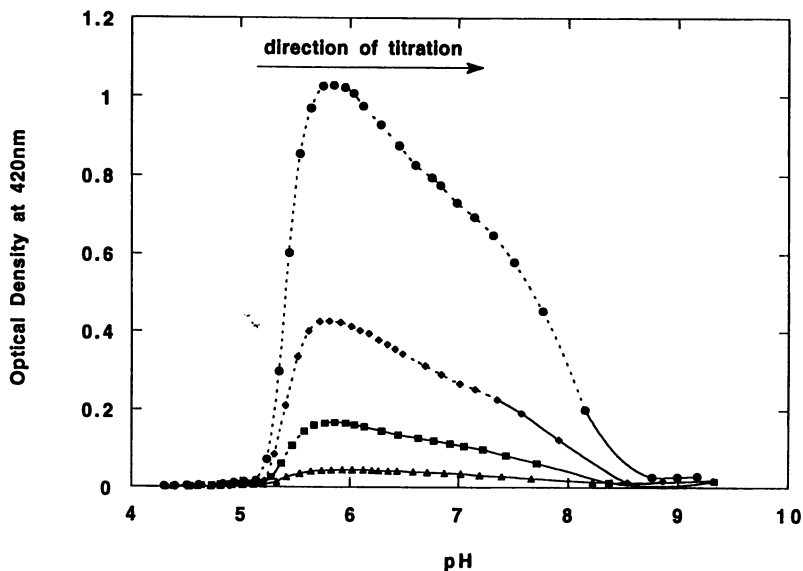


Figure 2(a). Self-aggregation of Polymer N at different polymer concentrations without added salt. From top to bottom: 0.040, 0.020, 0.010 and 0.004% w/w polymer. Dotted lines indicate unstable optical density readings.

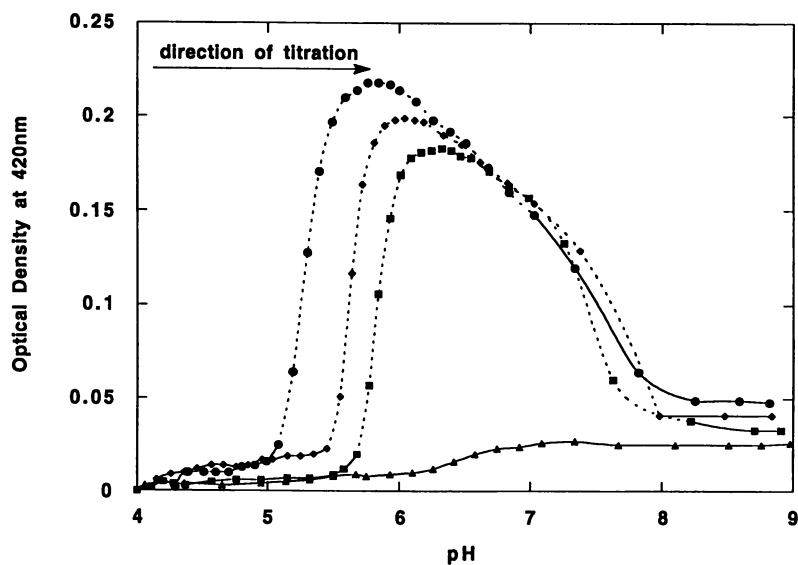


Figure 2(b). Self-aggregation of 0.01% w/w Polymer N at different salt concentrations. From top to bottom: 0.00, 0.10, 0.35 and 0.75M KCl. Dotted lines indicate unstable optical density readings.

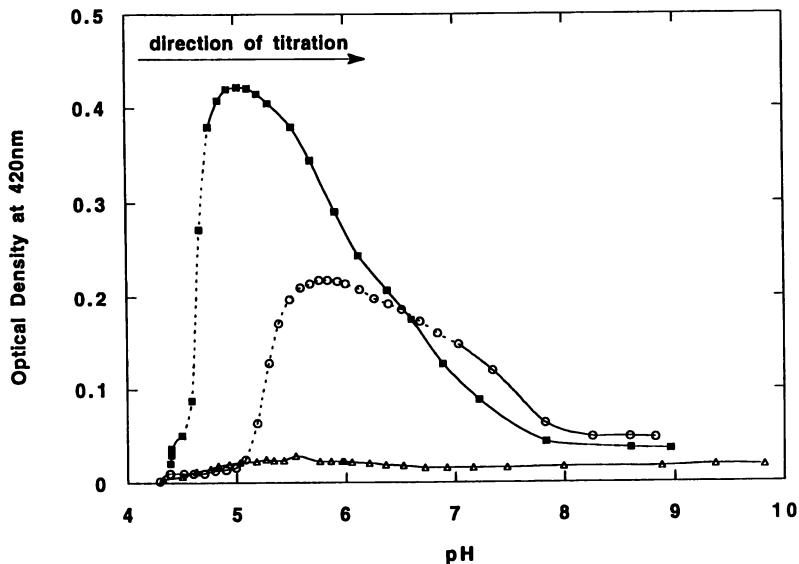


Figure 3(a). Optical densities of 0.010% Polymer N (open circles), 0.050% STI (open triangles) and mixture containing 0.025% STI and 0.005% w/w Polymer N (filled squares) without added salt. Dotted lines indicate unstable optical density readings.

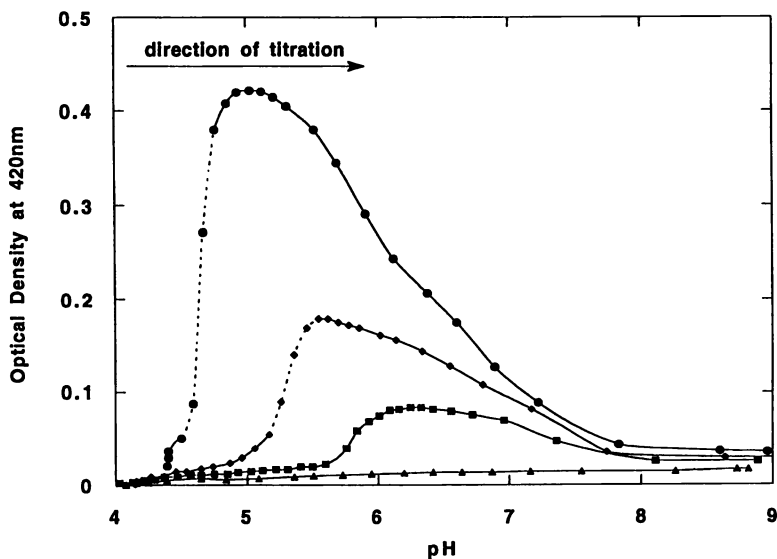


Figure 3(b). Complexation of 0.025% STI with 0.005% w/w Polymer N at different salt concentrations. From top to bottom: 0.00, 0.10, 0.35 and 0.75M KCl. Dotted lines indicate unstable optical density readings.

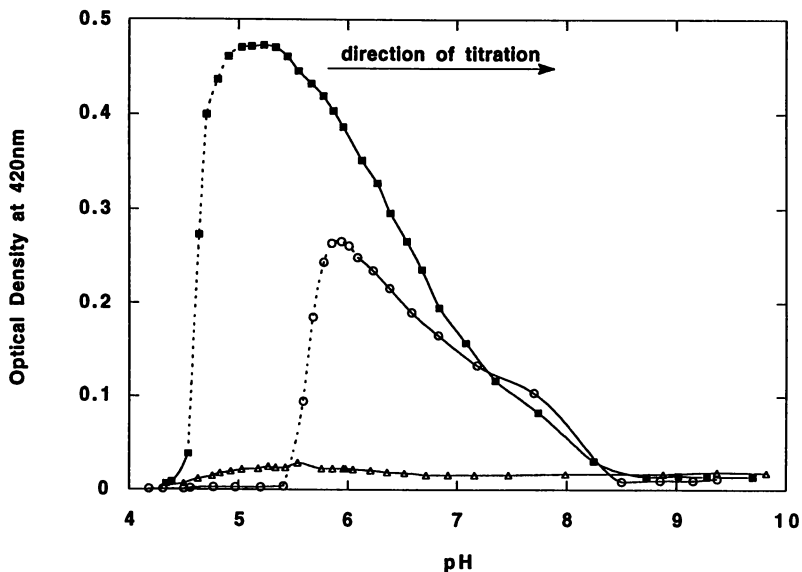


Figure 4(a). Optical densities of 0.010% Polymer B (open circles), 0.005% STI (open triangles) and mixture containing 0.005% Polymer B and 0.025% w/w STI (filled squares) without added salt.

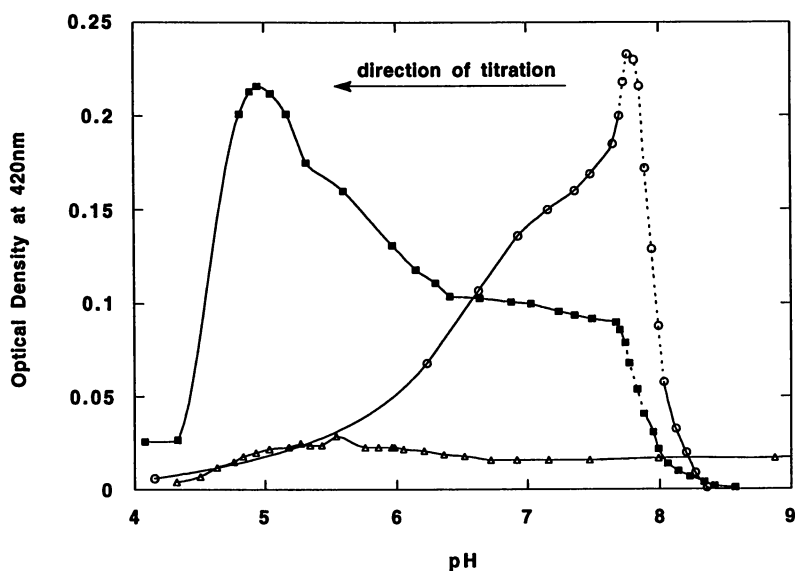


Figure 4(b). Back titrations of Figure 4(a). Optical densities of 0.010% Polymer B (open circles), 0.050% STI (open triangles) and mixture containing 0.005% Polymer B and 0.025% w/w STI (filled squares) without added salt.

is the back titration of Figure 4(a) in which the pH was changed from high to low values. Pure polymer solution aggregated at pH 8.0. In the protein-polymer mixture, a first increase in optical density was observed at pH 8.0, due to polymer aggregation, and a second more pronounced increase was observed at pH 5-6 due to polymer-protein aggregation.

In another experiment (not presented here) which involved Polymer R and STI, neither polymer nor polymer-protein interaction was observed because of the lack of charge localization of the random copolymer (low charge density).

Figure 5 shows quantitatively the extent of complexation between Polymer B and STI at pH 4.8 and 5.1. These pH's are near the pH of maximum optical density of Figure 4(a). The units of the axes are inverse absorbance at 280 nm. The straight-line correlation between the experimental points suggests that the complexation follows the Langmuir model (11). This can be understood by considering the protein as the adsorbate and the polyampholyte as the adsorbent with a fixed number of binding sites which become saturated as the protein concentration increases. This also seems to imply that the number of polymer molecules available for binding is independent of protein concentration. The latter can be realized only if all or most of the polyampholyte occurs in the precipitate. Unfortunately, we were not able to justify this hypothesis because it was impossible to analyze for the very low concentrations of the polymer in the supernatant or the very small amounts of precipitate. However, since in this set of experiments the protein/polymer mass ratio ranged from 2 to 20, we feel that most of the polyampholyte was associated with protein and precipitated. The y-intercepts of the lines correspond to the maximum amount of protein that can complexate with the given amount of polymer.

Unlike Figures 3-5, Figures 6 and 7 illustrate protein/polymer pairs in which the polymer is more acidic than the protein and, therefore, the polymer-protein critical pH is reached after the polymer critical pH (for forward titrations).

Figure 6 presents the optical densities of pure Polymer A and of mixtures of Polymer A with two different concentrations of ribonuclease, 0.025 and 0.25%, with no added salt. The optical density of pure protein solution (not shown) was lower than 0.01. As seen by the sharp changes in optical density, pure polymer aggregates at pH 4.6 and goes back to solution at pH 6.6. The curves of the mixtures preserve the increase in optical density due to pure polymer aggregation and additionally exhibit a peak due to polymer-protein interaction which is 4 to 6 times more intense than that of pure polymer. The critical pH for polymer-protein interaction is 6.2 and drops to 6.1 when the protein concentration is increased by 10 times. By increasing the pH, approaching the isoelectric point of the protein, the polymer-protein complex falls apart as indicated by the decrease in the optical density. The occurrence of the polymer-protein interaction within the pH interval defined by the polymer and protein isoelectric points, where they bear opposite net charges, implies that the interaction is mainly electrostatic. The insensitivity of the critical pH to protein concentration suggests that, for the given polymer, the onset of polymer-protein interaction is defined by a critical protein net charge rather than a combination of protein quantity and charge.

Figure 7 demonstrates the interaction between Polymer A and lysozyme. Lysozyme is more basic than ribonuclease A and has an isoelectric point of 11.0. The bottom curve (open triangles) was obtained for pure protein and shows that lysozyme, in the absence of polymer, does not precipitate. The middle curve (open circles) corresponds to pure polymer which precipitates over a pH range of 4.6 to 6.6 which spans the isoelectric point of 5.4. The upper curve (filled squares), which corresponds to the mixture of protein and polymer, implies that there is an interaction between the protein and the polymer because the optical density of the mixture is much greater than that of the average of the protein and the polymer and also because the critical pH of the mixture of 6.4 is very different from that of polymer alone, 4.6.

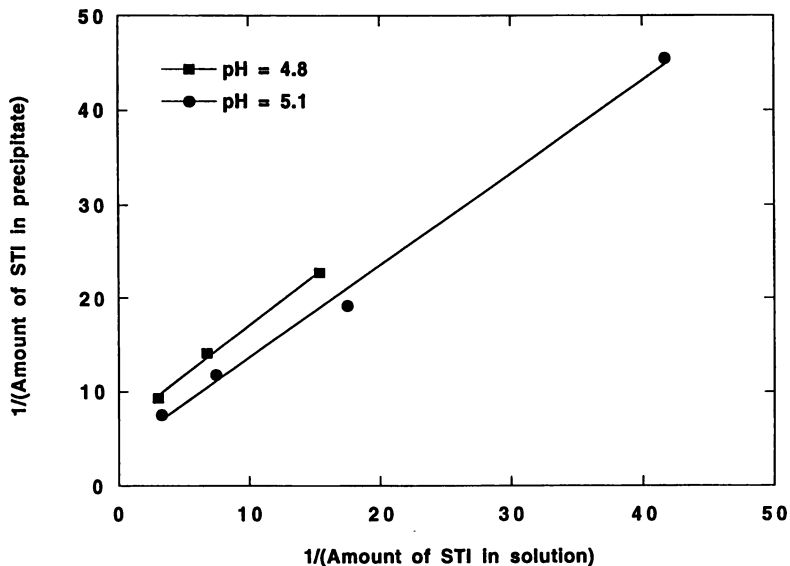


Figure 5. Langmuir plot of the complexation of 0.005% Polymer B with STI at initial concentrations ranging from 0.010% to 0.100% w/w without added salt and at two pH levels.

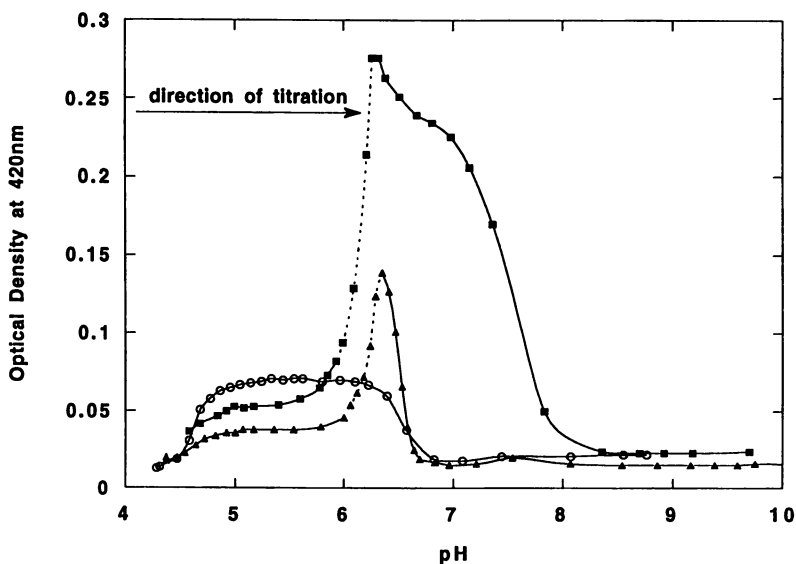


Figure 6. Optical densities of 0.010% Polymer A (open circles) and mixtures of 0.005% Polymer A with 0.025% (filled triangles) and 0.250% w/w ribonuclease (filled squares) without added salt.

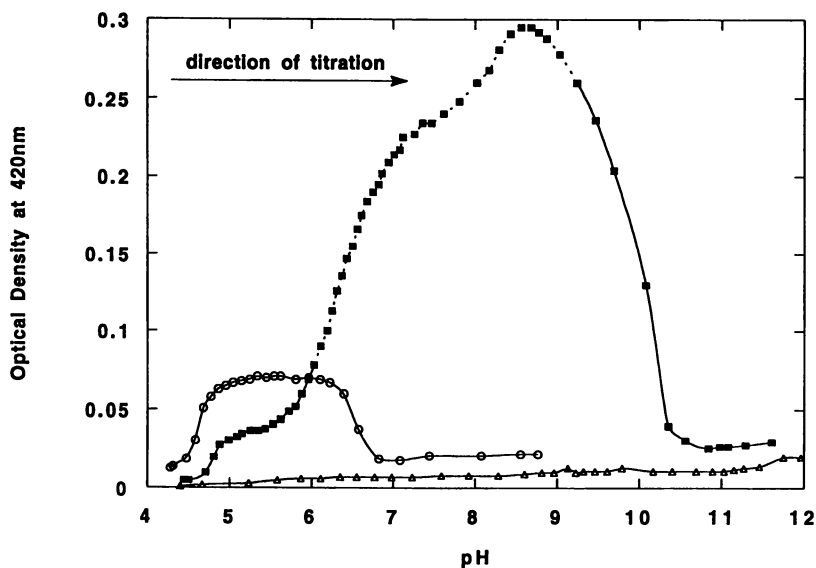


Figure 7. Optical densities of 0.010% Polymer A (open circles), 0.050% lysozyme (open triangles) and mixture containing 0.025% lysozyme and 0.005% w/w Polymer A (filled squares) without added salt.

## Conclusion

We have demonstrated that low-molecular-weight block acrylic polyampholytes, a new class of charged copolymers, at certain conditions of pH and salt concentration, interact strongly both with themselves and with proteins and precipitate. The pH-range for interaction is determined by the polymer and protein net charge. Pure polymer self-aggregates around the isoelectric pH, even at the very low polymer concentrations used in this investigation, typically 0.01% w/w. Pure protein does not show any aggregation behavior around its isoelectric pH for the protein concentrations employed in this study, typically 0.05% w/w. Polymer-protein mixtures interact in a pH-range between the isoelectric point of the protein and the self-aggregation pH of the polymer. Increasing salt concentration suppresses the polymer-polymer and protein-polymer interaction, confirming that the main driving force for self-aggregation and polymer-protein complexation is electrostatic. Like the homopolyelectrolyte-protein interaction, the polyampholyte-protein interaction can be used for protein separation processes, exploiting the selective complexation of the polymer with proteins of opposite charge. However, the self-aggregation of the polymer will provide the ability for polymer removal and recycling at the end of the process. Although we have not been able yet to determine the polyampholyte distribution between the supernatant and precipitated phases for the low polymer loadings employed, we plan to use higher polyampholyte (and protein) concentrations, typically 1%, and we expect to be able to analyze both phases for polyampholyte by ion-exchange chromatography. One disadvantage of these polymers for the proposed separation process is the low molecular weight. It is expected that block polyampholytes with molecular weight of typically 50,000 will be more efficient both in terms of self-aggregation and polymer-protein interaction.

## Literature Cited

1. Park, M. P.; Muhoberac, B. B.; Dubin, P. L.; Xia, J. *Macromolecules* **1992**, *25*, 290.
2. Strege, M. A.; Dubin, P. L.; West, J. S.; Flinta, C. D. In *Protein Purification*; Ladisch, M. R.; Willson, R. C.; Panton, C. C.; Builder, S. E., Eds., ACS Symposium Series 427, Washington, DC 1990; 66-79.
3. Strege, M. A.; Dubin, P. L.; West, J. S.; Flinta, C. D. In *Downstream Processing and Bioseparation*; Hammel, J.-F.; Hunter, J. B.; Sikdar, S. K., Eds., ACS Symposium Series 419, Washington, DC 1990; 158-169.
4. Dubin, P. L.; Ross, T. D.; Sharma, I.; Yegerlehner, B. E. In *Ordered Media in Chemical Separations*; Hinze, W. L.; Armstrong, D. W., Eds., ACS Symposium Series 342, Washington, DC 1987; 162-169.
5. Clark, K. C.; Glatz, C. E. In *Downstream Processing and Bioseparation*; Hammel, J.-F.; Hunter, J. B.; Sikdar, S. K., Eds., ACS Symposium Series 419, Washington, DC, 1990; 170-187.
6. Shieh, J.; Glatz, C. E. *Polym. Prepr.* **1991**, *32*, 606.
7. Xia, J.; Dubin, P. L.; Kim, Y.; Muhoberac, B. B.; Klimkowski, V. J. *J. Phys. Chem.* **1993**, *97*, 4528.
8. Parker, D. E.; Glatz, C. E.; Ford, C. F.; Gendel, S. M.; Suominen, I.; Rougvie, M. A. *Biotech. Bioeng.* **1990**, *36*, 467.
9. Sternberg, M.; Hershberger, D. *Biochim. Biophys. Acta* **1974**, *342*, 195.
10. Morawetz, H.; Hughes, W. L., Jr. *J. Phys. Chem.* **1952**, *56*, 64.
11. Scopes, R. K. *Protein Purification*; Springer Advanced Texts in Chemistry; Springer-Verlag: New York, NY, 1988; pp 81-84.

RECEIVED September 7, 1993

## Chapter 20

# Electrical Transport in Polyelectrolyte–Surfactant Complex Solutions at Various Degrees of Complexation

Jož Škerjanc and Ksenija Kogej

Department of Chemistry, University of Ljubljana, 61000 Ljubljana,  
Slovenia

The indirect moving boundary method was used to determine the transport number of the polyion in aqueous solutions of poly(styrenesulfonic acid), in which various portions of the charged groups on the polyion were blocked by the cetylpyridinium cations. From the transference and conductivity experiments, which were performed with the same solutions, the fraction of the free counterions,  $f_c$ , was calculated. It has been found that up to 50% complexation of the polyion, and for a given constant concentration, the values of the fraction of the free hydrogen ions are constant within the limits of the experimental error. At higher coverage, however, the shielding of the polyion by the surfactant aggregates becomes more extensive and  $f_c$  sharply increases.

Interactions between surfactants and polyelectrolytes have been the subject of some recent studies from this laboratory (1,2). It has been found that cationic surfactant, cetylpyridinium cation, is almost quantitatively associated with the anionic polyelectrolyte, poly(styrenesulfonic acid). Utilizing this finding samples of poly(styrenesulfonic acid) in aqueous solutions in which various portions of charged groups on the polyion were blocked by surfactant cations were prepared. For these solutions the osmotic coefficient, the apparent molar volume, the enthalpy of dilution, and the electrical conductivity were determined (2) as functions of polyelectrolyte concentration. In the present contribution these studies were accomplished by measurements of the transport number of the polyion. From the experimental transport numbers and measured electrical conductances of the same solutions the fraction of free counterions was calculated.

0097-6156/94/0548-0268\$06.00/0

© 1994 American Chemical Society



## Experimental Section

**Materials.** Poly(styrenesulfonic acid), HPSS, was prepared from its sodium salt, NaPSS, with a molecular weight of about 70 000 and a degree of sulfonation 1.0, supplied by Polysciences, Inc. (Warrington, PA). For purification and preparation of solutions, dialysis and ion-exchange techniques were used as described in detail elsewhere (3).

*N*-Cetylpyridinium chloride (CPC), puriss, obtained from Kemika (Zagreb, Croatia), was repeatedly recrystallized from acetone.

The poly(styrenesulfonate)-cetylpyridinium complex was prepared by mixing equivalent amounts of HPSS and CPC solutions. The resulting white precipitate of PSS-CP complex was washed repeatedly with water to remove HCl and finally dried by lyophilization. By dissolution of weighed amounts of the complex in the HPSS stock solutions, the samples with various degrees of free sulfonate groups on the polyion,  $f$ , were obtained.

**Apparatus.** For the conductivity measurements a Jones conductance bridge, Leeds & Northrup Co., was used, and the transport number of the polyion constituent was determined by the indirect moving boundary method. The apparatus and the method have been described previously (4). All measurements were performed at  $25 \pm 0.002$  °C.

## Results and Discussion

Experimental molar conductivities,  $\Lambda$ , and transport numbers of the polyion constituent,  $T_p$ , are presented as functions of concentration,  $c$ , in Figures 1 and 2 for various values of  $f$ . It is seen that  $\Lambda$  increases and  $T_p$  decreases with increasing  $f$  and concentration. From the conductivity and transference experiments we can obtain the fraction of free counterions,  $f_c$ , following the idea of the association of counterions with the polyion (5,6). In our notation, the relation between  $\Lambda$  and  $f_c$  is given by (7)

$$f_c = \Lambda / f(\Lambda_p + \Lambda_c) \quad (1)$$

where  $\Lambda_p$  is the monomolar conductivity of the polyion constituent, equal to  $\Lambda_p = \Lambda T_p$  and  $\Lambda_c$  is the molar conductivity of the free counterions. In equation 1  $\Lambda_c$  is still an unknown and may be, to a good approximation (8), equated to the corresponding value for the same counterion in a solution of a 1:1 electrolyte at a concentration equal to that of the free counterions,  $f_c c$ . In the computations of  $f_c$  the data (9) for the molar conductivities and transport numbers of hydrochloric acid solutions were used, and the values of  $f_c$  were obtained by iteration.

The results of the computations are presented in Figure 3. It can be seen that the values of  $f_c$  does not depend on the degree of complexation,  $1 - f$ , for values of  $f$  higher than 0.5. This finding confirms our previous observations (2), and indicates that surfactant molecules are not bound at random, but that they are "trapped" in the form of smaller or larger aggregates in the regions of high electrostatic potential

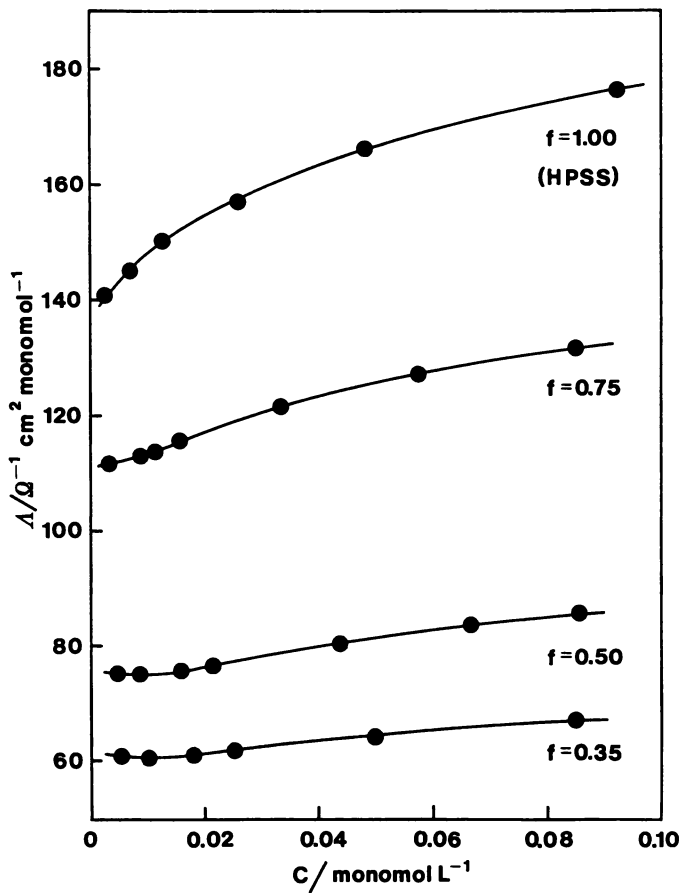


Figure 1. Concentration dependence of the molar conductivity of the HPSS-CP complex in water at 25 °C for various degrees of complexation,  $f$ .

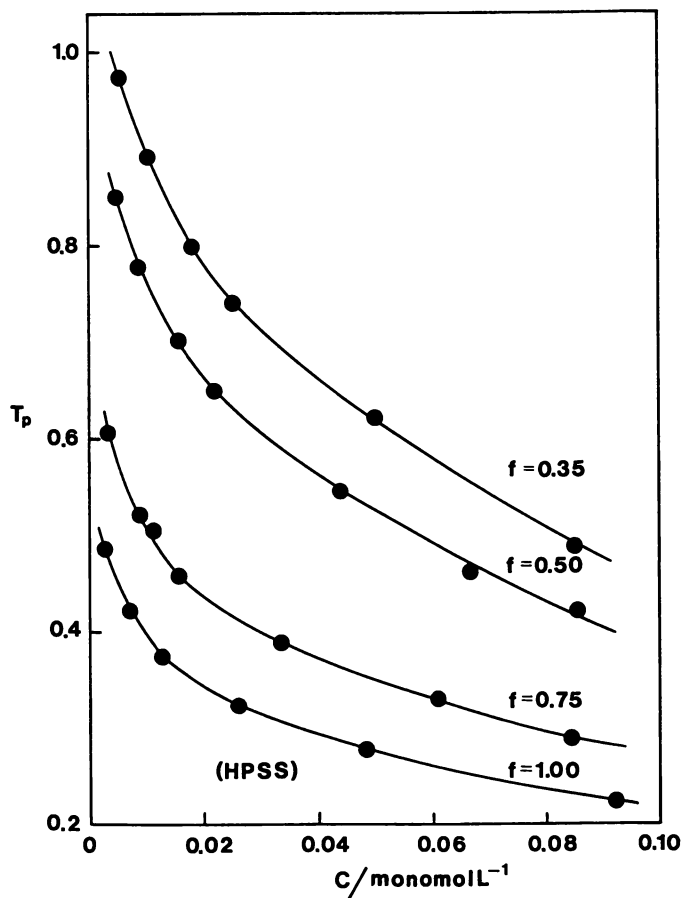


Figure 2. The polyion constituent transport number in aqueous solutions of HPSS-CP complex at 25 °C.

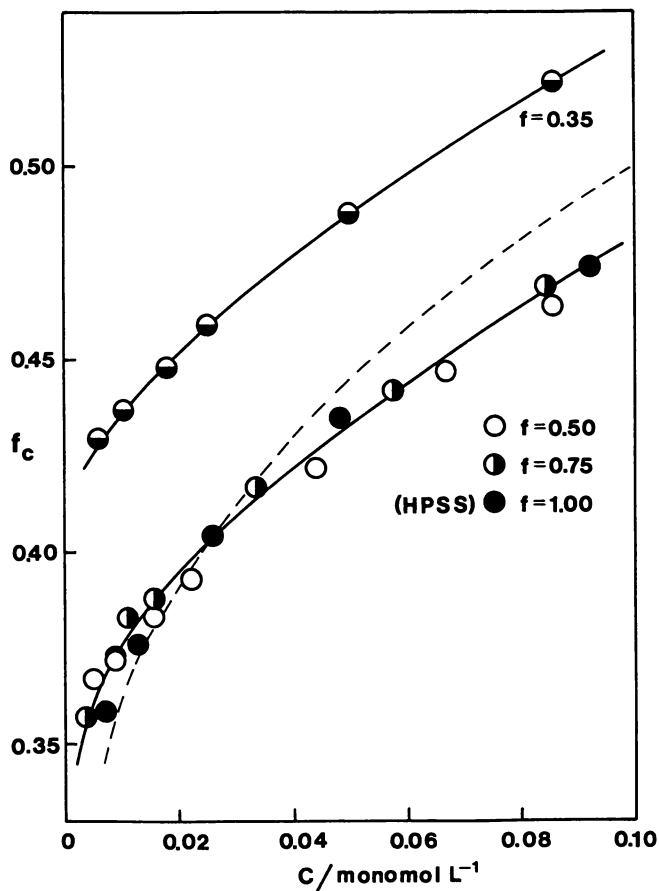


Figure 3. Concentration dependence of the fraction of free hydrogen counterions at 25 °C in aqueous solutions of HPSS-CP complex. Dashed line: calculated values (equation 7).

close to the macroion, making this part of the macroion thermodynamically inactive. The remaining part of the polyion behaves as a fully charged rod with the unchanged charge density. At complexations higher than 50% the shielding of the polyion by the surfactant aggregates becomes more extensive due to the steric factors, and more than the equivalent number of ionic groups on the macromolecule is blocked by the detergent aggregates. As a consequence, the values of the fraction of the free hydrogen ions increase.

By a phenomenological approach it has been shown (10) that the fraction of apparently free counterions,  $f_c$ , can be approximated by the ratio  $D_c/D_c^o$ , where  $D_c$  and  $D_c^o$  are the macroscopic self-diffusion coefficients of the counterion in the presence and absence of the polyion, respectively. It can be estimated (11,12) from equation 2

$$\frac{D_c}{D_c^o} = \frac{1}{\langle \exp z\Phi \rangle \langle \exp -z\Phi \rangle} \quad (2)$$

where  $\Phi (= -e_o\psi/kT)$  is the reduced potential,  $z$  is the charge number of the counterion,  $\psi$  is the electrostatic potential,  $e_o$  is the proton charge,  $k$  is the Boltzmann constant,  $T$  is the absolute temperature, and the brackets denote volume averages over the polyion cell. Using for  $\psi$  the expressions given by the cylindrical polyelectrolyte cell model (13-15) after lengthy integration the following expression for  $D_c/D_c^o \approx f_c$  is obtained (10,16):

$$f_c \approx \frac{D_c}{D_c^o} = 2 \frac{[\exp(2\gamma) - 1]^2}{\lambda [g_1 \exp(4\gamma) - g_2]} \quad (3)$$

$$g_1 = \frac{13 - \beta^2}{(4 - \beta^2)(1 - \beta^2)} \quad (4)$$

$$g_2 = \frac{(\lambda - 3)^2 + 4 - \beta^2}{(4 - \beta^2)[(\lambda - 1)^2 - \beta^2]} \quad (5)$$

In these equations  $\beta$  is the integration constant,  $\gamma$  is the concentration parameter related to the analytical concentration by  $c \exp(2\gamma) = (\pi a^2 b N_A)^{-1}$  ( $= 3.264$  monomol/L for polystyrenesulfonates),  $a$  is the radius of the polyion,  $b$  is the length of a monomeric unit,  $N_A$  is the Avogadro constant, and the charge density parameter  $\lambda$  is given by

$$\lambda = \alpha e_0^2 / \epsilon k T b \quad (6)$$

where  $\epsilon$  is the relative permittivity of the solvent.

For values of  $\gamma$  higher than 1 ( $c < 0.44$  monomol/L for polystyrenesulfonates) equation 3 can be approximated to 1% or better by

$$f_c \sim \frac{D_c}{D_c^0} = 2 \frac{[1 - \exp(-2\gamma)]^2}{\lambda g_1} \quad (7)$$

From equation 7 computed values of  $f_c$  are presented in Figure 3. In computations the numerical values typical for aqueous solutions of polystyrenesulfonates have been used:  $a = 0.8$  nm,  $b = 0.253$  nm and  $\lambda = 2.83$  at 298.15 K with  $\epsilon = 78.54$ . Figure 3 shows a semiquantitative agreement between calculated and experimental values of  $f_c$  for complexations lower than 0.5, a finding which is in agreement with the discussion above and with the results of previous conductivic and transference studies with pure polystyrenesulfonates (17).

At the end it should be noted that for  $c = 0$  experimental values of  $f_c$  appear to approach the limiting value of 0.31 predicted by the infinite line-charge model, which provides the following expression for  $f_c$  (18,19)

$$f_c = 0.87/\lambda \quad \lambda > 1 \quad (8)$$

A comment has to be given at this point. It has been shown several times that for vanishing polyelectrolyte concentrations the expressions for various thermodynamic properties predicted by the cylindrical cell model reduce to the limiting laws given by the line-charge model. A brief examination of equations 3 - 7 shows, however, that theoretical values for  $f_c$  predicted by the two models differ considerably. Thus, in the limit of zero concentration  $\gamma \rightarrow \infty$ ,  $\beta = 0$  for  $\lambda > 1$  (6), and equation 4 gives for  $g_1$  the value 13/4. So equations 3 or 7 reduce to

$$f_c = 8/13\lambda = 0.62/\lambda \quad \lambda > 1 \quad (9)$$

From this equation predicted limiting value 0.22 is for about 30 % lower than the value given by equation 8, and seems to be below the range to which the experimental values of  $f_c$  tend at zero concentration.

## Literature Cited

- (1) Škerjanc, J.; Kogej, K.; Vesnaver, G. *J. Phys. Chem.* **1988**, *92*, 6382.
- (2) Škerjanc, J.; Kogej, K. *J. Phys. Chem.* **1989**, *93*, 7913.
- (3) Škerjanc, J.; Pavlin, M. *J. Phys. Chem.* **1977**, *81*, 1166.
- (4) Dolar, D.; Špan, J.; Isaković, S. *Biophys. Chem.* **1974**, *1*, 312.
- (5) Huizenga, J. R.; Grieger, P. F.; Wall, F. T. *J. Am. Chem. Soc.* **1950**, *72*, 2636.
- (6) Katchalsky, A. *Pure Appl. Chem.* **1971**, *26*, 327.
- (7) Kurucsev, T.; Steel, B. J. *Rev. Pure Appl. Chem.* **1967**, *17*, 149.
- (8) Darskus, R. L.; Jordan, D. O.; Kurucsev, T. *Trans. Faraday Soc.* **1966**, *62*, 2876.
- (9) Lobo, V. M. M. *Handbook of Electrolyte Solutions, Part A and Part B*, Elsevier, Amsterdam, 1989.
- (10) Schmitt, A.; Varoqui, R. *J. Chem. Soc., Faraday Trans. 2* **1973**, *69*, 1087.
- (11) Lifson, S.; Jackson, J. L. *J. Chem. Phys.* **1962**, *36*, 2410.
- (12) Jackson, J. L.; Coriell, S. R. *J. Chem. Phys.* **1963**, *38*, 959.
- (13) Fuoss, R. M.; Katchalsky, A.; Lifson, S. *Proc. Natl. Acad. Sci. USA* **1951**, *37*, 579.
- (14) Alfrey, T. Jr.; Berg, P. W.; Morawetz, H. *J. Polym. Sci.* **1951**, *7*, 543.
- (15) Lifson, S.; Katchalsky, A. *J. Polym. Sci.* **1954**, *13*, 43.
- (16) In equation A8 of Reference 10 the square in the numerator of equation 3 is missing.
- (17) Špan, J.; Bratko, D.; Dolar, D.; Feguš, M. *Polym. Bull.* **1983**, *9*, 33.
- (18) Manning, G. S. *Biopolymers* **1970**, *9*, 1543.
- (19) Manning, G. S. *J. Phys. Chem.* **1975**, *79*, 262.

RECEIVED August 6, 1993

## Chapter 21

# Structure of Polyelectrolyte Solutions at Intermediate Charge Densities

W. Essafi<sup>1</sup>, F. Lafuma<sup>2</sup>, and C. E. Williams<sup>1</sup>

<sup>1</sup>Laboratoire pour l'Utilisation du Rayonnement Electromagnétique, Centre National de la Recherche Scientifique, Commissariat à l'Energie Atomique, Ministère de l'Education Nationale, University of Paris-Sud, F91405 Orsay, France

<sup>2</sup>Laboratory of Macromolecular Physical Chemistry, Ecole Supérieure de Physique et de Chimie Industrielle, 10, rue Vauquelin, F75231 Paris, France

We report a small angle X-ray scattering (SAXS) study of the structural properties of semi-dilute solution in water of poly(styrene-co-cesium styrene sulfonate) of various compositions. It is found that there is a striking continuity of all structural properties, e. g. scattering peak position and intensity, as a function of polymer concentration and of ion content, from 100% to 30%, the limit of solubility. The more intense peaks all have a hint of an associated second order peak, an observation that indicates that the correlations are more pronounced than predicted by the simple correlation hole model for highly charged polyelectrolytes. However there is no evidence of the microphase separation of weakly charged polymers. Finally, the effect on the structure of added salt is reported. It is suggested that the hydrophobicity of the polystyrene backbone could have a definite influence on the structure.

In the last few years, there has been a substantial theoretical and experimental effort to understand the structure of semi-dilute solutions of highly charged polyelectrolytes in water. In salt free solutions, the highly charged chains are usually described as forming a transient network, similar to that of semi-dilute solutions of neutral polymers, except that each macromolecule is surrounded by a depletion volume or "correlation hole" from which other chains are excluded by the screened repulsive electrostatic interactions (1) This model relies on the fact that each individual chain, that was highly stretched when dilute, becomes more flexible as the concentration increases and remains stiff at the local scale only. How rigid is the chain is still a much debated question, outside the scope of this note. Most structural investigations have been focused on polystyrene sulfonate, considered as a model polyelectrolyte. Extensive neutron (2, 3) and light scattering measurements (4, 5) have shown qualitative agreement with the theoretical predictions of this isotropic model without long range order. For instance for all polymer concentrations,  $c_p$ , above that of chain overlap, a broad halo is visible whose position,  $q^*$ , scales as  $c_p^{1/2}$  over many orders of magnitude in concentration. However, no really satisfactory quantitative agreement has been found and a detailed model is still lacking. In the light of new puzzling experimental data (6, 7) it has even been suggested more recently that the solution might not be homogeneous and that ordered and disordered regions could coexist in

0097-6156/94/0548-0278\$06.00/0

© 1994 American Chemical Society



the solution (two-state model). All theoretical models for highly charged polyelectrolytes assume that the solutions properties are dominated by long range coulombic interaction between charges and the hydrophobicity of the backbone is not taken into account.

On the other hand, for weakly charged polymers in a poor solvent, the delicate balance between hydrophobic and electrostatic interactions may lead to a phase separation, at a mesoscopic scale, into oppositely charged polymer-rich and polymer-poor domains. The theoretical models (8, 9) have been found adequate to describe the properties of semi-dilute solutions of poly(acrylic acid) and poly(methacrylic acid) (10). For both systems the hydrophobic effects are rather small and the degrees of ionization were kept very low. Here also, the scattering pattern is characterized by a rather broad single peak, related to pretransitional concentration fluctuations and whose position varies with charge content. The microphase transition itself has not been observed. It should be noted that no theory exists, up to now, that would be able to describe the behaviour of polyelectrolytes in the whole range of charge content.

In order to gain insight into the effect of hydrophobicity and to attempt to bridge the gap between these two extreme models, the properties of poly(styrenesulfonate-*co*-styrene) have been investigated in the intermediate range of charge content, between 100% and 30%, the limit of solubility in water. This polymer has a very hydrophobic backbone as shown by the fact that partially sulfonated polystyrene of lower charge content (< 20%), is only soluble in organic solvents and behaves as an ionomer; its properties are then dominated by the dipolar attraction between undissociated ion pairs. Herein, small angle x-ray scattering is used to provide an experimental description of the structural characteristics of semi-dilute solutions of this polymer as a function of charge content, polymer concentration and added salt concentration.

## Materials and Methods

Samples of poly(styrene-*co*-styrene sulfonate) of various composition have been prepared by postsulfonation of polystyrene (PS) according to a procedure described elsewhere (11). The precursor polymer was a commercial polystyrene (CdF-Chimie) of molecular weight 250,000 and polydispersity of 2. It was first purified by centrifugation of a solution ( $90\text{ g l}^{-1}$ ) in 1,2 dichloroethane (DCE) followed by precipitation in ethanol of the clear supernatant. For sulfonation, 5g of PS were dissolved in 70ml of DCE and the requisite amounts of acetic anhydride and sulfuric acid were added to the solution at  $50^\circ\text{C}$ ; the mixture was stirred for 60 minutes to obtain the polystyrene sulfonate acid which was subsequently converted into a sodium salt by addition of a sodium hydroxide solution. The mixture was then dialysed until its conductivity was close to that of distilled water. Finally, the concentrated solution was freeze dried to obtain poly(styrene-*co*-sodium styrene sulfonate), abbreviated NaPSS. The samples were characterized by elemental analysis in order to determine the degree of sulfonation, or equivalently, the charge content  $f$ , defined as the ratio of the number of sulfonated monomers to the total number of monomers; it varies between 0.27 and 0.9 for this investigation. Poly(styrene-*co*-cesium styrene sulfonate), CsPSS, was obtained by ion exchange of the corresponding NaPSS on a DOWEX  $\text{H}^+$  resin followed by neutralisation with cesium hydroxide.

Salt-free semi-dilute solutions were prepared by dissolving the polyelectrolyte in deionized  $\text{H}_2\text{O}$  at  $60^\circ\text{C}$  for 30 minutes, then let to rest for two days prior to the measurements.

Small angle X-ray scattering (SAXS) experiments were performed on beam line D22, at LURE, using the DCI synchrotron radiation source. Data were obtained with pinhole collimation and recorded with a linear detector of 512 cells. The scattering vector  $q$  varied from 0.008 to  $0.2\text{ \AA}^{-1}$  [ $q = (4\pi/\lambda) \sin(\theta/2)$ , where  $\theta$  is the observation angle and  $\lambda$ , the wavelength was  $1.37\text{ \AA}$ ].

The scattering data were normalized to constant beam intensity and corrected for transmission, sample thickness, parasitic and background scattering, according to a standard procedure. The resulting scattering profiles are obtained as normalized intensities  $I$  vs. scattering vector  $q$ . Conversion to absolute scattering units involves a simple multiplicative factor.

## Results

**Effect of Charge Content and Polymer Concentration.** Figure 1 shows the evolution of the scattering profiles as a function of charge content,  $f$ , for salt-free solutions at a constant monomer concentration  $c_p = 0.32$  monomol  $l^{-1}$  of NaPSS (12). For all charge contents, a maximum appears in the scattering profile at a finite scattering vector  $q^*$  whose position shifts continuously to lower values as  $f$  decreases; concomitantly, the intensity at  $q^*$  increases and the peak narrows, i.e.  $\Delta q/q^*$  decreases.  $I(0)$ , the intensity extrapolated to  $q=0$ , increases as  $f$  decreases, as expected for samples containing fewer charges, since it is related to the osmotic pressure  $\pi$  in the solution and is proportional to  $c_p(\partial c_p/\partial \pi)$ . At large  $q$ 's, all scattering profiles coincide indicating that at small spatial scales the monomer-monomer correlations are independent of  $f$ .

For each charge content, the polymer concentration was varied in a range between 0.03 and 0.6 monomol  $l^{-1}$ . A typical set of scattering profiles is shown on figure 2 for a CsPSS sample with  $f = 0.35$ . The same evolution is observed at each  $f$ :  $I(q)/c$  extrapolated at  $q = 0$  increases as  $c$  decreases; the peak is visible even at the lowest concentrations and its position  $q^*$  shifts to larger  $q$ 's as  $c_p$  increases; the intensity scattered per monomer also decreases as  $c_p$  increases and the peak broadens.

One striking feature of this set of data is the appearance of a very weak associated second order scattering shoulder at a position  $q_2$  of the order of  $1.8q^*$ , best seen in a  $I(q)q^2$  vs  $q$  representation (figure 3). It is clearly visible for small  $f$  ( $< 0.5$ ), when the total scattered intensity is maximum and the main peak is situated at low  $q$ 's. It is impossible to know whether it is absent at high  $f$  ( $> 0.7$ ) or too small to be visible above the background. Both CsPSS and NaPSS show the same trend.

For each  $f$  the position of the intensity maximum is found to vary as  $c_p^a$  with  $a$  between 0.4 and 0.45 for both NaPSS and CsPSS (figure 4). Because of the limited concentration range that could be investigated and of a possible systematic error in the position of the peak at low angle when  $I(0)$  is more intense, this result is compatible with the  $c_p^{1/2}$  dependency usually found for charged polyelectrolytes. The  $f$ -dependence of  $q^*$ , for samples containing a constant number of chains, scales like  $f^b$  but, unlike the preceding case, the exponent is dependent on the cation type:  $b$  equals 0.9 for NaPSS and 0.7 for CsPSS.

**Effect of Added Salt.** So far the reported data have been obtained in "salt-free" conditions, i.e. where only the counterions contribute to the ionic strength of the solution. By adding a simple electrolyte, it is possible to increase the ionic strength and considerably screen out the electrostatic interactions. A typical evolution of the structure factor is shown in figure 5 for NaPSS ( $f = 0.67$ ) in the presence of an increasing amount of NaCl,  $c_s$ , at a fixed polymer concentration of  $0.32$  mol  $l^{-1}$ .

As  $c_s$  increases the maximum in the structure factor shifts slightly to smaller  $q$ -values while the intensity at  $q^*$  increases; the peak is wiped out for a ratio  $c_p/c_s$  which is a strong function of  $f$ . The maximum of intensity is then centered on  $q = 0$  and simultaneously, its intensity  $I(0)$  increases.  $q^*$  varies approximately as  $c_s^{-1}$ . This behaviour appears to be quite general for all  $c_p$  and  $f$ . A more systematic study is in progress.

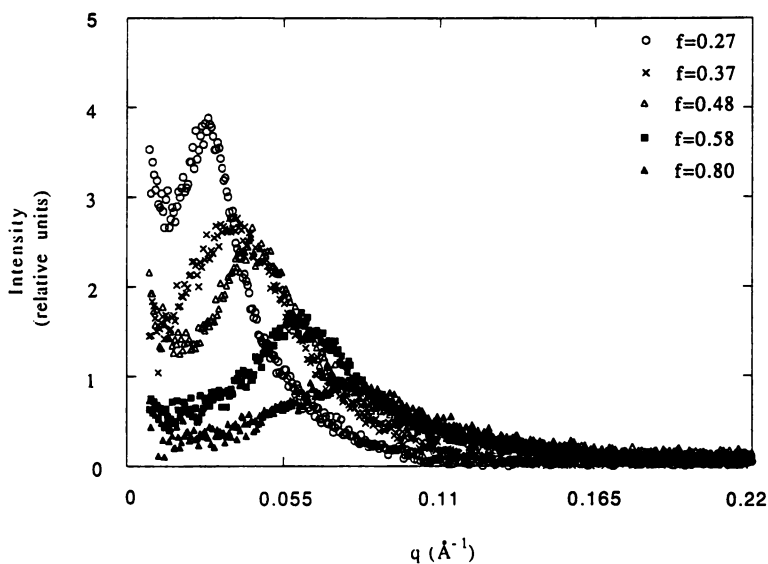


**Figure 1.** Normalized SAXS profiles for NaPSS at various charge contents  $f$  between 0.27 and 0.8. The monomer concentration is constant at  $0.32 \text{ mol l}^{-1}$ .

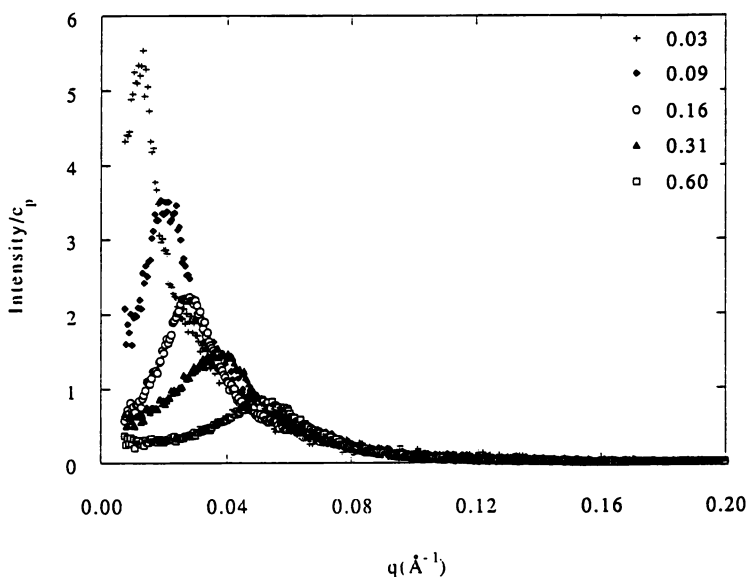


**Figure 2.** Normalized scattered intensities per monomer for CsPSS at  $f=0.35$  as a function of polymer concentration. Concentrations are noted on the figure in  $\text{monomol l}^{-1}$ .

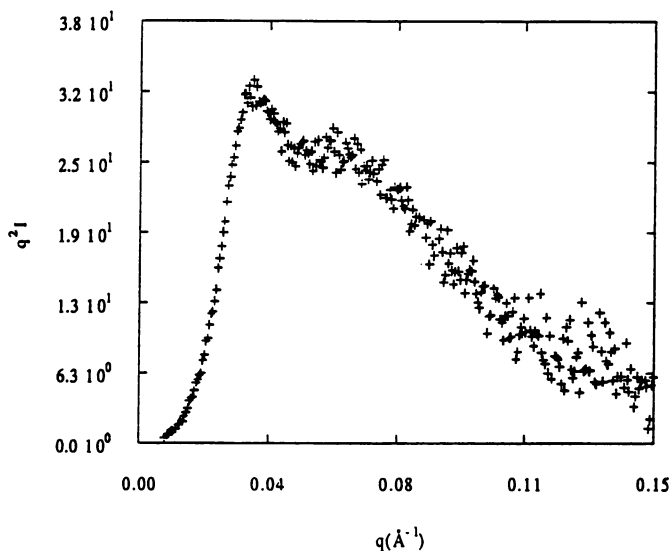


**Figure 3.** Kratky plot of the intensity scattered by a solution of CsPSS at  $f = 0.35$  and  $c_p = 0.16$  monomol  $l^{-1}$  showing the existence of two peaks in the structure factor.

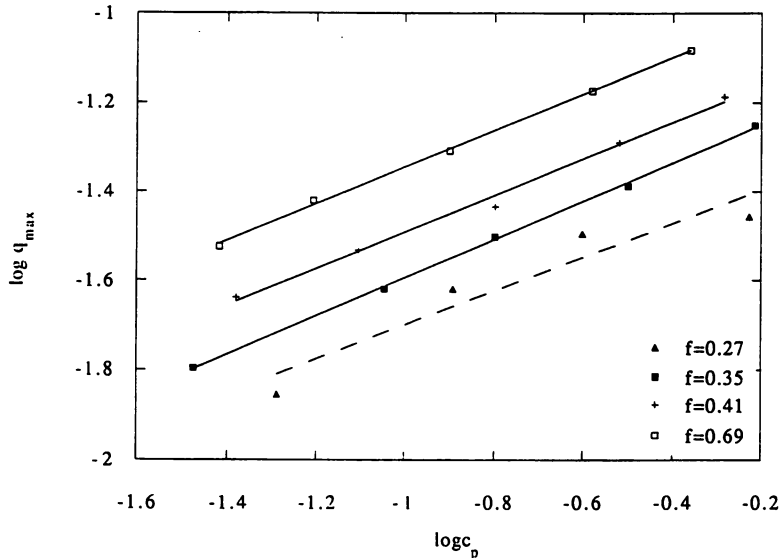


**Figure 4.** Scattering vector corresponding to the peak position plotted as a function of polymer concentration for  $f = 0.27, 0.35, 0.41$  and  $0.69$  (log-log representation). The full straight lines correspond to the best fits with slopes of  $0.4, 0.42$  and  $0.43$ .

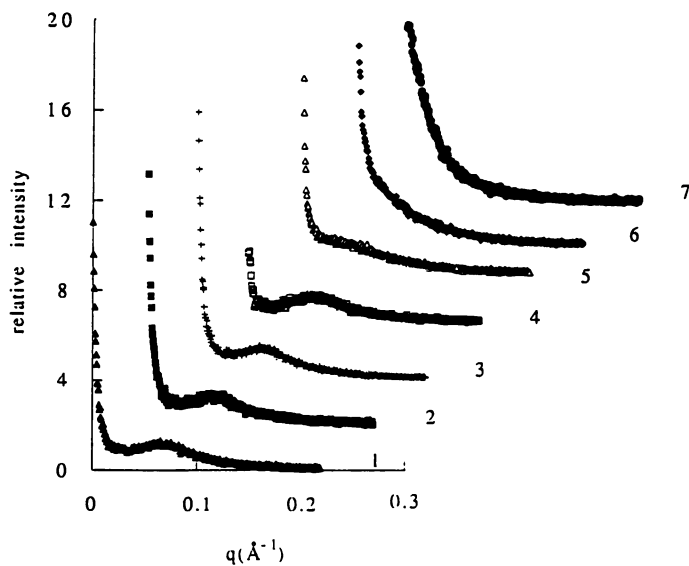


**Figure 5.** Evolution of the scattering profiles as a function of increasing salt concentration for a sample of NaPSS at  $f=0.67$  and  $c_p=0.32$  monomol  $l^{-1}$ . The concentrations of increase from (1) to (7) and correspond to 0,  $10^{-3}$ ,  $6 \cdot 10^{-3}$ ,  $10^{-2}$ ,  $10^{-1}$ ,  $3 \cdot 10^{-1}$  and 1 mol of NaCl.

**Effect of Counterions.** The effect of charge content and polymer concentration have been investigated on both NaPSS and CsPSS samples. The same general qualitative behaviour is observed, although the absolute value of  $q^*$  depends on the type of cation. As noted earlier,  $q^*$  scales as  $c_p^{1/2}$  for both ions but at the same concentration the peak for the sodium salt is narrower and displaced to higher  $q$ 's. It is also less intense, as might be expected since the counterions are likely to contribute to the scattering and sodium is a lighter element than cesium. Because the precise origin of the X-ray contrast for polyelectrolytes is difficult to ascertain in the absence of a detailed model, we have compared X-ray and neutron scattering data of the same sample of protonated NaPSS dissolved in D<sub>2</sub>O. With the latter technique, the chain is visible whereas the counterions are not. The peak was found at exactly the same position, indicating that the counterions do "decorate" the chain and thus a appreciable number of them are in the close vicinity of the chain. However the scattered intensity was so much weaker that it was not possible to be sure of the presence of the second order shoulder.

## Discussion

A striking feature of these SAXS data is the continuity of all structural properties as the proportion of charged monomers  $f$  varies from 0.27 to 1. This implies that a unique model should be able to describe the semi-dilute solutions of *this* polyelectrolyte when it is fully charged as well as when one in every three monomers is charged. The structure of semi-dilute solutions of fully charged PSS, as revealed by previous neutron scattering experiments (2, 3) had usually been described in terms of the isotropic model first introduced by de Gennes *et al.* (1). However, if a qualitative agreement exist here as well for the fully charged PSS, important discrepancies have been found here for the less charged samples which are discussed in what follows.

The shape and the width of the peak and the hint of a second order are indicative of stronger correlations than predicted by a correlation hole effect. In the original model, the total structure factor  $S(q)$  reaches a maximum value at  $q^*$ , of the order of the inverse of the Debye-Hückel screening length  $\kappa^{-1}$ , where  $\kappa^2 = 4\pi l_B (fc_p + 2c_s)$  and  $l_B$  is the Bjerrum length; for  $q > q^*$ ,  $S(q)$  decreases as  $q^{-2}$ , then as  $q^{-1}$  as  $q$  increases. This behaviour reflects the flexible character of the chain at large scale and its rigidity at short scale. The presence of a maximum in intensity is not due to some order in the solution but rather to the fact that no two monomers belonging to different chains can approach each other closer than  $\kappa^{-1}$ . Hence the term "correlation hole effect". Experimentally, it is found that the peak can be fitted reasonably well with a lorentzian line shape; a  $q^{-2}$  dependence as been found (within experimental error) only in the tail of the peak and, surprisingly, no  $q^{-1}$  dependence could be detected. At low  $f$  this behaviour could be masked by the second order shoulder but it is not visible either at high  $f$  when no shoulder is seen. Therefore it appears that the observed SAXS structure factor does not show the monomer-monomer correlations characteristic of a rigid chain (rodlike) at short length. It is interesting to note that no rodlike behaviour has been found either in a recent molecular dynamics simulation of the structure factor of polyelectrolyte solutions above  $c^*$  (13). However a  $q^{-1}$  behaviour has been reported in a neutron scattering investigation of quaternized poly(2-vinylpyridine) (14). Clearly more experimental and theoretical effort has to be devoted to this question.

Although both  $c_p$  and  $f$  change the ionic strength of the solution and are equivalent as far as the electrostatic interactions are concerned, they do not have the same effect on the structure of the solution. The observed variation of  $q^*$  with  $c_p^{1/2}$  is predicted whenever the characteristic length associated with the peak is related to the screening length  $\kappa^{-1}$  and is generally found for all charged polyelectrolytes. It is

not therefore a very severe criterion for a specific model. The fact that the effect of  $f$  is counterion dependent, at least for Na and Cs, is puzzling; it could reflect a difference in condensation for these ions. Indeed condensation should take place for most of our samples: for the fully charged chain, the average distance between charges is of the order of a monomer size (2.5Å) and much smaller than the Bjerrum length of 7.14Å in water at 25°C, and a considerable fraction of the counterions should be condensed. For the lowest  $f$ , one in every three monomers is charged; since the charges are spaced from the backbone and can alternate along the chain, their average distance is more than three bond lengths and slightly larger than  $l_B$ . In the absence of a model that takes explicitly into account the effect of  $f$ , it is tentatively proposed that two characteristic distances appear in this problem, the electrostatic length  $\kappa^{-1}$  for the solution and a length related to the chain itself that would also depend on the presence of condensed counterions.

Although the charge content of these polymers is too high for them to qualify as weakly charged polyelectrolytes, we did compare our data to the predictions of the mesophase model (8, 9, 10). In this model the perturbation introduced by the charged monomers is small, the chain is assumed to remain almost gaussian and the structure factor can be calculated exactly. A broad peak appears which reflects the fact that concentration fluctuations of characteristic length  $2\pi/q^*$  are favoured in the system; at the microphase transition it would transform into a Bragg peak corresponding to the periodicity of polymer-rich and polymer-poor regions. The relevant parameter,  $q^{*2} + \kappa^2$ , is predicted to vary as  $f c_p^{1/2}$ . No such relation is found for any of our data.

The hydrophobicity of the polystyrene backbone is likely to play an important role in the organization of the solution. Indeed fluorescence measurements of a small amount of pyrene molecules dissolved in the solution show that its environment is rather hydrophobic even when the chain is fully charged; the ratio of the intensities of the first to third peak of the fluorescence emission spectrum which is sensitive to the polarity of the pyrene local environment, is 1.46 for a  $c_p$  of 0.038 mol l<sup>-1</sup> compared to 1.9 for pure water. Furthermore there is no discontinuity in the intensity ratio as a function of  $f$  which would show the existence of a structural transition; it decreases smoothly as  $f$  decreases (to be published). If the local dielectric constant close to the backbone is low, some ion-pairs can remain associated as dipoles and further increase the chain insolubility.

## Conclusion

This SAXS investigation of semi-dilute solutions in water of poly(styrenesulfonate) at intermediate charge densities has shown a striking continuity of all structural properties from the fully charged polyelectrolyte to the chain where 30% of the monomers only are charged. This implies that a single model should describe the solution properties for all charge contents. No adequate model seems to exist for the moment. It has been found that the interchain monomer-monomer correlations are stronger than those due to a simple correlation hole effect and that the intrachain ones do not show rodlike behaviour even when highly charged. No transition to a microphase separated structure has been found, although the hydrophobic backbone of polystyrene seems to have a definite influence on the structure of the solution.

In order to have a deeper understanding of the structure of these polyelectrolytes, complementary experiments are in progress to test the single chain configuration by small angle neutron scattering and the counterion environment by nuclear magnetic resonance.

## References and Notes

1. de Gennes, P.G.; Pincus, P.; Velasco, R. M; Brochard, F., *J. Physique*, **1976**, *37*, 1461.
2. Nierlich, M.; Williams, C. E.; Boué, F.; Cotton, J. P.; Daoud M.; Farnoux, B.; Jannink, G.; Picot, C.; Moan, M.; Wolf, C.; Rinaudo, M.; de Gennes, P. G., *J. Physique*, **1979**, *40*, 701.
3. Jannink, G.; *Makromol. Chem., Macromol. Symp.*, **1986**, *67*, 1; and references therein
4. Drifford, M.; Dalbiez, J. P., *J. Phys. Chem.*, **1984**, *88*, 5368; *J. Phys. Lett. (France)*, **1985**, *46*, L311.
5. Sedláč, M.; Amis, E. J, *J. Chem. Phys.*, **1992**, *96*, 826.
6. Ise, N., *Angew. Chem., Int. Ed. Engl.*, **1986**, *25*, 323.
7. Sedláč, M., *Macromolecules*, **1993**, *26*, 1158.
8. Borue, V.; Erukhimovich, I., *Macromolecules*, **1988**, *21*, 3240.
9. Joanny, J. F.; Leibler, L., *J. Physique*, **1990**, *51*, 545.
10. Moussaid, A.; Schosseler, F.; Munch, J. P.; Candau, S. J., *J. Phys II France*, **1991**, *1*, 637.
11. Makowski, H. S.; Lundberg, R. D.; Singhal, G. S., US Patent 3870841, 1975, to EXXON Research and Engineering Company.
12. The weight of dissolved polymer has been calculated so that the number of chains is kept constant for all charge contents
13. Stevens, M.J.; Kremer, K., to be published
14. Förster, S.; Schmidt, M.; Antonietti, M., *Polymer*, **1990**, *31*, 781.

RECEIVED August 22, 1993



## Chapter 22

# Weakly Ionized Polymers in a Poor Solvent Dynamics in Relation to Structure

A. Moussaid<sup>1</sup>, F. Schosseler, J. P. Munch, and S. J. Candau

Laboratoire d'Ultrasons et de Dynamique des Fluides Complexes, Unité de Recherches Associée au Centre National de la Recherche Scientifique, 851, Université Louis Pasteur, 4 rue Blaise Pascal, 67070 Strasbourg Cédex, France

The static structure factor and the cooperative diffusion coefficient  $D_c$  of weakly charged poly(acrylic acid) in deuterated water were measured as a function of temperature, polymer concentration and salt content for a fixed neutralization degree  $f = 0.05$ . Results show that  $D_c$  cannot be deduced from the structure of the solution by simply modeling the components of the system as particles moving in a continuous viscous fluid.

Water-soluble polymers can exhibit in aqueous solutions a large variety of behaviors due to the amphiphilic nature of their constituents (1). A particular example is provided by polyacids with a vinylic backbone like polyacrylic acid (PAA).

In this case the hydrophobic nature of the backbone makes the solubilization of the uncharged chains (in acidic conditions) very difficult: light scattering measurements have shown (2) that the compensation temperature ( $\Theta$  temperature) of water-PAA solutions is around 15°C if 0.2 M/L HCl is added to shift the acido-basic equilibrium of the solution and prevent the ionization of the chains. If ordinary water ( $H_2O$ ) is replaced by heavy water ( $D_2O$ ) and HCl by DBr, the compensation temperature increases up to around 27°C (R. Skouri, unpublished data).

Thus the solubilization of PAA in water at room temperature is due to the electrostatic repulsion between ionized carboxylic groups along the chains, the fraction of these charged groups increasing with the pH of the solution. At high pH, the linear charge density on the chains is large and the behavior of PAA solutions (3-4) is similar to that observed for other strong polyelectrolyte solutions (5). For lower pH values, however, when there is only a small fraction of dissociated groups (about a few per cent), the electrostatic interactions have the same order of magnitude as the hydrophobic forces.

A naive guess would predict that the onset of weak electrostatic forces will not affect drastically the behavior of the neutral chains in poor solvent but mainly change the effective compensation temperature with no dramatic effect on the phase diagram of the system.

<sup>1</sup>Current address: Dutch State Mines Research, P.O. Box 18, 6160 MD Geleen, Netherlands

However this simple picture was not confirmed when the problem of weakly charged polyelectrolytes was addressed theoretically a few years ago (6-7). Instead it has been predicted that the presence of charged groups prevents any macroscopic phase separation of the system : upon a decrease in the solvent quality a microscopic phase separation should occur with the formation of polymer-rich and polymer-poor microdomains (6,7).

The basic reasons for that behavior lie in the overall electroneutrality requirement and the large entropy associated to the small counterions. Hydrophobic forces would tend to promote large scale fluctuations in polymer concentration and macroscopic phase separation. However polymer concentration fluctuations are coupled to charge density fluctuations because the polymer chains carry ionized groups. Due to the global electroneutrality condition, these charge density fluctuations have to be compensated by the small counterions which are compelled to follow the polymer chains in polymer-rich regions. Thus large scale fluctuations in polymer concentration are forbidden since they are paid by either an increase in electrostatic energy or a decrease in the entropy of the small counterions. Instead the balance between electrostatic and entropic costs favors fluctuations with finite wavelength  $\lambda^*$  or equivalently non-zero associated wavevectors  $q^* = 2\pi/\lambda^*$ . If the solvent quality decreases further, the spatial extent of these fluctuations remains fixed by the ionic strength but their amplitude and lifetime increase until finally microdomains with periodicity  $\lambda^*$  appear at the critical point (6,7).

From the above picture a maximum centered at  $q = q^*$  is expected in the solution structure factor  $S(q)$  measured in a scattering experiment. Here  $S(q)$  is the Fourier transform of the polymer-polymer pair correlation function and  $q$  is the scattering wavevector defined as  $q = 4\pi/\lambda \sin(\theta/2)$ ,  $\lambda$  being the wavelength of incident particles and  $\theta$  the scattering angle.

In the vicinity of the transition, the balance of repulsive coulombic forces and attractive hydrophobic forces gives a weak net interaction and polymer chains can reasonably be considered as nearly gaussian. This simplification allows the analytical calculation of the structure factor  $S(q)$  within the random phase approximation (6,7).

Detailed small angle neutron scattering (SANS) experiments have shown the relevance of this theory to describe the structure of weakly charged PAA solutions (8) and gels (9,10). In the remaining parts of this paper, we will first describe briefly experimental details, then show some typical results about the structure of PAA solutions and finally present and discuss the dynamics of these solutions in connection with our information about their structure.

## Experimental Part

A stock solution is prepared by radical polymerization of acrylic acid in  $D_2O$  at a concentration  $C_m = 1.11$  M/L. The reaction is initiated by ammonium peroxydisulfate and proceeds in an oven ( $70^\circ C$ ) for 12 hours after careful bubbling of nitrogen through the monomer solution (8-10).

Solutions with the desired polymer concentration  $C_p$ , salt concentration  $C_s$  and ionization degree  $\alpha$  are obtained by dilution of the stock solution with the appropriate amount of  $D_2O$  containing sodium hydroxide (NaOH) to set the ionization degree  $\alpha$  and, if desired, sodium bromide (NaBr) as added salt. The ionization degree is defined as the fraction of ionized monomers and is calculated in the usual way from the neutralization degree  $f$ , i.e. the stoichiometric ratio of NaOH to monomers, and the dissociation constant,  $K_a = 5.6 \cdot 10^{-5}$ , of acrylic monomers in  $H_2O$ . The error made by estimating the ionization degree in rather concentrated  $D_2O$  solutions from the monomer dissociation constant in light water was discussed in detail elsewhere (8). In this paper, only results obtained on solutions with  $f = 0.05$  are presented. Then the

ionization associated to the spontaneous dissociation of acrylic acid is about 2% of the total ionization and the relative error on  $\alpha$  is certainly smaller than that value.

SANS experiments have been performed on spectrometer PACE, at Laboratoire Léon Brillouin (Laboratoire commun CEA-CNRS). The experimental procedure and the data treatment have been described elsewhere (8-10).

Quasi-elastic light scattering (QELS) data have been obtained with an ALV-5000 correlator, the light source being an argon ion laser operating at 4880Å. For the light scattering experiment, the reaction bath was filtered through 0.2  $\mu\text{m}$  filters prior to the polymerization reaction and the final diluted solutions were carefully centrifuged before the measurements. Apart from these precautions, which are not necessary for the SANS experiments, the samples for SANS and QELS measurements were prepared in the same way and, in particular,  $\text{D}_2\text{O}$  was used as the solvent in both cases. This is important since, as mentioned earlier, the effective compensation temperature differs in protonated and deuterated water.

Intensity correlation functions showed usually a single mode decay with a rather broad distribution of decay times. Therefore the data were processed with the method of cumulants yielding typical variance values between 0.1 and 0.3. However for high salt concentration or low temperature, a second slower relaxation mode appeared in the spectrum of decay rates, thus making the analysis in cumulants very unreliable. Values of the cooperative diffusion coefficient were obtained as the mean value of  $\langle \Gamma(q) \rangle / q^2$  where  $\langle \Gamma(q) \rangle$  is the mean value of decay rates resulting from the cumulant analysis. In all the experiments  $\langle \Gamma(q) \rangle / q^2$  appeared independent of the scattering wavevector.

### Structure Factor of the Solutions

The scattering curves measured in SANS experiments show features in very good agreement with the predictions of the model. In practice, the intensity scattered by small ions can be neglected since their contrast relatively to the solvent and their concentrations are small. Then the total scattering intensity  $I(q)$  is simply proportional to the structure factor  $S(q)$  associated to polymer-polymer correlations (11).

First of all a maximum is observed for a finite wavevector  $q^*$  (Figure 1). The position and the amplitude of this maximum depend on the ionization degree  $\alpha$ , the polymer concentration  $C_p$  and the salt content  $C_s$  (8-10).

As  $\alpha$  and  $C_p$  decrease, the peak shifts to smaller  $q$  values and its amplitude increases : this behavior reflects the growing likelihood for fluctuations of polymer concentration with larger amplitude and wavelength as the number of charges per unit volume decreases.

For given  $\alpha$  and  $C_p$ , the same behavior for the maximum is observed if the salt concentration increases. This results from a lower electrostatic cost associated to fluctuations of polymer concentration since salt ions contribute to the screening of the electrostatic interactions beyond distances of the order of the Debye-Hückel length  $\kappa^{-1}$ , where

$$\kappa^2 = 4\pi\lambda_B (\alpha\phi + 2\phi_s) \quad (1)$$

$\lambda_B$  being the Bjerrum length ( $\lambda_B \approx 7.1 \text{ \AA}$ ),  $\phi$  and  $\phi_s$  respectively the polymer and salt concentrations (in  $\text{\AA}^{-3}$ ). Thus larger (both in amplitude and spatial scale) fluctuations of polymer concentration are allowed as the screening by small salt ions increases. For sufficiently high salt concentration, the maximum in  $S(q)$  is observed at  $q=0$ , which means that the system recovers a behavior similar to that of neutral polymers in poor solvent, i.e. macroscopic phase separation (6,7).

More quantitatively the peak position  $q^*$  is predicted (6,7) to follow equation 2 :

$$q^{*2} + \kappa^2 = \left(\frac{48\pi\lambda_B}{\alpha^2}\right)^{1/2} \alpha\phi^{1/2} \equiv r_0^{-2} \quad (2)$$

which is well obeyed in the experiments. In equation 2,  $\alpha$  stands for the statistical unit length of the neutral polymer chains. Equation 2 predicts a weaker effect of polymer concentration on the peak position ( $q^* \sim \phi^{1/4}$ ) than in strongly charged polyelectrolytes ( $q^* \sim \phi^{1/2}$ ) (5,12), which is compatible with the observations (Figure 1).

The equation determining the peak position does not contain any parameter linked to the solvent quality since the latter influences solely the amplitude of polymer concentration fluctuations and not their length scale which is fixed only by the ionic strength. This is indeed observed in the SANS experiments where the peak position is independent of the temperature contrary to its amplitude which increases as the solvent becomes poorer (8-10).

The comparison between theory and experiment can be pursued further by fitting (8) the scattering curves with the following equation :

$$I(q) = KS(q) = \frac{K}{4\pi\lambda_B \alpha^2} \frac{q^2 + \kappa^2}{r_0^4 (q^2 + \kappa^2)(q^2 - \frac{12\phi h}{\alpha^2}) + 1} \quad (3)$$

where  $S(q)$  is the calculated structure factor,  $K$  the contrast between polymer and solvent,  $r_0$  a characteristic length defined by equation 2 and  $h(T,\phi)$  a virial term which describes the interaction of neutral polymer chains in the poor solvent and depends only on temperature and polymer concentration  $\phi$ .

Continuous lines in Figure 1 result from the fit of equation 3 to the experimental data with  $K$ ,  $\alpha$  and  $h$  as free parameters. The agreement appears very satisfactory. Moreover detailed investigation (8) has shown that, for  $f=0.05$ , parameters  $K$  and  $\alpha$  are, as expected, independent of  $C_p$ ,  $C_s$  and  $T$ , within the experimental accuracy. A simple form for  $h(T,\phi)$  would be the classical expression used for  $\Theta$  solvents :

$$h(T,\phi) = -(2v\tau + 3w\phi) \quad (4)$$

$v$  being the excluded volume parameter,  $w$  the three-body interaction parameter and  $\tau = (T-\Theta)/\Theta$  the reduced distance to compensation temperature  $\Theta$ . The linear dependence of  $h$  on temperature was confirmed experimentally but its concentration dependence appeared more complicated than predicted by equation 4, presumably due to the rather high polymer concentration range investigated (8). Nevertheless  $h$  appears to be independent of salt concentration within a good approximation as shown in Figure 2.

Thus the good description of the scattering curves is not obtained at the expense of a lack in physical significance for the fitting parameters. These ones have not only the right functional dependence, i.e.  $K$  and  $\alpha$  are constants and  $h$  depends only on  $T$  and  $\phi$ , but also good orders of magnitude. In particular,  $K$  can be estimated to 9 barns from tabulated values of scattering length densities and partial molar volumes while the fitted values range between 8 and 10 barns (8). Similarly the value  $\alpha \approx 9\text{\AA}$  is very reasonable for the statistical unit length of a vinylic polymer.

In view of this agreement, it was tempting to try to describe the dynamics of these systems on the basis of this simple model.

### Dynamic Properties

A simple way to model the dynamics of these systems is to consider the motion of monomers, counterions and coions as the motion of particles in a continuous viscous medium. Then the relaxation of the fluctuations of component concentrations can be

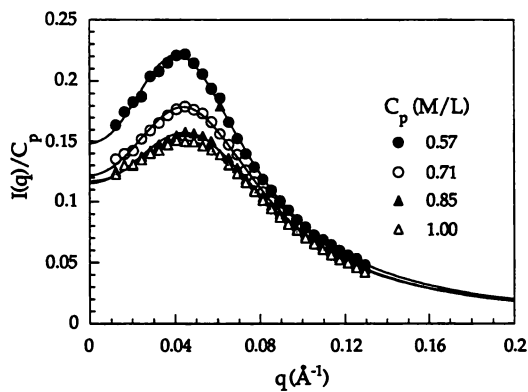


Figure 1 : Evolution of SANS intensity with polymer concentration.

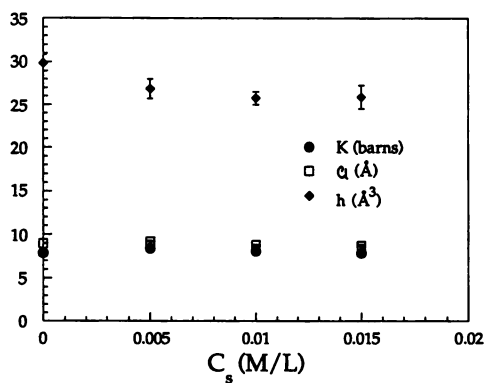


Figure 2 : Variation of the fitting parameters  $K$ ,  $Q$  and  $h$  with salt concentration.

described by a Langevin equation and backflow effects can be treated through the Oseen tensor. The linear response approximation then establishes simple relationships between the relaxation rates of concentration fluctuations and the partial structure factors of the system (13,14).

In principle, there are three different components in the system : monomers, counterions ( $\text{Na}^+$ ) and salt ions ( $\text{Na}^+$  and  $\text{Br}^-$ ), the small amount of  $\text{H}^+$  ions resulting from the spontaneous dissociation of the monomers being neglected. This implies three eigenvalues for the matrix of relaxation rates and thus three characteristic decay rates which have been discussed in detail by Ajdari et al (14).

The fastest relaxation mode is linked to the restoration of electroneutrality through the motion of small ions and is the so-called plasmon mode. The second mode is a diffusive one and tends to equilibrate the electrochemical potential of each species. Since the polymer chains usually move much more slowly than the small ions, this second mode deals essentially with the mutual repartition of counterions and salt ions in the whole volume occupied by polymer chains in a given configuration and corresponds to time scales where the Donnan equilibrium is restored. Finally the slowest relaxation mode is related to the collective motion of polymer chains, with electroneutrality and Donnan equilibrium being preserved (14).

A complete calculation shows that the three relaxation modes are not always well separated, in particular for fluctuations with large associated wavevectors, when the system is close to microphase separation transition or when salt is added. However, not too close from the transition, the decay of long wavelength (vanishing wavevector) fluctuations of polymer concentration is simply expressed in terms of the polymer-polymer pair correlation  $g(r)$  by means of a cooperative diffusion coefficient  $D_c$  (10,14):

$$D_c = \frac{\int d^3r g(r) \frac{kT}{6\pi\eta r}}{\int d^3r g(r)} = \frac{kT}{6\pi\eta} S^{-1}(0) \frac{1}{(2\pi)^3} \int d^3q \frac{4\pi}{q^2} S(q) \quad (5)$$

where  $\eta$  is the solvent viscosity,  $k$  the Boltzmann constant and the second equality results from Parseval's theorem. The integral in equation 5 can be performed analytically and the final result reads :

$$D_c = \frac{kT}{6\pi\eta} \frac{[1 - \frac{h}{4\pi\lambda_B} (\frac{\kappa}{\alpha})^2]^{1/2} \{\kappa^2 r_0^2 + [1 - \frac{h}{4\pi\lambda_B} (\frac{\kappa}{\alpha})^2]^{1/2}\}}{\kappa^2 r_0^3 \{2[1 - \frac{h}{4\pi\lambda_B} (\frac{\kappa}{\alpha})^2]^{1/2} - \frac{12\phi r_0^2 h}{q^2} + \kappa^2 r_0^2\}^{1/2}} \quad (6)$$

Although equation 6 has no simple form, it contains only quantities like ionization degree, polymer concentration and salt content, which are known a priori, or like  $\alpha$  and  $h$ , which can be obtained by fitting the static structure factor  $S(q)$ , as described above. No free parameter is left so that, within the linear response approximation and the simple model of particles moving in a continuous viscous fluid, the cooperative diffusion coefficient  $D_c$  is completely determined by the static scattering experiment. On the other hand,  $D_c$  is classically measured in a QELS experiment as the limiting value for vanishing wavevectors of  $\Gamma(q)/q^2$ . Therefore our experiments provide a direct test of the above dynamical model.

Table I shows the comparison between calculated and measured values of  $D_c$ . Values of the parameters  $\alpha$  and  $h$  used to compute  $D_c$  are those reported in reference (8). The variation of  $\text{D}_2\text{O}$  viscosity with temperature has been calculated by taking the

same relative changes as those tabulated for H<sub>2</sub>O (15). As can be seen from this table, the measured values are systematically lower than the calculated ones by a factor of about 3 to 5. As far as the general trends are concerned, the decrease of  $D_c$  as the salt content increases or as the temperature decreases is correctly predicted. However, equation 6 gives a weak maximum in the concentration dependence of  $D_c$  while experimentally a monotonous decrease is observed. These behaviors are better seen in Figure 3 where both the measured and the calculated  $D_c$  values have been normalized by their value for  $C_p = 0.707$  M,  $T = 20^\circ\text{C}$  and  $C_s = 0$ .

**Table I. Comparison of measured and calculated  $D_c$  values**

$C_p$ (M/L)	$C_s$ (mM/L)	T ( $^\circ\text{C}$ )	$D_c$ meas. <sup>a</sup>	$D_c$ calc. <sup>a</sup>	ratio
0.995	0	20	3.25	16.5	0.20
0.848	"	"	3.87	16.8	0.23
0.707	"	"	4.6	17.0	0.27
0.707	5	"	3.75	13.2	0.28
"	10	"	3.47	11.7	0.30
"	15	"	3.07	10.1	0.30
"	30	"	1.57	-	-
0.566	0	"	4.72	16.1	0.29
0.707	"	10	3.15	11.6	0.27
"	"	15	3.6	-	-
"	"	30	6.91	23.7	0.29
"	"	40	9.98	37.2	0.27
"	"	45	10.6	-	-

<sup>a</sup>  $D_c$  values in  $10^{-7}$  cm<sup>2</sup>/s

A slow relaxation mode not predicted by the model has been observed in the intensity correlation function for the lowest temperature or the highest salt contents. Such a slow mode is not uncommon for neutral (16) or ionized (17) polymers in a poor solvent. In our operating conditions, the amplitude of this slow decay process was not large enough to disturb the measurements but at higher salt concentration ( $C_s \geq 40$  mM) it made the determination of the faster decay rate very difficult.

At that point it can be remarked that  $S(q)$ , as given by equation 3, could be considered as a purely phenomenological description of the experimental curves. Then making the assumption of particles moving in a continuous viscous fluid would still yield equation 5. In principle, even if no analytical form was available for  $S(q)$ , it would still be possible to perform numerically the integration in equation 5 and to compare the results with the experimental values. Also it must be noted that the knowledge of the fitting parameters allows one to extrapolate  $S(q)$  to the  $q$  range investigated by the light scattering technique. These extrapolated values agree with the experimental light scattering data within a possible 10 to 20% variation. Therefore one can rule out any steep variation of  $S(q)$  at small  $q$  values ( $q < 10^{-2}$  Å<sup>-1</sup>) and the disagreement between measured and calculated  $D_c$  values is only indicative of a failure of equation 5, independently of any assumption concerning the structure of weakly charged polymers in a poor solvent.

From Figure 3, it can be seen that, apart from the numerical factor, the most serious qualitative disagreement concerns the concentration dependence. One could then assume that this factor is in some way also linked to an improper treatment of polymer concentration effects and correct artificially that error by normalizing the calculated and measured  $D_c$  as in Figure 3. Then, concerning temperature and salt influence, equation 5 appears to describe the experimental variations in a satisfactory way, i.e. within a

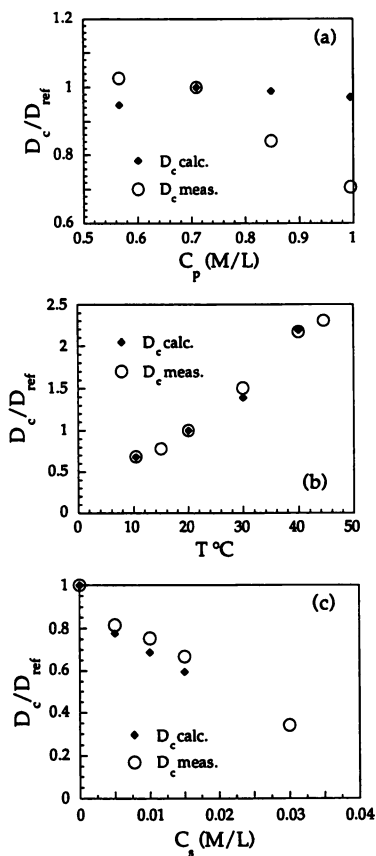


Figure 3 : Comparison of normalized measured and calculated  $D_C$  values as a function of polymer concentration (a), temperature (b) and salt concentration (c).  $D_{ref}$  is the measured or the calculated value for  $C_p=0.707$  M,  $T=20^{\circ}C$  and  $C_s=0$ .



15% relative error for a two to five-fold variation. However this normalization is hard to justify.

It can be worth noticing that the neglect of the two faster relaxation modes cannot be responsible for the disagreement since taking them into account would increase further the calculated decay rate.

Several levels of approximation are involved in the derivation of equation 5. One of them consists in preaveraging the hydrodynamic interactions over the equilibrium configuration of the system (13). For dilute  $\Theta$  solutions, this approximation introduces only a small error at large  $q$  and has no influence on the small  $q$  behavior (18). It is likely that this is also true in more concentrated systems and cannot explain our numerical factor. Probably the same can be said about the decoupling approximation which is made in an earlier step of the theoretical treatment and which assumes that density and velocity correlations are decoupled (13).

From an other point of view, the existence of a rather broad distribution of decay rates and the appearance, under certain conditions, of a slow decay mode might indicate that the system keeps some common features with semi-dilute  $\Theta$  solutions of neutral chains whose dynamics is not yet fully understood (13,16). The above model does not predict any of these features and in particular a single exponential decay is expected. It has been suggested that the non-exponential shape of the intensity correlation function is due to the existence of knots and self-entanglements in  $\Theta$  solvent (13,19). This makes the theory of dynamics in these systems more difficult since the distance between these topological interactions is not necessarily linked to the usual correlation length of excluded volume interaction (13,19). The same remark could be applied to weakly charged chains in a poor solvent where the length  $r_0$  characterizes the screening of electrostatic interactions and  $\lambda^*$  is the mean distance between regions with higher polymer concentration. A characteristic distance for topological interactions would then seem more likely linked to the latter than to the former. It is often argued that the effect of topological interactions should not show up in the short time decay of the intensity correlation function (13) but this might not be always true for systems with a microscopic structure when  $\lambda^* \sim 100 \text{ \AA}$ .

To conclude, the simple model cannot explain the experimental results and it is clear that a new theoretical effort is needed to understand better the dynamics of weakly ionized chains in a poor solvent.

### Acknowledgments

We are grateful to J.P. Cotton, our local contact on PACE for kind assistance during the experiments and for sharing his experience about polyelectrolyte systems. Illuminating discussions with J.F. Joanny and L. Leibler are acknowledged.

### Literature Cited

1. Strauss, U.P., in *Polymers in Aqueous Media: Performance through Association*; Glass, J.E., Ed.; Advances in Chemistry Series 223; American Chemical Society: Washington, DC, 1989.
2. Silberberg, A.; Eliassaf, J.; Katchalsky, A., *J. Polym. Sci.*, **1957**, *23*, 259.
3. Ise, N.; Okubo, T.; Hiragi, Y.; Kawai, H.; Hashimoto, T.; Fujimura, M.; Nakajima, A.; Hayashi, H., *J. Am. Chem. Soc.*, **1979**, *101*, 5836.
4. Kitano, T.; Taguchi, A.; Noda, I.; Nagasawa, M., *Macromolecules*, **1980**, *13*, 57.
5. Nierlich, M.; Williams, C.E.; Boué, F.; Cotton, J.P.; Daoud, M.; Farnoux, F.; Jannink, G.; Picot, C.; Moan, M.; Wolff, C.; Rinaudo, M.; de Gennes, P.G., *J. Physique*, **1979**, *40*, 701.
6. Borue, V.; Erukhimovich, I., *Macromolecules*, **1988**, *21*, 3240.
7. Joanny, J.F.; Leibler, L., *J. Phys. France*, **1990**, *51*, 545.

8. Moussaid, A.; Schosseler, F.; Munch, J.P.; Candau, S.J., *J. Phys. II France*, **1993**, *3*, 573.
9. Schosseler, F.; Ilmain, F.; Candau, S.J., *Macromolecules*, **1991**, *24*, 225.
10. Schosseler, F.; Moussaid, A.; Candau, S.J., *J. Phys. II France*, **1991**, *1*, 1197.
11. Jannink, G., *Makromol. Chem., Macromol. Symp.*, **1986**, *67*, 1.
12. de Gennes, P.G.; Pincus, P.; Velasco, R.M.; Brochard, F., *J. Phys. France*, **1976**, *37*, 1461.
13. Doi, M.; Edwards, S.F., *The Theory of Polymer Dynamics*, Oxford University: Oxford, 1986.
14. Ajdari, A.; Leibler, L.; Joanny, J.F., *J. Chem. Phys.*, **1991**, *95*, 4580.
15. *Handbook of Chemistry and Physics*, 53rd edition, Weast, R.C., ed., CRC Press: Cleveland, Ohio, 1972.
16. For a review see for example, Joanny, J.F.; Candau, S.J., in *Comprehensive Polymer Science*, Booth, C.; Price, C., eds., Pergamon Press, 1989, vol. 2, chap. 7.
17. Sedláč, M.; Konák, C.; Stepánek, P.; Jakes, J., *Polymer*, **1987**, *28*, 873; **1990**, *31*, 253.
18. Han, C.; Akcasu, A.Z., *Macromolecules*, **1981**, *14*, 1080.
19. Brochard, F.; de Gennes, P.G., *Macromolecules*, **1977**, *10*, 1157.
20. Brochard, F., *J. Phys. France*, **1983**, *44*, 39.

RECEIVED August 6, 1993

## Chapter 23

# Light-Scattering Results on Polyelectrolyte Conformations, Diffusion, and Interparticle Interactions and Correlations

Wayne F. Reed<sup>1</sup>

Centre de Recherches sur les Macromolécules Végétales, B.P. 53X, 38041  
Grenoble, France

This work summarizes static and dynamic light scattering results on the dilute solution properties of polyelectrolytes. These data allow estimates of how  $\langle S^2 \rangle$ ,  $A_2$ , and  $R_h$  vary with moderate to high salt concentration  $C_s$ , and linear charge density  $\xi$ . Combination of electrostatic persistence length (EPL) and electrostatic excluded volume (EEV) theories, with no adjustable parameters, accounts fairly well for  $\langle S^2 \rangle$  and  $A_2$  vs.  $C_s$  and  $\xi$ . Preliminary Size Exclusion Chromatography results confirm EPL/EEV predictions vs. molecular mass  $M$ . EEV effects are predominant in many situations. The behavior of  $R_h$  is more complex and not readily interpretable with current models. Observations of broad angular scattering maxima at extremely low  $C_s$  are interpreted in terms of liquid-like correlations.

When static and dynamic light scattering (SLS and DLS, respectively) results are carefully extrapolated to zero polyelectrolyte concentration,  $\langle S^2 \rangle$ ,  $A_2$  and  $R_h$  are obtained.  $\langle S^2 \rangle$  is the mean square radius of gyration,  $A_2$  is the second virial coefficient (with cgs units of Mole  $\times$  cm<sup>3</sup>/g<sup>2</sup>), and  $R_h$  is the hydrodynamic radius. This chapter presents results on a variety of polyelectrolytes and compares them with existing theories and simulations.

The scope of this work is highly restricted in the sense that all experiments were done at  $T=25^\circ\text{C}$  and at low polymer concentration  $C_p$ , so that only a tiny part of the polyelectrolyte phase diagram is explored. Furthermore, light scattering allows observation of these systems only over a limited range of scattering vector  $q$ , at low values. While neutron and x-ray scattering can reveal structure on shorter length scales than light scattering, they nonetheless require, in practice, much higher concentrations (usually in excess of  $10^{-2}$  g/cm<sup>3</sup>, compared to light scattering, which can often descend

<sup>1</sup>Current address: Physics Department, Tulane University, New Orleans, LA 70118

below  $10^{-5}$  g/cm<sup>3</sup>). Thus, light scattering is well suited to dilute solution studies where the behavior of isolated polyelectrolyte chains and interaction at low, hard volume concentrations is investigated. A good understanding of such properties should enhance the investigation of the diverse, fascinating and often useful phenomena which occur when polyelectrolytes interact at different concentrations and temperatures with multivalent ions, oppositely charged polyelectrolytes, neutral polymers, micelles and other colloids.

Statistical Mechanics, as well as many ingenious and simpler representations, have led to rapid advances in the understanding of neutral polymer properties such as molecular dimensions, elasticity and viscosity. The large number of conformational states in a polymer has also stimulated the use of Monte Carlo simulations, in which the properties of a subset of states is explored, which, if properly chosen, give a good approximation to the full parent distribution of states and properties.

The presence of electrical charge on polyelectrolytes introduces long range forces which considerably complicate the picture both theoretically and experimentally compared to neutral polymers. At high salt concentration  $C_s$ , the monomeric charges of the polyelectrolytes are largely shielded from each other so that conformations and properties are expected to approach those of neutral polymers. As  $C_s$  is lowered, the shielding decreases and the repulsion between charged monomers should make the chain stretch out,  $\langle S^2 \rangle$  being an experimental measure of this. Since the total free energy includes electrostatic and entropic terms, the latter of which is least favorable in the totally stretched out (all-trans) conformation, the polyelectrolyte will not suddenly suffer a random coil-to-rod transition as  $C_s$  is lowered, but rather will gradually stiffen and  $\langle S^2 \rangle$  will increase, as the entropic term balances the electrostatic term at each  $C_s$ . The argument is similar for increasing the linear charge density, or charge parameter  $\xi$ , at fixed  $C_s$ . ( $\xi$  is the number of elementary charges per Bjerrum length,  $\lambda_B$ ).

Since  $A_2$  measures the excluded volume between interacting particles, it is expected that it will likewise increase with decreasing  $C_s$  and/or increasing  $\xi$  due both to the increase of  $\langle S^2 \rangle$  and the electrostatic repulsion between polyelectrolytes. At extremely low  $C_s$  the EEV between polyelectrolytes becomes so large that liquid-like correlations can arise which produce broad angular scattering maxima.

The effects of  $C_s$  and  $\xi$  on  $R_h$  are less easily predictable, because  $R_h$  ultimately measures the total hydrodynamic friction of an isolated polyelectrolyte, and this latter quantity is a complicated combination of static dimensional properties and hydrodynamic perturbations among monomers or frictional elements along the chain.

The experimental investigation of dilute solutions of polyelectrolytes has run into several hurdles and ambiguities, which have led to some disagreement and irreproducibility in the literature. Although mostly mundane in origin, these hurdles must be decisively cleared before consistent experimental profiles of polyelectrolyte behavior emerge. As the light scattering data become more reliable, however, it turns out that the dilute solution properties of well-dispersed, linear polyelectrolytes are not

particularly mysterious, and generally follow qualitative expectations. A concise, definitive theory embracing all the experimentally observed dimensional, interactive and hydrodynamic properties of dilute solutions, however, has not yet been established.

Relevant notions from certain theories are now briefly summarized before the experimental results are presented.

### Summary of Theoretical Notions

**Electrostatic Persistence Lengths.** Landau and Lifschitz [1] treated the thermal conformational fluctuations of an elastic rod, and introduced the notion of 'persistence length',  $L_p$ , which is the contour distance along the polymer which determines how quickly the thermodynamically averaged cosine  $\langle \cos\phi \rangle$  of the direction vectors at the ends of a chain separated by contour distance  $l$  decays;

$$\langle \cos\phi \rangle = \exp(-l/L_p) \quad (1)$$

e.g. for  $l=L_p$  the average angle between the direction vectors at the ends of the segment is  $68.4^\circ$ .  $L_p$  and the total contour length of the rod  $L_r$ , serve to calculate the unperturbed  $\langle S^2 \rangle_0$

$$\langle S^2 \rangle_0 = (L_r L_p)/3 - L_p^2 + 2L_p^3/L_r - 2(L_p^4/L_r^2)[1 - \exp(-L_r/L_p)] \quad (2)$$

This is the basis of the 'wormlike chain' model and serves as a bridge between the rod limit where  $L_p \gg L_r$  and  $\langle S^2 \rangle_0 = L_r^2/12$ , and the random coil limit where  $L_r \gg L_p$  and  $\langle S^2 \rangle_0 = L_r L_p/3$ .

Treatments have been made of the local stiffening of polyelectrolyte chains in terms of the increase in electrostatic energy when a straight, charged rod is curved and the charges approach each other [2,3]. To first order, using Debye-Hueckel screening the electrostatic persistence length  $L_e$  is

$$L_e = \frac{\xi^2 \kappa^{-2}}{12\lambda_B} \{3 - 8/y + \exp(-y)[y + 5 + 8/y]\} \quad (3)$$

where  $y = \kappa L_r$  and  $\lambda_B = 7.2\lambda$  in water at  $25^\circ\text{C}$ . For  $L_r \gg \kappa^{-1}$

$$L_e(\text{\AA}) \cong (\xi/\kappa)^2/28.8, \text{ or } L_e \propto \xi^2/C_s \quad (4)$$

In this treatment

$$L_p = L_0 + L_e \quad (5)$$

where  $L_0$  is the intrinsic persistence length of the polymer and can be due to such effects as fixed bond angles, rotameric states, helical structure, etc.

**Electrostatic Excluded Volume (EEV).** Equation 2 applies only to semi-rigid molecules in which there are no excluded volume effects. Excluded volume effects, which modify polymer properties, are based on interactions between distant segments along a polymer which, via chain flexibility, are located in each others' spatial vicinity. Net repulsion among segments (e.g. polyelectrolytes in a 'good solvent'), increases the overall dimensions of the polymer. The 'perturbed' mean square radius of gyration is then  $\langle S^2 \rangle$  and has

often been related to  $\langle S^2 \rangle_0$  by the static expansion parameter  $\alpha_s$  [4]

$$\langle S^2 \rangle = \alpha_s^2 \langle S^2 \rangle_0 \quad (6)$$

$\alpha_s^2$  has been the object of intense theoretical and experimental investigation, for which varying results have been obtained. We restrict attention to one particular combination of results introduced in reference 5.

The Gupta-Forsman [6] relation between  $\alpha_s$  and the perturbation parameter  $z$ , which has worked well in several cases is, for  $N_k \geq 2$ ,

$$\alpha_s^5 - \alpha_s^3 \cong \frac{134}{105} (1 - 0.885 N_k^{-0.462}) z \quad (7)$$

where  $z$  is given in the long chain limit by [4]

$$z = (3/2\pi L_k^2)^{3/2} \beta N_k^{1/2} \quad (8)$$

$L_k$  and  $N_k$  are the length of a Kuhn statistical segment and the number of them in the polymer, respectively. In the coil limit  $L_k = 2L_p$ . Fixman (oral presentation at ACS meeting, Denver, March 1993) has recently used a Monte Carlo approach to compute  $z$  for a finite numbers of chain segments. In equation 8,  $\beta$  is the excluded volume between two Kuhn segments, which in the case of EEV measures the electrostatic interactions over all mutual configurations, as suggested by Odijk and Houwaart [7]. Fixman and Skolnick [8] approximated the EEV between charged rod-like segments of length  $L_k$  as

$$\beta = 8L_p^2 \kappa^{-1} \int_0^{\pi/2} \sin^2 \theta \int_0^{w/\sin \theta} x^{-1} (1 - e^{-x}) dx d\theta \quad (9)$$

where  $w = 2\pi \xi^2 \kappa^{-1} e^{-\kappa d}$ ,  $d$  being the rod diameter.

Static light scattering measures  $\langle S^2 \rangle$  and not  $\langle S^2 \rangle_0$ , so that  $L_p$  cannot be determined directly from equation 2. If, however, the experimental value of  $\langle S^2 \rangle$  is substituted for  $\langle S^2 \rangle_0$  in equation 2 the resulting  $L_p$  has been termed the 'apparent total persistence length',  $L_p'$  (sometimes represented as  $L_T$ ). Apparent persistence lengths have been discussed at length in earlier works [9-11].

In the coil limit of equation 2, the apparent and true persistence lengths are related to each other by

$$L_p' = \alpha_s^2 L_p \quad (10)$$

Since for EEV  $\alpha_s^2 \geq 1$ ,  $L_p' \geq L_p$ ; i.e. for positive excluded volume,  $L_p'$  is always an upper bound on  $L_p$ .

**Electrostatic Excluded Volume and  $A_2$ .** Yamakawa [4] used the perturbation theory of excluded volume to express  $A_2$  as

$$A_2 = (N_A N_k^2 \beta / 2M^2) h_0(\bar{z}) \quad (11)$$

where  $N_A$  is Avogadro's number and

$$h_0(\bar{z}) = [1-(1+3.9\bar{z})^{-4.68}]/1.83\bar{z} \quad (12)$$

where  $\bar{z} = z/\alpha_s^3$  and  $\beta$ ,  $z$  and  $\alpha_s$  are calculated as outlined above. The use of  $z/\alpha_s^3$  is Yamakawa's first order attempt at including intramolecular excluded volume into the intermolecular excluded volume problem. Under assumptions discussed in refs. 10,12 the total  $A_2$  of the polyelectrolyte can be approximated as the sum of  $A_2$  from equation 11 and  $A_{2,HS}$ , where  $A_{2,HS}$  is the high ionic strength limit of  $A_2$ , obtained from experimental extrapolation of  $A_2$  to infinite  $C_s$ .

**Hydrodynamic Radius  $R_h$ .** Numerous theories exist for the hydrodynamic friction factor  $f$  of polymers [13,14]. For an isolated, impermeable spherical particle,  $R_h$  is related to  $f$  by

$$f = 6\pi\eta R_h \quad (13)$$

where  $\eta$  is the viscosity of the supporting solvent. Measurements of  $R_h$  by DLS can in principle be related to  $f$  when the apparent hydrodynamic radius  $R_{app}$  is extrapolated to  $C_p=0$ . For a polymer, such an  $R_h$  is the hydrodynamic radius of a hydrodynamically equivalent spherical particle.

Two simplifying limits for polymer coils are mentioned here; the case where there is no hydrodynamic perturbation between frictional segments, often termed 'free-draining', and the limit where the hydrodynamic perturbations are so strong that effectively only the 'outermost' polymer segments in a coil contribute to  $f$ , which is often termed the 'non-draining' case. (Ref. 15 calculates that even in this latter limit there is appreciable differential solvent flow 'within' the polymer coil, and proposed the term 'least-draining' for this limit). In the 'free-draining' case, for a polymer of mass  $M$ ,

$$R_h \propto M \quad (14)$$

since each increment of mass of a polymer adds independently to  $f$ , which is proportional to  $R_h$ . For the non-draining case,

$$R_h \propto M^{0.5} \quad (15)$$

**Angular Maxima for Static and Dynamic Scattering.** A useful approximation often employed in scattering theory is that the total intensity  $I(q)$  is the product of the structure factor  $S(q)$  and the particle form factor  $P(q)$ ,

$$I(q) \propto S(q) P(q) \quad (16)$$

If a model for the radial distribution function of particles  $g(r)$  can be found or modeled, then  $S(q)$  can be calculated by

$$S(q) = 1 + 4\pi n \int_0^{\infty} [g(r)-1][\sin(qr)/qr]r^2 dr \quad (17)$$

where  $n$  is the number density of particles. One of the simplest forms of  $g(r)$  is for a hard sphere of radius  $R$ , for which  $g(r)=0$  for  $r \leq R$  and  $g(r)=\text{constant}$  for  $r > R$ .  $S(q)$  is then from equation 17

$$S(q) = [1 - 24C_v J_1(2qR)/2qR] \quad (18)$$

where  $C_v (=4\pi R^3 C_p N_A/3M)$  is the volume fraction of particles ( $C_p =$  polymer concentration in  $g/cm^3$ ), and  $J_1(2qR)$  is the first order spherical Bessel function, which manifests damped oscillations [16]. Thus, even hard spheres will manifest oscillations in  $S(q)$  at high enough volume concentrations. Broad maxima in  $I(q)$  using x-rays are in fact typical of simple liquids, and hence the term 'liquid-like correlations' can often be used to describe the origins of broad scattering maxima in dynamic systems with no long range order. Peak widths in the case of liquid-like correlations can be interpreted in terms of the average mean square deviation from simple Bragg spacing, by the 'Guinier disorder parameter' [17,18].

$1/D_{app}(q)$  is expected to follow  $S(q)$ , with deviations being due essentially to hydrodynamic effects [19].

## Experimental

**Scattering Apparatus.** SLS and DLS measurements were made using the vertically polarized 488nm line of an Argon ion laser. Computer programs were written to control a Brookhaven BI-2030 autocorrelator and a stepping motor. A Wyatt Technology Dawn-F, operating in batch mode with 15 monitored scattering angles and a vertically polarized 632nm He-Ne laser, and controlled by specially written software was also used for SLS. Absolute Rayleigh scattering ratios  $I(q)$  can be made by scaling relative scattered intensities to the relative scattering of a reference solvent whose Rayleigh ratio is known; e.g. for toluene it is 0.00001407 at  $\lambda=632$  nm, and 0.0000396 at  $\lambda=488$ nm at  $T=25^\circ C$ , where all experiments were performed.

Preliminary results on polyelectrolyte conformations vs.  $C_s$  and  $M$  using the Dawn F multi-angle laser light scattering (MALLS) instrument, coupled to a Size Exclusion Chromatography (SEC) apparatus (Waters 150C) are given below.

**Polyelectrolytes and Solution Preparation.** Sigma Co. bacterial hyaluronate (HA) was used, for which  $M_w \sim 1.3 \times 10^6$  daltons, the linear mass density  $m/b$  is 40  $g/(Mole \times \lambda)$ ,  $\xi = 0.72$  and the polydispersity ratio  $M_w/M_n \approx 1.2$  [9]. Variably ionized, sodium polyacrylate (NaPAA) was from Rhone Poulenc with  $M_w \approx 5 \times 10^6$ ,  $m/b = 28$ , and  $\xi$  ranging from 0.015 to 0.77 [10]. Sodium polystyrene sulfonate (NaPSS) from Pressure Chemical Co. was used with  $M_w \approx 780,000$ ,  $m/b = 81$ ,  $M_w/M_n \approx 1.2$  (some degradation in mass and increase in polydispersity over the manufacturer's specifications was found), and  $\xi \approx 1.0$  (i.e. assumed to be at the counterion condensation limit) [12]. Proteoglycan monomers (PGM) of  $M_w \sim 1.5 \times 10^6$ , consisting of a protein backbone of mass around 300,000 covalently bound to which are relatively short, highly charged glycosaminoglycan side chains (weights up to 20,000) were supplied by Dr. Anna Plaas (Shriners Hospital, Tampa, Fla.) [18].

Polyelectrolyte solutions were made at low concentration, seldomly exceeding 1 mg/ml, in aqueous solutions of desired ionic strength. The monovalent salt usually used was NaCl. Pure water was deionized (conductivity less than 1  $\mu S$ ) and doubly distilled and was withdrawn from a Corning Megapure I still through a 0.22 $\mu m$  Millistack (Millipore) filter. The polyelectrolyte was allowed to



dissolve in solution at least 24 hours under gentle agitation before experiments were performed.

Some investigations of the effects of  $C_s$  were also alternatively performed by adding small amounts of stock solutions of fixed  $C_s$  to the polyelectrolyte solutions in pure water. The practical range for determinations of  $\langle S^2 \rangle$  and  $A_2$  by SLS and of  $R_h$  by DLS was generally  $C_s = 0.001M$  to  $1.0M$ .

**The Problem of Aggregates.** Because well dispersed polyelectrolytes scatter weakly at low  $C_s$ , the complete elimination of aggregates and impurity particles is crucial for avoiding spurious scattering at low  $C_s$ , which can give rise to a detectable 'slow mode',  $D_s$  in DLS [9,10,12,18,20]. Even tiny traces of such aggregates/particles can significantly distort data at low  $C_s$ . Techniques such as viscometry and fluorescence recovery after photobleaching are closer to being number averaging techniques, and are far less sensitive to aggregates than light scattering, which generally measures weight and z-averages of scatterer populations.

The manner in which the dry polyelectrolyte is prepared, and how it is subsequently handled in solution are critical as regards the problem of aggregates and other particles. Lyophilisation, for example, can create large aggregate populations [9]. Particular attention must also be paid to solution quality after such handling steps as dialysis, freezing, sonicating, etc.

Attention should always be paid to the visual quality of the scattering from polyelectrolyte solutions, and monitoring of absolute scattering intensity (e.g. with respect to a standard such as toluene) at each stage of preparation and manipulation is highly recommended. At no added salt a good polyelectrolyte solution should scatter scarcely above the pure solvent level at all angles, except for the case of denser polyelectrolytes which give pronounced angular scattering maxima. In the latter case it is usually possible to visually observe low scattering intensity at forward angles, increasing as the eye scans to higher angles.

Proper filtration seems to be one of the keys to preparing aggregate-free polyelectrolyte solutions. For many years it was customary to use standard  $0.2\mu m$  membrane filters, applying manual or low, controlled pressure to syringes, or even using slow, gravity feed. Unfortunately, populations of aggregates and other particles can often survive such filtration, as well as centrifugation, leading to the problems at low  $C_s$  mentioned above. With the rapid advance in filtration technology, however, there is currently available a wide variety of hydrophilic membranes with pore sizes down to  $0.025\mu m$ . Experience has shown that a certain amount of trial and error is necessary to establish which pore size membrane of which chemical composition is best suited for complete or at least maximum aggregate/particle removal from any given polyelectrolyte whose dry material is produced in a given way [20]. Pore size alone is not always the sole criterion. Recently, for example, it was found that filtration of succinoglycan (a bacterial, polyelectrolytic saccharide) through a  $0.1\mu m$  cellulose nitrate membrane allowed crystal clear measurements of static and dynamic angular scattering peaks to be made. In such solutions the autocorrelation exhibited a single, fairly rapid decay time, for which  $1/D_{app}(q)$  showed an angular peak coincident with  $I(q)$ . When the same solutions were filtered with a  $0.1\mu m$  polyvinylidene difluoride membrane (or through a  $0.2\mu m$  cellulose nitrate membrane),

however, enough aggregates survived to predominate over the static peak, and produce a spurious slow mode of diffusion co-existing with the faster mode (I. Morfin, W.F. Reed, M. Rinaudo and R. Borsali, manuscript submitted to *J. Physique*).

Naturally, when experimenting with different types of filters and filtration techniques, common sense measures must be taken to monitor changes in solution concentration before and after filtration, and to verify that no significant shearing or degradation of the polymers is occurring. A quick and simple first step in checking for obvious degradation in solutions prepared and filtered at low  $C_s$ , is to add a small amount of concentrated, clean salt solution to the sample to bring it to a high  $C_s$  (say 0.1M) and, having taken any concentration changes due to filtering and salt addition into account, verify that it recovers the same SLS and DDL behavior as a polyelectrolyte solution of the same concentration originally at the same high  $C_s$ , filtered through a larger pore size membrane, or merely centrifuged (the scattering from small aggregate populations at high  $C_s$  is usually negligible compared to the scattering from the polyelectrolyte chains themselves). When available, direct SEC determinations of population distributions before and after specific filtration measures can be valuable for assessing possible degradation effects.

The generality of the 'removability' of the slow mode by membrane filtration was tested on a variety of polyelectrolytes at zero or low  $C_s$ , generally at concentrations below 2 mg/ml; Chondroitin sulfate, Heparin, NaPAA, NaPSS, and PLL [20]. It was found that whenever a slow mode existed for any of these, it could be eliminated by filtration through a sufficiently small pore size membrane, after which it never re-appeared. Filtering through membranes with pores larger than that needed for elimination of the slow mode led to  $R_{app}$  which increased with increasing pore size [20].

It was concluded in references 9,10, 12, 18 and 20 that the slow mode represents a tiny population of polyelectrolyte aggregates and/or other particles, incompletely removed by centrifugation and filtration, whose feeble scattering at very low  $C_s$  is autocorrelable against the extremely weak scattering of the well-dispersed polyelectrolyte molecules themselves. As is well known, when  $C_s$  increases, the  $A_2$  of the polyelectrolyte drops drastically (e.g. figure 3) and the scattered intensity increases enormously. It appears that this increase in intensity from the well dispersed polyelectrolytes overwhelms the feeble aggregate scattering, leading to the impression that the 'slow mode' disappears; i.e. when the sun shines you can't see the stars.

The physical nature of the aggregates has not been clearly established, although they may sometimes involve entanglements of polymers. The conclusion in references 9,10,12 and 20 is that they are already present, or at least nascent, in the dry polyelectrolyte material and that they are stable for long periods in solutions of low  $C_s$ , and hence susceptible to removal by filtration. In some cases the aggregates may irreversibly dissolve at high  $C_s$  and/or over long periods of time.

**Estimating  $\langle S^2 \rangle$  and Apparent Persistence Lengths.** Because of their generally weak scattering at low to moderate  $C_s$ , it is often difficult to apply successive dilution methods in SLS, such as that of Zimm, to obtain  $\langle S^2 \rangle$ ,  $M$  and  $A_2$  for polyelectrolytes. Reference 9

introduced a set of approximations for estimating these parameters from single concentration determinations of the absolute scattering  $I(q)$ .

Namely, if the scatterers resemble ideal Gaussian scatterers as a first approximation, and the polydisperse population is such that  $q^2 \langle S^2 \rangle > 3$ , for the majority of the weight fraction, and it can be experimentally demonstrated or assumed that the slope of  $K C_p / I(q)$  in isoionic dilution is independent of  $C_p$  for  $C_p < C_p$  ( $C_p$  = overlap concentration), then

$$K C_p / I(q) \approx 1/2 M_n + \gamma q^2 / 2 + 2 A_2 C_p \quad (19)$$

where, for ideal random coils,

$$\gamma = \langle S^2 \rangle / M \quad (20)$$

Importantly equation 19 yields  $\gamma$ , which is independent of  $M$  and hence also of the sample's polydispersity, rather than the highly polydispersity dependent  $\langle S^2 \rangle_z$  measured at low values of  $q^2 \langle S^2 \rangle$ . Total apparent persistence lengths in the coil limit are  $L_p' = 3 \langle S^2 \rangle / L_r$ , or, in terms of monomer mass per unit contour length,  $m/b$

$$L_p' = \frac{6m}{b} \frac{d[K C_p / I(q)]}{dq^2} \quad (21)$$

Significantly, this result is also independent of polydispersity. As  $C_s$  increases for semi-flexible polyelectrolytes there is typically a marked drop in the slope of  $K C_p / I(q)$  and of the  $q=0$  intercept. The slope as a function of  $C_s$  is independent of  $C_p$ , provided the latter is low enough. The constancy of the behavior of the slope vs.  $C_s$  should be verified for various low values of  $C_p$ .

If  $M_n$  is determined by static methods at high  $C_s$ , then  $A_2 = A_2(C_s)$  can be obtained from the same single concentration experiments via equation 19. Whereas the slope of  $K C_p / I(q)$  is independent of  $C_p$  at low  $C_p$ , the intercept is not.  $A_2$  as determined by equation 19 should naturally be, however, independent of  $C_p$ .

### Summary of Main Results

1. In the Coil Limit  $\langle S^2 \rangle \propto \xi C_s^{-0.5}$ . This approximate relation was found against  $C_s$  for HA [9], NaPSS [12] and PG [18], and against  $C_s$  and  $\xi$  for NaPAA [10]. It is in serious disagreement with equation 4 for unperturbed electrostatic persistence lengths, which predicts  $\langle S^2 \rangle_0 \propto \xi^2 / C_s$  in the coil limit.

Far better agreement with the experimental  $\langle S^2 \rangle$  is found, however, by including EEV effects via equation 6:  $L_e$  is computed by equation 3 and then used to calculate  $\langle S^2 \rangle_0$  from equation 2.  $\alpha_s$  is then computed on the basis of EEV theory, in this case according to equations 7-9. Some results of these computations and experimental data are shown in Figures 1 and 2.

It is important to note that this procedure for calculating  $\langle S^2 \rangle$  involves *no* adjustable parameters. The *fixed* parameters entering the calculations in equations 2 through 9 are the dielectric constant of water  $\epsilon$ , the polymer's linear mass density  $m/b$ , charge parameter  $\xi$ , apparent intrinsic persistence length  $L_0$ , and rod diameter  $d$ .  $\epsilon$  is assumed to be that of pure water (reasonably well known and constant for  $C_s$  not too high) and is used in the

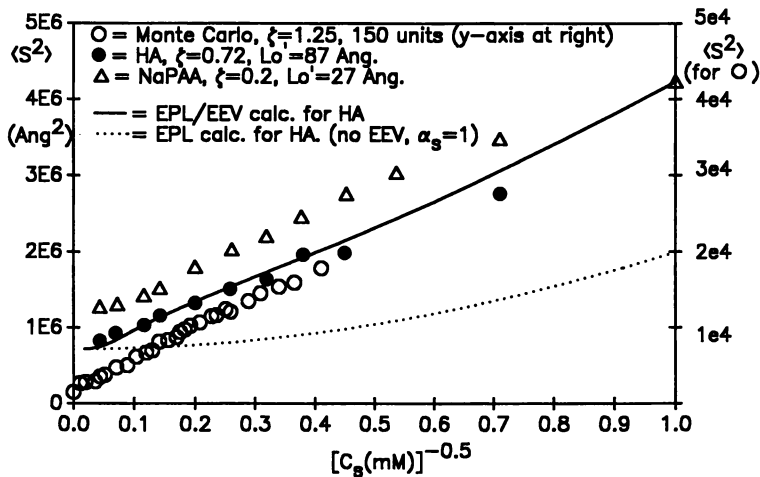


Figure 1.  $\langle S^2 \rangle$  vs.  $C_s^{-0.5}$ .  $\langle S^2 \rangle$  in  $\text{\AA}^2$  and  $C_s$  in mM of NaCl. Experimental and Monte Carlo results.

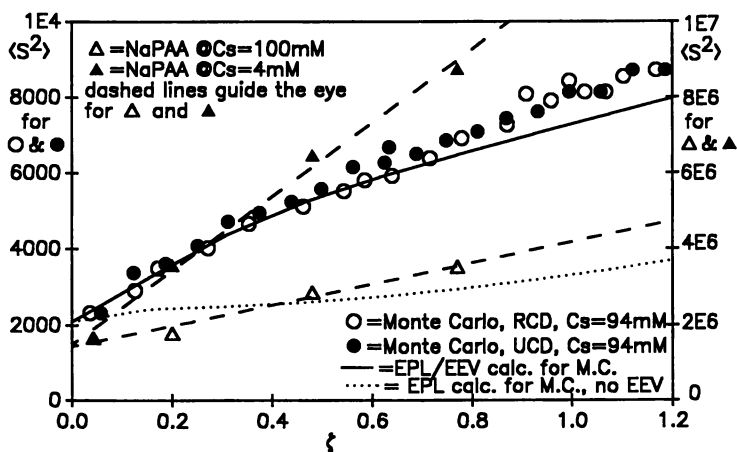


Figure 2.  $\langle S^2 \rangle$  vs.  $\xi$ , NaPAA and Monte Carlo.  $\langle S^2 \rangle$  in  $\text{\AA}^2$ .

computation of  $\lambda_b$  and  $\kappa$ .  $\xi$  and  $m/b$  are reasonably well known from the chemical structure of the monomers, and  $L_0$ , which is used as an approximation to  $L_0$  in equation 5, is obtained by extrapolating experimental  $\langle S^2 \rangle$  values to infinite  $C_s$ . The calculation of  $\beta$  in equation 9 is not very sensitive to  $d$  when a range of reasonable values for  $d$  is used based on the monomer chemical structure.

Interestingly, Monte Carlo calculations [11] using linearized screened potentials, discrete charges and zero hard core excluded volume also give, in the coil limit,  $\langle S^2 \rangle \propto \xi C_s^{-0.5}$ . Figures 1 and 2 include some results from these simulations.

As explained in reference 11, two distinct modes of ionization were used in the simulations: 1) Uniform charge density (UCD), in which all monomers are taken as ionized and the value of the charge on each monomer is adjusted to a fraction of the elementary charge  $e$ . 2) Random charge density (RCD), controlled by pH-pK influence on the total free energy of the polyelectrolyte, in which a monomer bears either one or no elementary charges. In addition to

confirming the scaling law  $L_e' \propto \xi$ , the results of  $\langle S^2 \rangle$  vs.  $\xi$  are surprisingly similar for the two types of ionization. This provides an argument for the validity of mean-field type approximations in calculating polyelectrolyte properties.

Because 'apparent' persistence lengths combine both local stiffening and long range effects, they may be considered objectionable quantities by some theorists. Even when not in the coil limit experiments and Monte Carlo results indicated that the apparent electrostatic persistence length  $L_e'$  varies as  $\xi/C_s^{0.5}$ . Its remarkable empirical consistency makes it a valuable experimental quantity.

The computation of  $A_2$  described in equations 11 and 12 likewise involves no adjustable parameters, and gives excellent agreement with experimental values of  $A_2$ . Figure 3 shows experimental and computed values of  $A_2$  for HA and NaPSS.

**EEV Effects Appear Dominant in Determining  $\langle S^2 \rangle$  and  $A_2$  of Long Polyelectrolytes at Moderate Ionic Strengths.** For  $C_s \sim 0.001M$  to  $1M$  the combined EPL/EEV theories give excellent predictions of  $A_2$  vs.  $C_s$  (and  $\xi$ , reference 10), fair estimates of  $\langle S^2 \rangle$  vs.  $C_s$ , and poorer matches vs.  $\xi$ . The importance of the EEV effects can be seen in the dotted lines in Figures 1 and 2, which show how badly off the values of  $\langle S^2 \rangle$  are when computed only with EPL effects and all EEV effects are ignored. In fact, over much of the range of  $C_s$  generally accessible to SLS (0.001M to 1M), EPL effects are often negligible compared to EEV effects.

Oddly, the approximate theories employed actually contain more 'structure' or curvature than the experimental data [9,11]. Further refinements to the theory, which capture the apparent simplicity of the behavior of  $\langle S^2 \rangle$  may be possible.

The current data in general make a stronger case for EEV effects than for EPL effects over the range of  $C_s$  investigated. In order to study EPL more directly, EPL must clearly dominate over EEV. For the polyelectrolytes studied here, it would be necessary to descend below  $C_s = 0.001M$ , which is difficult with SLS for both theoretical (e.g. onset of strong liquid-like correlations) and practical (e.g. very feeble scattering) reasons. Techniques such as transient birefringence have been tried for NaPSS [21], for example. There

may be difficulties with the hydrodynamic model employed in the interpretation of such data, however, as discussed in the next section.

Our attempts to observe EEV effects via SLS have failed. Although there is considerable difference among scattering theories for isolated polymers with excluded volume, all agree in that the asymptotic value of  $1/I(q)$  should vary as  $q^{-2/\mu}$ , where  $\mu$  is the exponent in the scaling relation

$$\langle S^2 \rangle = aM^\mu \quad (22)$$

Recent Monte Carlo simulations, however, indicate that it may be extremely difficult to measure EEV effects directly by single wavelength light scattering, and that over the accessible range of  $q^2 \langle S^2 \rangle$ ,  $1/I(q)$  may appear quite linear within experimental error, even for fairly large polymers [22].

**2. There is no Simple Relationship Between  $\langle S^2 \rangle$  and  $R_h$ .** The qualitative dependence of  $D$  on  $C_s$ , and  $\xi$  agrees with theories such as 'coupled modes' [23], but the limit of  $D$  at  $C_p=0$ ,  $D_0$ , is puzzling, and does not fall neatly into either of the limiting cases of 'free-draining' and 'non-free draining'. Figure 4 shows  $D$  vs.  $C_s$  for HA and NaPSS at different  $C_s$ .

As regards  $D_0$  (and hence  $R_h$  via  $D_0 = kT/6\pi\eta R_h$ ), three types of behavior have been observed: i)  $D_0$  is independent of  $C_s$  and  $\xi$  (HA [9], NaPAA [10], Chondroitin sulfate and heparin [12]), even though  $\langle S^2 \rangle$  is measured to be a smoothly changing function of  $C_s$  and  $\xi$ . ii) Behavior intermediate to i) and 'non-draining' was found for NaPSS [12] and poly-L-lysine (PLL) (Y. Tong and W.F. Reed, unpublished results). iii)  $1/D_0 \propto \langle S^2 \rangle^{0.5}$ , the 'non-draining' case, which behavior was exhibited by the 'bushy' PGM among the studied polyelectrolytes [18].

Cases i) and ii) do not seem easily explainable by current theories. Simple free-draining for case i) seems contradicted by the approximate scaling law of  $D_0 \propto M^{0.5}$  [12], which is the signature of the non-draining limit. For case ii), NaPSS gave  $D_0 \propto M^{0.3}$  for all  $C_s$ . Misinterpretation of the autocorrelation data due to the presence of internal modes also seems unlikely, since  $D_0$  follows the same trends even when extrapolated to zero scattering vector  $q$  [9,10,12].

A definitive solution to this puzzle is still lacking. Some type of draining effect seems to be implicated, and it is observed that the 'bald' polyelectrolytes, i.e. those such as HA and NaPAA which have no bulky sidegroups, tend towards case i), whereas PGM, which have long polysaccharide sidegroups attached to a protein backbone, falls into case iii), and NaPSS and PLL, which have slightly bulky sidegroups fall into the intermediate case ii). Figure 5 gives examples of  $D_0$  vs.  $C_s$  for each case.

In the meantime, it is important to realize that DLS measurements of many polyelectrolytes, even when extrapolated to  $C_p=0$ , may not accurately reflect their actual static dimensions. It should be noted that this is not an experimental ambiguity, such as may be caused by incomplete removal of aggregates/other particles at low  $C_s$ , but more of a refusal of polyelectrolytes to fall neatly within the limiting cases and theoretical approximations which seem to have worked well for neutral polymers in organic solvents.

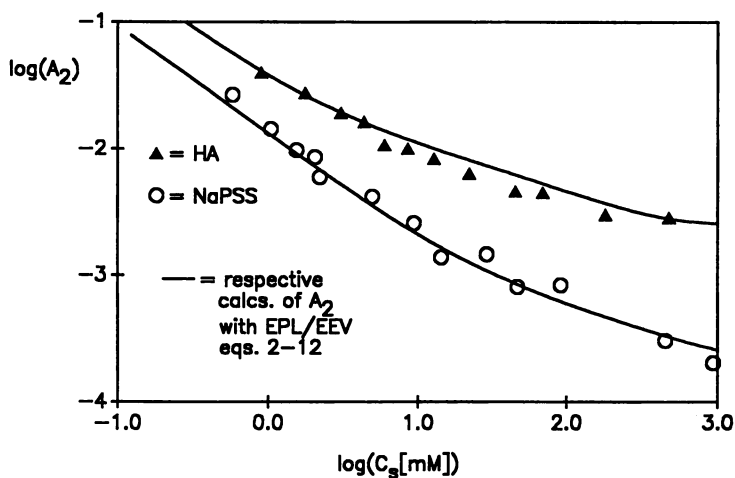


Figure 3.  $A_2$  (Mole-cm<sup>3</sup>/g<sup>2</sup>) vs.  $C_s$ , HA and NaPAA.

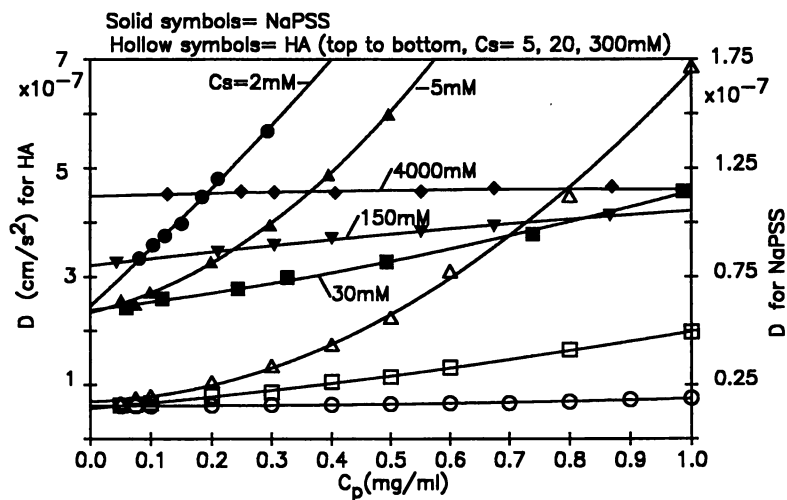


Figure 4.  $D$  vs.  $C_p$  at different  $C_s$  for hydrodynamic case i) HA and ii) NaPSS.

**3. Broad Angular Scattering Maxima are Sometimes Observed at Low Cs.** These scattering peaks of  $I(q)$  and  $1/D(q)$  at extremely low  $C_s$  and  $C_p$  have been observed by light scattering for several semi-flexible polyelectrolytes; PGM [18], NaPSS [24], NaPAA (Y. Tong, M. Rawiso and W.F. Reed, unpublished results), and others. With sufficient experimental care and cleanliness such maxima are probably observable for most polyelectrolytes.

Typical  $I(q)/Kc$  and  $1/D(q)$  vs.  $q$  plots for PGM are shown in Figure 6.  $q$  at the scattering maximum varied as  $C_p^{1/3}$  at mass concentrations of 0.06 to 0.32 mg/ml, and estimated corresponding volume fractions of 0.005 to 0.03. This  $C_p^{1/3}$  dependence is most simply interpreted in terms of cubic spacing, in which the average distance between (highly mobile) scatterers determines the location of  $q_p$ , and should apply for even anisotropic particles for  $C_p \ll C_p^*$ . When rod-like particles interact for  $C_p > C_p^*$  cylindrical 'packing' in two dimensions predicts  $q_p \propto C_p^{1/2}$ . Such a crossover from  $C_p^{1/2}$  to  $C_p^{1/3}$  in passing from overlapping to dilute solutions has been documented for rigid cylinders (tobacco mosaic virus [25]), DNA [26], and semi-flexible polyelectrolytes [27].

**The Existence of the Scattering Maximum Suggests Liquid-Like Correlations between Particles.** These correlations between nearest neighbors are most likely due to electrostatically enhanced volume of the polyelectrolytes.  $P(q)$  was obtained experimentally in reference 18, so that  $S(q)$  could be computed by equation 16.  $S(q)$  retained a peak. In this liquid-like correlation interpretation, the broad peak widths are due chiefly to the dynamic, mobile particles having large root mean square deviations from the average equi-distant Bragg spacing. Reference 28 used a simple effective square well potential whose radius  $R_{eff}$  depends on the strength of the electrostatic interactions between scatterers, which gives the broad, damped oscillations of equation 18. These correlations quickly disappear when  $C_s$  is increased and the effective volumes collapse. While long range order or 'domains' are not excluded, it is not necessary to invoke them to explain the peaks.

Whereas ordered phases in solutions of latex spheres [29,30] form at low hard volume fractions and low  $C_s$ , it is not obvious that such phenomena will occur for linear polyelectrolytes which are in general much less massive and have quite different spatial charge and mass distributions. In fact, as a qualitative observation, increasing the volume mass and charge density of the individual scatterers seems to increase the detectability and contrast of the scattering maxima. Latex spheres, for example, have such high optical contrast that video microscopy allows direct visualisation of their long range order. These systems are used as macroscopic analogues for studying solid state phenomena such as phase transitions, symmetries of long range order, two dimensional phenomena, defects, etc. [31,32].

**The Peaks for the Polyelectrolyte Appear Unrelated to Any 'Slow Mode' of Diffusion.** When a slow relaxation mode  $D_s(q)$  was present in the autocorrelation function of PGM at zero or very low  $C_s$ , for example, it could be filtered away with a  $0.1\mu\text{m}$  membrane filter and still the angular maxima of  $I(q)$  and  $1/D(q)$  remained [18]. As mentioned above, the same result has been recently found for succinoglycan (Morfin, Reed, Rinaudo and Borsali, manuscript



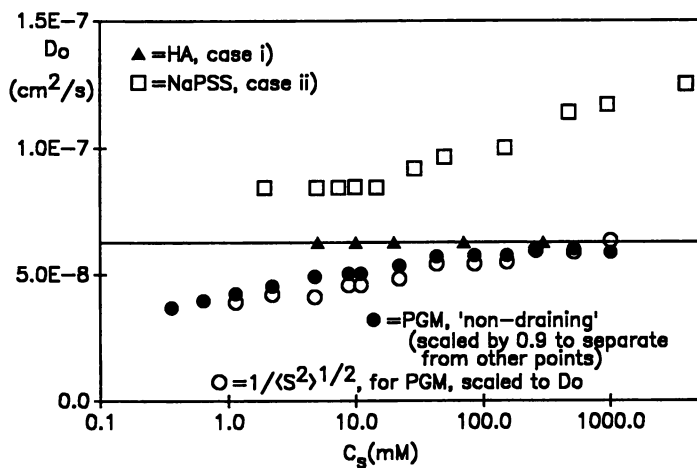


Figure 5.  $D_0$  vs.  $C_s$  illustrating case i) HA, case ii) NaPSS, and iii) PGM.

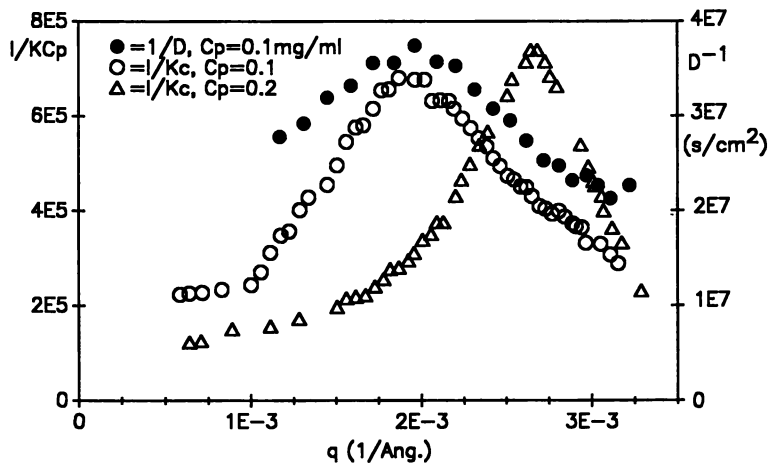


Figure 6.  $I/KC_p$  (units of grams/mole) and  $1/D(q)$  peaks for PGM.

submitted). The lack of any slow diffusive mode in the presence of  $I(q)$  and  $1/D(q)$  peaks further suggests that the peaks are due to highly mobile particles. The peaked  $1/D(q)$  for clean solutions of PGM and succinoglycan is quite different from that of the often reported, angularly flat or monotonically increasing  $D_r(q)$  for polyelectrolytes at low  $C_s$  [23,33, 34].

**4. Preliminary SEC Experiments Further Confirm EPL/EEV Approach.** Figure 7 is a three dimensional plot of  $\langle S^2 \rangle$  on the z-axis, vs.  $M$  and  $1/C_s^{0.5}$  on the x- and y-axes. The meshed surface shows the results of the EPL/EEV calculations according to the procedure outlined above, with no adjustable parameters. The data points are for HA from SEC/MALLS experiments, in which the system was equilibrated for at least 12 hours at the  $C_s$  of the eluant used.

The meshed surface lies astonishingly close to the experimental  $\langle S^2 \rangle$ , so that the applicability of the EPL/EEV approach to polyelectrolyte conformations is established with respect to  $M$ , as well as  $C_s$  and  $\xi$ .

### Summary

For polyelectrolytes in the coil limit  $\langle S^2 \rangle \propto \xi/C_s^{0.5}$  at moderate ionic strengths (0.001M to 1M). The apparent electrostatic persistence length  $L_e$  varies as  $\xi/C_s^{0.5}$  when extracted from equation 2 using  $\langle S^2 \rangle$  even for polymers not in the coil limit. Independent Monte Carlo results confirm this trend. This smooth behavior is fairly well described by combining the results of electrostatic persistence length and electrostatic excluded volume theories. The computations using these theories involve no adjustable parameters. The preliminary confirmation of the EPL/EEV theories against  $M$  using SEC further support their use. The future application of SEC in this direction may be important. The combined EPL/EEV theories also provide excellent predictions of  $A_2$  vs.  $C_s$  and  $\xi$ . The moderate success of the combined EPL/EEV theories may ultimately only represent an operationally viable computational procedure, and does not mean that such effects are in fact experimentally separable.

Since all these results were in the approximate range  $C_s = 0.001M$  to 1.0M, extrapolations of both experimental results and theoretical computations to lower  $C_s$  may not be valid. A recent assesment of the limitations of the conditions implicit in equation 3 for  $L_e$ , for example, indicate that semi-flexible polyelectrolytes may be much more flexible at very low  $C_s$  than equation 3 predicts (Barrat, J.L.; Joanny, J.F. submitted to *Eurorophysics Letters*). Only further experiments will tell.

At extremely low  $C_s$  interpolyelectrolyte correlations become strong, and are reminiscent of 'liquid-type' correlations.

The hydrodynamics of even isolated polyelectrolyte chains is complex and a theory which accounts for cases i) and ii) discussed above is desirable.

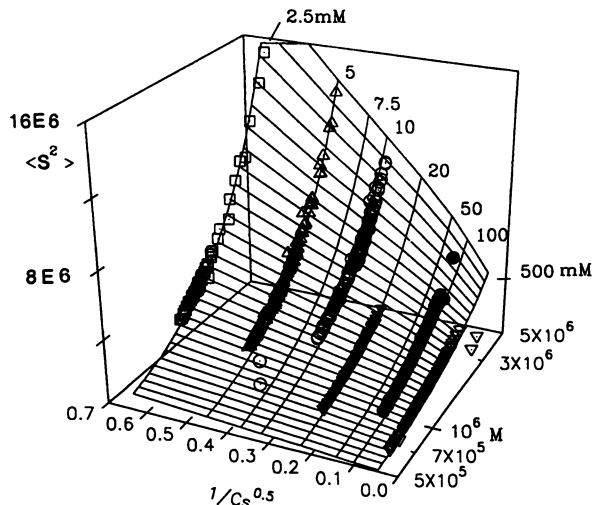


Figure 7. 3-D plot of  $\langle S^2 \rangle$  vs.  $1/C_s^{0.5}$  and  $\log(M)$ . The mesh is for EPL/EEV calculations with HA parameters (none adjustable), and the points are preliminary SEC/MALLS results for HA at the values of  $C_s$  indicated, for each iso-ionic curve.

#### Acknowledgments

Supported by NSF MCB 9116605, and Elf Aquitaine and the French Centre National de la Recherche Scientifique during the author's leave as Professeur de l'Academie des Sciences, 1992-93. The author acknowledges many co-workers, especially Chris Reed, Snehasish Ghosh, Robert Peitzsch, Xiao Li, Jeanne François, Redouane Borsali, Isabelle Morfin and Marguerite Rinaudo.

#### Literature Cited

1. Landau, L.D.; Lifshitz, E.M. *Course of Theoretical Physics, Part 1*, 3rd ed., Pergamon Press, N.Y., 1980, Vol. 5, Sect 127
2. Odijk, T. *J. Polym. Sci. Phys. Ed.*, 1977, 15, 477
3. Skolnick, J.; Fixman, M. *Macromole.*, 1977, 10, 9444.
4. Yamakawa, H. *Modern Theory of Polymer Solutions*; Harper & Row: N.Y.C., 1972
5. Reed, C.E.; Reed, W.F. *J. Chem. Physics*, 1990, 92, 6916
6. Gupta, S.K.; Forsman, W.C. *Macromole.*, 1972, 5, 779
7. Odijk, T.; Houwaart, A.C. *J. Polym. Sci. Phys. Ed.*, 1978, 16, 627
8. Fixman, M.; Skolnick, J. *Macromolecules*, 1978, 11, 8638
9. Ghosh, S.; Li, X.; Reed, C.E.; Reed, W.F. *Biopolymers*, 1990, 28, 1101 1101

10. Reed, W.F.; Ghosh, S.; Medjhadi, G.; François, J. *Macromole.*, **1991**, *24*, 6189
11. Reed, C.E.; Reed, W.F. *J. Chem. Physics*, **1991**, *94*, 8479
12. Peitzsch, R.M.; Burt, M.; Reed, W.F. *Macromole.*, **1992**, *25*, 806
13. Kirkwood, J.G.; Riseman, J. *J. Chem. Physics*, **1948**, *16*, 565
14. Debye, P. *Phys. Rev.*, **1947**, *71*, 486
15. Mulderje, J.J.H.; Jalink, H.L. *Macromole.*, **1987**, *20*, 1152
16. Doty, P.; Steiner, R.F. *J. Chem. Phys.*, **1952**, *20*, 85
17. Guinier, A. *X-Ray Diffraction in Drystals, Imperfect Crystals and Amorphous Bodies*; W.H. Freeman, N.Y., **1963**
18. Li, X.; Reed, W.F. *J. Chem. Physics*, **1991**, *94*, 4568
19. Felderhof, B.U. *J. Phys. A*, **1978**, *11*, 929
20. Ghosh, S.; Peitzsch, R.M.; Reed, W.R. *Biopolymers*, **1992**, *32*, 1105
21. Degiorgio, V.; Mantegazza, F.; Piazza, R. *Europhys. Lett.*, **1991**, *75*
22. Reed, C.E.; Reed, W.F. *J. Chem. Physics*, **1992**, *97*, 7766
23. Lin, S.C.; Li, W.I.; Schurr, M.J. *Biopolymers*, **1978**, *17*, 1041
24. Drifford, M.; Dalbiez, J.P. *J. Phys. Chem.*, **1984**, *88*, 5368
25. Maier, E.E.; Krause, R.; Deggelmann, M.; Hagenbüchle, M.; Weber, R.; Fraden, S. *Macromole.*, **1992**, *25*, 1125
26. Wang, L.; Bloomfield, V.A. *Macromole.*, **1991**, *24*, 5791
27. Krause, R.; Maier, E.E.; Deggelmann, M.; Hagenbuechle, M.; Schulz, S.F.; Weber, R. *Physica A*, **1989**, *160*, 135
28. Benmouna, M.; Weill, H.; Benoit, H.; Akcasu, Z. *J. Phys. (Paris)* **1982**, *43*, 1679
29. Krieger, I.M.; Hiltner, P.A. in *Polymer Colloids*, Editor, Fitch, R.M., Plenum Press, N.Y., **1971**
30. Ise, N. *Angew. Chem. Int. Ed. Engl.*, **1987**, *25*, 323
31. Murray, C.A.; Sprenger, W.O.; Wenk, R.A. *Phys. Rev. B*, **1990**, *42*, 668
32. Murray C.A., Ed. K. Strandbourg *Bond Orientational Order in Condensed Matter Systems*, Editor, K. Strandbourg, Springer Verlag, **1992**, Ch. 4
33. Förster, S.; Schmidt, M.; Antonietti, M. *J. Phys. Chem.*, **1992**, 4008
34. Schmitz, K. *Dynamic Light Scattering by Macromolecules*, Ch. 10 Academic Press **1990**

RECEIVED September 16, 1993

## Chapter 24

# Viscometric Behavior of Sodium Polygalacturonate in the Presence of Low Salt Content

A. Malovikova<sup>1</sup>, M. Milas<sup>2</sup>, M. Rinaudo<sup>2</sup>, and R. Borsali<sup>2</sup>

<sup>1</sup>Institute of Chemistry, Slovak Academy of Sciences, 84238 Bratislava, Slovakia

<sup>2</sup>Centre de Recherches sur les Macromolécules Végétales, Centre National de la Recherche Scientifique, and Joseph Fourier University, BP 53X, 38041 Grenoble Cédex, France

The dependency of the reduced viscosity as a function of the polyelectrolyte concentration is not yet well understood. This paper describes the viscometric behavior of low molar mass sodium polygalacturonates in the presence of very diluted salt concentrations; the reduced viscosity passes through a maximum whose location is predicted. At high salt concentrations, the intrinsic viscosity scales as  $C_S^{-1/2}$ ; this variation is related to the intrinsic persistence length of the molecule found equal to 90 Å for infinite salt content. The contribution of the polyelectrolyte chain to the ionic strength is controlled by  $C_p/\lambda$  where  $C_p$  is the polyelectrolyte concentration (expressed in equiv/l) and  $\lambda$  its charge parameter.

The viscosity of dilute solutions of polyelectrolytes was discussed for a long time but still their behavior is not yet well understood. When a solution is diluted, the reduced viscosity first decreases then passes through a minimum and increases. This increase was interpreted by the empirical Fuoss law (1). For very dilute solutions, usually a maximum exists as discussed previously by Pals and Hermans (2), and Goring and Rezanowicz (3). This maximum is shifted to higher polyelectrolyte concentration in the presence of low salt content ( $10^{-5}$  M -  $10^{-4}$  M). No definitive interpretation of this phenomenon is available today.

The same type of behavior is observed when isoionic dilution is used in order to get the intrinsic viscosity from linear extrapolation of the reduced viscosity at low ionic concentration. These two processes depend on the ionic concentration and exist whatever is the type of polyelectrolyte and even in non aqueous polar solvent (4-7).

This paper describes the viscometric behavior of low molar mass sodium polygalacturonates in dilute solutions.

### Experimental

Two samples of sodium Na- polygalacturonate (PGA) were used for this study. Sample 1 was prepared by alkali deesterification of commercial citrus pectin (Genu Pectin, Medium Rapid Set, Type A, Copenhagen, Denmark) and sample 2 was sodium salt of polygalacturonic acid from orange purchased from Sigma, U.S.A. Their characteristics are  $[\eta] = 93.3$  ml/g in

0097-6156/94/0548-0315\$06.00/0

© 1994 American Chemical Society

NaCl 0.1 M,  $\overline{M}_w = 25.500$  and 86% of galacturonic acid units for sample 1 and  $[\eta] = 85.7$  ml/g in NaCl 0.1 M,  $\overline{M}_w = 22.455$  and 95% of galacturonic acid units for sample 2. The polydispersity  $\overline{M}_w / \overline{M}_n$  is equal to 1.65 and 3.1 for samples 1 and 2 respectively.

The viscometer used was an Ubbelohde capillary and the experiments were performed at 25°C. All solutions have shown a newtonian behavior. For isoionic dilutions or dilutions in water the initial solution, at the concentration  $C \approx 7 \times 10^{-4}$  g/ml, was prepared with deionized and redistilled water and was progressively diluted with the same water or with the appropriate NaCl solutions.

The molecular weight distributions and  $\overline{M}_w$  values were obtained from gel permeation chromatography using a multidetection equipment as described in a previous paper (8).

## Results and discussion

**Isoionic dilution.** If one considers an initial polyelectrolyte concentration  $C_{pi}$  (expressed in equiv/l) in pure water, the dilution is performed with NaCl solution with molar concentration  $C_s$  such as  $X C_{pi} = C_s$ . Depending on the X value, the dilution gives for the reduced viscosity vs  $C_p$  a convex downwards curve "a", a linear dependence "b" or a concave upwards curve "c". If X is too low, one gets a curve of type "a"; if X is too high, the type "c" is obtained. For a given value of X which allows a dilution at a constant polyelectrolyte environment, one gets a linear dependency ("b"). An example is given in Figure 1 using sample 1.

Curve of type (b) corresponds to the isoionic dilution and is obtained with an average value of  $X \approx 0.77$  in this case. One suggests to relate this value to the free fraction of charge of this polyelectrolyte. The thermodynamics properties of polyelectrolytes are controlled by their charge parameter  $\lambda$  defined by the relation:

$$\lambda = \frac{ve^2}{DLkT}$$

where  $v$  is the number of ionic charge on a chain with a contour length  $L$ ;  $e$  is the electronic charge,  $D$  the dielectric constant and  $kT$  the Boltzmann term. From the chemical structure of PGA, one calculates the charge parameter and finds  $\lambda = 1.40$ ; from Manning theory, the uncondensed fraction of counterions is equal to  $1/\lambda$ . This will also contribute to the ionic strength of the solution and the Debye length  $K^{-1}$ .

The agreement between  $X$  and  $1/\lambda$  is good and allows a prediction of the isoionic condition given by  $C_T = \frac{C_p}{\lambda} + C_s$  ( $C_s$  the molarity of salt excess and  $C_T$  the total ionic concentration for monovalent electrolyte). This result is different from the conclusion of Pals and Hermans (2) who suggested that  $X$  should be equal to  $\phi$  ( $\phi$  = osmotic coefficient defined as the ratio between the experimental osmotic pressure and the theoretical one for a given polyelectrolyte solution in absence of external salt).

Then, following Hess and Klein (4,a) and Cohen et al (4,b) the reduced viscosity can be expressed by the relation :

$$\frac{\eta_{sp}}{C_p} \sim \frac{C_p}{K^3} \sim \frac{C_p}{(C_p/\lambda + C_s)^{3/2}} \quad (1)$$

Depending on the monomeric structure unit,  $C_p$  can be converted easily from equiv/l to g/ml.

In fact this relation corresponds to the Fuoss law in the absence of salt content i.e  $\frac{\eta_{sp}}{C_p} \sim C_p^{-1/2}$  and describes the linear dependence of the reduced viscosity with  $C_p$  in isoionic condition i.e at fixed environment. The slopes obtained from the dependence of the reduced viscosity on the polymer concentration are given in Table I. The ratio of the slopes

obtained for 2 different initial polymer concentrations are in very good agreement with the respective  $(C_T)^{-3/2}$  ratio as calculated using relation (1).

**Table I. Characteristic behavior of the polymer (sample 1) in isoionic dilution confirming the validity of relation (1)**

$C_T$	$(C_T)^{-3/2}$ (equiv/l) <sup>-3/2</sup>	Experimental slope (ml/g) <sup>2</sup>	Slope exp/ $(C_T)^{-3/2}$	$[\eta]_{ml/g}$	$k'$
$1.42 \times 10^{-3}$	18688	$0.5 \times 10^6$	26.75	80	78
$0.84 \times 10^{-3}$	41075	$1.05 \times 10^6$	25.56	95	110

$C_p$  equiv/l x 0.2 = C g/ml

The Na-polygalacturonate behaves as a polyelectrolyte with an effective charge proportional to  $1/\lambda$ . Then, from the above discussions, the linear dependence of the reduced viscosity and the relative value of the slopes of  $\eta_{red}(C)$ , the isoionic dilution must take into account the contribution of  $C_p/\lambda$ .

The role of the possible hydrolysis of the polyelectrolyte and the salt impurities in the water used for dilution do not perturb this conclusion at least under such experimental conditions i.e. presence of external salt.

**Dilution at low salt concentration.** In Figure 2 is plotted the variation of the reduced viscosity as function of polymer concentration at different salt concentrations ( $C_s$ ).

During dilution, in the domain of low polymer concentrations, the reduced viscosity increases then passes through a maximum at  $C_{max}$  and decreases again ; this sharp increase is usually interpreted in terms of Fuoss's relation :

$$\frac{\eta_{sp}}{C} = \frac{A}{1+B\sqrt{C}} \quad (2)$$

It is interesting to consider in which regime of polymer concentration these results are obtained. One can determine an overlap concentration  $C^*$  for this polyelectrolyte assuming fully extended chains :

$$C^* = \frac{Na \overline{M_w}}{4/3\pi(L/2)^3} = 1.52 \times 10^{-4} \text{ g/ml} \quad (3)$$

with  $L$  the contour length of the molecule deduced from the molecular weight.

In Table II, the values of the polyelectrolyte concentration of the maximum in the reduced viscosity are given for different salt concentrations ; for these data, it is shown that in water, if the molecule is assumed to be fully extended,  $C_{max}$  is lower than  $C^*$ .

We also calculate the intrinsic viscosity of the extended molecule assuming a cylindrical volume with a length  $L$  and a diameter  $d = 10 \text{ \AA}$ .

$$[\eta] = \frac{2}{3} Na \frac{V}{M} \Lambda(L/d) = 155 \text{ ml/g} \quad (4)$$

where  $\Lambda(L/d)$  is a function of the axial ratio  $L/d$  given by Broersma. (9)

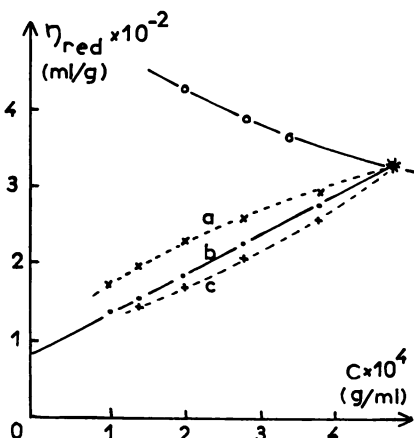


Figure 1. Variation of the reduced viscosity of sodium polygalacturonate as a function of polymer concentration diluted with pure water, O, and with different salt concentrations  $X C_{pi}$  with (a) :  $X = 0.6$ ; (b) :  $X = 0.75$ ; (c) :  $X = 0.9$  (sample 1).

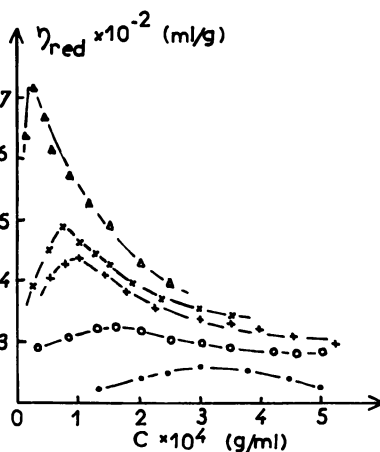


Figure 2. Variation of the reduced viscosity of sodium polygalacturonate as a function of polymer concentration at different NaCl concentrations ●,  $5 \times 10^{-4}$  M; ○,  $2 \times 10^{-4}$  M; +,  $1 \times 10^{-4}$  M; x,  $5 \times 10^{-5}$  M; Δ,  $1 \times 10^{-5}$  M (sample 1).



Table II. Values of the polymer concentration, the reduced viscosity and the ratio between polymer and NaCl concentrations at the maximum of the reduced viscosity as function of the NaCl concentration (sample 1)

$C_s \times 10^4$ (NaCl) mol/l	$C_p^{max} \times 10^5$ equiv/l	$(\eta_{sp}/C)^{max}$ ml/g	$C_p^{max}/C_s$
H <sub>2</sub> O	2.59	1178	-
0.1	9.55	720	9.55
0.5	27.0	485	5.40
1	39.7	440	3.97
2	63.6	320	3.18
5	119	255	2.38
7	191	219	2.73

$$C^* = 1.54 \times 10^{-4} \text{ g/ml} = 7.7 \times 10^{-4} \text{ equiv/l}$$

From this result and since the maximum of the reduced viscosity is found always higher than the calculated  $[\eta]$  (Table II) one directly understands that electroviscous effects between extended chains, having the same electrostatic charge, have an important impact on the behavior of dilute solutions. In addition, one can compare the Debye length  $K^{-1}$  (in absence of external salt) with the contour length of the molecule :

$$K^{-1} \approx 713 \text{ \AA} > L = 580 \text{ \AA} \quad (5)$$

In the range of polymer concentration corresponding to the peak, the molecule must be fully extended; these results are valid because of the low weight average molecular weight of the polymer sample.

From relation (1), the derivative allows to predict the position of the maximum for a given  $C_p^{max}/C_s$  :

$$C_p^{max} = 2\lambda C_s \quad (6)$$

where  $C_p$  and  $C_s$  are expressed in equiv/l.

The position of the maximum depends on the presence of external salt ( $C_s$ ). In Table II, are given the ratios  $C_p^{max}/C_s$  determined for each curve ; this ratio goes to a limit very close to  $2\lambda = 2.8$ . At very low salt content, experimental errors are not negligible and come from the estimation of possible hydrolysis or impurities (10) (about  $10^{-5}$  equiv/l from the pH and solvent conductivity).

**Role of the ionic concentration on the intrinsic viscosity.** The intrinsic viscosity of sample 2 was determined for various salt excess. The experimental values are given in Table III. The intrinsic viscosity decreases when ionic concentration increases following the relation :

$$[\eta]_{C_s} = [\eta]_{\infty} + S C_s^{-1/2}. \quad (7)$$

The slopes  $S$  depend directly on the flexibility of the chain. The intrinsic viscosity  $[\eta]_{\infty}$  obtained by extrapolation to infinite salt excess is assumed equivalent to  $[\eta]$  in  $\theta$ -conditions as previously discussed (11,12) ; considering Yamakawa-Fujii theory (13),  $[\eta]_{\theta}$  can be calculated from the wormlike chain model assuming a known value of the intrinsic persistence length ( $L_p$ ) :

$$[\eta]_{\theta} = \phi (Lr, dr) \left(\frac{M_L}{2Lp}\right)^{-3/2} M^{1/2} \quad (8)$$

**Table III. Variation of the intrinsic viscosity of polygalacturonate as function of salt concentration. Comparison between experimental and calculated values (sample 2)**

$C_s (M)$ (NaCl)	$[\eta]_{exp}^{ml/g}$	$[\eta]_{calc}^{ml/g}$	$\alpha_{\eta}^3$
0.01	122	118.3	1.40
0.05	92.3	93.6	1.221
0.1	85.7	84.8	1.166
0.2	81.5	77.8	1.089
$\infty$	69	70.75	
$L_p = 90\text{\AA}$	$L = 490\text{\AA}$	$M_L = 46 \text{ g/\AA}$	$\lambda = 1.55$

where  $Lr$  and  $dr$  are respectively the reduced values of the length and diameter of the chain ( $Lr = L/2 L_p$ ;  $dr = d/2L_p$ ),  $M_L$  the mass per unit length. The confrontation between the experimental value of  $[\eta]_{\infty}$  and calculated  $[\eta]_{\theta}$  allows the determination of  $L_p$ .

A good agreement is found for  $L_p = 90\text{\AA}$ . This value was also found for guluronic rich alginate (14) or pectins (15).  $L_p = 90\text{\AA}$  was also found to be more realistic to interpret the dependence of the radius of gyration as a function of the molecular weight (8). The values of  $[\eta]_{C_s}$  were also estimated from the analysis proposed by Odijk (16):

$$[\eta]_{C_s} = [\eta]_{\theta} \left(\frac{L_T}{L_p}\right)^{3/2} \alpha_{\eta}^3 (\phi_{C_s}/\phi_{\infty}) \quad (9)$$

where  $L_T$  is the total persistence length which takes into account also for the electrostatic contribution, the term  $(\phi_{C_s}/\phi_{\infty})$  accounts for the change in the draining when the ionic concentration changes, and  $\alpha_{\eta}$  is the expansion factor.

The calculated values are given in Table III and the agreement is good.

## Conclusion

This paper discusses the viscometric behavior of low molecular weight polygalacturonates in dilute solutions in absence and in presence of low salt concentrations. The large increase in the reduced viscosity is due to the long range electrostatic repulsions.

First, isoionic dilution is found to involve the contribution of a fraction  $1/\lambda$  (when  $\lambda > 1$ ) of the polyelectrolyte charge to the ionic concentration. Then the total ionic concentration  $C_T = C_p/\lambda + C_s$  controls the environment of the polyelectrolyte and experiments carried out satisfying this condition allows the linear extrapolation of  $n_{red}(C)$  and therefore the determination of  $[\eta]$  in the range of low salt concentrations.

Furthermore, when the polyelectrolyte is diluted with a salt solution, the reduced viscosity passes through a maximum at a given polymer concentration such as  $C_p/C_s = 2\lambda$  ( $C_p$  expressed in equiv/l). This result is also original and confirms the role of  $\lambda$  in the control of electrostatic behavior. Finally, the effect of the salt concentration on the intrinsic viscosity was analyzed and interpreted in terms of a wormlike chain model recently developed on hyaluronate (12). The validity of this treatment is again confirmed and the polygalacturonate is characterized by an intrinsic persistence length about  $90\text{\AA}$ .

**Literature cited**

- (1) Fuoss R.M. *J. Polym. Sci.* **1948**, *3*, 603 ; *ibid.* **1949**, *4*, 96.
- (2) Pals D.T.F., Hermans J.J. *Rec. Trav. Chim.* **1952**, *71*, 433.
- (3) Goring D.A.I., Rezanowich. A. *J. Colloid Sci.* **1960**, *15*, 472.
- (4)a. Hess W., Klein R. *Adv. Phys.* **1983**, *32*, 173
- b. Cohen J., Priel Z., Rabin T. *J. Chem. Phys.* **1988**, *88*, 7111
- (5) Yamanaka Y., Araie M., Matsioka H., Kitano H., Ise N., Yamaguchi T., Sacki, S. . Tsubokawa M. *Macromolecules* **1991**, *24*, 6156 .
- (6) Ganter J.L.M.S., Milas M., Rinaudo M. *Polymer* **1992**, *33*, 113
- (7) Malovikova A. , Milas M., Rinaudo M., Borsali R., *Polymer Preprint* **1993**, *34*, 1011.
- (8) Malovikova A. , .Milas M., . Rinaudo M. *Carbohydrate Polym.* **1993** (in press).
- (9) Broersma S., *J. Chem. Phys.* **1960**, *32*, 1626 .
- (10) Vink H. *Polymer* . **1992**, *33*, 3711 .
- (11) Rinaudo M. *Polym. Bull* **1992**, *27*, 585.
- (12) Fouissac E., Milas M., Rinaudo M., Borsali R. *Macromolecules* . **1992**, *25*, 5613
- (13) Yamakawa, H., . Fujii M. *Macromolecules* . **1974**, *7*, 128.
- (14) Rinaudo M. In "*Gums stabilisers for the food industry*" G.O. Philipp, D.J. Wedlock, P.A. Williams Ed ; IRL Press : Oxford, U.K., **1992**, Vol.6 ; 51-61
- (15) Axelos H., Thibault J.F. *Int. J. Biol. Macromol.* **1991**, *13*, 77.
- (16) Odijk T. *Biopolymers* . **1979**, *18*, 3111.

RECEIVED August 6, 1993

## Chapter 25

# Structure and Dynamics of Linear Flexible Polyelectrolytes in Salt-Free Solution as Seen by Light Scattering

Eric J. Amis<sup>1</sup>, Diane E. Valachovic<sup>1</sup>, and Marián Sedláčik<sup>1,2</sup>

<sup>1</sup>Department of Chemistry, University of Southern California, Los Angeles, CA 90089-0482

<sup>2</sup>Institute of Experimental Physics, Slovak Academy of Sciences, 043 53 Košice, Czechoslovakia

Two sets of light scattering experiments were performed on salt-free aqueous solutions of sodium poly(styrene sulfonate) (NaPSS): a molecular weight dependence study and a concentration dependence study (1, 2). In the first experiments, thirteen NaPSS samples of different molecular weight, ranging from  $M_w = 5\,000$  to  $1\,200\,000$ , were studied  $c = 10 - 45.6$  g/L. Two diffusion coefficients,  $D_f$  (fast) and  $D_s$  (slow), were observed for all systems. The fast diffusive mode is a coupled polyion-counterion diffusion that is dominated by counterion dynamics.  $D_f$  is found to be independent of molecular weight. The slow diffusive mode reflects the dynamics of large, multi-chain domains in solution. In contrast to the fast mode,  $D_s$  is molecular weight dependent as  $D_s \sim c^{-\nu}$ , where  $\nu \sim M_w^{\mu}$ . This molecular weight dependence contradicts the isotropic models of de Gennes and Odijk (3, 4). Apparent domain dimensions are calculated from angular dependencies of  $D_s$  and the scattered light intensity. Domain size is molecular weight independent. In the second study, the concentration dependence of polyelectrolyte solution behavior was examined for three NaPSS samples ( $M_w = 5\,000$ ,  $100\,000$  and  $1\,200\,000$ ) from  $c = 0.01 - 45.6$  g/L. A critical concentration  $c_{cr} \cong 0.5$  g/L was established and found to be independent of  $M_w$ . Above  $c_{cr}$  a strong polyion-counterion coupling exists and domains form in solution.  $D_f$  is independent of concentration, whereas  $D_s$  increases upon dilution. The excess intensity of scattered light ( $I$ ) exhibits a power dependency on concentration with an exponent slightly greater than 1. The angular dependence of the normalized reciprocal scattering intensity ( $I(0)/I(\theta)$ ) weakens as the domain size diminishes with dilution. At  $c = c_{cr}$  the angular dependence ceases. Below  $c_{cr}$  repulsive Coulombic interactions dominate solution structure.  $D_f$  decreases from high values and finally merges with  $D_s$ .  $I$  scales with concentration to a power much less than 1, and ( $I(0)/I(\theta)$ ) decreases with angle to form a broad minimum.

0097-6156/94/0548-0322\$06.00/0

© 1994 American Chemical Society

Both experimentally and theoretically, polyelectrolyte solutions have proven challenging to study due to the strong long-range electrostatic interactions within these systems. Polyelectrolyte solutions are multicomponent systems comprised of polymers with ionic substituents (polyions), the associated counterions, coions, and solvent. Polyions can be negatively or positively charged with counterions of opposite charge. Coions possess the same charge as the polyions and originate from the dissociation of low molecular weight salt in solution. The presence of low molecular weight salt strongly influences the behavior of polyelectrolytes. Ionic salt species electrostatically screen the charges along a polyion chain. At high-salt concentrations polyelectrolytes behave almost as neutral macromolecules in solution. However, low-salt or salt-free polyelectrolyte solutions exhibit rather unusual behavior.

**Experimental Observations on Salt-free Polyelectrolyte Solutions.** Using the technique of dynamic light scattering, Lin, Lee and Schurr (5) found that when the salt concentration in solution decreases below a certain critical level, the diffusion coefficient of charged macromolecules drops by more than an order of magnitude over a small change in added salt concentration. This steep reduction of the diffusion coefficient was described by the authors as an "ordinary-extraordinary" (O-E) transition, which gives reference to the extraordinary behavior of the diffusion coefficient seen at low salt concentrations. It was later found that for highly charged polymer chains below a critical salt concentration, the diffusion coefficient is actually split into two components (modes) rather than becoming depressed (6-8). The fast diffusive mode has been interpreted as the diffusion of polyions electrostatically coupled to dynamics of all charged species in solution, including counterions, coions, and the polyions themselves (6-8). This coupling phenomenon was described prior to the discovery of the O-E transition in order to explain the high diffusion coefficient values measured for charged molecules as compared to uncharged or highly salted molecules (9). The slow diffusive mode has been attributed to the presence of domains comprised of multiple chains in solution (6-8). Both the slow diffusion coefficient and the scattering intensity from moderately concentrated, salt-free polyelectrolyte solutions ( $c \sim 1$  to 100 g/L) possess angular dependencies that are characteristic for relatively large particles on the  $q^{-1}$  length scale (where  $q$  is the scattering vector  $q = (4\pi\eta/\lambda_0)\sin(\theta/2)$  with  $\eta$  the refractive index of the solvent,  $\lambda_0$  the wavelength of incident light *in vacuo*, and  $\theta$  the scattering angle). It is well known that light scattering on independent small polymer chains (molecular weights as low as 5 000) cannot possibly produce the angular dependence that is associated with the slow diffusive mode.

Other experimental results further confirm the unusual behavior of low-salt polyelectrolyte solutions. Small-angle x-ray scattering and small-angle neutron scattering (10-12) have been performed on polymers of a variety of compositions and all show a maximum in the angular dependency of the scattered radiation as the salt concentration is lowered. A molecular weight independent maximum in the concentration dependence of the reduced viscosity for low-salt solutions is also seen (13, 14). Regions of order and disorder have been microscopically observed within solutions of ionic latex particles (10). The existence of attractive forces necessary for creating ordered regions of particles within an otherwise randomly ordered latex solution has been suggested (10).

**Theoretical Models of Polyelectrolyte Behavior in Solution.** The first model for highly charged polyelectrolyte chain behavior was developed for dilute solutions (15). It was suggested that due to the unscreened electrostatic repulsion of like charges along the chain, the polyions are fully stretched as rigid rods and form a local ordered array of parallel close-packed chains. Recent experimental and

theoretical investigations showed that this is not the case. Instead chains are flexible to some degree.

De Gennes *et al.* used scaling concepts to develop the isotropic model (3). At the lowest concentrations, the polyelectrolyte chains are fully stretched and randomly oriented due to weak intermolecular interactions. At higher concentrations, the polyions form a three dimensional periodic lattice through electrostatic interactions. At still higher concentrations, chains bend, overlap, and form an entangled network with a characteristic correlation length  $\xi$ , which is similar to that in semidilute solutions of neutral polymers. Direct contacts between chains is not allowed due to the electrostatic repulsive interactions. Since there is no preferential orientation of the polyelectrolytes, the solution structure is isotropic.

Odijk (4, 16) further refined the isotropic model by introducing the concept of the electrostatic persistence length. The total persistence length of a chain ( $L_p$ ) is then defined as a sum of the electrostatic persistence length ( $L_e$ ) and an intrinsic persistence length ( $L_0$ ) for an uncharged chain. The theory is based on two assumptions: (i) the charges along one chain only increase its persistence length and do not effect its interactions with the surrounding chains and, (ii) uncondensed counterions only screen intramolecular electrostatic interactions. Two critical concentrations are introduced. The first concentration defines the point at which the stiff polyion chains begin bending to form a network ( $c_0^*$ ). Above a second critical concentration ( $c^{**}$ ) that is well within the semidilute region, the partially anisotropic net structure dissolves into a fully isotropic solution. The  $c^{**}$  concentration is defined by the equality  $L_e = \xi$ . For  $c < c^{**}$  the electrostatic persistence length of the polyion chain is much larger than the correlation length. This is equivalent to the chain inside the blob being fully stretched. For  $c > c^{**}$ ,  $L_e \ll \xi$ , and thus the chain inside the blob is flexible.

Witten and Pincus (17) considered polyion screening in addition to counterion screening. Their results show only one length-scale in solution as  $L_p \cong \xi \cong \kappa^{-1}$ , where  $\kappa^{-1}$  is the Debye-Hückel screening length.

A two-state, three-dimensional model for polyelectrolyte solutions was suggested by Ise (10). This model was developed in order to explain microscopically observed ordered domains of ionic latex particles within a disordered solution. Attractive forces required for domain formation are explained as the result of the presence of oppositely charged counterions between like-charged particles (18). The broad maxima seen in the angular dependencies of scattered radiation have been attributed to the three-dimensional ordering. While linear polyelectrolytes are too small to be seen by ultramicroscopy, it is assumed that the polyions possess relatively compact conformations due to intramolecular attractive forces and in some sense resemble the solution structure of ionic spherical particles.

The importance of counterions in the behavior of low-salt polyelectrolyte solutions has also been emphasized by Schmitz (6). In this model, the fluctuations in counterion distribution along the parent polyion induce dipole-dipole attractive interactions between polyions. The coupled polyion-polyion dynamics result in an extremely slow diffusive mode for low-salt polyelectrolyte solutions observed by dynamic light scattering.

The behavior of polyelectrolytes depends strongly upon several physical parameters: salt concentration (5-7, 10, 12), charge density on the chains (8, 19, 20), polyion concentration (7, 8, 10-14), dielectric permittivity of solvent (20), temperature (19), and polyion molecular weight (7, 8, 21). Although different molecular weight polyelectrolyte samples have been studied at various concentrations, a detailed investigation of the effect of molecular weight and concentration was missing. A thorough study of the molecular weight and polyion concentration effects on the fast and slow dynamic modes (1, 2) is presented in this paper.

## Experimental Section

Thirteen different samples of commercially prepared, relatively monodisperse ( $M_w/M_n < 1.1$ ) sodium poly(styrene sulfonate) (NaPSS), ranging in molecular weight from  $M_w = 5\,000$  to  $1\,200\,000$ , were chosen for this study (1, 2). The percentage of sulfonation (ratio of sulfonated units to the total number of monomer units) was in the interval of 85% to 100%. The actual effective charge density along the chains, is much less than these numbers due to counterion condensation. All samples were purified by mixed-bed ion-exchange resins to remove ionic impurities. Purified NaPSS samples were dissolved in deionized water (resistivity of 18 M $\Omega$  cm) and filtered through 0.2  $\mu$ m filters to remove dust particles before dynamic light scattering measurements.

Light scattering was performed on a modified commercial homodyne spectrometer, consisting of a Brookhaven Instruments BI200SM light-scattering goniometer and a BI2030AT multi-bit correlator with 264 channels. Static light scattering measurements were carried out by photon counting with a counter attached to the same experimental system.

Homodyne intensity and correlation functions were taken in a "multi-sample time" regime in which four different sample times were used simultaneously. By combining two "multi-sample time" functions, the resulting composite correlation functions ( $G^{(2)}(\tau)$ ) covered a broad time interval from 0.1  $\mu$ s to several seconds. Correlation curves were analyzed by the CONTIN program. Decay times and relative amplitudes of different modes were calculated from the moments of the distribution of relaxation times obtained by CONTIN analysis.

The majority of correlation functions were double exponentials, yielding fast and slow diffusive modes. The characteristic relaxation times were usually separated by several orders of magnitude. This separation allowed also a second order cumulant analysis of the "long time part" of the correlation curve. Figure 1 shows a typical example of a CONTIN analysis. Repeated fitting of the data by CONTIN and cumulant fits gave closely matched results. Diffusion coefficients were calculated from the decay times  $\tau$ , as  $D = \tau^{-1}q^{-2}$ .

## Molecular Weight Dependence of Polyelectrolyte Solution Behavior

The correlation functions for all molecular weight samples displayed double exponential behavior at relatively high polymer concentration ( $c = 45.6$  g/L). Figure 2 shows the molecular weight dependence of two diffusion coefficients associated with two diffusive modes: a relatively fast one ( $D_f$ ) and a relatively slow one ( $D_s$ ). For clarity of presentation, the discussion will be divided into two parts: (i) solution dynamics associated with  $D_f$  and (ii) solution dynamics associated with  $D_s$ .

**Solution Dynamics Associated with  $D_f$ .** Figure 3 clearly shows that the fast process is diffusive as the relation  $\tau_f^{-1} = D_f q^2$  holds. Since the contribution of the fast mode to the total scattered light intensity for the lowest molecular weight samples was very small ( $\sim 5\%$ ), precise values of  $D_f$  were difficult to obtain. Therefore, a dashed line is drawn in the low molecular weight region in Figure 2. A striking feature of the molecular weight dependence of  $D_f$  is that the diffusion coefficient remains constant while  $M_w$  changes several orders of magnitude. This indicates that  $D_f$  is not affected significantly by chain hydrodynamics. Instead, the coupling of polyion and counterion dynamics is the dominant effect resulting in  $D_f$ . The coupled-diffusion theories predict that under some circumstances highly charged polyions can diffuse at the same rate as their counterions. In reality, our  $D_f$  values are slightly lower than the diffusion coefficient  $D_c$  of a  $\text{Na}^+$  counterion ( $5.5 \times 10^{-6}$

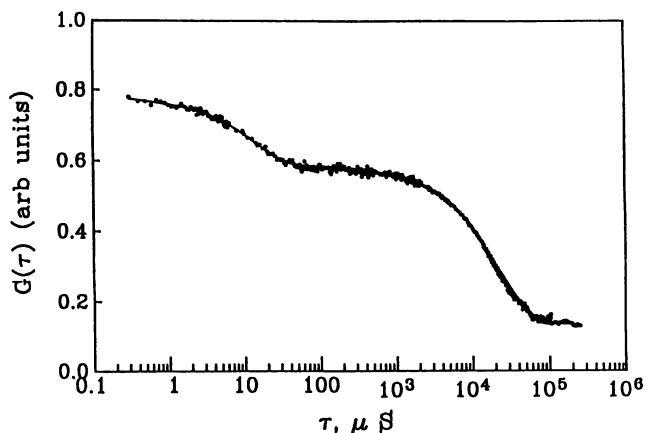


Figure 1. Example of a composite correlation function  $g^{(1)}(\tau)$  covering several decades of time. The  $g^{(1)}(\tau)$  data is overlaid by the fit obtained by the CONTIN program. Composite correlation functions were obtained by the combination of two "multi-sample time" correlation functions.

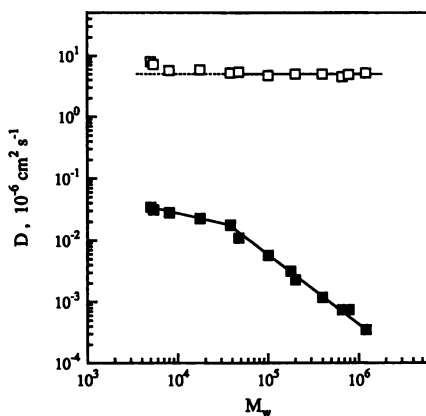


Figure 2. Dependence of fast diffusion coefficient,  $D_f$  ( $\square$ ), and the slow diffusion coefficient,  $D_s$  ( $\blacksquare$ ), on molecular weight.  $c = 45.6$  g/L;  $\theta = 90^\circ$ .



$\text{cm}^2\text{s}^{-1}$  vs.  $2 \times 10^{-5} \text{ cm}^2\text{s}^{-1}$ ). For the conditions of our experiments simple coupled-diffusion theory gives  $D_f = D_c/2$ , which is still a factor of two faster than our measurement value. Nevertheless, the independence of  $D_f$  on  $M_w$  can be understood qualitatively based on the coupled-diffusion concept.

At fixed polymer concentration  $c = 45.6 \text{ g/L}$ , the lowest molecular weight sample is not entangled for purely geometrical reasons. The highest molecular weight sample, though, is expected to be entangled, unless the chains are completely collapsed. Therefore, a  $c^*$  crossover concentration, or equivalent  $M_w^*$  at fixed concentration, is reached within the range we have investigated. This is not reflected in  $D_f$  behavior. For low molecular weight samples  $D_f$  could correspond to motion of individual isolated polyions. For high molecular weight samples,  $D_f$  corresponds to counterion accelerated motion of segments of chains (blobs) in an entangled network.

**Solution Dynamics Associated with  $D_s$ .** The relaxation time  $\tau_s$  associated with the slow diffusive process does not follow a  $q^2$  dependence as  $\tau_f$  does. Instead,  $\tau_s$  follows the relation  $\tau_s^{-1} = aq^2 + bq^4$ . The slow apparent diffusion coefficient (calculated as  $D_s = \tau_s^{-1}q^{-2}$ ), therefore, possesses a linear angular dependence as shown in Figure 3. We note that the extrapolation of  $D_s$  in Figure 3 to zero angle does not pass through the origin as it would if  $\tau_s$  had a  $q^3$  dependence that is characteristic of internal relaxation modes. The angular dependence of  $D_{\text{app}}$  has previously been predicted and experimentally measured (23) for particles with a radius of gyration  $\langle S^2 \rangle^{1/2} \cong q^{-1}$ . In this case,  $D_{\text{app}}$  obeys the formula

$$D_{\text{app}} = D_0(1 + C \langle S^2 \rangle_{\text{app}} q^2) \quad \text{for } q(\langle S^2 \rangle_{\text{app}}^{1/2}) \leq 1 \quad (1)$$

where  $D_0$  is the diffusion coefficient in the  $q \rightarrow 0$  limit and the coefficient  $C$  is sensitive to the scatterer's structure. Maximum and minimum values of  $C$  correspond to polydisperse chains with a most probable length distribution ( $C = 0.200$ ) and monodisperse infinite arm star molecules ( $C = 0.098$ ). For monodisperse linear chains  $C = 0.173$  (23).

Apparent radii of gyration were calculated from angular dependencies of  $D_s$  using marginal values of  $C$  ( $C = 0.098$  and  $0.200$ ) and also from static light scattering measurements using the following formula:

$$P(\theta)^{-1} \cong 1 + 1/3 (\langle S^2 \rangle_{\text{app}}) q^2 \quad q \rightarrow 0 \quad (2)$$

where  $P(\theta)$  is the particle structure factor and the slope of  $1/3$  is independent of the internal structure of the scatterers.

A summary of  $\langle S^2 \rangle_{\text{app}}^{1/2}$  values for different molecular weight NaPSS samples are listed in Table I. Systematically lower values of the apparent radius of gyration are obtained from DLS for the range of theoretical  $C$  values as compared to those values obtained from SLS. It should be noted that this discrepancy has also been reported for neutral isolated molecules in dilute solution (23). Qualitatively, the results obtained from static and dynamic measurements in our study are the same. The  $\langle S^2 \rangle_{\text{app}}^{1/2}$  values calculated from static and dynamic methods also possess very similar molecular weight dependence (Figure 4). The theoretical  $C$  values may simply be too high. It should be noted here that equations (1) and (2) are derived for isolated particles in dilute solutions. This condition may not hold true for domains. Radii of gyration are thus apparent values which are still useful in determining relative sizes of correlated regions within solution.

Relatively large values of  $\langle S^2 \rangle_{\text{app}}^{1/2}$  are calculated for even the lowest molecular weight ( $M_w = 5000$ ; degree of polymerization of only 24). These small chains, if fully extended, would have lengths of 6 nm. Clearly, the apparent radii of

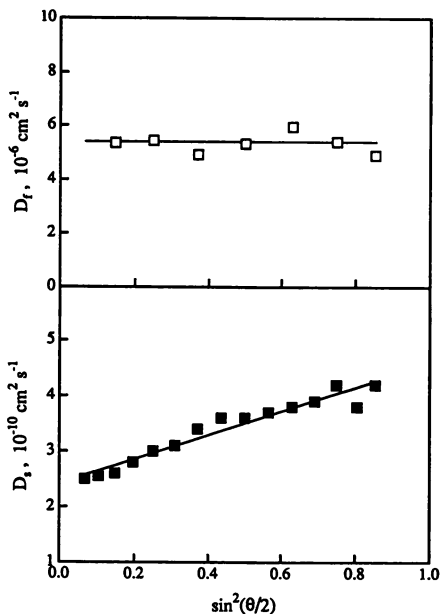


Figure 3. Dependence of diffusion coefficients  $D_f$  (□) and  $D_s$  (■) on scattering angle  $\theta$ .  $M_w = 1\,200\,000$ ;  $c = 45.6 \text{ g/L}$ .

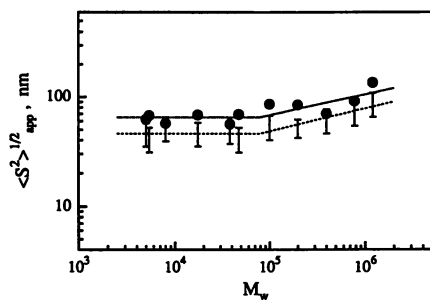


Figure 4. Dependence of apparent radius of gyration ( $\langle S^2 \rangle^{1/2}_{\text{app}}$ ) from static (●) and dynamic (○) light scattering on chain molecular weight. Bars indicate the range of values from the limits of the theoretical expression.  $c = 45.6 \text{ g/L}$ .

gyration that correspond to the slow diffusive mode reflect the size of domains (clusters) comprised of individual molecules within solution. Domains of a size of 50 nm have also been measured in salt-free solutions of poly(methacrylic acid) (PMA) (8). The radius of gyration of a single chain  $\langle S^2 \rangle^{1/2} = 5.3$  nm was reported by SANS (24), using deuterium labeled PMA under the same experimental conditions. This strongly indicates that  $\langle S^2 \rangle^{1/2}_{app}$  measured by DLS and SLS correspond to multi-chain domains.

**Table I.** Values of Apparent Radius of Gyration for Different Molecular Weight Samples at  $c = 45.6$  g/L

$M_w$ ( $10^3$ g mole $^{-1}$ )	$a\langle S^2 \rangle^{1/2}_{app}$ (nm)	$b\langle S^2 \rangle^{1/2}_{app}$ (nm)	
		$C = 0.2$	$C = 0.098$
5.4	67	31	52
8	57	39	65
17.4	68	35	58
38.2	56	37	61
47.3	69	31	52
100	85	40	67
200	84	32	54
400	70	46	77
780	91	54	90
1 200	135	65	109

<sup>a</sup> Determined from static light scattering

<sup>b</sup> Calculated from  $q$  dependence of  $D_s$  from dynamic light scattering for two limiting values of  $C$  constant in Eq. (1).

The dimensions of the domains ( $\langle S^2 \rangle^{1/2}_{app}$ ) do not have a strong molecular weight dependence as seen in Figure 4 for  $c = 45.6$  g/L. In order for the domain size to stay relatively constant over the broad range of molecular weights, more of the lower molecular weight (smaller) chains must be present within the domain compared to higher molecular weight (larger) chains. An explanation for the constant domain size may arise from the model that counterions play a key role in the domain formation process. Just as the domain dimensions are independent of molecular weight, the molar concentration of counterions is independent of chain molecular weight for the same polymer concentration. As will be discussed below, dimensions of domains change with polymer concentration.

From comparison of Figures 2 and 4 it can be seen that the slow diffusion coefficient changes two orders of magnitude while  $\langle S^2 \rangle^{1/2}_{app}$  remains constant. This indicates that the slow diffusion does not correspond to a simple Brownian diffusion of permanent aggregates through solution.

Figure 2 shows a discontinuity at  $M_w = 40$  000, where the slope of the dependence changes from -0.3 to -1.1. We do not currently have any explanation for this observation. A much weaker and possibly related discontinuity might be

recognized at  $M_w \cong 70\,000$  in Figure 4. This discontinuity in  $D_s$  clearly does not correspond to a dilute-semidilute transition. The position of the discontinuity does not change with concentration.

### Concentration Dependence of Polyelectrolyte Solution Behavior

The concentration dependencies of both the static and dynamic behavior were examined for salt-free solutions of NaPSS over the concentration range of  $c = 0.01$  to  $45.6$  g/L. To interpret correctly experimental data, it was necessary to determine the concentration regimes studied. The calculation of an overlap concentration:

$$c^* = M_w / [(4/3)\pi N_A \langle S^2 \rangle^{1/2}]^3 \quad (3)$$

where  $N_A$  is Avogadro's number, requires the value of the radius of gyration of a chain. This poses a problem, since the actual chain conformation of polyions in solution is still a highly discussed issue. Results from calculations of the electrostatic persistence length depend on the model of the chain and on the method of calculation of the Debye-Hückel screening length (25). As indicated in the previous paragraph, the broad ranges of molecular weight and concentration used in this work are expected to cover both dilute and semidilute regimes, although an accurate calculation of  $c^*$  is not possible.

**Behavior of the Fast Diffusive Mode.** Figures 5-7 show the concentration dependencies of  $D_f$  and  $D_s$  for NaPSS samples of  $M_w = 5\,000$ ,  $100\,000$  and  $1\,200\,000$ . Only the slow diffusion coefficient  $D_s$  is shown for the  $M_w = 5\,000$  sample, due to the difficulty in obtaining precise fast diffusion coefficient  $D_f$  values. Figure 8 shows results for  $D_f$  obtained from the other molecular weight samples.

These figures clearly show that at relatively high concentrations  $D_f$  is found to be independent of concentration. From Figures 6 and 7 it can be seen that the fast diffusion coefficient continues to be independent of polyion concentration for  $c = 0.5$  to  $45$  g/L. However, below  $c = 0.5$  g/L,  $D_f$  decreases from the relatively high values, arising from counterion coupling, to lower values, more typical for polymer chains. The fast mode finally merges with the slow mode at  $c \cong 0.01$  g/L.

The behavior of  $D_f$  at high concentrations remains independent of concentration, even though two distinct solution regimes were included because of the broad range of molecular weights studied. For high concentrations of low molecular weight samples, entanglements are not expected. However, solutions of high molecular weight samples at the same concentrations must contain entanglements. Coupled-diffusion theories (25) are consistent with the low molecular weight result. The coupled-diffusion coefficient is dependent only on the ratio of polyion to counterion concentration, which is equal to the polyion effective charge. The fast mode for the high molecular weight samples cannot be identified as a gel mode of the transient network. In this case  $D_f$  would be expected to increase with concentration. The isotropic model (4) predicts  $D \sim 1/\zeta \sim c^{1/2}$  or  $\sim c^{3/8}$ . Evidently, the electrostatic coupling effect is very pronounced and overwhelms the chain hydrodynamics.

The decrease of  $D_f$  below  $c = 0.5$  g/L corresponds to a decoupling of polyion and counterion dynamics. As polymer concentration decreases, the free counterions are less and less in the neighborhood of polyions since there is more space to diffuse away. As a result, the polyions at lower concentrations experience less of an influence by the ion cloud responsible for the fluctuations of the local electric field. Theoretical expressions for the coupled-diffusion coefficient predict no concentration dependence. This discrepancy might be caused by the fact that the derivation of the formula for coupled-diffusion coefficient (25) requires fluctuations

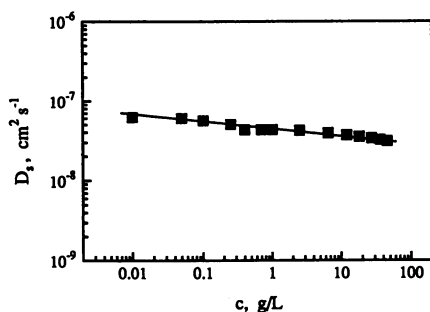


Figure 5. Dependence of the slow diffusion coefficient,  $D_s$  (■), on concentration.  $M_w = 5\,000$ ;  $\theta = 90^\circ$ .

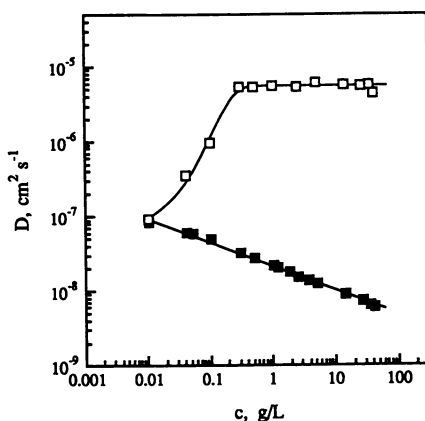


Figure 6. Dependence of the fast diffusion coefficient,  $D_f$  (□), and slow diffusion coefficient,  $D_s$  (■), on concentration.  $M_w = 100\,000$ ;  $\theta = 90^\circ$ .

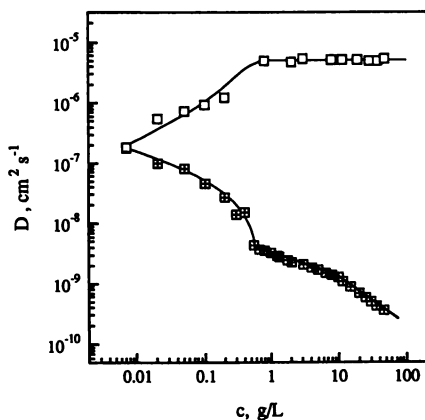


Figure 7. Dependence of the fast diffusion coefficient,  $D_f$  (□), and slow diffusion coefficient,  $D_s$  (■), on concentration.  $M_w = 1\,200\,000$ ;  $\theta = 90^\circ$ .

in concentration of ionic species which are much smaller than the average value. This requirement holds in relatively concentrated solutions, but not necessarily in more dilute ones.

**Behavior of the Slow Diffusive Mode.** Figures 5-7 and Figure 9 demonstrate that in general  $D_s$  tends to decrease with increasing concentration. The higher the molecular weight, the more pronounced the decrease. At higher concentrations ( $c > 10$  g/L) the concentration dependence of  $D_s$  follows the power relation  $D_s \sim c^{-\nu}$  where  $\nu \sim M_w^\mu$  ( $\mu = 0.35$ ). The empirical relationship between  $D_s$ ,  $c$  and  $M_w$  can be written as

$$D_s = c^{-b} M_w^\mu \quad (4)$$

with  $b = 0.0061$ . This contradicts the expectation of the isotropic model based on scaling arguments (3, 4). According to the model, the concentration scaling of the behavior of an entangled polyelectrolyte solution should not depend on molecular weight. The assumption of the isotropic model is that electrostatic interactions are important at length scales equal to or smaller than  $\xi$  for our concentration region. Present experimental results show that interactions on a much larger scale than  $\xi$  are substantial and that the molecular weights of individual coils are still "recognized" within the network. These large-scale interactions are considered to give rise to domains.

At lower concentrations ( $c < 10$  g/L) the trend of increasing  $D_s$  with dilution continues steadily for samples with  $M_w = 5\,000$  and  $100\,000$  (Figures 5, 6). The slow diffusion coefficient of the  $M_w = 1\,200\,000$  sample also increases upon dilution, yet displays two distinct discontinuities in the slope (Figure 7). At the first discontinuity (near  $c \cong 10$  g/L) the exponent of the power dependence changes, whereas at the second transition ( $c \cong 0.5$  g/L)  $D_s$  rapidly increases. Discontinuities similar to the one at  $c \cong 10$  g/L for the  $M_w = 1\,200\,000$  sample are reported for the slow diffusion coefficients of poly(methacrylic acid) (PMA) of  $M_w = 400\,000$  at  $c \cong 4$  g/L (8) and for NaPSS of  $M_w = 100\,000$  at  $c \cong 8$  g/L (26). Currently, we have no explanation for this discontinuity (1, 2). The discontinuity at  $c = 0.5$  g/L will be discussed in detail below.

**Behavior of the Scattered Light Intensity.** Figure 10 shows the concentration dependencies of scattering intensities for the  $M_w = 100\,000$  sample. Qualitatively the same results were obtained for  $M_w = 5\,000$  and  $M_w = 1\,200\,000$  (1, 2). All intensities show a transition at  $c = 0.5$  g/L, which is similar to the changes in diffusion coefficients at  $c = 0.5$  g/L. This indicates that there is a critical concentration  $c_{cr} = 0.5$  g/L at which the solution behavior changes qualitatively. The slopes of  $\log I$  vs.  $\log c$  dependencies for  $c > c_{cr}$  are not strongly influenced by molecular weight, whereas for  $c < c_{cr}$ , the higher the molecular weight, the smaller the slope. This is seen for  $I \sim c^a$ , where  $a = 1.08, 1.15,$  and  $1.26$  for  $c > c_{cr}$ , and  $a = 0.57, 0.45,$  and  $0.26$  for  $c < c_{cr}$  in order of increasing molecular weight, respectively.

It follows from the general light scattering theory (27) that the total scattered light intensity ( $I_t$ ) from non-interacting scatterers is linearly proportional to the number of particles in the scattering volume. Hence,  $I_t$  is linearly proportional to the solution concentration, and scales with concentration by the relation  $I \sim c^a$ , where  $a = 1$ . Interactions effect the total scattering, leading to either a lower or higher scattering intensity as compared to the sum of scattering intensities for a collection of individual particles. This effect is referred to as interparticle or intermolecular interference. Repulsive interactions result in a lower total intensity ( $a < 1$ ), while attractive interactions lead to  $a > 1$ . The same conclusion can be made also from a thermodynamic approach to light scattering (1, 2).

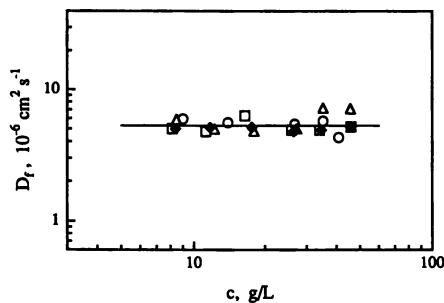


Figure 8. Concentration dependence of the fast diffusion coefficient,  $D_f$ , for molecular weights: ( $\Delta$ ) 5 000; ( $\square$ ) 38 200; ( $\circ$ ) 100 000; ( $\blacklozenge$ ) 1 200 000.

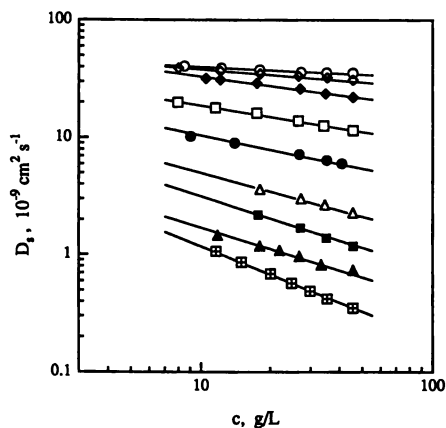


Figure 9. Concentration dependence of the apparent slow diffusion coefficient,  $D_s$ , for molecular weights: ( $\circ$ ) 5 000; ( $\diamond$ ) 5 400; ( $\blacklozenge$ ) 17 400; ( $\square$ ) 47 300; ( $\bullet$ ) 100 000; ( $\Delta$ ) 200 000; ( $\blacksquare$ ) 400 000; ( $\blacktriangle$ ) 780 000; ( $\boxtimes$ ) 1 200 000.

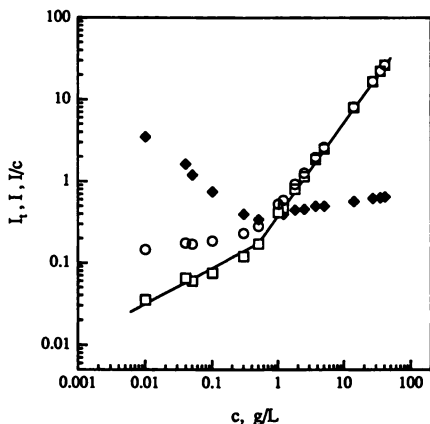


Figure 10. Concentration dependence of total scattering intensity  $I_t$  ( $\circ$ ), excess scattering intensity  $I$  ( $\square$ ) (after subtraction of solvent scattering) and reduced intensity  $I/c$  ( $\blacklozenge$ ) ( $c$  is concentration in  $\text{g/L}$ ).  $M_w = 100\,000$ . Intensities are extrapolated to zero angle and normalized by the scattering intensity of a benzene standard.

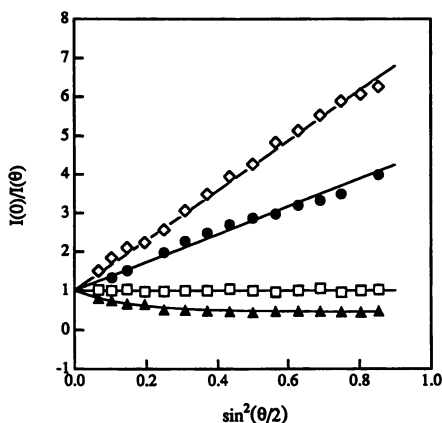


Figure 11. Dependence of the normalized reciprocal excess scattering intensity on scattering angle.  $M_w = 1\,200\,000$ . Concentrations: ( $\diamond$ )  $45.6\text{ g/L}$ , ( $\bullet$ )  $11.6\text{ g/L}$ , ( $\square$ )  $0.4\text{ g/L}$ , and ( $\blacktriangle$ )  $0.01\text{ g/L}$ .



For  $c > c_{cr}$ , the total scattered light intensity is dominated by the slow mode and it thus follows the ratio of the relative scattering amplitudes  $A_s$  and  $A_f$  with  $A_s \gg A_f$ . Values of the exponent  $a$  are close to 1, indicating that domains are relatively independent scatterers that show some weak correlations between domains. The fact that the exponent  $a$  is slightly larger than 1 reflects again the increasing size of domains with increasing concentration. This is demonstrated in Figure 11. For  $c < c_{cr}$  the domains gradually "dissolve" and a liquid-like ordering begins to dominate the solution structure, giving rise to broad minima in reciprocal scattering intensity (Figure 11 and references 22, 28). Screened repulsive interactions between polyions result in a small value of the exponent  $a$ . The larger the molecular weight, and hence the polyion charge, the smaller the exponent  $a$ .

## Conclusion

A regime description of the concentration and molecular weight dependence of salt-free NaPSS solutions based on light scattering results can be considered. Three regimes are distinguished. At very low concentrations (regime III), intermolecular interactions are very weak due to large separations between polyions. A concentration-independent angular dependence of the scattering intensity corresponding to the chain form factor is obtained (28). With increasing concentration the intermolecular interactions between polyions strengthen and result in strong correlations between their positions (regime II). This is reflected in a maximum in the angular dependence of scattering intensity (22, 28), a minimum in the angular dependence of the effective diffusion coefficient (22), and weak concentration dependence of total scattering intensity (1, 2). A further increase of concentration above a critical value  $c_{cr}$  results in formation of multichain domains and a strong coupling of polyion and counterion dynamics (regime I). This results in the presence of two diffusive modes, in pronounced angular dependencies of the scattering intensity and the slow diffusion coefficient, and in a strong concentration dependence of the scattering intensity. The critical concentration  $c_{cr}$  is independent of molecular weight. The molecular weight dependence of the transition from regime III to regime II cannot be established fully because of lack of experimental data for lower molecular weights. Light scattering experiments probing the structure and dynamics of solutions at length scales proportional to  $q^{-1}$  do not give any indication of a dilute-semidilute transition. This is because the chain hydrodynamics are overwhelmed by electrostatic effects.

## Acknowledgement

This work was supported by the Petroleum Research Fund administered by the American Chemical Society.

## Literature Cited

- 1 Sedláč, M.; Amis, E. J. *J. Chem Phys.* **1992**, *96*, 817.
- 2 Sedláč, M.; Amis, E. J. *J. Chem Phys.* **1992**, *96*, 826.
- 3 de Gennes, P. G.; Pincus, P.; Velasco, R. M.; Brochard, F. *J. Physique* **1976**, *37*, 1461.
- 4 Odijk, T. *Macromolecules.* **1979**, *12*, 688.
- 5 Lin, S. C.; Lee, W. I.; Schurr, J. M. *Biopolymers* **1978**, *17*, 1041.
- 6 Schmitz, K. S.; Lu, M.; Gauntt, J. J. *Chem. Phys.* **1983**, *78*, 5059.
- 7 Drifford, M.; Dalbiez, J. P. *Biopolymers* **1985**, *24*, 1501.
- 8 Sedláč, M.; Koňák, Č.; Štěpánek, P.; Jakeš, J. *Polymer* **1987**, *28*, 873.

- 9 Schmitz, K. S. *An Introduction to Dynamic Light Scattering by Macromolecules*; Academic Press, Inc.: San Diego, CA, 1990.
- 10 Ise, N. *Angew. Chem. Int. Ed. Engl.* **1986**, *25*, 323.
- 11 Kaji, K.; Urukawa, H.; Kanaya, T.; Kitamaru, R. *J. Phys. (Paris) Colloq.* **1988**, *49*, 993.
- 12 Nierlich, M.; Williams, C. E.; Boue, F.; Cotton, J. P.; Daoud, M.; Farnoux, B.; Jannink, G.; Picot, C.; Moan, M.; Wolff, C.; Rinaudo, M.; de Gennes, P. G. *J. Phys.* **1979**, *40*, 701.
- 13 Fuoss, R. M. *J. Polym. Sci.* **1949**, *3*, 603. and *J. Polym. Sci.* **1949**, *4*, 96.
- 14 Cohen, J.; Priel, Z.; Rabin, Y. *J. Chem. Phys.* **1988**, *88*, 7111.
- 15 Lifson, S.; Katchalsky, A. *J. Polym. Sci.* **1954**, *13*, 43.
- 16 Odijk, T. *J. Polym. Sci. Polym. Phys. Ed.* **1977**, *15*, 477.
- 17 Witten, T.; Pincus, P. *Europhys. Lett.* **1987**, *3*, 315.
- 18 Sogami, I.; Ise, N. *J. Chem. Phys.* **1984**, *81*, 6320.
- 19 Sedlák, M.; Koňák, Č.; Štěpánek, P.; Jakeš, J. *Polymer* **1990**, *31*, 253.
- 20 Sedlák, M.; Koňák, Č.; Labský, J. *Polymer* **1991**, *32*, 1688.
- 21 Förster, S.; Schmidt, M.; Antonietti, M. *Polymer* **1990**, *31*, 781.
- 22 Drifford, M.; Dalbiez, J. P. *J. Phys. Chem.* **1984**, *88*, 5368.
- 23 Burchard, W. *Adv. Polym. Sci.* **1983**, *48*, 1.
- 24 Pleštil, J.; Ostanevich, Yu. M.; Bezzabotov, V. Yu.; Hlavatá, D.; Labský, J. *Polymer* **1986**, *27*, 839.
- 25 Schmidt, K.S.; *Macroions in Solution and Colloidal Dispersion*, VCH Publishers 1993.
- 26 Drifford, M.; Dalbiez, J. P. *J. Phys. Lett.* **1985**, *46*, L311.
- 27 Kratochvil, P. *Classical Light Scattering From Polymer Solutions*; Elsevier: Amsterdam, 1987.
- 28 Krause, R.; Maier, E.E.; Deggelmann, M.; Hagenbuchle, M.; Schulz, S.F.; and Weber, R. *Physica A*, **1989**, *160*, 135.

RECEIVED August 6, 1993

## Chapter 26

# Extraordinary Behavior of Salt-Free Solutions of Strongly Charged Polyelectrolytes

Marián Sedlák

Institute of Experimental Physics, Slovak Academy of Sciences, 043 53  
Košice, Slovakia

The extraordinary behavior of salt-free polyelectrolyte solutions as observed by light scattering, i.e. existence of the slow mode and angular dependencies of scattering intensity, is discussed in light of three series of experiments. Results on binary mixtures of NaPSS with different molecular weights indicate that the slow mode originates as a result of intermolecular interactions and cannot be explained on the basis of purely intramolecular processes or stable particles/impurities in solution. A comparison between data obtained on samples filtered through filters with different pore sizes demonstrates that results are influenced by the filtration procedure, however, the origin of the slow mode is in electrostatic interactions, not in filterable aggregates. The third series of experiments deals with a possible role of non-electrostatic interactions in the mechanism of the slow mode due to the hydrophobicity of a polyion backbone. Results are not in favor of this assumption.

The issue of the extraordinary behavior of salt-free solutions of strongly charged polyelectrolytes has been rather controversial for recent years. Taking into account the complexity of the problem, this situation is not so surprising. The multicomponent nature of polyelectrolyte solutions is reflected in many types of interactions: intramolecular interactions between segments of the same macromolecule, intermolecular interactions between different macromolecules, interactions between polyions and counterions, electrostatic screening by counterions, co-ions and even by polyions themselves, polymer-solvent interactions, and entropic forces (mainly due to the presence of counterions). This complexity becomes "more visible" in the limit of low salt concentrations, where unscreened interactions are strong and long-range.

Experimental data obtained by numerous techniques is at variance with what is typical for neutral macromolecules and even for polyelectrolytes at high salt concentrations. Typical examples are peaks in the concentration dependence of reduced viscosity (1,2) and angular maxima in experiments of small-angle X-ray or small-angle neutron scattering(3,4). Other less frequent techniques show also rather unusual results(5). Static and dynamic light scattering, which were used as main experimental techniques in our investigation, belong to the most sensitive tools for the study of these systems. A characteristic feature of static light scattering data is a

0097-6156/94/0548-0337\$06.00/0  
© 1994 American Chemical Society

pronounced angular dependence of scattered light, even for very small molecules (e.g.  $M_w = 5000$  (6)). The occurrence of two dynamic modes with widely separated characteristic times is typical for dynamic light scattering (7,8,9). The relatively fast one is on the order of several microseconds and the relatively slow one is on the order of  $10^3$  to  $10^5$  microseconds. The slow mode appears when the salt concentration decreases below some critical value. This was referred to as an ordinary-extraordinary transition (10). The existence of the slow mode and pronounced angular dependencies of scattering intensity was interpreted as a result of formation of multichain domains (clusters, temporal aggregates) in solution (7-9).

Results of various theoretical treatments of salt-free polyelectrolyte solutions differ qualitatively according to accepted approximations (11-13). Most of general theoretical calculations for polyelectrolyte systems do not predict any experimentally observed "extraordinary behavior" and are thus restricted to low charge densities and/or higher salt concentrations.

The aim of the present paper is to contribute to the understanding of the extraordinary phenomena which are currently a subject of frequent scientific discussions.

## Experimental

Sodium poly(styrenesulfonate) (NaPSS) with  $M_w = 5\ 000$ ,  $47\ 000$ ,  $100\ 000$  and  $1\ 200\ 000$  was from Pressure Chemical (Pittsburgh, PA). Poly(acrylic acid) (PAA) with  $M_w = 90\ 000$  and poly(methacrylic acid) (PMA) with  $M_w = 30\ 000$  were prepared by radical polymerization. All samples were thoroughly purified by mixed-bed ion exchange resins. According to our previous experience (6), even dialyzed grades of commercially available NaPSS contain several percent of  $\text{Na}_2\text{SO}_4$  as an impurity. Consequently, rather different results are obtained without and with an ion exchange purification. The acidic form of poly(styrenesulfonate) was converted after the purification back to the sodium salt by titration with sodium hydroxide. Polyacids were neutralized by NaOH and LiOH to various degrees of ionization. Deionized water with resistivity of  $15\ \text{M}\Omega\text{cm}$  was used as a solvent. Binary mixtures with given compositions  $x = c(\text{P}2)/(c(\text{P}1)+c(\text{P}2))$  where  $c(\text{P}1)$  and  $c(\text{P}2)$  are concentrations of polymer 1 and polymer 2, respectively, were prepared by mixing of binary solutions. Samples were gently shaken and allowed to stand and mix sufficiently. Solutions were filtered through 0.1- and 0.2-  $\mu\text{m}$  polycarbonate membrane filters from Nuclepore. These filters were chosen because the pores are well-defined and relatively monodispersed. This was important especially for the investigation of the influence of the filter pore size on the solution behavior.

The light scattering measurements were made using a Carl Zeiss Jena ILA 120-1 argon laser with 200 mW at 514.5 nm. A laboratory made goniometer was used to collect data from  $30^\circ$  to  $150^\circ$  for both static and dynamic light scattering experiments. The scattering cell was thermostated in the temperature range  $10^\circ\text{C}$  to  $80^\circ\text{C}$  with a precision of  $\pm 0.1^\circ\text{C}$ . Scattering intensities were measured by photon counting and normalized using a doubly distilled and filtered benzene as a standard. Photon correlation measurements used an ALV5000 correlator with a transputer board for numerical analysis of correlation curves by CONTIN program. Correlation curves were in most cases multi-exponential. Characteristic decay times  $\tau_i$  and their relative amplitudes  $A(\tau_i)$  were evaluated through the moments of distribution functions of decay times  $A(\tau)$ . Diffusion coefficients were then calculated as  $D_i = (1/\tau_i)q^{-2}$  where  $q$  is the scattering vector defined as  $q = (4\pi n/\lambda_0)\sin(\theta/2)$ , with  $n$  the solution refractive index,  $\lambda_0$  the laser wavelength, and  $\theta$  the scattering angle.

## Results and Discussion

**Light Scattering from Binary Mixtures of Polyelectrolytes.** The slow diffusion coefficient  $D_s$  at relatively high polymer concentrations ( $\sim 10$  g/L) strongly depends on molecular weight (in the range of two orders of magnitude)(6). Hence upon mixing of two samples with appreciably different molecular weights, two peaks in the spectrum of relaxation times corresponding to two slow diffusion coefficients could be (in principle) separated, even in the case of some shifts with respect to positions from binary solutions. The main stimulus for performing experiments on binary mixtures of polyelectrolytes with different molecular weights was to prove or rather disprove this possibility.

NaPSS was chosen for these experiments because of the availability of well-defined monodispersed samples and very detailed experimental data on molecular weight dependencies(6). Fractions with  $M_w = 5\ 000$ ,  $100\ 000$ , and  $1\ 200\ 000$  were used.

A set of solutions with a total polymer concentration  $c = 25$  g/L and various mixture compositions  $x = c(P2)/(c(P1)+c(P2))$  was prepared [ $c(P1)$  and  $c(P2)$  are concentrations of polymer 1 with  $M_w = 5\ 000$  and polymer 2 with  $M_w = 1\ 200\ 000$ , respectively]. Static and dynamic light scattering measurements were performed on these samples. Distribution functions of characteristic times  $A(\tau)$  obtained from correlation curves for selected values of  $x$  are presented in Figure 1. As can be seen, the peak corresponding to the fast mode ( $D_f$ ) does not change its position with  $x$ , although the relative amplitude slightly increases with  $x$ . More importantly, only one peak corresponding to the slow mode ( $D_s$ ) was observed in all cases. The position of the peak shifts towards longer times with  $x$  going from 0 to 1, while the amplitude remains high and the slow mode dominates the spectrum.

In addition to the fast and slow modes, a third mode clearly develops upon mixing of two polyelectrolyte samples. The relative amplitude of this mode reaches a maximum around  $x = 0.5$  and decreases to zero in the limits  $x \rightarrow 0$  and  $x \rightarrow 1$ . As will be discussed later, this mode is diffusive in nature and hence it is marked as  $D_m$  in Figure 1. Figure 2 shows the dependence of the slow diffusion coefficient  $D_s$  on the mixture composition  $x$ .  $D_s$  gradually decreases with increasing  $x$ . The fast diffusion coefficient  $D_f$  is independent of  $x$  (not shown).

Static light scattering measurements yielded linear dependencies of the normalized inverse scattering intensity  $I(0)/I(\theta)$  on  $\sin^2(\theta/2)$ , where  $\theta$  is the scattering angle. Apparent radii of gyration  $\langle S^2 \rangle^{1/2}$  were calculated according to the formula

$$I(0)/I(\theta) = 1 + C \langle S^2 \rangle \sin^2(\theta/2) \quad \theta \rightarrow 0 \quad (1)$$

with  $C = 1/3(4\pi n/\lambda_0)^2$ , and are summarized in Table I. No dependence of  $\langle S^2 \rangle^{1/2}$  on  $x$  was observed.

Our interpretation of the existence of the slow diffusive mode and angular dependencies of scattering intensity is based on an idea of formation of multichain domains, where the slow diffusive mode corresponds to the dynamics of creation and annihilation of domains (slow, long-range fluctuations in refractive index), and the apparent radius of gyration obtained from angular dependencies corresponds roughly to the size of domains. Domains are not considered to be stable particles, but rather temporal objects. Detailed discussions supporting this temporal nature of domains goes beyond the scope of this presentation. Briefly it can be noted that while  $D_s$  is strongly dependent on molecular weight (two orders in magnitude), the apparent size of a domain is independent of molecular weight. A different relationship between the size and the diffusion coefficient holds for stable particles.

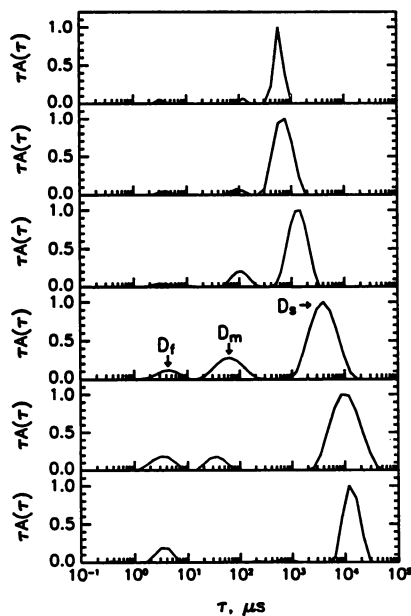


**Figure 1.** Spectra of relaxation times for binary mixtures of two polyelectrolyte samples in water: P1 = NaPSS,  $M_w = 5\,000$ , P2 = NaPSS,  $M_w = 1\,200\,000$ . The total polymer concentration was  $c = 25\text{ g/L}$ . The mixture composition  $x = c(P2)/(c(P1)+c(P2))$  was from top to bottom  $x = 0, 0.046, 0.188, 0.488, 0.824, 1.0$ . All measurements were performed at  $\theta = 90^\circ$ . Three diffusive modes present for  $0 < x < 1$  are marked as  $D_f$ ,  $D_m$ , and  $D_s$ .

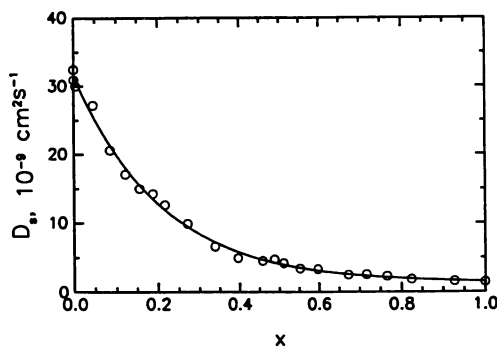


**Figure 2.** Dependence of slow diffusion coefficient  $D_s$  on mixture composition  $x$  of the binary mixture of NaPSS samples with  $M_w = 5\,000$  and  $M_w = 1\,200\,000$  in water.

In the case of a low molecular weight sample ( $M_w = 5\ 000$ ), domains could be visualized as temporal particles consisted of many chains (on the order of hundreds or more), surrounded by solvent with single polyions. In the case of the high molecular weight sample ( $M_w = 1\ 200\ 000$ ), the overlap is highly probable and domains could be visualized as regions of higher density and/or higher order in the net. The process of creation and annihilation of domains is much slower in the net where the motion of chains is more restricted than in a not-entangled solution of very short and mobile chains.

Regardless this hypothesis, two general conclusions can be made from the present data: (1) the slow mode is not caused by any stable species (particles) in solution; and (2) it does not correspond to an intramolecular (or purely intramolecular) process. In both cases two peaks would be expected. The existence of only one fairly narrow peak oppositely confirms the intermolecular interaction character of the slow mode. The independence of  $D_f$  and  $\langle S^2 \rangle^{1/2}$  on the mixture composition  $x$  is consistent with the independence of these quantities on molecular weight ( $\delta$ ).

Admitting that the model of the visualization of domains is correct, we can further speculate on what happens upon mixing of two solutions. The addition of a small amount of the high molecular weight sample into a solution of the low molecular weight sample ( $x \sim 0$ ) causes incorporation of long chains into domains and a relatively rapid slowing-down of the process of creation of domains as longer chains are less mobile than short ones. Oppositely, addition of a small amount of the low molecular weight sample into a net in the solution of the high molecular weight sample ( $x \sim 1$ ) accelerates the process. The change in the rate of the process is, however, not as pronounced as for  $x \sim 0$ . It seems that the slower motion (i.e. the motion of longer chains) is crucial for the final effect.

Table II shows results for mixtures of three different samples. Again, it can be seen that  $D_f$  and  $\langle S^2 \rangle^{1/2}$  are independent of the combination of polymer samples.  $D_s$  of the mixture appears to be a geometrical average of  $D_s$  values from corresponding binary solutions. More combinations would be helpful to prove exactly this conclusion, but still, geometrical averages are much closer to real data than arithmetic averages. The geometrical average means that lower values of the diffusion coefficient are more weighted. This is consistent with the above mentioned statement that the slower motion is crucial for the final effect in the domain formation.

Another set of experiments was performed on the total polymer concentration dependence. The results will be published in a separate paper (14). Here we can briefly mention that the concentration dependence of quantities characterizing the extraordinary phenomena resembles those from binary solutions. The "medium" diffusive mode marked as  $D_m$  in Figure 1 gets quickly in influence with decreasing the total polymer concentration (Figure 2). This new mode will be also discussed in detail (14). According to our experimental data, it was interpreted as a polyelectrolyte interdiffusion. It was proved that the main effect of the interdiffusion is caused by electrostatic interactions (14).

**On the possible role of non-electrostatic interactions in the mechanism of the slow mode.** Although there is an increasing number of experimental data on the slow mode, the mechanism of this mode is not clearly understood yet. The question is what type of interactions play a key role in the process of domain formation. As light scattering is sensitive to fluctuations in solution refractive index, domains can be visualized as regions with a different refractive index than the rest of the solution. This can be caused by a different density and/or different degree of order inside the domain. The question is how these regions arise.

An attractive interaction between charged particles through the intermediary of counterions was proposed by Ise (13). This idea was created on the basis of a very extensive experimental work, mainly naked eye observations of charged latex

**Table I. Dependence of the Apparent Radius of Gyration of Domains  $\langle S^2 \rangle^{1/2}$  (nm) on Mixture Composition  $x$** 

$x$	0.000	0.0005	0.085	0.217	0.488	0.766	1.000
$\langle S^2 \rangle^{1/2}$	86.6	84.5	83.6	90.0	84.0	93.7	109.8

The mixture composition is  $x = c(P2)/(c(P1)+c(P2))$ , and the molecular weight ( $M_w$ ) of the NaPSS were  $P1 = 5\ 000$  and  $P2 = 1\ 200\ 000$ . The total polymer concentration was  $c = 25\ \text{g/L}$ .

**Table II. Values of Fast ( $D_f$ ) and Slow ( $D_s$ ) Diffusion Coefficients and Apparent Radius of Gyration of Domains  $\langle S^2 \rangle^{1/2}$  for Mixtures of Three Different NaPSS Samples**

Sample	$M_w$	$D_f$ ( $10^{-6}\ \text{cm}^2/\text{s}$ )	$D_s$ , ( $10^{-9}\ \text{cm}^2/\text{s}$ )	$\langle S^2 \rangle^{1/2}$ (nm)	$\langle D \rangle$ ( $10^{-9}\ \text{cm}^2/\text{s}$ )
P1	5 000	5.6	44.0	62.4	
P2	100 000	5.7	20.6	59.4	
P3	1 200 000	5.5	4.15	87.9	
P1+ P2		5.7	30.7	65.6	30.1
P1+ P3		5.7	15.8	65.1	13.5
P2+ P3		5.5	8.3	84.3	9.3

The mixture composition was  $x = 0.5$  with a total polymer concentration of  $c = 5\ \text{g/L}$ .  $\langle D \rangle$  is the geometrical averages defined as  $\langle D \rangle = (D_i D_j)^{1/2}$  where  $D_i$  and  $D_j$  are values of the slow diffusion coefficient for samples  $P_i$  and  $P_j$ , respectively.

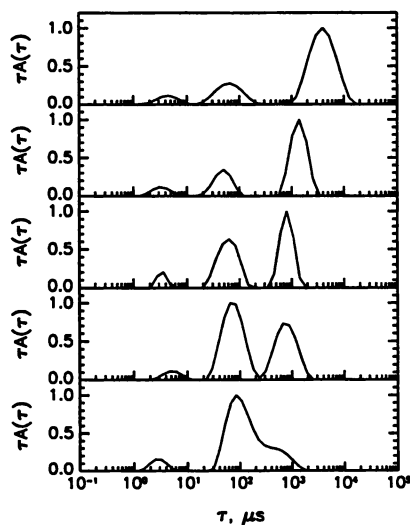


**Figure 3.** Spectra of relaxation times for binary mixtures of two polyelectrolyte samples in water:  $P1 = \text{NaPSS}$ ,  $M_w = 5\ 000$ ,  $P2 = \text{NaPSS}$ ,  $M_w = 1\ 200\ 000$ . The mixture composition  $x = c(P2)/(c(P1)+c(P2))$  was 0.488. The total polymer concentration in  $\text{g/L}$  was from top to bottom  $c = 25.0, 15.0, 3.8, 1.7,$  and  $0.58$ . All measurements were performed at  $\theta = 90^\circ$ .



particles. Authors believe that the mechanism could be the same for linear polyelectrolytes, where individual chains have a compact conformation due to intramolecular attractive interactions and the system resembles a solution of charged spheres. Schmitz (7) explained the existence of "temporal aggregates" as a result of fluctuating forces created by counterion dynamics. The instantaneous distribution of counterions around a charged chain is asymmetrical and hence dipole attractive interactions are possible.

Recently an issue of the hydrophobicity of a polyelectrolyte chain backbone in a polar solvent was discussed (15-17). Theory was developed for weakly charged polyelectrolytes (15,16) and it was shown that formation of mesophases (microscopic dense regions) or micelles originating as a result of aggregation of hydrophobic parts of chains between charges, is possible. Thus a question arose if this mechanism could play some role in the domain formation in solutions of strong polyelectrolytes.

Combinations of two polymers [poly(acrylic acid) and poly(methacrylic acid)] and two solvents (water and methanol) were taken into consideration. Water is a better solvent for PAA than methanol. In the case of PMA, the situation is opposite, i.e. methanol is a better solvent than water (18,19). It has been shown (9,20) that while domains are very pronounced in aqueous PMA solutions, they do not form in methanolic PMA solutions. This could be explained according to above mentioned ideas by a weaker or no aggregation of chain backbones in a better solvent (methanol).

In this case, results for PAA should be opposite, i.e. the tendency to form aggregates should be higher in methanol than in water. Therefore measurements were performed on methanolic and aqueous PAA solutions. Samples were neutralized by lithium hydroxide in water and by lithium methoxide in methanol. Figure 4 shows spectra of relaxation times for PAA solutions neutralized to degree of neutralization  $\alpha = 0.2$  in methanol (a) and water (b). The polymer concentration was  $c = 20$  g/L in both cases. As can be seen, there is a pronounced difference in these spectra. While the situation in water is typical for strongly charged salt-free polyelectrolytes, (the slow and fast modes are widely separated and the slow mode dominates), the methanolic sample shows a relatively broad spectrum with less pronounced slow mode. Quantitatively, the slow diffusion coefficient in the methanolic solution is "less slow" and the ratio  $A_s/A_f$  of amplitudes corresponding to slow and fast modes, respectively, is much lower (Table III). Clearly, the extraordinary behavior is less pronounced in methanol. This can be also supported by results of static light scattering obtained on the same samples. Figure 5 shows angular dependencies of normalized reciprocal excess scattering intensities for both samples. In the case of the aqueous solution, a pronounced dependence yields apparent radius of gyration of 64 nm, while in the case of the methanolic solution, there is a very slight angular dependence at the experimental recognition threshold ( $\langle S^2 \rangle^{1/2} \sim 26$  nm).

These results clearly do not support an assumption that the hydrophobic aggregation due to the hydrophobic nature of the polymer backbone is the main factor in domain formation.

Another way to verify the possible role of hydrophobic interactions in domain formation is to change solvent quality by a change in temperature. The tendency to form domains should be accordingly temperature-dependent. However, results of temperature dependencies also contradict the idea of the hydrophobic aggregation. Table IV shows results obtained by static and dynamic light scattering on an aqueous solution of NaPSS ( $M_w = 47\ 000$ ) at different temperatures.  $D_{fc}$  and  $D_{sc}$  are values of diffusion coefficients corrected for a change in solvent viscosity and kinetic effects according to the formula

$$D_{ic} = D_i(T) (\eta(T)T_0 / \eta(T_0)T) \quad (2)$$

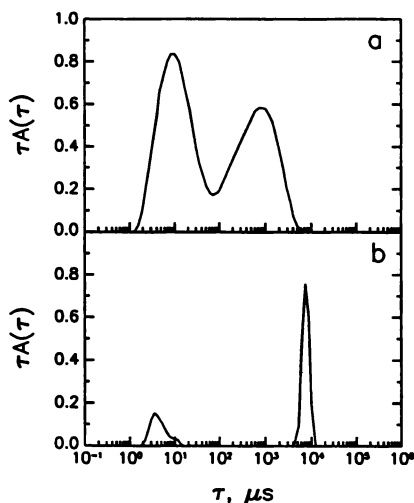


**Figure 4.** Spectra of relaxation times for solutions of poly(acrylic acid) ( $M_w = 90\,000$ ) with the degree of neutralization  $\alpha = 0.2$  and concentration  $c = 20\text{ g/L}$  in methanol (a) and water (b). Both measurements were performed at  $\theta = 90^\circ$ .

**Table III.** Values of  $\langle S^2 \rangle^{1/2}$ ,  $D_f$ ,  $D_s$ , and the Ratio of Scattering Amplitudes  $A_f/A_s$  for Solutions of Poly(acrylic acid)<sup>a</sup> in Water and Methanol

solvent	$D_f$ ( $10^{-6}\text{ cm}^2/\text{s}$ )	$D_s$ ( $10^{-9}\text{ cm}^2/\text{s}$ )	$A_f/A_s$	$\langle S^2 \rangle^{1/2}$ (nm)
water	3.8	2.66	6.0	64
methanol	2.1	26.9	0.7	26*

\* very weak angular dependence at the experimental recognition threshold

<sup>a</sup>  $M_w = 90\,000$ ,  $c = 20\text{ g/L}$ ,  $\alpha = 0.2$

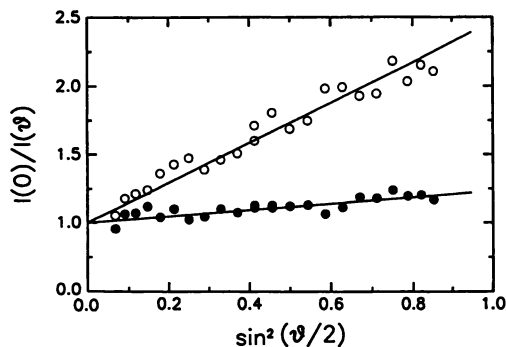


**Figure 5.** Dependence of the normalized reciprocal excess scattering intensity on scattering angle: solutions of poly(acrylic acid) ( $M_w = 90\,000$ ) with the degree of neutralization  $\alpha = 0.2$  and concentration  $c = 20\text{ g/L}$  in methanol (a) and in water (b).

where  $i = f, s$ ,  $\eta(T)$  is viscosity of water at temperature  $T$ , and  $T_0$  is a reference temperature  $T_0 = 25^\circ\text{C}$ .

Values of  $D_{ic}$  from Table IV are independent of temperature, which means that all changes in  $D_f$  and  $D_s$  are only due to changes in temperature and solvent viscosity. Also the ratio  $A_s/A_f$  is roughly constant. The tendency to form domains is not temperature - dependent in a broad temperature interval, though the solvent quality changes and there is a lower critical temperature around  $70^\circ\text{C}$ . A macroscopic demixing phase separation accompanied by an increase of scattering intensity begins above  $70^\circ\text{C}$ .

The same kind of independence of the tendency to form domains on temperature was observed on systems NaPSS in formamide and NaPSS in dimethylsulfoxide. A detailed analysis will be given in a separate paper (21). Also previously published data on aqueous solutions of PMA do not indicate a temperature dependence of the tendency to form domains (22). It seems that in the case of strongly charged polyelectrolytes with high charge densities the effect of the hydrophobicity of a chain backbone is overcompensated by the hydrophilic nature of numerous charged groups along the chain.

**On the influence of sample filtration on the slow mode behavior.** Recently it was reported (23-26) that the slow mode is caused by the presence of impurities or entanglements in solution and is "removable" by filtration through a proper size filter. Usually a  $0.1\ \mu\text{m}$  pore size filter used instead of conventional  $0.2\ \mu\text{m}$  filters was reported as sufficient to "remove" completely the slow mode. Authors note that "there is number of ways that these aggregates can form, including lyophilization prior to dispersal in solvent, and no impurities need be involved." The aggregates did not reappear after removal, at least on a time scale of days (23-26). (On the other hand, a gradual reappearance of the slow mode after filtration was reported in other papers. (27,28)). The "loss" of the slow mode as ionic strength of the solution increases was explained as a result of the weak scattering signal from impurities or entanglements getting buried in the sharply increasing scattering from polyelectrolyte molecules.(26)

To verify these conclusions, experiments with well defined samples of PMA ( $M_w = 30\ 000$ ) and NaPSS ( $M_w = 5000$ ) filtered through both  $0.1-$  and  $0.2\ \mu\text{m}$  filters were performed. The choice of the two polymers for our experiments was motivated by the fact that both samples can be prepared with sufficient purity and they have been extensively investigated (6,8,9,20,22). The NaPSS sample with extremely low molecular weight  $M_w = 5\ 000$  was chosen to minimize the influence of relatively small filter pores on single chains during filtration. Our aim was to investigate only the influence on domains (aggregates). Individual molecules should pass freely through the filter. Finally, we took advantage of the fact that PMA is a weak polyelectrolyte and various degrees of ionization can be reached under salt-free conditions by neutralization with a proper alkali

Figure 6a shows the correlation function and the spectrum of characteristic times for the solution with degree of neutralization  $\alpha = 0$ , which was filtered through a  $0.1\ \mu\text{m}$  filter. Figure 6b corresponds to the sample with  $\alpha = 0.4$ . This sample was prepared by adding several drops of NaOH through a  $0.1\ \mu\text{m}$  filter to the scattering cell with the original solution with  $\alpha = 0$ . Clearly, the addition of thoroughly purified NaOH results in a pronounced slow mode as can be seen from the comparison of Figures 6a and 6b. The excess scattering intensity shows an angular dependence for  $\alpha = 0.4$ , contrary to the case with  $\alpha = 0$  (not shown here).

The sample with  $\alpha = 0.4$  was filtered again through a  $0.1\ \mu\text{m}$  filter and measurements were repeated. The corresponding correlation function and the spectrum of characteristic times are shown in Figure 6c. Figures 6b and 6c differ very little, and also values of diffusion coefficients calculated from these spectra are

**Table IV. Temperature Dependence of  $D_f$ ,  $D_s$ ,  $A_f/A_s$ , and Total Scattering Intensity  $I$  for NaPSS in Water**

T, (°C)	$D_f$ , ( $10^{-6}$ cm <sup>2</sup> /s)	$D_s$ , ( $10^{-9}$ cm <sup>2</sup> /s)	$A_f/A_s$	$I$	$D_{fc}$ , ( $10^{-6}$ cm <sup>2</sup> /s)	$D_{sc}$ , ( $10^{-9}$ cm <sup>2</sup> /s)
10	2.6	14.8	9.5	19.6	4.0	22.8
17.5	3.3	17.4	11.2	19.5	4.2	22.1
25	4.1	19.8	9.7	19.5	4.1	19.8
40	5.7	30.4	14.4	19.6	4.0	21.2
55	7.2	37.4	9.6	19.8	3.9	18.5
65	9.7	49.1	10.1	19.5	4.2	21.2
70	10.9	53.0	10.0	19.5	4.3	21.0
74	10.8	51.9	-	25.0	4.0	19.3
77	11.2	57.8	-	30.0	4.0	20.5
81	15.5	73.0	-	42.0	4.1	23.9

$M_w = 47\ 000$ ,  $c = 20$  g/L. The scattering intensities are in arbitrary units.  $D_{fc}$  and  $D_{sc}$  are corrected for a change in solvent viscosity and kinetic effects.

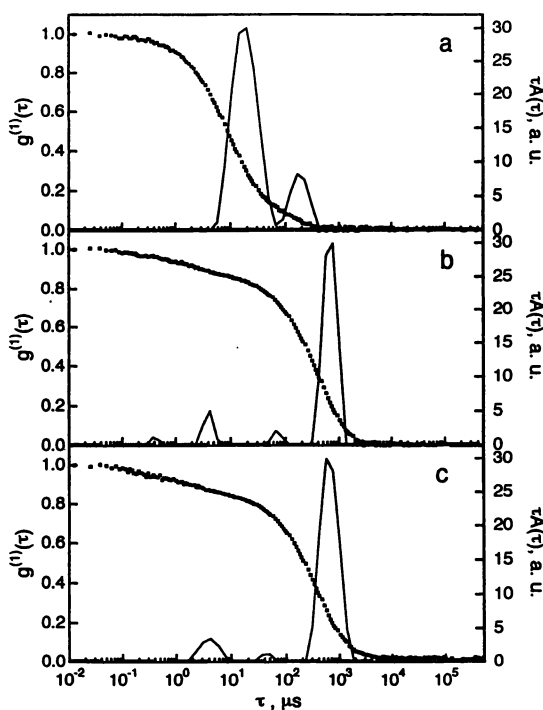


**Figure 6.** Composite correlation functions and spectra of relaxation times for solutions of poly(methacrylic acid) ( $M_w = 30\ 000$ ). a) sample with  $\alpha = 0$ , filtered through a  $0.1\ \mu\text{m}$  filter; b) sample with  $\alpha = 0.4$ , neutralized by adding an aliquot amount of NaOH through a  $0.1\ \mu\text{m}$  filter; c) sample with  $\alpha = 0.4$ , filtered once more through a  $0.1\ \mu\text{m}$  filter.

Table V.  $D_f$ ,  $D_s$ ,  $A_f/A_s$ ,  $\langle S^2 \rangle^{1/2}$ , and  $I$  for Different Concentrations NaPSS<sup>a</sup>

c (g/L)	$D_f$ , ( $10^{-6}$ cm <sup>2</sup> /s)	$D_s$ , ( $10^{-9}$ cm <sup>2</sup> /s)	$A_f/A_s$	$\langle S^2 \rangle^{1/2}$ , (nm)	$I$
2	5.52	80.0	8.3	26	0.31
4	5.77	70.1	6.9	34	0.72
8	5.60	66.2	6.5	37	1.44
16	5.79	51.5	9.2	62	2.90
22	6.27	48.0	7.5	75	4.20

a -  $M_w = 5\ 000$ . All samples were filtered through a 0.1  $\mu$ m filter.

Table VI.  $D_f$ ,  $D_s$ ,  $A_f/A_s$ ,  $\langle S^2 \rangle^{1/2}$ , and  $I$  for Different NaPSS<sup>a</sup> Concentrations

c (g/L)	$D_f$ , ( $10^{-6}$ cm <sup>2</sup> /s)	$D_s$ , ( $10^{-9}$ cm <sup>2</sup> /s)	$A_f/A_s$	$\langle S^2 \rangle^{1/2}$ , (nm)	$I$
2	5.67	46.0	40	48	1.50
4	5.89	42.1	36	64	3.51
8	5.64	38.2	36	72	7.20
16	6.01	35.9	45	87	14.5
22	6.05	34.0	40	105	21.0

a - NaPSS,  $M_w = 5\ 000$ . All samples were filtered through a 0.2  $\mu$ m filter.

relatively close ( $D_f = 4.90 \times 10^{-6}$  cm<sup>2</sup>/s,  $D_s = 31.0 \times 10^{-9}$  cm<sup>2</sup>/s for Figure 6b, and  $D_f = 4.80 \times 10^{-6}$  cm<sup>2</sup>/s,  $D_s = 37.3 \times 10^{-9}$  cm<sup>2</sup>/s for Figure 6c). It can be concluded that the repeated filtration of the sample had no pronounced effect on the results of these measurements.

A more detailed investigation was performed with the NaPSS sample. Solutions with  $c = 2$  to 22 g/L filtered through both 0.1- and 0.2  $\mu$ m filters were investigated. Results are summarized in Tables V and VI. It can be concluded that while filtration through a smaller pore size filter has no effect on the fast diffusive mode corresponding to the diffusion of individual chains which are not altered by filtration, it has a modest disruptive effect on domains which are smaller in size, scatter less light and the slow diffusion coefficient is higher after filtration. Domains are most pronounced when no filter is used and samples are centrifuged prior to measurements (29). Filtration of solutions suppresses the slow mode and the effect is stronger for 0.1  $\mu$ m filters than for 0.2  $\mu$ m filters.

Repeated measurements on samples filtered through a 0.1  $\mu$ m filter have not shown considerably different results after couple of hours. However, repeated measurements on a scale of longer times might be a task for further investigation.

It can be concluded that the origin of the slow mode is of electrostatic nature and that it is not possible to explain it as a result of the presence of impurities or stable entanglements in solution. Impurity or aggregate free solution of neutral PMA exhibits a pronounced slow mode after adding several drops of clean (impurity or aggregate free) solution of NaOH. The only change introduced into the solution by this procedure is charging of PMA chains.

Another simple arguments disproving the idea of filterable aggregates may be advanced as well. Apparent radii of gyration of domains are dependent on solution ionic strength, degree of ionization, and polymer concentration (7, 30-32). Thus a simple dilution of solution can "destroy" domains. The intensity of the slow mode and the tendency to form domains is also dependent on dielectric permittivity of solvent (20, 33, 34) as this quantity strongly influences effective charges and charge interactions. Results obtained on binary mixtures of polyions presented in this paper are again in contradiction with the idea of filterable aggregates.

Numerous arguments can be also found in reference 35. The most convincing ones are that the ordinary-extraordinary transition is fully reversible (some samples have undergone three or more complete cycles from extraordinary to ordinary regime and back (10)), and that the extraordinary regime can be disrupted by applying a sinusoidal electric field (36).

Our conclusion is that although the slow mode cannot be filtered out in the sense of removing stable particles from solution, a small quantitative difference in data is observed when using a 0.1  $\mu\text{m}$  filter instead of a 0.2  $\mu\text{m}$  filter. Generally, pressure filtration through a 0.1  $\mu\text{m}$  filter corresponds to applying mechanical forces on domains. Investigation of the influence of these forces on the stability of domains can be a new challenging task on the way towards understanding the behavior of low-salt polyelectrolyte solutions.

## References

1. Cohen, J.; Priel, Z.; Rabin, Y. *J. Chem. Phys.* **1988**, *88*, 7111.
2. Eisenberg, H.; Pouyet, J. *J. Polym. Sci.* **1954**, *13*, 85.
3. Ise, N. *Angew. Chem. Int. Ed. Engl.* **1986**, *25*, 323.
4. Benmouna, M.; Weil, G.; Benoit, H.; Akcasu, Z. *J. Phys. (Paris)* **1982**, *43*, 1679.
5. Schmitz, K. S. *Macroions in Solution and Colloidal Suspension*; VCH Publishers: New York, NY, **1993**.
6. Sedlak, M.; Amis, E. J., *J. Chem. Phys.* **1992**, *96*, 817.
7. Schmitz, K. S.; Lu, M.; Gauntt, J., *J. Chem. Phys.* **1983**, *78*, 5059.
8. Drifford, M.; Dalbiez, J. P., *Biopolymers* **1985**, *24*, 1501.
9. Sedlak, M.; Konak, C.; St'panek, P.; Jakes, J. *Polymer* **1987**, *28*, 873.
10. Lin, S. C.; Lee, W.; Schurr, J. M., *Biopolymers* **1978**, *17*, 1041.
11. Lifson, S.; Katchalsky, A., *J. Polym. Sci.* **1954**, *13*, 43.
12. Odijk, T. *Macromolecules* **1979**, *12*, 688.
13. Sogami, I.; Ise, N., *J. Chem. Phys.* **1984**, *81*, 6320.
14. Sedlák, M.; to be published
15. Borue, V.; Erukhimovich, I., *Macromolecules* **1988**, *21*, 3240.
16. Joanny, J. F.; Leibler, L., *J. Phys. France* **1990**, *51*, 545.
17. Rabin, Y., Weizmann Institute, personal communication, 1991.
18. Katchalsky, A.; Eisenberg, H., *J. Polym. Sci.* **1951**, *6*, 145.
19. Horsky, J.; Petrus, V.; Bohdanecky M., *Macromol. Chem.* **1986**, *187*, 2621.
20. Sedlák, M.; Konak, C.; Labsky J., *Polymer* **1991**, *32*, 1688.
21. Sedlák, M.; to be published
22. Sedlák, M.; Konak, C.; Stepanek, P.; Jakes, J., *Polymer* **1990**, *31*, 253.
23. Li, X.; Reed, W. F., *J. Chem. Phys* **1991**, *94*, 4568.
24. Reed, W. F.; Ghosh, S.; Medjahdi, G.; Francois, J., *Macromolecules* **1991**, *24*, 6189.
25. Ghosh, S.; Li, X.; Reed, C. E.; Reed, W. F., *Biopolymers* **1991**, *30*, 1101.
26. Peitzsch, R. M.; Burt, M. J.; Reed, W.F., *Macromolecules* **1992**, *25*, 806.
27. Nicolai, T.; Mandel, M., *Macromolecules* **1989**, *22*, 2348.
28. Nicolai, T.; Mandel, M., *Macromolecules* **1989**, *22*, 438.
29. Sedlák M.; unpublished results
30. Forster, S.; Schmidt, M.; Antonietti, M., *Polymer* **1990**, *31*, 781.
31. Sedlak, M. Ph.D. Thesis.
32. Sedlák, M.; Amis, E. J., *J. Chem. Phys.* **1992**, *96*, 826.
33. Austin, M. Ph.D. Thesis.
34. Sedlák, M.; Amis, E. J., in preparation.
35. Schmitz, K.S., *Biopolymers*, **1993**, *33*, 953.
36. Schmitz, K. S.; Ramsay D. J., *Macromolecules* **1985**, *18*, 933.

RECEIVED August 6, 1993

## Chapter 27

# Determination of Cluster Size in Polyelectrolyte Solutions by Small-Angle Neutron Scattering

Hideki Matsuoka<sup>1</sup>, Dietmar Schwahn<sup>2</sup>, and Norio Ise<sup>3</sup>

<sup>1</sup>Department of Polymer Chemistry, Kyoto University, Kyoto 606-01, Japan

<sup>2</sup>Institut für Festkörperforschung, Forschungszentrum Jülich, Postfach  
1913, D-5170 Jülich, Germany

<sup>3</sup>Fukui Research Laboratory, Rengo Company Ltd., 10-8-1, Jiyugaoka,  
Kanazu-cho, Sakai-gun, Fukui 919-06, Japan

Small-angle neutron scattering measurements were performed for sodium polystyrenesulfonate-D<sub>2</sub>O solutions. A steep upturn behavior was observed at very small-angle regions below 0.01 Å<sup>-1</sup> which could not be measured by our previous X-ray experiments. This upturn reflects the existence of ordered clusters and its size was estimated to be around 400 - 1000 Å by Guinier, Debye-Bueche, and Porod analyses. Model calculations were also performed to estimate the number density of the clusters by using absolute scattering intensity.

Small-angle X-ray scattering (SAXS) and neutron scattering (SANS) curves for polyelectrolyte solutions at low ionic strengths showed a single, broad but distinct peak.<sup>(1-4)</sup> This peak was taken as implying a more or less ordered arrangement of ionic solutes, though in solutions. In other words, this was an interparticle interference peak although the degree of order was not high. The average interparticle distance ( $2D_{exp}$ ) was calculated from the peak position by the Bragg Equation. At low polymer concentrations,  $2D_{exp}$  value was smaller than the average distance calculated from the concentration ( $2D_0$ ) when the charge number and molecular weight of the polymer were high.<sup>(1,2)</sup> This relation implies that the ordered regions were not formed throughout the solution but existed as localized clusters. We have been calling this structure a "two-state structure"<sup>(1,2)</sup>. A similar kind of structure was often observed directly for ionic latex dispersions by ultramicroscope technique.<sup>(1,2)</sup> However, no further signs of the cluster structure have been detected in conventional scattering measurements of ionic polymer solutions.

In a previous study, we performed SANS measurements by a scattering camera which could detect scattering at very small angles that were not covered by the conven-

0097-6156/94/0548-0349\$06.00/0

© 1994 American Chemical Society

tional SAXS apparatus.(5) Sodium polystyrenesulfonate (NaPSS) having a narrow molecular weight distribution was chosen as a sample since we carried out earlier SAXS measurements for the same material and found an interference peak.(6) The SANS curves obtained for NaPSS in D<sub>2</sub>O solutions showed a steep upturn behavior in very small-angle regions while an interference peak was also observed at the same positions as in our previous SAXS results. According to basic scattering theory, the strong scattering at very small angles is due to a density fluctuation of a very large size in the system. This upturn is compatible with the localized clusters in the two-state structure; other model proposed earlier,(7) cannot account for the upturn since it assumes a uniform distribution of solutes.

In the present paper, the upturn behavior was confirmed at various polymer and salt concentrations. Guinier method, Debye-Bueche method and model calculations with the absolute scattered intensity were employed to analyze the upturn behavior and to estimate the size and other structural parameters of the cluster structure.

### Experimental Section

**Materials** NaPSS was purchased from Pressure Chemicals (Pittsburgh, PA). The molecular weight was 100,000 by the supplier. The sample was purified by ultrafiltration until the filtrate showed no UV absorbance. The purified sample was filtered by a glass filter of mesh G3 and then freeze-dried. D<sub>2</sub>O used as solvent was Merck Art.2919 (99.75%, Darmstadt, FRG). Sodium chloride used as an added salt was also of Merck, pro analyze grade, lot 527K785404.

**SANS Measurements** The SANS apparatus used was a KWS 2 system in Forschungszentrum Jülich. This has a long camera distance of 20m, which enables us to cover very small-angle regions. The details of the system were fully described elsewhere.(8) The SANS cell used was made of quartz, Hellma Präzisions-Küvetten, thickness 5.00 mm. The cells were washed with detergents and also cleaned by ultrasonication before use. The scattered intensities were collected at three or four detector distances (say, 2m, 4m, 8m, and 20m). Those data were gathered and analyzed by a computer system (ELLAVAX system). The absorption correction was done using the results of transmission measurements. The calibration for the absolute intensity was performed by using a standard Lupolen sample.

### Results

Figure 1 shows the polymer concentration dependence of the SANS curves of NaPSS-D<sub>2</sub>O solutions. The ordinate ( $d\Sigma(q)/d\Omega = I(q)$ ) is the absolute intensity of scattered neutrons, and the abscissa,  $q$ , is the scattering vector in  $\text{\AA}^{-1}$ :  $q=4\pi\sin\theta/\lambda$  ( $2\theta$  : the scattering angle,  $\lambda$ :wave length). An interference peak was observed at practically the same  $q$  as our previous SAXS measurements(6). In the very small-angle regions, i.e.  $q < 0.01 \text{\AA}^{-1}$  which could not be studied by SAXS, a clear, strong upturn behavior was observed for all profiles.

Figure 2 shows the salt concentration dependence of SANS profile. An interference peak could be observed at



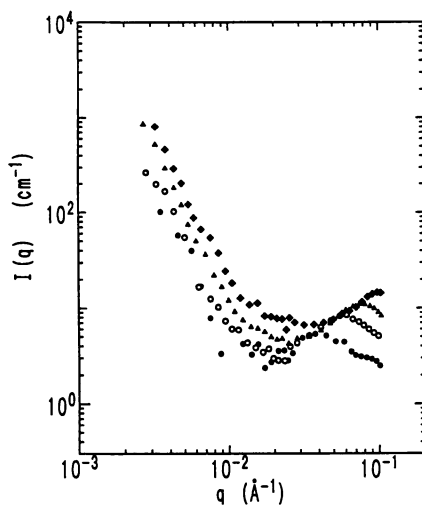


Figure 1 Concentration dependence of SANS curves of NaPSS in  $D_2O$  solutions. ●:0.01 g/ml, ○:0.02, ▲:0.04, ◆:0.08.

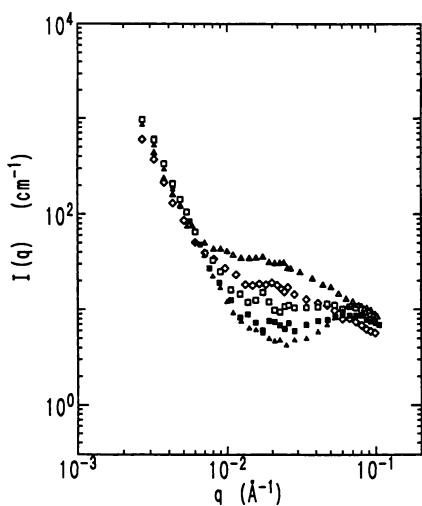


Figure 2 Salt concentration dependence of SANS curves of NaPSS in  $D_2O$  solutions. [NaCl]= ▲:0M, ■:0.05, □:0.1, ◇:0.5, △:0.5.

fairly large angle regions when the salt concentration is low, indicating that a more or less ordered arrangement of ionic polymers was maintained in the solution. A steep upturn at very small-angle regions could be also observed under all conditions.

### Discussion

**Guinier Analysis** The Guinier analysis(9) is a most convenient way to analyze the upturn behavior. The radius of gyration ( $R_g$ ) of the cluster can be estimated although the value obtained is approximate for a scatterer which has a heterogeneous internal structure. An example of the Guinier plot ( $\ln(d\Sigma(q)/d\Omega (=I(q)))$  vs.  $q^2$ ) is shown in Figure 3. From the slope of the straight line at small-angle regions,  $R_g$  of the cluster was calculated by the following Equation;

$$I(q) = I(0) \exp(-1/3)R_g^2 q^2 \quad (1)$$

For the case of Figure 3 in which the straight line was fitted for the first three data points,  $R_g$  can be calculated to be  $686\text{\AA}$ . If we draw the straight line for the first four data points,  $R_g$  becomes  $648\text{\AA}$ . If we assume that the cluster is spherical and that the inside of the cluster is homogeneous in this large scale, the radius ( $R$ ) of the spherical cluster can be obtained by the simple Equation,  $R^2 = (5/3)R_g^2$ .(9) These results are summarized in Table I. After the estimation of the intermolecular distance between polystyrenesulfonate ions in the clusters ( $2D_{\text{exp}}$ ) from the peak position by the Bragg Equation, the average number of polymers in one cluster ( $N$ ) was calculated by  $N = (4\pi R^3/3)/(2D_{\text{exp}})^3$ . Though this Equation is valid for simple cubic system, the  $N$  values obtained here may be approximate, since the single, broad peak implies that the degree of order is not high so as to enable us to determine the lattice systems. However, since  $2D_{\text{exp}}$  values should be valid as an "average" distance, the calculation of  $N$  here would be justified. The  $N$  values obtained are summarized in Table II. At higher salt concentrations,  $N$  values could not be calculated because the intermolecular interference peak was no longer observed; the ordered arrangement of the polymer molecules was destroyed by the screening effect of the simple ionic salts, which means that the ordering phenomena is of an electrostatic origin.

Figure 4 shows the polymer concentration dependence of  $R_g$ . With increasing polymer concentration,  $R_g$  increased monotonically. The fact that the cluster became larger with increasing concentration is reasonable if the enhanced interparticle electrostatic interaction is taken into account. The slight decrease at 0.08 g/ml condition may be due to the limited small-angle resolution, since the linearity at this concentration was not so good as under the other conditions.

The salt concentration dependence of  $R_g$  is shown in Figure 5. The  $R_g$  value was independent of added salt in the concentration range studied here. This may mean that there remains still some density fluctuation even when the ordered structure is destroyed by salt effect.

The forward scattering intensity,  $\frac{d\Sigma(0)}{d\Omega} = I(0)$ , is

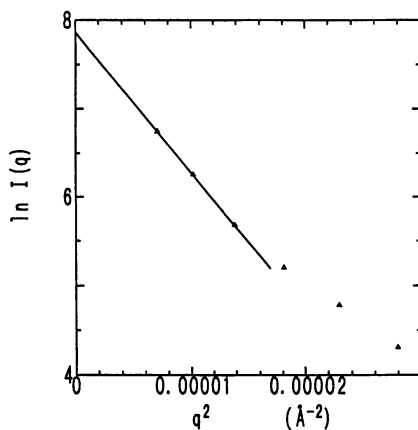


Figure 3 Guinier plot of SANS curve of NaPSS in  $D_2O$  solutions.  $[NaPSS]=0.04$  g/ml,  $[NaCl]=0M$ .

Table I  
Structural Parameters of Clusters of NaPSS in  $D_2O$  Solutions

[NaPSS] (g/ml)	[NaCl] (M)	Guinier				Debye-Bueche		
		$R_g$ (Å)	$R$ (Å)	$I_G(0)$ ( $cm^{-1}$ )	$R_G$ (Å)	$a$ (Å)	$I_{DB}^{(0)}$ ( $cm^{-1}$ )	$R_{DB}$ (Å)
0.01	0	407	525	190	416	217	231	437
0.02	0	516	666	530	534	306	772	587
0.04	0	686	886	2590	660	739	20290	1104
0.08	0	(630)	(813)	3040	613	934	81170	1395
0.04	0.05	664	857	2700	627	508	6610	784
0.04	0.1	683	882	2860	673	502	7690	863
0.04	0.3	671	866	1720	659	624	6610	922
0.04	0.5	631	814	1620	638	638	10740	1024

Table II  
Interparticle Distance ( $2D_{exp}$ ) and Number of Polymers in the Cluster (N)

[NaPSS] (g/ml)	[NaCl] (M)	$2D_{exp}$ (Å)	N	
			Guinier	Debye-Bueche
0.01	0	166	130	9.4
0.02	0	103	1100	110
0.04	0	85	4700	2750
0.08	0	64	8600	13000
0.04	0.05	94	3200	660
0.04	0.1	(132)	(1250)	(230)
0.04	0.3	---	---	---
0.04	0.5	---	---	---

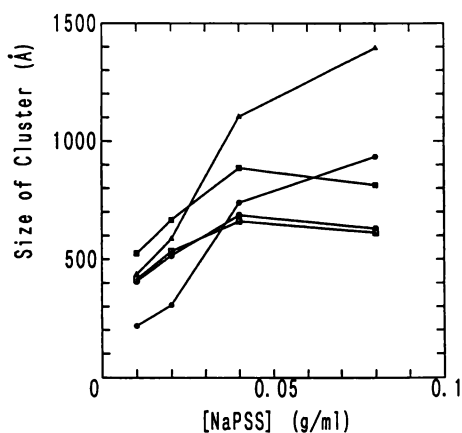


Figure 4 Concentration dependence of cluster sizes.  
 ○ :  $R_g$ , ■ :  $R$ , ● :  $a$ , □ :  $R_G$ , ▲ :  $R_{DB}$ .

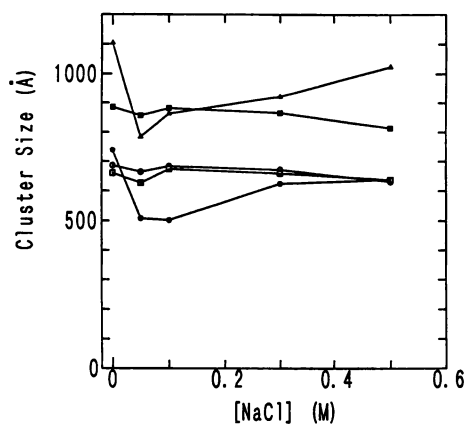


Figure 5 Salt concentration dependence of cluster sizes. Symbols are same as Fig. 4.

related to the number density ( $n$ ), the volume ( $V$ ) of the scatterer and the scattering contrast ( $\Delta\rho$ ) as follows;

$$I(0) = n V^2 (\Delta\rho)^2 \quad (2).$$

The intensity was estimated and denoted by  $I_G(0)$ , which was determined by the extrapolation of the Guinier straight line into  $q \rightarrow 0$ . Its polymer and salt concentration dependencies are shown in Table I.  $I_G(0)$  became larger with increasing polymer concentration and with decreasing salt concentration.

**Debye-Bueche Analysis of the Upturn** Since the Guinier plots were not very linear, we reanalyzed the data by the Zimm and Debye-Bueche methods. The linearity of the Zimm plot ( $I^{-1}(q)$  vs.  $q^2$ ) at  $q^2 < 0.0001$  was not so bad for all data, but the intercept of the straight line at  $q=0$  was negative for some data, which was physically unreasonable. Therefore we excluded this analysis from further consideration. On the other hand, the Debye-Bueche plot ( $I^{-1/2}$  vs.  $q^2$ ) showed an excellent linearity. An example is shown in Figure 6. Since the Debye-Bueche Equation is shown as follows, (10)

$$I(q) = I(0) / (1 + a^2 q^2)^2 \quad (3),$$

where  $I(0)$  is the extrapolated scattering at  $q=0$ , we can obtain the correlation length ( $a$ ) from the ratio of the slope to the intercept of the straight line. The Debye-Bueche approximation is given by the exponential correlation function,  $\gamma(r) = e^{-r/a}$ , which is the Fourier transform of  $I(q)$  and corresponds to a completely random size distribution of the particles. The  $a$  values thus estimated are listed in Table I and plotted in Figures 4 and 5. The  $a$  values changed from 200 Å to 900 Å with increasing concentration which was consistent with  $R_g$  values quantitatively. The  $I(0)$  values were also estimated from the intercept and denoted as  $I_{DB}(0)$  (Table I).

**Porod Analysis** As is seen in the double logarithmic plot (Figures 1 and 2), we could find a rather excellent linearity for upturn behavior. This means that the upturn follows a power law: i.e.  $I(q) \sim P q^{-\alpha}$  where  $P$  is the Porod constant. Since the slope  $\alpha$  was found to be about 4, (this means that the cluster surface was rather smooth; in other words, the Porod law(11) held), the  $P$  values, which is related to the surface area ( $S$ ) of the scatterer by the following Equation(9), are estimated by  $Iq^4$  vs.  $q$  plot (Figure 7).

$$P = 2\pi\phi(S/V)(\Delta\rho)^2 \quad (4)$$

Combining Equations 2 and 4, we obtain

$$P / I(0) = 2\pi S / V^2 \quad (5).$$

If we assume a spherical shape of the scatterer, then

$$P / I(0) = 9 / (2R^4) \quad (6).$$

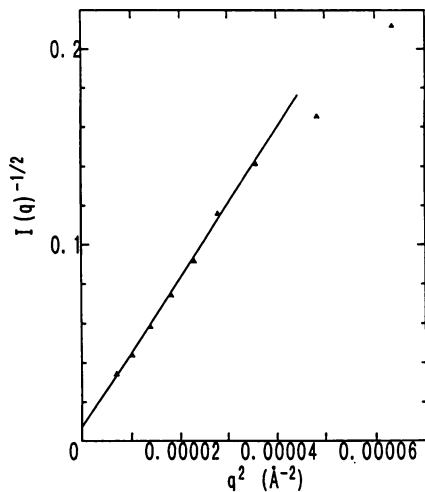


Figure 6 Debye-Bueche plot of SANS data of NaPSS in  $D_2O$  solution.  $[NaPSS]=0.04g/ml$ ,  $[NaCl]=0M$ .

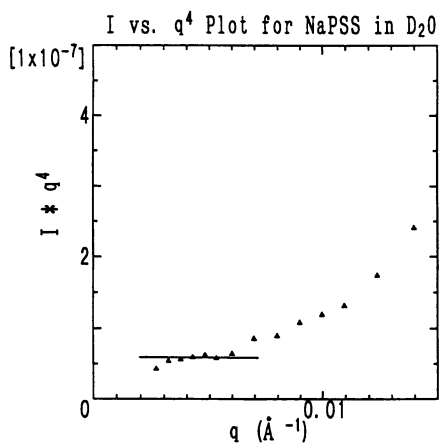


Figure 7 Porod plot of SANS data of NaPSS in  $D_2O$  solutions.

By this Equation, we can evaluate the radius of the cluster  $R$  independently in addition to Guinier and Debye-Bueche methods. We can calculate two kinds of  $R$  values,  $R_G$  and  $R_{DB}$ , by using  $I_G(0)$  and  $I_{DB}(0)$  values, respectively. These values thus obtained are summarized in Table I and plotted in Figures 4 and 5. The  $R_G$  values were again in the range of 400–700 Å which were very close to  $R_g$  values. The  $R_{DB}$  values were also not very different from the  $R_g$  values. This consistency may reflect the validity and correctness of our analyses.

A comment may be necessary on the fact that the upturn follows the Porod law. This means that the cluster has a sharp, smooth interface. This may be surprising since the cluster is not homogeneous but contains regularly arranged PSS molecules and the solvent. We cannot deny the possibility that a combination of effects by surface roughness and by non-sharp change of the density between the inside and the outside of the cluster gave an apparent slope of 4. However, we believe that the good agreement between  $R_g$  and  $R_G$  supports our analysis. As seen in Figure 7, the Porod region is outer than Guinier region (the first three points).

**The Origin of the Upturn** By the simple analyses mentioned above, it was found that the upturn in SANS curves corresponded to the scatterer sizes of 500 – 900 Å and 200–900 Å by Guinier method and Debye-Bueche method, respectively. The results by the Porod analysis support the validity of these analyses. Now, it may be necessary to consider some other possibilities as the origin of the upturn. The first possibility is dust in the solvent ( $D_2O$ ). However, this may be completely ruled out by the fact that the scattering from the solvent showed no upturn. In addition, the scattering curve shown had the solvent scattering already subtracted. The second is the dust in the polymer. This is also impossible because  $R_g$  and  $a$  values and the forward scattering intensity,  $I(0)$ , showed substantial polymer concentration and salt concentration dependencies. It is obvious that dust should not show such dependencies. The third is colloidal polymer aggregates formed by ionic impurities in the solution. Previously, Nierlich et al.(7) and Boue et al.(12) also observed a similar upturn behavior for NaPSS- $D_2O$  solutions by SANS, and they attributed it to ionic impurities in  $D_2O$ . According to their interpretation, the ionic impurities in  $D_2O$  caused formation of aggregates of polymers in solution and the scattering from them gave rise to an upturn. However, the aggregate formation should reduce the concentration of the polymer forming ordered structure. This reduction in concentration must affect the intermolecular distance ( $2D_{exp}$ ) and hence the peak position in the scattering curve. However, the peak positions in the present SANS curves were almost the same as those of our previous SAXS results.<sup>6</sup> Moreover, the peak position was sensitive towards the concentration of simple ionic salt. It seems definitely infeasible that the SAXS and SANS curves have an interference peak at the same position and, in addition, these curves displayed the upturn due to ionic impurities. Nierlich et al.(7) reported that an upturn could be observed for the system with added salt, but nothing about the peak profile for

the system was mentioned. It is not clear whether the peak was observed at the same position or whether the peak was detected or not. Thus we cannot accept their explanation of the upturn in terms of ionic impurities. For these reasons, it is most reasonable to think that the upturn is due to the cluster formation. However, we must be careful about the use of isotopes ( $D_2O$  for the present case) for SANS measurements. This cannot be avoided to get enough scattering contrast. For long time, it was believed that H and D have chemically the same properties. However, recently, it was found to be incorrect. For example, it was reported that polystyrene - deuterated polystyrene systems are sometimes microphase separated. (13)

**Comparison with DLS Results** The time correlation function obtained by dynamic light scattering (DLS) gives us information on dynamic modes and hence diffusion coefficients of solutes in solutions and dispersions. It was first reported by Lin, Lee, and Schurr(14) that there existed a slow mode in polyelectrolyte solutions (poly-L-lysine in their case) at low ionic strengths. They found a steep drop of the apparent diffusion coefficient with decreasing salt concentration and this phenomenon has been called "ordinary-extraordinary transition". Drifford et al.(15) reported that there were two dynamic (fast and slow) modes, at low ionic strength for NaPSS solutions. It was thought that the slow mode represents a translational motion of (temporal) cluster. Sedlak and Amis(16), and Sedlak(17) claimed that the size of the cluster in NaPSS ( $M_w=5000 - 1200000$ ) solutions at about 0.04 g/ml was in the range of 1000-2000 Å. Matsuoka et al. also found two or three dynamic modes for bovine serum albumin(18) and NaPSS solutions(19) and claimed that the slow mode corresponded to clusters of size of 2000-3000 Å (20). These values are of the same order of magnitude as our present SANS results.

**Model Calculation of the Structure** The approximate size of the cluster has been determined. However, the number or number density of the clusters in solution is still unknown. The information can be obtained by analyses using the absolute scattered intensity. Here, we calculated the number density,  $n$ , by using the results of Guinier analysis, since agreements between simple Guinier ( $R_g$ ) and Porod ( $R_G$ ) analyses were rather good. We assumed the structural model as shown in Figure 7 on the basis of the "two-state structure" model which we earlier proposed. In a cluster whose radius is  $R$ , NaPSS molecules are arranged in a more or less ordered manner. The average separation is  $2D_{exp}$ . This cluster has an average scattering length density of  $\rho_{cluster}$ , which should be in between the that

for  $D_2O$  ( $\rho_{D_2O}$ ) and that for NaPSS molecules ( $\rho_{NaPSS}$ ). In

the disordered regions, some macroions are distributed, and this region has an average scattering length density of  $\rho_{dis}$ . In general, the scattered intensity of neutrons at  $q=0$  is given by Equation 2.

For the model shown above,  $n$  corresponds to the number density of the ordered cluster,  $V$  to the volume of



the cluster ( $=4\pi R^3/3$ ), and  $\Delta\rho = \rho_{D_2O} - \rho_{NaPSS}$ . The scattering length density for each region is represented as follows by those of solvent ( $\rho_{\text{solv}} (= \rho_{D_2O})$ ) and polymer ( $\rho_{\text{polymer}} (= \rho_{NaPSS})$ ):

$$\rho_{\text{cluster}} = \phi_c \rho_{\text{polym}} + (1 - \phi_c) \rho_{\text{solv}} \quad (7)$$

$$\rho_{\text{dis}} = \phi_d \rho_{\text{polym}} + (1 - \phi_d) \rho_{\text{solv}} \quad (8)$$

Hence,

$$\begin{aligned} \Delta\rho &= \rho_{\text{cluster}} - \rho_{\text{dis}} \\ &= (\phi_c - \phi_d)(\rho_{\text{polym}} - \rho_{\text{solv}}) \end{aligned} \quad (9),$$

where  $\phi_c$  and  $\phi_d$  are volume fractions of polymer in the clusters and in the disordered region, respectively.

By using Equation 9, Equation 2 becomes

$$I(0) = \frac{d\Sigma(0)}{d\Omega} = n v^2 (\phi_c - \phi_d)^2 (\rho_{\text{polym}} - \rho_{\text{solv}})^2 \quad (10)$$

and  $\phi_c$  can be written as

$$\phi_c = (N M_w / (N_A d)) / V \quad (11),$$

where  $N$  is the number of polymers in one cluster ( $= V / (2D_{\text{exp}}^3)$ ),  $M_w$  the molecular weight of polymer,  $N_A$  the Avogadro number, and  $d$  the density of the polymer. The total number of polymer in clusters ( $N^*$ ) and the total number of polymers in disordered regions ( $N_{\text{dis}}$ ) are

$$N^* = n N \quad (12)$$

$$N_{\text{dis}} = N_{\text{tot}} - N^* \quad (13)$$

where  $N_{\text{tot}}$  is the total number of polymers in the system. The volume fraction of disordered regions,  $V_{\text{dis}}$ , is

$$V_{\text{dis}} = 1 - v n \quad (14)$$

Hence,

$$\phi_d = (N_{\text{dis}} M_w / (N_A d)) / V_{\text{dis}} = (N_{\text{dis}} M_w / (N_A d)) / (1 - v n) \quad (15)$$

By using Equations 11, 12 and 14, Equation 10 reduces to;

$$\frac{d\Sigma(0)}{d\Omega} = n v^2 \left( \frac{M_w}{N_A d} \right)^2 \left( \frac{N/V - (N_{\text{tot}} - N^*)}{(1 - v n)} \right)^2 (\rho_{\text{polym}} - \rho_{\text{solv}})^2 \quad (16)$$

If we define

$$\alpha \equiv \left( \frac{M_w}{N_A d} \right)^2 (\rho_{\text{polym}} - \rho_{\text{solv}})^2 \quad (17),$$

then

$$\frac{d\Sigma(0)}{d\Omega} = \alpha n v^2 \left( \frac{N/V - (N_{\text{tot}} - N n)}{(1 - v n)} \right)^2 \quad (18)$$

When we define

$$\beta \equiv N - v N_{\text{tot}} \quad (19),$$

then

$$n^{1/2} = \frac{(-\beta \alpha^{1/2} \pm \alpha \beta^2 + 4V(d\Sigma(0)/d\Omega))}{(2(d\Sigma(0)/d\Omega))^{1/2} V} \quad (20)$$

By Equation 20, the number density of the cluster,  $n$ , can be estimated. Here, we used  $\phi_{D20} = 6.05 \times 10^{10}$ , and  $\phi_{NaPSS} = 2.09 \times 10^{10} \text{ cm}^{-2}$ .

The results are summarized in Table III. The general trend of this model calculation is as follows; At low polymer concentration, a large number of relatively smaller clusters are distributed in the system. The difference in the number densities of the polymers between the clusters and the disordered regions are rather large. With increasing polymer concentration, the size of the cluster becomes larger. However, the number density of the clusters become smaller.

**Void Model** As is well known from the Babinet principle, it cannot be determined by simple scattering experiments that the density difference ( $\Delta\rho$ ) is positive or negative. For the present case, it is certain that there exists a large scale density fluctuation in the system, but we cannot claim conclusively that the upturn is solely due to a cluster of high polymer density: the opposite case, i.e. void structure of low polymer density, cannot be excluded. Actually, for some cases, void structures were observed by ultramicroscope for ionic polymer latex dispersions at low ionic strengths.<sup>(20,21)</sup> Hence, we performed a similar model calculation for a void structure.

Figure 9 shows a model of the void structure used in this calculation. For simplicity, we assumed that no polymers were contained in voids and they coexisted with ordered particles. Voids are spheres of radius  $R$ . For the case of void structure, Equation 2 is also valid with the number density of voids,  $n_{\text{void}}$ , and the volume of the void,  $V$ .  $\Delta\rho$  for this case is defined by

$$\begin{aligned} \Delta\rho &= \rho_{\text{order}} - \rho_{\text{solv}(D20)} \\ &= \phi_{\text{order}} (\rho_{\text{polym}} - \rho_{\text{solv}}) \end{aligned} \quad (21)$$

since  $\phi_{\text{order}}$  is given by

$$\phi_{\text{order}} = (c/d)/V_{\text{order}} = c/(d(1-V_{\text{void}} n_{\text{void}})) \quad (22),$$

Equation 21 can be written

$$\Delta\rho = c (\rho_{\text{polym}} - \rho_{D20}) / (d(1-V_{\text{order}} n_{\text{void}})) \quad (23).$$

Then,

$$I(0) = n_{\text{void}} (V_{\text{void}})^2 \alpha / (1-V_{\text{void}})^2 \quad (24)$$

$$\text{where } \alpha \equiv (c/d)(\rho_{\text{polym}} - \rho_{D20}) \quad (25),$$

which gives us  $n_{\text{void}}$  values. The results are summarized in Table III.

The  $n$  value decreased with increasing polymer concentration, which is easily acceptable, while  $n_{\text{void}}$  was not so sensitive towards salt concentration under the conditions studied here. Certainly, with the experimental data available now, it is definitely impossible to conclude whether the void structure really contributes to the

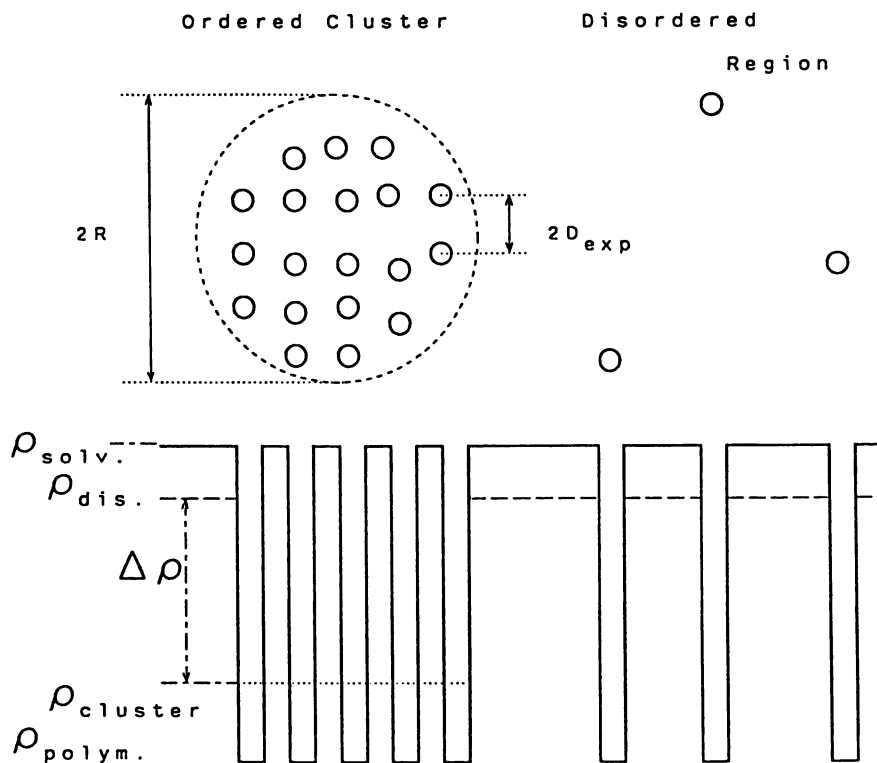


Figure 8 Structural model used for absolute intensity calculation.

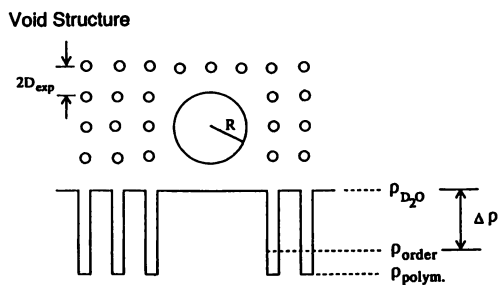


Figure 9 Void model used for absolute intensity calculation.

August 10, 2012 | http://pubs.acs.org  
 Publication Date: December 13, 1993 | doi: 10.1021/bk-1994-0548.ch027

Table III  
Number Density (n) of Clusters and Voids

[NaPSS] (g/ml)	[NaCl] (M)	n	n <sub>void</sub> (10 <sup>12</sup> cm <sup>-3</sup> )
0.01	0	346	838
0.02	0	14.9	269
0.04	0	4.1	117
0.08	0	1.46	51.5
0.04	0.05	8.50	95.2
0.04	0.1	(110)	86.2
0.04	0.3	----	67.4
0.04	0.5	----	88.9

appearance of the upturn, although the model calculation did not provide unacceptable results. Judging from the microscopic observation of the latex dispersions, clusters and void structure are simultaneously present in real solutions. Further study is necessary and in progress in order to clarify the true nature of ionic distribution in polyelectrolyte solutions.

### Conclusions

A steep upturn at very small-angle regions was observed for NaPSS in D<sub>2</sub>O solutions. This upturn reflects the existence of large scale density fluctuation such as ordered clusters. The size of the cluster was estimated by both Guinier and Debye-Bueche analyses. The radius was in the range of 200 - 1000 Å, and increased with increasing polymer concentration. The radii estimated by the simple Guinier method and by using the Porod analysis agreed very well. The linearity of the Debye-Bueche plot was excellent. The number density of the cluster, n, was also calculated by using absolute scattered intensity and decreased with increasing polymer concentration. Both the radius and the number density of clusters were independent of added salt in the concentration range studied here. The possibility of void structure was also considered.

### Acknowledgments

This work is supported by a Grant-in-Aid for Specially Promoted Research (no.63060003) and an International Scientific Research Program from the Ministry of Education, Science and Culture, Japan, and a partial support of the traveling expenses from the Japanese-German Culture Institute, to which our gratitude is due. D.S. would like to thank Yamada Science Foundation for a fellowship. H.M. expresses his sincere thanks to Ms.Rita Thomas, Messers Gerd Meier and Günter Pohl, and other members of the Institute of Festkörperforschung for their kind cooperation and support during his stays in Jülich.

## References

- 1) Ise, N. *Angew. Chem.* 1986, 25, 323. : Ise, N.; Matsuoka, H.; Ito, K. *Macromolecules* 1989, 22, 1 : Ise, N.; Matsuoka, H.; Ito, K.; Yoshida, H.; Yamanaka, J. *Langmuir* 1990, 6, 296.
- 2) Ise, N.; Okubo, T. *Acc. Chem. Res.* 1980, 13, 303.
- 3) Ise, N.; Okubo, T.; Yamamoto, K.; Kawai, H.; Hashimoto, T.; Fujimura, M.; Hiragi, Y. *J. Amer. Chem. Soc.* 1980, 102, 7901.
- 4) Plestik, J.; Mikes, J.; Dusek, K.; *Acta Polym* 1979, 30, 29.
- 5) Matsuoka, H.; Schwahn D.; Ise, N. *Macromolecules* 1991, 24, 4227.
- 6) Ise, N.; Okubo, T.; Kunugi, S.; Matsuoka, H.; Yamamoto, K.; Ishii, Y. *J. Chem. Phys.* 1984, 81, 3294.
- 7) M. Nierlich et al., *J. Physique*, 1979, 40, 701.
- 8) Alefeld, B.; Schwahn, D.; Springer, T. *Nucl. Instrum. Methods Phys. Res.* 1989, A274, 210.
- 9) Guinier, A.; Fournet, G. *"Small-angle Scattering of X-rays"* Wiley, NY, 1955
- 10) Debye, P.; Bueche, A.M. *J. Appl. Phys.* 1949, 20 518.
- 11) Porod, G. *Kolloid Z.* 1951 124, 83.
- 12) Boue, F. et al., *Proc. Symp. Neutron Inelastic Scattering*, 1977, 1, 563.
- 13) Schwahn, D.; Hahn, K.; Sheib, J.; Springer, T. *J. Chem. Phys.* 1990, 93, 8383.
- 14) Lin, S.-C.; Lee, W.I.; Schurr, J.M. *Biopolymers*, 1978, 17, 1041.
- 15) Drifford, M.; Dalbiez, J.P.; *J. Physique*, 1985 46, L-311.
- 16) Sedlack, M.; Amis, E. *J. Chem. Phys.* 1991, 96 817.
- 17) Sedlack, M. *Macromolecules*, in press.
- 18) Matsuoka, H.; Hattori, N.; Ise, N. in preparation.
- 19) Matsuoka, H.; Tomita, H.; Ise, N. in preparation.
- 20) Ito, K.; Yoshida, Y.; Ise, N. *Chem. Lett.*, 1992, 2081.
- 21) Dosho, S. et al., 1993 *Langmuir*, 9, 394.

RECEIVED August 6, 1993

## Chapter 28

# Phase Diagram of Ionic Colloidal Crystals

T. Okubo

Department of Polymer Chemistry, Kyoto University, Kyoto 606-01, Japan

Very large single crystals (3 to 8 mm) are observed with the naked eye in the highly deionized colloidal suspensions of monodisperse polystyrene and silica spheres. Deionization is carefully made with the mixed beds of ion-exchange resins more than three weeks. Two kinds of single crystals, i.e., block-like crystals from homogeneous nucleation in the bulk phase far from the cell wall and the pillar-like ones from the heterogeneous nucleation along the cell wall are observed. Size of the single crystals increases sharply as the concentration of spheres decreases, and is largest at the concentration slightly higher than the critical concentration of melting ( $\phi_c$ ).  $\phi_c$  and the melting temperature ( $T_m$ ) have been measured again for the *completely* deionized suspensions. New  $\phi_c$  values are very small compared with the previous data, whereas  $T_m$  values are high. Important role of the long Debye-screening length around spheres and the intersphere *repulsion* is strongly supported.

Ionic colloidal suspensions display the extraordinary structures in particle distribution, such as gas-like, liquid-like and solid-like [crystal-like and amorphous solid-like (or glass-like)] distributions, especially in deionized state (1-4). The suspensions showing the crystal-like structures are ideal systems for model studies of metals, since the colloidal structures are analyzed with the optical techniques and their forces are readily manipulated by controlling the composition of the suspension. Furthermore, phase transition phenomena such as crystallization and melting occur sharply. A study of the extraordinary structures of colloidal particles is also helpful in understanding fundamental properties of states of substances and electrostatic interactions of macro-ionic systems. The two essentially important factors in the characteristic properties for colloidal systems are an electrostatic interparticle repulsion and an expanded electrical double layers around the particle in the deionized state. These factors are quite different from the features of real metals.

Observation with the naked eye of the iridescent colors and single crystals (or crystallites) is beautiful and impressive! Colloidal crystals are surrounded by grain boundaries and are quite similar to the morphology of metals. Iridescent colors of the crystal-like suspension, which are ascribed to the Bragg diffraction of visible

0097-6156/94/0548-0364\$06.00/0  
© 1994 American Chemical Society

light by the arrayed lattice planes. Lattice spacing of the colloidal crystals is very long by several thousands times compared with that of metals and in the range of light wavelengths. The colors change from reddish to bluish as the concentration of colloidal particles increases in many cases.

In this report we deionized the colloidal suspensions as completely as possible with the Bio-Rad mixed beds of cation- and anion-exchange resins coexisted more than three weeks. Very big colloidal single crystals, 3 to 8 mm in size have been observed with the naked eyes, for the first time, for the completely deionized suspensions in a test tube of 13 mm in outer diameter! Furthermore, the critical concentrations of melting for the completely deionized colloidal suspensions was significantly low compared with the reference values hitherto, and the melting temperature was quite high. Importance of the complete deionization on the appearance of the colloidal single crystals and their phase equilibria is discussed in this report.

### Experimental Section

**Materials.** D1C25, D1C27, D1B76, D1K88, D1B72 and D1B28 were polystyrene spheres purchased from Dow Chemical Co. Colloidal silica spheres of CS-81 and CS-91 were gift from Catalyst & Chemicals Ind. Co.(Tokyo). Diameters( $d$ ), standard deviation( $\delta/d$ ) are listed in Table I with other characteristics. The values of  $d$  and  $\delta$  were determined from an electron microscope. The charge densities of the spheres were determined by conductometric titration with a Wayne-Kerr autobalance precision bridge, model B331, mark II(Bognor Regis, Sussex). Strongly acidic and weakly acidic groups coexisted. All these spheres were carefully purified several times using an ultrafiltration cell(model 202, membrane: Diaflo-XM300, Amicon Co.). Then the samples were treated on a mixed bed of cation- and anion-exchange resins[Bio-Rad, AG501-X8(D), 20-50 mesh] for at least one month. Water used for the purification and for suspension preparation was deionized by using cation- and anion-exchange resins[Puric-R, type 10, Organo Co., Bedford, MA), and further treated with the ion-exchange resins of Bio-Rad. Colloidal suspension was prepared in a test tube(disposable culture tube, borosilicate glass, Corning Glass Works, Corning, N.Y., 11 and 13 mm, inside and outside diameters) shielded tightly with Parafilm(American Can Co., Greenwich, CT). The sample suspensions were treated with a small amount of Bio-Rad resins more than three weeks with up-and-down mixing several times a day.

**Table I. Characteristics of Colloidal Spheres Used**

Sphere	diameter		$\delta/d$	charge density ( $\mu\text{C}/\text{cm}^2$ )	
	$d(\text{nm})$	$\delta$		strong acid	weak acid
D1C25	85	6	0.07	1.5	1.0
D1C27	91	6	0.066	2.0	1.4
D1B76	109	3	0.028	2.1	0.71
D1K88	137	16	0.12	0.58	0.60
D1B72	173	7	0.04	1.0	----
D1B28	212	3	0.014	1.29	0.36
CS-81	103	13.2	0.13	0.38	----
CS-91	110	4.5	0.041	0.48	----

**Close-up Photographing and Video Films.** Photographing of colloidal crystals in a test tube was made with a Canon EOS10 camera, macro-lens(EF50

mm,  $f=2.5$ ) and life-size converter EF(5). Light source was a pocket-type flash light. Velvia film[Fuji chrome, RVP135, ISO=50] was used for color transparencies. Close-up video films were taken with a video-camera recorder(Hi-8, CCD-V800, Sony). Color photographs from the video films were reproduced with a color printer(NV-MP1, Panasonic). Microscopic photographs were taken with a metallurgical microscope, type PME3-211U of Olympus Co.(Tokyo) and a Plan-Neofluar objective-lens(100x, oil) of Carl-Zeiss, Germany.

**Reflection Spectroscopy.** The reflection spectra of an incident angle of ninety degree were recorded on a multichannel photodetector(MCPD-110B, Otsuka Electronics, Hirakata, Osaka) connected to a Y-type optical fiber cable. The instrument was operated by a microcomputer(MC8000, Otsuka Electronics).

**Determination of Melting Temperature.** The test tubes containing the completely deionized suspension were immersed into a water bath which was made from smooth quartz glass and contained deionized water, a cooling tube and a heater(6-8). Temperature of the bath was raised very slowly from 8 °C to 92 °C during three or four hours. Melting temperature was determined with the naked eye,i.e., the brilliant iridescent colors and/or colloidal single crystals disappeared distinctly at the melting point.

## Results and Discussion

Figure 1 shows a close-up photograph of the colloidal single crystals appeared for the monodispersed silica spheres, CS-91. The suspensions were deionized with the Bio-Rad resins for eighteen days in an observation test tube. Picture was taken one hour after up-and-down mixing of the suspension. Very big and beautiful single crystals are observed for the very diluted suspension, 0.0008 in volume fraction of spheres. Changes in colors from bluish to reddish is due to the changes of incident angles of light through the curved wall of test tube. These patterns of single crystals changed rapidly with very slow rotation of the test tube. Two kinds of single crystals are observed, very large block-like crystals and the pillar-like ones. The former appears in the bulk phase far from the cell wall, and grows up from the homogeneous nucleation mechanism. On the other hand, the latter is from heterogeneous nucleation along the cell wall. Shapes of the former were quite various. Triangle, cubic-like, pentagonal, hexagonal, and even cone-like single crystals have been observed. Figure 2 shows typical shapes of the single crystals in the completely deionized suspension of CS-81 spheres. Size is between 1.5 and 3 mm. It should be noted here that the fundamental features of the single crystals do not depend on the kind of spheres examined, polystyrene or silica spheres.

Figure 3 shows the colloidal single crystals of CS-91 spheres at different concentrations, from the top, 0.0007, 0.0008 and 0.001 in volume fraction. Size of the single crystals decreased as sphere concentration increased, though their size is highly dispersed.

Figure 4 shows the changes in size of single crystals of monodisperse polystyrene spheres(D1B76) as a function of sphere concentration. The suspensions were completely deionized more than three weeks after suspension preparation. Circles in the figure show the rough values of average sizes taken with a ruler from the close-up pictures. Very large single crystals were observed for suspensions at the concentrations a bit higher than the critical concentration of melting,  $\phi_c=0.00016$  at 25 °C. Size of the single crystals decreased very sharply as sphere concentration increased. Note here that the very large crystals appeared in the narrow range of diluted concentrations. This observation is understandable, because size should increase as number of nuclei decreases and then as sphere concentration decreases. The nucleation rate( $J$ ) for the homogeneous nucleation mechanism is given by eq 1.



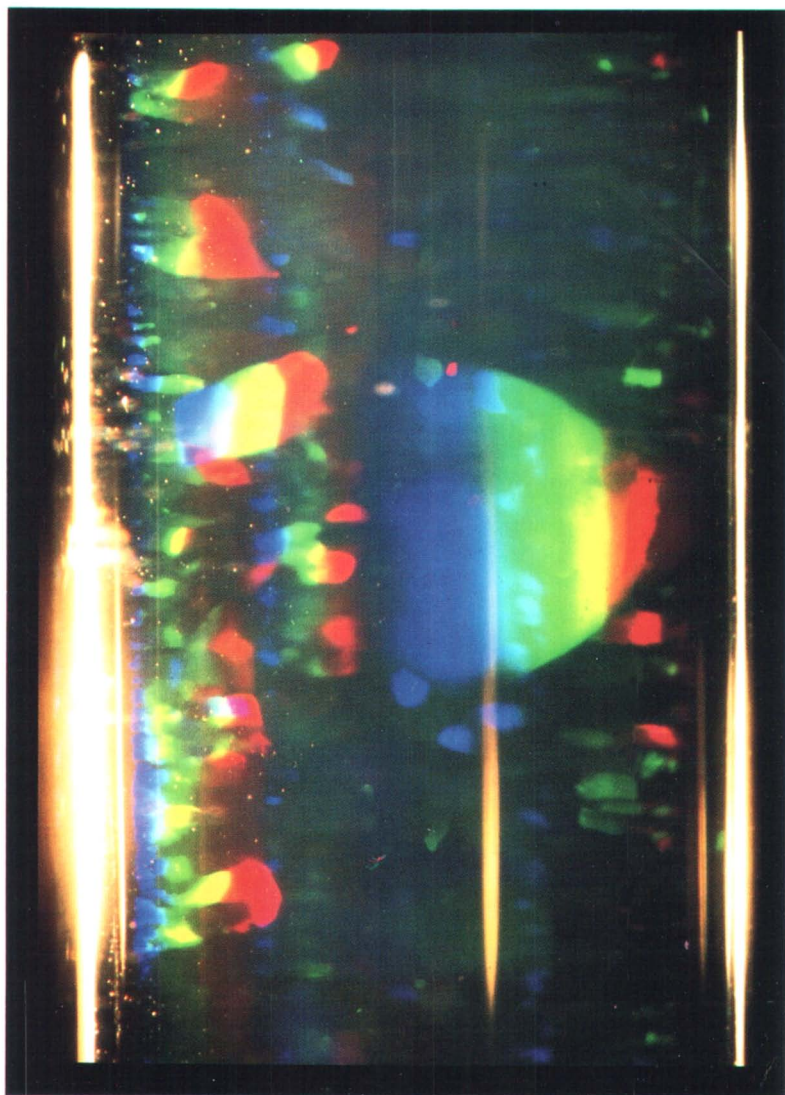


Figure 1. A close-up color picture of CS-91 suspension with the resins at  $\phi=0.000829$ . Picture was taken 18 days after suspension preparation and 1 hour after up-and-down mixing. exposure=1 s, iris=22. Distance between bright outside lines is 13 mm. Brilliant colors are ascribed to the Bragg diffraction of visible light by the lattice planes of colloidal single crystals. The lattice spacing is just in the range of light wavelengths.

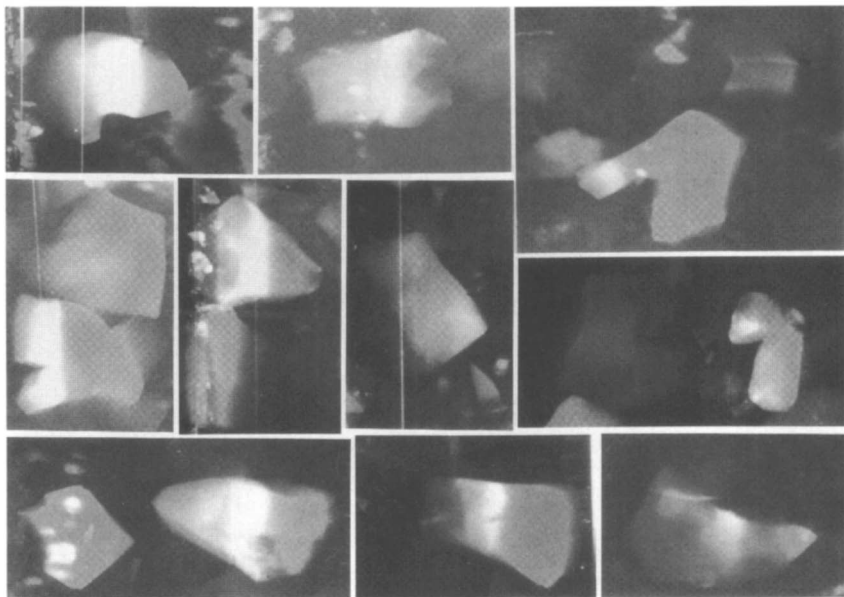
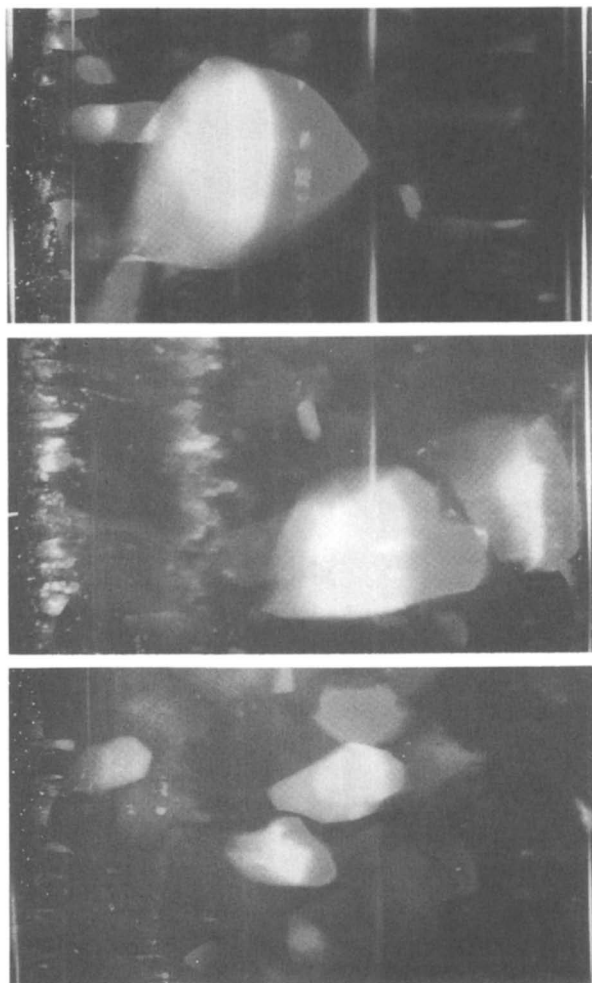


Figure 2. Examples of the colloidal single crystals observed for CS-81 suspensions with the resins.  $\phi=0.00144$ . Pictures were taken 11 days after suspension preparation and more than 10 hours after up-and-down mixing. exposure=2 s, iris=22.



**Figure 3.** Close-up pictures of CS-91 suspension with ion-exchange resins 3 weeks after suspension preparation. From the top,  $\phi=0.000682$ ,  $0.000833$ , and  $0.00114$ . 62 min, 15 min, and 4 min after up-and-down mixing, respectively. Distance between the bright outside lines is 13 mm.

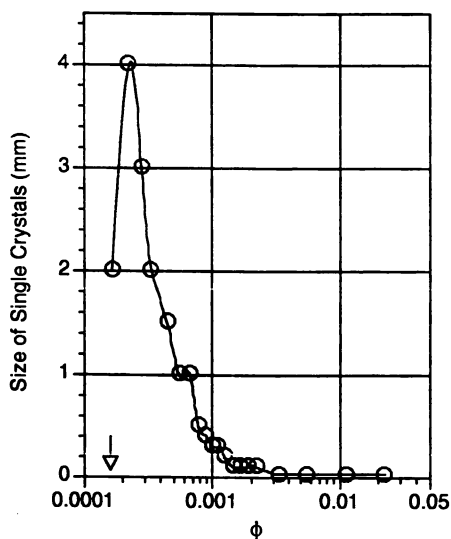


Figure 4. Plots of size of single crystals in the deionized D1B76 (diameter=109 nm) suspension against sphere concentration. Arrow shows the critical concentration of melting,  $\phi_c=0.00016$ . (Adapted from reference 19.)

$$J = K \exp(\Delta G/kT), \quad (1)$$

where  $K$  is the kinetic coefficient.  $\Delta G$  is the critical activation free energy for nucleation.  $\Delta G$  is given by eq 2(9).

$$\Delta G \propto (\ln r)^{-2}, \quad (2)$$

where  $r$  is  $\phi/\phi_c$ .  $\phi_c$  is the critical concentration of melting. Combination of eqs 1 and 2 supports the observation shown in Figure 4.

When sphere concentration is comparatively high, the size becomes small. Figure 5 shows the examples of single crystals of alloy structures appeared for the binary mixtures of monodisperse polystyrene spheres, 85 nm(D1C25) and 173 nm (D1B72)(10). Size of the single crystals formed from the two component spheres is now small, in the order of hundred micrometers, and these photographs are taken using a metallurgical microscope. When sphere concentration is much high, single crystals become very small and can not be recognized with the naked eyes. However, strong brilliant colors are observed as is shown in Figure 6. In this picture large black and brown particles are the ion-exchange resins coexisted.

Colloidal crystals are broken very easily by shearing forces induced by up-and-down mixing. This occurs because the elastic moduli of the crystals are very small in the order of  $10^{-2}$  and  $10^3$  Pa for typical cases(2). When the suspension leaves to stand after up-and-down mixing, small crystals appear again and grow up further to large crystals with time. As is shown in Figure 7 small crystals from the homogeneous nucleation are spherical at the beginning, and their shape becomes squarish for the large crystals. Aastuen et al.(11) reported the nearly spherical growing single crystals having rough interfaces with a time-independent interface velocity.

Figure 8 shows growing process of the pillar-like single crystals along the cell wall. Single crystals from the homogeneous nucleation are not observed. Crystal growth along the cell wall can be also analyzed from the sharpened peaks in the reflection spectra with time. Figure 9 shows the typical changes in the spectra in the course of crystallization. The mean size of the single crystals are estimated from the half-width of the reflection peak by using Scherrer's equation. As is clear in this figure crystallization is fast. Size of single crystals thus estimated is shown in Figure 10. Size increased linearly with time at the beginning. The rate coefficient increased as sphere concentration increased. Furthermore, an induction period appeared. Further analyses are now in progress in our laboratory.

Table II compiles the critical concentrations of melting( $\phi_c$ ) for the aqueous suspensions of polystyrene spheres, which have been deionized with the Bio-Rad resins more than three weeks(data C). The data A and B are our previous ones for the suspensions treated in the observation cells without resins(12) and with resins shortly for one hour(6), respectively. Clearly, the  $\phi_c$  values decreased substantially, one thirties when three experiments are compared. This finding is rather surprising because the concentrations of the diffusible simple ions are not so different to each other, ranging from  $10^{-7}$  to  $10^{-6}$  mole/dm<sup>3</sup>. This table demonstrates that very careful and complete deionization process of the suspension is essential to obtain the reliable value of  $\phi_c$ .

Ionic groups on the colloidal surfaces leave their counterions in the suspension, and these excess charges accumulate near the surfaces forming an electrical double layer. The double layer consists of two regions; an inner region composed of adsorbed counterions(the Stern layer) and a diffuse region containing the remainder of the excess counterions(Gouy-Chapman layer). The counterions in the diffuse region are distributed according to a balance between their thermal motion and the

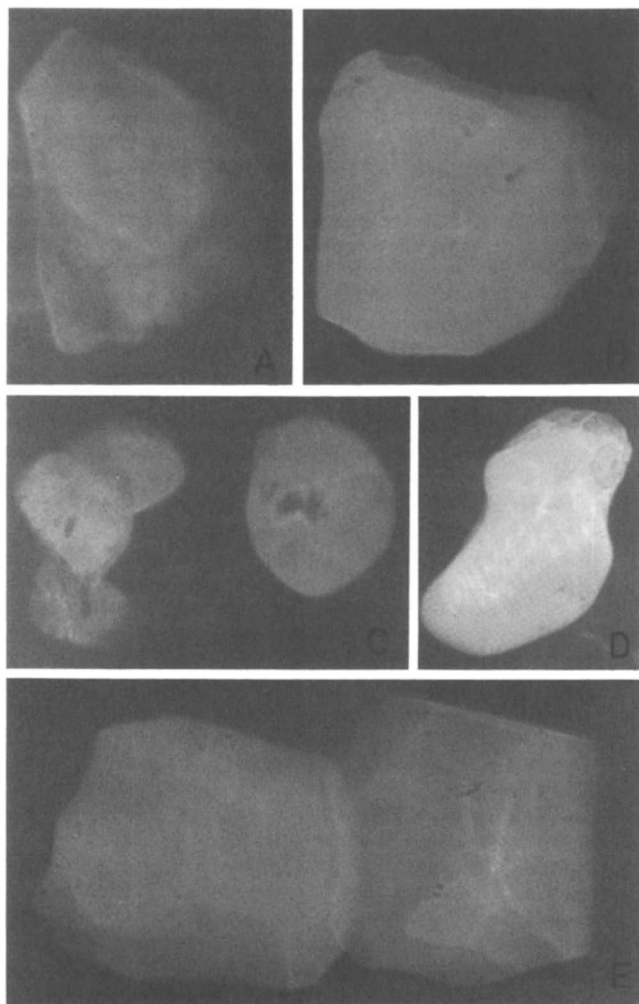
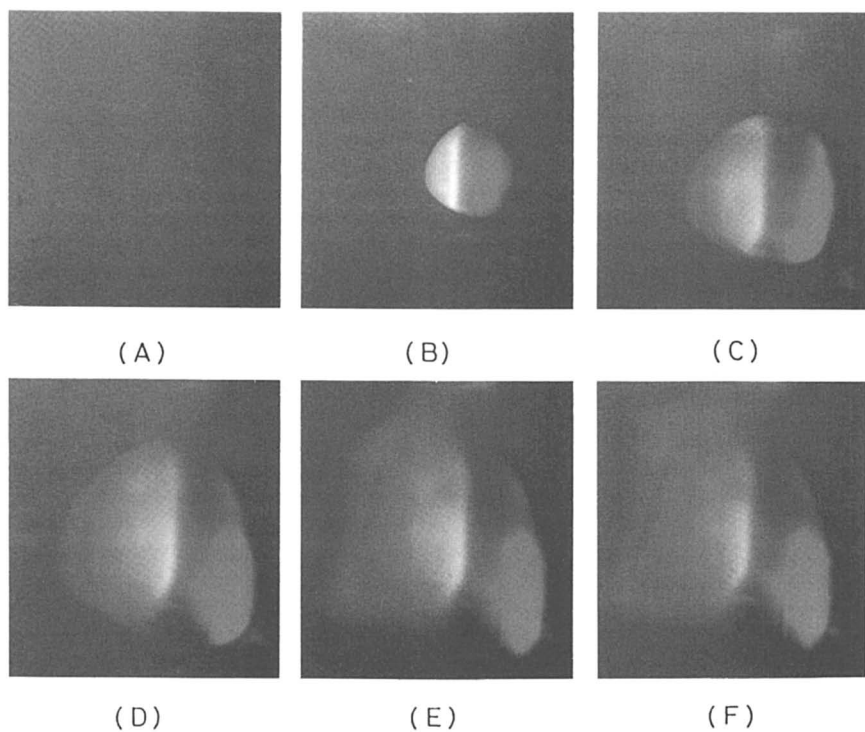


Figure 5. Microscopic photographs of single crystals for binary mixture of D1C25 ( $d=85$  nm,  $\phi=0.0136$ ) and D1B72 (173, 0.0205).



**Figure 6.** Close-up photograph of D1B76 ( $d=109$  nm,  $\phi=0.1$ ) suspension in the presence of the Bio-Rad resins. Outside diameter of the vessel is 15 mm.



**Figure 7.** Close-up photographs from video camera for CS-91 suspension with the Bio-Rad resins in the course of crystal growth.  $\phi=0.000984$ , 3 weeks after suspension preparation. A, 2 min after mixing; B, 4; C, 6; D, 8; E, 11; and F, 20. Size of each frame of the picture is 3 mm  $\times$  3 mm.



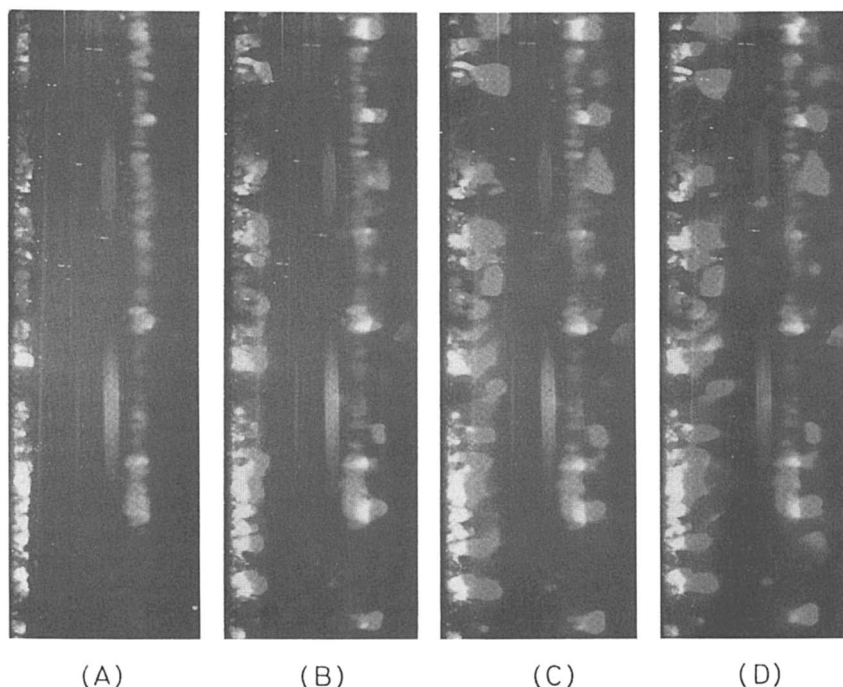


Figure 8. Close-up photographs for CS-91 suspension with ion-exchange resins in the course of crystal growth.  $\phi=0.000682$ . A, 7 min after mixing; B, 15; C, 26; and D, 62. Width of each frame is 7 mm.

**Table II. Critical Concentrations of melting( $\phi_c$ ) of Deionized Suspensions of Polystyrene Spheres at 25 °C**

Sphere	A	$\phi_c$ B	C
D1C25	0.005	0.002	0.0014
D1C27	0.002	0.001	0.0003
D1B76	0.005	0.001	0.00016
D1K88	---	0.001	0.00037
D1B28	---	0.002	0.00035
D1B72	0.025	0.0015	0.00038

A) without resins, B) with resins for 1 hr,  
C) with resins coexisted for more than 3 weeks(this work).

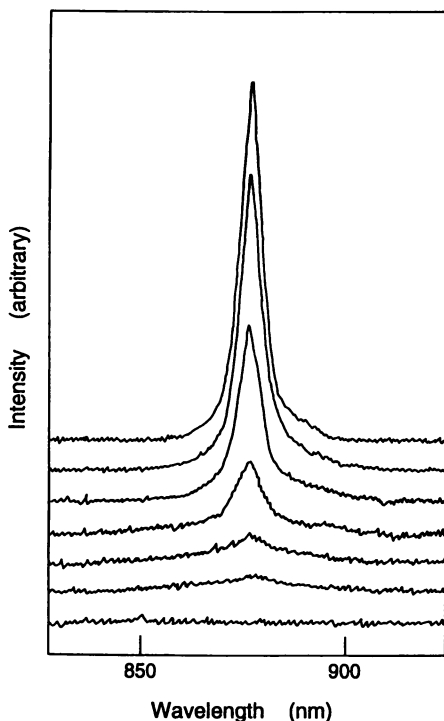


Figure 9. Reflection spectra in the course of crystal growth for CS-91 suspension with ion-exchange resins at 23 °C.  $\phi=0.00262$ , 9 days after suspension preparation. From the bottom curve 15 s after mixing, 20 s, 25 s, 30 s, 35 s, 45 s, and 300 s.

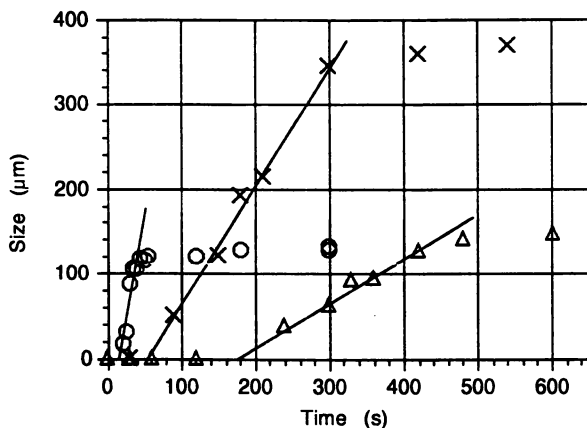


Figure 10. Size of single crystals for CS-91 suspension estimated from the half-width of the reflection peak shown in Figure 9. O:  $\phi=0.00262$ , x: 0.00179,  $\Delta$ : 0.00143.

forces of electrical attraction with the colloidal spheres. The thickness of the diffuse double layer is approximated by the Debye-screening length,  $\lambda_{DH}$

$$\lambda_{DH} = (4\pi e^2 n / \epsilon k T)^{-1/2}, \quad (3)$$

where  $e$  is the electronic charge,  $\epsilon$  is the dielectric constant of the solvent,  $k$  is the Boltzmann constant and  $n$  is the concentration of free-state cations and anions in suspension, and given by  $n = n_c + n_s + n_o$ , where  $n_c$  is the concentration (number of ions per  $\text{cm}^3$ ) of diffusible counterions,  $n_s$  is the concentration of foreign salt, sodium chloride, for example,  $n_o$  is the concentration of both  $\text{H}^+$  and  $\text{OH}^-$  from the dissociation of water. In order to estimate  $n_c$ , the fraction of free-state counterions ( $\beta$ ) must be known, and has been estimated from the conductometric, transference and electrophoretic measurements hitherto (13). Note that the maximum in the  $\lambda_{DH}$  values, which were estimated from  $l$  values observed using the relation,  $l = d + 2 \times \lambda_{DH}$ , was ca. 1  $\mu\text{m}$  in water. The similar value of  $\lambda_{DH}$  (1.2  $\mu\text{m}$ ) was also estimated from eq 3 by taking  $n_o = 2 \times 10^{-7}$  (moles/liter)  $\times N_A \times 10^{-3} \text{ cm}^{-3}$ , where  $N_A$  is Avogadro's number.

According to the effective hard-sphere model, which is a simple but very convenient one for the deionized colloidal suspension, crystal-like ordering is formed when the effective diameter ( $d_{eff}$ ) of the spheres containing the Debye-screening length is close to or larger than the intersphere distance ( $l$ ), i.e.,  $d_{eff}$  [diameter( $d$ ) +  $2 \times \lambda_{DH}$ ]  $> l$ . Figure 11 shows comparison of the  $d_{eff}$  values estimated using eq 3 and the intersphere distance at the critical concentration of melting ( $l_c$ ). The agreement between  $d_{eff}$  and  $l_c$  is excellent, though the deviation can not be neglected when  $l_c$  is extremely large, i.e., larger than 2  $\mu\text{m}$ . This supports the validity of the effective hard-sphere model. Systematic comparison of  $d_{eff}$  and  $l$  values has supported the validity of the effective hard-sphere model strongly (2, 14, 15). The Debye-screening length is, therefore, essentially an important factor for the formation of colloidal crystal.

Phase diagram between crystal-like and liquid-like structures, which plots the sphere concentration against concentration of sodium chloride added, is shown in Figure 12. This figure also shows the change in size of single crystals. Concentrations of the diffusible simple ions (most of them will be hydronium and hydroxide ions in aqueous media) in suspension with and without ion-exchange resins coexisted are estimated to be close to  $2 \times 10^{-7}$  moles/liter and  $1 \times 10^{-6}$  moles/liter, respectively. Clearly,  $\phi_c$  values increase substantially by the addition of a small amount of sodium chloride.

Williams et al. (16) have measured, for the first time, the melting temperature of colloidal crystals of monodisperse polystyrene spheres as a function of sphere concentration. Heat of melting and entropy change were 4 to 5 kcal/mole and 10 to 16 e.u., respectively. This author measured the melting temperature for the *completely* deionized colloidal crystals. Figure 13 shows the three sets of melting temperatures measured by Crandall et al. (16) (open circles), ours (6) and this work for the deionized suspensions of monodisperse polystyrene spheres purchased from Dow Chemical Co. (diameter=109 nm for all data). Clearly, melting temperature increased with years reported. A small amount of ionic impurities lowered melting point to below room temperature. Data shown by crosses were obtained two or three hours after suspension preparation in the quartz observation cell with the Bio-Rad resins. It is clear that the reliable data of melting temperature for the *completely* deionized suspension can be obtained after the resin treatment more than three weeks.

Figure 14 shows the plots of the energy parameter,  $kT/U_a$  against the ionic parameter,  $l$ . These parameters are given by eqs 4 and 5, respectively.

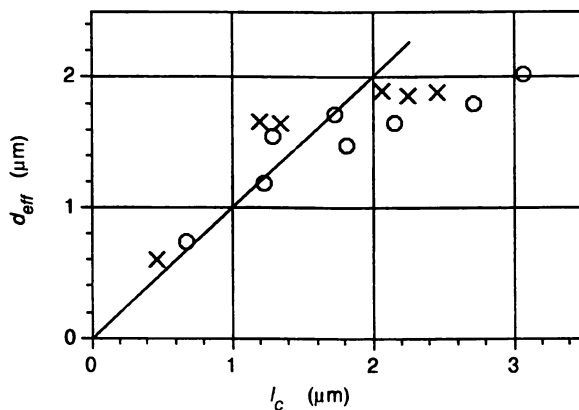


Figure 11. Comparison of  $d_{eff}$  and  $l_c$ .  $\circ$ : polystyrene spheres,  $\times$ : silica spheres.

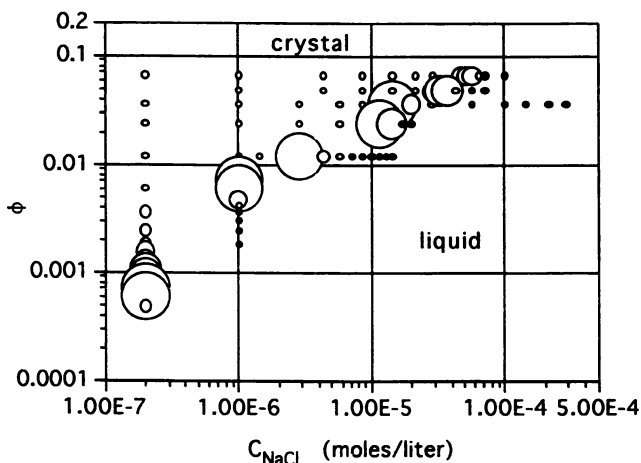


Figure 12. Phase diagram of CS-81 suspension as the  $\phi$  vs. salt concentration plots. Very large open circles: size of single crystal is larger than 3 mm; large circles: 1.5 to 3 mm; medium circles: 0.7 to 1.5 mm; small circles: 0.2 to 0.7 mm; very small circles: smaller than 0.2 mm; very small filled circles: liquid state.

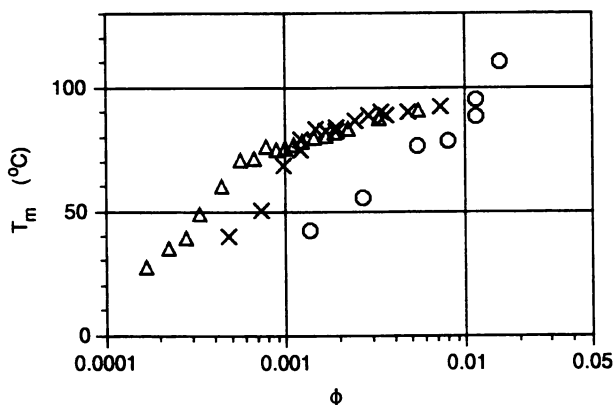


Figure 13. Plots of melting temperature of deionized suspensions of monodisperse polystyrene spheres ( $d=109$  nm) against sphere concentration ( $\phi$ ). O: Crandall et al. (15), x: Okubo (6),  $\Delta$ : this work. (Adapted from references 18 and 19.)

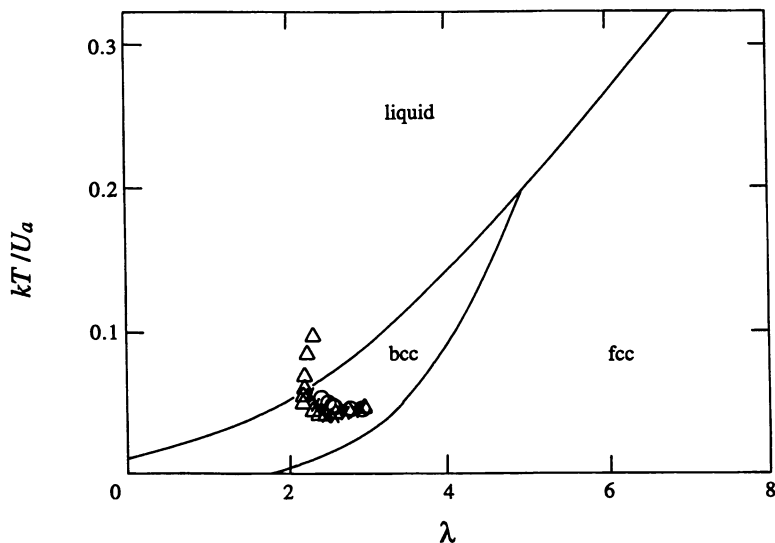


Figure 14. Plots of  $kT/U_a$  against  $\lambda$ . O: experimental data for the phase transition of deionized suspension of polystyrene spheres ( $d=109$  nm) between liquidlike and crystallike structures (Williams et al. (15)); x: data for the transition of D1B76 suspension between liquidlike and bcc structures (6),  $\Delta$ : this work.  $\beta=0.1$ ,  $Z=490$ , —: theory (16). (Adapted from reference 18.)

$$kT/U_a = (\epsilon l k T / \alpha^2 e^2) \exp(\lambda) \quad (4)$$

$$\lambda = \kappa l \quad (5)$$

where,  $\kappa$  is the inverse of Debye-screening length,  $l$  is the average intersphere separation, and  $\alpha$  is the effective charge number of a colloidal sphere obtained as the stoichiometric number of charges ( $Z$ ) multiplied by the  $\beta$ -values, i.e.,  $\alpha = \beta Z$ . The solid curves in Figure 14 are the theoretical ones separating liquid-like and crystal-like [body-centered-cubic (bcc)] structures. Open circles are the experimental reported by Williams et al. (16) for the phase transition between liquid-like and crystal-like structures. Crosses are the data reported previously by us (6). Agreement between the theory (17) and the experiment is satisfactory. However, sphere concentration dependence is not explained so nicely with the theory (18, 19).

### Acknowledgments

This research was supported by a grant-in-aid from the Japanese Ministry of Education, Science and Culture. The author is also grateful to the Kawasaki Steel 21st Century Foundation and Iketani Science and Technology Foundation for financial support.

### Literature Cited

1. Pieranski, P. *Contemp. Phys.* 1983, 24, 25-73.
2. Okubo, T. *Acc. Chem. Res.* 1988, 21, 281-286.
3. Ottewill, R.H. *Langmuir* 1989, 5, 4-9.
4. Russel, W.B.; Saville, D.A.; Schowater, W.R. *Colloidal Dispersions*; Cambridge Univ. Press: Cambridge, 1989.
5. Okubo, T. *Naturwissenschaften* 1992, 79, 317-320.
6. Okubo, T. *J. Chem. Phys.* 1991, 95, 3690-3697.
7. Okubo, T. *J. Chem. Phys.* 1992, 96, 2261-2268.
8. Okubo, T. *Colloid Polymer Sci.* 1992, 270, 1018-1026.
9. Boistelle, R.; Astier, J.P. *J. Crystal Growth* 1988, 90, 14-30.
10. Okubo, T. *J. Chem. Phys.* 1990, 93, 8276-8283.
11. Aastuen, D.J.W.; Clark, N.A.; Cotter, L.A.; Ackerson, B.J. *Phys. Rev. Lett.* 1986, 57, 1733-1736.
12. Okubo, T. *J. Chem. Soc. Faraday Trans.* 1990, 86, 2871-2876.
13. Okubo, T. *J. Colloid Interface Sci.* 1988, 125, 380-385.
14. Okubo, T. *J. Chem. Phys.* 1987, 87, 5528-5533.
15. Okubo, T. *J. Chem. Phys.* 1989, 90, 2408-2415.
16. Williams, R.; Crandall, R.S.; Wojtowicz, P.J. *Phys. Rev. Lett.* 1976, 37, 342-351.
17. Kremer, K.; Robbins, M.O.; Grest, G.S. *Phys. Rev. Lett.* 1986, 57, 2694-2697.
18. Okubo, T. *Colloid Polym. Sci.*, in press.
19. Okubo, T. *Prog. Polym. Sci.*, in press.

RECEIVED September 16, 1993

## Chapter 29

# Phase Diagram of Polyelectrolyte Solutions in Presence of Multivalent Salts

M. Delsanti, J. P. Dalbiez, O. Spalla, L. Belloni, and M. Drifford

Commissariat à l'Énergie Atomique, Centre d'Étude de Saclay, Service  
de Chimie Moléculaire, 91191 Gif-sur-Yvette Cédex, France

Aqueous solutions of sodium poly(styrene sulfonate) with multivalent added electrolytes present complex behaviors. Phase diagrams were experimentally investigated. At a given polymer concentration, there exist lower and upper limits of added electrolyte concentration between which phases separation occurs. This behavior was studied as a function of polymer concentration and for different valencies of the added cation. The two phases region increases as the valency increases. In presence of an excess of added monovalent salt, the two phases region is reduced and can disappear.

Mixtures of entities having opposite charges are important in several applications. In the recent years, a developing field of research was the study of polymer/polymer and polymer/spherical particle (surfactant or colloid) mixtures (1-3). Most studies were carried out on systems made of polyelectrolyte and oppositely charged surfactant. In such systems, the solution is usually homogeneous in default of surfactant. Upon further addition of surfactant the dispersion phase separates. With a large excess of surfactant the dispersion becomes again homogeneous. In the present work, our goal is to study simple situations where the two entities are well known: the polyelectrolyte is an anionic linear polymer, the poly(styrene sulfonate), and the particles of opposite charge are various cations of different valencies:  $\text{Na}^+$ ,  $\text{Ca}^{2+}$ ,  $\text{La}^{3+}$ , and  $\text{Th}^{4+}$ . The ionic radii of all these cations are within 10% identical (4). These systems can be considered as simple systems in the sense that attractive interactions between the anionic polyelectrolyte and the cations are dominated by electrostatic interactions. Mixtures of polyelectrolyte with small cations were already studied in particular with polyacrylic and polymethacrylic acids (5-6). In these systems, phase separation with added salt, called salting out, was observed. In order to see if this behavior is general, it is important to study phase behaviors of various polyelectrolyte/salt systems. In this paper is reported the systematic study of the phase diagrams of the following mixtures:  $\text{NaPSS}/\text{NaCl}$ ,  $\text{NaPSS}/\text{CaCl}_2$ ,  $\text{NaPSS}/\text{LaCl}_3$ ,  $\text{NaPSS}/\text{Th}(\text{NO}_3)_4$ , and  $\text{NaPSS}/\text{LaCl}_3/\text{NaCl}$ .

0097-6156/94/0548-0381\$06.00/0  
© 1994 American Chemical Society

## Experimental Section

The sodium poly(styrene sulfonate) samples (NaPSS) were purchased from Pressure Chemical and had molecular weights  $M_w$  ranging between 4,000 and 1,600,000 daltons. The polydispersity index  $M_w/M_n$  of all these samples was smaller than 1.1 and their nominal degree of sulfonation was 1. The sample mostly used, in the determination of phase diagrams had a molecular weight  $M_w = 780,000$  and a polydispersity index  $M_w/M_n = 1.1$ . The added salts used in the preparation of the solutions, NaCl, CaCl<sub>2</sub>, LaCl<sub>3</sub>, and Th(NO<sub>3</sub>)<sub>4</sub>, are of analytical grade. Influence of addition of univalent salt (NaCl) on the phase diagram of NaPSS/LaCl<sub>3</sub> system was studied using a NaPSS sample purchased from Aldrich. This polymer prepared by radical polymerization exhibited a large molecular weight distribution. This sample was characterized, in our laboratory, by aqueous gel permeation chromatography with a small angle light scattering detector on line. The molecular weight was of 70,000 daltons and the polydispersity index  $M_w/M_n$  was equal to 2.5. Degree of sulfonation was measured by counterions titration and found to be equal to  $0.96 \pm 0.04$  close to 1 the nominal value. To purify and eliminate extra free ions, all the sodium salts of poly(styrene sulfonate) were dialysed against deionized water. The NaPSS plus salt solutions were prepared by using a deionized water upon passing it through MilliQ Millipore system of pore size 0.22 micron (18 M ohm cm). The pH was adjusted to a value of 3 by adding HCl or HNO<sub>3</sub> acid; in this way lanthane and thorium cations were not hydrolyzed (7, 8).

Phase diagrams were determined, at a temperature close to 25°C, by visual inspection of solutions and, in some cases, by light scattering measurements at a given scattering vector equal to  $0.0023 \text{ \AA}^{-1}$  (scattering angle of 90° in the present experimental set up). In general, the visual aspect of a two phases system is characterized by a small viscous drop of concentrated polystyrene at the bottom of the cell. Experimental investigations were generally limited to polymer concentration ranging between 0.001 and 0.5 mol/l. Thus, sharp boundaries at the lowest and highest polymer concentrations in phase diagrams reported in the different figures have no physical meaning and are only due to the limitation in the polymer concentration investigated. At a given NaPSS concentration, as salt concentration increased, the intensity scattered by solutions drastically increased near the appearance of the two phases region. We must point out that it is not clear if it is the spinodal or the binodal line which was experimentally determined. As a first approximation, we can assume that it is the unstable region which was determined and thus experimental phase boundary is closer to the spinodal line. In all cases, the phase separation is reversible upon salt concentration variations.

## Results

The main results are summed up in Figure 1, where boundaries of the two phases region and the intensity of the light scattered by NaPSS solutions of molecular weight 780,000 daltons at a polymer concentration  $C_p = 0.0338$  Monomer mol/l is plotted against the concentration  $C_s$  of the different added salts (thorium, lanthane, calcium, and sodium salts). At a given polymer concentration, the intensity of the light scattered by the solution increases as the salt concentration increases. In the case of tetravalent and trivalent cations, there exists a salt concentration region between  $C_s^*$  and  $C_s^{**}$  where solutions phase separate. For divalent and monovalent cations, the mixtures remain homogeneous. In the case of divalent cations, the scattered intensity only presents a broad maximum. For monovalent cation, no such behaviors are



observed, the intensity of the light scattered by solutions monotonically increases with increasing salt concentration (at least in the investigated domain  $C_S < 1$  mol/l).

**Polymer Concentration Dependence of  $C_{S3}^*$  and  $C_{S3}^{**}$ .** For a given molecular weight ( $M_w = 780,000$ ), the variation of the salt concentration region, where phase separation occurs, is plotted as a function of polyelectrolyte concentration in Figures 2 and 3 for NaPSS/LaCl<sub>3</sub> and NaPSS/Th(NO<sub>3</sub>)<sub>4</sub> systems, respectively. In both systems, the lower salt concentration limit of the two phases region  $C_{S3}^*$  increases when polymer concentration increases and is proportional to the polymer concentration. We have:

$$C_{S3}^*/C_p = 0.23 \pm 0.03 \quad (1. a)$$

$$C_{S4}^*/C_p = 0.12 \pm 0.01 \quad (1. b)$$

for NaPSS/LaCl<sub>3</sub> and NaPSS/Th(NO<sub>3</sub>)<sub>4</sub> systems, respectively. In the experimental range of polymer concentration investigated, the upper salt concentration limit of the two phases region  $C_{S3}^{**}$  is nearly independent of the polymer concentration. The upper limits could be approximated by the following empirical relations:

$$C_{S3}^{**} \approx 0.30 \times C_p^{0.033} \quad (2. a)$$

$$C_{S4}^{**} \approx 1.14 \times C_p^{0.090} \quad (2. b)$$

for NaPSS/LaCl<sub>3</sub> and NaPSS/Th(NO<sub>3</sub>)<sub>4</sub> systems, respectively.

**Molecular Weight Dependence of  $C_{S3}^*$  and  $C_{S3}^{**}$ .** Systematic studies of the evolution of phase diagram as a function of molecular weight were not performed. However, molecular weight dependence of the lower and upper limits in salt concentration,  $C_{S3}^*$  and  $C_{S3}^{**}$ , at two given polymer concentrations (0.1 and 0.01 mol/l) were established for the NaPSS/LaCl<sub>3</sub> system (see Figure 4). Whatever is the polymer concentration, the lower limit  $C_{S3}^*$  is molecular weight independent between 4,000 and 1,600,000 daltons. Figure 4 shows also that a decrease in molecular weight results in a decrease of the upper limit salt concentration  $C_{S3}^{**}$ . The decrease is less pronounced at the highest polymer concentration. In other words, at a given polyelectrolyte concentration, the extension of the two phases region decreases as the size of the polymer decreases. This effect is more pronounced as the polyelectrolyte concentration is lowered.

**Modification of the Phase Diagram of NaPSS/LaCl<sub>3</sub> System in Presence of Added NaCl Salt.** We study now how the phase diagram NaPSS/LaCl<sub>3</sub> presented in Figure 2 changes in presence of different added NaCl salt concentrations. The mixtures are five components systems : four different ionic species and the water. The requirement of charge neutrality reduces the number of variables by one and thus we have 3 independent variable concentrations. To fully describe these systems, 3 independent concentrations are needed . Figure 5 represents different cross sections of the three dimensional phase diagram which correspond to different added NaCl concentrations. The NaPSS sample used in this study ( $M_w = 70,000$ ) is very polydisperse and consequently, the observed phase diagrams, reported in Figure 5, can be only considered as apparent phase diagrams. To comparison, we have reported in the same figure the phase diagram obtained with NaPSS of molecular weight 780,000 (see Figure 2). Figure 5 clearly shows that addition of univalent salt results

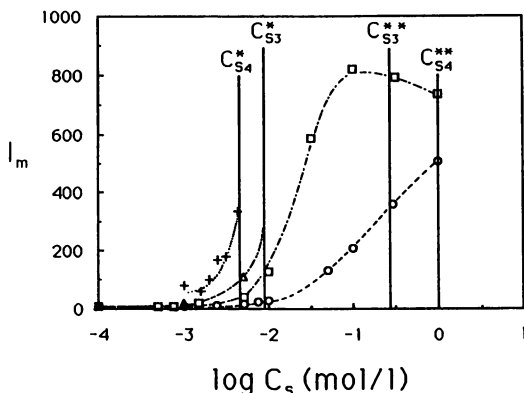


Figure 1. Typical variation of the light intensity scattered per polystyrene monomer,  $I_m$ , as a function of salt  $C_s$  for various multivalent cations of valency  $z$ : (circle) NaCl,  $z = 1$ ; (square)  $\text{CaCl}_2$ ,  $z=2$ ; (triangle)  $\text{LaCl}_3$ ,  $z = 3$ ; (cross)  $\text{Th}(\text{NO}_3)_4$ ,  $z = 4$ . Solid vertical lines represent the boundaries of the two phases region for mixtures with cations of valency  $z \geq 3$ . A phase separation appears when  $C_{S_z}^* \leq C_s \leq C_{S_z}^{**}$ . In all cases, the monomer concentration is  $C_p = 0.0338$  Monomer mol/l.

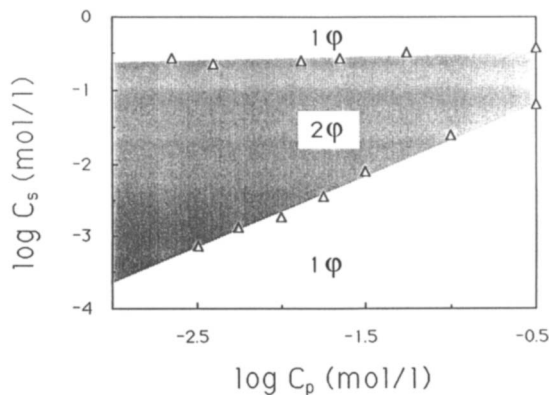


Figure 2. Phase diagram of NaPSS/ $\text{LaCl}_3$  ( $M_w = 780,000$ ) system. Hatched region represents the two phases region.

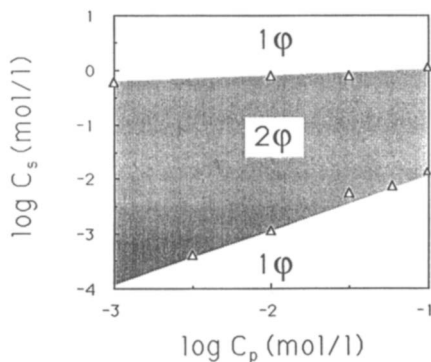


Figure 3. Phase diagram of NaPSS/Th(NO<sub>3</sub>)<sub>4</sub> ( $M_w = 780,000$ ) system. Hatched region represents the two phases region.

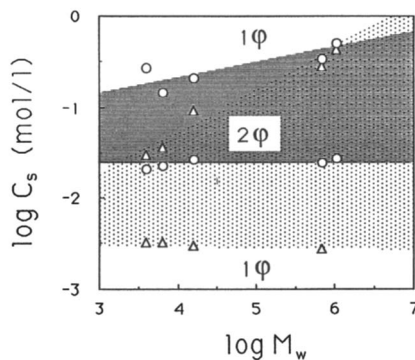
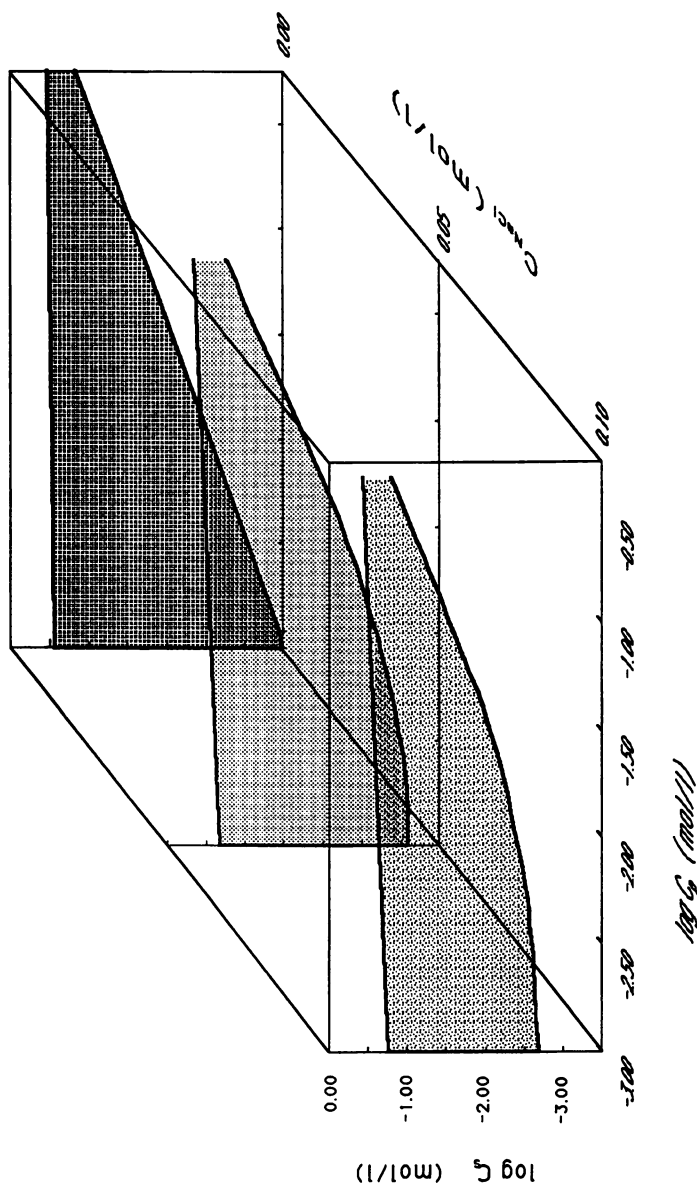


Figure 4. Molecular weight dependence of the lower and upper limits salt concentration  $C_{S3}^*$  and  $C_{S3}^{**}$  of the two phases region, for the system NaPSS/LaCl<sub>3</sub>, at given polymer concentrations. Hatched regions represent the two phases regions. The polymer concentrations are 0.1 mol/l (circle) and 0.01 mol/l (triangle).



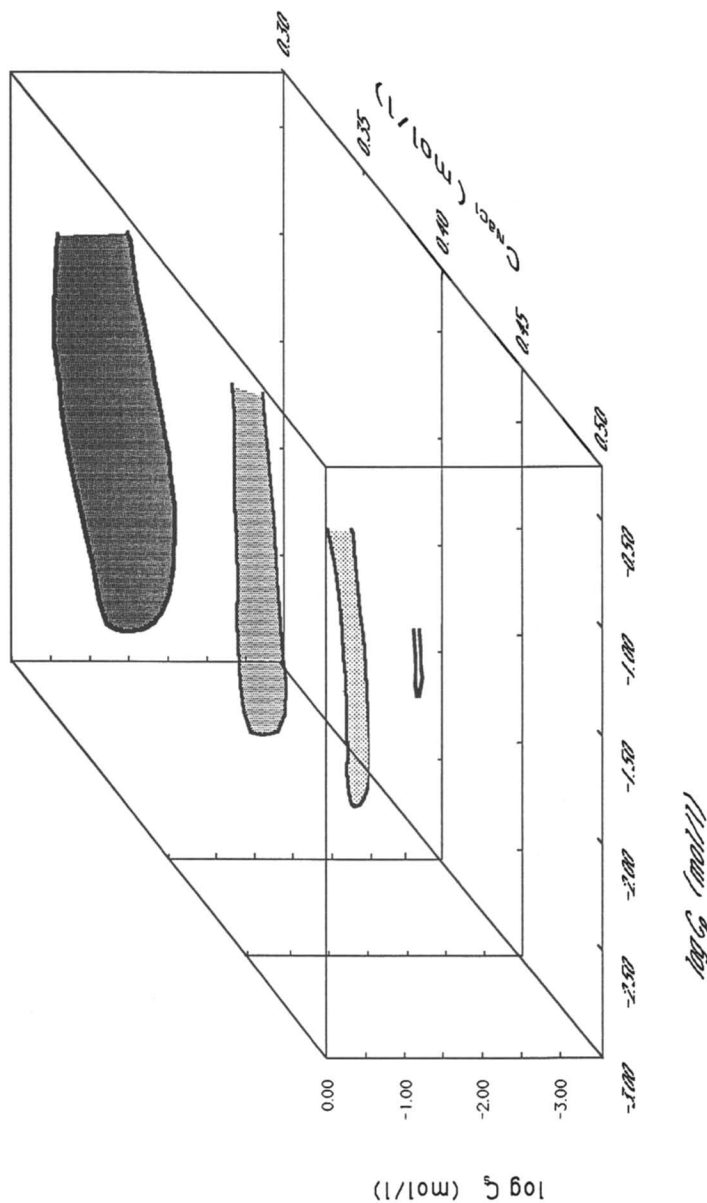


Figure 5. Shrinkage of the two phases region in presence of an univalent salt for the system NaPSS/LaCl<sub>3</sub> ( $M_w = 70,000$ ). Hatched regions represent the different two phases regions obtained for various amounts of added NaCl : 0.05, 0.1, 0.3, 0.4, 0.45, and 0.5 mol/l. To comparison, at zero NaCl concentration the phase diagram given in Figure 2 is reported. The narrowest two phases region corresponds to the largest NaCl concentration.

in a drastic reduction of the two phases region. Increasing sodium concentration, the disappearance of the phase separation firstly occurs at the lowest polymer concentration whereas at the highest polymer concentration the two phases region remains. At 0.5 mol/l of added NaCl, the two phases region is practically cancelled. A close inspection of Figure 5, reveals that for a given polymer concentration, the lower phase boundary  $C_{S3}^*$  changes more than the upper phase boundary  $C_{S3}^{**}$  when a given amount of salt is added. Let us consider a polymer concentration of 0.01 mol/l: changing the sodium concentration from 0.05 mol/l to 0.45 mol/l leads to a relative variation of the upper limit ( $\Delta C_{S3}^{**}/C_{S3}^{**}$ ) and of the lower limit ( $\Delta C_{S3}^*/C_{S3}^*$ ) of the order of - 0.7 and + 25, respectively.

## Discussion

The results presented above rise two main questions. Why anionic polyelectrolyte solutions with univalent counterions phase separate with addition of salt having multivalent cations? Why phase separation disappears at high concentration of added salt? In this section we do not give theoretical explanations of observed phenomena. We only discuss the general characteristics of the phase separation. We show that the underlying mechanisms are not of the same nature for the lower and upper lines  $C_S^*$  and  $C_S^{**}$  (at least at the lowest polymer concentration).

At first sight, the most simple parameters which should control the attractive forces between monomers and thus phase separation are the effective electrical charge per monomer (effective degree of ionization) and the Debye screening length which is related to the ionic strength. To estimate these two quantities, the binding of counterions must be known. That may be done by using the simple Manning's model of condensation (9-11). The polyelectrolyte is assumed to be an infinite isolated thread, with a uniform linear charge density, in a sea of counterions of valency  $z$ . According to this model, a fraction of counterions is trapped in the close vicinity of the polyelectrolyte backbone with absence of binding fluctuations. When the distance between structural unity charges  $b$  ( $= 2.5 \text{ \AA}$  for PSS) is smaller than  $z\lambda_B$ , where  $\lambda_B$  is the Bjerrum length ( $= 7 \text{ \AA}$  in water), a fraction of counterions is condensed and the mean distance between effective unity charges  $b_{\text{eff}}$  is adjusted to  $z\lambda_B$ . For mixtures of univalent and multivalent counterions of valency  $z > 1$  (for instance  $\text{Na}^+$  and  $\text{La}^{3+}$ ), cations of highest valency dominate in the population of bound counterions. When the concentration of multivalent cations is high enough, the effective distance between charges is adjusted to  $z\lambda_B$ . In term of the Manning's charge parameter  $\xi = \lambda_B/b$ , the structural value for the polystyrene sulfonate is  $\xi_S = 2.8$  and the effective values are  $\xi_{\text{eff}} = 1$  ( $= \alpha\xi_S$ ) in presence of univalent cation,  $1/3$  for trivalent and  $1/4$  for tetravalent. In Figure 6 are reported, according to this model, the fraction of free counterions and the effective degree of ionization,  $\alpha = b/b_{\text{eff}}$ , of the NaPSS when trivalent and tetravalent cations are added. All these quantities are only function of the ratio of the concentration of the multivalent counterions to the concentration of the structural charges  $[\text{SO}_3^-]$  of the NaPSS. Three domains can be roughly distinguished, the boundaries between these domains being:

- $C_S'/C_P = (1-b/\lambda_B)/z$ , concentration at which all the univalent cations are free,
- $C_S''/C_P = (1-b/z\lambda_B)/z$ , concentration at which the condensation of multivalent cations ceases.

In between these two concentrations,  $\xi_{\text{eff}}$  decreases from 1 to  $1/z$ . The binding predicted by this crude model was experimentally well verified for NaDextranSulfate/LaCl<sub>3</sub> system when  $[\text{La}^{3+}]/[\text{SO}_3^-] < 0.2$  (12).

To estimate the ionic strength,  $I$ , we take into account all the free mobile ions present in the solution : Na<sup>+</sup>, Cl<sup>-</sup> ( or NO<sub>3</sub><sup>-</sup> ), H<sup>+</sup>, La<sup>3+</sup> ( or Th<sup>4+</sup> ). In the case of mixtures of NaPSS plus one salt, we have explicitly :

$$I = zC_S/2 + z^2F_X C_S/2 + F_{\text{Na}} C_P/2 + 10^{-\text{pH}} \quad (3)$$

where  $F_X$  and  $F_{\text{Na}}$  represent the fraction of free multivalent La<sup>3+</sup>(or Th<sup>4+</sup>) and univalent sodium cations, respectively (see Figure 6).

Let us first consider the lower boundary of the two phases region  $C_S^*$ . Using the equation 3 for the ionic strength, it is possible to roughly estimate the Debye screening length  $\lambda_{\text{DH}}$  in the lower one phase region. It appears that in both systems, NaPSS/LaCl<sub>3</sub> and NaPSS/Th(NO<sub>3</sub>)<sub>4</sub>, the screening length  $\lambda_{\text{DH}}$  is always larger than 6 Å which is larger than the distance between structural charges. Thus, it is reasonable to expect that the lower limit of the two phases regions is intimately related to electrostatic effects. The parameter which seems to drive the lower phase separation is the condensation of multivalent cations which among other things reduces the effective charge and thus decreases the hydrophilicity of the polymer, carbonated backbone of PSS being recognized as hydrophobic. One could imagine that phase separation occurs when the effective charge parameter becomes lower than a threshold value. We will show that this hypothesis is incorrect. Indeed, the ratio  $C_S^*/C_P$  where phase separation occurs (equation 1) correspond to  $\xi_{\text{eff}} = 0.8$  for added La<sup>3+</sup> and  $\xi_{\text{eff}} = 1$  for added Th<sup>4+</sup>. It is important to note that these values are not much smaller than one. On the other side, the effective charge parameter reaches the value 1/2 for divalent cations while no precipitation is observed for added CaCl<sub>2</sub> salt. According to Figure 1, nothing happens to the scattered intensity for NaPSS/CaCl<sub>2</sub> system during the decrease of  $\xi_{\text{eff}}$  from 1 to 1/2 ( $0.32 < C_S/C_P < 0.41$  which corresponds at a given polymer concentration  $C_P = 0.0338$  mol/l to  $0.011 < C_S$  (mol/l)  $< 0.014$ ). Furthermore if the notion of effective charge threshold were essential, the ratio  $C_{S3}^*/C_{S4}^*$  should be (in first approximation) inversely proportional to the ratio of the valency of cations:  $C_{S3}^*/C_{S4}^* = 4/3$ . In fact, experimentally, a better empirical approximation is  $C_{S3}^*/C_{S4}^* \approx (4/3)^2$ . Thus it is clear that the notion of effective uniform charge is not sufficient to explain the lower boundary of the phase diagram. Presence of supplementary attractive forces related to condensation of multivalent cations is needed. It is certainly necessary to introduce the inhomogeneous or discrete aspect of the distribution of the condensed multivalent ions on the backbone.

We now turn our attention to the upper one phase region of the phase diagrams and the upper line  $C_S^{**}$ . Assuming that the condensation model is always valid, and using equation 3 to calculate the ionic strength, we find a screening length which is always smaller than 3 Å (in both systems). Another manner to evaluate the screening length  $\lambda_{\text{DH}}$ , without assuming any particular structure of the solutions, is to estimate that the ionic strength is at least larger than the ionic strength due to the mobile anions Cl<sup>-</sup> ( or NO<sub>3</sub><sup>-</sup> ) :  $I > zC_S/2 + 10^{-\text{pH}}/2$ . Using experimental relations 2 , we obtain  $\lambda_{\text{DH}} < 5.5$  and  $\lambda_{\text{DH}} < 3$  Å for NaPSS/LaCl<sub>3</sub> and NaPSS/Th(NO<sub>3</sub>)<sub>4</sub> systems, respectively. Due to the high ionic strength, electrostatic interactions can be neglected in first approximation. The properties of the solutions must be interpreted

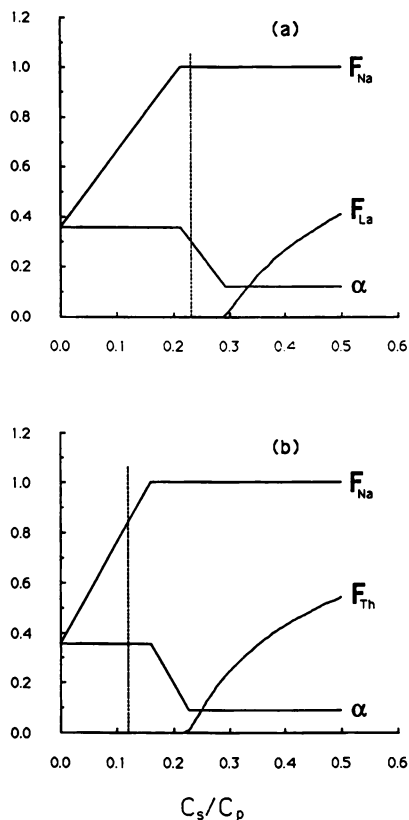


Figure 6. According to condensation model, the variation of the fractions of free ions and the effective degree of ionization  $\alpha$  of PSS are reported as a function of reduced variable  $C_s/C_p$  which is the ratio of the salt concentration to the polymer concentration (solid lines).

(a) NaPSS/LaCl<sub>3</sub> system,  $F_{La}$  is the fraction of free La<sup>3+</sup> ions,

(b) NaPSS/Th(NO<sub>3</sub>)<sub>4</sub> system,  $F_{Th}$  is the fraction of free Th<sup>4+</sup> ions.

In both cases  $F_{Na}$  represents the fraction of free Na<sup>+</sup> ions and dashed vertical lines correspond to the lower salt concentration  $C_s^*$  of the two phases region.



considering the polymer as a neutral polymer taking into account the osmotic effects of small mobile ions. The line  $C_S^{**}$  strongly depends on the valency of the added cation:  $C_{S4}^{**}/C_{S3}^{**} \approx (4/3)^4$ .

It is interesting to note that results obtained with the 3 different multivalent cations are experimentally consistent together. Using the experimental values of  $C_S^*$  and  $C_S^{**}$  given in equations 1 and 2 for trivalent and tetravalent cations, extrapolation to divalent cations (assuming power laws) leads to  $C_{S2}^* = 0.02$  and  $C_{S2}^{**} = 0.06$  mol/l at a given polymer concentration of 0.0338 mol/l. These values roughly correspond to the salt concentration region where a broad maximum is observed in the intensity of the light scattered by NaPSS/CaCl<sub>2</sub> solutions. However, this apparent agreement may be fortuitous.

The shrinkage of the two phases region in presence of univalent cation can be understood by the fact that ionic strength increases and binding of multivalent cations decreases (10-12) in presence of an excess of univalent cations. The changes are more pronounced in the lower part of the two phases regions. This behavior confirms the fact that the lower line  $C_S^*$  is closely related to the condensation of multivalent cations whereas the upper line  $C_S^{**}$  is relatively insensitive to changes in electrostatic interactions. The upper limit  $C_S^{**}$ , as it is for neutral polymers demixions (13), is molecular weight dependent, this dependency decreasing as the polymer concentration increases. To describe the upper limit of the two phases region, it is also necessary to take into account translational entropy of mixing of the individual polymers, at least in the dilute polymer concentration regime. In opposite, the lower limit  $C_S^*$  is molecular weight independent whatever is the concentration. This suggests that the free energy of the system is dominated by free energy coming from local electrostatic interactions.

## Conclusion

From data reported here, it is clear that phase diagrams strongly depend on the valency of the added salts. The lower boundary of the two phases region is essentially driven by attractive interactions of electrostatic origin (molecular weight independent). The upper limit of the two phases region is certainly less directly related to local electrostatic interactions (molecular weight dependent). The mechanism of the attraction which is responsible of the phase transition has not yet been totally elucidated. A full explanation needs further experimental investigations. We must state that there is a lack of theoretical works on the phase behavior of such simple mixtures of entities having opposite charges and we may expect that the present experimental data will be useful for the development of future theoretical works.

## Literature Cited

- (1) Piculell, L.; Lindman, B. *Advances in Colloid and Interface Science* **1992**, *41*, 149.
- (2) Blaakmeer, J.; Bohmer M.R.; Cohen Stuart, M.A.; Fleer, G.J. *Macromolecules* **1990**, *23*, 2301.
- (3) Guyot, A.; Audebert R.; Botet, R.; Cabane, B.; Lafuma, F.; Jullien, R.; Pefferkorn, E.; Pichot, C.; Revillon, A.; Varoqui, R. *J. Chim. Phys.* **1990**, *87*, 1859.
- (4) Marcus, Y. *Chem. Rev.* **1988**, *88*, 1475.
- (5) Ikegami, A.; Imai, N. *J. Polym. Sci.* **1962**, *36*, 133.
- (6) Michaeli, I. *J. Polym. Sci.* **1960**, *XLVIII*, 291.

- (7) Baes, C.F.; Mesmer, R.E. *The Hydrolysis of Cations*; John Wiley: New York, NY, 1976.
- (8) Rich, R.L. *J. Chem. Educ.* **1985**, *62*, 44.
- (9) Manning, G.S. *J. Chem.* **1969**, *51*, 924.
- (10) Belloni, L.; Drifford, M.; Turq, P. *Chem. Phys.* **1984**, *83*, 147.
- (11) Belloni, L. Thèse 3<sup>o</sup> cycle, Paris, **1982**.
- (12) Mattai, J.; Kwak, J.C.T. *J. Phys. Chem.* **1984**, *88*, 2625.
- (13) For instance, de Gennes, P.G. *Scaling Concepts in Polymer Physics*; Cornell University Press: Ithaca, NY, 1979.

RECEIVED August 6, 1993

## Chapter 30

# Adsorption and Viscoelastic Properties of Thermosetting Cationic Polyelectrolytes

D. I. Devore, N. S. Clungeon, and S. A. Fischer

Henkel Corporation Research and Development, 300 Brookside Avenue,  
Ambler, PA 19002

Crosslinking of polyaminoamide or polyamine with epichlorohydrin forms thermosetting cationic polyelectrolyte resins which are essential to the production of wet strength in paper products. The adsorption and thermosetting of these resins are shown to be dependent on pH and temperature. The resin crosslinking reactions can be characterized by established viscoelastic network theory. The tensile properties imparted to paper by essentially monolayer coverage with resin are shown to be consistent with an additivity rule for independent networks.

Polyaminoamide-epichlorohydrin (PAAE) and polyamine-epichlorohydrin (PAE) are important thermosetting resins for producing wet strength properties in paper in neutral to alkaline paper furnishes. Wet strengthened paper is resistant to rupture when saturated with water. The resins are critical to the performance of such common household products as paper towels, milk cartons, hamburger wrappers, and pizza boxes. The resins are also used in a variety of water treatment applications as coagulants and flocculants. These resins constitute a unique class of cationic polyelectrolytes having both quaternary and tertiary amine functional groups which impart pH-independent and pH-dependent properties, respectively. The resins are low viscosity and water soluble up to concentrations exceeding 45% solids.

The mechanism by which these resins produce wet strength in paper has been under investigation for some time, and two distinct mechanisms have been proposed (1,2): 1) the formation of an independent network of homo-crosslinked resin which is bound to the paper fibers through physisorption; and, 2) the formation of covalent bonds between the resin and cellulosic functional groups on the paper fibers (i.e., chemisorption). Our investigation of resin reactions with model cellulosic compounds, and of tensile properties of resin treated

0097-6156/94/0548-0394\$06.00/0  
© 1994 American Chemical Society

paper, provided support for the physisorbed, homo-crosslinked network mechanism (3).

Environmental factors related to epichlorohydrin, a Class 1 carcinogen, are making this chemistry a more critical issue today (4). Epichlorohydrin reacts with water and hydrochloric acid to form chloropropanediol (CPD) and dichloropropanol (DCP), respectively, and both of these are under investigation for their carcinogenic activities. These compounds are obviously organochlorines and as such can have an impact on the total organic halide (TOX) in a paper mill's water system; TOX is a critical parameter which is monitored in paper mill effluents according to strict environmental regulations.

In this study, the molecular and mechanical properties of commercial PAEE and PAE resins are related to their activities in developing wet strength in paper. Adsorption isotherms for the resins are measured on cellulose and on a paper furnish as a function of pH. The crosslinking kinetics are determined for neat resin films by applying the theory of rubber-like elasticity (5) to the observed stress-strain tensile properties of the films. Wet tensile strengths imparted to paper by these resins are shown to be a function of curing time, and the curing rates are compared to those of the resin films. The wet tensile strengths obey an additivity rule (3) which, when combined with the results obtained in this study, strongly supports the existence of physisorbed networks of independent resin and paper fibers.

### Experimental

The two resins in this study were synthesized by reacting polyaminoamide or polyamine backbones with epichlorohydrin (6,7) and were designated as resins A and B, respectively. Resin structures were determined from NMR spectra, obtained with a Varian 4VXR-400S spectrometer, and other analytical methods (3). The cationic charge densities of the resins were determined by titration with the potassium salt of polyvinylsulfate (PVSK) (8).

Adsorption isotherms were obtained at 60°C on 3% cellulose (Sigmacell 100, Sigma Chemicals) by PVSK titration of supernatants filtered through 0.45 micron nylon filters. Adsorption isotherms were also obtained at 25°C on 2% bleached softwood kraft pulp slurries which were adjusted to pH 7 and 10 with NaOH. The anionic charge density of the cellulose was determined by back-titration with PVSK using excess polydiallyldimethylammonium chloride (pDADMAC).

Paper handsheets were prepared with the Mark IV Dynamic Handsheet Mold (Paper Chemistry Laboratory) (9) using a bleached softwood kraft pulp at pH 7. The handsheets were cured at 70°C and 50% relative humidity (RH) for 16 hr or 32 hr and the tensile strengths were measured on an Instron Tester either dry (dry tensile, DT) or after 1 hr soaking in deionized water (wet tensile, WT).

Resin films were cast in aluminum pans coated with "no stick" corn oil to prevent adhesion. This method permits coherent resin films to be easily peeled off the surface and avoids difficulties encountered with other methods (10) and surfaces such as glass and metals to which the resins bind irreversibly. Resin solutions were prepared from 34% solids solutions adjusted to pH 7 or 10 with

NaOH. The resins were cured at 70°C and 50% RH for 16 hr to 168 hr. The film tensile properties (breaking strength, elongation at break, and Young's modulus) were measured at 25°C on the Instron Tester.

## Results and Discussion

Simplified structures for resins A and B are illustrated in Figure 1, based on the  $^1\text{H}$  NMR spectra shown in Figure 2. Resin A contains quaternary azetidinium rings as well as quaternary and tertiary chlorohydrin groups; resin B contains quaternary and tertiary chlorohydrins, but no azetidinium. The amounts of epichlorohydrin added into the resin reaction processes are sufficient to assure that all secondary amines have reacted. The processes by which these reactions are accomplished on a commercial scale are critical to assuring that environmental exposure to organochlorines is minimized (4,6).

The cationic charge densities of resins A and B are strongly dependent upon the pH, as shown in Figure 3. This is due to protonation of the tertiary amines in the resin backbones. At high pH, the backbones are deprotonated and only the quaternary ammonium groups (azetidinium or dichlorohydrin) are charged. Resin B has a higher charge density than resin A because of the shorter chain lengths in its backbone.

Both resins are completely and irreversibly adsorbed on cellulose at resin dosages up to 35 mg/L, and there is little difference in their adsorption up to very high dosages, as shown in Figure 4. The small difference in adsorption in this case is apparently due to molecular weight (weight-average molecular weights for resins A and B, obtained by GPC, are 66,500 and 34,700, respectively) and not to charge density effects.

Resin adsorption is consistent with monolayer coverage of cellulosic anionic charge sites. From PVSK back-titration, the anionic charge density of the cellulose at pH 7 is -.012 mequiv/g, and the zero-point-of-charge is at pH 2.0, in accord with proton titration data (11). This cellulose anionic charge density represents the anionic carboxylic acid charge sites accessible to the cationic polyelectrolytes. In typical commercial papermaking processes, resin dosages on the order of 100 mg/L are used, which for resin A at pH 7 would amount to 50% neutralization of the anionic charge on the 3% cellulose dispersion. Therefore, over the dosage range of practical interest, there are 1 or fewer resin cationic charge sites per cellulose anionic charge site.

Resin adsorption on paper fibers follows the same behavior observed for cellulose (4), and as shown in Figure 5, there is a pH dependency. Adsorption of both resins A and B is greater at pH 10 than pH 7, and there is a greater difference for resin B than resin A. The observed pH effects are due to a relatively large increase in the anionic charge density of the cellulosic carboxylic groups with increased pH, coupled with a relatively small decrease in cationic charge densities of the resins over the range from pH 7 to pH 10 (Figure 3).

The tensile strengths imparted to paper by the resins reach plateaus as the dosages increase, as shown in Figure 6; the wet tensile (WT) is always less than the dry tensile strength (DT). This behavior is in accord with the adsorption properties. For the paper furnish used in this study, resin A produces far more

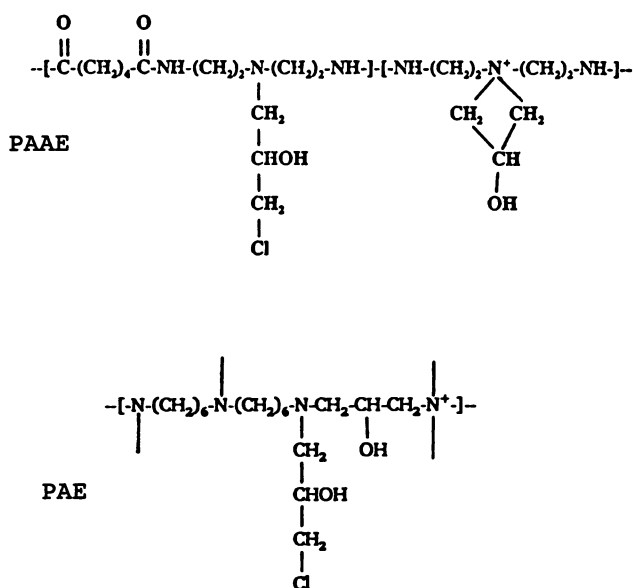


Figure 1. Resin A, polyaminoamide-epichlorohydrin (PAAE), and Resin B, polyamine-epichlorohydrin (PAE), simplified structures.

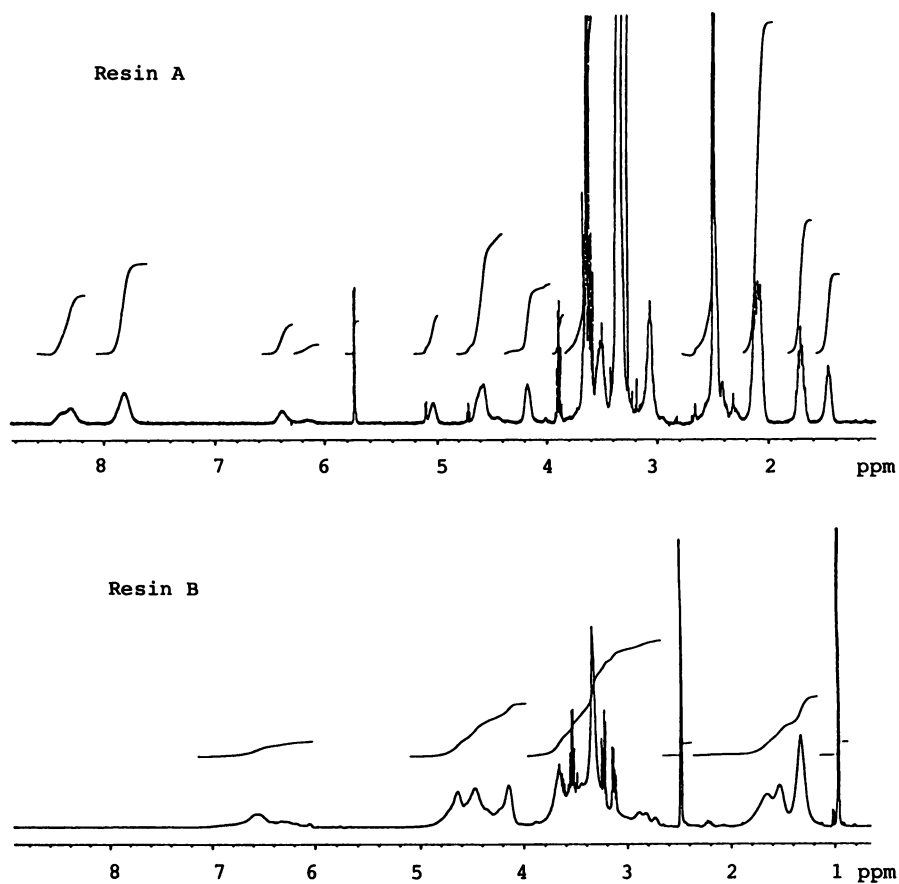


Figure 2.  $^1\text{H}$  NMR spectra: Resin A; Resin B.

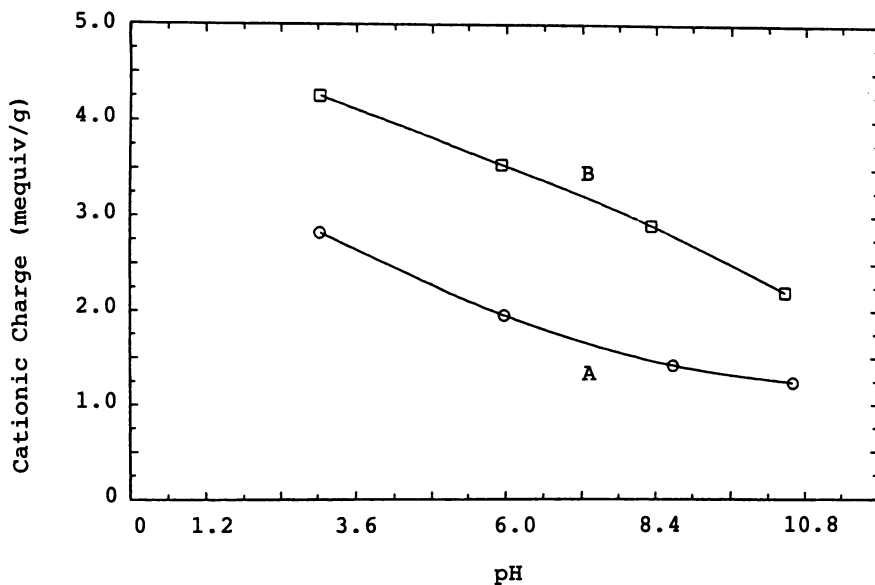


Figure 3. Effect of pH on resin cationic charge densities.

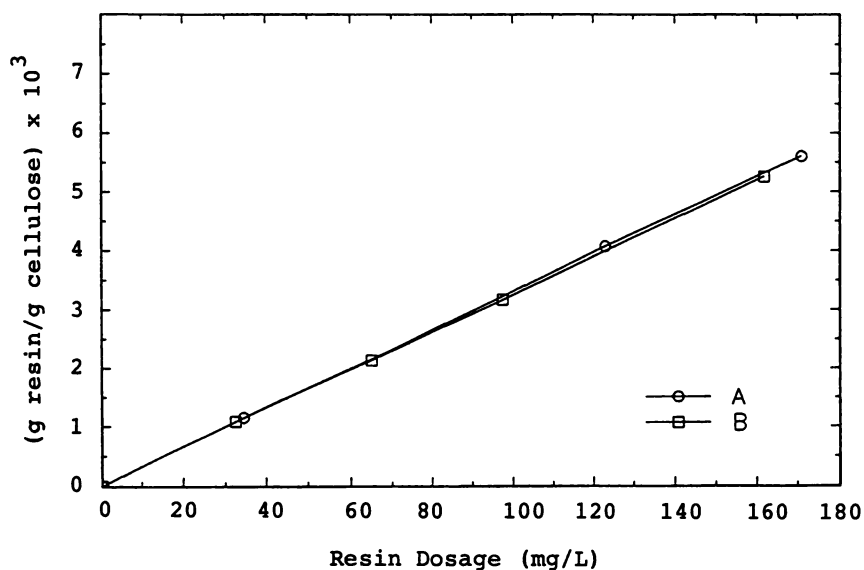


Figure 4. Adsorption isotherms for Resins A and B on cellulose.



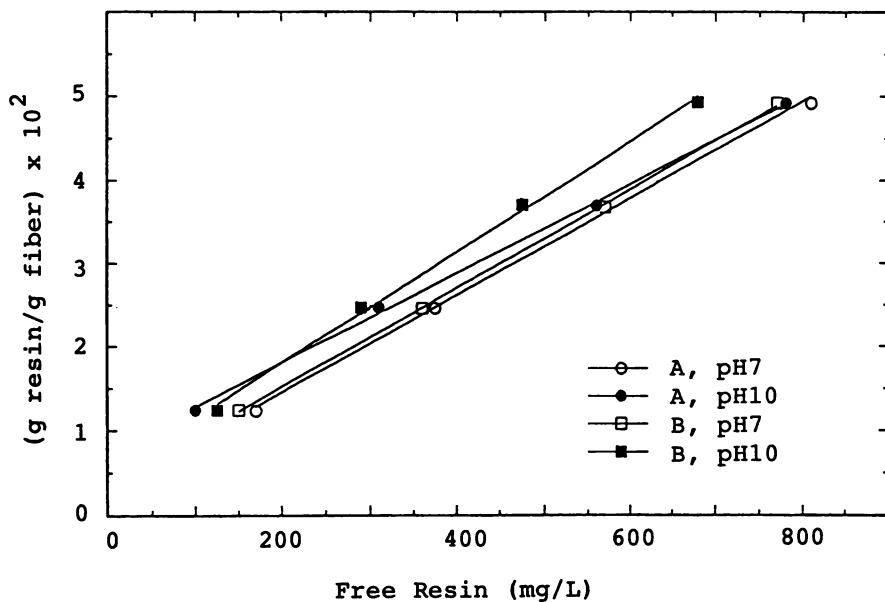


Figure 5. Adsorption isotherms for Resins A and B on bleached softwood pulp as a function of the pH of the pulp furnish.

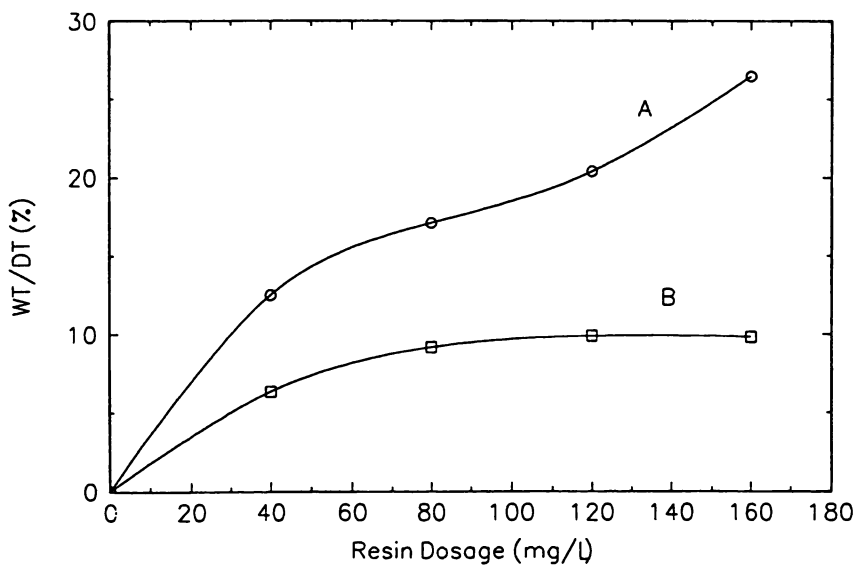


Figure 6. Effects of initial resin dosages on the ratio of wet tensile strength (WT) to dry tensile strength (DT) of handsheets.

wet strength than resin B. This relative performance difference has been observed in most (but not all) paper furnishes tested, and is accounted for below on the basis of the mechanical properties of the crosslinked resins themselves.

An examination of the tensile data for this and many other tested paper furnishes leads to an additivity rule for the tensile strengths (3):

$$DT_r = (WT_r - WT_b) + DT_b \quad (1)$$

where the subscripts r and b refer to resin-treated and untreated (blank) handsheets, respectively. Additivity rule behavior is frequently observed for polymer blends, and here implies independent networks of the resins and paper fibers contributing to the total tensile strength.

A critical factor in the wet strength produced by a resin is the time that the handsheet is cured at a given temperature. This is shown in Figure 7 for handsheets made with resins A and B at pH 7. From NMR and other studies, there is no evidence of covalent bond formation between the resins and the paper fibers (3). Hence, the curing behavior of the paper handsheets is indicative of resin self-crosslinking. Applying the additivity rule, Equation 1, to the data in Figure 7 by calculating  $\ln(WT_r - WT_b)$  vs. time gives pseudo-first order curing rate constants for handsheets made with either resin of approximately  $2 \times 10^{-6}/\text{sec}$ .

The tensile strengths of the resins themselves are directly dependent upon the curing time and pH. The molecular weights between crosslinks,  $M_c$ , are shown in Figure 8 for films of resins A and B. The  $M_c$  values are based on elastic network theory (5), using the film tensile strengths,  $f^*$ , and elongations at break,  $\ell/\ell_i$  (ratio of final to initial film lengths):

$$f^* = (vkT/V) [ (\ell/\ell_i) - (\ell/\ell_i)^2 ] \quad (2)$$

and,

$$M_c = d/(v/V) \quad (3)$$

where  $k$  is the Boltzman constant,  $T$  the absolute temperature,  $d$  the resin film density, and  $(v/V)$  is the number of chains per unit volume in the network.

The crosslinking rates for the films of resins A and B follow pseudo first-order kinetics. The rate constants obtained from the data in Figure 8 are  $3.8 \times 10^{-6}/\text{sec}$  for resin A at both pH 7 and pH 10, while those for resin B are  $5.0 \times 10^{-6}/\text{sec}$  at pH 7 and  $8.3 \times 10^{-6}/\text{sec}$  at pH 10. The difference in pH effects may be ascribed to the different basicities of the backbone amines in the resins. The resin crosslinking rate constants are comparable to the curing rate constants obtained above for the paper handsheets. Resin A contains azetidinium groups which rapidly open and crosslink with free resin tertiary amine groups under the curing conditions used to form the paper handsheets; the observed pseudo-first order rate constant for the azetidinium reaction, based on NMR studies, is  $4.6 \times 10^{-4}/\text{sec}$ , and this reaction is complete in about 1 hr at  $70^\circ\text{C}$  (3). Resin B contains no azetidinium groups, so crosslinking (thermosetting) occurs only

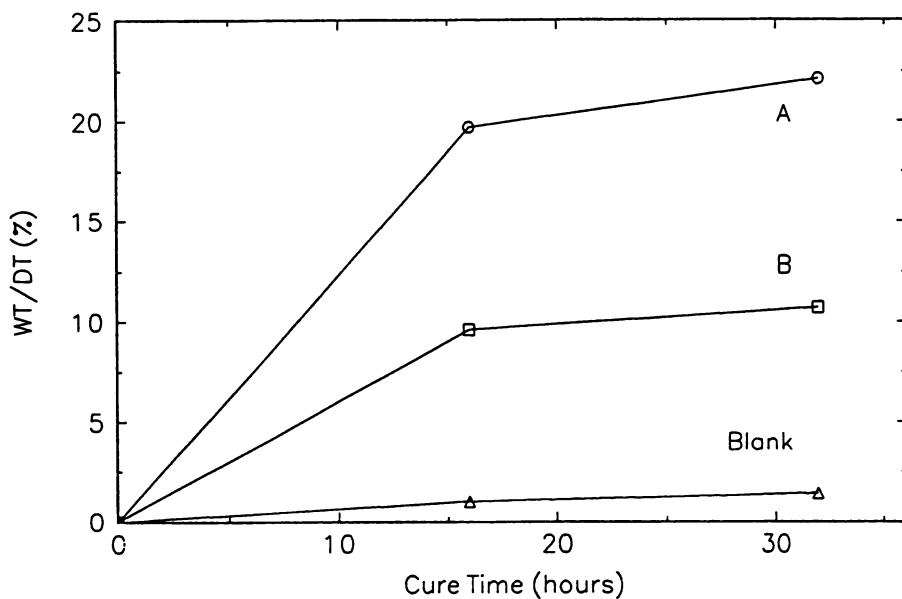


Figure 7. Effects of curing time on the tensile strength ratio of handsheets made with Resins A and B or untreated (blank).

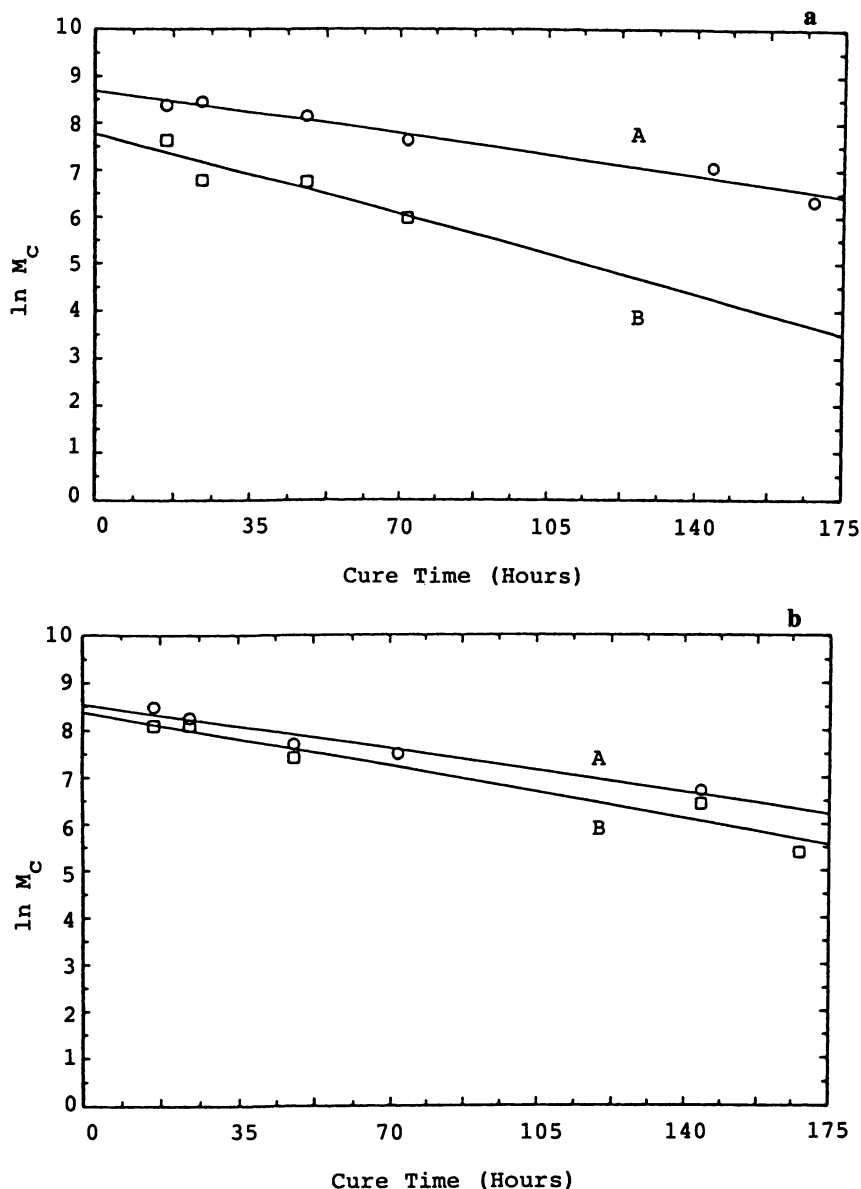


Figure 8. Crosslinking kinetics of films of Resins A and B: a) molecular weight between crosslinks,  $M_c$ , vs. curing time at pH 10.0; b) at pH 7.0.

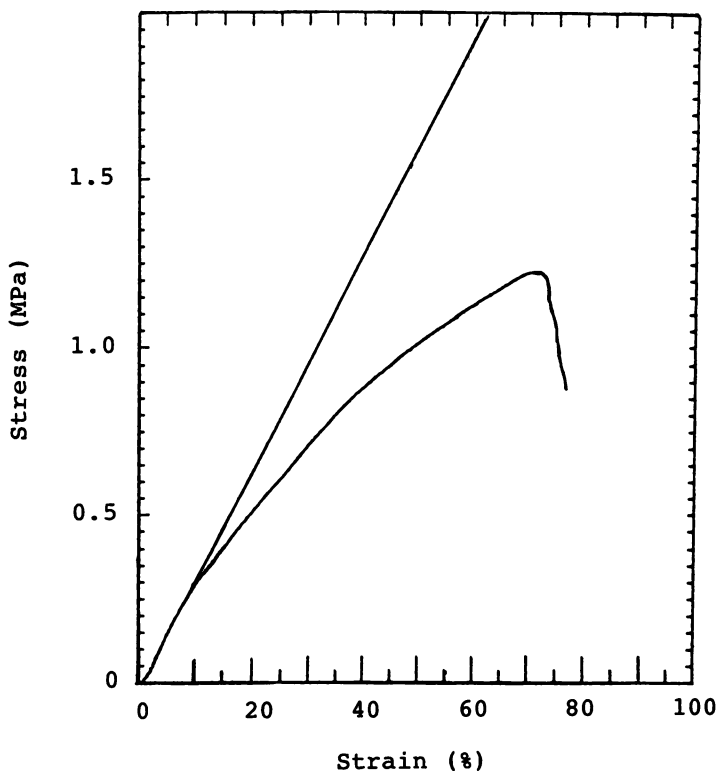


Figure 9. Stress-strain behavior of film of Resin A at pH 7 cured for 24 hours at 70°C; elastic modulus given by initial slope (straight line).

through the slower reaction of chlorohydrin groups with tertiary amines, and it is this reaction rate which is observed in the resin film curing.

The  $M_c$  values at the longest curing time tested, 168 hr, are very close to the monomer molecular weights for the fully crosslinked resins. This lends support to the use of elastic network theory to describe these resin films, however, further direct NMR analysis of crosslinking in the films would be desirable. The elastic moduli of the resin A and B films increased from 2 - 3 MPa after 16 hr curing time to approximately 100 MPa after 168 hr curing time. A typical stress-strain curve is shown in Figure 9 for the resin A film cured for 24 hr at pH 7. The elastic moduli for these resins, given by the initial slopes of the stress-strain curves, are relatively low compared to those of other thermosetting polymers (12).

The differences in wet tensile strengths achieved by resins A and B in the paper handsheets (Figures 6 and 7) are due to the relative mechanical strengths of the resin films. After 16 hr curing, the tensile strength of the resin A film at pH 7 is 1.22 MPa, while that of the resin B film is only 0.62 MPa. These film

strengths are in good agreement with the paper handsheet tensile strength quantity,  $(WT_r - WT_b)$ , in the additivity rule (Equation 1), which can thus be identified with the independent contribution of the resin network to the paper's wet strength.

### Conclusions

From the adsorption and tensile properties of PAAE and PAE resins, the effects of curing time on resin-treated paper handsheets, and the additivity rule for the wet strengths, it is concluded that these resins form independent networks with paper fibers. Resin A produces greater wet tensile strength than resin B because cured resin A itself has inherently greater tensile strength than resin B. The resins are bound to the paper fibers through electrostatic attraction of the resin cationic groups and cellulosic anionic groups. This physisorption is dependent upon pH, which affects the charge densities of the resins and the cellulose, as well hydrogen bonding between them.

### Literature Cited

1. Westfelt, L., *Cellulose Chem. Technol.*, **1979**, *13*, 813
2. Neal, C.W. *TAPPI Notes, Wet and Dry Strength Short Course*; TAPPI Press: Atlanta, **1988**; pp.1-24.
3. Devore, D.I.; Fischer, S.A. *Tappi J.*, August, **1993** (in press)
4. Devore, D.I.; Clungeon, N.S.; Fischer, S.A. *Tappi J.*, **1991** *74(12)*, 135
5. Mark, J.E.; Eisenberg, A.; Graessley, W.W.; Mandelkern, L.; Koenig, J.L. *Physical Properties of Polymers*, ACS: Washington, D.C., 1984
6. Devore, D.I.; Fischer, S.A. *U.S. Patent 5,189,142* (Feb. 23, **1993**)
7. Fischer, S.A.; Grinstein, R. *U.S. Patent 5,120,773* (June 9, **1992**)
8. Wang, L.K.; Shuster, W.W. *Ind.Eng.Chem.Prod.Res.Dev.*, **1975** *14(4)*, 312
9. Penniman, J.G.; *Dynamic Handsheet Mold Mark IV Operating Manual*; Paper Chemistry Laboratory: Carmel, NY, 1988
10. Bates, N.A. *Tappi J.*, **1969**, *52(6)*, 1162
11. Budd, J.; Herrington, T.M. *Coll. Surf.*, **1989**, *36*,273
12. Billmeyer, F.W., Jr. *Textbook of Polymer Science*, 3rd Ed.; John Wiley: New York, 1984; p.480

RECEIVED August 6, 1993

## Chapter 31

# Polyelectrolyte Adsorption and Stability of Latex Suspensions

S. Bárány<sup>1</sup>, A. A. Baran<sup>1</sup>, I. Solomentseva<sup>2</sup>, and L. Velichanskaya<sup>2</sup>

<sup>1</sup>Institute of Chemistry, University of Miskolc, 3515 Miskolc-Egyetemváros, Miskolc, Hungary

<sup>2</sup>Institute of Colloid and Water Chemistry of the Ukrainian Academy of Sciences, 42 Vernadsky Boulevard, Kiev 252680, Ukraine

Complex investigations of polyethylenimine (PEI) and carboxymethylcellulose sodium salt (CMC) adsorption and their effects on the sedimentation rate, volume of sediment, electrokinetic potential and degree of aggregation of homodisperse polystyrene and melamineformaldehyde copolymer particles, respectively, were carried out. The adsorption isotherms are of high-affinity type and may be described by the Hesselink theory of polyelectrolyte adsorption. Based on calculated values of the adsorption layer thickness and segment densities in polymer coils and adsorbed layers, the conclusion that considerable deformation of CMC (less for PEI) during adsorption is made. It is shown that the flocculation of suspensions by polyelectrolytes takes place far from the isoelectric point of particles. The role of electrostatic, structural and steric forces in the mechanism of stabilization of dispersions by oppositely charged polyelectrolytes is discussed.

The adsorption of macromolecules from solution onto solids is not merely of academic interest but it is also a basic phenomenon in many applied processes such as the stabilization and flocculation of dispersions, filtration, flotation, dewatering, etc. The effect of polymers on colloidal stability is connected with the structure of adsorbed layers and their influence on the surface forces acting between particles ///. There are a number of studies concerning the relationship between nonionic polymer

0097-6156/94/0548-0406\$06.00/0  
© 1994 American Chemical Society

adsorption and stability of dispersions. At the same time we have much less information about the structure of polyelectrolytes on surfaces and its dependence on the electrolyte concentration in the system as well as about the mechanism of stabilization/flocculation of dispersions by polyelectrolytes and their mixtures with electrolytes.

Our work aimed to study the regularities of polyelectrolyte adsorption from aqueous and electrolyte solutions and its effect on the electrokinetic potential and degree of aggregation of oppositely-charged particles, and to establish the mechanism of stabilization/flocculation in relevant systems. The suspensions of homodisperse spherical particles of melamine-formaldehyde copolymers (MF) and polystyrene (PS) containing different amounts of sodium carboxy-methylcellulose (CMC) and polyethylenimine (PEI) were used.

### Materials and methods

The utilised samples of carboxy-methylcellulose salt were of different degrees of polymerization (numerators, column I of Table I) and of different degrees of substitution of hydroxyl groups by carboxyl ones (denominators).

The CMC macroions in aqueous and electrolyte solutions form hydrodynamically permeable coils, the effective hydrodynamic radius ( $R_h$ ) of which was calculated from Debye-Büche theory /2/. Macromolecules of PEI in solution are non-permeable hard spheres. The expression for calculation of  $R_h$  of this polymer is given in /3/.

The characteristics of the samples investigated in solution and in adsorbed layer are summarised in Table I and II.

The positively charged MF and negatively charged emulsifier-free PS particles were obtained by traditional methods and were purified by dialysis. Their characteristics are given in Table III.

The values of the surface charge density were determined by potentiometric titration of MF and PS particles in  $\text{OH}^-$  and  $\text{H}^+$  forms, respectively. The electrophoretic mobility of particles in polymer-free suspensions was measured by microelectrophoresis, and with polyelectrolyte additions by macroelectrophoretic methods. The adsorbed amount was calculated from the material balance of polyelectrolyte in the system before and after contact with the solids particles. The concentration of polyelectrolytes in solution was measured interferometrically. As a measure of dispersion stability the coagulation value of electrolytes (the minimum concentration of salt at which the light



transmission coefficient of dispersion (I) reaches the 50 % value two hours after the electrolyte addition) was taken.

**Table I. Parameters of CMC in Solution and in Adsorbed Layers on Melamine-formaldehyde**

Sample	$M \times 10^{-3}$	$R_h$ , nm	a, nm	h, nm	$\rho_a \times 10^{-2}$ mgcm <sup>-3</sup>	$\rho_c$ , mgcm <sup>-3</sup>	$\rho_a/\rho_c$
800/86	176	89	550	105	146	114	128
530/83	116	70	550	95	117	134	87
239/81	52	42	200	40	155	279	55
239/81	52	42	550	70	96	279	34
239/81	52	42	1050	76	90	279	32
520/55	114	60	550	86	150	210	71
548/140	120	85	550	110	34	78	43

**Table II. Parameters of PEI in Solution and in Adsorbed Layers on Polystyrene**

$M \times 10^{-3}$	$R_h$ , nm	a, nm	h, nm	$\rho_a \times 10^{-2}$ mgcm <sup>-3</sup>	$\rho_c \times 10^{-2}$ mgcm <sup>-3</sup>	$\rho_a/\rho_c$
10	8.6	118	6.8	206	498	0.42
50	22.2	118	15.1	146	146	1.0
80	29.6	118	16.0	150	98	1.53
140	42.2	118	19.7	155	59	2.63
140	42.2	231	29.0	105	59	1.78
140	42.2	351	34.7	88	59	1.47

The adsorption layer thicknesses were calculated from the sedimentation rate of the particles and from the volume of the close-packed sediment of polymer-containing particles. The first method

enables us to calculate the thickness value ( $h$ ) of a hydrodynamically non-permeable adsorption layer from the coefficient of sedimentation of particles  $S_p$  /4/ :

$$S_p = \frac{2a^3 (\rho_1 - \rho_0) + 2 (3ha^3 + 3h^2a + h^3) (\rho_2 - \rho_0)}{9\eta_0 (a + h)} \quad (1)$$

where  $a$  is the radius of particles,  $\rho_1$  is their density,  $\rho_0$  is the density of the medium,  $\eta_0$  is its viscosity,  $\rho_2$  is the density of the polymer layer.

For polymer-free dispersion:

$$S_0 = \frac{2a^2 (\rho_1 - \rho_0)}{2\eta_0} \quad (2)$$

and for the case when the density of the polymer layer is close to that for the medium (as is valid for our system):

$$S_0/S_p = (a + h)/a \quad (3)$$

For polystyrene particles with  $\rho_2 \approx \rho_0$  the sedimentation rate coefficients were determined by ultracentrifugation at 10 000, 6 000 and 3 000 rpm for particles of diameter  $\sim 0.2$ ,  $\sim 0.5$  and  $\sim 0.7 \mu\text{m}$ , respectively.

The equilibrium volumes of polymer-free and polymer-containing particles were measured in capillaries of 1.7 - 2.0 mm in diameter at 7-8 days (for particles with  $a = 1050 \text{ nm}$ ) or 50-60 days (for smaller particles) after beginning the sedimentation. The thicknesses were calculated from the equation:

$$h = \frac{\Delta v \times 0.62}{S \times M_p} \quad (4)$$

where  $\Delta v$  is the increase of the volume of particles due to the polymer adsorption,  $S$  is the specific surface area and  $M_p$  is the mass of the particles.

**Table III. Characteristics of Melamine-formaldehyde Copolymer and Polystyrene Particles**

Particle	Density, $\text{gcm}^{-3}$	Mean $d$ , nm	Surface group	Surface charge density, $\mu\text{Ccm}^{-2}$	Zeta-potential mV, at pH=6.8
MF	1.3292	400	$-\text{NH}_3^+$	94	+ 72
		1100			
		2100			
PS	1.0541	200	$-\text{SO}_3^-$	12	- 40
		490			
		690			

## Results and discussion

**Adsorption.** The preliminary tests showed that the polymer-free suspensions of MF or PS were aggregatively stable. Adsorption equilibrium of polyelectrolytes was reached after 4 hours, and increasing the concentration of the particles from 10 to 50  $\text{gdm}^{-3}$  did not considerably change the plateau values of adsorption.

The adsorption isotherms of the polyelectrolytes studied on the surface of oppositely-charged particles are of high-affinity type, and reach a plateau value ( $\Gamma_\infty$ ) at high polymer concentrations (Figures 1,2). The adsorbed amount ( $\Gamma$ ) increases with molecular mass; this dependence may be described by the empiric Perkel-Uhlmann relationship:

$$\lg \Gamma_\infty = \alpha \lg M + b \quad (5)$$

where  $\alpha$  and  $b$  are constants;  $M$  is the molecular mass. The value of  $\alpha$  for MF-CMC and PS-PEI systems is 0.35 and 0.33, respectively. This

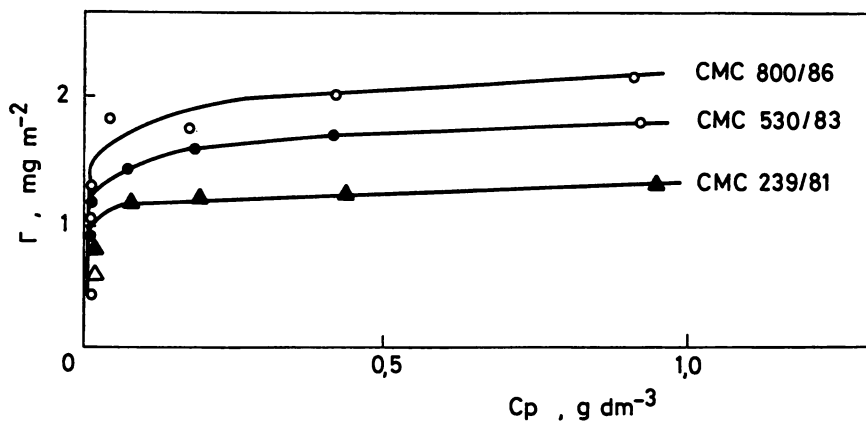


Figure 1. Adsorption isotherms of different CMC samples (indicated) on melamine-formaldehyde copolymer particles.

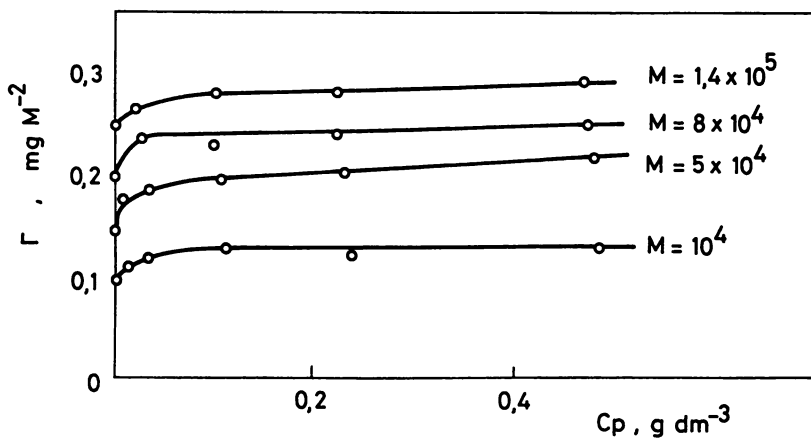


Figure 2. Adsorption isotherms of PEI of different molecular mass (indicated) on polystyrene particles.

provides indirect evidence that the adsorption of the polymers in question is in the form of a statistic coil /5/.

The maximum adsorbed amount of PEI ( $0.1 - 0.3 \text{ mgm}^{-2}$ ) is much less than that for CMC ( $1-2 \text{ mgm}^{-2}$ ). The latter values are characteristic for adsorbed polymers /1, 5/. The calculated area occupied by a PEI molecule in a close-packed monolayer is approximately the same as the cross-section of this molecule in solution /3/. In the case of CMC adsorption we have an another picture: the calculated  $\Gamma_{\infty}$  value for the CMC 239/81 sample (for example) with  $R_h = 70 \text{ nm}$  is  $0.02 \text{ mgm}^{-2}$ , which is two orders of magnitude lower than the experimental value. Similar behavior is seen for the other samples of CMC as well. This is evidence of a strong deformation of CMC coils at their transition to a surface.

The dependence of the adsorbed amount on the electrolyte concentration in the system reveals a minimum at about  $0.05-0.1 \text{ M NaCl}$  (Figures 3, 4). The adsorption in  $0.5-1.0 \text{ M}$  salt solutions exceeds the  $\Gamma_{\infty}$  values typical for aqueous solutions by several times.

The extreme "adsorption versus electrolyte concentration" dependences may be explained by the Hesselink theory of polyelectrolyte adsorption on charged surfaces /6/. According to this theory the adsorbed amount of polyelectrolytes depends on non-electrostatic and electrostatic terms of adsorption energy, i.e. on the surface charge densities before and after adsorption, surface potential, degree of dissociation of functional groups, etc. With increasing salt concentration the electrostatic attraction between the surface and the oppositely-charged polyelectrolytes decreases due to the screening of the charge of the macroions and suppression of the electric double layer of the adsorbent. This is a reason for the initial decrease of the adsorbed amount to the minimum of the curves of Figure 4. On the other hand, increase of the electrolyte content is accompanied by deterioration of the solvent quality, with an increase of "salting-out" and decrease of the dimensions of the polymer coil. All of these factors promote the polyelectrolyte adsorption (see increases after minima of curves in Figure 4).

The interaction of the polymer-covered particles is determined not only by the adsorbed amount but the structure (primarily the thickness) of adsorbed polymer layers and the density of segments within its limits. We have used two independent methods for determination of the polyelectrolyte layers thickness- the measurement of the effect of polymer

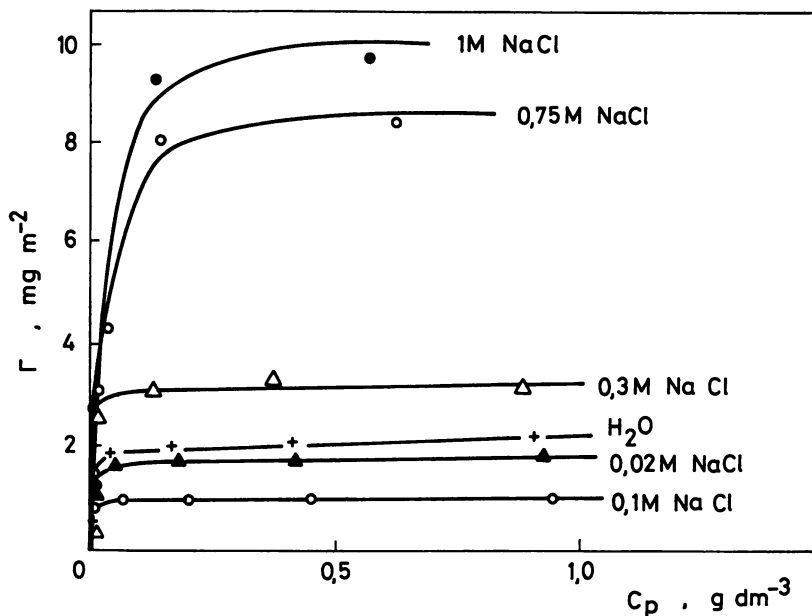


Figure 3. Adsorption isotherms of CMC 800/86 on MF particles from water and sodium chloride solutions of different concentration (indicated).

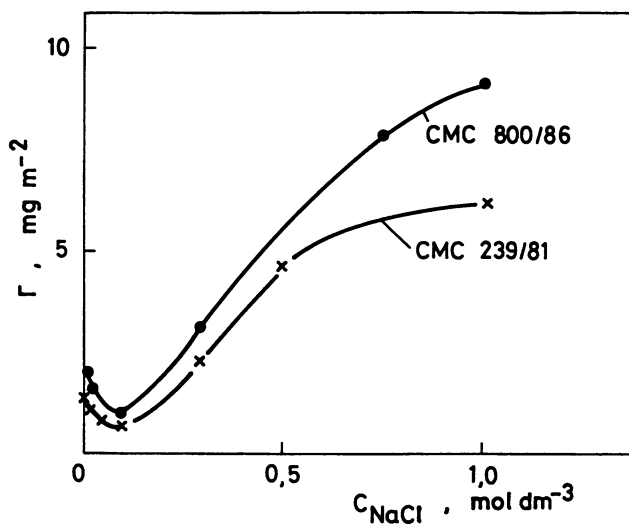


Figure 4. Dependences of the maximum adsorbed amount of CMC 239/81 and 800/86 on MF particles on the sodium chloride concentration in the system.

adsorption on the rate of sedimentation and on the volume of a close-packed sediment (see above).

Figure 5 shows an example of dependence of the polymer layer thickness on the equilibrium concentration of CMC in solution, and on the amount of adsorbed polymer. Both methods mentioned give similar values of  $h$ . Three regions on  $h(C_p)$  plots may be distinguished: the initial region at low polymer contents with poor dependence of the layer thickness on the polymer concentration; the intermediate region with sharp increase of  $h$  with  $C_p$  (here the precise determination of the  $h$  value is not possible owing to intensive flocculation) and a region at relatively high polyelectrolyte concentrations where some decrease of the layer thickness with increasing polymer content takes place. The great difference between thicknesses of layers at the beginning and at the end of the flocculation region is evidence of the change of conformation of the adsorbed layer in the transition region mentioned.

With increasing ionic strength of the solution the  $h$  values decrease, especially at NaCl concentrations above 0.25–0.3 M (Figure 6). This is in spite of the fact that at these electrolyte contents the adsorption amount of polyelectrolytes increases sufficiently (Figures 3, 4). Meanwhile it is obvious that the increase of the ionic strength leads to the compression of the polymer coil and to increase of its density. For characterization of changes in packing of segments in adsorbed layers we have introduced two parameters: (1) the amount of polymer in a unit volume of the macromolecular coil  $\rho_c$  and (2) that of the adsorbed layer  $\rho_a$  expressed in  $\text{mgcm}^{-3}$ . The values of these parameters for PEI and CMC on the surfaces of PS and MF, respectively, are summarized in Table I and II.

The dependence of  $\rho_a$  on NaCl concentration is characterised by a gently sloping minimum and a sharp increase of this parameter at salt content more than 0.3 M (Figure 6). At sodium chloride concentration of 1 M the value of  $\rho_a$  reaches  $200 \text{ mgcm}^{-3}$ , whereas at these conditions the magnitude of  $\rho_c$  is only  $2.2 \text{ mgcm}^{-3}$ .

It may be supposed that the polyelectrolyte segments localized near the interface undergo maximum deformation due to the electrostatic attraction between the oppositely charged segments and the surface groups. According to Hesselink /6/ in such cases the part of the surface covered by segments is  $\sim 0.8$  (80 %). Starting from this value and from the area occupied by CMC unit (5.15 nm /2/) and the M of this unit (242 for the CMC with degree of substitution of 81) we have estimated that in

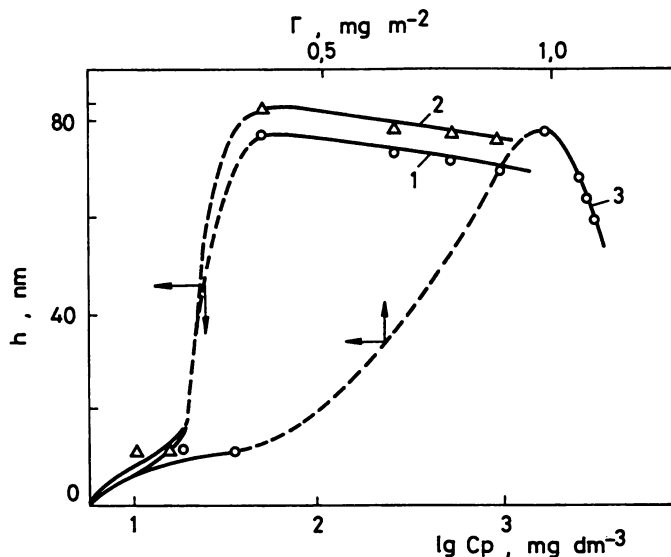


Figure 5. Dependences of the CMC 239/81 adsorption layer thickness on MF particles ( $a=550$  nm) on the polymer concentration in suspension (1,2) and on the adsorbed amount (3). The values of  $h$  were determined from the rate of sedimentation (1) and from the increase of the volume of the close-packed sediment (2).

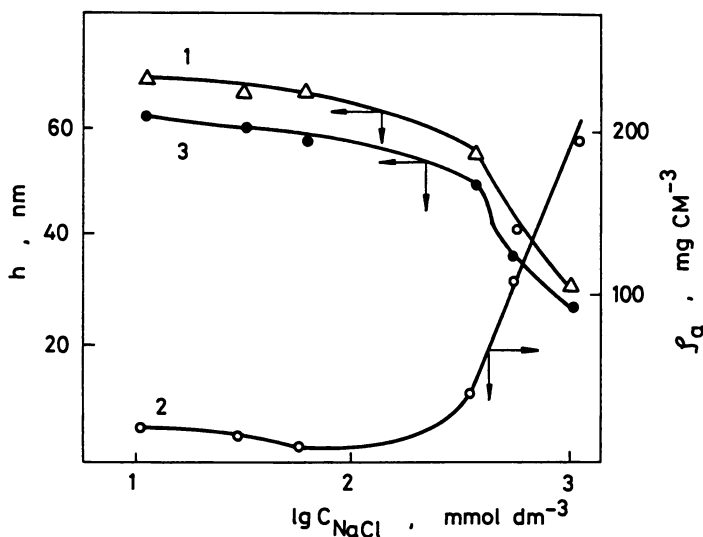


Figure 6. Dependences of the plateau values of the CMC 239/81 adsorption layer thickness (1,3) on MF particles and of the amount of polymer in a unit volume of the adsorbed layer (2) on the NaCl concentration. The values of  $h$  were determined from the volume of the close-packed sediment (1) and from the rate of sedimentation.



the nearest (first) layer to the surface is adsorbed  $\sim 0.6 \text{ mgm}^{-2}$ . Then, using the expression /6/:

$$h = (1 - P) \times V_c \times N_s \quad (6)$$

the thicknesses of the different CMC samples on the MF surface were calculated. Here  $V_c$  is the volume of polymeric coil,  $P$  is the fraction of segments tightly bound to the surface,  $N_s$  is the number of polymer molecules adsorbed per unit area. The calculated values of  $h$  in all cases exceed the experimental magnitudes of thickness by 1-2 orders of magnitude. It shows the strong deformation of the polyelectrolyte not only near the surface but in the peripheral region of the adsorbed layer. As a measure of this deformation we have used the ratio of  $\rho_a/\rho_c$ . For the CMC samples this ratio is much more than unity (see Table I), so it means that during adsorption the carboxy-methylcellulose salts undergo very strong deformation. The degree of this deformation increases with increasing molecular mass of the samples, and with decreasing the macrochain rigidity and the curvature of particles.

In the case of PEI adsorption on polystyrene particles we see the same trends, but the ratio of  $\rho_a/\rho_c$  is much less than that for CMC (Table II). This may be due to the fact that PEI samples have lower molecular masses than CMC, the higher flexibility of the polymeric chain, and the lower energy of adsorption of segments on the surface.

**Electrokinetic potential.** The adsorption of polyelectrolytes changes the surface charge density, the Stern potential value and the electrokinetic potential of dispersed particles *///*. Usually the accumulation of a superequivalent amount of oppositely charged segments on a surface (in the Stern layer) cause the overcharge of the surface of the particles. Such behavior has been observed for the adsorption of CMC on MF and of PEI on PS particles (Figure 7): increasing the amount of the oppositely charged polyelectrolyte in the suspension leads to a sharp decrease of the zeta- -potential, and then to the change of the sign of the potential particles. At high electrolyte concentrations an almost constant value of  $\zeta$  is reached. These effects are more pronounced for the highly charged rigid carboxy--methylcellulose salts. In the intermediate polymer concentration region (dotted lines of Figure 7), an intensive flocculation of the dispersions takes place and the determination of the exact values of the zeta-potential is very difficult. The effect of the polyelectrolyte

adsorption on the electrokinetic potential of the particles increases with the increase of  $M$  and of the charge of the macromolecules as well as with the increase of the radius of curvature of the particles.

**Stability.** Figure 8 illustrates the dependence of the stability of polystyrene latex (characterized by the coagulation value of NaCl) on the PEI concentration in the system. It can be seen that with increasing salt content the stability of the suspension initially decreases, at PEI concentration of 0.3-1.0 mgdm<sup>-3</sup> an intensive flocculation takes place, then the stability rises again and in a narrow interval of the polyelectrolyte concentration unlimited growth of the coagulation values of the electrolyte is achieved. It is impossible to coagulate the dispersion even by concentrated salt solution in this region. The destabilizing and stabilizing effects of polyelectrolytes increases with increasing molecular mass in good accordance with the adsorption data. Similar dependences were obtained for the other systems investigated.

The most natural and widely accepted explanation of destabilization of dispersions by oppositely charged polyelectrolytes is a reduction in the effective charge and potential of the particles, i.e. the mechanism analogous to the neutralization coagulation of sols by multiply charged counterions. The sharp decrease of the  $\zeta$ -potential of particles in the presence of the increasing amount of CMC or PEI seems to verify this suggestion. But our calculations using the DLVO theory show that the energetic barrier between the PS or MF particles disappears only at an approximate zeta-potential value of 5 mV, whereas the aggregation of particles with adsorbed polyelectrolytes occurs at relatively high  $\zeta$ -potential magnitudes (about 30-40 mV, see Figure 7). Thus, the combination of results permits the conclusion that the most probable cause of the destabilization of dispersions by oppositely charged polyelectrolytes is not a lowering of the charge and the potential of the particles, as is frequently assumed, but most probably the formation of bridge bonds between the particles through the adsorbed macroions. Also in favor of the hypothesis are the results on the increase in the degree of flocculation with an increase in the molecular mass of the sample and in the concentration of the dispersed phase. It is also possible that the flocculant (at least its first portions) is bound to the surface by a large number of contacts, unfolding on it with the formation of a mosaic structure of approximately equal numbers of charges of opposite sign.

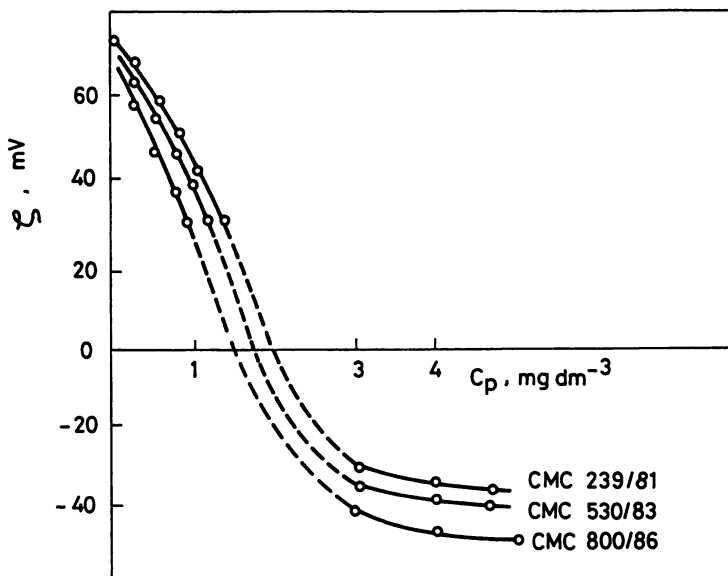


Figure 7. Dependences of the zeta-potential of MF particles on the concentration of different CMC samples (indicated) in the system.

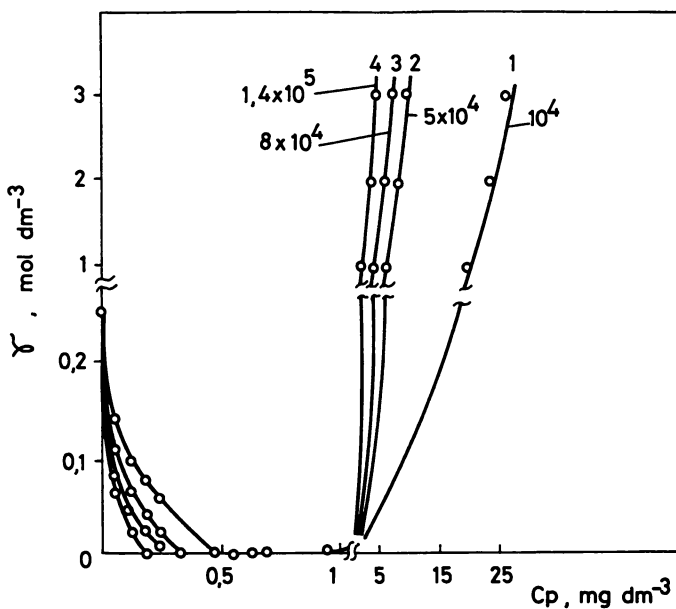


Figure 8. Dependences of the NaCl coagulation values for PS suspensions on the concentration of PEI of different molecular mass (indicated) in the system.

Using these ideas, Gregory was able to explain many features of the flocculation of lattices and bacteria by cationic polyelectrolytes /8/.

Stabilization of colloidal dispersions by adsorbed polymers may be due to the simultaneous influence of at least three main factors: electrostatic repulsion, hydrophilization of the surface, and steric stabilization.

The electrostatic factor plays an important role at low ionic strengths. It is confirmed by the increase of the zeta-potential values of particles with increasing polyelectrolyte content within the zone of stabilization (after the surface overcharge). Adsorption of macroions of CMC and PEI containing hydrophilic functional groups leads to the hydrophilization of the surface of the particles. The stabilizing effect of adsorbed hydrophilic macromolecules may be attributed to the effect of structural forces or structural components of the disjoining pressure /1, 9/. These are repulsive forces and they arise when overlapping of water layers of the interacting particles takes place and the structure of water in the overlapping zone changes. This mechanism of stabilization is of special importance for dispersions and emulsions with adsorbed non-ionic surfactants /10, 11/. The contribution of this mechanism is essential is at low surface coverages with a polymer and at low electrolyte concentrations as it was shown for hydrophobic sols containing water-soluble polymers (1, 9). In concentrated electrolyte solutions these factors can not play an important role due the screening of the charge of the macroions, which suppresses the electric double layer of the particles themselves, and decreases the hydration's degree of the polyelectrolyte molecules. The extremely high stability of suspensions at high surface coverages by polyelectrolytes even in saturated salt solutions is caused by steric repulsion forces of adsorbed macromolecules. This is connected with a formation in electrolyte solutions, as was shown above, of thick and dense adsorption layers of polyelectrolytes.

### Literature Cited

1. Baran, A.A. *Polymer-containing disperse systems* (in Russian), Naukova Dumka : Kiev , SU, 1986; pp 206.
2. Solomentsava, I. M.; Kocherga, I. I.; Baran, A. A. *Ukrainski Khimicheskii Zhurnal* 1982, vol. 47, pp 265-270.
3. Gembitsky, P. A.; Zhuk, D. S.; Kargin, V. A. *Polyethylenimine* (in Russian), Nauka : Moscow, SU, 1971; pp 203.

4. Garvey M. J.; Tadros, Th. F.; Vincent, B. J. *Colloid a. Interf. Sci.* **1974**, vol. 49, pp 69-74.
5. Lipatov, Yu. S.; Sergeeva, L. M. *Adsorption of polymers* (in Russian), Naukova Dumka : Kiev, SU, 1972; pp 196.
6. Hesselink, F. Th. *J. Colloid a. Interf. Sci.* **1977**, vol. 60, pp 448-465.
7. Solomentseva, I. M.; Velichanskaya, L. A. *Kolloidnii Zhurnal* **1983**, vol. 45, pp 800-806.
8. Gregory, J. J. *Colloid a. Interf. Sci.* **1973**, vol. 42, pp 448-456.
9. Baran, A. A.; Solomentseva, I. M. *Kolloidnii Zhurnal* **1974**, vol. 36, pp 1035-1040.
10. Derjagnin, B. V.; Churaev, N. V.; Muller, V. M. *Surface Forces* (in Russian), Nauka: Moscow, SU, 1985; pp 399.
11. Rabinovich, Ya. I.; Baran, A. A. *Colloids a. Surfaces* **1991**, vol. 59, pp 47-57.

RECEIVED August 6, 1993

## Chapter 32

# Structure and Stability of Weakly Charged Polyelectrolytes at a Solid-Liquid Interface

R. Varoqui

**Institut Charles Sadron Centre de Recherche sur les Macromolécules,  
Ecole d'Application des Hauts Polymères, Centre National de la Recherche  
Scientifique, Université Louis Pasteur, Strasbourg 6, Rue Boussingault,  
67083 Strasbourg Cédex, France**

We derive the concentration profile and the stability conditions of a layer of charged macromolecules adsorbed at a solid liquid interface. The interface is modeled as a dense layer of polymer segments in equilibrium with a dilute polyelectrolyte solution. In the case of weak electrostatic potentials, the self-consistent field equation for the configuration probability of a chain and the Poisson-Boltzmann equation can be linearized. Examples of numerical solutions obtained within the approximation of the fundamental mode are shown for different parameter values. Two cases are considered : (i) the surface is charged and interacts with oppositely charged polymer segments by long range coulombic forces ; (ii) the surface potential is of short range. By combining the numerical integration and simple thermodynamic arguments, we derive an analytical expression for the layer thickness in terms of the charge and Debye-Hückel parameters and express the conditions of stability of the polymer layer.

It is known that polyelectrolytes readily adsorb from solution on oppositely charged surfaces (1). It is also found that polyelectrolytes at low degrees of ionization adsorb on neutral surface (2-3). Adsorption gives rise to a marked alteration of the interfacial properties which is of great theoretical and practical interest (4). In the present paper we shall deal with the theory of that phenomena.

In a large number of experiments, it has commonly been observed that adsorption plateaus at bulk polymer concentrations corresponding to fairly dilute solutions (5-7) (polymer volume fractions at adsorption saturation were found of the order of  $10^{-4}$  or even lower). From the experimental side, adsorption has therefore been mainly studied for dilute solutions. In our treatment we shall focus on that situation and model the interface as a distinct polymer phase in thermodynamic equilibrium with a dilute solution. In dilute solutions, polymer molecules tend to remain as discrete units without appreciable overlap with each other. We suppose, on the other hand, that the surface phase which is formed by polymer loops of different size which overlap, resembles to a semi-dilute solution which allows a mean-field description. Strong adsorption is indeed most often the rule at low bulk polymer concentration. Because of the large number of units in a chain, the finite fraction of segments in the

0097-6156/94/0548-0421\$06.00/0  
© 1994 American Chemical Society

region of negative potential gives rise to a huge free-energy gain per molecule which invariably results in large adsorption amounts.

In this treatment, the probability of chain end distribution is coupled with the Poisson-Boltzmann equation as was done before (8-9). It comes out from the treatment that, once the number of adsorbed polymers per unit surface area is fixed, only a few parameters such as surface and polymer charge densities, Debye-Hückel and segment length, are needed to describe the segment density profile and the layer thickness. The present theory does not specifically aim at elucidating the surface excess. The derivation of this parameter which is related to the volume fraction and to the free-energy of the polymer in the solution, would need a detailed description of the polyelectrolyte shape and the small ion distribution in solution, a difficult problem. The adsorption amount remains here as a parameter (which is usually determined experimentally from the change in the concentration of the solution in equilibrium with the adsorbate). In other theoretical treatments one additional step was taken: the polyelectrolyte solution was schematized as an array of charged plates and a continuously decreasing segment density near the surface, reaching smoothly the bulk concentration, was assumed in a lattice model (10). In that theory, the adsorbed amount of polymers and the concentration profile of segments depended crucially on the more or less realistic model chosen to describe the polyelectrolyte in solution.

### Theoretical Formalism

In the self-consistent field theory (see for example references (11-12)) the distribution function  $G(\mathbf{r}', \mathbf{r}, N)$  for a flexible chain of  $N$  units to start at point  $\mathbf{r}'$  and to end at point  $\mathbf{r}$  is a Green function:

$$\left[ \frac{\partial}{\partial N} - \frac{a^2}{6} \Delta - e^{-\beta U(\mathbf{r})} + 1 \right] G(\mathbf{r}', \mathbf{r}, N) = \delta(\mathbf{r}' - \mathbf{r}) \delta(N) \quad (1)$$

$a$  is the length of a segment,  $\beta = (k_B T)^{-1}$  with  $k_B$  the Boltzmann constant and  $T$  the temperature,  $U(\mathbf{r})$  is the potential acting on a segment at point  $\mathbf{r}$ . The general form of  $U(\mathbf{r})$  is:

$$\beta U(\mathbf{r}) = \alpha \psi(\mathbf{r}) + v c(\mathbf{r}) + w(\mathbf{r}) \quad (2)$$

$\alpha e N$  is the total electrical charge of the polymer,  $e$  being the elementary charge and  $\alpha$  the degree of ionization of a segment,  $0 < \alpha < 1$ .  $\alpha \psi(\mathbf{r})$  is the reduced electrostatic energy of a segment ( $\psi(\mathbf{r}) = \beta e \tilde{\psi}(\mathbf{r})$ ,  $\tilde{\psi}(\mathbf{r})$  being the electrostatic potential),  $v$  is the excluded volume of non-electrostatic origin and  $c(\mathbf{r})$  the concentration of segments,  $w(\mathbf{r})$  is the reduced surface potential of van der Waals-London origin. We suppose in the following that  $\psi(\mathbf{r}) \gg v c(\mathbf{r})$ , which restricts somewhat the treatment in so far as segment-segment interactions are resumed totally into electrostatic interactions. This simplification is correct if in aqueous environment, the solvent behaves with respect to non-charged segments more or less as a poor solvent.

Equation 1 must be complemented with the Poisson-Boltzmann equation:

$$\Delta \psi(\mathbf{r}) = -4\pi L_B \{ \alpha c(\mathbf{r}) - C [\exp(-\psi(\mathbf{r})) - \exp(+\psi(\mathbf{r}))] \} \quad (3)$$

$C$  is the concentration of a uni-univalent added electrolyte,  $L_B$  is the Bjerrum length and  $\epsilon$  the dielectric constant:

$$L_B = \beta \epsilon^{-1} e^2 \quad (4)$$

We restrict our considerations to weak potentials, i.e.,  $\beta U(\mathbf{r}) \ll 1$ , then equations 1 and 3 can be linearized and  $G(\mathbf{r}', \mathbf{r}, N)$  expanded in the spectral expansion:

$$G(\mathbf{r}', \mathbf{r}, N) = \sum_{\lambda} \varphi_{\lambda}(\mathbf{r}) \varphi_{\lambda}(\mathbf{r}') \exp(-E_{\lambda} N) \quad (5)$$

The eigenfunctions  $\varphi_{\lambda}$  and eigenvalues  $E_{\lambda}$  satisfy the homogeneous equation:

$$\left[ \frac{a^2}{6} \Delta - \beta U(r) \right] \varphi_{\lambda}(r) = -E_{\lambda} \varphi_{\lambda}(r) \quad (6)$$

It can be shown explicitly that if the polymer is confined within a length  $L$ , small compared to the size of the polymer in solution (which is usually satisfied for long chains,  $N \gg 1$ ), the lowest eigenvalue  $E_0$  and corresponding eigenfunction  $\varphi_0(\mathbf{r})$ , - which will be denoted simply  $E$  and  $\varphi(\mathbf{r})$  in the following - dominate the spectral expansion. For the problem at hand, the following set of differential equations is then obtained:

$$\frac{a^2}{6} \varphi''(x) = [x\psi(x) + w(x) - E] \varphi(x) \quad (7)$$

$$\psi''(x) = -4\pi\alpha L_B \varphi^2(x) + \kappa^2 \psi(x) \quad (8)$$

$\kappa^{-1}$  is the Debye-Hückel length:

$$\kappa^{-1} = (8\pi L_B C)^{-1/2} \quad (9)$$

Equation 8 is the linear Poisson-Boltzmann equation. We address here to large surfaces, ignoring any concentration fluctuations in directions parallel to the surface;  $\varphi(\mathbf{r})$  and  $\psi(\mathbf{r})$  are then functions of the coordinate  $x$  in a direction normal to the surface.  $\varphi^2(x)$  is, when properly normalized, the segment concentration  $c(x)$ . Linearization of equations 1,3 restricts the treatment to weakly charged systems. The set of coupled differential equations were first proposed by Podgornik and the author in separate papers (8-9). The foundations of the self consistent mean field equations were analyzed in the first paper through elaborated field theories. Analytical expressions for the polyelectrolyte expansion at non-charged surfaces were derived by solving these equations using a perturbation method (9). In the following we shall discuss on the basis of numerical solutions and scaling analysis the main features characterizing the adsorption of charged chains, namely the concentration profile, the average layer thickness and the critical adsorption conditions. We shall treat the case of charged surfaces and non-charged surfaces separately.

### Application to Charged Surfaces : $\sigma \neq 0, w = 0$

We suppose  $w = 0$  and the surface charge density  $\sigma < 0$ ,  $\sigma$  being the charge per unit



area of the surface.  $\alpha$  is taken positive and in that situation attraction of the chains toward the surface occurs through long range electrical forces between opposite charges.

**Numerical solution.** Integration of equations 7-8 was performed using the following boundary conditions:

$$\varphi(0) = 0 \quad (10)$$

$$\psi'(0) = -4\pi L_B \sigma e^{-1} \quad (11)$$

$$\varphi(x)_{x \rightarrow \infty} = 0 \quad (12)$$

Boundary condition 10 is the proper condition to be used in the case of adsorption (see ref. 13).

The relation for  $\psi(0)$  is obtained after multiplication of the left and right hand side of equations 7-8 by  $\varphi'(x)$  and  $\psi'(x)$  respectively followed by integration from 0 to  $\infty$ . This yields:

$$\kappa^2 \psi^2(0) + (4/3\pi) L_B (a\varphi'(0))^2 - (\psi'(0))^2 = 0 \quad (13)$$

$\varphi'(0)$  was chosen to keep the normalization condition on  $\varphi^2(x)$ :

$$\Gamma = \int_0^{\infty} \varphi^2(x) dx \quad (14)$$

with  $\Gamma$  the total amount of segments per unit area.  $E$  was adjusted to make  $\varphi(x)$  and  $\psi(x)$  to converge uniformly to zero for  $x \rightarrow \infty$ . In Figure 1 are shown different curves (1), (2) and (3) which represent the calculated profile as a function of distance  $x$  for  $\sigma e^{-1} = -2.10^{-4} \text{ \AA}^{-2}$ ,  $\kappa^{-1} = 120 \text{ \AA}$  ( $C = 3.2 \times 10^{-4}$  moles/liter),  $a = 4.8 \text{ \AA}$ ,  $\alpha = 0.2$  and different adsorption amounts  $\Gamma$ :  $7.9 \times 10^{-4} \text{ \AA}^{-2}$  (1),  $2.6 \times 10^{-4} \text{ \AA}^{-2}$  (2) and  $3.6 \times 10^{-5} \text{ \AA}^{-2}$  (3). For the parameter values used, there is no perceptible difference using full P.B. equation (—) or its linear version (\*). The parameters were chosen to be arbitrarily small. The surface charge density  $\sigma$  is in line of what one would expect for minerals not too far from their isoelectric point (for a more detailed account on this question, the reader is referred to reference (14)).

Some qualitative conclusions can be drawn from an inspection of Figure 1:

(i) At weak electrostatic screening ( $\kappa^{-1} = 120 \text{ \AA}$ ), the average layer thickness defined by equation 15 is of the order of  $20 \text{ \AA}$

$$L = \Gamma^{-1} \int_0^{\infty} x \varphi^2(x) dx \quad (15)$$

So, even at rather low surface charge density, the polymer is confined within a thin surface layer. The chains are somewhat more expanded when  $\Gamma$  increases:  $L = 21.7 \text{ \AA}$ ,  $18.4 \text{ \AA}$  and  $17.5 \text{ \AA}$  for the situations described by curves (1), (2) and (3) respectively. It is clear that when  $\Gamma$  increases, the space charge density in the vicinity of the surface increases and this gives rise to enhanced intramolecular

coulombic repulsions and consequently to more expanded conformations; the effect is nevertheless weak.

ii) The variation of the electrostatic potential for different surface coverage is shown in Figure 2. At the low electrolyte concentration of  $3.2 \times 10^{-4}$  moles/liter, the charge density close to the surface is dominated by the  $4\pi\alpha L_B \phi^2(x)$  term in equation 8 which generates a positive potential, this potential opposes to a large part the potential of the surface charges- compare curves 1 and 5 in Figure 2. When the overall potential becomes small, the full P.B. equation gives the same result as the linearized P.B. equation.

As observed in Figure 3, most of the small counterions (positive monovalent ions in our case) are displaced towards the solution phase by the large polyion after adsorption. The polyion acts therefore as an effective ion-exchanger at the largest  $\Gamma$  value.

iii) The value of  $\Gamma = 7.9 \times 10^{-4} \text{ \AA}^{-2}$  corresponds to an upper limit. Increasing further this value by a few percent, leads to a situation for which no solution can be found with  $\phi(x)$  and  $\psi(x)$  converging to zero at large  $x$  with an associated negative value for the energy  $E$ . It has been shown long ago that the onset of adsorption for uncharged polymers fulfils the condition of a phase transition and critical adsorption parameters were indeed described (15-16). The ratio of surface charge density and polymer charge density,  $10e^{-1}/\Gamma\alpha$ , is here about 1.2 at the critical  $\Gamma$ .

It is hard to set by numerical calculations a rational to define precisely the critical adsorption conditions. To proceed further with this point, we shall use a simple scaling argument which goes back to Flory (17) and which will also prove useful for the derivation of an analytical expression for the layer thickness under the condition of weak electrostatic screening.

**Scaling analysis.** The free-energy of the layer is the sum of an electrostatic ( $F_e$ ) and a conformational contribution ( $F_c$ ):

$$F = F_e + F_c \quad (16)$$

$$\beta F_e = \frac{1}{2} \int_0^{\infty} e^{-1} \rho(x) \psi(x) dx \quad (17)$$

$$\beta F_c \equiv \left[ \Gamma (a/L)^2 - k_B^{-1} \Delta S_i \right] \quad (18)$$

$\rho(x)$  is the charge density,  $\Delta S_i$  the entropy change of small ions and  $(a/L)^2$  the confinement energy per segment (17-18). Ignoring for the moment numerical coefficients, we derive  $F_e$  for a constant charge density  $\rho_0$  of segments in a distance  $L$ , i.e.:

$$\beta F_e = \frac{1}{2} \int_0^L \rho_0 e^{-1} \psi(x) dx - (\kappa^2 / 8\pi L_B) \int_0^{\infty} \psi^2(x) dx \quad (19)$$

$$\psi''(x) = -4\pi L_B \rho_0 e^{-1} + \kappa^2 \psi(x) \quad , \quad x < L \quad (20)$$

$$\psi''(x) = \kappa^2 \psi(x) \quad , \quad x > L \quad (21)$$

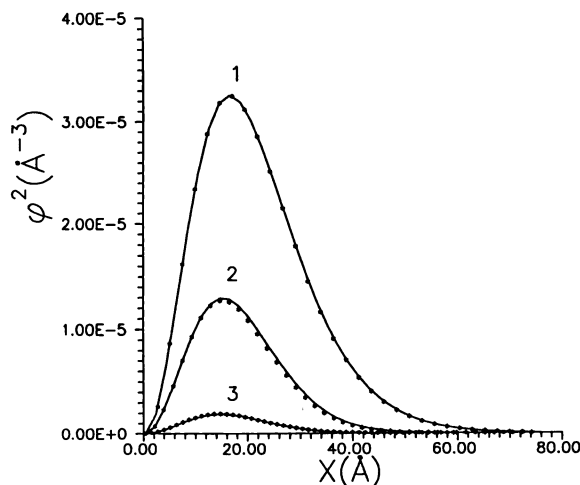


Figure 1: Segment density profile determined for different amount of polymer adsorbed with  $\alpha = 0.2$ ,  $\sigma e^{-1} = -2.10^{-4} \text{\AA}^{-2}$ ,  $\kappa^{-1} = 120 \text{\AA}$ ,  $a = 4.8 \text{\AA}$ :  $\Gamma = 7.9 \times 10^{-4} \text{\AA}$  (1),  $\Gamma = 2.6 \times 10^{-4} \text{\AA}^{-2}$  (2),  $\Gamma = 0.37 \times 10^{-4} \text{\AA}^{-2}$  (3). (—) full P.B., (\*\*\*) linearized P.B.

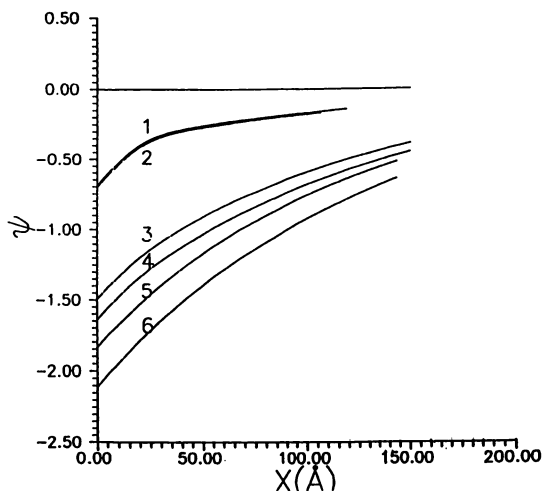


Figure 2: Reduced potential as a function of distance  $x$  from surface with  $\sigma e^{-1} = -2.10^{-2} \text{\AA}^{-2}$ ,  $\kappa^{-1} = 120 \text{\AA}$ ,  $a = 4.8 \text{\AA}$ :  $\Gamma = 7.9 \times 10^{-4} \text{\AA}^{-2}$ , (1) full P.B., (2) linearized P.B.;  $\Gamma = 2.6 \times 10^{-4} \text{\AA}^{-2}$ , (3) full P.B., (4) linearized P.B.;  $\Gamma = 0$  (bare surface), (5) full P.B., (6) linearized P.B.

Giving now attention to a situation for which  $\kappa^{-1} \gg L$ , it can be shown that the contribution of the small ions to the free-energy has only a weak dependence on  $L$  (of order  $(\kappa L)^2$ ) and we obtain:

$$\beta F = \Gamma(a/L)^2 + \pi L_B \kappa^{-1} \alpha \Gamma [\sigma e^{-1} (1 - \kappa L/2) + 2\alpha \Gamma (1 - 2\kappa L/3)] \quad (22)$$

$$\left. \frac{\partial F}{\partial L} \right|_{\Gamma, \alpha, \kappa} = 0 \quad (23)$$

With

$$e^{-1} \rho_0 = \frac{\alpha \Gamma}{L} \quad (24)$$

we obtain for the box-like distribution:

$$L = (2a^2 / \pi L_B)^{1/3} [\alpha e^{-1} |\sigma| / 2 - (4/3) \alpha^2 \Gamma]^{-1/3}, \quad \kappa L \ll 1 \quad (25)$$

The following condition must be fulfilled in order that  $F < 0$ :

$$\alpha |\sigma| \sigma^{-1} (\pi L_B)^{-1} \kappa (a/L)^2 + 2\alpha^2 \Gamma \quad (26)$$

or making use of expression (25) for  $L$ :

$$\alpha |\sigma| \sigma^{-1} \kappa (\pi L_B)^{-1/3} [a(\alpha |\sigma| \sigma^{-1} / 4 - (2/3) \alpha^2 \Gamma)]^{2/3} + 2\alpha^2 \Gamma \quad (27)$$

This condition fixes the critical parameter values. Using correct numerical coefficients for the exact profile (numerical coefficients can be assessed from the numerical integration for situations with  $L \ll \kappa^{-1}$ ), we obtain the expression for the average thickness  $L$ :

$$L = (2a^2 / \pi L_B)^{1/3} (5.17)^{1/3} \sigma^{-1} [\alpha \sigma^{-1} - 6.33 \alpha^2 \Gamma]^{-1/3}, \quad \kappa L \ll 1 \quad (28)$$

Values of  $L$  calculated according to equation 28 for  $e^{-1} \sigma = -2.10^{-4} \text{ \AA}^{-2}$ ,  $\kappa^{-1} = 120 \text{ \AA}$  and different  $\alpha$  and  $\Gamma$  values are reported in Table I ( $L_{\text{app}}$  in the last column) and compared to the exact values ( $L_{\text{ex}}$  in the third column) obtained by numerical resolution. The agreement is very good ; as long as  $L$  is less than  $0.4 \kappa^{-1}$ , the difference does not exceed 3%. However, the accuracy decreases when  $\kappa^{-1}$  becomes of the same order of magnitude than  $L$ .

**Table I. Average layer thickness calculated as a function of  $\alpha$  and  $\Gamma$  for  $|\sigma e^{-1} = 2.10^{-4} \text{ \AA}^{-2}$ ,  $\kappa^{-1} = 120 \text{ \AA}$**

$\alpha$	$\Gamma(\text{\AA}^{-2}).10^4$	$L_{ex}(\text{\AA})$	$L_{app}(\text{\AA})$
0.05	1.62	28.72	27.89
0.1	0.76	22.33	22.20
0.2	7.92	21.65	21.50
0.2	0.37	17.49	17.49
0.2	2.57	18.40	18.37
0.4	0.79	14.10	14.10
0.05*	$4.3 \times 10^{-4}$	43.67	43.63
0.1**	$1.6 \times 10^{-3}$	24.40	21.80

\* Calculated for  $\kappa^{-1} = 70 \text{ \AA}$ , ( $\kappa L \cong 0.3$ )

\*\*Calculated for  $\kappa^{-1} = 500 \text{ \AA}$  and  $\sigma e^{-1} = -10^{-4} \text{ \AA}^{-2}$ .

**Layer thickness in presence of electrolyte.** We have discussed in the previous section the situation in which  $\kappa L \ll 1$ . No simple analytical expression can be derived when  $\kappa^{-1}$  is close to or less than  $L$ . Numerical calculations show that  $L$  increases sharply when the screening of coulombic forces becomes effective-see Figures 4 and 5. However, if  $\kappa^{-1}$  decreases, it appears that the thickness of the layer cannot increase beyond a certain limit owing to the fact that below a critical  $\kappa_C^{-1}$  value, no solution can be found for  $\phi(x)$  in the vicinity of the surface. For the parameter values used in Figure 4,  $\kappa_C^{-1}$  is found by numerical calculation to be equal to  $19.5 \text{ \AA}$ . Equation 33 in paragraph 3.4 gives  $\kappa_C^{-1} = 14.8 \text{ \AA}$ , this value is slightly smaller because electrostatic interactions between the segments are neglected in that equation.

Because the layer becomes unstable at low surface energies, expanded layers cannot be reached just by decreasing  $\kappa^{-1}$  as might be expected at first sight. Instead, suppose  $\kappa^{-1} \rightarrow \infty$ ,  $\alpha \sigma \rightarrow 0$  and  $|\sigma e^{-1}| \gg \alpha \Gamma$ , then, as can be checked by inspection of equation 28, the loop size increases beyond limits.

**Approximate treatment.** Equation 7 was solved in a previous study (20) with the potential  $\psi(x) = 4\pi L_B \kappa^{-1} \sigma e^{-1} \exp(-\kappa x)$ ; this is the potential of the surface charges, the contribution to the potential of the polymer charges - the  $4\pi \alpha L_B \phi^2(x)$  term in

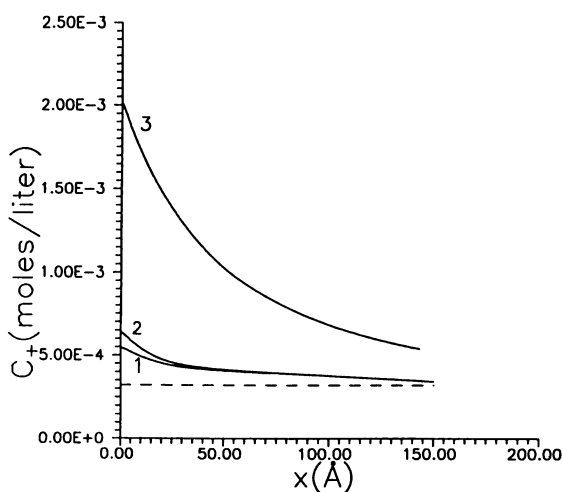


Figure 3: Concentration of monovalent counterions vs distance to surface with  $\sigma e^{-1} = -2.10 \cdot 10^{-2} \text{ \AA}^{-2}$ ,  $\kappa^{-1} = 120 \text{ \AA}$ : (3)  $\Gamma = 0$ , full P.B.;  $\Gamma = 7.9 \times 10^{-4} \text{ \AA}^{-2}$ ,  $\alpha = 0.2$ , (2) full P.B., (1) linearized P.B.

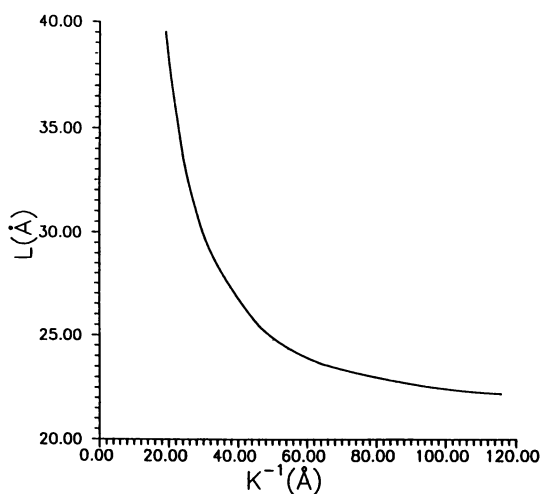


Figure 4: Layer thickness as a function of  $\kappa^{-1}$ :  $\alpha = 0.1$ ,  $a = 4.8 \text{ \AA}$ ,  $\Gamma = 7.56 \times 10^{-6} \text{ \AA}^{-2}$ .

equation 8 - being neglected. This gives the following equation for  $\varphi(x)$ :

$$\frac{a^2}{6} \varphi''(x) = [4\pi L_B \kappa^{-1} \sigma e^{-1} \alpha \exp(-\kappa x) - E] \varphi(x) \quad (29)$$

Equation 29 can be transformed into a Bessel equation with following solution:

$$\varphi(x) = J_\nu [\kappa^{-1} a^{-1} (24\theta)^{1/2} \exp(-\kappa x / 2)] \quad (30)$$

$$\theta = 2\pi |\sigma| e^{-1} \alpha L_B \kappa^{-1} \quad (31)$$

$J_\nu$  is a Bessel function of order  $\nu$  and the eigenvalue  $\nu$  is fixed by the condition  $\varphi(0) = 0$ , i.e.,

$$J_\nu [\kappa^{-1} a^{-1} (24\theta)^{1/2}] = 0 \quad (32)$$

The critical adsorption energy is given by:

$$\kappa^{-1} a^{-1} (24\theta_c)^{1/2} = 2.404 \quad (33)$$

$$\alpha |\sigma| e^{-1} (2.404a)^2 \kappa^3 L_B^{-1} / 48\pi \quad (34)$$

Apart from numerical coefficients, equation 34 reduces to equation 27 when  $\Gamma$  is set equal to zero. For comparison, the density profile calculated by equations 7-8 and equation 30 are reported in Figure 6, curves 1 and 2 respectively. Neglecting the  $\varphi^2(x)$  term in the P.B. equation results, as expected, in less expanded layers; the effect on the average layer thickness is not large, but it has a pronounced effect on the free-energy  $E$ :  $E = -0.34$  and  $E = -0.06$  for curves 1 and 2 respectively. With the free-energy of segment-segment interactions included, we are in fact near to the threshold of the adsorption/desorption transition.

It is important to note that the adsorption of one single chain was considered in reference (18). When for a single chain in presence of a large surface (large when compared to the polymer size), the segment-segment interactions are neglected, the distribution function becomes:

$$G(r', r, N) = \frac{3}{2\pi N a^2} \exp\left\{-\left[3\left[(y' - y)^2 + (z' - z)^2\right] / 2Na^2\right]\right\} \varphi_n(x) \varphi_n(x') \exp(-EN) \quad (35)$$

The probability distribution in the direction parallel to the surface is gaussian. In reality, because of the segment-segment interactions,  $\psi$  must also be a function of coordinates  $y, z$ :  $\psi \equiv \Psi(x, y, z)$ , and the single chain problem is therefore considerably more involved. If we let  $N \rightarrow \infty$ ,  $S \rightarrow \infty$  with  $N/S = \text{const.}$ , then the equivalence  $\Gamma = N/S$  becomes correct and the one chain problem can be treated formally along the previous lines.

In another treatment, electrostatic interactions between segments were handled in the one chain problem by replacing in equation (29) the step length  $a$  by a new step length  $a_1$ , (21):

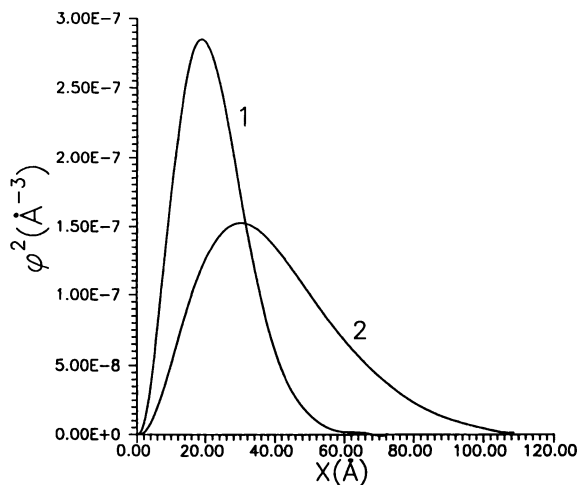


Figure 5: Segment density profile for two different values of  $\kappa^{-1}$ ,  $\sigma e^{-1} = -2.10^{-4} \text{ \AA}^{-2}$ ,  $a = 4.8 \text{ \AA}$ ,  $\alpha = 0.1$ ,  $\Gamma = 7.06 \times 10^{-6} \text{ \AA}^{-2}$ : (1),  $\kappa^{-1} = 100 \text{ \AA}$ ; (2),  $\kappa^{-1} = 20 \text{ \AA}$ .

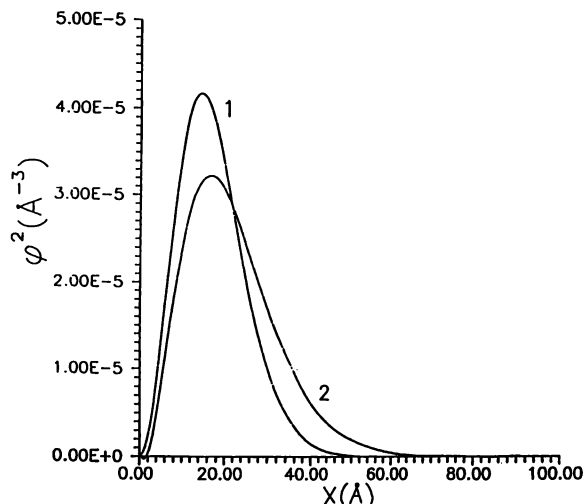


Figure 6: Segment density profile for  $\sigma e^{-1} = -2.10^{-4} \text{ \AA}^{-2}$ ,  $\kappa^{-1} = 120 \text{ \AA}$ ,  $a = 4.8 \text{ \AA}$ ,  $\alpha = 0.2$ ,  $\Gamma = 7.9 \times 10^{-4} \text{ \AA}^{-2}$ . (1) exact profile; (2) profile calculated according to relation (30).



$$\frac{a_1^2}{6} \varphi''(x) = [4\pi L_B \kappa^{-1} \sigma \vartheta^1 a_1 a^{-1} \alpha \exp(-\kappa x) - E] \varphi(x) \quad (36)$$

the length  $a_1$  was obtained from the sum of a non-electrostatic excluded volume  $\xi_{ev}$  and an electrostatic excluded volume contribution  $\xi_c$ :

$$a_1^{3/2} (1/a - 1/a_1) = \xi_{ev} + \xi_c \quad (37)$$

$\xi_{ev}$  and  $\xi_c$  were derived from the configuration of the chain in solution. Limiting laws at adsorption criticality were found to depend on the chain length through the renormalized step  $a_1$ . In this equivalent chain model, segment-segment interactions are not evaluated in the adsorbed state, and this model does therefore not comply with the P.B. equation 8.

#### Application to uncharged surfaces $\sigma = 0, w \neq 0$

Weakly charged polyelectrolytes can possibly adsorb onto non-charged surfaces through short range forces, van der Waals-London attractive forces, hydrogen-bonds, hydrophobic forces etc... (examples are reported in references (2-3) in which the mechanism of adsorption onto cellulose-acetate of a copolymer of maleic acid and of poly(glutamic-acid) were investigated at various degrees of ionization). For  $w \neq 0$ , the eigenfunction  $\varphi(x)$  and the potential  $\psi(x)$  must satisfy following equations:

$$\frac{a^2}{6} \varphi''(x) = [\alpha \psi(x) + w(x) - E] \varphi(x) \quad , \quad x < x_0 \quad (38)$$

$$\frac{a^2}{6} \varphi''(x) = [\alpha \psi(x) - E] \varphi(x) \quad , \quad x > x_0 \quad (39)$$

$x_0$  is the effective range of the surface force. For a given potential shape,  $\varphi(x)$  may be computed for  $x < x_0$  by solving the eigenvalue equation in the attractive region. However since the range of attraction is assumed to be small ( $x_0$  is of the order of monomer size), the layer profile is essentially defined for  $x > x_0$ . It is therefore convenient to assume a delta function for  $w(x)$ ,  $w(x) = w\delta(x-x_0)$ , with  $w < 0$  (see for instance de Gennes in reference (16)). Expressing the "contact" energy in the form of a delta function imposes a boundary condition at  $x = x_0$ :

$$\frac{1}{\varphi} \frac{d\varphi}{dx} \Big|_{x=x_0} = 6wa^{-2} \quad (40)$$

A slightly different notation will then prove useful. For an uncharged chain, ( $\alpha = 0$ ), the profile  $\varphi(x)$  is a simple exponential:

$$\varphi^2(x) = A \exp(-x/L_1) \quad (41)$$

$$L_1 = 2a(6|E_0|)^{-1/2} \quad (42)$$

$$w = -a^2 / 12L_1 \quad (43)$$

The chain at zero charge is confined within an exponential of length  $L_1$  and the strength of interaction is defined by the length  $L_1$ . Let us express as before the free-energy  $F$  in a scaling form:

$$\beta F = \Gamma(a/L)^2 - a^{-1}|w|\Gamma(a/L) + 2\pi\alpha^2\Gamma^2L_B(\kappa^{-1} - 2L/3) \quad (44)$$

Since the monomers are spread over a thickness  $L$ , we expect the fraction of bound monomers to be proportional to  $a\Gamma/L$ , and the second term in the r.h.s. of equation 44 expresses the "contact" energy. Proceeding as previously, one finds:

$$1/L^3 - 1/24L_1L^2 + 2\pi\alpha^2\Gamma L_B a^{-2}/3 = 0 \quad , \quad \kappa L \ll 1 \quad (45)$$

$$1/12L_1L > 1/L^2 + 2\pi\alpha^2\Gamma L_B a^{-2}\kappa^{-1} \quad , \quad \kappa L \ll 1 \quad (46)$$

Equation 46 defines an upper limit  $\Gamma_{\max}$  for  $\Gamma$  at fixed  $\alpha$  and  $\kappa$  in terms of an upper limit value  $L_{\max}$  for  $L$ :

$$1/12L_1L_{\max} = 1/L^2 + 2\pi\alpha^2\Gamma_{\max}L_B\kappa^{-1}a^{-2} \quad (47)$$

After substitution in equation 45, a relation for  $L_{\max}$  is obtained:

$$1/L_{\max} = 1/2 \left[ \lambda + (\lambda^2 - \kappa/9L_1)^{1/2} \right] \quad (48)$$

$$\lambda = 1/24L_1 + \kappa/3 \quad (49)$$

Since  $L > L_1$ , the condition  $L_1\kappa \ll 1$  is also satisfied so that the r.h.s. in equation 48 becomes a function of solely the length  $L_1$ , which means that  $L_{\max}$  is of the order of  $L_1$ . Since the chain is most expanded at weak screening, we do in fact not expect  $L$  much different of  $L_1$  at all  $\kappa^{-1}$  values. When  $L = L_1$  is substituted in equation 46,  $\Gamma_{\max}$  is obtained as a function of  $\kappa$ ,  $\alpha$  and  $L_1$ :

$$\Gamma < \Gamma_{\max} \quad (50)$$

$$\Gamma_{\max} \equiv a^2\kappa/\alpha^2L_1^2L_B \quad (51)$$

Because of  $L \equiv L_1$ , a perturbation calculation can be made to determine the concentration profile. Since this has been described before (9), we shall skip all details here. It was shown that an approximate solution for  $\varphi(x)$  is:

$$\varphi(x) = A \exp \left[ - \int \sqrt{f(x)} dx \right] / [f(x)]^{1/4} \quad (52)$$

$$f(x) = (6/a^2)[-E + \alpha\psi_1(x)] \quad (53)$$

$$\psi_1 = \alpha L_B \Gamma L_1 \kappa^{-2} \left[ \exp(-x/L_1) - \kappa^{-1} / L_1 \exp(-\kappa x) \right] / (L_1^2 - \kappa^{-2}) \quad (54)$$

A is a normalization constant and E is defined by:

$$\left[ 6a^{-2}(-E + \alpha\psi_1(0)) \right]^{1/2} = 1/2L_1 \quad (55)$$

If the function  $f(x)$  is negative the Wentzel -Kramer-Brillouin solution 52 oscillates and the function  $\varphi(x)$  does not converge to zero at infinity. In order to have bound states we must impose  $f(x) > 0$ , we again reach then an upper limit for  $\Gamma$  :

$$\Gamma_{\max} = a^2 (L_1 + \kappa^{-1}) / (24\alpha^2 L_1^2 \kappa^{-2} L_B) \quad (56)$$

This condition holds now at any  $\kappa$  value. Apart from numerical coefficients, this is identical with equation 51 when  $\kappa L_1 < 1$ . It is gratifying to note that one reaches from the scaling concepts and the completely different perturbation approach essentially the same conclusion.

### Conclusion

We have discussed the structure of a dense polyelectrolyte layer at the interface between a solid and a dilute polymer solution. It was possible by combining numerical solutions and simple thermodynamic arguments to derive analytical expressions with numerical coefficients included for the layer thickness and a relation between parameters at the critical adsorption point. The derivation was made for two different situations:

i) charged surfaces: polyelectrolytes are then generally adsorbed into flat layers. At low electrolyte concentration, the thickness depends only weakly -to a power of 0.33-on the charge density and adsorption amount. Under conditions of weak electrostatic screening and at low surface and polymer charge densities, one expects however large loops to be formed. Strong electrolyte screening causes chains to desorb.

ii) short range interactions: the segment density profile does not deviate much from an exponential profile when the surface attracts the chain via short range forces. An analytic expression is derived for the segment density profile by a perturbation calculation in the Wentzel- Kramer -Brillouin approximation. From the free-energy balance, it appears that the adsorption is characterized by a limiting value of total segments adsorbed per unit surface area which decreases with the square of the polymer charge and is inversely proportional to  $L_1^2 \kappa^{-1}$  at low electrolyte content and inversely proportional  $L_1 \kappa^{-2}$  at high electrolyte content. The typical length  $L_1$  varies inversely with the adsorption strength and  $\kappa^{-1}$  is the Debye-Hückel length.

### Acknowledgements

The author is grateful to Professor P. G. de Gennes for a conversation regarding the problem addressed. Acknowledgements are also made to Professor J. F. Joanny and A. Johner for valuable discussions.

**Literature Cited**

- (1) Cohen Stuart M.A.; Fleer G.J.; Lyklema J.; Norde W.; Scheutjens J.M.H.M. *Adv. Colloid and Interf. Sci.* **1991**, *34*, 477.
- (2) Pefferkorn E.; Dejardin Ph.; Varoqui R. *J. of Colloid and Interf. Sc.* **1977**, *63*,353.
- (3) Pefferkorn E.; Schmitt A.; Varoqui R. *Biopolymers* **1982**, *21*, 1451.
- (4) Napper D. H. *Polymeric Stabilization of Colloid Dispersions*; Colloid Science, Academic Press: New York, **1983**.
- (5) Girot G.; Lamarche J.; Foissy A.. *J. of Colloid and Interf. Sc.* **1988**, *121*, 275.
- (6) Pefferkorn E.; Jean-Chronberg A.C.; Chauveteau G.; Varoqui R. *J. of Colloid and Interf. Sc.* **1990**, *137*, 66.
- (7) Wang T. K.; Audebert R. *J. of Colloid and Interf. Sc.* **1987**, *119*, 459.
- (8) Podgornik R. *J. Phys. Chem.* **1992**, *96*, 884.
- (9) Varoqui R.; Johner A.; Elaissari A. *J. Chem. Phys.* **1991**, *94*, 6873.
- (10) Van der Schee H. A.; Lyklema J. *J. Phys. Chem.* **1984**, *88*, 6661.
- (11) Edwards S. F. *Proc. Phys. Soc.* **1965**, *85*,613.
- (12) Freed K. F. *Adv. Chem. Phys.* **1972**, *22*,1.
- (13) DiMarzio E. A.. *J. Chem. Phys.* **1965**, *42* ,2101.
- (14) Hunter R.J. *Zeta Potential in Colloid Science. Principles and Applications*; Academic Press: London, New York, **1981**.
- (15) Hoeve C.A.J.; DiMarzio E.A.; Peyser P. *J. of Chem. Phys.* **1965**, *42*, 2558.
- (16) de Gennes P. G. *Rep. Prog. Phys.* **1969**, *32*, 187.
- (17) Flory, J. P. *Principles of Polymer Chemistry*; Cornell University Press: Ithaca, New York ,**1953**.
- (18) de Gennes P. G. *Scaling Concepts in Polymer Physics*; Cornell University Press: Ithaca, London ,**1979**.
- (19) Wittmer J.; Joanny J. F. *Macromolecules* (submitted).
- (20) Wiegel F. W. *J. Phys. A: Math. Gen.* **1976** , *10*, 299.
- (21) Muthukumar M. *J.Chem. Phys.* **1987**, *86*, 7230.

RECEIVED August 6, 1993

## Chapter 33

# Adsorption of Neutral Polymers and Polyelectrolytes on Model Colloid Particles by Electrooptics

I. B. Petkanchin

Institute of Physical Chemistry, Bulgarian Academy of Sciences, 1040  
Sofia, Bulgaria

The adsorption of polymers and polyelectrolytes modifies the electric surface properties of colloidal particles-e.g. their charge, electric polarizability and the dynamic properties of electric double layer. These changes lead to a change of the suspension stability. The electro-optic method of investigation gives the possibility to obtain information for electric dipole moments of the particles as well as on their dimensions. The influence of neutral polymer (polyacrylamide) and polyelectrolytes (carboxy-methyl cellulose) on the surface properties of model oxide particles, clays and mica is studied electro-optically. From the transient electro-optical measurements the thickness of the neutral adsorbed polymer layer is calculated. The changes of the electric surface properties and their dynamics are established. The results obtained show the connection of the particles electric moments with the conformational properties of the adsorbed layers.

Recently, the influence of neutral polymers and polyelectrolytes on the stability of colloid systems, attracts the attention of many researchers (1). This interest concerns the fundamental problems arising from interaction of surfaces with polymers leading to changes in the suspension stability. Besides, stabilisation or destabilisation of disperse systems is widely used in many technological processes. The better understanding of the interactions is related to the conformation state of adsorbed

0097-6156/94/0548-0436\$06.00/0  
© 1994 American Chemical Society

macromolecules, their transition from bulk solution to the interface and as well as the changes of surface electric properties of the particles. The adsorbed neutral polymers cause alteration of the dynamic properties of particles electric double layer (edl) whereas polyelectrolytes provoke additional changes in the static properties. Many experimental methods exist for determination of the adsorbed polymer layer thickness (quasi elastic light scattering, sedimentation, ellipsometry, electrophoresis) (2,3). In the present paper, the electric light scattering method (ELS) is used for determination of adsorbed layer thickness on model colloid particles ( $\beta$ -FeOOH, mica, kaolinite). The obtained values are in good agreement with those derived from other methods. An additional information is also obtained, the changes of particles surface electric moments and their dynamics in presence of adsorbed neutral polymer or polyelectrolyte.

### Electric Light Scattering Method

The application of an electric field (d.c. or a.c.) on a suspension from anisometric particles causes orientation of the particles. The orientation is due to the interaction of particles electric moments ("permanent" and induced) with the applied electric field. The particles orientation changes the optical properties of the system as a whole. The "permanent" dipole moment could be related with structural charge asymmetry or with interfacial processes connected with ions movements and macromolecular adsorption. These processes are manifested in electro-optical investigation as an interfacial "permanent" dipole moment (4,5). Some electroosmotic effects of the surrounding liquid should be also considered, which also would contribute to the polarisation mechanism (6). The induced dipole moment and the polarisation mechanism resp are related to ions movement in the diffuse double layer (7). The electro-optical effect  $\alpha$  is defined as (7):

$$\alpha = \frac{I_E - I_0}{I_0} \quad (1)$$

where  $I_E$  and  $I_0$  are the intensities of the scattered light when an electric field of strength  $E$  is applied to the suspension and without field resp. The electro-optical effect for elongated particles with length  $l$  and thickness  $b$ , at low degree of orientation, in the limit of Rayleigh-Debye-Gans

approximation, is given by (7,8):

$$\alpha = \frac{A(Kl, Kb)}{I_0(Kl, Kb)} (\mu + \delta^2) E^2 \quad (2)$$

where  $A(Kl, Kb)$  and  $I_0(Kl, Kb)$  are optical functions, depending on particles dimensions, particles optical properties and on the geometry of light scattering experiment.  $K = (2\pi/\lambda) \sin(\theta'/2)$ ,  $\lambda$  is incident light wave length in the disperse medium,  $\theta'$  - angle of observation;  $\mu = (p^2)/(kT)^2$ ,  $\delta = (\gamma_1 - \gamma_2)/(kT)$ ,  $p$  and  $\gamma_1$  are the permanent dipole moment and electric polarizability along particle symmetry axis;  $\gamma_2$  - electric polarizability along the transverse axis;  $k$  - Boltzmann constant;  $T$  - Kelvin temperature. The dependence of the electro-optical effects on the field frequency i.e. dispersion dependence gives the possibility to separate different polarisation mechanisms connected with "permanent" and induced dipole moments. From Equation 2 particles electric moments could be estimated if particles dimensions are known. The initial slope of  $\alpha/E^2$  dependence is proportional to particle electric polarizability at field frequencies (plateau region) where contributions from "permanent" dipole moments have already relaxed.

The transient electro-optical effect, following the switching off of the electric field is connected with particles disorientation and is given by (9).

$$\alpha_t = \alpha_0 \exp(-6D_r t) \quad (3)$$

where  $\alpha_0$  and  $\alpha_t$  are the steady state electro-optical effect and its value after time  $t$ ,  $D_r$  - rotational diffusion coefficient,  $\tau$  - relaxation time of particles disorientation.

The rotational diffusion coefficient  $D_r$  for thin circular discs with diameter  $B$  and thickness  $d$  ( $B \gg d$ ) is given by Perrin (10):

$$D_r = \frac{3kT}{4\eta B^3} \quad (4)$$

For ellipsoidal particles  $D_r$  is given by (11):

$$D_r = \frac{3kT}{4\pi\eta l^3} (2 \ln 2p - 1) \quad (5)$$

where  $l$  is the particle long dimension,  $b$  is the transverse axis;  $p=l/b$  and  $\eta$  is the medium viscosity. The polymer layer thicknesses (hydrodynamic values) were estimated from electro-optical data, using Equations (3), (4) and (5).

## Objects

**Kaolinite.** The particles of Na-kaolinite (GZA-IV-France) present hexagonal thin discs with dimensions obtained from Electron Microscopy, length- 250 nm, width- 160 nm and thickness- 25 nm (12). The two basal surfaces of kaolinite are with different structure, one composed from Al-O-OH octaheders and the other from Si-O tetraheders. The latter surface carries the most amount of the total negative charge due to isomorphous substitution (13). The edge of the disc has a pH dependent charge due to dissociation of Al-OH groups. This means that the particles have a charge asymmetry (structural permanent dipole moment) across the disc plane.

**Mica.** The suspensions were prepared from freshly cleaved muscovite by wet grinding and converted to K-form (14). The mica suspensions were investigated 24 hours after addition of PAM, at pH=5.9 and ionic strength  $10^{-4}$  KCl. The mica particles present thin discs with an average diameter of 500 nm and thickness of 50 nm. Muscovite was the same used in surface forces apparatus (15). The elementary layer of mica is composed from two silicon-oxygentetrahedral layers and in between octaheders of aluminium-oxygen layers. Both basal surfaces have the same structure and there is no reason for charge asymmetry across the disc plane.

**$\beta$ -ferric hydroxide.** The particles ( $\beta$ -FeOOH) were prepared by acid hydrolysis of FeCl<sub>3</sub> (16). The obtained ellipsoidal particles are with length around 352 nm, axial ratio 4 and are rather monodisperse, (17).

**$\gamma$ -Al<sub>2</sub>O<sub>3</sub>, SiO<sub>2</sub>.** The particles of  $\gamma$ -Al<sub>2</sub>O<sub>3</sub> and SiO<sub>2</sub> (Aerosil) are obtained through flame hydrolysis (18). Both oxides give aggregates built from monodisperse spheres, with a diameter of about 20 nm. The aqueous dispersions of these oxides give stable and reproducible electro-optical effects, because of the existence of fractal anisometric aggregates (19).

The surface charge of oxide particles is due to ionisation of surface hydroxyl groups. The  $\gamma$ -Al<sub>2</sub>O<sub>3</sub> particles are positively charged at pH 4-8 whereas Aerosil particles are negatively charged at the same pH.



The particles' concentration of the suspension was for  $\beta$ -FeOOH -  $4 \times 10^{-3}$  g.dm<sup>-3</sup>, mica -  $10^{-2}$  g.dm<sup>-3</sup>, kaolinite -  $2 \times 10^{-2}$  g.dm<sup>-3</sup>, aerosil -  $10^{-1}$  g.dm<sup>-3</sup> and  $\gamma$ -Al<sub>2</sub>O<sub>3</sub> -  $10^{-2}$  g.dm<sup>-3</sup> where the electro-optical effect do not depend on particles' concentration.

**Neutral polymer.** The used neutral polymer - polyacrylamide (PAM) with different molecular weights  $1.2 \times 10^6$  and  $3.7 \times 10^5$  was fractionated and kindly supplied by Dr. R.Varoqui (CNRS - France).

The suspensions are stabilized in presence of neutral polymer which was proved by addition of NaCl.

**Polyelectrolyte.** Na carboxymethylcellulose (Na CMC) was used with molecular weight -  $10^5$ , degree of substitution 0.65 - 0.9 and degree of polymerization - 1000. We used also NaCMC-1 (Blanose 12M31RD) from Hercules (France) with molecular weight MW  $2.5 \times 10^5$ , degree of substitution 1.2 and degree of polymerization around 1000.

**Electric surface properties of colloid particles and thickness of the adsorbed neutral polymer.**

The dependence of the electro-optical effect  $\alpha$  on the field frequency at constant field strength reveals polarisation mechanisms with different relaxation times. The relaxation time of particles orientation due to permanent dipoles or interfacial "permanent" dipoles is in the order of particles' relaxation time of disorientation. Particles orientation due to induced dipole moments is determined by the movement of diffuse layer charges. The relaxation time of the induced dipole moment, the electric polarizability resp. depends on ions mobility and is given by  $\tau_{\gamma} = l^2/2D$  where  $l$  is the long particle dimension and  $D$ -ions' diffusion coefficient (7). Figure 1 presents a normalised (to electro-optical effect without polymer- $\alpha_0$ ) dispersion dependence for  $\beta$ -FeOOH particles in presence of polyacrylamide (MW= $1.2 \times 10^6$ ) with different concentration at  $E = 1.8 \times 10^4$  V.m<sup>-1</sup>. An increase of ( $\alpha_p$  - electro-optical effect in presence of PAM) the low frequency effect upon polymer adsorption is observed. The relaxation time of the low frequency dispersion (10 Hz - 1kHz) coincides with particle relaxation time of disorientation showing the interfacial nature of this dispersion. The high frequency range (above 3 kHz) of the dispersion dependence is connected with the relaxation of the electric polarizability. A shift of polarizability relaxation frequency to higher frequency in

comparison to the suspension without PAM is observed. In other words the relaxation time of polarizability decreases when polymer is adsorbed. At  $4 \times 10^{-4} \text{g.dm}^{-3}$  PAM ( $\Phi$ ) no relaxation of the electro-optical effect, electric polarizability resp. is observed.

On the inset of Figure 1 a dispersion dependence of  $\alpha_p$  for  $\beta$ -FeOOH in presence of  $8 \times 10^{-5} \text{g.dm}^{-3}$  PAM is given. The value  $\alpha_s$  of the plateau electro-optical effect is proportional to the particles electric polarizability because all contributions from "permanent" dipole moments have already relaxed. The quantity  $\alpha_{ad}$  is defined as  $\alpha_{ad} = \alpha_{10\text{Hz}} - \alpha_s$ . It consists of contributions to the polarization mechanism connected with the interface and with electro-osmotic effects. A similar trend of the dispersion dependence shown in Figure 1 is observed for mica in presence of PAM. In the case of kaolinite particles with transversal to the disc plane charge asymmetry, the adsorption of PAM diminishes this asymmetry.

On Figure 2  $\alpha_s$  as a function of  $C_{\text{PAM}}$  for all objects is presented. The electro-optical effect  $\alpha_s$  in the plateau region of the dispersion dependence is proportional to the electric polarizability. A region, where  $\alpha_s$  is constant exists for kaolinite,  $\beta$ -FeOOH and  $\gamma$ -Al<sub>2</sub>O<sub>3</sub>, (20). After this constant region a decrease of the electric polarizability is observed with the further increase of PAM concentration. One exception is mica where the decrease of  $\alpha_s$  is not so well expressed. One can suppose that electric polarizability of mica is predominantly determined by the potassium ions adsorbed in the Stern plane and that is why  $\gamma$  only slightly depends on the adsorbed neutral polymer. The changes of the electrophoretic mobility ( $U_e$ ) with PAM concentration are shown on Figure 3. The similarity of  $\alpha_s$  and  $U_e$  dependences could be seen, as proving the connection of electric polarizability with diffuse ions movement in the case of oxides and kaolinite. The decrease of  $U_e$  could be related with the shift of slipping plane to the bulk solution in presence of adsorbed polymer layer. An effective electrokinetic thickness ( $\delta_u$ ) of polymer layer could be calculated from the electrophoretic mobility decrease when polymer layer thickness is smaller than double layer thickness (21). A good coincidence was obtained between  $\delta_u$  and those obtained by electro-optic measurements in the case of Na-kaolinite and  $\beta$ -FeOOH (12,22)

The appearance of  $\alpha_{ad}$  at low field frequencies is typical for  $\beta$ -FeOOH particles and mica. On Figure 4  $\alpha_s$  and  $\alpha_{ad}$  for  $\beta$ -FeOOH in presence of PAM at two different molecular weights are given. A non-monotonic change of  $\alpha_{ad}$  and its dependence on the molecular weight of the

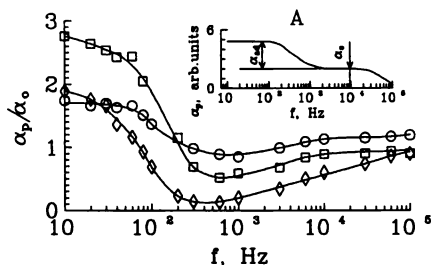


Figure 1. Normalized dispersion dependence ( $\alpha_p/\alpha_0$ ) of  $\beta$ -FeOOH particle at different PAM concentrations,  $\circ$  -  $8 \times 10^{-5}$ ,  $\square$  -  $2 \times 10^{-4}$  and  $\diamond$  -  $4 \times 10^{-4}$   $\text{g} \cdot \text{dm}^{-3}$ ,  $E = 1.8 \times 10^4 \text{V} \cdot \text{m}^{-1}$ ,  $\text{pH} = 4$ , ionic strength  $10^{-4}$ .

A - Dispersion dependence of  $\beta$ -FeOOH particles in presence of  $8 \times 10^{-3}$   $\text{g} \cdot \text{dm}^{-3}$  PAM.

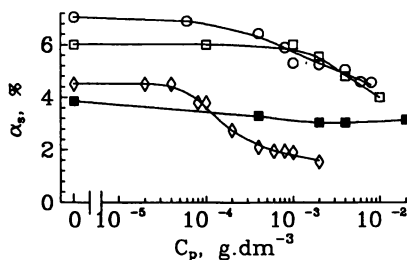


Figure 2. Dependence of the electro-optical effect  $\alpha_s$  for  $\gamma$ - $\text{Al}_2\text{O}_3$  -  $\circ$ , Na-kaolinite -  $\square$ ;  $\beta$ -FeOOH -  $\diamond$  and mica -  $\blacksquare$  on PAM concentration.

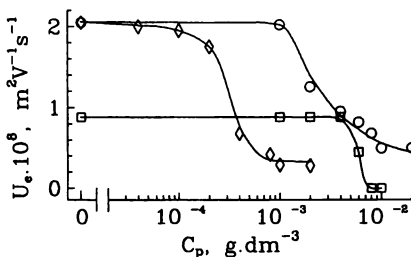


Figure 3. Dependence of the electrophoretic mobility  $U_e$  for Na-kaolinite -  $\circ$ ,  $\beta$ -FeOOH -  $\diamond$  and mica -  $\square$  on PAM concentration.

adsorbed polymer are observed. For comparison the changes of  $\alpha_s$  are also given.

Using the transient electro-optical effect and knowing the particles form, the thicknesses of the adsorbed polymer layer were calculated. The results obtained are given in Figure 5. The results for  $\delta_\tau$  are in good agreement with those obtained with other methods like quasielastic light scattering (22). The non-defined form of  $\gamma\text{-Al}_2\text{O}_3$  particles not allowed to calculate  $\delta_\tau$ . A sharp increase of  $\delta_\tau$  in the concentration region of PAM where electric polarizability decreases and changes in its relaxation frequency is observed. In the same concentration interval  $U_e$  also decreases. From the change of the slopes of  $\delta_\tau$  vs.  $\lg C_{\text{PAM}}$  curves one can suppose a conformational changes of the adsorbed polymer layer (23). At low concentration of PAM the adsorbed macromolecules are in flat conformation and do not influence the electric polarizability and electrophoretic mobility (Figures 2 and 3). At the same time  $\alpha_{\text{ad}}$  steeply increases from zero reaching a maximum and after that decreases (Figure 5). The maximum of  $\alpha_{\text{ad}}$  corresponds to a transition from a flat adsorbed layer to a thick and dense (loops and tails are built). This layer could probably change the ions distribution in electric double layer (edl). Considering the probable changes of the static edl properties in presence of neutral polymer one can suppose: a) decrease of the dielectric constant and disturbance of water molecules ordering; b) competition between the charge determining ions (in case of oxides-protons) with polymer molecules for adsorption places leading to a decrease of the surface charge and changes of space ions distribution; c) competition between counterions and polymer molecules in the dense part of edl; d) appearance of an adsorption potential because of the probable orientation of amide group. The neutral polymer decreases the hydrodynamic tangential flow of liquid and as well as the tangential surface current (21).

### **Electric surface properties of colloid particles in presence of polyelectrolyte**

The interactions of polyelectrolytes with charged colloid particles, besides the specific forces give rise the appearance of electrostatic forces. The

latter would influence the conformation of the adsorbed polyelectrolyte. The variation of pH and electrolyte concentration is of importance for the surface electric properties of the substrate as well as for the polyelectrolyte conformation on the particle surface. The electrostatic forces depend on the sign of charge of the particle and polyelectrolyte. When the particles and polyelectrolytes have different sign of charges, the adsorption causes a decrease of the surface charge, and respectively of suspension stability upon polyelectrolyte concentration increase.

The electro-optical effect of  $\gamma$ -Al<sub>2</sub>O<sub>3</sub> suspension was studied at increasing concentration of NaCMC-1 at pH=6 and ionic strength 10<sup>-5</sup>. The initial slopes of ( $\alpha/E^2$ ) dependences at field frequency 1 kHz are presented in Table I at increasing NaCMC-1 concentration. Simultaneously the relaxation time of disorientation was followed and the values are given also in Table I.

It can be seen that the relaxation time of disorientation increases with  $C_p$  increase till the isoelectric point (2 - 2.5×10<sup>-3</sup>g.dm<sup>-3</sup>) and after that  $\tau$  decreases. The variation of  $\tau$  is connected with destabilization of the suspension. At higher concentrations 5×10<sup>-3</sup> - 10<sup>-2</sup>g.dm<sup>-3</sup> the particles are recharged (negative) and the suspensions are stable. The electrophoretic mobility ( $U_0=2\times 10^{-8}\text{m}^2\text{V}^{-1}\text{s}^{-1}$ ) also decreases, reaching the isoelectric point and after that increases till  $U_e=-2\times 10^{-8}\text{m}^2\text{V}^{-1}\text{s}^{-1}$  at  $C_p=10^{-2}\text{g.dm}^{-3}$ . The same dependence is observed for the electric polarizability. It is interesting to be noted, the difference in the initial slopes when the suspensions are stable from the both sides of the isoelectric point, at 5×10<sup>-4</sup>g.dm<sup>-3</sup> and at 10<sup>-2</sup>g.dm<sup>-3</sup> NaCMC-1. Considering that the increased relaxation time from 3ms to 5ms is due to the adsorbed polyelectrolyte layer it means a 50% increase of the layer thickness at 10<sup>-2</sup>g.dm<sup>-3</sup> NaCMC-1 in comparison with 5×10<sup>-4</sup>g.dm<sup>-3</sup>. Besides this the counterions in both cases are different (cations and anions) and probably with different mobility. Another reason for the decreased initial slope could be the condensation of a part of the counterions on the adsorbed polyelectrolyte.

The dependence of the electro-optical effect  $\alpha$  on the field frequency for aerosil in presence of NaCMC is shown in Figure 6 at  $E=4.4\times 10^4\text{ V.m}^{-1}$ , pH=4.5 and ionic strength 5×10<sup>-4</sup>. There is clearly seen the increase of  $\alpha$  with NaCMC concentration increase. This shows that the polyelectrolyte is adsorbed on aerosil, regardless of the electrostatic repulsion between aerosil and NaCMC carrying the same (negative) sign of charge. The adsorption is due to specific interactions. The increased negative surface

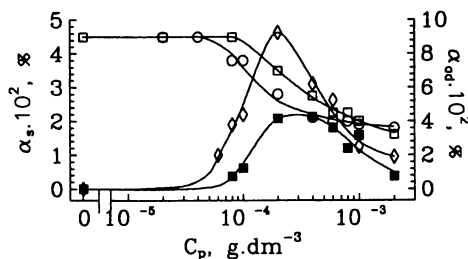


Figure 4. Dependence of  $\alpha_s$  (O,  $\square$ ) and  $\alpha_{ad}$  ( $\diamond$ ,  $\blacksquare$ ) for  $\beta$ -FeOOH on PAM concentration for MW=1.2 $\times$ 10<sup>6</sup> (O,  $\diamond$ ) and MW=3.7 $\times$ 10<sup>5</sup> ( $\square$ ,  $\blacksquare$ ).

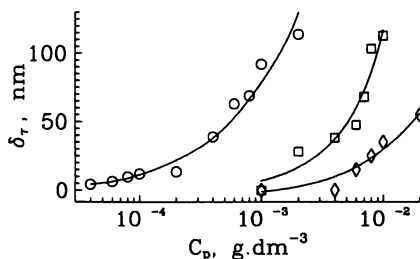


Figure 5. Dependence of adsorbed layer thickness on PAM concentration: O -  $\beta$ -FeOOH;  $\square$  - kaolinite;  $\diamond$  - mica.

TABLE I.

Initial slope of  $(\alpha/E^2)$  dependence and relaxation time  $\tau$  to  $\gamma$ -Al<sub>2</sub>O<sub>3</sub> particles at different NaCMC-1 concentration ( $C_p$ )

$C_p \times 10^4$ , g.dm <sup>-3</sup>	0	5	10	15	20-25	30	50	100
$(\partial\alpha/\partial E^2)$ , V <sup>-2</sup> m <sup>2</sup>	18.3	17.1	17.1	14	0	2.3	2.7	8.6
$\tau$ , ms	2-3	3	4	6	-	15	5	5

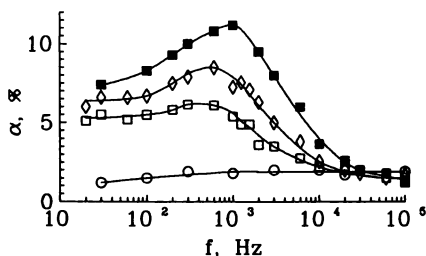


Figure 6. Dependence of  $\alpha$  on field frequency for aerosil in presence of NaCMC: ○ - without; □ - 0.03 g.dm<sup>-3</sup>; ◇ - 0.05 g.dm<sup>-3</sup> and ■ - 0.1 g.dm<sup>-3</sup> NaCMC;  $E = 4.4 \times 10^4 \text{ V.m}^{-1}$ , pH = 5.5, ionic strength  $2 \times 10^{-4}$ .

charge of the particles is also observed by the increase of the electrophoretic mobility (24).

Significant changes of the dispersion dependence in presence of polyelectrolyte are observed. The plateau region is shortened in comparison with this for aerosil (100 Hz - 10 kHz). A decrease of the relaxation frequency of the induced dipole moment is observed. This fact could be explained with by decreased mobility of the ions in diffuse double layer. A possible reason could be condensation of counterions on specific parts of the polyion (25).

The low frequency part of dispersion dependence shows a tendency of straightening. One can suppose a changes in the hydrodynamic conditions near to the interface resulting in changes of the "electro-osmotic" contribution to the orientating moment (4).

The measured relaxation times of disorientation in presence of NaCMC at pH 4.5 and 5.5 and ionic strength  $5 \times 10^{-4}$  are near to those without polyelectrolyte - in the range of 5-6ms. This is an indication that the adsorbed layer is with small thickness corresponding to a flat conformation of the macromolecules. It is known that the polyelectrolytes give a layer with smaller thickness than the neutral polymers (26). It is quite naturally to propose a flat conformation because the polyelectrolyte have a form of rods at low ionic strength.

## Conclusion

The decrease of the induced dipole moment and its relaxation time coincide with the sharp changes in the layer thickness when transition from flat to thick and dense layer occurs.

An additional electro-optical effect is observed at low field frequencies. Its maximal value is in the region of conformational transition. The electric light scattering method is useful in studying adsorbed polymer layers through their influence on particles surface electric properties and their dynamics resp.

### Acknowledgement

This work has been supported by the National Fund "Scientific Researches" at Bulgarian Ministry of Education and Science (Grant № X-44/1991).

### References

1. Vincent B, S-G Whittington in *Surface and Colloid Science*, vol 12, E Matijevic (Ed), Plenum Press, 1982.
2. Fleer G.I., Lyklema J in *Adsorption from Solution at the Solid/Liquid Interface*, Parfitt G and Rochester C.H. (Eds) Academic Press, New York, 1983, p.153.
3. Kawaguchi M., Takahashi A., *Adv.Coll.Interface Sci.*,1991,37,219-317.
4. Petkanchin I. in *Macromolecules, Colloids, Liquid Crystals and Biological Systems*, Watanabe H. (Ed) Hirokawa Publ.Co., Tokyo, 1988, 337-342.
5. van de Ven T.G.M., in *Colloid and Molecular Electro-Optics*, Jennings B.R., Stoylov S.P. (Eds) IOP Publishing Ltd., Bristol, 1991, p.71.
6. Shilov N.V., *Dokl.Acad.Nauk SSSR*, 1971, 200, 1161.
7. Stoylov S., Shilov V.N., Dukhin S.S., Sokerov S., Petkanchin I., *Electro-optica Kolloidov*, Naukova Dumka, Kiev, 1977.
8. Petkanchin I., Bruckner R., Sokerov S., Radeva Ts., *Colloid Polym. Sci.*, 1979, 257, 160.
9. Stoylov S.P., *Colloid Electro-Optics*, Academic Press, London, 1991.
10. Perrin F., *J.Phys.Radium*, 1934, 5, 497.
11. Broersma S., *J.Chem.Phys.*, 1981, 74, 6989.
12. Radeva Ts., Petkanchin I., Varoqui R., Stoylov S., *Coll. Surf.*, 1989,41,353
13. van Olphen A., *An Introduction to Clay Colloid Chemistry*, Interscience Publs, New York, 1963.

**American Chemical  
Society Library**

**1155 16th St., N.W.**

**Washington, D.C. 20036**

In Macro-Ion Characterization; Schmitz, K.;



14. Radeva Ts., Netzel J., Petkanchin I., Stoylov S., *J.Coll.Int.Sci.*, in press.
15. Israelachvili J.N., Tandon R.K., White L.R. *Nature (London)* **1979**, 277, 120; *J.Coll.Int.Sci.*, **1980**, 78, 430; Klein J. *Nature (London)* **1980**, 288, 248.
16. Zocher H., Heller W., *Zeitschrift fur Anorg.Chemie*, **1930**, 186, 75.
17. Radeva Ts., Petkanchin I., Varoqui R. in *Colloid and Molecular Electro-Optics*, Jennings B.R., Stoylov S.P. (Eds) IOP Publishing Ltd, Bristol, 1991, p.111.
18. Iler R.K. in *Surface and Colloid Science*, Matijevic E (Ed) John Willy Intersci.Publ., New York, 1973, p.1-100.
19. Buleva M., Petkanchin I., Sonntag H., Stoylov S., *Colloid Polym.Sci.*, **1979**, 257, 324-327.
20. Radeva Ts., Stoimenova M., *Colloid and Surfaces*, **1991**, 54, 235.
21. Koopal L., Hlady V., Lyklema J., *J.Coll.Int.Sci.*, **1988**, 121, 49.
22. Radeva Ts., Petkanchin I. and Varoqui R., *Langmuir*, **1993**, 9, 170.
23. Cohen Stuart MA, Cosgrove T., Vincent B., *Adv.Coll.Int.Sci.*, **1986**, 24, 143.
24. Petkanchin I., Buleva M., *Commun.Dept.Chem., Bulg.Acad.Sci.*, **1991**, 24, 570-575.
25. Wall F.T., Terayama H., Techakumpuch S., *J.Polym.Sci.*, **1956**, 20, 477.
26. Cohen Stuart M., *J.Phys.France*, **1988**, 49, 1001.

RECEIVED August 6, 1993

## Chapter 34

# Proteins at the Interfaces of Poly(styrene–acrolein) Latexes and Solvent

S. Slomkowski<sup>1</sup>, D. Kowalczyk<sup>1</sup>, T. Basinska<sup>1</sup>, and F. W. Wang<sup>2</sup>

<sup>1</sup>Center of Molecular and Macromolecular Studies, Sienkiewicza 112,  
90–363 Lodz, Poland

<sup>2</sup>Polymers Division, National Institute of Standards and Technology,  
Gaithersburg, MD 20899

The behavior of human serum albumin (HSA) and gamma globulins ( $\gamma$ G) at the interfaces of poly(styrene/acrolein) latex particles and solvent is described. It is shown how the relative amounts of proteins bound to the latex surfaces by hydrophobic adsorption and by covalent immobilization are affected by the chemical composition of the latex particles. The competition in adsorption of "monomeric", "dimeric" and "oligomeric" HSA is also described. Studies of fluorescently marked HSA and  $\gamma$ G at interfaces of latex particles and solvent indicate that, after attachment, protein molecules first lose their internal fluidity and only later change their conformation.

In medical and veterinary applications of polymeric materials, it is essential to understand what happens to various macromolecules, vital for functions of an organism, when the macromolecules approach the polymeric surface. One of these applications entails using polymeric latexes and microspheres for diagnostic purposes. Latexes with the appropriate antibodies, adsorbed and/or covalently immobilized at their surfaces, are used for detection of the corresponding antigens in standard agglutination tests (1). Recently, the new, so called "dry tests" have been designed (e.g. the tests for detection of antigens against the HIV and hepatitis viruses (2)). In these tests the only liquid being used is the liquid from the analyzed sample.

Regardless of the actual design of the test, it is crucial to establish whether the required biologically active compounds could be adsorbed or covalently immobilized at the surface of the prospective latex particles. Special attention has to be paid to the microheterogeneity of the surface of polymeric composite materials, because this often leads to the distribution of the protein attachments to the patches with different chemical composition (3). Not less important is to determine the character and degree of changes occurring in the bioactive molecules upon attachment to the surface. In the

0097–6156/94/0548–0449\$06.00/0  
© 1994 American Chemical Society

case of proteins with localized active sites, like enzymes and gamma globulins, adsorption with the active centers directed towards the surface results in blocking access to these centers and in effect in the loss of their biological activity. Similarly, in other proteins some epitopes could be blocked making them inaccessible for antibodies (3-5). There are many studies indicating that proteins change their conformations at the solid-solvent interfaces, and that these changes may persist even after protein desorption (3,4,6-15). Finally, one has to remember that some proteins may form the dimeric and oligomeric structures composed of monomeric units and that the attachment of these complex forms of proteins to the latex may be different from that of the monomers.

In this paper we describe our studies on the behavior of human serum albumin (HSA) and human gamma globulins ( $\gamma$ G) at the interfaces of poly(styrene/acrolein) latexes (PSA). HSA is the blood protein responsible, among other activities, for transport of the lipophilic compounds. Moreover, recent determination of the 3D structure of HSA (16) makes this protein especially interesting candidate for the studies of interactions of complex proteins with solid surfaces. Gamma globulins are the vital constituents of immune systems. The PSA latexes were chosen for our studies because, depending on the composition of the surface, on these particles proteins could be adsorbed and/or immobilized (by reacting with aldehyde groups from acrolein monomeric units). The poly(styrene/acrolein) latexes synthesized previously (17,18), were obtained by grafting polyacrolein onto the polystyrene core. Thus, their surface was composed of polyacrolein and for approaching proteins these particles were not different from the pure polyacrolein latexes. Our recent development of the simultaneous emulsion polymerization of styrene and precipitation polymerization of acrolein (Basinska, T.; Slomkowski, S.; Delamar, M. *J. Bioactive Biocompatible Polym.* in press) did open the way to the suspensions of electrostatically stabilized particles containing both polystyrene and polyacrolein in the surface layer. In some experiments, for comparison, we also used the poly(styrene/acrolein) latexes stabilized sterically with poly(vinylpyrrolidone).

In our investigations we wanted to find direct evidence of the attachment of proteins to the polyacrolein rich areas of the PSA particles. We wanted to clarify whether there are any preferences for adsorption and/or covalent immobilization of proteins onto these latexes. Our aim was to find out whether there is any discrimination between immobilization of complex protein macromolecules and small organic molecules in reaction with the aldehyde groups of the PSA latexes. We were interested in the competition between different quaternary structures of HSA ("monomer", "dimer", and "oligomers") during adsorption onto the polystyrene latex. Finally, we wanted to investigate the conformational changes in proteins due to their interaction with latexes.

## Experimental

Polystyrene and poly(styrene/acrolein) latexes were synthesized according to the procedure described in our earlier paper (Basinska, T.; Slomkowski, S.; Delamar, M. *J. Bioactive Biocompatible Polym.* in press). X-ray photoelectron spectroscopy (XPS) has been used for determination of the polyacrolein units in the surface layer. The details of the application of the XPS method for the poly(styrene/acrolein) latexes are

described elsewhere (Basinska, T.; Slomkowski, S.; Delamar, M. *J. Bioactive Biocompatible Polym.* in press). Human serum albumin (HSA) (Cohn fraction V), human gamma globulins ( $\gamma$ G) (Cohn fractions II and III), 1,3-bis(1-pyrene)-propane (BPP), 1-pyrene-carboxyaldehyde (PCA), and dimethylaminonaphthalene-1-sulfonylhydrazide (dansylhydrazine (DHZ)) were commercial products used without further purification. Incorporation of the BPP probe and/or PCA label into the HSA and  $\gamma$ G molecules was performed in the way described earlier (19). Proteins (HSA and/or  $\gamma$ G) were attached to the latexes by incubation of the required amount of protein in phosphate buffer saline (PBS, pH = 7.4) with the latex suspension in water. The total volume of the mixture was adjusted to 10 mL with PBS. The water to PBS ratio in the mixture never exceeded 1:9. The modified Lowry method was used for determination of the surface concentration of proteins attached to the latex particles (20,21). HPLC traces of proteins were registered using a phosphate buffer with pH = 7 as an eluent at a flow rate 0.5 mL/min.

## Results

### Basic Characteristics of the Polystyrene and Poly(styrene/acrolein) Latexes.

Values of number average diameters ( $D_n$ ) and polydispersity parameter ( $D_w/D_n$ ) for different latexes are given in Table I. Figure 1 illustrates the relation between fraction of acrolein in the whole PSA latex (for the latex stabilized electrostatically) and fraction of acrolein in the surface layer (determined by XPS).

Data collected in Table I indicate that latexes used for protein attachment were monodisperse ( $D_w/D_n$  close to 1). It is worth noting that for both kinds of latexes (stabilized electrostatically and sterically) the increased fraction of acrolein in the polymerization mixture leads to latex particles with smaller diameter. The relation between the fraction of polyacrolein monomeric units in the whole latex ( $f_{PA}(\text{whole})$ ) and in the surface layer ( $f_{PA}(\text{surface})$ ) (cf Figure 1) suggests radial inhomogeneity of the particles, with significant enrichment of the surface layer in polyacrolein.

The sulfate anions on the surface of electrostatically stabilized latexes come from the potassium persulfate used as an initiator. Latexes synthesized by precipitation polymerization and stabilized with polyvinylpyrrolidone are neutral however, this does not exclude presence of the positively and negatively charged microdomains at their surface, assuming that they balance each other.

### Immobilization of 2,4-Dinitrophenylhydrazine in the Surface Layer of PSA Latexes.

2,4-Dinitrophenylhydrazine (DNPH) is known as an analytical reagent for determination of aldehyde groups (23,24). In reaction with aldehydes DNPH forms Schiff bases with 2,4-dinitrophenyl moiety (2,4-dinitrophenylhydrazone) with characteristic absorption in UV region ( $\lambda_{\text{max}} = 360 \text{ nm}$ ) (22).

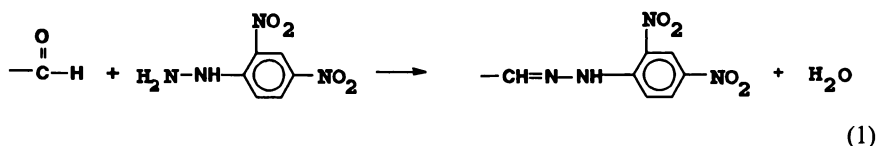


Table I. Basic data characterizing the poly(styrene/acrolein) latexes

Latex	$f_A$ (fraction of acrolein units in the polymerization mixture)	$\bar{D}_n^*$ $\mu\text{m}$	$\bar{D}_v/\bar{D}_n$	$[-\text{SO}_4^-]$ $\text{mol}/\text{m}^2$
Latexes stabilized electrostatically				
PSA1E	0	0.52	1.005	$3.39 \cdot 10^{-6}$
PSA2E	0.049	0.51	1.010	$2.52 \cdot 10^{-6}$
PSA3E	0.091	0.49	1.002	$1.38 \cdot 10^{-6}$
PSA4E	0.145	0.36	1.002	$2.57 \cdot 10^{-6}$
PSA5E	0.206	0.38	1.007	$2.14 \cdot 10^{-6}$
PSA6E	1.000	0.31	1.003	$3.24 \cdot 10^{-6}$
Latexes stabilized sterically (with poly(vinylpyrrolidone))				
PSA1S	0.085	1.58	1.001	0
PSA2S	0.157	1.51	1.001	0
PSA3S	0.200	1.36	1.002	0

\* Diameters determined from SEM microphotographs.

$$\bar{D}_n = \sum D_i n_i / \sum n_i; \quad \bar{D}_v = \sum D_i^3 n_i / \sum D_i^2 n_i$$

We wanted to check whether DNPH, known to be suitable for immobilization onto the PSA latexes which are stabilized electrostatically (21) (Basinska, T.; Slomkowski, S.; Delamar, M. *J. Bioactive Biocompatible Polym.* in press) could penetrate the polyvinylpyrrolidone layer of the sterically stabilized PSA particles and became immobilized on their surface. With this purpose we incubated in ethanol known amounts of different PSA latexes with known amounts of DNPH. The surface concentration of immobilized DNPH has been determined either from the UV measurements of depletion of DNPH from the solution or by determination of the attached DNPH in isolated DNPH labelled particles. In the latter case particles were washed thoroughly with ethanol from any unbound DNPH and dried to the constant weight. The incorporated DNPH was determined from UV spectra of particles dissolved in  $\text{CH}_2\text{Cl}_2$ . Results of these measurements are collected in Table II.

Table II. Surface concentration of DNPH immobilized onto different PSA latexes

Latex	PSA1E	PSA2E	PSA3E	PSA4E	PSA5E	PSA6E
[DNPH] $\times 10^6$ , mol/m <sup>2</sup>	0	2.20	2.28	1.76	2.51	1.96
Latex	PSA1S	PSA2S	PSA3S			
[DNPH] $\times 10^5$ , mol/m <sup>2</sup>	1.41	1.59	2.80			

From Table II it is evident that, with the exception of latex PSA1E (pure polystyrene latex), the surface concentration of DNPH immobilized onto the PSA latexes stabilized electrostatically does not change significantly with the fraction of polyacrolein (even from the pure polyacrolein PSA6E latex). It is worth noting that the surface concentration of DNPH immobilized onto the PSA latexes stabilized sterically (with polyvinylpyrrolidone) is roughly ten times higher than for latexes with electrostatic stabilization. Presumably, the outer layer composed of polyvinylpyrrolidone and polyacrolein can be easily and deeply penetrated by DNPH.

**Competitive Adsorption of "Monomeric", "Dimeric", and "Oligomeric" HSA onto the Polystyrene (PSA1E) Latex.** HSA is the mixture of "monomer" (macromolecules with  $M_w = 69\ 000$ ), "dimer" ( $M_w = 138\ 000$ ), and "oligomers" composed of more than two "monomer" macromolecules. For our studies we used HSA with fractions of "monomer", "dimer", and "oligomers" equal to 0.772, 0.161, and 0.067 respectively. The oligomeric HSA was difficult for quantitative determination, due to its low fraction. However, we noticed that the BPP probe is preferentially incorporated into "oligomeric" HSA which facilitates the UV detection of these species in HPLC analysis. It is known that in the HSA macromolecules the domain III is at pH = 7 the least charged one (+2) (24,25). This domain is known also to be responsible for binding the alkyl chain surfactants (24,25) and other aromatic ligands (16). Thus, it seems reasonable to assume that in oligomeric HSA the close arrangement of domains III from different macromolecules forms compartment enhancing the incorporation of the hydrophobic BPP probe. Values of the fractions of "monomeric", "dimeric", and "oligomeric" HSA which became adsorbed to the polystyrene (PSA1E) latex are collected in Table III. These data indicate that, at the conditions when there is not enough space on the surface of the latex particles to adsorb the whole amount of protein, "oligomers" are adsorbed preferentially, then "dimer", and eventually "monomer". Similar dependence has been observed earlier for the bovine serum albumin (26). Presumably, in aggregates of HSA the domains III are arranged into the superstructures having the higher number of the centers involved in attachment to the surface of the latex particles, what in effect, due to the cooperative character of adsorption, facilitates attachment of these species.

Table III. Competitive adsorption of different forms of HSA onto the polystyrene (PSA1E) latex ([HSA] = 49 mg/L)

[PSA1E] mg/mL	Adsorbed [HSA] %	Fraction of adsorbed		
		"monomer" %	"dimer" %	"oligomers" %
0.10	4	0	42.3	51.2
0.24	8	0	47.3	82.4
0.65	18	9.3	28.9	99.4
1.03	26	12.4	69.2	100
1.75	35	27.5	57.6	100

**Attachment of HSA and  $\gamma$ G onto the PSA Latexes.** In experiments, in which proteins were attached to latexes at the same latex concentrations, we noticed that the dependence of the surface concentration of attached protein ( $\Gamma$ ) on the protein concentration in solution is characterized by a steep initial increase of  $\Gamma$ , when all added protein molecules find enough space for attachment, and a plateau, at the conditions when apparently the whole surface of latex particles becomes saturated with protein molecules. An example, illustrating the dependence of  $\Gamma$  on the protein concentration, for attachment of HSA and  $\gamma$ G onto the PSA latex is given in Figure 2.

In spite of the apparent simplicity the dependencies of  $\Gamma$  on the protein concentration in solution usually cannot be characterized by one adsorption equilibrium constant. This is because many proteins are not symmetrical, contain domains with different properties (different hydrophobicity and hydrophilicity, positive or negative charge) and, depending on the microstructure of the surface available for adsorption and pH of the medium, could be attached via various domains (25,27). In effect the attached protein macromolecules could form the flat layer or could protrude from the surface. Any possible orientation of adsorbed protein molecules is characterized by its own equilibrium constant (4,28). The maximal surface concentration of attached protein corresponding to plateau ( $\Gamma_{\max}$ ) can be used as a convenient parameter for the quantitative comparison of the protein attachment to various latexes. The relation between  $\Gamma_{\max}$  and fraction of polyacrolein in the surface layer is given in Figure 3. For both proteins used for attachment onto the PSA latexes  $\Gamma_{\max}$  decreases with increasing  $f_{PA}(\text{surface})$ . However, for HSA apparently denaturated easier on the surface than gamma globulins this dependence is more complex.

We postulated that in the case of the poly(styrene/acrolein) latexes some of attached HSA is adsorbed and the remaining part is covalently immobilized. We found that HSA adsorbed onto the pure polystyrene latex (PSA1E) can be removed when treated with 3% sodium dodecylsulfate (SDS). Time required for the complete desorption of HSA from PSA1E at room temperature was 2 h. Thus, we assumed that from the latexes with attached HSA SDS should remove the adsorbed protein leaving

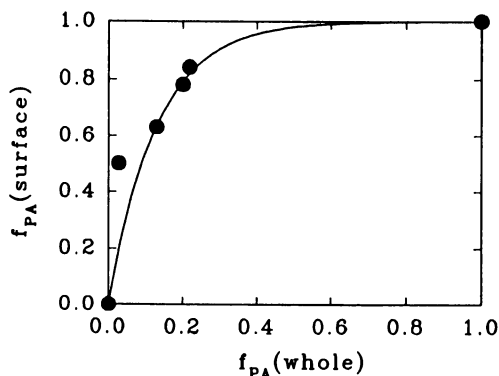


Figure 1. Dependence of the fraction of polyacrolein in the surface layer ( $f_{PA}(\text{surface})$ ) on the fraction of polyacrolein in the whole latex ( $f_{PA}(\text{whole})$ ).

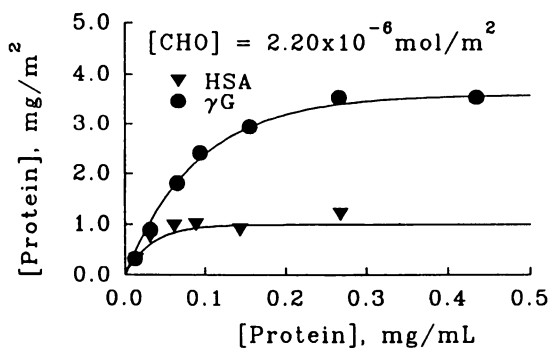


Figure 2. Dependence of the surface concentration of attached HSA and  $\gamma G$  on the concentration of these proteins in solution. Latex: PSA2E ( $[PSA2E] = 3 \cdot 10^{-3}$  g/mL).

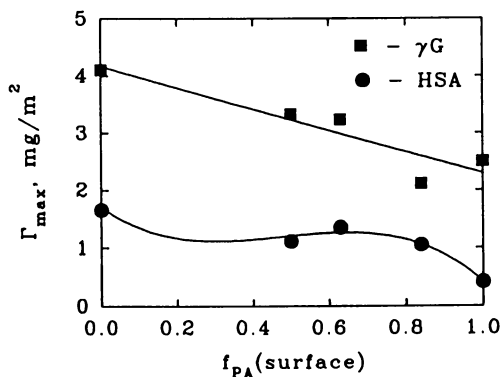


Figure 3. Dependence of  $\Gamma_{max}$  on the fraction of polyacrolein in the surface layer.



the protein immobilized covalently. In each experiment the total surface concentration of attached HSA ( $\Gamma$ ) was determined first and then HSA adsorbed by physical interactions ( $\Gamma(a)$ ) was removed with SDS and determined in the usual manner (29). The surface concentration of HSA immobilized covalently was calculated from the difference ( $\Gamma(c) = \Gamma - \Gamma(a)$ ). These experiments enabled us to determine the dependencies of  $\Gamma(a)$  and  $\Gamma(c)$  on the concentration of the appropriate protein during immobilization, and eventually to find values of  $\Gamma_{\max}$  for adsorbed and covalently immobilized HSA. Values of these parameters are collected in Table IV.

Table IV. The maximal surface concentrations of total ( $\Gamma_{\max}$ ), adsorbed ( $\Gamma_{\max}(a)$ ), and covalently immobilized ( $\Gamma_{\max}(c)$ ) HSA

Latex	$\Gamma_{\max}$ mg/m <sup>2</sup>	$\Gamma_{\max}(a)$ mg/m <sup>2</sup>	$\Gamma_{\max}(c)$ mg/m <sup>2</sup>
PSA1E	1.63	1.63	0
PSA2E	1.07	0.61	0.46
PSA3E	1.48	0.33	1.15
PSA5E	1.28	0.18	1.10

Data in Table IV indicate that, as it could be expected, the maximal surface concentrations of adsorbed HSA are lower for latexes with lower fraction of polystyrene in the surface layer. Moreover, we noticed that the surface concentration of adsorbed protein approaches a plateau at lower concentrations of HSA in solution (in experiments with [Latex] = 3 mg/mL for [HSA] < 0.1 mg/mL) than in the case of the covalent immobilization.

All attempts to immobilize HSA and  $\gamma$ G onto the PSA latexes stabilized with polyvinylpyrrolidone (PSA1S, PSA2S, and PSA3S) were unsuccessful. If any protein has been attached to these latexes, its surface concentration was lower than 10<sup>-2</sup> mg/m<sup>2</sup>.

**Attachment of HSA and/or  $\gamma$ G onto the PSA Latex Labelled with Dansylhydrazine (DHZ).** Dansyl groups introduced onto the surface of latex particles could be used as reporter molecules. The emission spectra of dansyl fluorophores provide information on the local environment of this label. Like DNPH also the DHZ molecules could be immobilized only in areas in which polyacrolein is present (reaction with aldehyde groups of polyacrolein). Thus, changes in the emission of dansyl groups, after incubation of the labelled latex with HSA and/or  $\gamma$ G, will indicate directly that protein molecules became attached to these areas.

The PSA4E latex was labelled with DHZ in ethanol in the similar manner as it was described for DNPH. The emission spectrum of immobilized dansyl groups was registered after transferring the PSA4E(DHZ) latex to the PBS buffer. For excitation

at  $\lambda = 345$  nm the immobilized dansyl groups emitted light with maximum at  $\lambda = 485.5$  nm (the emission of dansylhydrazine in ethanol was at  $\lambda = 509.9$  nm). The PSA4E(DHZ) latex was incubated with proteins and the emission spectra of the latex - protein systems were registered again. The emission spectra of PSA4E(DHZ) measured before and after incubation with HSA and/or  $\gamma$ G are shown in Figure 4.

Spectra in Figure 4 indicate that the intensity of the emission of dansyl label located on the surface of latex particles is strongly enhanced (80%) when protein is added to the latex suspension. This effect we attribute to the adsorption of HSA and/or  $\gamma$ G onto the polyacrolein patches of the PSA latex. In effect, dansyl fluorophores labelling the polyacrolein patches became screened by proteins from quenchers.

Dansyl, a label with the life time ca 10 ns, is recommended for the studies of the local fluidity of surrounding medium by polarization of the emission (30). When rotation of dansyl fluorophore becomes restricted by the matrix the excitation with the polarized light leads to polarized emission. Polarization of PSA4E(DHZ)-HSA registered in the region from 350 nm to 600 nm is given in Figure 5. Absence of any measurable polarization indicates that in spite of the attachment of HSA the dansyl group can easily rotate within the life time of this label in the excited state.

#### **Kinetics of the HSA and $\gamma$ G Transformation due to the Protein-Latex Interaction.**

BPP and PCA are convenient markers suitable for probing the fluidity and polarity of their nearest environment (31-36). When introduced into the protein macromolecules they enable monitoring of the conformational rearrangements of proteins. In matrix with very low fluidity the emission spectrum of BPP is characterized by signal of the pyrene fluorophore at 378 nm with a typical fine structure. In media with low fluidity the emission spectrum of BPP contains the signal of pyrene-pyrene excimer (structureless with  $\lambda_{\max} = 480$  nm). The emission of PCA in nonpolar hydrocarbons has a characteristic signal with maximum at 378 nm. In solvents with higher polarity this signal is shifted to the longer wavelengths and becomes broader. Finally, in water the emission signal of PCA is very broad with maximum at 489 nm (33). Thus, any conformational changes of protein containing BPP probe and/or PCA label, which lead to changes of local fluidity in the vicinity of BPP or in the exposure of PCA to the hydrophilic environment, would be reflected by the corresponding emission spectra.

The detailed studies of conformational alteration of HSA and  $\gamma$ G containing BPP probe or PCA label are described elsewhere (Kowalczyk, D.; Slomkowski, S.; Wang, F.W. *J. Bioactive Biocompatible Polym.* in press). Here we would like only to summarize the main results of these investigations.

We found that incubation of proteins labelled with BPP (HSA(BPP) and  $\gamma$ G(BPP)) with PSA1E and PSA3E is accompanied with reduction of the intensity of emission of excimer, indicating the loss of internal fluidity in the protein molecules. Incubation of HSA(PCA) and  $\gamma$ G(PCA) with the same latexes indicated the conformational changes of proteins resulting in screening the PCA label from the hydrophilic environment. It has been established also that these conformational changes in protein molecules persist even after the exchange between the adsorbed (and conformationally altered) protein molecules and protein molecules in solution, with the native conformation. Even in experiments when only the small (e.g. 5%) fraction of protein is at a given moment attached to the latex surface, the whole protein becomes eventually conformationally changed.

The emission spectra of proteins (marked with BPP and/or PCA) in the initial and altered conformation were used for evaluation of the fractions of protein in the initial and in the conformationally changed states at any intermediate stage of their transformation.

Process of the conformational changes of HSA and  $\gamma$ G due to their contact with PSA latexes could be illustrated by the Scheme 1. In this scheme  $P_i$  and  $P_i(A)$  denote the protein molecules in the initial conformational state, in solution and attached onto the polymer surface respectively,  $P_T$  and  $P_T(A)$  denote the corresponding protein molecules in the denatured conformation. Because the emission spectra of HSA and  $\gamma$ G, denatured on the latex particles do not return to their original pattern (at least within ten hours after separation of protein from the latex) we assume that transfer from the state  $P_T$  to  $P_i$  in solution, after desorption, is slow and could be neglected in Scheme 1. This observation does not exclude the possibility that the chains of denatured proteins refold upon desorption. It proves only that BPP probes and/or PCA labels are in different environment in protein macromolecules before and after protein contact with the surface of the latex. Possibly, denaturation on the latex surface opens the way for BPP and PCA to the otherwise inaccessible subdomains of protein macromolecules.

In experiments in which proteins were incubated with small amounts of latexes, providing space only for attachment of the small fraction of proteins present in solution, the kinetics of the overall conformational changes could be analyzed assuming the steady state for the concentrations of attached protein ( $P_i(A)$  and  $P_T(A)$ ). At these conditions the following equation describes the kinetics of the conformational changes (Kowalczyk, D.; Slomkowski, S.; Wang, F.W. *J. Bioactive Biocompatible Polym.* in press):

$$d([P_i + P_i(A)])/dt = -k_{eff} \cdot [P_i] \quad (2)$$

where

$$k_{eff} = \frac{k_A \cdot k_T \cdot S \cdot P_T}{k_D + k_T \cdot P_T} \quad (3)$$

In equation (3)  $S$  denotes the surface of the latex not occupied and available for attachment and  $P_T$  the probability that in the vicinity of attached molecule there is enough space allowing the conformational rearrangement. For  $[P_i(A)] \ll [P_i]$  equation (2) has a very simple solution  $\ln([P_i]_0/[P_i]) = k_{eff} \cdot t$ .

An example of the dependence of  $k_{eff}$  on the latex concentration (and thus on the total surface of the latex) is given in Figure 6.

The initial increase of  $k_{eff}$  is attributed to the larger surface on which the conformational changes may occur. Maximum can be attributed to different orientation of protein molecules at the surface. It has been found that in IgG macromolecules, constituting the main fraction of  $\gamma$ G, the most hydrophobic are the Fc fragments ( $CH_3$  and  $CH_2$  domains) and thus, these protein macromolecules are attached to the hydrophobic surface via the  $CH_3$  domain (37,38). The  $F(ab^1)_2$  parts including the VH, VL,  $CH_1$ , and CL subdomains are hydrophilic. Below and above the isoelectric point the  $F(ab^1)_2$  portions of IgG are positively or negatively charged. However, at pH close

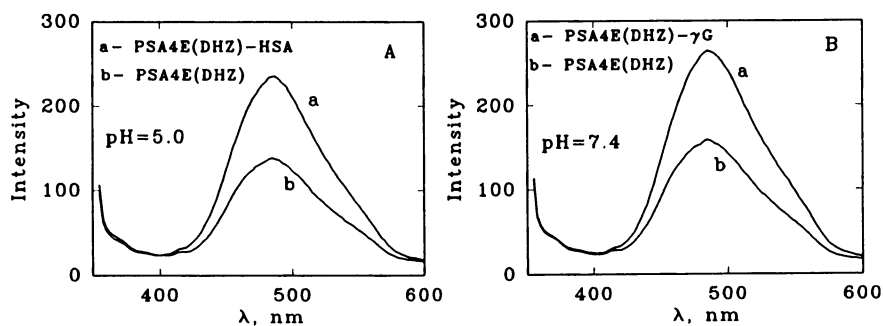


Figure 4. Emission spectra of PSA4E(DHZ), A - PSA4E(DHZ)-HSA, and B - PSA4E(DHZ)- $\gamma$ G systems. Excitation at 345 nm. Conditions: [PSA4E(DHZ)] =  $7 \cdot 10^{-4}$  g/mL, [HSA] =  $50 \mu\text{g/mL}$ , [ $\gamma$ G] =  $50 \mu\text{g/mL}$ .

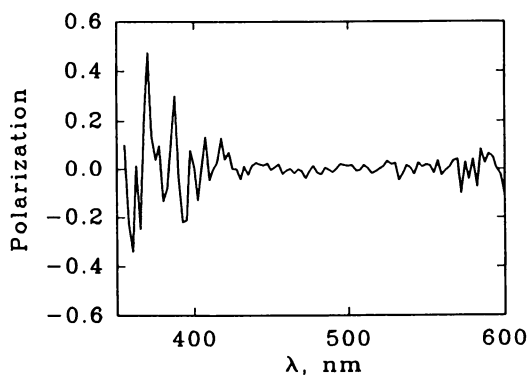
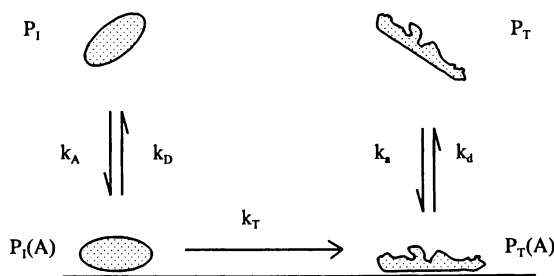


Figure 5. Polarization for PSA4E(DHZ)-HSA. Conditions: [PSA4E(DHZ)] =  $3 \cdot 10^{-3}$  mg/L, [HSA] =  $50 \mu\text{g/mL}$ , pH = 5.0.



Scheme 1

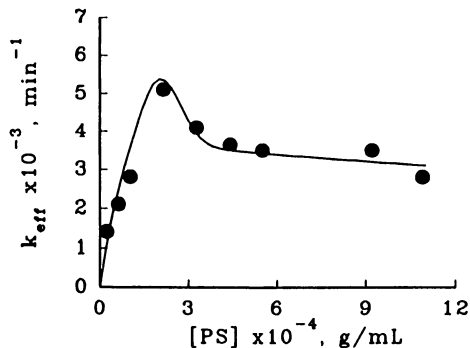


Figure 6. Dependence of  $k_{\text{eff}}$  on the concentration of PSA3E latex for  $\gamma\text{G(BPP)}$ . Conditions of kinetic experiments:  $[\gamma\text{G(BPP)}]_0 = 75 \text{ mg/L}$ , PBS (pH = 7.4).

to 7 (for rabbit IgG at pH = 7.8), it is at the conditions at which we studied the protein - polymer interactions, the IgG macromolecules are in the collapsed conformation (arms of the  $\text{F(ab)}_2$  fragment are held together (37) and being neutral are to the lesser extent solvated with the water molecules. When there is only small surface available for attachment (low latex concentration) the IgG molecules are attached via the  $\text{CH}_3$  domains and thus, are protruding from the surface. In this way the higher number of them could be attached. However, due to the small area of the contact between each protein molecule and the polymer surface the attachment is weak and allows the fast exchange. In systems with higher concentration of the latex the protein molecules could be probably attached in a manner involving also other subdomains (side-on) with better contact with the surface, more efficient attachment, and thus slower exchange. For experiments with high concentration of the latex  $k_{\text{eff}}$  became independent of the latex concentration. Presumably, at these conditions all protein molecules became attached to the latex in the initial period and the steady-state approximation is no longer valid.

It is known that whereas the adsorbed protein molecules could be rather easily exchanged with protein molecules in solution, apparently becoming desorbed, the desorption in absence of any proteins or surface active agents in solution is strongly reduced (4,6). Thus, in experiments with the high latex concentrations the whole process could be reduced to one reaction enabling determination of  $k_{\text{T}}$ .



and described by simply equations (Kowalczyk, D.; Slomkowski, S.; Wang, F.W. *J. Bioactive Biocompatible Polym.* in press)

$$d[P_i(A)]/dt = -k_T \cdot [P_i(A)] \quad (5)$$

$$\ln([P_i(A)]_0/[P_i(A)]) = k_T \cdot t. \quad (6)$$

Values of  $k_T$  measured for conformational changes of HSA(BPP), HSA(PCA),  $\gamma$ G(BPP), and  $\gamma$ G(PCA) attached to PSA1E and PSA3E latexes are collected in Table V.

Table V. Values of the rate constant of conformational changes of HSA and  $\gamma$ G attached to the surface of PSA latexes ( $k_T$  in  $\text{min}^{-1}$ )

	HSA(BPP)	HSA(PCA)	$\gamma$ G(BPP)	$\gamma$ G(PCA)
PSA1E	$2.06 \cdot 10^{-3}$	$1.19 \cdot 10^{-3}$	$3.10 \cdot 10^{-3}$	$1.22 \cdot 10^{-3}$
PSA3E	$4.04 \cdot 10^{-3}$	$1.35 \cdot 10^{-3}$	$6.40 \cdot 10^{-3}$	$2.40 \cdot 10^{-3}$

It is worth noting that values of  $k_T$  are higher for proteins with BPP probe than for these marked with the PCA label. Moreover, values of  $k_T$  are higher for proteins attached onto the latex with aldehyde groups (PSA3E) than for these adsorbed onto the pure polystyrene (PSA1E) latex.

## Discussion

Studies of the chemical composition of the PSA latexes indicate that surface layer of these particles is considerably enriched in polyacrolein. Presumably, it is due to the higher hydrophilicity of polyacrolein (in comparison with polystyrene) resulting in their preferential exposure to the protonic media (like water or ethanol) used for the synthesis of latexes. Similar observations have been reported in the literature for the synthesis of latexes from styrene and hydroxyethylacrylate giving particles with the surface layer strongly enriched in hydrophilic polyhydroxyacrylate (39). We did show that the swollen outer layer of PSA latexes stabilized with polyvinylpyrrolidone can be easily penetrated by small molecules of DNPH finding their way to the aldehyde groups. In effect, the concentration of DNPH immobilized in the surface layer of particles stabilized with polyvinylpyrrolidone is even higher than for the pure polyacrolein (PSA5E) latex stabilized electrostatically with apparently much less permeable surface layer. It has been established that adsorption of proteins to the surface of polymers covered with hydrophilic poly(ethylene oxide) is strongly hindered (4,40-42). We found that the hydrophilic polyvinylpyrrolidone layer prevents also the covalent immobilization of proteins, even if the aldehyde groups, easily accessible by small DNPH molecules, are incorporated into it.

Studies of attachment of HSA and  $\gamma$ G onto the PSA latexes and studies of the conformational changes of these proteins in the presence of latex particles conform to the following picture. At the very beginning, when there is the large unoccupied surface

available for the incoming protein, there are several subpopulations of proteins attached via different domains. Some of these conformations require more space on the surface than the other. When the whole surface becomes covered the new protein molecules could approach the polymeric surface only when those already attached become reoriented in such a way that they are protruding from the surface, making space for newcomers. The driving force for this reorientation comes from the minimalization of free energy of the whole protein latex system taking into account the difference of free energy between the states at which the small number of protein macromolecules is bound by interactions involving more than one domain, with remaining protein macromolecules free in the solution, and the states at which the larger number of protein macromolecules becomes attached via weaker (presumably involving one domain) interactions. Reorientation of protein molecules on the interface during adsorption has been observed earlier (8,11,28). Reorientation, accompanying attachment of new protein molecules, occurs easily for the polystyrene particles onto which proteins are only adsorbed. In the case of latex particles with polyacrolein in the surface layer some of the protein macromolecules become covalently immobilized in the side-on orientation and thus they cannot make space for more protein molecules. Thus, it is easy to understand why the higher content of polyacrolein in the surface layer results in lower concentration of attached proteins.

We found that areas of the latex surface onto which HSA is only adsorbed are saturated at lower concentration of protein in solution than in the case of areas suitable for the covalent immobilization. Presumably, adsorption is controlled by diffusion of HSA to the surface whereas many encounters of HSA molecules with the hydrophilic polyacrolein patches should occur before eventually the reaction of aldehyde groups from the latex and amine groups of HSA becomes successfully completed. It is worth noting that the rotation of dansyl labels introduced into the polyacrolein patches (evidenced by lack of the polarization of dansyl emission) is not hindered by attachment of HSA. Apparently, protein molecules immobilized covalently to the hydrophilic polyacrolein leave enough space for free rotation of dansyl fluorophore.

Different values of  $k_T$  for the same protein - latex system resulting from the studies involving BPP probe and PCA label are not surprising. Emission from BPP provides information on the internal fluidity of the protein molecule whereas emission from PCA indicates changes of the exposure of the label to water, resulting from the conformational changes of proteins. Moreover, it seems reasonably to assume that the hydrophobic BPP probe is incorporated, under the thermodynamic control of partition between different domains, into the hydrophobic domain III in HSA and/or domain  $CH_3$  in IgG whereas the PCA label is incorporated into different domains, under the kinetic control determined by the reaction of aldehyde groups of PCA with  $-NH_2$  groups in protein macromolecules. For both latexes and for both investigated proteins values of  $k_T$  obtained from experiments with BPP are higher than in the case of PCA label. Apparently, in the first step of the attachment to the surface, protein molecules first lose their internal fluidity and only in the second step they change their conformation. It is also worth noting that the covalent immobilization leads to faster conformational changes than the hydrophobic adsorption.

The work was supported by the M.Sklodowska-Curie Fund, Grant PAN/NIST-90-42.

## Literature Cited

1. Polysciences. Inc., Data Sheet No. 238, 1984 with over 70 references to original papers on application of latexes in medical diagnostics.
2. Tarcha, P.J.; Misun, D.; Finley, D.; Wong, M.; J.J. Donovan, J.J. In *Polymer Latexes; Preparation, Characterization, and Applications*; Daniels, E.S.; Sudol, E.D.; El-Aasser, M., Eds; ACS Symp.Ser. 1992, 492, 347.
3. Sakurai, Y.; Akaile, T.; Kataoka, K.; Okano, T. In *Biomedical Polymers - Polymeric Materials and Pharmaceuticals for Biomedical Use*; Goldberg, E.P.; Nakajima, A., Eds; Academic Press, New York, 1980, p. 335.
4. Andrade, J.D.; Hlady, V. *Adv.Polym.Sci.* **1986**, 79, 1.
5. Pye, E.K.; Chance, B. In *Methods in Enzymology - Immobilized Enzymes*; Mosbach, K., Ed.; Academic Press, 1976, vol. 44, p. 357.
6. Lundström, I.; Ivarsson, B.; Jönsson, U.; Elvig, H. In *Polymer Surfaces and Interfaces*; Feast, W.J.; Munro, H.S., Eds; Wiley, New York, 1987, p. 201.
7. Gabel, D.; Steinberg, I.Z.; Katchalsky, E. *Biochemistry* **1971**, 10, 4661.
8. Soderquist, M.E.; Walton, A.G. *J.Colloid Interface Sci.* **1980**, 75, 386.
9. Bagchi, P.; Birnbaum, S.M. *J.Colloid Interface Sci.* **1981**, 83, 460.
10. Chan, B.M.C.; Brash, J.L. *J.Colloid Interface Sci.* **1981**, 84, 263.
11. VanDulm, P.; Norde, W. *J.Colloid Interface Sci.* **1983**, 91, 248.
12. Bohnert, J.L.; Horbett, T.A. *J.Colloid Interface Sci.* **1986**, 111, 363.
13. Jennissen, H.P. *J.Colloid Interface Sci.* **1986**, 111, 570.
14. Norde, W.; MacRitchie, F.; Nowicka, G.; Lyklèma, J. *J.Colloid Interface Sci.* **1986**, 112, 447.
15. Sandwick, R.K.; Schray, K.J. *J.Colloid Interface Sci.* **1987**, 115, 130.
16. He, X.M.; Carter, D.C. *Nature*, **1992**, 358, 209.
17. Colvin, M.; Smolka, A.; Rembaum, A.; Chang, M. In *Microspheres: Medical and Biological Applications*; Rembaum, A.; Z.A.Tökès, Z.A., Eds.; CRC, Boca Raton, Fl., 1988; p.1.
18. Gritskova, I.A.; Gusev, S.A.; Grzywa, E., Teleshov, E.N.; Shuman-skii, E.N.; Grzywa-Niksinska, I. *Polimery*, **1991**, 36, 229.
19. Kowalczyk, D.; Slomkowski, S.; Wang, F.M. *ACS Polym.Prep.* **1992**, 33(1), 846.
20. Basińska, T.; Slomkowski, S. *J.Biomater.Sci., Polymer Edn.* **1991**, 3, 115.
21. Slomkowski, S.; Basinska T. In *Polymer Latexes; Preparation, Characterization, and Applications*; Daniels, E.S.; Sudol, E.D.; El-Aasser, M.S.; ACS Symp.Ser. **1992**, 492, 328.
22. Lohman, F.H. *Anal. Chem.* **1950**, 30, 972.
23. Cheronis, N.D.; T.S.Ma, T.S. *Organic Functional Group Analysis by Micro and Semimicro Methods*; Interscience, New York, 1964; p. 145.
24. Peters, T., Jr. *Adv.Protein.Chem.* **1985**, 37, 161.
25. Andrade, J.D.; Hlady, V.; Wei, A.-P.; Gölander, C.-G. *Croat.Chim.Acta*, **1990**, 63, 527.
26. J.Zsom, R.L. *J.Colloid Interface Sci.* **1986**, 111, 434.



27. Andrade, J.D.; Hlady, V.; Wei, A.-P.; Ho, C.-H.; Lea, A.S.; Jeon, A.S.; Lin, Y.S.; Stroup, E. *Clinical Mat.* **1992**, *11*, 67.
28. Waldman-Meyer, H.; Knippel, E. *J. Colloid Interface Sci.* **1992**, *148*, 508.
29. Lowry, O.H.; Rosenbrough, N.J.; Farr, A.L.; Randall, R.J. *J. Biochem.* **1952**, *193*, 26.
30. Lakowicz, J.R. *Principles of Fluorescence Spectroscopy*; Plenum Press, New York, 1983; p. 16
31. Turro, N.; Arora, K.A. *Polymer*, **1986**, *27*, 783.
32. Winnik, M.A. In *Photophysical and Photochemical Tools in Polymer Science*; Winnik, M.A., Ed.; Reidel Publishing Co., Dordrecht, 1985; p. 293.
33. Lianos, P.; Cremel, G. *Photochem. Photobiol.* **1980**, *31*, 429.
34. Kalayasundaram, K.; Thomas, J.K. *J. Phys. Chem.* **1977**, *81*, 2176.
35. Almgren, M.; Grieser, F.; Thomas, J.K. *J. Am. Chem. Soc.* **1980**, *102*, 3188.
36. Turro, N.J.; Kuo, P.-L. *Langmuir*, **1985**, *1*, 179.
37. Bagchi, P.; Birnbaum, S.M. *J. Colloid Interface Sci.* **1981**, *83*, 460.
38. Schwartz, L.M. *Compendium of Immunology*; Van Nostrand Reinhold Co., New York, 1980, vol. 1, chapter III.
39. Okubo, M.; Yamamoto, Y.; Kamei, S. *Colloid Polym. Sci.* **1989**, *267*, 861.
40. Gregonis, D.E.; Buerger, D.E.; Van Wagenen, R.A.; Hunter, S.K.; Andrade, J.D. *Biomaterials* **84**, *Trans. Soc. Biomaterials*, **1984**, *7*, 766.
41. Jeon, S.I.; Lee, J.H.; Andrade, J.D.; DeGennes, P.G. *J. Colloid Interface Sci.* **1991**, *142*, 149.
42. Jeon, S.I.; Andrade, J.D. *J. Colloid Interface Sci.* **1991**, *142*, 159.

RECEIVED August 6, 1993

## Chapter 35

# Dynamics of DNA Molecules under Gel Electrophoresis

T. Kotaka, S. Adachi, K. Igarashi, and T. Shikata

Department of Macromolecular Science, Faculty of Science, Osaka University, Toyonaka, Osaka 560, Japan

Under biased sinusoidal field gel electrophoresis (BSFGE) that utilized sinusoidal field of strength  $E_s$  and frequency  $f$  superposed on steady bias field of  $E_b$ , large DNA fragments with size  $M > 20$  kbp exhibit peculiar behavior, especially when  $E_s > E_b$ . A most intriguing case was what we called *pin-down* phenomenon in which mobility of a particular DNA became minimum at a particular frequency (pin-down frequency) specific to  $M$ , gel concentration and field conditions. To examine the dynamics of DNA molecules under BSF conditions, we conducted frequency-domain electric birefringence measurements and were able to locate a few orientational relaxation modes related to the peculiar electrophoretic behavior. Direct observation *via* fluorescence microscopy also revealed the features of DNA molecules moving through gel network.

Gel electrophoresis is currently the most important technique available to molecular geneticists for size dependent separation of chromosomal DNA fragments. The technique also provides an intriguing problem for polymer physicists in relation with molecular dynamics of uniformly charged macromolecules moving through obstacles. In fact, steady field electrophoresis in agarose gel is a powerful tool for separating short DNA fragments according to their size  $M$  but ineffective for large fragments with  $M > 20$  kilobasepairs (kbp) (1). For large DNAs the steady-field mobilities  $\mu_s$  are independent of  $M$ . Thus for the separation of large fragments, various pulsed-field (PFGE) methods (2-5) were developed as motivated with an idea that alteration of the direction and/or the timing of the pulse field may activate some specific modes of motion that are dependent on  $M$  of DNA molecules moving through the gel. We also developed a new version which we called *biased sinusoidal field gel electrophoresis* (BSFGE) (6-8) that utilized sinusoidal field of strength  $E_s$  and frequency  $f$  superposed on steady bias field of  $E_b$ . The field was then defined as:

$$E(t) = E_b + E_s \sin(2\pi ft) \quad (1)$$

and we defined the effective mobility  $\mu$  in BSFGE as:

$$\mu = (\text{distance migrated } X/\text{cm}) / [(\text{time elapsed } t/\text{h})(E_b/V\text{cm}^{-1})] \quad (2)$$

0097-6156/94/0548-0466\$06.00/0  
© 1994 American Chemical Society

In such studies we were able to find some interesting features of BSFGE. A most striking case was that under a low bias condition of  $E_s > E_b$  (for example,  $E_s = 7.5$  V/cm;  $E_b = 2.5$  V/cm; and gel concentration  $C_{\text{gel}}$  of 1 wt%) the mobility  $\mu$  of DNA with  $M > 20$  kbp exhibits a minimum at a particular frequency dependent on  $M$  and  $C_{\text{gel}}$  as well as on  $E_b$ . This means that DNA fragments with  $M$  either smaller or larger than this particular one move faster under these particular conditions. We called this phenomenon, *pin-down* phenomenon; the frequency, pin-down frequency  $f_p$ ; and the minimum mobility, pin-down mobility  $\mu_p$ . We then attempted to examine dynamical features of DNA molecules by conducting frequency-domain electric birefringence (FEB). We also attempted to make direct observation of moving DNA molecules under gel electrophoresis via fluorescence microscopy.

## Gel Electrophoresis

**Experimental.** Experiments were conducted on commercially available DNA samples with  $M$  from 200 basepairs (bp) to 1.9 megabasepairs (Mbp) purchased from Pharmacia, LKB (Uppsala, Sweden) and Nippon Gene Co. Ltd. (Tokyo, Japan). In particular we examined bacteriophage  $\lambda$  DNA of 48.5 kbp and T4 dC DNA of 166 kbp. Agarose was a DNA/RNA separation grade (Pharmacia, LKB). The buffer was a standard 50 mM TBE which consisted of 50 mM [tris(hydroxymethyl)-amino]methane (tris base), 50 mM boric acid, and 1 mM ethylenediaminetetraacetic acid (EDTA) disodium salt. Usually 0.5 mg/L ethidium bromide (EB) was added to the buffer to visualize DNA bands with a UV illuminator.

A submerge type cell was used mainly at 20°C. To generate BSF we employed a high speed, high voltage bipolar power amplifier and a conventional function generator. The details were described elsewhere (7) and will not be repeated here.

**Behavior in Steady Field Gel Electrophoresis.** In steady field gel electrophoresis,  $M$  dependence of steady field mobility  $\mu_s$  is known to be divided into three regimes (5,7,8): The first one is Ogston regime I for small size DNAs that do not entangle with gel strands and moves rather freely so that  $M$  dependence of  $\mu_s$  is small; the second one is entangled-but-unstretched regime II for intermediate size DNAs for which  $\mu_s \propto M^{-1}$  and efficient size-dependent separation is possible; and the third case is entangled-and-stretched regime III for large DNAs with  $M > 20$  kbp for which  $M$  dependence of  $\mu_s$  is again lost.

Figure 1 illustrates an example of  $\log \mu_s$  vs  $\log M$  under a steady field of strength  $E = 2.5$  V/cm in 1.0 wt% agarose gel at four different temperatures ranging from 13 to 37°C. The results show the three regimes exist as mentioned above. In these three regimes,  $\mu_s$  increases almost uniformly with increasing temperature, and the features of their  $M$  dependences are essentially unchanged. In fact, apparent activation energy  $E^*$  estimated from the Arrhenius plot of  $\log \mu_s$  vs  $1/T$  is of the same order of 10 to 6 kJ/mol for DNA with  $M$  of 1.35 to 166 kbp. Incidentally,  $E^*$  of water viscosity is also of the order of 8 kJ/mol. This result suggests that the friction from the medium determines the temperature dependence of  $\mu_s$ . Figure 1 also includes pin-down mobility  $\mu_p$  data of 166 kbp T4 dC phage DNA (solid symbols), on which we will discuss later.

**Behavior under BSF Conditions.** In BSFGE we examined frequency  $f$  dependence of  $\mu$  defined by equation 2 under varying  $E_b$ , sinusoidal field strength  $E_s$  and  $f$ , and found several interesting features in  $\mu$  vs  $\log f$  relations (7,8).

**High to Comparable Bias Conditions.** In BSFGE of a high bias with  $E_s < E_b$  (for example,  $E_s = 2.5$  V/cm and  $E_b = 7.5$  V/cm),  $\mu$  of DNAs of any size were independent of  $f$  and coincided with the steady field values  $\mu_s$  (7). On the other

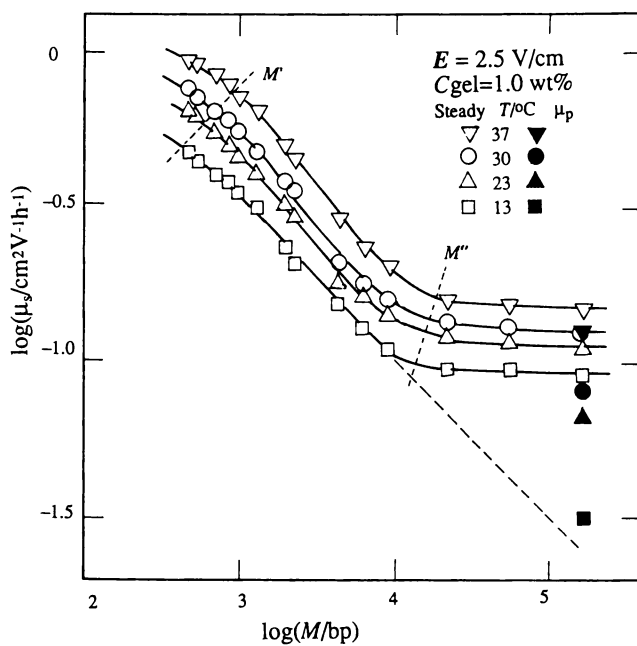


Figure 1. Plot of  $\log \mu_s$  vs  $\log M$  at different temperatures as indicated. Solid symbols represent  $\mu_p$  data.

hand, in BSFGE of a comparable bias with  $E_s \equiv E_b$  (for example,  $E_s = 7.5$  V/cm,  $E_b = 7.5 \sim 5.0$  V/cm), each  $\mu$  vs  $\log f$  curve exhibited a peak  $\mu_M$  at a frequency  $f_M$  (around 10 Hz in 1.0 wt% gel) independent of  $M$  but strongly dependent on  $C_{\text{gel}}$ , while  $\mu$  in the low- and high- $f$  sides coincided with  $\mu_s$  (7,8). As  $C_{\text{gel}}$  was increased from 0.5 to 2.0 wt%,  $f_M$  rapidly shifted to the high  $f$  side and the peak flattened out (7). The peak height  $\Delta\mu_M (= \mu_M - \mu_s)$  was nearly constant for large DNAs in the regimes II and III, but increased with decreasing  $M$  for small DNAs in Ogston regime I (7).

**Low Bias Conditions.** In BSFGE of a low bias field with  $E_s > E_b$ , three interesting features emerge. Figure 2 illustrates an example in which  $E_s = 7.5$  V/cm,  $E_b = 2.5$  V/cm and  $C_{\text{gel}} = 1.0$  wt%. We see that (i) the low  $f$  values  $\mu_0$  ( $\equiv \mu$  at  $f \rightarrow 0$ ) are significantly enhanced, but (ii) the high  $f$  values  $\mu_\infty$  ( $\equiv \mu$  at  $f \rightarrow \infty$ ) remain essentially the same as  $\mu_s$ . The most striking finding is (iii) pin-down phenomenon in which  $\mu$  vs  $\log f$  curve of large DNAs with  $M > 20$  kbp exhibits a minimum  $\mu_p$  at  $f_p$  dependent on  $M$ ,  $C_{\text{gel}}$  as well as on the field strengths in such a way that  $f_p \propto M^{-1} C_{\text{gel}}^{-1} E_b E_s^\alpha$  with  $\alpha = 0$  for  $E_s <$  a certain critical value ( $\equiv 10$  V/cm at  $E_b = 2.5$  V/cm) and  $\alpha = 2 \sim 3$  for  $E_s >$  the critical value (8).

On the other hand, the pin-down mobility  $\mu_p$  at a fixed  $E_b$  first decreases with increasing  $E_s$  and levels off at high  $E_s$ . When these  $\mu_p$  data were plotted in  $\log \mu_p$  vs  $\log M$  plots, we see that the leveled-off values of  $\mu_p$  are found on the extrapolated portion of the steady-field regime II curve. This result implies that the particular DNA at the pin-down condition assumes an entangled-but-unstretched conformation as a result of the field reversal at a proper timing  $f_p^{-1}$ , otherwise the DNA belonging to the regime III category assumes a stretched conformation (8).

Figure 3 shows  $\mu$  vs  $\log f$  curves in  $E_s = 7.5$  V/cm,  $E_b = 2.5$  V/cm and  $C_{\text{gel}} = 1.0$  wt% at four different temperatures from 13 to 37°C. We see that with increasing temperature  $f_p$  shifts to the high  $f$  side and  $\mu_p$  becomes larger. These  $\mu_p$  data are plotted in Figure 1 with the solid symbols. We see that only 13°C data point appears close to the extrapolated portion of the regime II curve (dotted line), and with increasing temperature  $\mu_p$  becomes closer to the regime III value of  $\mu_s$ . This result means that the temperature dependence of  $\mu_p$  is larger than that of  $\mu_s$ . In fact,  $E^*$  for  $\mu_p$  is of the order of 15 kJ/mol that is about twice as large as those of  $\mu_s$ .

### Frequency-Domain Electric Birefringence.

To examine the features of moving DNA molecules under BSF conditions, we conducted frequency-domain electric birefringence (FEB) measurements with a home-made FEB apparatus. The apparatus consisted of a semiconductor laser with 670 nm wavelength, a polarizer, a 3 mm or 1 mm optical path-length quartz Kerr cell of 50 mm length and 5 mm width, a quarter-wave ( $\lambda/4$ ) plate, an analyzer and a photodiode connected to a fast Fourier transform (FFT) analyzer (Hitachi, VC2420).

In each run the Kerr cell was filled with agarose gel of a desired concentration, and both ends of the cell were filled with the TBE buffer and connected with salt bridges to electrode baths. A DNA solution was applied on the top of the Kerr cell, and a small steady field was applied to bring the DNA band to the center of the cell illuminated with laser beam. Then the steady field was shut off ( $E_b = 0$ ), and a sinusoidal field of desired  $E_s$  and  $f$  was applied with the same bipolar power amplifier used in BSFGE experiments.

Birefringence  $\Delta n$  induced by a sufficiently weak sinusoidal field of strength  $E_s$  and frequency  $f$  ( $\omega = 2\pi f$ ) consists of a direct current (dc) component  $\Delta n_{\text{dc}}$  and an alternating current (ac) component  $\Delta n_{\text{ac}}$  of  $2\omega$  with a phase lag of  $\delta$  (9,10). The dynamic Kerr coefficient  $K$  is then given as

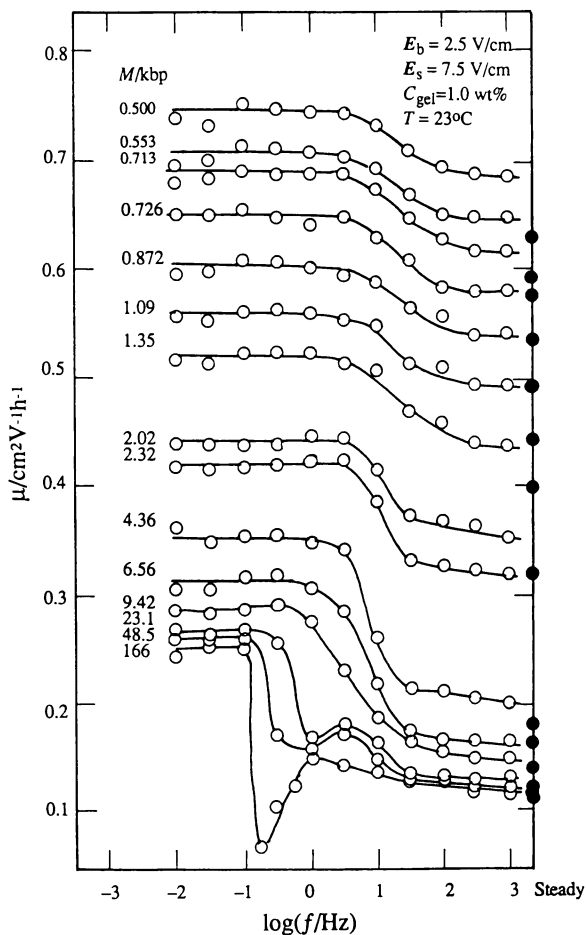


Figure 2. Plot of  $\mu$  vs  $\log f$  under a low-bias BSF condition for DNAs of different  $M$  as indicated. Solid symbols represent  $\mu_s$  data.

$$K = 2\Delta n / |E_s|^2 = K_{dc} + K' \sin(2\omega t) + K'' \cos(2\omega t) \quad (3)$$

with  $K_{dc} = \Delta n_{dc} / |E_s|^2$ ;  $K' = 2\Delta n_{ac} \sin\delta / |E_s|^2$ , and  $K'' = 2\Delta n_{ac} \cos\delta / |E_s|^2$

The birefringence is proportional to the orientation function of DNA molecules and the dynamic Kerr coefficients represent the orientation function related to rotational diffusion of the DNA molecules in agarose gel.

We measured  $\Delta n$  as a function of  $2f$  and determined  $K'$  and  $K''$  by equation 3 for 21 kbp fragment, 48.5 kbp  $\lambda$  DNA and 166 kbp T4 dC DNA. We plotted  $\log(-K'')$  vs  $\log(2f)$  for the three samples. In the plots we found a small mode always appearing at the same highest frequency  $f_e$  independent of  $M$  of all the samples. Thus we shifted the curves for 21 kbp and 48.5 kbp DNAs vertically so that the small modes (marked as  $f_e$ ) appearing around  $f \approx 10$  Hz were superposed onto the  $f_e$  mode of 166 kbp DNA. The results are shown in Figure 4.

In Figure 4, we see three relaxation modes for 21 and 48.5 kbp DNAs, but only two modes for 166 kbp DNA. The first mode at the highest frequency  $f_e$  is independent of  $M$  as mentioned above but dependent on  $C_{gel}$  in such a way that  $f_e \propto C_{gel}^{-1.3}$ . This result means that this first mode is presumably related to vibrational motion of DNA segments between entanglement points of DNA molecules with gel strands or the motion of DNA molecules induced by the motion of gel strands. Thus we may call this mode *gel* mode. (However the signals cannot be from gel strands alone, because the signals from the gel strands themselves are very weak as compared to those from DNA molecules.) The second mode appearing at a frequency  $f_p'$  close to  $f_p$  of each DNA shifts to the low  $f$  side with increasing  $C_{gel}$  as well as with  $M$  in such a way that  $f_p' \propto C_{gel}^{-1} M^{-1}$ , which is the same as that of  $f_p$ . This second mode seems to be related to the pin-down phenomenon, and we call this mode *pin-down* mode. The third mode appearing at the lowest frequency  $f_R$  also rapidly shifts to the low  $f$  side with increasing  $C_{gel}$  and  $M$  in such a way that  $f_R \propto C_{gel}^{-1.4} M^{-3}$ . Thus we could not locate the  $f_R$  mode for 166 kbp T4dC DNA in 1.0 wt% gel.

Figure 5 shows double logarithmic plots of the characteristic times  $\tau$  ( $\approx 1/2\pi f$ : defined as the reciprocal angular frequency of each mode) vs  $M$  relation determined from FEB experiments. Figure 5 also shows the relaxation time data (solid symbols) obtained by Strum and Weil (11) via time-domain electric birefringence (TEB) in 0.7 wt% agarose gel. First we notice that  $\tau_e$  of the gel mode is independent of  $M$ . For this gel mode,  $f_e$  was close to  $f_M$  at which we saw an enhancement in  $\mu$  in BSFGE under comparable bias conditions (7). The enhancement appears for all DNAs even those belonging to the Ogston I regime that cannot entangle with the gel strands. Thus the gel mode is presumably related to the motion of the gel strands. For the pin-down mode,  $\tau_p'$  is proportional to  $C_{gel}M$  that is equivalent to the behavior of  $f_p$  ( $\propto C_{gel}^{-1} M^{-1}$ ). When a sinusoidal field of  $f_p$  is applied, the stretching of DNA molecules (of a particular size) along the field can be effectively suppressed due to the field alteration at the proper timing of  $f_p^{-1}$ . Thus at this pin-down mode the particular DNA molecules may assume rather tightly coiled-conformation so that their  $\mu$  sharply reduces to exhibit pin-down phenomenon at this particular  $f_p$ . On the other hand,  $\tau_R$  corresponding to the  $f_R$  mode exhibits  $M^3$  dependence that was predicted by de Gennes for diffusion of long chain molecules through fixed obstacles and called reptation (12). Thus this mode may be called *reptation* mode.

### Fluorescence Microscopy of Moving DNA Molecules

To observe dynamical structure of moving DNA molecules in gel electrophoresis, we utilized fluorescence microscopy proposed by Yanagida *et al.* (13), developed by Schwartz and Koval (14) and by Yoshikawa *et al.* (15). In fact, experiments were

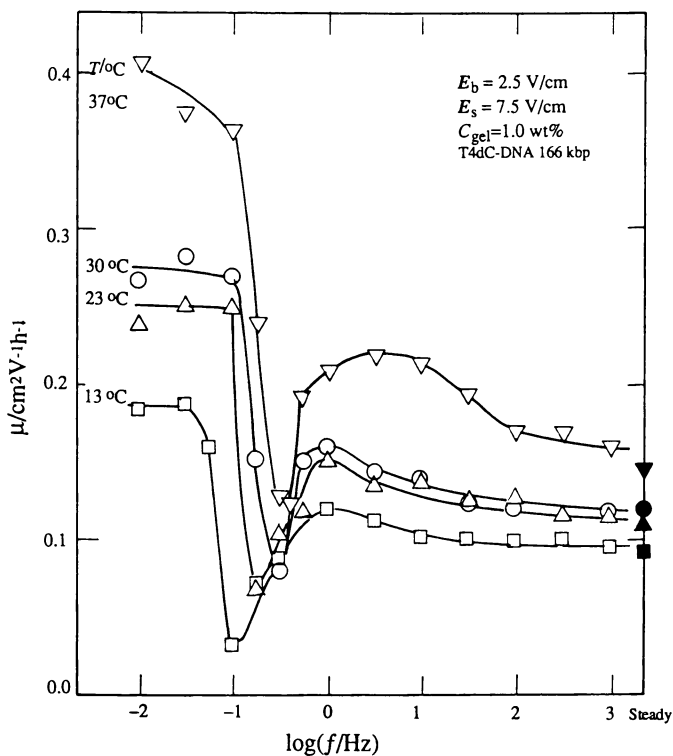


Figure 3. Plot of  $\mu$  vs  $\log f$  for 166 kbp T4dC DNA at different temperatures as indicated.

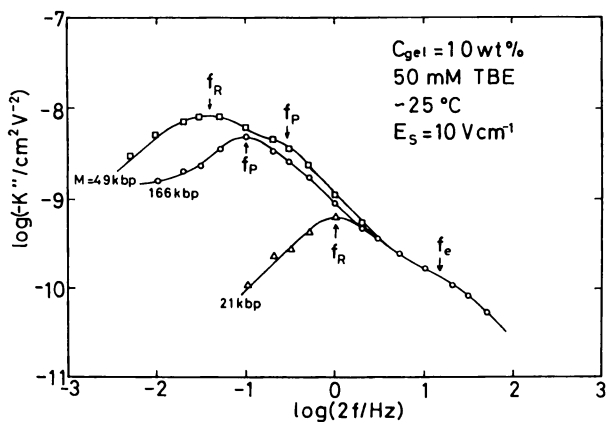
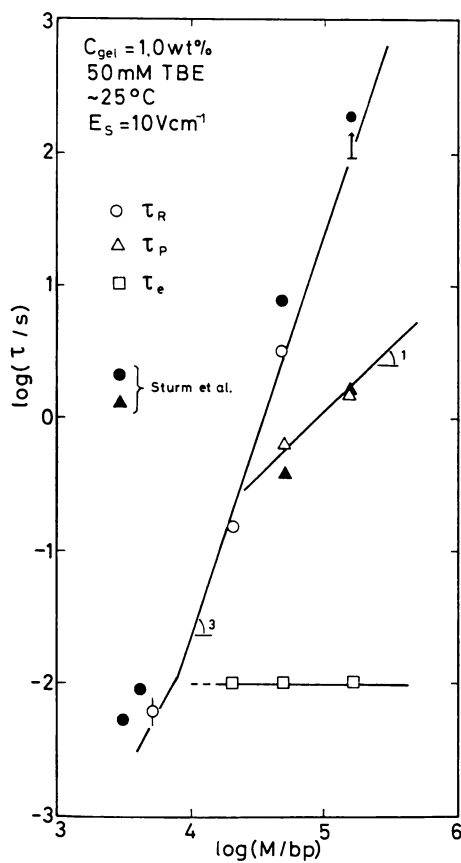


Figure 4. Plot of  $\log(-K'')$  vs  $\log(2f)$  in FEB experiments.



Figure 5. Plot of  $\log(\text{FEB relaxation times})$  vs  $\log M$ .

conducted in Prof. Yoshikawa's laboratory at Nagoya University according to their routine (8,15,16). Observation was made primarily on T4 dC-DNA in 0.5 wt% agarose gel containing 50 mM TBE buffer, 4 % (v/v) 2-mercapto-ethanol and a fluorescent dye, ethidium bromide (EB). Nikon TMD microscope was used with a high sensitivity SIT TV camera (Hamamatsu Photonics, Hamamatsu, Japan). EB complexed T4 dC-DNA (DNA:EB) were illuminated with 520 nm light and emitted fluorescence of 580 to 620 nm were observed. The images were recorded on a video tape from which hard copies were made.

Figure 6 shows traces of video images of T4dC-DNA:EB moving under (a) a steady field of  $E = 10.5$  V/cm, a BSF field of  $E_s = 7.5$  V/cm and  $E_b = 2.5$  V/cm at (b) the pin-down frequency  $f_p (\cong 0.215$  Hz) and at (c) low  $f (= 0.0316$  Hz  $< f_p$ ) together with the field conditions. The figures are self-explanatory: Under a steady field, a DNA molecule initially in coiled-up conformation forms an U-shaped hook structure with elongated arms around an (invisible) obstacle. The arms are pulled by the field but the molecule stays at the same position for some time until the balance between the arms is broken. Once the balance is broken and the molecule becomes J-shaped conformation, then the longer arm pulls the shorter one quickly to pass around the obstacle and the molecule resumes the initial coiled-up conformation, as seen in Figure 5(a) (16). The process is highly nonuniform: Under a given steady field a short chain (but long enough to entangle with gel strands) rapidly repeats stretching-and-contracting motions but migrates a shorter distance per step, whereas a large fragment does it slowly but jumps a larger distance in one step. In effect, they migrate on an average with the same rate. Under a BSF pin-down condition the particular DNA molecule with initially coiled-up conformation begins to being stretched out, but coils up again as the field is reversed at the timing of  $f_p^{-1}$  resonant to the characteristic time  $\tau_p'$  of the molecule. Thus, as seen in Figure 5 (b) the DNA molecule almost always assumes a coiled conformation. Under such a situation only the bias field contributes to its forward migration and the coiled molecule moves very slowly. This explains why  $\mu$  is comparable to the value of  $\mu_s$  extrapolated from the regime II curve, where the DNA molecule is believed to be assuming entangled-but-unstretched, coiled conformation. However, at low  $f (< f_p)$  a DNA molecule spends a sufficient time under a strong effective field for repeating measuring worm-like (stretching-and-contracting) motion before the field is reversed. Thus it exhibits an enhanced mobility. This observation nicely fits to the picture deduced from the results of steady field and BSFGE experiments as well as from FEB experiments described above.

### Concluding Remarks

Under steady field GE, large DNA molecules migrate virtually at the same rate independent of  $M (> 20$  kbp) and cannot be properly separated. By superposing a sinusoidal field of adequate frequency and strength onto the steady field, we can activate certain internal modes of motion of the DNA molecules. Especially in a DNA fragment of a particular size  $M$  at the pin-down condition the stretching-and-contracting mode of the DNA molecule is resonant to the timing of the field alteration. Thus the DNA molecule assumes an unstretched, coiled conformation and migrates slower than those either of the larger or smaller sizes. Near BSF pin-down conditions  $\mu$  becomes sensitive to  $M$  and size dependent separation of large DNA fragments becomes possible. The pin-down frequency  $f_p$  varies as  $f_p \propto M^{-1} C_{gel}^{-1} E_b E_s^0$  as long as  $E_s$  is not too large (7,8). This feature allows us to design BSF conditions appropriate for separating giant DNA fragments.

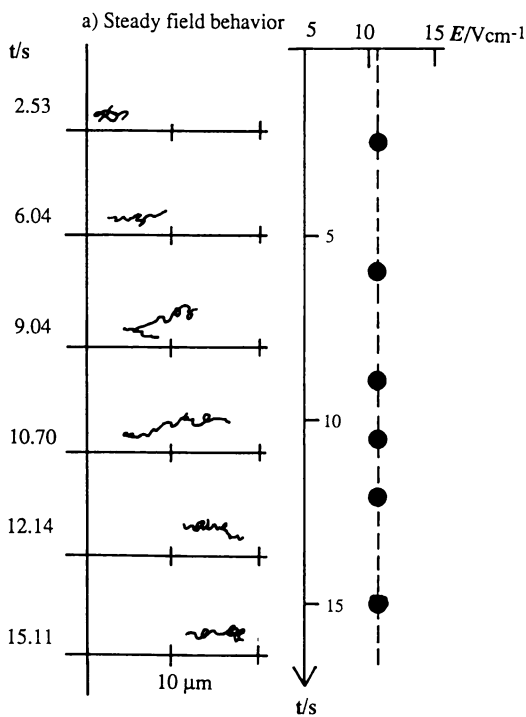
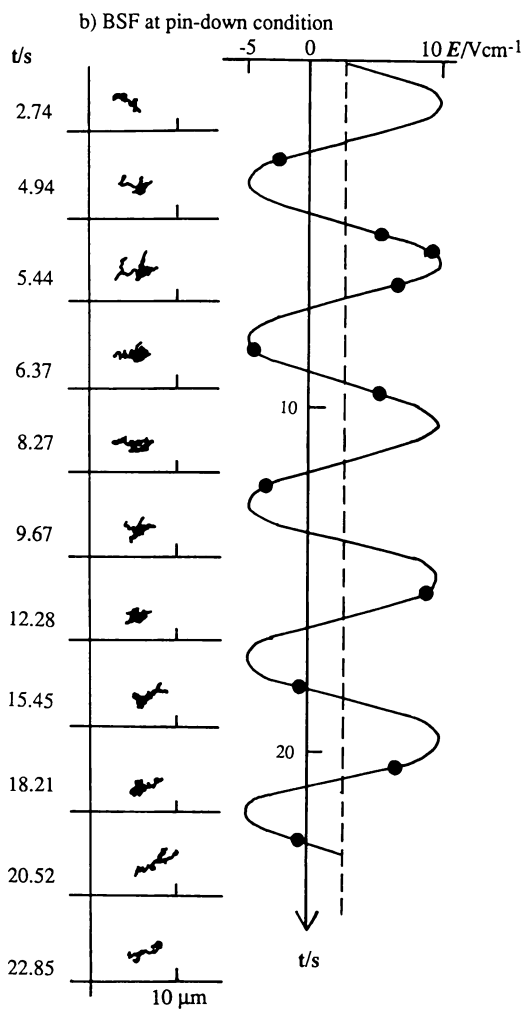
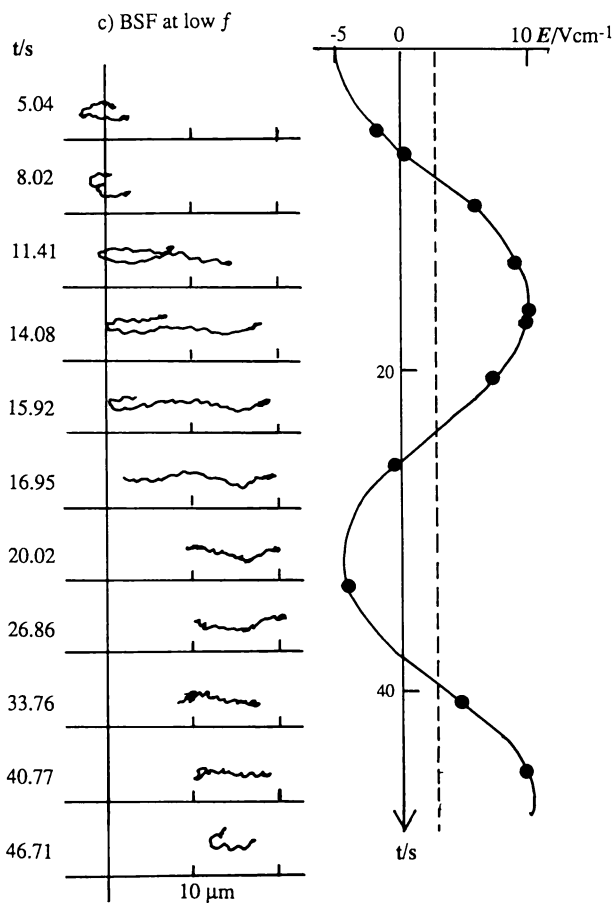


Figure 6. Traces of T4dC DNA : EB moving under (a) a steady field of  $E = 10$  V/cm; a BSF field of  $E_s = 7.5$  V/cm and  $E_b = 2.5$  V/cm at (b) the pin-down frequency  $f_p (\cong 0.215$  Hz) and at (c) low  $f (= 0.0316$  Hz  $< f_p$ ).  
*Continued on next page*

Figure 6. *Continued.*

Figure 6. *Continued.*

**Acknowledgement.** We thank the Ministry of Education, Science and Culture (Mombusho), Japan for financial support through a Grant 01470107.

### Literature Cited.

- (1) McDonnell, M.W.; Simon, M.N.; Studier, F. W. *J. Mol. Biol.* **1977**, *110*, pp. 114-146.
- (2) Schwartz, D.C.; Cantor, C.R. *Cell* **1984**, pp 77-84.
- (3) Carle, G.F.; Frank, M.; Olson, M. V. *Science* **1986**, *232*, pp 65-68.
- (4) Lalande, M.; Noolandi, J.; Turnmell, C.; Rousseau, J., Slater, G.W. *Proc. Natl Acad. Sci. USA* **1987**, *84*, pp 8011-8015.
- (5) Slater, G.W.; Rousseau, J.; Noolandi, J.; Turnmel, G.; Lalande, M. *Biopolymers* **1988**, *27*, pp 509-524.
- (6) Shikata, T.; Kotaka, T. *Biopolymers* **1991**, *31*, pp 253-254.
- (7) Shikata, T.; Kotaka, T. *Macromolecules* **1991**, *24*, pp 4868-4873.
- (8) Kotaka, T.; Adachi, S.; Shikata, T. *Electrophoresis* **1993**, *14*, pp 313-321.
- (9) Parus, S.J.; Shick, R.A.; Matsumura, M.; Morris, M.D. *Analytical Chemistry* **1988**, *60*, pp 1932-1635.
- (10) Ookubo, N.; Hirai, Y.; Ito, K.; Hayakawa, R. *Macromolecules* **1989**, *22*, pp 1359-1366.
- (11) Strum, J.; Weil, G. *Phys. Rev. Lett.* **1989**, *62*, pp 1484-1486.
- (12) De Gennes, P.-G. *J. Chem. Phys.* **1971**, *55*, pp 572-579.
- (13) Yanagida, M.; Hiraoka, Y.; Katsura, I. *Cold Spring Harbor Symp. Quant. Biol.* **1983**, *47*, pp 117-187.
- (14) Schwartz, D.C.; Koval, M. *Nature* **1989**, *338*, pp 520-522.
- (15) Matsuzawa, Y.; Ninagawa, K.; Yoshikawa, K.; Doi, M. *Nucleic Acids Res. Symp.* **1990**, *ser. 22*, pp 77-78.
- (16) Kotaka, T.; Adachi, S.; Matsuzawa, Y.; Yoshikawa, K. *Rep. Progr. Polym. Phys., Jpn* **1992**, *35*, pp 687-688.

RECEIVED September 7, 1993

## Chapter 36

# Effect of Gel Structure on Matrix Orientation in Pulsed Electric Fields

Nancy C. Stellwagen and John Stellwagen

Department of Biochemistry, University of Iowa, Iowa City, IA 52242

The orientation of four polymeric gels, LE agarose, HEEO agarose,  $\beta$ -carrageenan (a stereoisomer of agarose), and polyacrylamide, has been studied in pulsed electric fields, using the technique of transient electric birefringence. Orientation is observed for all four polymeric gels when pulses of a few V/cm are applied to the gels for a few seconds. The birefringence decay curves typically contain two or three components of alternating sign. The relaxation times correspond to the orientation of fibers and/or fiber clusters ranging up to  $\sim 10 \mu\text{m}$  in size. The three polysaccharide gels exhibit orientation anomalies in rapidly reversing electric fields, which appear to be due to electric field-induced structural rearrangements. Cross-linked polyacrylamide gels exhibit normal orientation behavior in reversing electric fields.

Agarose gels are widely used as a non-convective medium for DNA gel electrophoresis (1). In order to avoid orientation and reptation effects, pulsed alternating electric fields must be used to separate DNA molecules larger than  $\sim 20$  kilobase pairs (reviews: 2-4). Molecular weight separation occurs under these conditions because the DNA molecules are forced to change their direction of migration every time the electric field changes direction; the time required for reorientation is dependent on DNA molecular weight. Various theories (2-5) have been proposed to describe the center-of-mass velocity and the dynamics of large DNA molecules during pulsed field gel electrophoresis (PFGE). Although the theories are based on quite different physical models of gel electrophoresis (2), they all assume that the agarose matrix is fixed in space and time while the DNA molecules move. However, this assumption is not correct; the agarose matrix itself is extensively oriented when pulsed electric fields of the amplitude and duration used for PFGE are applied to the gels (6-8). Therefore, it is necessary to understand the orientation of the agarose gel matrix in pulsed electric fields in order to have a complete understanding of the mechanism of PFGE.

The orientation of the agarose gel matrix is conveniently characterized by the technique of transient electric birefringence (TEB). This technique, which is based on refractive index differences rather than on the presence of specific chromophores in the gels, allows one to estimate the size of the orienting particles and their extent of orientation in the electric field (9). Unfortunately, agarose gels exhibit highly anomalous electric birefringence signals in low voltage electric fields (6-8). In particular, the sign of the birefringence reverses when the electric field is reversed in

0097-6156/94/0548-0479\$06.00/0  
© 1994 American Chemical Society

polarity, in contrast to the behavior expected from the Kerr law. In order to understand the basis of this effect, the electric birefringence of agarose gels has been studied in low voltage and high voltage electric fields. The electric birefringence of several other gel-forming polymers has also been studied, to assess the effect of matrix structure on gel orientation.

### Polymer Gels

Four different gel-forming polymers have been studied: two types of agarose with different charge densities, LE agarose and HEE0 agarose,  $\beta$ -carrageenan, a stereoisomer of agarose, and polyacrylamide, a chemically crosslinked gel.

Agarose is an alternating copolymer of 1,3-linked  $\beta$ -D-galactose and 1,4-linked 3,6-anhydro- $\alpha$ -L-galactose (10). The backbone chain is substituted at irregular intervals with charged groups such as sulfate, carboxylate and pyruvate. LE (low electroendosmosis) agarose has a relatively low charge density; HEE0 agarose is more highly charged. Agarose molecules aggregate in the sol phase to form large fiber bundles (11-13), which condense to form a three dimensional matrix upon gelation (14).

$\beta$ -carrageenan, a stereoisomer of agarose, is an alternating copolymer of 1,3-linked  $\beta$ -D-galactose and 1,4-linked 3,6-anhydro- $\alpha$ -D-galactose. The backbone chains of the two polysaccharides differ because  $\beta$ -carrageenan has only D residues while agarose contains alternating D and L residues.  $\beta$ -carrageenan has a higher sulfate content than agarose, with correspondingly lower melting and gelation temperatures (15).

All polysaccharide gels were prepared by boiling the desired quantity of gel powder in distilled, deionized water in a microwave oven, as described elsewhere (16). LE agarose gels ranging from 0.3-2.0% in concentration were characterized; the results were virtually independent of gel concentration. HEE0 agarose and  $\beta$ -carrageenan gels were studied only at a concentration of 1.0%.

Unlike polysaccharide gels, polyacrylamide gels are chemically crosslinked. The gels studied here contained 6.9% total acrylamide (%T, acrylamide plus crosslinker) and 3% (w/w) N,N'-methylenebisacrylamide (Bis) crosslinker (%C). The polyacrylamide gels were cast in distilled, deionized water, using ammonium persulfate and TEMED (N,N,N',N'-tetramethylethylenediamine) as initiator and catalyst, respectively, as described (16).

### Experimental Methods

The theory of transient electric birefringence is described in detail elsewhere (9). Briefly, if a macromolecule (or a domain in a gel matrix) is asymmetric and polarizable, it can be oriented by an electric field. As a result, the refractive index of the sample becomes different in directions parallel and perpendicular to the direction of the electric field. In limiting low electric fields, the difference in refractive index, called the birefringence,  $\Delta n$ , is proportional to the square of the electric field strength, E, according to the Kerr law, equation 1:

$$\Delta n = n_{//} - n_{\perp} = K_{sp} n C_V E^2 \quad (1)$$

where  $K_{sp}$  is the specific Kerr constant, n is the refractive index of the sample, and  $C_V$  is the partial specific volume of the sample. The specific Kerr constant, which varies depending on the macromolecule orienting in the electric field, is the product of two terms, an optical anisotropy factor and an electrical orientation factor (17). Either term can be positive or negative, depending on the structure of the macromolecule and the amplitude and direction of its induced and/or permanent dipole moments.



After removal of the electric field, the birefringence signal decays to zero because of the randomizing effects of Brownian motion (9). The rate of decay of the birefringence in a polydisperse system is given by equation 2:

$$\Delta n/\Delta n_0 = \sum_i C_i \exp(-t/\tau_i) \quad (2)$$

where  $\Delta n$  is the birefringence at any time,  $t$ , after removal of the electric field,  $\Delta n_0$  is the birefringence at the moment the field is removed,  $\tau_i$  is the relaxation time of the  $i$ th particle and  $C_i$  is its relative contribution to the total birefringence signal. The birefringence relaxation times can be related to particle dimensions using standard equations (18), if some assumptions can be made about particle shape and if the axial ratio or diameter of the macromolecule is known (9).

The rise of the birefringence signal is more complicated than the decay, because the rise curves depend on the electric field strength and the electrical orientation factors of the macromolecules as well as the relaxation times (9). For agarose gels, the rise curves also depend on the pulse length, which determines the number and size of the components orienting in the electric field (16,19). Because of space limitations, the rise curves will not be discussed here. Only the amplitude of the birefringence in unidirectional electric fields, the decay curves, and the envelope of the birefringence signal obtained in rapidly reversing electric fields will be described.

The apparatus and methods used for the birefringence measurements have been described in detail previously (20). The Kerr cell was a shortened 1.00 cm quartz spectrophotometer cell, chosen for its negligible strain birefringence. The electrodes were parallel platinum plates separated by 2.0 or 4.0 mm, mounted on lexan supports of standard design (21). The cell was thermostated at 20°C; heating effects due to the applied pulses were negligible. Unidirectional and bipolar rectangular pulses ranging from 0.5-100 volts in amplitude and 10 msec to 300 seconds in duration were generated by a home-built Dual Pulser and Stimulator Controller. Successive pulses and pulse trains were separated by at least 10-30 minutes, to allow the birefringence signal to decay to zero between pulses. All birefringence signals were recorded without signal averaging; typical oscilloscope traces have been chosen to illustrate the results.

### LE Agarose Gels

**High Voltage Electric Fields.** Agarose gels oriented by short, high voltage electric fields (pulses of a few kV/cm applied to the gel for durations ranging up to 1 msec) exhibit positive birefringence signals with fast rise and decay times, as shown in Figure 1a. The terminal relaxation times varied between 10-220  $\mu$ sec, depending on pulse length and gel concentration (7). Terminal relaxation times of 220  $\mu$ sec correspond to the orientation of rod-like particles  $\sim$ 270 nm in length if the axial ratio,  $p$ , is assumed to be 100 (19). Particles of this size would correspond to small agarose aggregates or dangling ends of fibers orienting in the electric field.

When the electric field was rapidly reversed in polarity, the birefringence signal decreased transiently and then increased again to its steady state value, as shown in Figure 1b. Such reversing field behavior is typical of macromolecules orienting by a combined permanent dipole/induced dipole orienting mechanism (22). However, the birefringence saturation curve was best fit by the theoretical equation for pure permanent dipole orientation (17), as shown in Figure 2a, suggesting that the orientation of agarose gel fibers is primarily due to permanent dipole polarization. A similar discordance between the reversing field results and the saturation behavior has been observed in dilute agarose solutions (13).

**Low Voltage Electric Fields.** In low voltage electric fields, the sign of the birefringence of LE agarose gels varied randomly from one gel to another, for reasons that are not clear. The sign of the birefringence also varied at different locations within

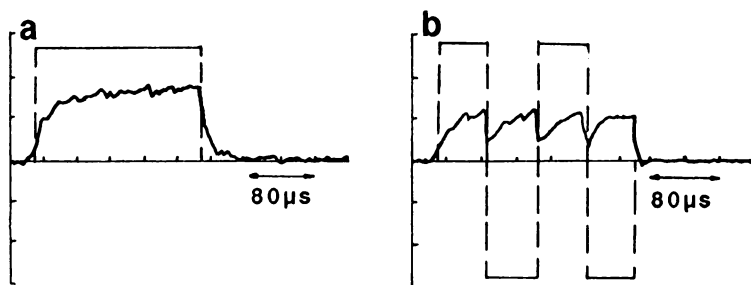


Figure 1. Oscilloscope traces of typical birefringence signals observed for 1.0% LE agarose gels in the high voltage regime, using  $E = 2.8$  kV/cm. (a), pulse length ( $t_p$ ) = 200  $\mu$ s; (b), two consecutive 60  $\mu$ s/60 $\mu$ s reversing pulses. In this and subsequent figures, the relatively noisy trace is the observed birefringence signal; the pulse is indicated by the trace with vertical dashed lines. The vertical scale is arbitrary but approximately constant for all traces in a given figure; the horizontal scale is indicated. The direction of positive birefringence is always up.

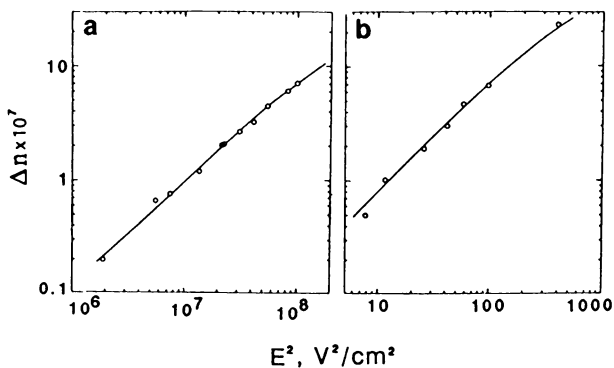


Figure 2. Log-log plot of the absolute value of the birefringence,  $\Delta n$ , as a function of  $E^2$ , compared with theoretical curves for permanent dipole orientation. The solid lines correspond to theoretical curves; the points represent the experimental data. (a), 1.0% LE agarose gel, high voltage regime,  $\mu_{app} = 2.5 \times 10^3$  D ( $8.4 \times 10^{-27}$  C m); (b), 0.6% agarose gel, low voltage regime,  $\mu_{app} = 1.54 \times 10^6$  D ( $5.1 \times 10^{-24}$  C m).

each gel, suggesting that the agarose matrix consists of multiple discrete, independently orienting domains.

**Relaxation Times.** The decay of the birefringence of LE agarose gels contained two or three components of alternating sign, depending on the pulse length and electric field strength (16). A typical birefringence signal is illustrated in Fig. 3a for a 1.0% LE agarose gel oriented by a 5 second pulse at  $E = 7.6$  V/cm. The decay of the birefringence was fitted as a sum of exponentials using a nonlinear least-squares fitting program (23), as shown in Fig. 3b. Birefringence decay curves containing three relaxation times (not shown) were measured at several different oscilloscope sweep speeds, to visualize the initial and final portions of the decay accurately. The relaxation times obtained from the analysis of several birefringence decay curves, measured under the same pulsing conditions at different oscilloscope sweep speeds, were then averaged to give the reported relaxation times. The relaxation times measured for a single gel under the same pulsing conditions usually agreed with  $\pm 5$ -6%; the standard deviations of the relaxation times measured for differently independently prepared gels of the same composition was  $\pm 10$ -30%, depending on the particular relaxation time. All relaxation times were independent of the pulsing history of the gel.

Typical relaxation times are given in Table I for 1.0% LE agarose gels oriented by an electric field of 7.6 V/cm. The coefficients of the various relaxation times alternated in sign, for reasons that are not clear. The particles giving rise to each relaxation time may have had optical factors of the opposite sign, because of anomalous diffraction (24,25). Alternatively, or in addition, each larger aggregate may have oriented in the opposite direction from that of its constituent particles, as commonly observed for aggregates of large polyelectrolytes (25-27). Further studies will be needed to distinguish between these possibilities.

**Table I. Average Birefringence Relaxation Times of Gel-Forming Polymers<sup>a)</sup>**

Polymers	$\tau_1$ , s	$\tau_2$ , s	$\tau_3$ , s
1% LE agarose	2	15	68
1% HEE0 agarose	6	29	62
1% $\beta$ -carrageenan	5	75	130
6.9% polyacrylamide	8	20	-

a)  $E = 7.6$  V/cm

The sizes of the LE agarose particles orienting in the electric field were estimated from their relaxation times by assuming the particles to be rod-like with an axial ratio ( $p$ ) of 10 or 100, bracketing the axial ratios observed for agarose molecules in solution (28), or by assuming the particles to be spherical ( $p=1$ ), as suggested by quasielastic light scattering experiments (29). The particle lengths are compiled in Table II. The results suggest that, regardless of the axial ratio, very large particles are orienting in the electric field. Comparisons of the relaxation times (19) with other data in the literature suggest that the particles with relaxation times of  $\tau_1$  and  $\tau_2$  may correspond to agarose fibers or fiber bundles, while the larger particles with the relaxation time of  $\tau_3$  probably correspond to clusters of fiber bundles (14) or microgel domains (30).

Table II. Variation of Particle Size in 1.0% Agarose Gels<sup>a)</sup>

Relaxation Time	L, $\mu\text{m}$ ( $p=100$ )	L, $\mu\text{m}$ ( $p=10$ )	D, $\mu\text{m}$ ( $p=1$ )
$\tau_1 = 7 \text{ s}$	6	4	2
$\tau_2 = 15 \text{ s}$	11	8	5
$\tau_3 = 68 \text{ s}$	18	13	8

a)  $E=7.6 \text{ V/cm}$

**Saturation of the Birefringence.** Birefringence saturation curves were measured for 1.0% agarose gels in both high and low voltage electric fields. In both voltage regimes, the amplitude of the birefringence increased approximately as  $E^2$ , as shown in Figure 4. However, the amplitude of the birefringence in the low field regime is 5-6 orders of magnitude larger than would have been predicted from the high field results. Since the optical anisotropy factor is approximately independent of the voltage regime in which the measurements are made (19), the large increase in the amplitude of the birefringence in low voltage electric fields must be due to an increase in the electrical orientation factor.

The birefringence saturation curve measured for a 0.6% LE agarose gel in the low voltage regime is compared with a theoretical curve calculated for permanent dipole orientation in Figure 2b. The apparent dipole moments, given in the caption of Figure 2, increased approximately as the 1.6 power of fiber length (19). Since this power law dependence is larger than the first order dependence expected for permanent dipole orientation, the fiber bundles orienting in the low voltage electric fields probably contain large overlapping aggregates of the fibers orienting in high voltage electric fields.

**Polarity of the Electric Field.** As previously described (6,8), the sign of the birefringence of agarose gels can be reversed from positive to negative (or *vice versa*) by reversing the polarity of the electric field. The resulting birefringence signal is approximately the mirror image of the original, as shown in Figure 5. The sign of the birefringence always follows the polarity of the electric field. Repeatedly pulsing the gel in one direction does not change the sign of the birefringence, while repeatedly reversing the polarity of the electric field causes the sign of the birefringence to reverse repeatedly. This anomalous change in the sign of the birefringence is not observed when short, high voltage reversing pulses are applied to the gel, as shown in Figure 1.

The change in sign of the birefringence upon reversal of the polarity of the electric field indicates that either the optical factor or the electrical orientation factor changes sign upon field reversal. A change in sign of the optical factor upon field reversal is unlikely, and is not observed under other pulsing conditions. A change in sign of the electrical orientation factor would indicate that the agarose fibers orient alternately parallel and perpendicular to the direction of the applied electric field, when the electric field is reversed in polarity.

**Symmetric Reversing Electric Fields.** When a train of symmetric, rapidly reversing pulses was applied to LE agarose gels, the sign of the birefringence oscillated in phase with the applied electric field, as shown in Figure 6. However, the frequency of the oscillations was only one-half that usually observed for macromolecules oriented

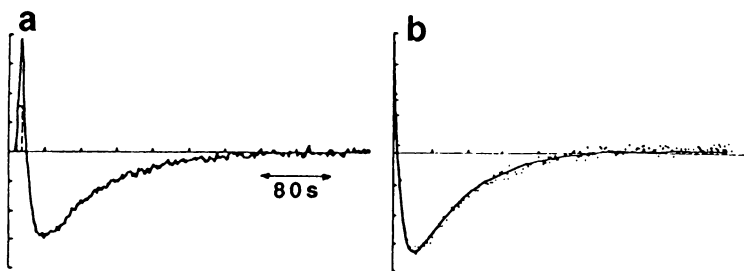


Figure 3. Typical electric birefringence signal observed for a 2.0% LE agarose gel. (a), observed birefringence signal,  $E = 7.6$  V/cm,  $t_p = 5$  s; (b), two-exponential fit of the decay curve. The points represent the experimental data and the solid line is the fitted curve. The fitted relaxation times and relative amplitudes are:  $\tau_1 = 8.8$  s,  $C_1 = +0.64$ ;  $\tau_2 = 60$  s,  $C_2 = -0.36$ .

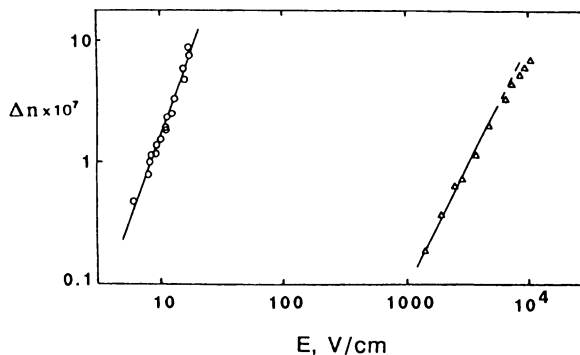


Figure 4. Log-log plots of the birefringence,  $\Delta n$ , of 1.0% LE agarose gels as a function of electric field strength,  $E$ . ( $\Delta$ ), high voltage regime,  $t_p = 250$   $\mu$ s; (o), low voltage regime,  $t_p = 5$  s. The slopes of the drawn lines are 2.0 (high field) and 2.7 (low field).

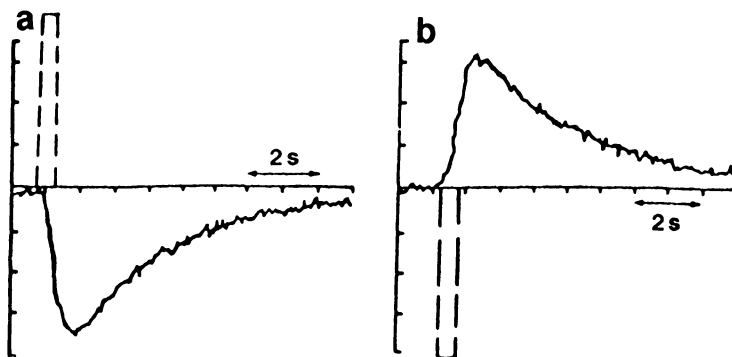


Figure 5. Reversal of the sign of the birefringence observed for a 1.0% LE agarose gel when the electric field is reversed in polarity.  $E = 50$  V/cm,  $t_p = 0.5$  s.

August 10, 2012 | http://pubs.acs.org  
 Publication Date: December 13, 1993 | doi: 10.1021/bk-1994-0548.ch036

by sinusoidal or reversing square wave pulses (9), because of the anomalous reversal of the sign of the birefringence upon field reversal.

The birefringence relaxation times observed after applying a reversing pulse train to the gel were approximately the same as observed with unidirectional pulses, indicating that particles of similar size were orienting in both types of electric fields. However, the relative proportions of the various components in the decay curves depended on the amplitude and duration of the reversing field pulses.

**Asymmetric Reversing Field Pulses.** The results observed when the reversing field pulses were equal in amplitude but unequal in duration depended markedly on the applied electric field strength, as shown in Figure 7. If the applied field was  $\leq 7$  V/cm, the amplitude of the birefringence gradually decreased to zero with increasing pulse number, as shown in Figure 7a. The decrease in the amplitude of the birefringence indicates either that the agarose fibers gradually stopped orienting in the electric field, or, more likely, that the fibers adopted an orientation midway between the orientations adopted in each field direction.

If the electric field strength was  $\geq 7$  V/cm, the amplitude of the birefringence envelope (the absolute value of the difference in the birefringence signal observed in the two field directions) increased sigmoidally to a value 5-10 times larger than observed when single pulses were applied to the gel, as shown in Figure 7b. The marked increase in the birefringence envelope, without a significant increase in the birefringence relaxation times, indicates that an increased number of agarose fibers were orienting in the electric field. Hence, asymmetric reversing pulses  $\geq 7$  V/cm appear to cause a fundamental change in agarose gel structure, probably junction zone breakdown. Agarose fibers released from the junction zones would be able to orient independently in the electric field, increasing the amplitude of the birefringence.

### HEEO Agarose Gels

The electric birefringence signals observed for HEEO agarose gels were qualitatively similar to those observed for LE agarose gels. The sign of the birefringence varied from one gel to another, and also varied at different locations within each gel. The decay curves contained several components of alternating sign, with typical relaxation times given in Table I. Since the relaxation times were similar to those observed for LE agarose gels, the sizes of the orienting fibers and/or microgel domains must be similar also.

The sign of the birefringence of HEEO gels usually reversed when the polarity of the electric field was reversed, as observed for LE agarose gels. Occasionally, only the relative proportions of the various components in the decay curves changed after field inversion, but not the net sign of the birefringence (manuscript in preparation). The results suggest that mirror image orientation behavior upon field inversion is correlated most strongly with the lower charge density of the LE agarose matrix.

In symmetric, rapidly reversing electric fields, the birefringence of HEEO agarose gels oscillated in phase with the applied electric field, as shown in Figure 8. If the electric field strength was  $\leq 4$  V/cm, the birefringence envelope was constant in amplitude and the mean birefringence was close to zero, as shown in Figure 8a. At higher electric field strengths, the birefringence envelope increased slowly with increasing pulse number, and the mean birefringence changed from negative to positive, as shown in Figure 8b. Hence, the results obtained with HEEO agarose gels in symmetric reversing fields paralleled those obtained with LE agarose gels, except that the amplitude of the mean birefringence was larger.

In asymmetric reversing electric fields, the birefringence of HEEO agarose gels oscillated in phase with the applied electric field, as shown in Figure 9. As with LE agarose gels, the qualitative shape of the birefringence signals depended critically on the applied voltage. If the electric field was  $\sim 4$  V/cm, the mean birefringence was close to zero, and the birefringence envelope remained constant with increasing pulse number, as shown in Figure 9a. These results differ from those obtained with LE

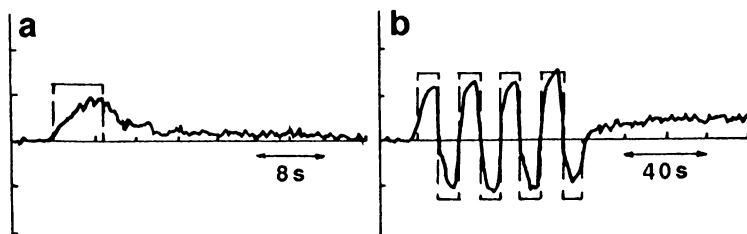


Figure 6. Electric birefringence of 1.0% LE agarose gels in symmetric rapidly reversing electric fields. (a),  $E = 2.9$  V/cm  $t_p = 5$  s; (b), four 10s/10s reversing pulses,  $E = 2.6$  V/cm.

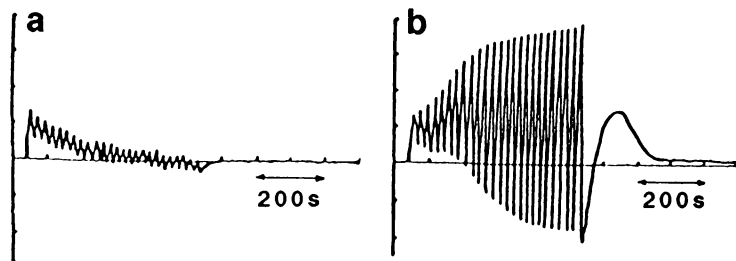


Figure 7. Birefringence signals observed for 1.0% LE agarose gels when trains of 15s/5s asymmetric reversing field pulses are applied to the gels. (a),  $E = 5.0$  V/cm; (b),  $E = 7.6$  V/cm. The pulse trains contained 25 pulses; only the birefringence signals are shown for clarity.

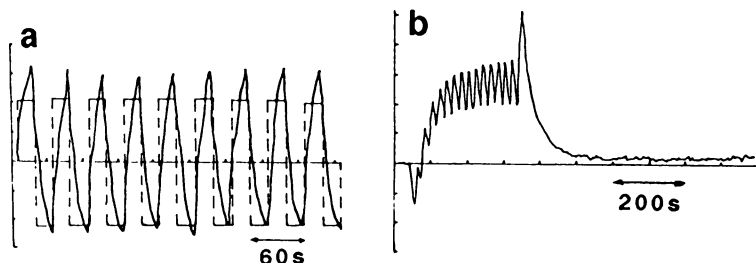


Figure 8. Typical birefringence signals observed for 1.0% HEEO agarose gels in symmetric reversing fields. (a),  $E = 3.8$  V/cm, nine 20s/20s reversing pulses; (b),  $E = 7.6$  V/cm, fifteen 10s/10s reversing pulses. In (b), the pulses are not shown for clarity.

agarose gels, where the birefringence envelope gradually decreased to zero in low voltage electric fields (Figure 7a). Above the threshold voltage of  $\sim 7$  V/cm, the mean birefringence and the birefringence envelope of HEEO agarose gels increased markedly with increasing pulse number (Figure 9b), as observed for LE agarose gels (Figure 7b). The results suggest that asymmetric reversing field pulses  $> 7$  V/cm disrupt the junction zones in both HEEO and LE agarose gels, allowing large numbers of agarose fibers and domains to orient in the electric field.

### Beta-carrageenan Gels

The electric birefringence of  $\beta$ -carrageenan gels exhibited both similarities and differences with the results observed for agarose gels. The amplitude of the birefringence was similar for agarose and  $\beta$ -carrageenan gels. Like agarose, the decay of the birefringence of  $\beta$ -carrageenan gels contained two or three components with different relaxation times and coefficients of alternating sign. Unlike agarose, the signs of the birefringence of the various components in the  $\beta$ -carrageenan decay curves were relatively consistent from one gel to another, although the relative proportions of each of the components varied between gels. The relaxation times observed for  $\beta$ -carrageenan gels were considerably larger than those observed for agarose gels, as shown in Table I. Hence,  $\beta$ -carrageenan fibers and fiber clusters appear to be larger than those of agarose.

Somewhat variable results were observed for  $\beta$ -carrageenan gels when the electric field was reversed in polarity. If a single reversing field pulse was applied to the gel, the birefringence signal frequently decreased in absolute value upon field reversal, and then began to increase toward the original steady state value, as shown in Figure 10a. In other gels, the birefringence signal oscillated in phase with the applied electric field, as observed for agarose gels. This variable behavior suggests either that the microscopic structure of  $\beta$ -carrageenan gels is less regular than agarose gels, or that the  $\beta$ -carrageenan sample contained a heterogeneous mixture of polysaccharides.

When trains of symmetric reversing field pulses were applied to  $\beta$ -carrageenan gels, the birefringence envelope gradually decreased to zero with increasing pulse number. However, the mean birefringence of  $\beta$ -carrageenan gels did not go to zero, but varied randomly with increasing pulse number. Since the relaxation times were unchanged, the slow variation of the mean birefringence must be attributed to electric field-induced changes in the  $\beta$ -carrageenan gel structure.

When asymmetric reversing pulses were applied to  $\beta$ -carrageenan gels, the mean birefringence and the birefringence envelope gradually began to oscillate in phase with the applied electric field, as shown in Figure 10b. If the electric field strength was  $\geq 7$  V/cm, the mean birefringence became large and positive and the birefringence envelope increased markedly with increasing pulse number. The results suggest that extensive junction zone breakdown also occurs for  $\beta$ -carrageenan gels in asymmetric reversing electric fields.

### Polyacrylamide Gels

The birefringence of polyacrylamide gels containing 6.9%T and 3%C was completely different from that observed for the polysaccharide gels. The birefringence signal increased monotonically during the pulse, as shown in Figure 11a. The amplitude of the birefringence was only about 1% as large as that of the polysaccharide gels, suggesting that the polyacrylamide gel fibers were much less free to orient in the electric field. Two components of similar magnitude and opposite signs were observed during the decay of the birefringence, as shown in Table I. However, no relaxation times corresponding to  $\tau_3$  were observed in the polyacrylamide gels, suggesting that polyacrylamide gels do not have the same type of domain structure as the polysaccharide gels.



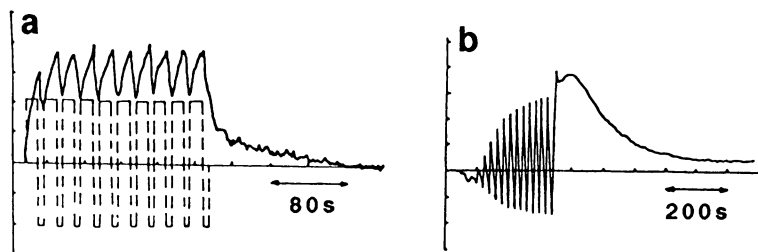


Figure 9. Typical birefringence signals of 1.0% HEEO agarose gels oriented by 15s/5s reversing pulses. (a),  $E = 3.8$  V/cm; (b),  $E = 7.6$  V/cm. The pulses in (b) are not shown.

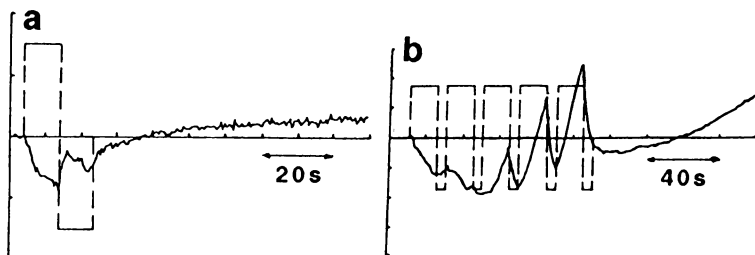


Figure 10. Typical birefringence signals observed for 1.0%  $\beta$ -carrageenan gels in symmetric and asymmetric reversing electric fields, with  $E = 7.6$  V/cm. (a), 10s/10s reversing pulse; (b), five 15s/5s reversing pulses.

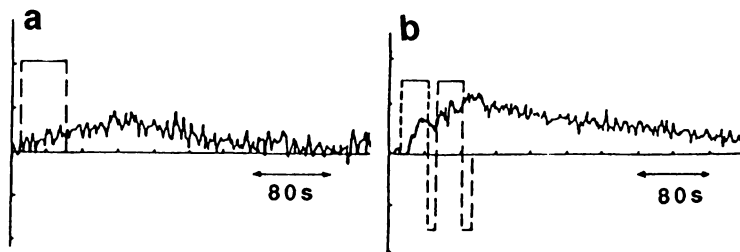


Figure 11. Typical birefringence signals observed for 6.9% polyacrylamide gels, with  $E = 7.6$  V/cm. (a), single pulse,  $t_p = 50$  s; (b), two 30s/10s reversing pulses.

When the electric field was reversed in polarity, the sign of the birefringence of the polyacrylamide gels did not change. In rapidly reversing electric fields, the birefringence signal continued to increase during both the positive and negative portions of the reversing field pulse, as shown in Figure 11b, because the steady state birefringence had not yet been reached. This type of orientation behavior, which was observed with both symmetric and asymmetric reversing field pulses, is expected from the Kerr law. Hence, the reversing field behavior of polyacrylamide gels is normal.

### Concluding Remarks

The results described here indicate that polysaccharide and polyacrylamide gels can be oriented by low voltage, pulsed electric fields of the amplitude and duration used for pulsed field gel electrophoresis. The decay curves of all gels contained several components with different relaxation times and coefficients of alternating sign. The relaxation times correspond to the orientation of fiber bundles and/or microgel domains ranging up to several tens of micrometers in size.

When the electric field applied to an agarose gel is reversed in polarity, the sign of the birefringence of each of the components in the decay curve reverses, giving a mirror image birefringence signal. As discussed above, either the optical factor or the electrical orientation factor of each component must change sign upon field reversal. The anomalous reversal of the sign of the birefringence upon field reversal is not observed for agarose gels oriented by short, high voltage pulses (Fig. 1b) or for agarose solutions (13); hence, the optical factor does not change sign upon field reversal.

Therefore, it seems likely that the change in sign of the birefringence of agarose gels upon field reversal is due to a change in sign of the electrical orientation factor, causing the agarose fibers and/or domains to orient in the opposite direction after field reversal. It seems likely that the orienting agarose fibers are semi-detached or completely detached from the matrix, either because they were never incorporated in the three dimensional gel structure or because of junction zone breakdown due to electric field-catalyzed hydrogen bond rearrangements. If the orienting agarose fibers become reattached to the matrix in new locations during or after the first pulse, and if the reattached gel fibers tend to orient in the opposite direction after field reversal, the anomalous change in sign of the birefringence would be explained. The loss of the birefringence signal after removal of the original pulse does not necessarily indicate that the fibers have returned to their initial positions in the gel matrix; only that their preferential direction of orientation in the electric field has been lost.

Electric field-induced structural rearrangements can also explain the "memory" effects exhibited by oriented agarose gels in electrophoresis (31,32) and field inversion (6,7) experiments. The "memory" of the original field direction persists for at least 12 hours after the orienting field has been removed from the gel. It is difficult to rationalize these results without postulating gel fiber rearrangements induced by the electric field.

The orientation of agarose gel fibers alternately parallel and perpendicular to the electric field, as evidenced by the change in sign of the birefringence upon field reversal, is observed for both LE and HEEO agarose gels, suggesting that charged residues on the agarose backbone chain are not responsible for the anomalous orientation effects. The similarity of the results observed for agarose and  $\beta$ -carrageenan gels suggests that the alternating D, L structure of the agarose backbone chain does not cause the orientation anomalies. In addition, the normal orientation behavior observed for polyacrylamide gels suggests that field-induced structural rearrangements cannot occur in chemically crosslinked gels.

The marked increase in the birefringence envelope when asymmetric reversing pulses greater than 7 V/cm are applied to agarose and  $\beta$ -carrageenan gels suggests that a common event is occurring in the two polysaccharide gels. Since the relaxation times are essentially unchanged when reversing electric fields are applied to the matrix, the increased amplitude of the birefringence indicates that an increased number of gel

fibers are orienting in the electric field. The results suggest that significant junction zone breakdown occurs above the threshold voltage of 7 V/cm when asymmetric reversing pulses are applied to polysaccharide gels. Similar results are not observed with symmetric reversing pulses, probably because the gel fibers are oscillating about a mean position in the gel matrix.

The results described here suggest that significant orientation of the agarose gel matrix occurs when pulsed electric fields of the amplitude and duration used for PFGE are applied to the gels. The reversing field results suggest that the agarose fiber bundles and domains orient alternately parallel and perpendicular to the electric field when the field is reversed in polarity. Comparison with other polymer gels suggests that the anomalous orientation behavior of agarose gels is probably due to field-induced rearrangements of the gel fibers. Recurring gel fiber rearrangements could create transient dynamic pores in the gel matrix, facilitating the migration of very large DNA molecules during PFGE. Further studies of agarose gels by electric birefringence and other techniques will be needed to clarify the importance of matrix orientation to the DNA molecular weight separations obtained during PFGE.

### Acknowledgments

The  $\beta$ -carrageenan, FMC BioProducts sample BRE-682, was generously provided by Dr. F. Kirkpatrick of FMC. The pulse generator was designed and built by Mr. Craig Fastenow of the Department of Biomedical Engineering at the University of Iowa. Financial support from Grant GM29690 from the National Institute of General Medical Sciences is also gratefully acknowledged.

### Literature Cited

1. Stellwagen, N. C. *Adv. Electrophoresis* **1987**, *1*, 177-224.
2. Cantor, C. R.; Smith, C. L.; Mathew, M. K. *Annu. Rev. Biophys. Biophys. Chem.* **1988**, *17*, 287-304.
3. *Pulsed-Field Gel Electrophoresis*; Burmeister, M.; Ulanovsky, L., Eds.; Meth. Mol. Biol.; Humana Press: Totowa, NJ, 1992; Vol. 12.
4. Levene, S.; Zimm, B. H., *Quart. Rev. Biophys.* **1992**, *25*, 171-204.
5. Deutsch, J. M. *Science* **1988**, *240*, 922-924.
6. Stellwagen, J.; Stellwagen, N. C. *Nucleic Acids Res.* **1989**, *17*, 1537-1548.
7. Stellwagen, N. C.; Stellwagen, J. *Electrophoresis* **1989**, *10*, 332-344.
8. Sturm, J.; Weill, G. *Phys. Rev. Lett.* **1989**, *62*, 1484-1487.
9. Fredericq, E.; Houssier, C. *Electric Dichroism and Electric Birefringence*; Clarendon Press, Oxford, 1973; pp 7-59.
10. Rees, D. A.; Morris, E. R.; Thom, D.; Madden, J. K. In *The Polysaccharides*; Aspinall, G. O., Ed.; Academic Press, New York, NY, 1982, Vol. 1; pp 196-290.
11. Leone, M.; Sciortino, T.; Migliore, M.; Fornili, S. L.; Vittorelli, M. B. *Biopolymers* **1987**, *26*, 743-761.
12. Stellwagen, N. C.; Stellwagen, D. *J. Biomol. Struct. Dyn.* **1990**, *8*, 583-600.
13. Dormoy, Y.; Candau, S. *Biopolymers* **1991**, *31*, 109-117.
14. Emanuele, A.; Di Stefano, L.; Giacomazza, D.; Trapanese, M.; Palma-Vittorelli, M. B.; Palma, M. U. *Biopolymers* **1991**, *31*, 859-868.
15. Renn, D. W.; Santos, G. A.; Dumont, L. E.; Parent, C. A.; Stanley, N. F.; Stancioff, D. J.; Guiseley, K. B. *Carbohydrate Polymers*; submitted.
16. Stellwagen, J.; Stellwagen, N. C. *Electrophoresis* **1992**, *13*, 595-600.
17. O'Konski, C. T.; Yoshioka, K.; Orttung, W. H. *J. Phys. Chem.* **1959**, *67*, 1558-1565.
18. Broersoma, S., *J. Chem. Phys.* **1981**, *74*, 6989-6990.
19. Stellwagen, J.; Stellwagen, N. C. submitted.
20. Stellwagen, N. C. *Biopolymers* **1991**, *31*, 1651-1667.
21. Pytkowicz, R. M.; O'Konski, C. T. *Biochim. Biophys. Acta* **1959**, *36*, 466-470.
22. Tinoco, I., Jr.; Yamaoka, K. *J. Phys. Chem.* **1959**, *63*, 423-427.

23. Swenson, C. A.; Stellwagen, N. C. *Biopolymers* **1988**, *27*, 1127-1141.
24. Meeten, G. H. *J. Colloid Interface Sci.* **1982**, *87*, 407-415.
25. Stoylov, S. P. *Colloid Electro-Optics*; Academic Press, San Diego, CA, **1991**.
26. O'Konski, C. T.; Zimm, B. H. *Science* **1951**, *111*, 113-116.
27. Kramer, U.; Hoffman, H. *Macromolecules* **1991**, *24*, 256-263.
28. Hickson, T. G. C.; Polson, A. *Biochim. Biophys. Acta* **1968**, *165*, 43-58.
29. Pines, E.; Prins, W. *Macromolecules* **1973**, *6*, 888-895.
30. Bulone, D.; San Biagio, P. L. *Chem. Phys. Lett.* **1991**, *179*, 339-342.
31. Holmes, D. L.; Stellwagen, N. C. *J. Biomol. Struct. Dyn.* **1989**, *7*, 311-327.
32. Stellwagen, N. C.; Stellwagen, J. *Electrophoresis* **1993**, *14*, 355-368.

RECEIVED August 6, 1993

## Chapter 37

# Cationic Polyelectrolyte Gel from Poly(ethylenimine)

## Effects of pH and Alkyl Sulfate Surfactants on Swelling Equilibria

Mitsuo Hirata<sup>1</sup>, Kazunori Yamada<sup>1</sup>, Kiyomi Matsuda<sup>1</sup>, and  
Etsuo Kokufuta<sup>2</sup>

<sup>1</sup>Department of Industrial Chemistry, College of Industrial Technology,  
Nihon University, Narashino, Chiba 275, Japan

<sup>2</sup>Institute of Applied Biochemistry, University of Tsukuba, Tsukuba, Ibaraki  
305, Japan

A cationic polyelectrolyte gel was prepared through the cross-linking of highly branched poly(ethylenimine) (PEI) with ethylene glycol diglycidyl ether. The swelling characteristics of the PEI gel were investigated as a function of pH as well as of the concentration of surfactants (sodium dodecyl sulfate and sodium 1-octanesulfonate) together with the viscosity changes in the PEI solution caused by these factors. Through comparison of its swelling and viscosity curves, the swelling behavior of the PEI gel is discussed in terms of a balance or competition between the repulsion and attraction between the polyelectrolyte chains in the networks. In the present system, the electrostatic force due to protonated or charged amine groups ( $-\text{NH}_3^+$ ,  $-\text{NH}_2^+$ ,  $-\text{NH}^+<$ ) can act as the repulsive force which swells the gel. On the other hand, the attractive force responsible for collapsing the gel may related to both (i) the hydrogen bonding of the deprotonated or uncharged amine groups ( $-\text{NH}_2$ ,  $-\text{NH}-$ ) and (ii) hydrophobic interaction, especially in cases in which the surfactants are bound to the polymer through electrostatic interaction.

Evidence has accrued which indicates that the volume of gels results from a balance between the repulsion and attraction between the cross-linked polymer chains within their networks, forces which arise from a combination of four intermolecular forces: ionic, hydrophobic, van der Waals, and hydrogen bonding (*1*). In the case of polyelectrolyte gels, the electrostatic interactions result in forces within the polymer networks which are either repulsive or attractive in nature, depending on the signs of the charges. Thus, the dissociation behavior of the ionizable groups attached to the networks is of primary importance for understanding the nature of the swelling of polyelectrolyte gels.

Many of the polyelectrolyte gels prepared in the past have consisted of ionic monomers or of their mixtures with non-ionic monomers, several of which have possessed the capability of causing hydrophobic interactions and hydrogen bonding in the networks. These polyelectrolyte chains contain only one species of ionic groups such as  $-\text{COOH}$ ,  $-\text{N}^+\text{R}_3\text{X}^-$ , and  $-\text{SO}_3\text{H}$  (one set of anionic and cationic groups

0097-6156/94/0548-0493\$06.00/0

© 1994 American Chemical Society

being introduced into ampholytic polyelectrolyte gels). In contrast to these previous polyelectrolytes, poly(ethylenimine) (PEI) is a branched polymer containing primary, secondary, and tertiary amine groups at an approximate ratio of 1:2:1 (2). The dissociation of PEI in aqueous solutions has been studied using potentiometric titration (3-5) and colloid titration (6), and is reported to be different from those of other polyacids and polybases. Thus, the study of the swelling behavior of a PEI gel is vital in order to understand the general characteristics of polyelectrolyte gels.

The authors have reported a method of preparing a PEI gel through the cross-linking of the polymer with ethylene glycol diglycidyl ether (EGDGE) (7). The present study focuses on the pH-induced swelling-deswelling changes of PEI gel originally due to the protonation and deprotonation of the three amine groups in the polyelectrolyte chains. In addition, the effects of surfactants (sodium dodecyl sulfate, SDS, and sodium 1-octanesulfonate, SOS) on the swelling-deswelling changes of PEI gel were also studied to elucidate the role of hydrophobic interactions as the attractive force in the collapse of polyelectrolyte gels.

The viscosity of aqueous PEI solutions was examined in these studies, the measurements of which were performed under the same conditions used in those for the swelling curves. A detailed understanding of the swelling characteristics of PEI gel could be obtained by comparing it with the viscometrically elucidated conformational changes of PEI chains.

## Experimental Section

PEI of M.W.=70,000 in 30 % solution, EGDGE of reagent grade as a cross-linker, and SDS and SOS as the surfactants were all obtained from commercial sources.

PEI gels were prepared through cross-linking PEI with EGDGE and mixing ratio of [amine group in PEI]:[epoxy group in EGDGE] was 15:1. The gelation was carried out at room temperature in a test tube into which glass capillaries with inner diameters of 0.13 mm had been inserted. After the gelation was completed, the gels were removed from the capillaries and washed thoroughly with water.

Gel diameters were determined using a microscope with a calibrated scale. The swelling ratios of the gel were expressed as a ratio of the diameters of each gel to a completely swollen gel at pH 3.

The viscosities of aqueous solutions of PEI were measured using an Ubbelohde viscometer with a flow time of more than 100 s for each solvent used in the measurements.

## Results and Discussion

**Viscosity changes.** As shown in Figure 1, the intrinsic viscosity of PEI decreases with an increase in pH, passing through a plateau level near pH 7. This result is directly related to pH-induced alteration in the conformation of the PEI chains via the deprotonation of the charged amine groups ( $-\text{NH}_3^+$ ,  $-\text{NH}_2^-$ ,  $-\text{NH}^{\delta-}$ ). The deprotonation of these charged amine groups should be dependent upon pH levels; this, therefore, is the reason for appearance of non-monotonic changes in the viscosity curve. However, the pH ranges in which the viscosity decreases (increases) through the deprotonation (protonation) are not sharply differentiated. From previous studies on the dissociation behavior of PEI in aqueous solutions using potentiometric and colloid titration methods, it is known that the acid/base equilibrium of PEI in an aqueous system is governed by a strong interaction of charged neighbors on uncharged groups along the branched polymer chain, i.e., "the nearest neighboring interaction," (5) originally proposed by Katchalsky and his co-workers (8). As a result, this type of the interaction affects the pH-induced expansion of collapse of PEI chains in aqueous solution.

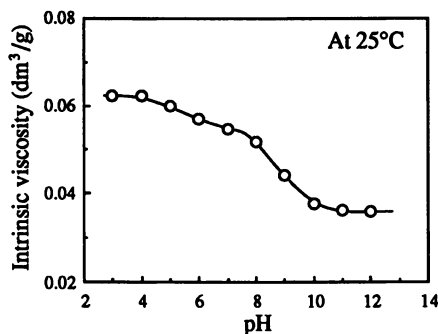


Figure 1 Dependence of intrinsic viscosity on pH for PEI. Ionic strength = 0.1 mol/dm<sup>3</sup>

Figure 2 shows the effects of the concentrations of the surfactants SDS and SOS on the reduced viscosities of PEI with amine groups completely protonated at pH 3. The addition of the surfactants brought about a decrease in the viscosity. However, there were marked differences between SDS and SOS in the viscosity changes induced at a concentration above 10<sup>-3</sup> mol/dm<sup>3</sup>; the magnitude of surfactant-induced decrease in the viscosity was larger in the case of SDS, with a longer alkyl chain than SOS. In addition, increases in temperature caused decreases in the viscosity. These results can be understood by assuming the collapse of the PEI chains as being due to the neutralization of the charged amine groups resulting from the binding of the surfactant anions, as well as being due to the hydrophobic interaction between the polymer-bound surfactant molecules. Therefore, SDS and SOS are useful for studying the effect of hydrophobic interactions as the attractive force in the collapse of PEI gels.

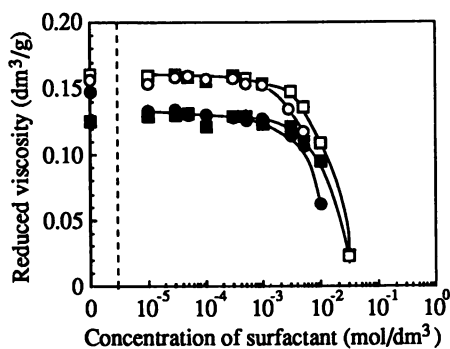


Figure 2 Surfactant-concentration dependence of reduced viscosity at pH 3 for PEI. Polym. Conc. = 5g/dm<sup>3</sup>; SOS : □(20°C) and ■(60°C); SDS : ○(20°C) and ●(60°C)

**Swelling curves.** The previous section showed that variations in pH level and surfactant concentration brought about conformational changes in PEI chains in aqueous solutions. Thus, the effects of these factors on the gel volume were studied

and discussed by comparing them with the experimental results regarding the conformation changes.

**Effects of pH.** Figure 3 shows the effect of pH on the equilibrated volume of the PEI gel. A large hysteresis appeared in the swelling curve during a cyclical pH change; i.e., 3 to 12 followed by 12 to 3. An increase in pH influenced the gel volume little at  $\text{pH} < 11$ , but collapsed the gel with a volume transition near  $\text{pH} 11$ ; a decrease in pH from 12 to 3 brought about a gradual increase in the gel volume. The latter result resembles the pH-induced viscosity change related to the protonation/deprotonation of the amine groups (see Figure 1). However, little change in the gel volume with an increase in pH from 3 to 10 (deprotonation process) was observed, a result which was not expected on the basis of the viscosity curve. This persistency is presumably due to the difficulty in deprotonating the charged amine groups attached to the cross-linked PEI chain networks (the nearest neighbor interaction). In addition, we would have to take into account the fact that the electrostatic force due to the charged amine groups is a "longer range interaction," thus, a slight amount of the charged groups remaining in the cross-linked PEI chains makes the collapse of the networks difficult due to an attractive force (We believe that the hydrogen bonding between the uncharged amine groups, i.e.,  $-\text{NH}_2$  and/or  $-\text{NH}-$ , acts as the attractive force; some experimental evidence concerning this subject will be reported elsewhere). This aspect observed in the PEI gel is apparently different from that of PEI ions in an aqueous solution.

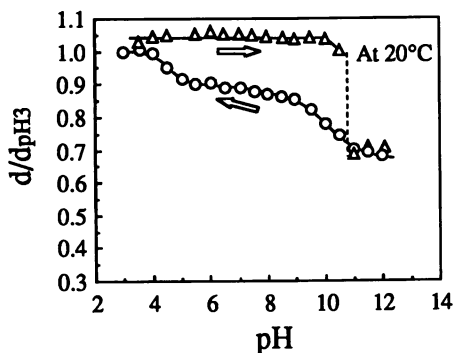


Figure 3 Dependence of swelling ratio on pH for PEI gel

**Effects of SDS and SOS.** The swelling behavior of the PEI gel was further studied as a function of the SDS and SOS concentrations and pH at 20 and 60°C (Figure 4). Gel previously swollen with HCl (pH 3) collapsed discontinuously in an aqueous medium with a certain concentration of the surfactants; the concentration of SDS was lower than that of SOS, with such surfactant effects being enhanced by a rise in temperature. These results agree with those obtained from the viscometric measurements (see Figure 2). It can thus be said that the gel collapse caused by the surfactant is due to both the neutralization of the charged amine groups and the hydrophobic interaction due to the binding of the surfactant molecules.

It is noteworthy that PEI gels show a tendency to increase their volume with added surfactant at 60 °C after having achieved their minimum volume values around  $10^{-3}$  mol/dm<sup>3</sup>. In particular, the PEI gel bound to SDS exhibited the tendency more clearly. It is known that precipitates formed by polyelectrolytes with positive charges and surfactants with negative charges upon the addition of excess surfactant can be redissolved due to the second layer of bound, outward-pointing surfactant ions which



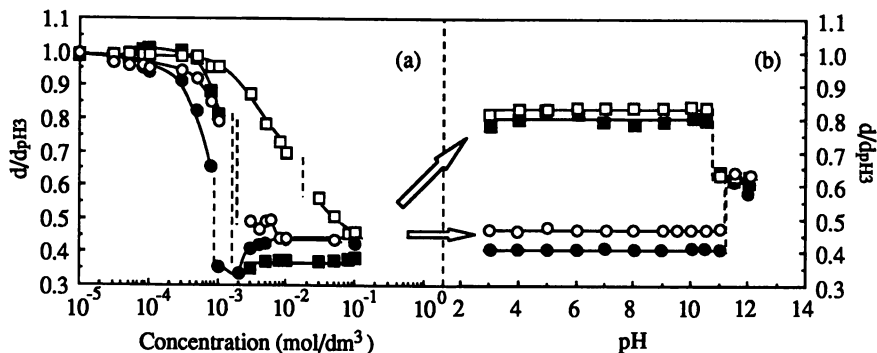


Figure 4 Changes in swelling ratio with surfactant concentrations and pH during washing process with aqueous surfactant-free solution for PEI gels.  
 SOS : □ (20°C) and ■ (60°C);  
 SDS : ○ (20°C) and ● (60°C)

are attached to the first bound layer through association with hydrophobic parts of the first layer (9). Therefore, it is thought that the increases in the volume of PEI gels at higher surfactant concentrations were brought about as a result of repulsion from negatively recharged complexed polymer chains.

The curves in Figure 4 show how the volume of a gel changed when the gel, which had been collapsed using surfactants (at  $10^{-1}$  mol/dm<sup>3</sup>), was washed with aqueous surfactant-free solutions adjusted to various pH levels. In the case of SDS, the volume remained constant at  $\text{pH} < 11$ , and increased discontinuously near  $\text{pH} 11$ . It would seem from this result that the dissociation of the bound SDS did not take place at  $\text{pH} < 11$ . However, the SOS-collapsed gel immediately reswelled when washed with a surfactant-free solution ( $\text{pH} 3$ ). After this, an unaltered volume was observed up to  $\text{pH} 11$ . Such differences may be related to the equilibrium for the surfactant binding to the PEI cations, the nature of which could be dependent upon the chain length of the surfactant molecules. Thus, it seems that the dissociation of the bound SDS from the polymer chains did not take place below  $\text{pH} 11$ , *i.e.* the collapsed volume was maintained even when the gel was immersed in surfactant-free solution through the hydrophobic interaction between the SDS molecules. However, it appears that it is difficult for the SOS molecules, with a chain length which is shorter than that of SDS, to bind strongly to the polymer chains (see temperature dependence); therefore, a part of the bound SOS would be dissociated to swell the gel through the weakened hydrophobic interaction.

A further interesting result to be seen in Figure 4 is that a gel which was collapsed with SOS and then reswollen by washing with SOS-free solution, again shrinks around  $\text{pH} 11$ , the  $d/d_{pH3}$  level being the same as that observed in Figure 3. This means that the discontinuous shrinking around  $\text{pH} 11$  is related to the hydrogen bonding between the  $-\text{NH}_2$  and/or  $-\text{NH}-$  groups in the PEI chains, because deprotonation followed by the dissociation of SOS from the charged amine groups would be possible at  $\text{pH} > 11$ .

## Conclusions and Future Topics

A polyelectrolyte gel has been prepared through the cross-linking of PEI, which is a branched polymer containing primary, secondary, and tertiary amine groups in the approximate ratio of 1:2:1. Effects of pH levels and surfactant concentrations on the

gel volume were investigated and discussed by comparing the results of viscometric studies for aqueous PEI solutions. It has become apparent that the swelling/deswelling changes of the gel result from a balance between the repulsion and attraction of cross-linked polymer chains in their networks. The electrostatic force caused by the pH-induced dissociation of three amine groups acts as the repulsive force, while the attractive force mainly results from hydrophobic interaction when the surfactants were bound to the polymer chains. In addition, hydrogen bonding should be considered an attractive force in this system.

The equilibrium for the surfactant binding to the PEI chains in solution and gel and the nature of the hydrogen bonding of the PEI chains in solution and gel should be investigated in greater detail in the future. Such studies would provide useful general information for understanding the interactions between cross-linked polyelectrolyte chains in gels.

### Acknowledgments

Many thanks are due to Mr. F. Kaneko for carrying out many of the measurements reported in this study.

### References

1. F. Ilmain, T. Tanaka, and E. Kokufuta, *Nature*, **349**, 400(1991).
2. R.L. Davidson, and M. Sittig, "Water-Soluble Polymers," 2nd Edn. (1968) p317.
3. E.J. Shepherd, and J.A. Kitchener, *J. Chem. Soc.*, **1956**, 2448(1956).
4. H. Thiele, and K.H. Gronau, *Makromol. Chem.*, **59**, 207(1963).
5. C.J. Bloys van Treslong, and A.J. Staverman, *Recl. Trav. Chim. Pays-Bas*, **93**, 171 (1974).
6. E. Kokufuta, *Macromolecules*, **12**, 350(1979).
7. F. Kaneko, K. Shimizu, K. Matsuda, K. Yamada, M. Hirata, and E. Kokufuta, *CSJ Ann. Meeting, 1992, Abstr.*, No.3C617 (in Japanese).
8. A. Katchalsky, J. Mazur, and P. Spitnik, *J. Polym. Sci.*, **23**, 513(1957).
9. E.D. Goddard, and K.P. Ananthapadmanabhan, "Interaction of Surfactants with Polymers and Proteins," CRC Press (1993) p171.
10. T. Izumi, and M. Hirata, *Colloid & Polym. Sci.*, **264**, 142(1986).

RECEIVED September 7, 1993

## Chapter 38

# Polyelectrolyte Chains in Swollen Gels

S. Sasaki, H. Ojima, and H. Maeda

Department of Chemistry, Faculty of Science, Kyushu University, 33,  
Hakozaki Higashi-ku Fukuoka 812, Japan

Our previous approach describing the swelling behavior of polyion gels in terms of the dimensionality  $d$  of the chain extension space is applied to the analysis of the expansion behavior of poly(acrylic acid) gels neutralized to various degrees in equilibrium with external salt solutions of different concentrations  $C_s$ . The results showed that  $d$  remained constant to be about 2.2 in the range of  $C_s$  between 10 and 50 mM while it reached about 3 at  $C_s$  of 0.1 M. Light scattering data on fully ionized gels also showed corresponding changes in a narrower range of  $C_s$  between 60 and 80 mM with respect to both the apparent diffusion constants and the scattered light intensities. A structural change of sodium polyacrylate gels was suggested in this range of  $C_s$ .

Ionic polymer gels expand tremendously at high ionization degrees and the degree of expansion depends strongly on the salt concentration (1). The gel volume is determined by a balance among the conformational contractile force, the electrostatic expanding force and the mixing free energy (2 - 5). We have proposed a novel approach according to which the expansion behavior of the gels can be related to the dimensionality  $d$  of the space for the microbrownian motion of cross-linked chains(6). Due to strong electrostatic repulsion, the space available for the random walk chains may be much reduced, which is expected to result in a dimensionality of less than 3. In the previous study, the expansion of carboxymethyl-dextran (CM-dextran) gels was successfully described in terms of a unique dimensionality  $d$  of about 1.5 irrespective of the degree of ionization and ionic strengths(6). The low dimensionality was ascribed to the stiff chain nature of the polymer skeleton itself.

Recently, Schosseler et al. have reported extensive characterization of polyacrylate gels including neutron scattering, light scattering and shear modulus measurements(7). In the present study, we have measured the volume of PAA gel as a function of the degree of ionization  $\alpha$  and the salt concentration outside the gel  $C_s$ . The results were analyzed on the basis of our approach modified to take the strong electrostatic interaction into account according to the Katchalsky theory(8,9). On fully ionized gels, dynamic light scattering measurements were carried out at different  $C_s$ .

0097-6156/94/0548-0499\$06.00/0

© 1994 American Chemical Society

## Theoretical

The conformational free energy  $F_{\text{conf}}$  of tractile chains is given by de Gennes (10, 11) as eq 1.

$$F_{\text{conf}} = n_p kT (R/R_F)^\delta \quad (1)$$

where  $n_p$ ,  $R$  and  $R_F$  denote the total number of polymer chains, their average end-to-end distances in the gel and in the standard state, respectively. The dimensionality  $d$  is related to the parameter  $\delta$  as

$$\delta = (d + 2)/(d - 1). \quad (2)$$

We have shown (6) that the contractile force  $P_{\text{el}}$  is given as eq 3 when  $R_F$  is constant,

$$P_{\text{el}} = -kT (\delta/3) A_V^{-\delta/3} R_F^{-\delta} (C_{\text{pm}}/D_p)^{(1-\delta/3)} \quad (3)$$

where the constant  $A_V$  relates  $R$  to the volume of a single polymer coil. In eq 3, where  $C_{\text{pm}}$  and  $D_p$  denote the residue concentration and the average degree of polymerization of crosslinked chains. The linear charge density of polyacrylate chains is generally much greater than that of CM-dextran. When the osmotic pressure of the gel is evaluated, we need to take the counterion condensation (8, 9, 12, 13) into account. This is effected by introducing the effective ionization degree  $\alpha_e$  which is given as eq 4 according to the theory of Katchalsky (8, 9).

$$\alpha_e = (1 - \beta^2) b / (2 \lambda_B). \quad (4)$$

Here  $b$  represents the distance between neighboring ionizable groups. The Bjerrum length  $\lambda_B$  is defined as  $\lambda_B = e_0^2 / \epsilon kT$  where  $e_0$  and  $\epsilon$  are the elementary charge and the dielectric constant of the solvent. The parameter  $\beta$  in eq 4 is given as eq 5.

$$\alpha \lambda_B / b = (1 - \beta^2) / [1 + \beta \coth\{(-\beta/2) \ln(\pi C_{\text{pm}} b a^2)\}] \quad (5)$$

Here  $\alpha$  and  $a$  denote the degree of ionization and the radius of polymer skeleton (taken to be 0.6 nm), respectively.

In the case of the ideal Donnan equilibrium, the osmotic term is given by eq. 6.

$$\pi_{\text{os}} = 2 kT C_s \left[ \sqrt{1 + (\alpha_e C_{\text{pm}} / 2C_s)^2} - 1 \right] \quad (6)$$

It is to be noted that  $C_s$  in the present study denotes the outside salt concentration in Donnan equilibrium with the gel and should not be confused with the inside salt concentration which is not easily measured. The latter generally differs from  $C_s$  as a result of the Donnan distribution of salt.

The gel volume is determined by a balance between the osmotic expanding force and the conformational contractile force  $P_{\text{el}}$  as eq 7.

$$\pi_{\text{os}} + P_{\text{el}} = 0 \quad (7)$$

Here we ignore the contribution from the mixing entropy of the solvent and polymer segments because the polymer concentration encountered in the present study was very low: the maximum volume fraction was about 0.02.

Introduction of eqs 3 and 6 into eq 7 leads to eq 8 .

$$\pi_{os} = kT (\delta/3) A_V^{-\delta/3} R_F^{-\delta} (C_{pm}/D_p)^{(1-\delta/3)} \quad (8)$$

Plotting  $\log \pi_{os}$  against  $\log C_{pm}$ , we expect a linear relation between them if  $R_F$  is constant. From the slope of the plot we can evaluate  $\delta$  and then  $d$  from eq 2.

## Experimental

Gels were prepared by radical copolymerization of acrylic acid (10 v/v%) and N,N'-methylenebis-(acrylamide), initiated by ammonium peroxydisulfate and was carried out at 70 °C. For swelling measurements, gels synthesized in a plate form of 1mm thick were rinsed thoroughly with distilled water after soaking in 1 - 5M HCl solutions for 12 hours, then freeze-dried, cut into small pieces and used. Gel swelling experiments were carried out at 25 ± 0.5°C. Gels were equilibrated with the solution for more than a week to until their volumes did not increase further. The gel volume  $V_t$  was evaluated assuming the gel density to be identical with the density of the outer solution. Values of  $V_t$  were in the range of 0.0005 - 0.002 dm<sup>3</sup> depending on  $C_s$  and  $\alpha$ .  $C_{pm}$  was calculated as  $Wd/(V_t/72)$  from the weight of dry gel  $Wd$ .

Dynamic light scattering measurements were carried out with a Malvern PCS 100SM system at 25±0.1 °C on fully ionized samples prepared in the following way. Solutions for polymerization were filtered through a membrane (0.22 μm) and gelation took place in a glass tube (inner diameter 5 mm). The gel was purified as above followed by neutralization and equilibration in 0.5 M NaCl and subsequently transferred into a light scattering cell. The gel volume was kept constant by confining it in the cell with a silicon rubber plug. There were two holes in the plug, through which two teflon tubings connected the gel to a reservoir of the salt solution of a constant concentration  $C_s$ . A salt solution was allowed to circulate between the reservoir and the gel. The plug was fixed not to move after the gel was equilibrated with a high salt concentration of about 0.5 M NaCl. Salt concentration was decreased in stepwise manner. When the salt concentration was changed, it took a long time before the equilibrium was attained; usually one to three weeks were required. The equilibration time became as long as one month when  $C_s$  was as low as 10 mM.

The time correlation function of the electric field of the scattered light  $g_1(t)$  was evaluated from the time correlation of the scattered light intensity by the Siegelt relation (14). No significant angular dependence was observed for a range between 60 - 120 degrees. Therefore, the data at 90° angle were used for the analysis.

The values of  $D_p$  were estimated from the ratio of the monomer to the crosslinking reagent. Gels of  $D_p$  110 and 140 were used for the swelling measurements and light scattering study, respectively.

## Results

**Expansion Behavior of Gels.** The dependencies of the gel volume per mole of monomeric unit,  $V (=1/C_{pm})$ , on  $\alpha$  are shown in Fig. 1 for different  $C_s$ .  $V$

increases with  $\alpha$ , but decreases with  $C_s$ . The increment of  $V$  with  $\alpha$  is reduced when  $\alpha$  is greater than about 0.3. This is consistent with the ion-condensation theory that the increment of  $\alpha_e$  with  $\alpha$  becomes very small when  $\alpha\lambda_B/b$  is greater than unity ( $\lambda_B/b$  is taken as 2.8 at 300K). The volume at high  $\alpha$  strongly depends on  $C_s$ . This indicates that the reduced increment of  $V$  at high  $\alpha$  is not caused by the full extension of the chains. When the persistence length does not significantly depend on  $\alpha_e$  nor on  $C_s$ , a linear relation between  $\log \pi_{OS}$  and  $\log C_{pm}$  is expected to hold from eq. 8. The data in Fig. 1 are plotted in Fig. 2 to examine the expected power relation. In Fig. 2, linearity of the data is not good and the data for different  $C_s$  values give different lines. These results differ from the previous one on CM-dextran gels (6). One reason for the difference will be the different ranges of  $d$  encountered. A value of  $d = 2.5$  corresponds to  $\delta = 0$ . Slopes of the plot in Fig. 2 are quite sensitive to a small change of  $\delta$  in this range. In the previous study,  $d$  was 1.4-1.5 while in the present study it varies between 1.7 and 3. The poor linearity in the present study may partly originate from the assumption of a constant  $R_F$ . The charges on the segments will make the persistence length longer and this effect depends on  $C_s$ . When  $R_F$  varies with  $\alpha$  or  $C_s$ , the expected linear relation does not hold any more. This effect is under study and the result will be presented elsewhere.

Values of  $\delta$  were  $5.3 \pm 0.4$ ,  $4.9 \pm 0.2$ ,  $3.8 \pm 0.2$ ,  $3.5 \pm 0.2$ ,  $3.1 \pm 0.1$  and  $2.4 \pm 0.2$  for the values of  $C_s$  of 1, 5, 10, 25, 50 and 100 mM. The corresponding values of the dimensionality  $d$  were  $1.7 \pm 0.1$ ,  $1.8 \pm 0.1$ ,  $2.1 \pm 0.2$ ,  $2.2 \pm 0.1$ ,  $2.4 \pm 0.1$  and  $3.2 \pm 0.5$ . The  $d$  value is roughly constant (about 2.2) in the range of  $C_s$  of 10 - 50 mM but increases to about 3 at 0.1M  $C_s$  and decreases to about 1.7-1.8 at low  $C_s$  of 1-5 mM. The strong electrostatic repulsive force between neighboring ionized chains may induce the vacancy of chain segments between them leading to a dimensionality near 2. At high  $C_s$ , the shielding effect reduces the vacancy region. When the shielding length is much smaller than the distance between the neighboring chains, the chain segments are randomly distributed in the 3-dimensional space ( $d = 3$ ). A transition of  $d$  in the range of  $C_s$  between 50 and 100 mM is obvious, while that between 5 and 10 mM is not conclusive in the present study. It may arise from the poor approximation of the osmotic pressure with eq 6 at low ionic strength. The dependence of  $d$  on  $C_s$  found in the present study is in contrast with the unique  $d$  value in the previous study on CM dextran gels.

**Dynamic Light Scattering Study.** The time correlation function of the electric field of the scattered light  $g_1(t)$  was measured on the fully ionized gels ( $\alpha=1$ ) at different external salt concentrations. In most cases, the observed  $g_1(t)$  was described in terms of two relaxation times, fast and slow mode, as in eq 9

$$g_1(t) = A_f \exp(-\Gamma_f t) + A_s \exp(-\Gamma_s t) \quad (9)$$

The apparent cooperative diffusion constant  $D_{app}$  of polymer network was evaluated from the fast mode according to eq 10

$$D_{app} = \Gamma_f / q^2 : q = (4\pi\tilde{n}/\lambda) \sin(\theta/2) \quad (10)$$

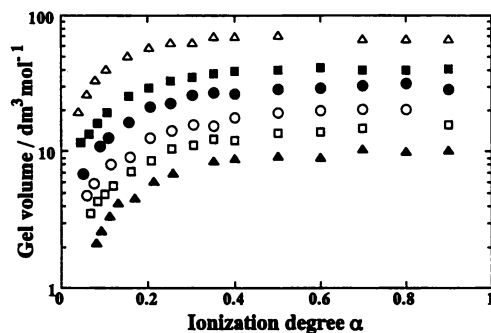


Figure 1. The dependence of gel volume per residue on the degree of ionization  $\alpha$  at different external NaCl concentrations  $C_s$ .  $C_s$ (M): ( $\Delta$ ) 0.001, ( $\blacksquare$ ) 0.005, ( $\bullet$ ) 0.01, ( $\circ$ ) 0.025, ( $\square$ ) 0.05 and ( $\blacktriangle$ ) 0.10.

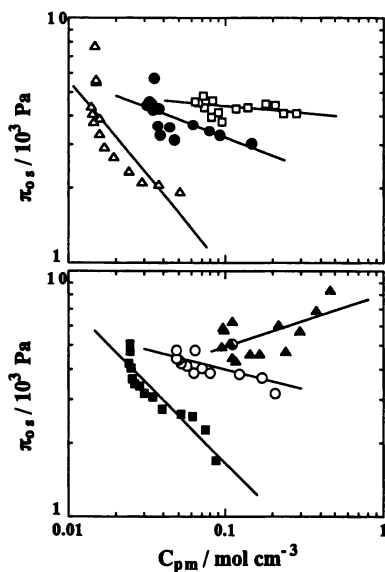


Figure 2. Plots of  $\log \pi_{0s}$  against  $\log C_{pm}$ . Identical symbols are used as shown in Figure 1.

Here,  $\bar{n}$ ,  $\lambda$  and  $\theta$  denote the refractive index of the gel, the wavelength in vacuo and the scattering angle. A probable contribution to the slow mode is considered to arise from dangling chains.

According to Tanaka et al.(15),  $D_{app}$  defined by eq 10 and the scattered light intensity  $I_s$  are related to the longitudinal modulus of gel  $K$  and the hydrodynamic friction factor (per unit volume)  $\zeta$  as follows.

$$I_s = kT (\bar{dn}/dC)^2 / K \quad (11)$$

and

$$D_{app} = K/\zeta \quad (12)$$

In Fig. 3,  $D_{app}$  is plotted against the reciprocal of  $I_s$ . A good linear relation is observed. This indicates that friction constant  $\zeta$  did not significantly depend on  $C_s$  in the present experiments. This is in contrast with the reported trend (7) that  $\zeta$  increased with both  $\alpha$  and  $C_{pm}$ . In Fig. 4, both  $D_{app}$  and  $I_s$  for the gel at  $\alpha = 1$  are shown as functions of  $C_s$  and compared with  $d$ . It is clearly seen that the change of  $d$  is correlated with the change in  $D_{app}$  and  $1/I_s$  in the range of  $C_s$  between 50 and 100 mM. Since  $\zeta$  is shown to be essentially unaltered in this range of  $C_s$ , the change of  $d$  corresponds to a change in  $K$ . Hence, a structural change of NaPA gel is suggested in the range of  $C_s$  between 60 and 80 mM where these three properties change significantly.

## Discussion

### Comparison with the Previous Study on CM-Dextran Gels.

In the previous study on CM-dextran, the predicted linear relation between  $\log \pi_{0s}$  and  $\log C_{pm}$  holds irrespective of  $\alpha$  and  $C_s$ , while it does not hold for different  $C_s$  in polyacrylate gels. In other words,  $d$  varies with  $C_s$  in the present study. Polyacrylate chains are much more flexible than CM-dextran chains and hence the persistence length may vary with  $C_s$  and  $\alpha$ . This may explain the rather poor fit to the predicted power relationship as well as the  $C_s$ -dependence of  $d$  in the present study. However, the dependence of the dimensionality on  $C_s$  in the range between 60-80 mM should be related to some structural change of the gel supposed to occur in this range of  $C_s$ . The latter view was supported in the present study by the dynamic light scattering data.

As to the contribution from the mixing entropy of chain segments with solvent, it is neglected in both studies but the reasons differ between them. In the present study, it is ignored simply because the polymer concentration was sufficiently low. In the previous study, this contribution was suggested to be negligible in spite of rather high polymer concentration, because the data accurately fitted the relation which neglected this contribution. It was supposed that CM-dextran chains were stiff enough not to mix well with the solvent. This picture was consistent with the observed low dimensionality about 1.5.



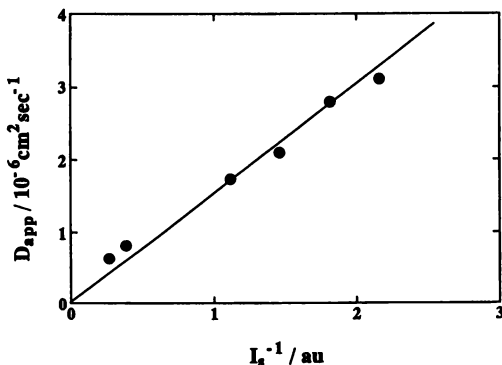


Figure 3. The relationship between the apparent diffusion constant  $D_{app}$  and the scattered light intensity  $I_s$ .

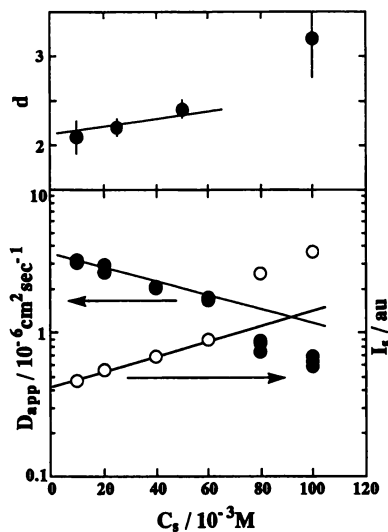


Figure 4. The dependence of the dimensionality  $d$ , the apparent diffusion constant  $D_{app}$  and the scattered light intensity  $I_s$  on the external salt concentration  $C_s$ .

**Evaluation of the Osmotic Pressure.** In the present study the osmotic pressure  $\pi_{OS}$  is approximately evaluated according to the assumption of the ideal Donnan equilibrium in combination with the counterion condensation. The osmotic pressure can be evaluated also on the basis of Manning's theory (12). It is pertinent to discuss Manning's approach in comparison with our present approach. A reasonable starting point common to both approaches is the additivity of the osmotic pressure, which is written in Manning's notation as follows.

$$\pi_{0s} = \phi_p n_e + 2n_s - 2n_s' \quad (13)$$

Here  $\phi_p$ ,  $n_e$ ,  $n_s$ ,  $n_s'$  denote the osmotic coefficient in the salt-free solution, polyelectrolyte equivalent concentration, the salt concentration inside the gel and that outside the gel, respectively. In eq 13 the osmotic coefficients of salt solutions are ignored for simplicity. The osmotic coefficient  $\phi_p$  (in our notation  $\alpha_e$ ) is given in the present study as eq 4 but in Manning's theory it is given in terms of the linear charge density parameter  $\xi$  (in our notation  $\lambda_B/b$ ).

It is necessary to express  $\pi_{0s}$  in terms of  $n_s'$  rather than  $n_s$ , since it is not  $n_s$  but  $n_s'$  that is experimentally controlled. In contrast with the ideal Donnan equilibrium,  $n_s$  is related to  $n_s'$  through a more exact Donnan equilibrium in Manning's theory as follows.

$$\gamma_{\pm} n_s (n_e + n_s) = (n_s')^2 \quad (14)$$

It is not easy, however, to solve eq 14 for  $n_s$  since the mean activity coefficient  $\gamma_{\pm}$  is given as a function of  $\xi$  and  $X (= n_e/n_s)$ .

It is not easy to express  $\pi_{0s}$  in terms of  $n_s'$  in Manning's approach, although it provides a better approximation than the values in this study. This is the reason why we calculate  $\pi_{0s}$  according to eq 6.

This work was partially supported by a Grant-in-Aid (No. 02403004) from the Ministry of Education, Science and Culture of Japan.

### Literature Cited

- 1) Kuhn, W.; Hargitay, B.; Katchalsky, A.; Eisenberg, H. *Nature* **1950**, *165*, 514
- 2) Katchalsky, A.; Lifson, S.; Eisenberg, H. *J. Polym. Sci.* **1951**, *7*, 571
- 3) Katchalsky, A.; Michaeli, I. *J. Polym. Sci.* **1955**, *15*, 69
- 4) Flory, P. J. *Principles of Polymer Chemistry*; Cornell University Press: **1953** Chap. 13.
- 5) Ricka, J.; Tanaka, T. *Macromolecules* **1984**, *17*, 2916
- 6) Sasaki, S.; Miyajima, T.; Maeda, H. *Macromolecules* **1992**, *25*, 3599.
- 7) Schosseler, F.; Ilmain, F.; Candau, S. J. *Macromolecules* **1991**, *24*, 225
- 8) Fuoss, R. M.; Katchalsky, A.; Lifson, S. *Proc. Nat. Acad. Sci. U. S.* **1951**, *37*, 579.
- 9) Lifson, S.; Katchalsky, A. *J. Polym. Sci.* **1953**, *13*, 43
- 10) de Gennes, P. -G. *Scaling Concepts in Polymer Physics*, Cornell Univ. Press **1979** Chap. 1.
- 11) Pincus, P. *Macromolecules* **1976**, *38*, 386
- 12) Oosawa, F. *Polyelectrolytes*, Marcel Dekker, Inc: **1971**, Chap. 2.
- 13) Manning, G. *J. Chem. Phys.*, **1969**, *51*, 924
- 14) Mandel, L. *Prog. Opt.* **1963**, *2*, 181
- 15) Tanaka, T.; Hocker, L. O.; Benedek, G. B. *J. Chem. Phys.* **1973**, *59*, 5151.

RECEIVED September 7, 1993

## Chapter 39

# Construction of Biochemo-Mechanical Systems Using Polyelectrolyte Gels

Etsuo Kokufuta<sup>1</sup>, Shingo Matsukawa<sup>1</sup>, Toyokichi Ebihara<sup>2</sup>, and Kiyomi Matsuda<sup>2</sup>

<sup>1</sup>Institute of Applied Biochemistry, University of Tsukuba, Tsukuba, Ibaraki 305, Japan

<sup>2</sup>Department of Chemistry, College of Industrial Technology, Nihon University, Narashino, Chiba 275, Japan

It would be of interest to develop a gel system that undergoes a swelling-shrinking transition in response to biochemical changes, i.e., "a biochemo-mechanical system" which converts biochemical energy into mechanical work. The present study deals with the design and synthesis of such gel systems using polyelectrolytes. Preparation was performed by immobilizing urease and glucose dehydrogenase into a cross-linked copolymer network consisting of N-isopropylacrylamide (NIPAAm) and acrylic acid (AA). The gels obtained undergo reversible swelling and shrinking in response to the enzyme reactions; the hydrolysis of urea by urease and the oxidation of glucose by glucose dehydrogenase, both of which bring about changes in pH within the gel and thereby the protonation or deprotonation of the COOH groups in the AA residues. As a result, a balance between the repulsive and attractive forces, which are respectively due to an electrostatic interaction of the COO<sup>-</sup> groups and a hydrophobic interaction of the NIPAAm residues, is shifted to a new state to swell or collapse the gel with the immobilized enzymes. In order to examine the potential use of such an enzymatically driven gel in biomedical fields, the release control of a protein such as insulin has been studied. It was found that the protein release occurs when urea was added to an aqueous bulk solution to initiate the enzyme reaction within the gel.

A chemical system that undergoes changes in shape due to a contractile or expanding force created in response to chemical environmental changes is called a "mechano-chemical or chemo-mechanical" system and is one in which chemical potential energy can be converted into mechanical work. Katchalsky and his co-workers were pioneers in the development of such systems using polyelectrolyte gels (1-3). However, the environmental changes that trigger a swelling or shrinking of the gel are not necessarily specific. For example, a volume change can be induced in polyelectrolyte gels by varying pH, but any acids and bases give similar results.

"Biochemo-mechanical systems," in which biochemical changes such as enzymatic reactions are used in place of the usual chemical changes for creating mechanical energies, are taken to be one development of chemo-mechanical systems (Kokufuta, E. *Adv. Polym. Sci.*, in press) (4-6). Since biochemical reactions are generally believed

0097-6156/94/0548-0507\$06.00/0  
© 1994 American Chemical Society

to be uniquely specific, the creation of mechanical energies in a biochemo-mechanical system is expected to be responsive to a specific kind of molecule. This aspect is not only technologically important in the biomedical and engineering fields, but will also provide a basis for a better understanding of the marvelous energy-converting mechanisms available only in biological systems. Here, a general paradigm for the design and preparation of biochemo-mechanical systems using polyelectrolyte gels with immobilized enzymes is described, together with their application in drug delivery devices.

### Design of Biochemo-Mechanical Systems Using Polyelectrolyte Gels

In order to apply polymer gels in the construction of biochemo-mechanical systems, we have tried to account for their volume changes by hypothesizing a balance between the repulsion and attraction of the cross-linked polymer chains in the networks which arise from a combination of four intermolecular forces: ionic, hydrophobic, van der Waals and hydrogen bonding (4,7). When a repulsive force, usually electrostatic in nature, overcomes an attractive force such as the hydrogen bonding or hydrophobic interaction between network chains, gel volume increases discontinuously in some cases or continuously in others. Conversely, a decrease in volume may occur when the attractive force becomes dominant. The variables that trigger the volume change influence these intermolecular forces and thereby the balanced state of the attractive and repulsive forces. This concept is extremely qualitative, but makes it possible for us to construct biochemically driven gel systems (Kokufuta, E. *Adv. Polym. Sci.*, in press) (4).

One possible approach for constructing biochemo-mechanical systems is the swelling-shrinking control of polyelectrolyte gels through a change in the balance between the ionic (repulsive) and hydrophobic (attractive) forces as a result of an enzyme-induced change in pH. For this purpose, urease and glucose dehydrogenase were selected and immobilized into a cross-linked copolymer network consisting of N-isopropylacrylamide (NIPAAm) and acrylic acid (AA). As shown in equation (1), when urea as the substrate is hydrolyzed by the immobilized enzyme, the resulting ammonium ions are expected to increase the pH within the gel. In contrast, a decrease in pH within the gel is anticipated due to the formation of gluconic acid from D-glucono- $\delta$ -lactone which was enzymatically produced through the oxidation of glucose (substrate) by glucose dehydrogenase with the aid of nicotinamide adenine dinucleotide (NAD<sup>+</sup>) [see equation (2)]. Thus, the gel may swell (or collapse) as a result of changes in the electrostatic repulsion between the polymer networks due to the dissociation of the COOH groups (or protonation of COO<sup>-</sup> groups) in the AA residues (see Figure 1). When the substrate is removed, the gel volume also varies due to hydrophobic interaction between the NIPAAm residues which become dominant as a result of the elimination of anionic charges from the networks.

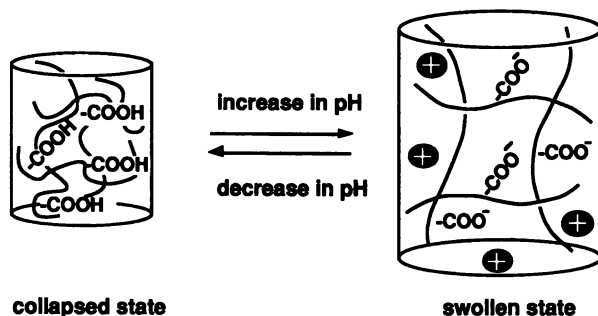
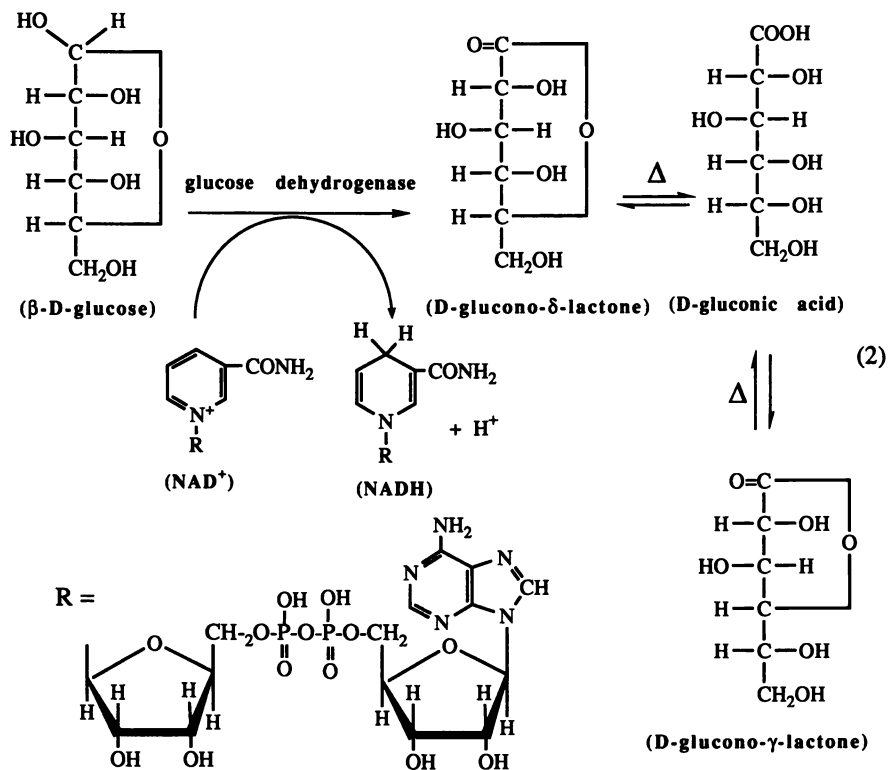
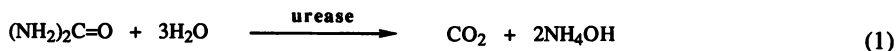


**Figure 1.** Schematic illustration for pH-induced volume change for NIPAAm/AA gel.



### Materials and Methods

Jack bean urease (EC 3.3.1.5, Sigma; Mw = 483,000) with an enzyme activity of 6,1000 units/g-protein was used (one unit of the activity liberates 1.0  $\mu$ mole of ammonia from urea per minute at pH 7.0 and 25 °C). Glucose dehydrogenase (EC 1.1.1.47, from *Bacillus* sp.; Mw = ca. 120,000) was purchased from Wako Pure Chemical Co., Japan; the activity of this enzyme was 6,5000 units/g, where one unit was defined as the activity producing 1.0  $\mu$ mole of NADH from NAD<sup>+</sup> per minute at pH 8.0 and 25 °C.

The immobilization was achieved by gelling an aqueous solution (1 ml) containing NIPAAm (75.6 mg, Kodak), AA (2.3 mg, Wako), N,N'-methylenebisacrylamide (1.33 mg, cross-linker, BioRad), N,N,N',N'-tetramethylethylenediamine (1.85 mg, accelerator, BioRad), ammonium persulfate (0.4 mg, initiator, Wako), and urease (20 mg) or glucose dehydrogenase (1.5 mg). The gelation took place at 0 °C for 1 h in a test tube into which glass capillaries with inner diameters of 0.1 mm had been previously inserted. After the gelation was completed, the gels were taken out of the capillaries, thoroughly washed with distilled water, then with buffers used for the

preparation of substrate solutions. All the samples were cut into cylinders of approximately 2 mm length and stored at 3 °C before use.

The substrate solution for urease was prepared by dissolving different amounts of urea in a  $\text{NH}_4\text{Cl}/\text{HCl}$  buffer solution (0.2 M; pH 4.0), while an aqueous solution (pH 8.1) containing 320 mM glucose, 160 mM  $\text{NAD}^+$  and 160 mM NaOH was used for the substrate solution for glucose dehydrogenase.

The gel samples with the immobilized enzymes were inserted into a glass cell together with the substrate solution, with measurement of gel diameters being started within 1 hour of that time. The diameter was determined using a microscope with a calibrated scale, the temperature being controlled to within 0.01 °C between 20 and 65 °C using circulating water.

A disk-like gel containing immobilized urease (1 mm thickness and 20 mm diameter) was used in the experiments for insulin release. The concentration of insulin released was determined at suitable time intervals by measuring the absorbance of the sample solution at 280 nm using a Hitachi U-3200 spectrophotometer. From a preliminary experiment it was confirmed that there was no release of the enzyme from the gel.

## Results and Discussion

**Effect of pH on Swelling Curve of NIPAAm/AA Gel.** The first requisite for the construction of the enzymatically driven gels is to examine pH changes in the volume of NIPAAm/AA gel without the immobilized enzyme. Figure 2 shows a typical example of temperature dependence of swelling ratio for a NIPAAm/AA gel in an aqueous solution under acidic and alkaline pH levels. Both the transition temperature and swelling ratio increase with an increase in the pH of the aqueous solution. This can be explained by assuming that a repulsive force due to the dissociation (or deprotonation) of the COOH in the AA residues overcomes an attractive force arising from a hydrophobic interaction between the NIPAAm residues. Therefore, it can be expected that an enzymatically induced change in pH within the gel phase would affect the swelling ratio of the present polyelectrolyte gel through shifting the balance between such repulsive and attractive forces.

**NIPAAm/AA Gel with Immobilized Urease.** Swelling curves were measured in the  $\text{NH}_4\text{Cl}/\text{HCl}$  buffer solutions, both with and without urea as the substrate (Figure. 3). In the absence of urea, the gel underwent a discontinuous volume transition at 32.4 °C. In contrast, the presence of urea brought about a continuous volume change, and the temperature causing the volume transition was shifted into a higher range. The dependence of the volumes of the enzyme-free and enzyme-loaded gels on the urea concentration at 33.4 °C showed that the latter gel swelled at urea concentrations > 1 mM, while the former collapsed in the presence of urea (Figure 4). This clearly indicated that the enzyme reaction contributed to the swelling and shrinking of the gel.

We attempted to regulate the gel volume reversibly by alternative immersion of the gel in urea-free and urea-containing buffer solutions (Figure 5). The cylindrical gel in the cell at 33.4 °C was shrunken in the urea-free buffer solution. The buffer was then quickly replaced with the urea solution using a syringe. The swelling of the gel, which began as soon as the urea was introduced into the cell, was completed within 15 minutes. The swollen gel collapsed again when the ambient solution was replaced with the urea-free buffer. The time needed for a complete collapse for the gel-size employed here was approximately 90 minutes. The swelling and collapsing were repeated several times with satisfactory reproducibility.

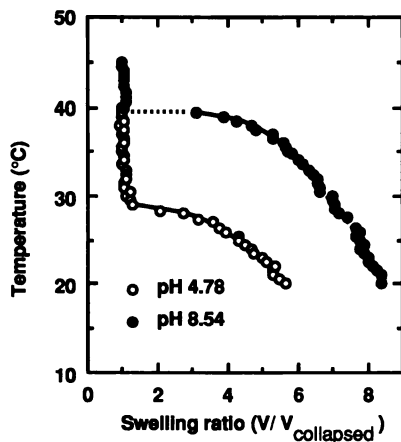


**Figure 2.** Swelling curves as a function of temperature for NIPAAm/AA gel in aqueous solutions at pH 4.78 and 8.54. These swelling curves were measured in a control experiment for glucose dehydrogenase-loaded gels; thus the aqueous phase contained the desired amounts of NaOH and gluconic acid other than both glucose (80 mM) and NAD<sup>+</sup> (80 mM).

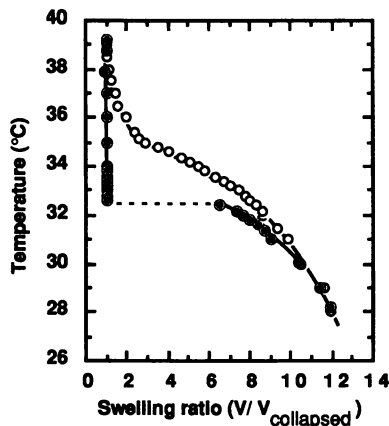


**Figure 3.** Swelling curves of urease-loaded gel in ammonium buffers (0.2 M, pH 4.0) in the presence (○) and absence (●) of urea (1 M) as the substrate. In the absence of urea, hysteresis was observed in the volume changes during heating and cooling procedures, indicating a discontinuous phase transition. The completely collapsed volume for each sample was determined at 50 °C. (Adapted from ref. 4)

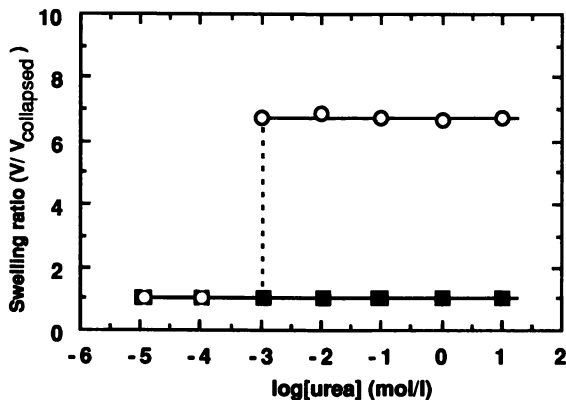


**Figure 4.** Effect of the urea concentration on the volume ratios of the gels with (O) and without immobilized urease (■) at 33.4 °C

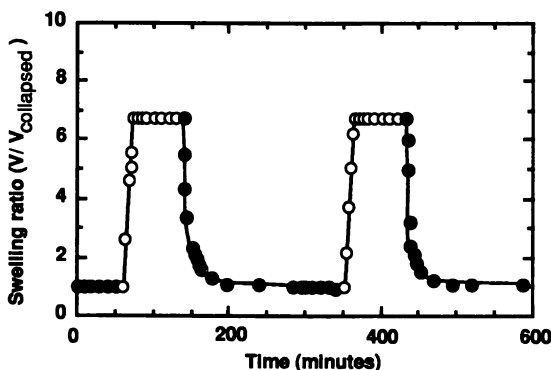


**Figure 5** Repeated swelling and shrinking control of the urease-loaded gel at 33.4 °C by the alternate use of urea-free (●) and urea-containing 0.2 M ammonium buffer solutions (○) at pH 4.0. The aqueous phase (80 ml) in the cell into which the gel sample was immersed was replaced within 2 minutes by 4 ml of another aqueous solution. To avoid temperature changes during the replacement, both aqueous phases were kept at almost the same temperature. (Adapted from ref. 4)

The urease-loaded gel reported here can be regarded as a biochemical-mechanical system. The immobilized urease catalyzes the hydrolysis of urea into ammonia and carbon dioxide [see equation (1)]. The carbon dioxide produced is soluble in water and partially turns into  $\text{HCO}_3^-$  and  $\text{CO}_3^{2-}$ . The gel phase is saturated with the following species:  $\text{NH}_4\text{OH}$ ,  $\text{NH}_4^+$ ,  $\text{HCO}_3^-$ ,  $\text{CO}_3^{2-}$ , and  $\text{Cl}^-$ , in which  $\text{NH}_4\text{OH}$ ,  $\text{NH}_4^+$ , and  $\text{Cl}^-$  originate partially from the buffer. The reaction should increase the pH of the gel phase because of an increase in the ammonia concentration. The carboxyl groups of the gel are then dissociated and result in an electrostatic repulsion between the polymer networks, bringing about an increase in the transition temperature. The gel was swollen when a certain amount of urea was present but collapsed in its absence if the



temperature was kept within a suitable range. In this system, the enzymatically produced chemical energy was converted into mechanical energy through the swelling-shrinking changes of the gel.

**NIPAAm/AA Gel with Immobilized Glucose Dehydrogenase.** Figure 6(a) shows the swelling curves of the glucose dehydrogenase-loaded gel in the presence and absence of glucose. At temperatures below 55°C, the gel volume decreased in the substrate solution containing NAD<sup>+</sup> as the coenzyme, with its pH initially adjusted to 8.5. This result means that the enzyme reaction shown in equation (2) brings about the protonation of the COO<sup>-</sup> groups in the cross-linked polymer networks. However, as can be seen from Figures 5 and 6(b), the time course of the volume change for the glucose dehydrogenase-loaded gel was very slow compared with the urease-loaded gel; i.e., more than 12 h were needed for the glucose dehydrogenase-loaded gel to collapse fully under the conditions used, while the swelling of the urease-loaded gel was completed within 15 minutes.

It seems that this time-consuming change in the gel volume is related to a slow decrease in pH during the enzymatic oxidation of glucose. This is because the time for a gel to swell or shrink has been shown to be proportional to the square of a characteristic length such as the radius of a spherical gel ( $\delta$ ), and also because the size of each gel used here was almost the same. On the other hand, there is a difference in the kinetics of the urease and glucose dehydrogenase-induced changes in pH; that is, a decrease in pH during the oxidation of glucose by glucose dehydrogenase takes place through thermal or non-enzymatic formation of gluconic acid from D-glucono- $\delta$ -lactone as the product of the enzyme reaction. In addition, the resulting gluconic acid partially turns into D-glucono- $\gamma$ -lactone without the aid of the enzymes. As a result, the rate of pH changes by glucose dehydrogenase is slower than that by urease. (We believe that this is the case at least under the experimental conditions employed, although it is preferable to compare the rate constants of enzyme reactions only under certain strict conditions of temperature, pH, substrate concentration, enzyme concentration and so on.)

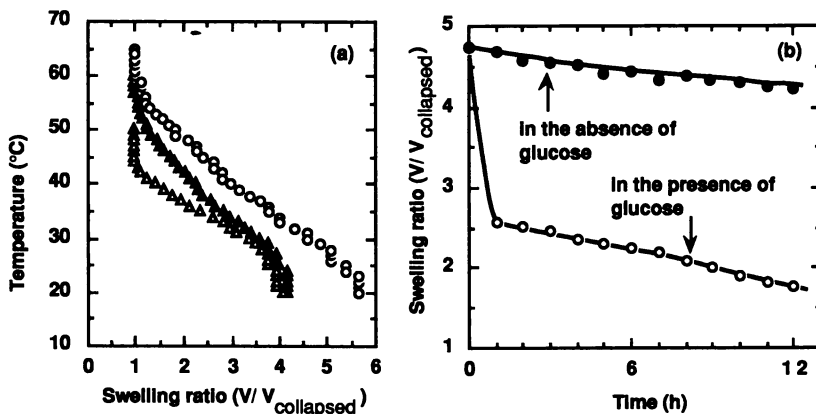


**Figure 6.** Changes in swelling ratios with temperature (a) and time (b) for glucose dehydrogenase-loaded NIPAAm/AA gel. The temperature dependence was measured in the absence (O) and presence of glucose ( $\Delta$ ), within 2 h after the initiation of enzymatic reaction;  $\Delta$ , after permitting the enzyme-loaded gel to stand for 12 h in a cell maintained at 37 °C). The time dependence was measured at 37 °C.

**Enzymatically Induced Volume Changes of Gels.** The observed changes in gel volume induced by immobilized enzymes can be explained according to the schematic illustration shown in Figure 7. The gel undergoes a volume change depending upon the concentrations of the products, i.e., pH levels in the present case, within or in the near vicinity of the gel phase but not in the bulk solution. When an enzymatically induced change in the product concentration is rapid (e.g., with urease), the gel volume immediately alters as a result of saturation of the gel phase with the products, with the volume remaining unchanged until the complete saturation of the bulk medium with the products [see (a) in Figure 7]. However, as shown in Figure 7(b), a time-consuming alteration in the product concentration results in a slow volume change, the magnitude of which is large for the initial state due to an increase in product concentrations within the gel phase. In the final state, the gel volume approaches a constant level since the bulk phase is approximately saturated with the products. Consequently, the regulation of rate of enzyme reaction within the gel phase plays an important role in the construction of enzymatically driven gels; this may be performed by varying the amount of immobilized enzymes and/or by the use of an accelerator.

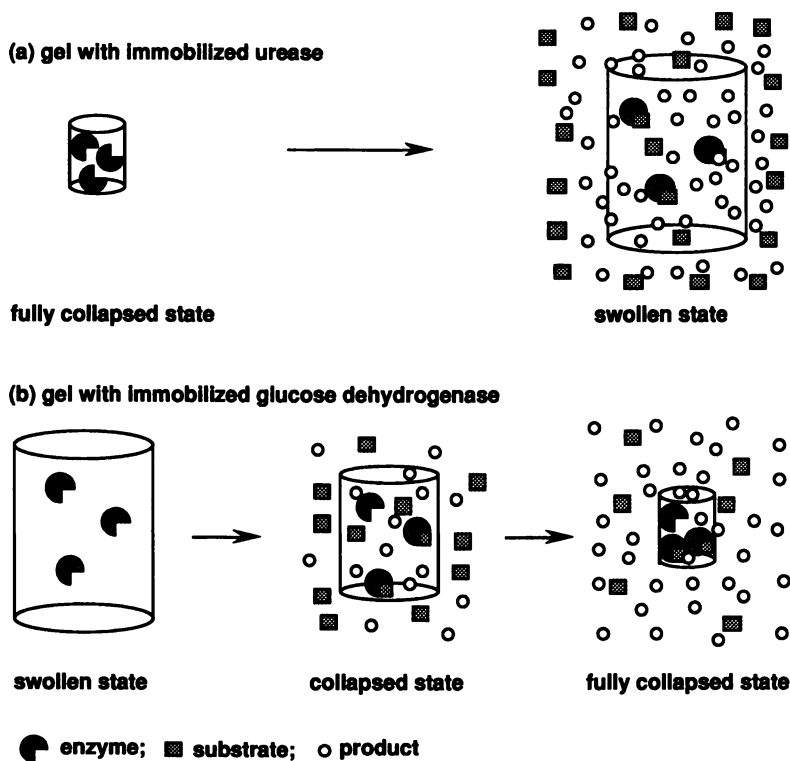


**Figure 7.** Schematic illustration for enzymatically induced volume change in NIPAAm/AA gels with immobilized urease and glucose dehydrogenase

**Enzymatically Controlled Protein Release from Urease-loaded NIPAAm/AA Gel.** The enzymatically driven gel not only provides a simulation of biological energy-conversion systems, but is also available for technological applications. For example, gels undergoing reversible swelling and shrinking changes in response to biochemical stimuli in the form of enzyme reactions may serve as drug delivery devices. In fact, the release of a protein such as insulin from the present gel system occurred when the substrate was added to an aqueous bulk solution to initiate the enzyme reaction within the gel (Figure 8).

Several studies have focused on the controlled release of insulin from stimulus-sensitive polymers in the form of gels and membranes, the structural or chemical properties of which vary in response to changes in environmental conditions, especially glucose concentration (9-16). The goal of these studies has been to develop glucose-sensitive drug delivery devices that are capable of administering insulin to diabetics. At present, we have not yet succeeded in controlling insulin release in response to glucose by use of the NIPAAm/AA gel with immobilized glucose dehydrogenase. However, from the results in Figure 8, we are able to suggest the potential use of our glucose dehydrogenase-loaded gel as a glucose-sensitive insulin delivery device. As a general concept, enzymatically driven gels could serve as drug delivery devices which function in response to pathogenic stimuli.

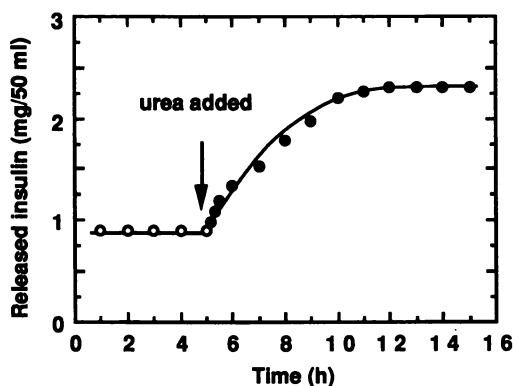


**Figure 8.** Biochemo-mechanically controlled protein release using urease-loaded gel. The experiment was carried out in a 0.2M ammonium buffer maintained at 33.4 °C using insulin (Mw = 5733) as a protein solute.

## Conclusions

A polyelectrolyte gel exhibiting a biochemo-mechanical function has been prepared by immobilizing urease or glucose dehydrogenase into a cross-linked copolymer network consisting of N-isopropylacrylamide and acrylic acid. The gel undergoes reversible swelling and shrinking (in some cases, discontinuous) in response to urea or glucose as the substrate. The system demonstrates a general scheme for a biochemo-mechanical system in which biochemical energy is converted into mechanical energy in the outer medium. In addition, the potential use of such biochemo-mechanical systems was suggested in the field of drug delivery devices which work in response to some pathogenic stimulus.

### Acknowledgments

The author wishes to thank Professor M. Hirata of Nihon University for valuable discussions and R. Craig for his critical reading of this manuscript. This research was supported in part at the University of Tsukuba by a grant to E. K. through a grant from the New Energy and Industrial Technology Development Organization (NEDO), Japan.

### Literature Cited

1. Kuhn, W.; Hargitay, B.; Katchalsky, A.; Eisenberg, E. *Nature* **1950**, 165, 514.
2. Steinberg, I. Z.; Oplatka, H.; Katchalsky, A. *Nature* **1966**, 210, 568.
3. Sussman, M. V.; Katchalsky, A. *Science* **1970**, 167, 45.
4. Kokufuta, E. *Prog. Polym. Sci.* **1992**, 17, 647.
5. Kokufuta, E.; Tanaka, T. *Macromolecules* **1991**, 24, 1605.
6. Kokufuta, E.; Zhang, Y.-Q.; Tanaka, T. *Nature* **1991**, 351, 302.
7. Ilmain, F. Tanaka, T.; Kokufuta, E. *Nature* **1991**, 349, 400.
8. Tanaka, T.; Fillmore, D. J. *J. Chem. Phys.* **1979**, 70, 1214.
9. Ishihara, K.; Kobayashi, M.; Shinohara, I. *Makromol. Chem., Rapid Commun.* **1983**, 4, 327.
10. Ishihara, K.; Kobayashi, M.; Ishimura, N.; Shinohara, I. *Polymer J.* **1984**, 16, 625.
11. Ishihara, K.; Muramoto, N.; Fujii, H.; Shinohara, I. *J. Polym. Sci., Polym. Lett. Edn.* **1985**, 23, 531.
12. Kost, J.; Horbett, T. A.; Ratner, B. D.; Singh, M. *J. Biomed. Mater. Res.* **1985**, 19, 1117.
13. Jeong, S. Y.; Kim, S. W.; Eenink, M. J. D.; Feijen, J. *J. Controlled Release* **1984**, 1, 57.
14. Sato, S.; Jeong, S. Y.; McRea, J. C.; Kim, S. W. *J. Controlled Release* **1984**, 1, 64.
15. Jeong, S. Y.; Kim, S. W.; Holmberg, D. L.; McRea, J. C. *J. Controlled Release* **1985**, 2, 143.
16. Kwon, I. C.; Bae, Y. H.; Kim, S. W. *Nature* **1991**, 354, 291-293.

RECEIVED September 17, 1993

## Chapter 40

# Biomimetic Macromolecular Actuators

Danilo De Rossi<sup>1,2</sup> and Piero Chiarelli<sup>1,2</sup>

<sup>1</sup>Centro "E. Piaggio", Faculty of Engineering, University of Pisa, 56126  
Pisa, Italy

<sup>2</sup>Institute of Clinical Physiology, CNR (Italian Research Council), 56126  
Pisa, Italy

The dichotomy of man-made machines and biological machines is not an engineering dogma anymore. Recent research efforts in the field of molecular engineering led to substantial advances to the endeavour of mimicking through synthetic pathways the functional characteristics of biological muscles. The effort to build sophisticated molecular engines has its foundation on methods techniques to synthesize, study and characterize new materials able to perform useful electromechanical work, starting from conformational changes on a molecular scale.

An overview of electron-conducting polymer and polyelectrolyte gels based-actuators is presented.

A continuum model of the electromechanical response and control strategies for polyelectrolyte gel actuators are discussed.

Organic materials can be used to create new sensors and actuators capable of measuring physical, chemical and biological parameters or of generating controllable forces and displacements. These novel transduction systems, which rise from research into intrinsic energy conversion characteristics of molecular aggregates and developments in molecular electronics, possess specific capabilities that may improve upon those of conventional materials. Whilst significant advances in solid state technology have allowed tremendous improvements in electronic processing, memory and display systems of modern instrumentation, this has not always been possible for transducers. In fact, transducers still remain highly specialized, delicate and costly and are often unreliable. Moreover, conventional transducers frequently limit the overall performance of an instrument and impose severe restrictions on its operating environment. For decades the electronic applications of macromolecules made almost exclusive use of their dielectric properties and electrical insulation capacities. This general view of polymers changed when metal-like conductivity in doped polyacetylene was discovered in 1977. Electronic and ionic macromolecular conductors now offer much broader uses as actuation elements and are the subjects of intense investigation in several laboratories worldwide.

Molecular based transducers are thus being studied in order to overcome measurement and actuation problems in fields such as bioengineering, advances robotics and pollution control, which inorganic materials cannot solve.

0097-6156/94/0548-0517\$06.00/0

© 1994 American Chemical Society

## Molecular Actuators

The layman's view of a machine is a large, unwieldy and inefficient piece of equipment which converts an input energy into a lot of heat and noise and some useful work. Micro actuators and nano machines should someday replace this image with one of quiet efficiency and compactness, performing critical and delicate tasks.

A great majority of the devices developed by man to convert chemical or electrical energy in mechanical work are thermochemical or electromagnetic machines. The physical principles exploited in such man-made machines are completely different from the ones which biological machines use to generate forces and accomplish work. Despite the advanced state of conventional motor technology, the development of mechanical actuators exhibiting biomorphic characteristics would provide a major advance and have important implications in several areas of technology. Although the end is not yet in sight, the two very promising young fields of nano and micro actuators are undergoing vigorous growth and popularity and some short term goals such as microweeder and micropositioners based on polymers are nearing realization.

**Nanoactuators.** The concept of nanoactuators was examined several years ago by K.E. Drexler, who is today one of the leading devotees of nanofabrication. Although it is by no means necessary to mimic nature's machines to the letter, they are near-perfect systems upon which we can model man-made nanomachines. The innate ability of biological organisms to move themselves is impelled by their exquisitely simple yet sophisticated biomolecular machines. Simple because the tiny machines found in nature are based on only a few molecules, and sophisticated because they are able to work in the environments present in vivo and use minimal energy to produce relatively large forces and displacements. Research in nanoactuation systems has only just begun to take off, with the participation of mainly Japanese and American groups. The ultimate man made molecular machine, according to Drexler (1), will eventually be self assembling and self repairing and will be used to direct chemical reactions, repair organs, construct computers, transport reagents and generally perform a whole range of useful functions. Obviously, such a machine will take many years to develop, in the meantime this field is still in its infancy, and current efforts are devoted to replicating biological machines in the laboratory in order to better understand such systems. Two pioneering examples are myosin sliding machines and flagellar rotary motors and will be briefly described.

**Flagellar Rotary Motor.** A group at the University of Tokyo has attempted to reconstruct the flagellar motor of bacteria in vitro (2) The flagellar motor, by which means a bacterium propels itself, is the only rotating type motor found in nature, and for its high speed and efficiency and low inertia merits study. The whole flagellum is composed of three parts: the filament, the hook which connects the filament to the motor, and the motor itself, as illustrated in (Figure 1).

The filament, which is not unlike a screw, was reconstructed in vitro by self assembly of its constituent proteins, which consist of identical subunits known as flagellin. The hook, which is a sort of universal flexible joint, is also made up of identical proteic subunits. It has not yet been possible to reconstruct the hook in a reproducible manner. Several disk-like structures make up the motor unit including a shaft-like element, a bush and a rotor. The motor can rotate at speeds of up to 12000 rpm.

By using genetic engineering techniques, genes encoding the rotor and shaft proteins were expressed in bacteria and amplified, and the rotor, but not as yet the shaft, was successfully self assembled.

These are the first promising attempts at reconstructing a biological motor and have led to a further understanding of its mechanisms. This type of research is a first step towards the realization of nanomolecular machines.

**Myosin Sliding Machines.** Muscle fibre consists of two protein containing filaments. One type of filament (the thin filament), contains the proteins actin, troponin and tropomyosin, and it consists of thin threads supporting globular proteins. A second type of filament, containing the protein myosin, consists of thicker rods that interdigitate with adjacent actin filaments. According to the sliding filament model of muscle contraction, during a contraction, actin filaments slide past myosin filaments through the generation of cross-bridges. In this manner, the entire muscle fibre contracts, and the process is driven by the hydrolysis of APT. In an attempt to comprehend this chemomechanical energy transduction process Ishijima et al. (3) have monitored the motions of individual actin filaments in vitro. In their experiments, a single fluorescent labelled actin filament is placed on a myosin coated surface. By means of fluorescent microscopy, the motions of the actin filament can be observed, and it is also possible to measure the force produced by a single myosin molecules. In this system then, the coupling of the APT cycle to interaction between actin and myosin can be examined directly, thus furnishing insights into molecular mechanisms which drive muscle contraction. In the future they can perhaps be applied to molecular machines.

**Microactuators.** There is growing demand, in fields such as anthropomorphic robotics, microrobotics and bioengineering, for muscle-like actuators with high power to weight ratios and a large degree of compliance. From a mechanical engineering point of view, muscle are very unconventional, actuators. They are neither pure force generators (like electric DC motors), nor pure motion generators (like stepper motors). In fact, they behave rather like springs with tuneable elastic parameters. This and the built-in compliance of muscles are winning features for achieving versatility and robustness and for affording the complexity of sensory-motor problems, such as motor redundancy, trajectory formation, negotiation of impacts and motor learning. All this, though, is achieved at the cost of precision.

Nonetheless, pure mechanical precision is unnecessary because what is of functional significance when confronted with an interacting object is a global characterization of the integrated sensory-motor system, rather than any accurate information on its location, shape or bulk and surface properties.

Pseudomuscular actuators are intended to reproduce the salient features of biological muscles. Hence it is desirable to target performances which equal or even exceed those of muscles. These objectives thus provide the following set requirements for actuators (4)

- large linear displacements
- durable, with long lifetimes and high stability
- built-in tuneable compliance
- High power/volume ratio, and power/weight (0.1-1 kW/kg)
- high force density (0.1 MPa)
- fast response time (a typical strain rate is 100%/s)
- convenient, high density and environmentally safe energy source
- efficient energy conversion (45-70%)

Some of the criteria above have been met, but most of them are far too ambitious to be approached by currently available materials. In spite of several major advances in actuator performances in the last few years, a number of technical breakthroughs are needed before efficient and reliable devices can be implemented. At present, there are four different major classes of macromolecular materials that exhibit mechanical transduction (see Table I), three of which are discussed below.

**Piezoelectric Polymers.** Piezoelectric polymers (5) are widely used as sensing devices and are common in medical ultrasonics.

Their use as low frequency actuators is however limited because of the high driving voltages required to produce small strains (typically 2 kV for a 1  $\mu\text{m}$  linear displacement) and their lack of a steady state response.

**Table I: Molecular Actuators**

<i>Micro</i>	<i>Nano</i>
electrostrictive materials	actin-myosin
polymer gels	flagellar motor
conducting polymers	proton pumps in membranes
piezoelectric polymers	

Nevertheless, they can be fast and highly reliable, and production technologies for piezoelectric polymers are quite advanced. In order to produce useful displacements, polyvinylidene fluoride, (PVDF) for example, can be formed into a bimorph. In (6), two small PVDF strips with opposing axes were bonded together to produce a 13  $\mu\text{m}$  displacement with an applied voltage of 300 V.

Their precision and reliability make piezoelectric polymers ideal for low mechanical impedance, small displacement, multidegree of freedom micromanipulators for cell handling (7), as illustrated in (Figure 2).

**Conducting Polymers.** Conducting polymers (CP) have only recently been used for actuation, but have already shown to possess very high force generation capabilities (8).  $\pi$ -electron conjugated polymers can exert tremendous forces, hundreds of times greater than those of muscles. In very thin CP fibres, where diffusion distances are minimized, response times can be compatible with the proposed application.

They do however tend to have lower strain (1-10%) than polyelectrolyte gels, but not as low as those of piezoelectric polymers. Pei and Inganäs (9) have investigated the mechanical properties of a bilayer CP strip of polypyrrole. On application of 0.8 V vs SCE the strip bent by 0.5 cm. The process was fairly slow, but reversible.

CP are rather solid compact polymers, and it is this which limits the response times of anything other than very thin fibres. To circumvent this, a number of different approaches to designing CP actuators are being investigated. The synthesis of a polymer gel incorporating a CP backbone has been accomplished (10).

However, this trial and error type approach may take several year before a useful polymer with adequate mechanical properties can be synthesized. Alternatively, it may be possible to produce a microporous CP structure, rather than a gel, using a phase inversion spinning process. This method would produce a polymer structure with a fast response time, at the expense of a slightly reduced force density.

**Polymer Gels.** Polyelectrolyte gels have received much attention since the early 50's, and, more recently have been incorporated into prototypes or demonstration robotic devices (11). A polyelectrolyte gel is a cross-linked polyelectrolyte network permeated by an aqueous solution.

The majority of gels investigated undergo chemomechanical (CM) conversion by ionization, redox reactions or photoisomerisation. Other mechanisms such as ion-exchange and phase or order-disorder transitions also exist (12). Under direct chemomechanical conversion, polymer gels are characterized by yielding large strain (50%) and force densities comparable to those in muscles. However, in spite of almost two decades of research, the mechanical strength and response times of these materials still leave much to be desired.



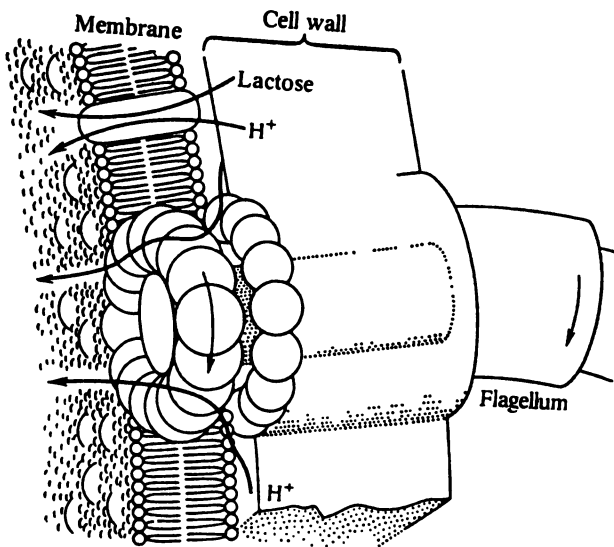


Figure 1. A natural flagellar rotary motor (adapted from ref. 26)

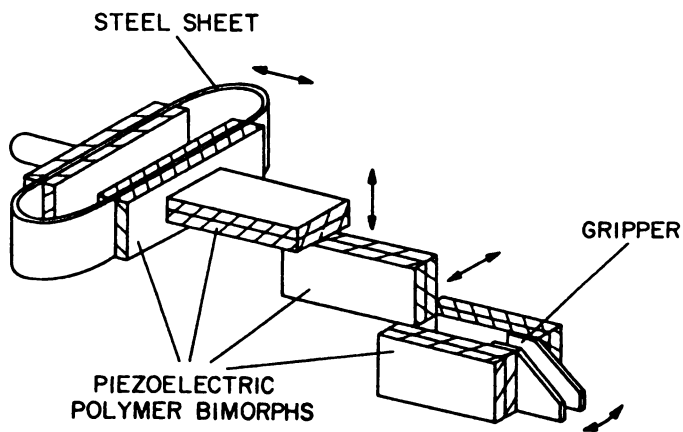


Figure 2. A micromanipulator that uses piezoelectric polymers

The CM conversion process is diffusion regulated so that the response time may be increased by drawing the gels into very thin fibres and assembling bundles composed of several fibres. This poses severe technical problems, not least breakage of the fibres. Present efforts in this field are dedicated to providing polymer gels with some sort of electrical drive in order to render them useful for various applications. In earlier attempts, metal electrodes were positioned in the gels. More recently, the electrochemomechanical (ECM) properties of a polymer gel with interpenetrating polypyrrole electrodes have been studied (13). In both cases although ECM conversion was achieved, the electro-chemical coupling mechanism was inefficient. To date no experimental evidence related to the feasibility of electrically triggered chemically fueled ECM conversion has been reported. This problem poses a major limiting on polyelectrolyte gels for application to actuators.

Notwithstanding recent advances in the science and technology of electrocontractile polyelectrolyte and conducting polymer gels, major progress has to be achieved in all aspects which are instrumental to the conception and implementation of muscle-like actuators.

These aspects embrace various disciplines and their intimate interrelations pose additional difficulties.

### **Pseudomuscular Gel Actuators For Advanced Robotics.**

In the course of a research aimed at developing muscle-like gel actuators, the following topics have been examined:

- analysis of mechanisms eliciting electromechanochemical response in gels
- formulation of continuum models describing gel rheology and electromechanochemistry
- reduction of model complexity to a lumped parameter description of gel fiber actuators, useful for control purposes
- formulation of control strategies for finger-like kinematic chains driven by polymeric actuators
- neural control of redundant, multi-actuator systems.

**Analysis of mechanisms eliciting electromechanochemical response in polyelectrolyte gels.** The effects of interactions of electric fields with polyelectrolytes in solution or gel form can be summarized as:

- a) orientation of dipolar species
- b) deformation of polarizable species and orientation of induced dipoles
- c) alterations of the degree of dissociation of weak acids and bases
- d) motion and redistribution of mobile charged species.

In addition, in the case of electric fields produced by electrodes in contact with the solution or gels:

- e) electrochemical reactions at the interfaces.

These effects can be associated with various modifications and structural readjustments at the molecular level which, in a gel, can manifest themselves macroscopically because of intermolecular bridges and crosslinks.

Estimates in terms of orders of magnitude, although approximated, can offer useful indications for a comparative evaluation of electric field dependence of the effects listed above.

It is clearly understood that the large variety of physical and chemical properties of various polyelectrolyte moieties would require a detailed analysis, specific for each compound. The following analysis, however, is based on large categorizations and, although limited in their applicability and accuracy, results are easily obtained in an handy form (14).

In its simplest form, the analysis is limited to synthetic polymers made by a unique monomeric unit possessing a permanent dipole moment which, as it occurs typically, has a value of a few Debye.

In the process leading from a single monomer to a structural unit in a linear polymeric chain the dipole moment  $d_0$  of the monomer changes because of a diverse electronic distribution in the molecule and, in general, the structural unit assumes a moment given by  $d = Vd_0$  (where  $V \sim 1$ ).

In the presence of an electric field each structural unit tends to rotate to align its dipole moment with the local field  $E$  and its energy decreases by an amount equal to  $d \cdot E$ . The interaction with the electric field affects the rotational mobility of the structural unit. Since the elastic properties of the chain deriving from this mobility originate from thermal agitation, we may consider as a term of comparison the average energy of a structural unit equal to  $KT$ .

We can so impose the condition:

$$dE \sim KT$$

Assuming  $V = 1$ ,  $d_0 = 3D$  and  $T = 300^\circ \text{K}$ , we obtain  $E \sim 10^6 \text{ V/cm}$ .

So, an electric field strength of  $10^3 \text{ V/cm}$  causes an approximate change of 1% of the average energy of the structural unit. Using similar arguments, the polarizability of an ionized polyelectrolyte chain and the influence of electric field changes on the dissociation constants in polyelectrolyte systems can be taken into account, leading to similar values of electric field strength needed to produce a 1% change in end-to-end distance in the macromolecule (see Table II).

Table II. Various Effects Related to Electric Field Dependence and TEFS\*

<i>Effect</i>	<i>electric field (E) dependence</i>	<i>TEFS*</i>
a) Deformation of chains containing permanent dipoles	$\Delta h/h \approx E m^{1/2} d_0 / 3kT$	$10^3 \text{ V/cm}$
b) Polarizability of a polyelectrolyte chain	$\Delta h/h \approx E^2 \alpha / 3kT$	$10^4 \text{ V/cm}$
c) Change in dissociation constant in a polyelectrolyte	$\Delta K_d/K_d \approx  E  e^3 / 8\pi\epsilon_0\epsilon(kT)^2$	$10^4 \text{ V/cm}$

$(A_p B \rightleftharpoons A_p^+ + B^-)$

\* Typical electric field strength causing 1% change

$h$  = change end-to distance;  $\epsilon_0$  = vacuum dielectric constant;  $\epsilon$  = dielectric constant

$e$  = electron charge;  $k$  = Boltzman constant;  $\alpha$  = chain polarizability

$T$  = temperature  $^\circ\text{K}$   $K_d$  = dissociation constant  $d_0$  = permanent dipole of a chain

Calculation performed as per Neuman (19).

The arguments so developed indicate that structural modifications caused by electric field effects of classes a), b) and c) can reasonably be excluded if the field strength is below  $10^2$  V/cm.

Low intensity electric fields (below 10 V/cm), however, have been shown to cause sizable size and shape changes in polyelectrolyte gels. The interpretation of the mechanisms governing contractile phenomena and volume phase transitions, which occur in polyelectrolyte gels when in direct contact with an electrode is, however, controversial. Tanaka et al. (15) attributed the volume phase transitions they observed in an ionized polyacrylamide gel under electric field to electrostatic attraction between the positive electrode and the negatively charged gel, leading to imbalance of the equilibrium swelling pressure.

We attempted to interpret experimental findings related to contractile activity in polyelectrolyte gels under electric excitation, using the model proposed by Tanaka, reaching the conclusion that the electrostatic attraction model is inadequate to describe the kinetic and electric field dependence of the observed phenomena. We investigated the origin of these electromechanical effects, and a conclusion has been reached which ascribes the observed contractile response primarily to spatio-temporal pH gradients created by electrochemical reactions as the electrodes (16).

**Continuum Models of Electrochemomechanical Response.** Theoretical models to analyze the transient electrochemomechanical (ECM) response of polyelectrolyte gels have been formulated and their adequacy tested in experiments.

Kinetic equations for chemical and electrochemical reactions and ion transport have been

coupled to formulae governing the contraction and swelling of gels. The dynamics of swelling of a gel can be analyzed by recurring to continuum models which have their foundations in the poroelastic theory formulated by Biot (17). Grodzinsky (18) developed a continuum model which extended to charged gels, and was aimed at describing mechanical transients occurring in response to changes in the composition of the fluid permeating and surrounding the gel. According to the model, the total stress  $\sigma_{ij}^T$  acting on a homogeneous, linear, isotropic gel can be expressed, in the small strain approximation, through the constitutive law:

$$\sigma_{ij}^T = K(c) \text{div}_i \delta_{ij} + 2\mu(c)(u_{ij} - 1/3 \text{div}_i u_{ij}) - (\beta(c) + P)\delta_{ij}$$

where  $K(c)$  and  $\mu(c)$  are respectively the bulk and shear moduli of the solid polymer network, which depend on the concentrations of the ionic solution in the gel interpenetrating liquid.  $\beta(c)$  is the chemical stress, which couples changes in local chemical concentrations to the local dilatation of the sample;  $u$  is the polymer displacement vector and  $\delta_{ij}$  the Kronecker index. The fluid pressure,  $P_f$ , is related to the difference between the hydrostatic pressure,  $P$ , inside the gel (relative to the bath pressure) and the osmotic pressure difference  $\Delta\pi$  (between the inside and the outside of the sample) as:

$$P_f = (P - \chi(c)\Delta\pi)$$

where  $\chi(c)$  is the membrane reflection coefficient. The fluid velocity is assumed to be related to the fluid pressure by Darcy's law:

$$U = - (1/f(c)\Delta P_f)$$

where  $U$  is the total-area averaged fluid velocity relative to the flow of fluid with respect to the solid matrix and  $1/f$  ( $C$ ) is the hydraulic permeability of the gel matrix ( $f$  is a polymer-solution friction coefficient).

Conservation of mass, assuming both liquid and solid fractions are incompressible materials, and conservation of momentum, usually neglecting inertial effects, complete the description of gel dynamics, thus leading to an equation of motion of the polymer network.

In order to account for electrochemical changes generated by electrodes for driving the actuator through modulation of the material coefficients and the chemical stress, electrodiffusion-reaction and continuity equations have to be considered:

$$J_i = -D_i \text{grad } C_i + (Z_i/|Z_i|) C_i \mu_i E + C_i v$$

and

$$\partial C_i / \partial t = -\text{div} J_i + G_i - R_i$$

where  $J_i$  is the flux of the species  $i$ ,  $Z_i$  its valence,  $\mu_i$  its mobility and  $D_i$  its diffusion coefficient.  $E$  and  $v$  are the local electric field and the local velocity of the fluid respectively.  $G_i$  and  $R_i$  are the generation and recombination rates for the chemical reactions.

The concentrations of ions inside the gel and in the external bath are linked through Donnan partition relationships. Coupling between the ion transport processes and the mechanical readjustment of the gel is taken into account by the dependence of the transport coefficients  $D_i$  and  $\mu_i$  from the local dilatation field of the polymer network, and, hence, the local water volume fraction.

Stating of appropriate initial and boundary conditions fully defines the problem.

The solution of the coupled equation system is a challenging task, even using numerical methods. However, under appropriate conditions, ion transport and mechanical readjustment phenomena can be decoupled because of the large difference in the values of their rate limiting constants.

Free swelling and stress relaxation experiments have been performed on thin cylindrical fibre, which are a suitable geometry for actuator construction. The elastic moduli and hydraulic permeability of the gel have thus been determined and used to calculate the isometric tensile force generated under rate limiting chemical stimuli (19).

In the case of gels with high elastic moduli, the rate limiting phenomena in ECM experiments generally resides in the electrodiffusion-reaction.

The requirement of high modulus fibre for actuator construction appears to favour a shorter mechanical time constant over the electrodiffusion-reaction time constant. This implies a working mechanism in which the active dynamics of the actuator is essentially governed by time needed to modulate (in space as well as in time) the gel material parameters by the electrochemically generated species (20).

The passive properties of the actuator are governed by the viscoelastic behavior in the following section.

**Dynamical Properties of Hydrogel Thin Fibres.** The free swelling and stress-relaxation behavior of thin fibres of a hydrogel can be analytically described starting from the equation of motion of the gel network in a motionless fluid phase approximation:

$$\rho \partial^2 u / \partial t^2 = \text{div } \sigma_{Tij}$$

where  $\rho$  is the density of the polymer network.

In the absence of chemical changes or concentration gradients, the chemical stress term can be omitted and the inertial term can usually be neglected, because phenomena are slow, to obtain the motion equation:

$$f \partial u / \partial t = (K + \mu / 3) (\text{grad}(\text{div}u)) + \mu \text{div}(\text{grad}u)$$

This equation, combined with the linear constitutive law of the gel, Darcy's law, the equations of conservation of mass of both the liquid and solid components, and initial and boundary conditions, has been used to predict the time course of the force developed in a stress-relaxation experiment performed on thin fibres of gel [19].

The analytical expressions for the time course of the force are very complicated. Much simpler expressions have been obtained in two limiting cases which are, respectively, the recoil force immediately after the application of a step deformation and the force at time infinity when fluid flow has ceased and only the elastic recoil force of the polymer exists.

The time constant for the stress-relaxation process above has also been calculated and has been shown to have a multiexponential behavior. The limiting (single exponential) time constant has been found to be (19).

where  $d$  is the fibre diameter and  $\alpha_0 = 0.767$ .

$$\tau_0 = (d^2 / 4\alpha_0^2 \pi^2) (f / \mu)$$

**A Lumped Parameter Model of the Mechanical Behavior of a Gel Fibre.** The continuum approach is useful for determining the concentration of chemicals and the stress in the gel in space and time. Since dynamic control of the actuator requires a fast feedback loop, the complex equations describing the phenomena have to be reduced to a manageable form by appropriate simplifications.

A lumped parameter model which is suitable for representing the passive viscoelastic behavior of a gel fibre is the standard viscoelastic solid (SVS) which is thought to hold when the solid polymer component behaves as an elastic material.

Referring to (Figure 3) the dynamic equations of the SVS can be expressed as:

$$F_a = (\mu_a / S l_0) (l_p + x - x')$$

$$F_b = (\mu_0 S / l_0) (l_p + x - l_0)$$

$$-(\mu_a S / l_0) (x') + F_a = 0$$

$$F = F_a + F_b$$

where  $l_0$  is the unstrained length,  $l_p$  the pretensioned length,  $x$  is the instantaneous length of the gel fibre, and  $x'$  is the fictitious instantaneous length at the point A'.  $S$  is the resisting cross section of the fibre and  $\mu_a$ ,  $\mu_b$ ,  $\pi_a$ , are the elastic and viscous moduli of the SVS, respectively.

The dependence of the parameters on the material coefficients of the gel, as they appear in the continuum model, can be deduced by assuming that, instantly, following the application of a step deformation, the gel fibre (at time  $t = 0^+$ ) behaves as an incompressible medium. Thus, by equating the resisting force of the linear viscoelastic solid submitted to a step elongation to the force calculated for the gel fibre at time  $t = 0^+$  (whose polymeric component has a bulk modulus  $k$ , a shear modulus  $\mu$ , and a polymer-solution friction coefficient,  $f$ ) we have:

$$\mu_a + \mu_b = 3 \mu$$

Also equating at time  $t = \infty$ , the asymptotic force value of the linear viscoelastic solid with the corresponding expression for the gel fibre, we obtain:

$$\mu_b = [9(k/\mu)/(1 + 3(k/\mu))] \mu$$

Then, by combining these equations it follows that

$$\mu_a = [3/(1 + 3(k/\mu))] \mu$$

Finally, by equating the time constant of the viscoelastic solid to the limiting stress-relaxation decay time constant of the gel fibre we obtain:

$$\tau_0 = (d^2/4\alpha_0^2\pi^2)(f/\mu) = (S/\alpha_0^2\mu^3)(f/\mu) = \eta_a/\mu_a$$

The expression for the viscous modulus is obtained as:

$$\eta_a = (S/\alpha_0^2\pi^3)[3(f/\mu)/1 + 3(k/\mu)] \mu$$

The expression above can be reasonably assumed to hold for the general case of an arbitrary force history.

An additional simplification which has been used consists in regarding  $f/\mu$  and  $K/\mu$  as substantially independent of the gel chemical status.

Thus, as a consequence of the assumptions above, the dynamic behavior of the contractile gel fibres, under electrochemically generated spatio-temporal gradients of ion concentration substantially relies upon a characterization of the terms  $\mu_a$ ,  $\mu_b$ ,  $\tau_a$ , as functions of gel proton and salt concentrations. Although the reduction of a contractile gel fibres to an SVS with tuneable parameters necessarily obscures some of the complexities of the real system, it makes it possible to devise and implement strategies and algorithms for the control of robotic end-effectors.

**Control Strategies for the Motion of Articulated Chain.** Throughout this work, the application of polyelectrolyte gels to pseudomuscular force-position actuators has been stressed.

We also investigated (20) on a lumped parameter model of a fibre bundle and a control scheme to move a finger-like articulated chain, in which joint rotation was imposed by an agonist-antagonist actuator couple working in a push-pull control configuration (Figure 4).

The SVS rest length, elastic and viscous coefficients were tuned by electrochemically generated pH changes with an experimentally determined sigmoidal function. With this system, each joint actuator-couple behaves as a pure negative position feedback loop with little damping and an offset. Then, we proposed the use of a linear time-invariant servo-system to control the chain, a solution which is satisfactorily used in many practical robotic applications.

On the basis of some macroscopic similarities between muscle structure and the parallel fibre actuator, we also devised and analyzed a control scheme based on the concept of recruitment (21). The recruitment scheme can be accomplished by progressively activating parallel subunits constituting the actuator. By modulating the number of driven actuators, from a fully contracted to a fully relaxed state, the total tensile force of the whole actuator can be controlled.

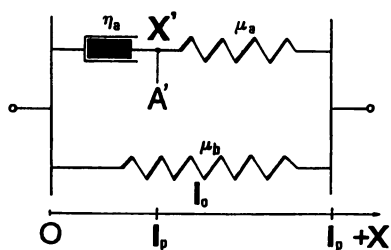


Figure 3. Lumped parameter model

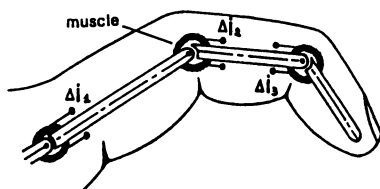


Figure 4. Finger-Like articulated chain



Although potentially more stable and precise than the previous scheme, recruitment control requires addressing of individual fibres or bundles in the actuator. The practical feasibility of this kind of actuator remains however, still to be demonstrated.

**Representing and Regularizing Motor Redundancy.** The importance of viscoelastic properties of muscle in human motor control has long been recognized although the proposition that the angular position of a joint is determined by the equilibrium point between the length-tension curve of the agonist and antagonist muscles is a notion that blurs the distinction between gesture and movement (22).

Using this approach, postures are coded by the distribution of neuromuscular activity in a series of equilibrium configurations that "attract" the different hand segments in response to mismatches, due either to external or internal disturbances (23).

A constraint, which may be an obstacle or a manipulated object, inhibits the planned movement and transforms it into a contact force. Therefore, movement and force planning can be causally related to the same mechanism.

The purpose of the neural controller we are developing (24) is to provide a computational architecture which naturally exploits the actuator-mechanical properties and is able to generate "synergies", i.e. to coordinate the activity of a multi-actuator redundant mechanical system. This problem includes, but goes well beyond, the so called "inverse kinematics" which is usually restricted to "open" kinematic chains for a single task (generation of assigned trajectories of the terminal element of the kinematic chain).

The neural controller that we are developing is based on a principle of motor control that is called "Passive Motion Paradigm" (PMP). This principle states that whatever the kinematic complexity of a motor system, if the actuators have viscoelastic properties, then the synergy of actuator commands necessary to carry out a desired movement can be obtained via the simulation of a passive movement, i.e. the movement determined by an external "virtual" disturbance. The basic underlying principle is that the elastic properties of muscles provide an effective analog mechanism for automatically and uniquely distributing the motion to all the parts according to the least variations of potential energy (a constraint that expresses passivity).

From these concepts, it is possible to outline a controller whose input is the "virtual" disturbance which represents the intended direction of the planned movement. It operates as an analogic computer, determining a succession of equilibrium configurations of the global actuator-mechanical system from which the control variables of the actuators are extracted.

In particular, the mechanism that we have proposed for implementing the PMP is a relaxation network, that, similar to the Hopfield networks (25), is attracted by configurations of minimum potential energy. We use spring-like elastic devices in the network not only for the pseudo-muscular actuators but also to express additional constraints such as joint limits. In this sense, we may conceive them as generalized "ligaments", in a sort of Eulerian representation of kinematic constraints.

We are currently working in order to implement the system in a parallel simulation environment. It is a neural network which can be conveniently implemented on a mid-grained architecture like a transputer system because the number of units is limited and each of them has a significant computational load. We expect to reach, with a suitable configuration, real-time performance, which can allow the model to operate as a neural controller of an artificial hand driven by a large number of pseudo-muscular actuators.

## Literature Cited.

- [1] Drexler, K.E. *Nanosystems: Molecular Machinery, Manufacturing and Computation*; John Wiley, New York, (NY), 1992, pp
- [2] Aizawa, S. I. "Reconstruction of the flagellar motor". Bionic Design International Workshop, Tsukuba, Japan, Jan 29-30, 1992.

- [3] Ishijima, A.; Doi, T.; Sakurada, K.; Yanagida, T. *Nature* 1991, *vol.* 352, pp. 301-396.
- [4] De Rossi, D.; Suzuki, M.; Osada, Y.; Morasso, P. *J. of Intell. Mater. Syst. and Struct.*, 1992, *vol.* 3, pp. 75-95.
- [5] Wang, T. T.; Herbert, J. M. In *The applications of ferroelectric polymers*; Glass A. M. Eds.; Blackie: Glasgow, 1988, pp.
- [6] Toda, M. *Trans. IECE of Japan E-61* 1978, *vol.* 7 pp. 513-518.
- [7] Umetani, Y.; Suzuki, H. "Piezoelectric micromanipulator in multi-degrees of freedom with tactile sensibility". *Proc. 10<sup>th</sup> ISIR Milan*, 1980, pp. 572-579.
- [8] Baugham, R.H.; Shacklette, L. W. Elsenbaumer, R. L.; Plichta, E.; Becht, C. Brédas, J. L. In *Conjugated Polymeric Materials*, Chance R.R. Ed.; Kluwer Academic Pub, Netherlands, 1990, pp. 559-582.
- [9] Pei, Q.; Inganás, O. *Advanced Materials*; 1992, *vol.* 4, pp. 277-278.
- [10] Yoshino, K.; Nakao, K.; Sugimoto, R. *Japanese J. of Applied Physics* 1989, *vol.* 28, pp.490-492.
- [11] *Polymer Gels: "Fundamentals and Biomedical Applications"*; De Rossi, D.; Osada, Y.; Yamauchi, A.; Kajiwara, K. Eds.; Plenum Press, London, UK, 1991.
- [12] Osada, Y. *Advances in Polymer Science*, 1987, *vol.* 82, pp.3-46.
- [13] Chiarelli, P.; Umezawa, K. In *Polymer Gels: "Fundamentals and Biomedical Applications"*; De Rossi, D.; Osada, Y.; Yamauchi, A.; Kajiwara, K. Eds.; Plenum Press, London, UK, 1991..
- [14] Neumann, E. In *Ions in Macromolecular and Biological Systems*; Everett D.H.; and Vincent B. Eds.; Univ. Park Press, Baltimore, 1978.
- [15] Tanaka, T.; Nishio, I.; Shao-Tang, S.; Ueno-Nishio, S. *Science*, 1982, *vol.* 218, pp.467-470.
- [16] De Rossi, D.; Chiarelli, P.; Buzzigoli, G.; Domenici, C.; and Lazzeri, L. *Trans. Am. Soc. Artif. Int. Organs. XXXII*, 1986, pp.157-162.
- [17] Biot, M. A. *J. Appl. Phys.*, 1955, *vol.* 26 pp.182-191.
- [18] Grodzinsky, A. *J.CRC Critical Rev. Biomed. Eng.*, 1983, *vol.* 9(2), pp.133-199.
- [19] Chiarelli, P.; De Rossi, D. *J. of Int. Material Systems and Structures*, 1992, *vol.* 3, N. 3 (1991) pp.
- [20] Genuini, G.; Casalino, G.; Chiarelli, P.; De Rossi, D. In *Kinematic and Dynamic Issue in Sensor Based Control*; G. E. Taylor Ed.; NATO ASI Series, Springer Verlag, Berlin, 1990, *vol.* F 57, pp. 341-360.
- [21] Casalino, G.; Chiarelli, P.; De Rossi, D.; Morasso, P.; Umezawa, K. "Progress in the design and control of pseudomuscular linear actuators", ARW-NATO: Robots and Biological Systems, il Ciocco Lucca, June 1989, pp.26-30.
- [22] Feldman, A. G. *Biophysics* 1966, *vol.* 11 pp.137-144.
- [23] Abend, W.; Bizzi, E.; Morasso, P. *Brain*, 1982, *vol.* 105, pp.331-348.
- [24] Casalino, G.; De Rossi, D.; Morasso, P.; Solari, M. paper presented at Int. Conf. on Advanced Robotics (ICAR 91), 1991, Pisa, Italy.
- [25] Hopfield, J. J. *Proc. Nat. Acad. Sci., U.S.A.*, 1982, *vol.* 79, pp.2554-2558.
- [26] Volkenshtein, M. V. *Biophysics*; MIR, Moscow, (Russia), 1983, p. 435.

RECEIVED August 6, 1993

## Author Index

- Adachi, S., 466  
Ahmed, Lasker S., 225  
Amis, Eric J., 322  
Ander, Paul, 180  
Anderson, John L., 67  
Arscott, Patricia G., 195  
Baran, A. A., 406  
Bárány, S., 406  
Basinska, T., 449  
Behilo, Kerrie, 180  
Belloni, L., 381  
Bloomfield, Victor A., 195  
Borsali, R., 315  
Bratko, D., 34  
Candau, S. J., 287  
Chiarelli, Piero, 517  
Clungeon, N. S., 394  
Cramer, S. M., 144  
Dalbiez, J. P., 381  
Daoud, M., 45  
Dautzenberg, H., 210  
Dawson, K. A., 34  
Delsanti, M., 381  
De Rossi, Danilo, 517  
Devore, D. I., 394  
Drifford, M., 381  
Dubin, Paul L., 225  
Ebihara, Toyokichi, 507  
Essafi, W., 278  
Fischer, S. A., 394  
Fisher, M. M., 114  
Gadam, S. D., 144  
Gao, Yueying Y., 98  
Hamielec, A. E., 162  
Hartmann, J., 210  
Hatton, T. A., 144,257  
Hertler, W. R., 144,257  
Hirata, Mitsuo, 493  
Hunkeler, D., 162  
Igarashi, K., 466  
Ise, Norio, 349  
Jang, C. J., 257  
Kamachi, M., 243  
Kogej, Ksenija, 268  
Kokufuta, Etsuo, 225,493,507  
Kotaka, T., 466  
Kowalczyk, D., 449  
Kremer, Kurt, 57  
Lafuma, F., 278  
Ma, Chenglie, 195  
Maeda, H., 499  
Malovikova, A., 315  
Matsuda, Kiyomi, 493,507  
Matsukawa, Shingo, 507  
Matsuoka, Hideki, 349  
Meyer, Ellen M., 131  
Milas, M., 315  
Morishima, Y., 243  
Moussaid, A., 287  
Munch, J. P., 287  
Nomura, S., 243  
Odijk, Theo, 86  
Ojima, H., 499  
Okubo, T., 364  
Patrickios, C. S., 144,257  
Pelton, R. H., 162  
Petkanchin, I. B., 436  
Reščič, J., 24  
Reed, Wayne F., 297  
Rinaudo, M., 315  
Rother, G., 210  
Sasaki, S., 499  
Schmitz, Kenneth S., 1,98  
Schosseler, F., 287  
Schwahn, Dietmar, 349  
Sedlák, Marián, 322,337  
Seki, M., 243  
Shaaban, Amer H., 180  
Shikata, T., 466  
Singh, Narinder, 98  
Škerjanc, Jože, 268  
Slomkowski, S., 449  
Solomentsev, Yuri, 67  
Solomentseva, I., 406  
Spalla, O., 381  
Stellwagen, John, 479  
Stellwagen, Nancy C., 479  
Stevens, Mark J., 57  
Strauss, Ulrich P., 154

- Valachovic, Diane E., 322  
 Varoqui, R., 421  
 Vasconcellos, Stephen R., 131  
 Velichanskaya, L., 406  
 Vlachy, V., 24  
 Wang, F. W., 449  
 Williams, C. E., 278  
 Woods, D. R., 162  
 Wu, X. Y., 162  
 Xia, Jiulin, 225  
 Yamada, Kazunori, 493  
 Zdanowicz, Vincent S., 154  
 Zhong, Yuanzhen, 154

## Affiliation Index

- Betz Industrial, 131  
 Bulgarian Academy of Sciences, 436  
 CNR (Italian Research Council), 517  
 Carnegie Mellon University, 67  
 Center of Molecular and Macromolecular  
 Studies, 449  
 Centre National de la Recherche  
 Scientifique, 315  
 Centre d'Etude de Saclay, 45,381  
 Centre de Recherches sur les Macromolécules  
 Végétales, 297,315  
 Cytec Industries, 114  
 Delft University of Technology, 86  
 Ecole Supérieure de Physique et de Chimie  
 Industrielle, 278  
 Henkel Corporation Research and  
 Development, 394  
 Indiana University—Purdue University at  
 Indianapolis, 225  
 Institut für Festkörperforschung, 57,349  
 Joseph Fourier University, 315  
 Kyoto University, 349,364  
 Kyushu University, 499  
 Massachusetts Institute of Technology,  
 144,257  
 Max-Planck-Institute of Colloid and Interface  
 Research, 210  
 McMaster University, 162  
 National Institute of Standards and  
 Technology, 449  
 Nihon University, 493,507  
 Osaka University, 243,466  
 Rengo Company Ltd., 349  
 Rutgers, The State University of New  
 Jersey, 154  
 Seton Hall University, 180  
 Slovak Academy of Sciences, 315,322,337  
 Ukrainian Academy of Sciences, 406  
 Université Louis Pasteur, 287,421  
 University of California—Berkeley, 34  
 University of Iowa, 479  
 University of Ljubljana, 24,268  
 University of Minnesota, 195  
 University of Miskolc, 406  
 University of Missouri—Kansas City, 1,98  
 University of Paris-Sud, 278  
 University of Pisa, 517  
 University of Southern California, 322  
 University of Tsukuba, 225,493,507  
 Vanderbilt University, 162

## Subject Index

### A

- Acrylamide, base-initiated polymerization  
 mechanism, 115–116  
 Acrylic polyampholyte(s)  
 chromatographic characterization, 145–152  
 description, 257  
 properties, 144–146f  
 structures, 144,146f  
 Acrylic polyampholyte(s)—*Continued*  
 use in protein separation, 257  
 Acrylic polyampholyte–protein interaction  
 back-titration, 259,263f,264  
 experimental procedure, 258  
 future work, 267  
 Langmuir plot of complexation, 264,265f  
 lysozyme complexation, 264,266f  
 optical densities, 259,262–263f

- Valachovic, Diane E., 322  
 Varoqui, R., 421  
 Vasconcellos, Stephen R., 131  
 Velichanskaya, L., 406  
 Vlachy, V., 24  
 Wang, F. W., 449  
 Williams, C. E., 278
- Woods, D. R., 162  
 Wu, X. Y., 162  
 Xia, Jiulin, 225  
 Yamada, Kazunori, 493  
 Zdanowicz, Vincent S., 154  
 Zhong, Yuanzhen, 154

## Affiliation Index

- Betz Industrial, 131  
 Bulgarian Academy of Sciences, 436  
 CNR (Italian Research Council), 517  
 Carnegie Mellon University, 67  
 Center of Molecular and Macromolecular  
 Studies, 449  
 Centre National de la Recherche  
 Scientifique, 315  
 Centre d'Etude de Saclay, 45,381  
 Centre de Recherches sur les Macromolécules  
 Végétales, 297,315  
 Cytec Industries, 114  
 Delft University of Technology, 86  
 Ecole Supérieure de Physique et de Chimie  
 Industrielle, 278  
 Henkel Corporation Research and  
 Development, 394  
 Indiana University—Purdue University at  
 Indianapolis, 225  
 Institut für Festkörperforschung, 57,349  
 Joseph Fourier University, 315  
 Kyoto University, 349,364  
 Kyushu University, 499  
 Massachusetts Institute of Technology,  
 144,257
- Max-Planck-Institute of Colloid and Interface  
 Research, 210  
 McMaster University, 162  
 National Institute of Standards and  
 Technology, 449  
 Nihon University, 493,507  
 Osaka University, 243,466  
 Rengo Company Ltd., 349  
 Rutgers, The State University of New  
 Jersey, 154  
 Seton Hall University, 180  
 Slovak Academy of Sciences, 315,322,337  
 Ukrainian Academy of Sciences, 406  
 Université Louis Pasteur, 287,421  
 University of California—Berkeley, 34  
 University of Iowa, 479  
 University of Ljubljana, 24,268  
 University of Minnesota, 195  
 University of Miskolc, 406  
 University of Missouri—Kansas City, 1,98  
 University of Paris-Sud, 278  
 University of Pisa, 517  
 University of Southern California, 322  
 University of Tsukuba, 225,493,507  
 Vanderbilt University, 162

## Subject Index

### A

- Acrylamide, base-initiated polymerization  
 mechanism, 115–116  
 Acrylic polyampholyte(s)  
 chromatographic characterization, 145–152  
 description, 257  
 properties, 144–146f  
 structures, 144,146f
- Acrylic polyampholyte(s)—*Continued*  
 use in protein separation, 257  
 Acrylic polyampholyte–protein interaction  
 back-titration, 259,263f,264  
 experimental procedure, 258  
 future work, 267  
 Langmuir plot of complexation, 264,265f  
 lysozyme complexation, 264,266f  
 optical densities, 259,262–263f

Acrylic polyampholyte–protein interaction—  
*Continued*  
 polyampholytes, properties, 258,260*t*  
 polymer concentration vs. turbidity,  
 259,261*f*  
 ribonuclease complexation, 264,265*f*  
 salt concentration vs. complexation,  
 259,262*f*  
 salt concentration vs. turbidity, 259,261*f*  
 time dependence of aggregation vs.  
 polymer concentration, 259,260*f*

Actuators, biomimetic macromolecular, *See*  
 Biomimetic macromolecular actuators

Adsorption of macromolecules from solution  
 onto solids, occurrence, 406

Adsorption of neutral polymers and poly-  
 electrolytes on model colloid particles by  
 electrooptics  
 adsorbed layer thickness vs. polyacrylamide  
 concentration, 443,445*f*  
 $\gamma$ -Al<sub>2</sub>O<sub>3</sub> preparation, 439  
 dispersion dependence of  $\beta$ -ferric hydroxide,  
 440–442*f*  
 electric light scattering method, 437–439  
 electrooptical effect  
 vs. (carboxymethyl)cellulose, 444,445*t*  
 vs. field frequency in (carboxymethyl)cell-  
 ulose, 444,446*f*  
 vs. polyacrylamide concentration,  
 441–443,445*f*  
 electrophoretic mobility vs. polyacrylamide  
 concentration, 441,442*f*  
 experimental description, 437  
 $\beta$ -ferric hydroxide preparation, 439  
 kaolinite preparation, 439  
 mica preparation, 439  
 neutral polymer preparation, 440  
 polyelectrolyte preparation, 440  
 reasons for interest, 436–437  
 SiO<sub>2</sub> preparation, 439–440

Adsorption of polyelectrolytes  
 dilute solution studies, 421  
 latex suspension effect, 406–419

Adsorption properties, thermosetting cationic  
 polyelectrolytes, 394–405

Agarose, description, 480

Agarose gels, use as nonconvective medium  
 for DNA gel electrophoresis, 479

Alcohol, DNA condensation effect,  
 202–206

Alkyl sulfate surfactants, swelling equilibria  
 effect for cationic polyelectrolyte gel from  
 polyethylenimine, 493–498

Amphiphilic polyelectrolyte(s)  
 hydrophobic photoactive chromophore  
 incorporation, 243–244  
 micellar structure formation, 243

Amphiphilic polyelectrolyte–surfactant  
 coulombic complexes  
 characterization in organic solution,  
 249–251*f*,253*f*  
 fluorescence from pyrene labels, 252,254*f*  
 hydrophobic self-organization of amphi-  
 philic polyelectrolytes in aqueous solu-  
 tion, 244–247*t*  
 photoinduced electron transfer, 252,254–255  
 preparation, 246,248–250*f*  
 proposed structure, 252,253*f*  
 reasons for interest, 244  
 unimolecular micelle evidence in amphi-  
 philic polyelectrolytes, 246,247*f*

Angular maxima for static and dynamic  
 scattering, description, 301–302

Apparent cooperative diffusion constant of  
 polymer network, definition, 502,504

Apparent diffusion coefficient  
 classification of profiles, 14–16*f*  
 interpretation of class 3 profiles, 17–19  
 NaBr concentration effect, 13–15*f*

Aqueous salt-free solutions, electric trans-  
 port of polyelectrolytes, 180–193

## B

Biased sinusoidal field gel electrophoresis  
 definitions, 466  
 features, 467

Biochemo-mechanical system(s), 507–508

Biochemo-mechanical system construction  
 using polyelectrolyte gels design, 508*f*,509  
 enzymatically controlled protein  
 release, 515*f*  
 enzymatically induced volume  
 changes, 514*f*  
 experimental procedure, 509–510  
 glucose vs. swelling, 513*f*  
 pH-induced volume change in gel, 508*f*  
 pH vs. swelling, 510,511*f*  
 urea vs. swelling, 510–513

- Biomimetic macromolecular actuators  
molecular actuators, 518–522  
pseudomuscular gel actuators, 522–529
- Birefringence, 480–481
- Block and graft copolymers, commercial importance, 114
- Bovine serum albumin–poly(dimethyldiallyl ammonium chloride), stoichiometric and nonstoichiometric complex formation, 225–241
- Branched polyelectrolyte conformation, random, *See* Randomly branched polyelectrolyte conformation
- C**
- $\beta$ -Carrageenan, description, 480
- $\beta$ -Carrageenan gels, electric birefringence, 488,489*f*
- Cation(s), multivalent, role in DNA condensation, 195–206
- Cationic polyelectrolyte gel from polyethylenimine, pH and alkyl sulfate surfactant effects on swelling equilibria, 493–498
- Cetylpyridinium–poly(styrenesulfonic acid) complex solutions, electrical transport, 268–274
- Chain of equal size spheres, electrophoresis, 78–82
- Characterization of polyacrylamide-*co*-sodium acrylate  
copolymer characterization procedure, 164  
dialysis procedure, 164  
experimental objectives, 162–163  
fractionation procedure, 164  
hydrolytic procedure, 164  
intrinsic viscosity determination procedure, 164  
light scattering characterization, 165–168*t*  
light scattering procedure, 165  
polyacrylamide characterization, 165,167*t*  
polymer preparation procedure, 163–164  
size exclusion chromatographic procedure, 164  
size exclusion chromatography, 169–176  
universal calibration method, 163  
viscometric characterization, 166,169,170*f*
- Charge densities, polyelectrolyte solution structure effect, 278–285
- Charged polymer chains, molecular dynamics simulations, 57–66
- Charged surfaces, weakly charged polyelectrolyte structure and stability at solid–liquid interface, 423–432
- Chemomechanical system, definition, 507
- Cholesteric phase, undulation-enhanced forces in hexagonal gels of semiflexible polyelectrolytes, 87–89*f*
- Chromatographic characterization of acrylic polyampholytes  
experimental description, 145  
frontal experiment(s), 149–152*f,t*  
frontal experimental procedure, 145,147  
gradient elution, 145–150*f*  
pH effect, 151,152*t*  
polymer type effect, 149–152*f*  
salt concentration effect, 151,152*t*
- Class 3 profile interpretations  
cluster domain, 18–19  
filterable aggregate, 17–18  
o–e transition, 19  
temporal aggregate, 18–19
- Cluster domain interpretation, class 3 profiles, 18–19
- Cluster size determination in polyelectrolyte solutions by small-angle neutron scattering  
comparison with dynamic light scattering results, 358  
experimental description, 350  
model calculation of structure, 358–362*t*  
polymer concentration vs. scattering curves, 350,351*f*  
salt concentration vs. scattering curves, 350–352  
small-angle neutron scattering measurement procedure, 350  
studies, 349–350  
upturn  
Debye–Bueche analysis, 355,356*f*  
Guinier analysis, 352–355  
origin, 357–358  
Porod analysis, 355–357  
void model structure, 360–362*t*
- Clustering of counterions around linear polyelectrolytes in solution, 24
- Coacervation, description, 226
- Colloidal crystals, morphology, 364–365
- Colloidal particles, adsorption of neutral polymers and polyelectrolytes by electrooptics, 436–446

Composite diffusion coefficient, direct macro-ion–macro-ion interactions in strong interaction limit, 103–104

Concentrated regime, randomly branched polyelectrolyte conformation, 53,54f

Concentration of polymers, role in polyelectrolyte complex formation, 210–223

Condensation, description, 195

Condensation of DNA, role of multivalent cations, 195–206

Condensed counterion, operational definition, 9

Conducting polymers, use as actuators, 520

Configuration of ionized macromolecule in solution, influencing interactions, 34

Conformation, randomly branched polyelectrolytes, 45–55

Continuum models of electrochemomechanical response, description, 524–525

Correlation hole effect, description, 284

Coulombic amphiphilic polyelectrolyte–surfactant complexes, *See* Amphiphilic polyelectrolyte–surfactant coulombic complexes

Counterion condensation  
description, 8–10  
theory of Manning, description, 180–181

Cylindrical polyon, ion–ion correlations in electrical double layer, 24–33

**D**

Debye–Bueche analysis, use for cluster size determination in polyelectrolyte solutions, 355,356f

Debye–Hückel length, characterization of screening effects, 45

Derjaguin–Landau–Verwey–Overbeek theory, interactions between macro-ions, 1–2

Diffusion coefficient,  $q$ -dependent  
apparent, *See*  $q$ -dependent apparent diffusion coefficient

Dilute solution(s) of polyelectrolytes  
light scattering studies, 297–313  
low salt content vs. viscometric behavior, 315

Direct macro-ion–macro-ion interactions in strong interaction limit, 103–104

DNA  
conformation, 195

DNA—*Continued*  
role of multivalent cations in condensation, 195–206

$\phi$ -DNA, production, 195–196

DNA molecular dynamics under gel electrophoresis  
behavior measurement  
biased sinusoidal field conditions, 467,469,470f,472f  
steady field gel electrophoresis, 467,468f

experimental frequency-domain electric birefringence procedure, 469

experimental gel electrophoretic procedure, 466

fluorescence microscopy, 471,474–477f

frequency-domain electric birefringence, 469,471,472–473f

Dry tests, 449

Dynamic Kerr coefficient, 469,471

Dynamic light scattering correlation function, slow modes, 13–19

Dynamic light scattering for dilute solution properties of polyelectrolytes, *See* Light scattering for dilute solution properties of polyelectrolytes

Dynamic properties  
hydrogel thin fibers, 525–526  
weakly ionized poly(acrylic acid) in deuterated water, 290,292–295

Dynamics, linear flexible polyelectrolytes in salt-free solution using light scattering, 322–335

Dynamics–structure relationship, water-soluble polymers, 287–295

**E**

Electric light scattering method, 437–439

Electric transport of polyelectrolytes in aqueous salt-free solutions  
calculated interaction parameter, 191,193f  
conductivity measurement, 185  
counterion mobility vs. charge density, 187,190–191f  
electric mobility vs. charge density, 187,189f  
electric mobility vs. concentration, 185,186t,188f  
equivalent conductance vs. charge density, 187,188–189f



- Electric transport of polyelectrolytes in aqueous salt-free solutions—*Continued*  
equivalent conductance vs. concentration, 183,184*f*,191,192*f*  
interaction parameter vs. charge density, 187,191,192*f*  
isotachophoretic procedure, 181–182  
polyelectrolyte preparation procedure, 182,184*r*  
polyion specific conductance vs. polymer concentration, 185,187,188*f*  
reduced viscosity vs. charge density, 187,190*f*  
specific conductance vs. concentration, 183,185,186*f*
- Electrical double layer, ion–ion correlations around cylindrical polyion, 24–33
- Electrical interactions, role of screening parameter, 5
- Electrical transport in polyelectrolyte–surfactant complex solutions  
apparatus, 269  
experimental procedure, 269  
fraction of free counterions vs. concentration, 269,272*f*–274  
molar conductivity vs. concentration 269–271*f*
- Electrochemomechanical response, continuum models, 524–525
- Electrolyte dissipation, description, 103
- Electrolyte ions, role in attraction between identical macro-ions, 11–12
- Electrooptical effect, definition, 437–438
- Electrooptics, adsorption of neutral polymers and polyelectrolytes on colloid particles, 436–446
- Electrophoresis, function, 67
- Electrophoresis of nonuniformly charged chains  
experimental description, 68,70  
polymer–colloidal complexes, 70–73  
slender particles, 73–85
- Electrophoretic mobility, definition, 67–68
- Electrostatic excluded volume, 299–300
- Electrostatic interactions, screening for randomly branched polyelectrolytes, 49–52
- Electrostatic persistence length  
description, 299  
stiff vs. flexible polyelectrolytes, 12–13
- Epichlorohydrin, carcinogenicity, 395
- Equal size sphere chain, electrophoresis, 78–82
- Excluded volume, electrostatic, 299–300
- Extraordinary behavior of salt-free polyelectrolyte solutions using light scattering  
binary mixtures, 339–342*t,f*  
experimental procedure, 338  
nonelectrostatic interactions, role in slow mode mechanism, 341,343–346  
sample filtration vs. slow mode behavior, 345–348
- F
- Filterable aggregate interpretation, class 3 profiles, 17–18
- Flagellar rotary motor, 518,521*f*
- Flexible polyelectrolytes, electrostatic persistence length, 12–13
- Fluid pressure and velocity, definition, 524
- Fluorescence from pyrene labels, amphiphilic polyelectrolyte–surfactant coulombic complexes, 252,254*f*
- Fluorescence microscopy, moving DNA molecules, 471,474–477*f*
- Frequency-domain electric birefringence, DNA molecular dynamics, 469,471–473*f*
- G
- Gel electrophoresis  
applications, 466  
DNA molecular dynamics, 467–470,472
- Gel permeation chromatography–low-angle laser light scattering, molecular weight distributions of water-soluble polyelectrolytes, 131–142
- Gel structure effect on matrix orientation in pulsed electric fields  
 $\beta$ -carrageenan gels, 488,489*f*  
experimental procedure, 480–481  
future work, 491  
HEEO agarose gels, 486–489*f*  
LE agarose gels, 481–487  
polyacrylamide gels, 488–490  
polymer gel preparation, 480
- Generalized diffusion equation, interacting hard sphere systems, 99

Gibbs free energy  
 comparison to Helmholtz free energy for describing macro-ion systems, 10–11  
 description, 7  
 Global screening parameter, definition, 4  
 $\gamma$ -Globulins  
 behavior at poly(styrene-acrolein) latex-solvent interfaces, 449–462  
 description, 450  
 Glucose dehydrogenase, use in biochemical-mechanical systems, 513–514f  
 Graft copolymer synthesis, 114  
 Grand canonical Monte Carlo method  
 calculation, 26–27  
 description, 25  
 Guinier analysis  
 description, 352  
 use for cluster size determination in poly-electrolyte solutions, 352–355

**H**

HEEO agarose gel structure effect on matrix orientation in pulsed fields  
 asymmetric reversing electric fields, 486,488,489f  
 symmetric reversing electric fields, 486,487f  
 Helmholtz free energy  
 comparison to Gibbs free energy for describing macro-ion systems, 10–11  
 description, 5–7  
 Hexagonal gels of semiflexible polyelectrolytes, undulation-enhanced forces, 86–96  
 Human serum albumin  
 behavior at poly(styrene-acrolein) latex-solvent interfaces, 449–462  
 description, 450  
 Hydrodynamic interaction, description, 103  
 Hydrodynamic radius, description, 301  
 Hydrogel thin fibers, dynamical properties, 525–526  
 Hydrolyzed alternating copolymers of maleic anhydride and alkyl vinyl ethers, 154–155  
 Hydrophobic polyelectrolytes, microdomain size determination by luminescence quenching, 154–160

**I**

Inner region, definition, 4  
 Interacting hard sphere systems, generalized diffusion equation, 99  
 Interparticle interactions, study problems, 98  
 Ion-exchange displacement chromatography of proteins, 144  
 Ion-ion correlations in electrical double layer around cylindrical polyion cell model, 25–26  
 comparison to other theories, 28,33  
 counterion-coion correlation, 28–31f  
 counterion-counterion correlation function, 27–31f  
 grand canonical Monte Carlo calculation, 26–27  
 grand canonical Monte Carlo method, 25  
 mean activity coefficient of bulk electrolyte, 27t  
 Poisson-Boltzmann equation, 26  
 rate constant ratio for energy transfer between cations vs. DNA concentration, 28,32f  
 studies, 24  
 Ionic colloidal crystal phase diagram  
 close-up photography procedure, 365–366  
 close-up video film procedure, 366  
 color vs. size, 371,373f  
 critical concentrations of melting for aqueous suspensions of spheres, 371,375t  
 crystallization vs. spectra, 371,376f  
 effective diameter vs. intersphere distance, 377,378f  
 electrical double layer near surface, 371,377  
 energy parameter vs. intersphere distance, 377,379f,380  
 experimental materials, 365t  
 growing process, 371,375f  
 melting temperature(s), 366,377,379f  
 phase diagram between crystalline and liquidlike structures, 377,378f  
 reflection spectroscopic procedure, 366  
 single crystals  
 close-up photograph, 366,367f  
 shapes, 366,368f  
 size estimation, 371,376f  
 size vs. shape, 371,374f

- Ionic colloidal crystal phase diagram—*Continued*  
size vs. sphere concentration, 366,369–372*f*
- Ionic colloidal suspensions, structures, 364
- Ionic polymer gels, degree of expansion vs. salt concentration, 499
- Isoionic dilution, sodium polygalacturonate, 316,317*t*,318*f*
- Isotropic phase, undulation-enhanced forces in hexagonal gels of semiflexible polyelectrolytes, 87–89*f*
- L**
- Langmuir theory, interactions between macro-ions, 1
- Latex suspensions, role of polyelectrolyte adsorption and stability, 406–419
- LE agarose gel structure effect on matrix orientation in pulsed fields  
asymmetric reversing field pulses, 486,487*f*  
electric fields  
  high-voltage, 481,482*f*  
  low-voltage, 481,483  
  polarity, 484,485*f*  
  symmetric reversing, 484,486,487*f*  
relaxation times, 483–485*f*  
saturation of birefringence, 484,485*f*
- Light scattering, structure and dynamics of linear flexible polyelectrolytes in salt-free solution, 322–335
- Light scattering characterization of polyacrylamide-*co*-sodium acrylate  
comparison to size exclusion chromatography, 172,175*t*,176*f*  
molecular weight method, evaluation, 166–168*t*  
refractive index increment determination, 165–166
- Light scattering for dilute solution properties of polyelectrolytes  
aggregate problem, 303–304  
angular maxima, 301–302  
apparatus, 302  
apparent persistence length estimation, 304–305  
broad angular scattering maxima occurrence, 310–312  
electrostatic excluded volume, 299–300
- Light scattering for dilute solution properties of polyelectrolytes—*Continued*  
electrostatic excluded volume vs. electrostatic persistence length theories, 307–308  
electrostatic persistence lengths, 299  
hydrodynamic radius, 301  
liquidlike correlations between particles, 310  
mean square radius of gyration estimation, 304–305  
mean square radius of gyration vs. hydrodynamic radius, 308,309*f*,311  
mean square radius of gyration vs. salt concentration, 305–307,309*f*  
polyelectrolyte preparation, 302–303  
reliability, 298–299,312,313*f*  
second virial coefficient, 300–301  
solution preparation, 302–303  
studies, 297–298
- Light scattering of polyelectrolyte complex formation  
concentration dependence, 219–223*f*  
data analysis for dynamic light scattering, 214,216–217  
data analysis for static light scattering, 212–215*f*  
degree of conversion, 217–219  
experimental materials, 211*t*  
light scattering procedure, 211–212
- Linear flexible polyelectrolytes in salt-free solution using light scattering  
concentration vs. behavior  
  fast diffusive mode, 330–333*f*  
  scattered light intensity, 332,334*f*,335  
  slow diffusive mode, 330–333*f*  
dynamics associated with fast diffusion coefficient, 325–328*f*  
dynamics associated with slow diffusion coefficient, 326–330  
experimental procedure, 323,325,326*f*  
molecular weight vs. behavior, 325–330  
theoretical models of behavior, 323–324
- Liquid–solid interface, structure and stability of weakly charged polyelectrolytes, 421–434
- Local screening parameters, definition, 4–5
- Long spheroid, electrophoresis, 76–77
- Low-angle laser light scattering–gel permeation chromatography, molecular weight distributions of water-soluble polyelectrolytes, 131–142

Low ionic strength buffers, quasi-elastic light scattering by polyelectrolytes, 98–111

Low salt concentration, viscometric behavior effect for sodium polygalacturonate, 317–319

Luminescence quenching, microdomain size determination of hydrophobic polyelectrolytes, 154–160

Lumped parameter model, mechanical behavior of gel fiber, 526–528*f*

Lysozyme, interaction with acrylic polyampholyte, 264,266*f*

## M

### Macro-ionic systems

attraction between identical macro-ions, 11–12

counterion condensation, 8–10

electrostatic persistence length, 12–13

Gibbs vs. Helmholtz free energy, 10–11

pairwise electrostatic energy, 5–7

screening parameter, definition, 3–4

slow modes in dynamic light scattering correlation function, 13–19

Macromolecular actuators, biomimetic, *See* Biomimetic macromolecular actuators

Macromolecular complex coacervation, 226

Manning distance, definition, 10

Manning theory, description, 8

Masses, distribution in randomly branched polyelectrolytes, 46–47

Matrix orientation in pulsed electric fields, gel structure effect, 479–491

Mean square distances, perturbative approach to polyelectrolyte configuration, 40–43

Mechanochemical system, definition, 507

### Microactuators

applications, 519

classes, 519,520*t*

conducting polymers, 520

piezoelectric polymers, 519–521*f*

polymer gels, 520,522

requirements, 519

Microdomain size determination of hydrophobic polyelectrolytes by luminescence quenching experimental procedure, 155–156

luminescence quenching, 157–140*t*

micelle size and related parameters, 158–160*t*

Microdomain size determination of hydrophobic polyelectrolytes by luminescence quenching—*Continued*

parameters of sample run, 158,159*t*

previous methods, 155

solubilization of quencher, 156,157*t*

Mixed polyion system with no added salt, *q*-dependent apparent diffusion coefficient, 101,102*t*

Mixtures of entities having opposite charges, 381

### Molecular actuators

microactuators, 519–522

nanoactuators, 518–519,521*f*

Molecular-based transducers, advantages, 517

Molecular dynamics simulations of charged polymer chains from dilute to semidilute concentrations

chain length independence, 60,62*f*

comparison of scaling predictions, 63,64*f*

comparison of simulation results to experimental results, 59–61*f*

form factor vs. monomer density, 63,65*f*

polyelectrolyte structure, schematic representation, 63,65*f*,66

saturation density, 60,63

simulation method, 58

theoretical models, 59

transition from stretched to coiled conformation, 60,64*f*

typical polymer configurations, 60,62*f*

Molecular weight characterization of polyelectrolytes, difficulties, 162

Molecular weight distributions of water-soluble polyelectrolytes using gel permeation chromatography—low-angle laser light scattering

diallyldimethylammonium chloride, 134,135*t*,138–140*f*

epichlorohydrin–dimethylamine results, 132–134,136–138

experimental procedure, 132,133*t*

intrinsic viscosity vs. weight-average

molecular weight, 134,140*t*,141*f*

linear correlation coefficient, 134,140*t*

Mark–Houwink constants, 134,140*t*

salt effect, 142

solvent effect for epichlorohydrin–dimethylamine polymers, 134,135*t*

- Molecular weight distributions of water-soluble polyelectrolytes using gel permeation chromatography–low-angle laser light scattering—*Continued*  
 solvent system selection, 142  
 scattering system parameters, 132,133†
- Motor redundancy, representing and regularizing, 529
- Multivalent cation role in DNA condensation  
 aggregation mechanism, 201–202  
 alcohol effect, 202–206  
 condensed particle effect, 196  
 cross-linking, 200–201  
 electrostatic force effect, 199  
 hydration structure force effect, 200  
 kinetic effect, 206  
 multivalent cation–DNA interaction, 196–199  
 reasons for study, 196  
 substance types involved, 195–196
- Multivalent salts, phase diagram of polyelectrolyte solutions, 381–391
- Muted diffusion coefficient, definition, 13
- Myosin sliding machines, description, 519
- N**
- Nanoactuators  
 development, 518  
 flagellar rotary motor, 518,521f  
 myosin sliding machines, 519
- Nematic phase, undulation-enhanced forces in hexagonal gels of semiflexible polyelectrolytes, 87–88
- Neutral polymers, adsorption on model colloid particles by electrooptics, 436–446
- Nonstoichiometric complex formation of bovine serum albumin–poly(dimethyldiallyl ammonium chloride)  
 complex diameter vs. polymer concentration, 234,235f  
 electrophoretic light scattering, 230,236–238  
 experimental materials, 227  
 formation and coacervation, mechanism, 238–241  
 ionic strength vs. turbidity, 231–233f  
 mass ratio vs. turbidity, 231,232f  
 optical microscopic procedure, 231  
 pH vs. turbidity, 231,232f
- Nonstoichiometric complex formation of bovine serum albumin–poly(dimethyldiallyl ammonium chloride)—*Continued*  
 quasi-elastic light scattering procedure, 228–229  
 sample preparation procedure, 227  
 static light scattering, 229–230,234,236†,237  
 studies, 227  
 turbidimetric titration procedure, 227–228
- Nonuniformly charged chains, geometries, 68,69f
- O**
- Oligomeric poly( $\beta$ -alanine), water-soluble vinyl terminated, *See* Water-soluble vinyl-terminated oligomeric poly( $\beta$ -alanine)
- Oosawa–Manning theories, 8–10
- Osmotic pressure, evaluation for polyelectrolyte chains in swollen gels, 505–506
- Outer region, definition, 4
- P**
- Packaging of DNA and RNA in viruses, need for understanding of condensation mechanisms, 196
- Pairwise electrostatic energy between macro-ions  
 Gibbs free energy, 7  
 Helmholtz free energy, 5–7  
 pairwise interaction potential, 7
- Passive motion paradigm, description, 529
- Persistence length, electrostatic, *See* Electrostatic persistence length
- Perturbative approach to polyelectrolyte configuration  
 configuration-dependent part of Hamiltonian, 35–36  
 experimental description, 35  
 mean square distances, 40–43  
 numerical results, 40–43  
 polyion structures, 35  
 renormalized exponents, 40,41†  
 scaling exponents, 40–42f  
 self-consistent perturbation approach, 36–40
- pH, swelling equilibria effect for cationic polyelectrolyte gel from polyethylenimine, 493–498

Phase diagram, ionic colloidal crystals, 364–380

Photoinduced electron transfer, amphiphilic polyelectrolyte–surfactant coulombic complexes, 252,254–255

Piezoelectric polymers, use as actuators, 519–521f

Pin-down phenomenon, description, 467

Poisson–Boltzmann cell theory equation, 26,422–423  
shortcomings, 24–25

Polyacrylamide gels, birefringence, 488–490

Polyacrylamide-*co*-sodium acrylate characterization, 162–176  
preparation, 162

Polyacrylate gels, characterization methods, 499

Poly( $\beta$ -alanine), water soluble vinyl terminated oligomeric, *See* Water-soluble vinyl-terminated oligomeric poly( $\beta$ -alanine)

Polyamine–epichlorohydrin applications, 394  
molecular and mechanical properties, 395–405

Poly(aminoamide)–epichlorohydrin applications, 394  
molecular and mechanical properties, 395–405

Polyampholytes, acrylic  
*See* Acrylic polyampholyte(s)  
*See* Acrylic polyampholyte–protein interaction

Poly(dimethyldiallyl ammonium chloride)–bovine serum albumin, stoichiometric and nonstoichiometric complex formation, 225–241

Polyelectrolyte(s)  
adsorption, 421  
adsorption on model colloid particles by electrooptics, 436–446  
counterion condensation, 8–10  
difficulties in studying, 57  
dilute solution properties using light scattering, 297–313  
electric transport in aqueous salt-free solutions, 180–193  
electrolyte ions and attraction between identical macro-ions, 11–12  
electrostatic persistence length, 12–13  
Gibbs vs. Helmholtz free energy, 10–11

Polyelectrolyte(s)—*Continued*  
hydrophobic, 154–160  
linear flexible, *See* Linear flexible polyelectrolytes in salt-free solution using light scattering  
need for simulations, 57–58  
pairwise electrostatic energy between macro-ions, 5–7  
quasi-elastic light scattering in low ionic strength buffers, 98–111  
screening parameter, 3–5  
semiflexible, *See* Semiflexible polyelectrolytes  
slow modes in dynamic light scattering correlation function, 13–19  
strongly charged, extraordinary behavior of salt-free solutions, 337–348  
thermosetting cationic, *See* Thermosetting cationic polyelectrolyte properties  
understanding fundamental interactions between macro-ions, 1

Polyelectrolyte adsorption and stability of latex suspensions  
adsorption  
layer thickness vs. polymer concentration, 414,415f  
vs. adsorbed amount, 414,415f  
vs. critical micelle concentration, 410,411f  
vs. electrolyte concentration, 412,413f  
vs. molecular mass, 410,411f,412  
density of adsorbed layer vs. NaCl concentration, 414,415f  
electrokinetic potential, 416–418f  
experimental procedure, 407–410  
maximum adsorbed amount vs. NaCl concentration, 406  
stability, 417–419  
studies, 406–407  
thickness vs. salt sample, 416

Polyelectrolyte chains in swollen gels  
apparent cooperative diffusion constant vs. scattered light intensity, 502,504,505f  
comparison with (carboxymethyl)dextran gel study, 504  
dynamic light scattering study, 502,504,505f  
expansion behavior of gels, 501–503f  
experimental procedure, 501  
gel volume determination, 500  
osmotic expanding force determination, 500–501  
osmotic pressure, evaluation, 505–506

- Polyelectrolyte complex formation  
influencing factors, 210  
light scattering studies, 210–223
- Polyelectrolyte configuration, perturbative approach, 34–43
- Polyelectrolyte conformation, randomly branched, *See* Randomly branched polyelectrolyte conformation
- Polyelectrolyte gel(s)  
composition, 493–494  
polyethylenimine, cationic, pH and alkyl sulfate surfactant effects on swelling equilibria, 493–498  
use in construction of biochemo-mechanical systems, 507–514
- Polyelectrolyte–protein complexes  
applications, 225–226  
stoichiometric and nonstoichiometric complex formation, 225–241  
studies, 226–227
- Polyelectrolyte solution(s)  
behavior, theoretical models, 323–324  
cluster size determination by small-angle neutron scattering, 349–362  
description, 323  
experimental observations on salt-free solutions, 323  
interparticle interference peak in small-angle X-ray and neutron scattering curves, 349  
salt concentration vs. behavior, 337–338  
salt vs. behavior, 323  
two-state structure, 349  
types of interactions, 337
- Polyelectrolyte solution(s) in multivalent salts  
phase diagram, 381–391  
solutions, 337–348
- Polyelectrolyte solution phase diagram in multivalent salts  
effective degree of ionization vs. salt polymer concentration ratio, 388–391  
experimental procedure, 382  
factors affecting phase separation, 388  
fraction of free ions vs. salt–polymer concentration ratio, 388,390f,391  
intensity vs. salt concentration, 382–384f  
molecular weight vs. salt concentration, 383,385f  
polymer concentration vs. salt concentration, 383–385f
- Polyelectrolyte solution phase diagram in multivalent salts—*Continued*  
salt concentration vs. phase diagram, 383,386–388
- Polyelectrolyte–surfactant complex solutions, electrical transport, 268–274
- Polyethylenimine, pH and alkyl sulfate surfactant effects on swelling equilibria for cationic polyelectrolyte gel, 493–498
- Polyion, cylindrical, ion–ion correlations in electrical double layer, 24–33
- Polyions with added electrolyte, *q*-dependent apparent diffusion coefficient, 100–102f
- Polymer(s), neutral, adsorption on model colloid particles by electrooptics, 436–446
- Polymer chains, charged, molecular dynamics simulations, 57–66
- Polymer–colloidal complexes, electrophoresis, 70–73
- Polymer concentration, role in polyelectrolyte complex formation, 210–223
- Polymer gels, use as actuators, 520,522
- Polymer theory, conventional model, 34–35
- Polymeric materials, medical and veterinary applications, 449
- Poly(styrene–acrolein) latex(es), 450
- Poly(styrene–acrolein) latex–solvent interfaces, behavior of proteins, 449–462
- Poly(styrenesulfonate-*co*-styrene) solutions, structure, 278–285
- Poly(styrenesulfonic acid)–cetylpyridinium complex solutions, electrical transport, 268–274
- Porod analysis, cluster size determination in polyelectrolyte solutions, 355–357
- Precipitation, description, 226
- Protein–acrylic polyampholyte interaction, *See* Acrylic polyampholyte–protein interaction
- Protein(s) at poly(styrene–acrolein) latex–solvent interfaces  
dansylhydrazine as reporter molecules, 456–457,459f,461  
2,4-dinitrophenylhydrazine immobilization in surface layer of poly(styrene–acrolein) latexes, 451–453f  
experimental procedure, 450–451  
human serum albumin, competitive adsorption onto polystyrene latexes, 453,454f  
human serum albumin and  $\gamma$ -globulin attachment onto poly(styrene–acrolein) latexes, 454–456,461–462

Protein(s) at poly(styrene-acrolein) latex-solvent interfaces—*Continued*  
transformation due to protein-latex interaction, kinetics, 457–458,460–462

polystyrene and poly(styrene-acrolein) latexes, characteristics, 451,452*t*,455*f*

Protein-polyelectrolyte complexes

applications, 225–226

stoichiometric and nonstoichiometric complex formation, 225–241

studies, 226–227

Pseudomuscular gel actuators for advanced robotics

continuum models of electrochemomechanical response, 524–525

control strategies for motion of articulated chain, 527–529

hydrogel thin fibers, dynamical properties, 525–526

lumped parameter model of gel fiber mechanical behavior, 526–528*f*

mechanisms eliciting electromechanochemical response in polyelectrolyte gels, 522–524

motor redundancy, representation, 529

Pulsed electric fields, gel structure effect on matrix orientation, 479–491

## Q

*q*-dependent apparent diffusion coefficient

linearized form, 101,103

modified form vs. cell model, 104–105

polyion system with no added salt, 101,102*t*

polyion(s) with added electrolyte, 100–102*t*

series expansion representation, 101

Quasi-elastic light scattering, description, 98

Quasi-elastic light scattering by polyelectrolytes in low ionic strength buffers

bovine serum albumin characterization procedures, 105–107,109*t*

composite diffusion coefficient vs. cell model, 103–104

dialysis bag preparation procedure, 105

electrolyte concentration vs. volume fraction coefficient, 110,111*f*

experimental description, 98

generalized diffusion equation

interacting hard sphere systems, 99

small ion-polyion coupled modes, 99–102*t*

Quasi-elastic light scattering by polyelectrolytes in low ionic strength buffers—*Continued*

KCl effect, 108,109*t*

light scattering measurement procedure, 106–107

linearized form of *q*-dependent apparent diffusion coefficient, 101,103

modified form of *q*-dependent apparent diffusion coefficient vs. cell model, 104–105

osmometry procedure, 106,109*t*

pH effect, 108,111*f*

series expansion representation of *q*-dependent apparent diffusion coefficient, 101

theoretical prediction, comparison with simplified mathematical models, 107

viscometry procedure, 106

## R

Randomly branched polyelectrolyte conformation

approximations, 46

concentrated regime, 53,54*f*

dilute solutions, 47–49

distribution of masses, 46–47

experimental description, 46

screening of electrostatic interactions, 49–52

semidilute regime, 52–54*f*

studies, 45

validity, 54–55

Randomly branched polymers, studies, 45

Ribonuclease, interaction with acrylic polyampholyte, 264,265*f*

Robotics, pseudomuscular gel actuators, 522–529

Rotational diffusion coefficient, definition, 438–439

## S

Salt-free polyelectrolyte solutions

experimental observations, 323

extraordinary behavior, 337–348

linear flexible polyelectrolytes, structure and dynamics, 322–335



- Scaling exponents, perturbative approach to polyelectrolyte configuration, 40–42f
- Scattered light intensity, definition, 504
- Screening effects, influencing factors, 45–46
- Screening of electrostatic interactions, randomly branched polyelectrolytes, 49–52
- Screening parameter  
definition in macro-ionic systems, 3–4  
global parameter, 4  
local parameter, 4–5  
role in electrical interactions, 5
- Second concentration, characterization of screening effects, 45–46
- Second virial coefficient, description, 300–301
- Self-consistent field theory, description, 422
- Semidilute regime, randomly branched polyelectrolyte conformation, 52–54f
- Semidilute solutions of highly charged polyelectrolytes, structure studies, 278–279
- Semiflexible polyelectrolytes  
definition and examples, 86  
undulation-enhanced forces in hexagonal gels, 86–96
- Single polyion species with no added salt,  $q$ -dependent apparent diffusion coefficient, 101
- Size exclusion chromatography of polyacrylamide-*co*-sodium acrylate  
charge density vs. elution volume, 172,173f  
comparison to light scattering data, 172,175t,176f  
elution volume and molecular weight of polyacrylamide, 169,170f  
hydrodynamic volume and elution volume of polyacrylamide and polyacrylamide-*co*-sodium acrylate, 169,171f,172  
molecular weight vs. elution volume, 172,174f
- Slender particles  
chain of equal size sphere, 78–82  
geometry, 73–75  
hydrodynamics, 75–76  
long spheroid, 76–77  
straight circular cylinder, 77–78  
torus, 81,83–85
- Sodium acrylate-*co*-polyacrylamide, characterization, 162–176
- Sodium polygalacturonate, low salt content vs. viscometric behavior, 315–320
- Sogami–Ise theory, interactions between macro-ions, 2–3
- Solid–liquid interface, structure and stability of weakly charged polyelectrolytes, 421–434
- Solvent–poly(styrene–acrolein) latex interfaces, behavior of proteins, 449–462
- Specific Kerr constant, calculation, 480
- Stability, weakly charged polyelectrolytes at solid–liquid interface, 421–434
- Stability of polyelectrolytes, latex suspension effect, 406–419
- Static light scattering for dilute solution properties of polyelectrolytes, *See* Light scattering for dilute solution properties of polyelectrolytes
- Static structure factor, weakly ionized poly(acrylic acid) in deuterated water, 289–291f
- Steady field electrophoresis in agarose gel, applications, 466
- Stiff polyelectrolytes, electrostatic persistence length, 12–13
- Stoichiometric complex formation of bovine serum albumin–poly(dimethyldiallyl ammonium chloride)  
complex diameter vs. polymer concentration, 234,235f  
electrophoretic light scattering, 230,236–238  
experimental materials, 227  
ionic strength vs. turbidity, 231–233f  
mass ratio vs. turbidity, 231,232f  
mechanism of formation and coacervation, 238–241  
optical microscopic procedure, 231  
pH vs. turbidity, 231,232f  
quasi-elastic light scattering procedure, 228–229  
sample preparation procedure, 227  
static light scattering, 229–230,234–237  
studies, 226  
turbidimetric titration procedure, 227–228
- Straight circular cylinder, electrophoresis, 77–78
- Strongly charged polyelectrolytes, extraordinary behavior of salt-free solutions, 337–348
- Structure  
linear flexible polyelectrolytes in salt-free solution using light scattering, 322–335

Structure—*Continued*

weakly charged polyelectrolytes at solid–liquid interface, 421–434

Structure–dynamics relationship, water-soluble polymers, 287–295

Structure of poly(styrenesulfonate-co-styrene) solutions

added salt effect, 280,283f

charge content effect, 280,281f,284–285

counterion effect, 284–285

experimental procedure, 279–280

hydrophobicity effect, 285

polymer concentration effect, 280–282f,284 studies, 278–279

Surfactant(s), alkyl sulfate, swelling equilibria effect for cationic polyelectrolyte gel from polyethylenimine, 493–498

Surfactant–amphiphilic polyelectrolyte coulombic complexes, *See* Amphiphilic polyelectrolyte–surfactant coulombic complexes

Surfactant molecule–water-soluble polymer complexes, applications, 243

Surfactant–polyelectrolyte complex solutions, electrical transport, 268–274

Swelling equilibria for cationic polyelectrolyte gel from polyethylenimine

experimental procedure, 493–494

future work, 498

surfactant concentration vs. pH, 495f

swelling ratio vs. pH, 496–497f

swelling ratio vs. surfactant concentration, 496,497f

viscosity vs. pH, 494,495f

Swollen gels, polyelectrolyte chains, 499–506

Synthetic polyelectrolytes, use in protein separation, 257

## T

Temporal aggregate interpretation, class 3 profiles, 18–19

Thermosetting cationic polyelectrolyte properties

adsorption isotherms, 396,399f

adsorption isotherms vs. pH, 396,400f

cross-linking kinetics of films, 401,403f,404

curing time vs. wet–dry tensile strength ratio, 401,402f

Thermosetting cationic polyelectrolyte properties—*Continued*

experimental procedure, 395–396

<sup>1</sup>H-NMR spectra, 396,398f

initial resin dosage vs. wet–dry tensile strength ratio, 396,400f,401

pH vs. cationic charge densities, 396,399f

stress–strain behavior of film, 404f,405

structures, 396,397f

Thermosetting resins, 394

Torus

definition, 81

electrophoresis, 81,83–85

Transducers, limitations, 517

Transient electric birefringence, 479–480

Two-state structure, polyelectrolyte solutions, 349

## U

Uncharged surfaces, weakly charged polyelectrolyte structure and stability at solid–liquid interface, 432–434

Undulation-enhanced forces in hexagonal gels of semiflexible polyelectrolytes

cholesteric phase, 87–89f

experimental objective, 86

hexagonal phase, 88–92

isotropic phase, 87–89f

nematic phase, 87–89f

van der Waals forces, 92–96

Urease, use in biochemo-mechanical systems, 510–514

## V

van der Waals forces, undulation-enhanced forces in hexagonal gels of semiflexible polyelectrolytes, 92–96

Vinyl-terminated oligomeric poly( $\beta$ -alanine), water soluble, *See* Water-soluble vinyl-terminated oligomeric poly( $\beta$ -alanine)

Vinyl-terminated prepolymers, use in graft copolymer synthesis, 114–115

Viscoelastic properties, thermosetting cationic polyelectrolytes, 394–405

Viscometric behavior of sodium polygalacturonate  
dilution at low salt concentration, 317–319  
experimental procedure, 315–316  
ionic concentration vs. intrinsic viscosity, 319,320*t*  
isoionic dilution, 316–318*f*  
Viscometric characterization of polyacrylamide-*co*-sodium acrylate, Mark–Houwink equations, 166,169,170*f*  
Viscosity of charged macro-ions, shear rate effect, 98  
Volume of gels, factors, 493

## W

Water-soluble polymer(s)  
dynamics–structure relationship, 287–295  
factors affecting behavior, 287–288  
molecular weight distribution(s) using gel permeation chromatography–low-angle laser light scattering, 131–142  
molecular weight distribution vs. performance, 131  
Water-soluble polymer–surfactant molecule complexes, applications, 243  
Water-soluble vinyl-terminated oligomeric poly( $\beta$ -alanine)  
acrylamide dimer homopolymerization procedure, 117  
acrylamide dimer synthetic procedure,116–117  
bentonite suspension flocculation procedure, 117–118  
bentonite suspension flocculation using cationic poly(acrylamide dimer), 126,128,129*t*  
Water-soluble vinyl-terminated oligomeric poly( $\beta$ -alanine)—*Continued*  
characterization procedure, 117  
experimental description, 116  
kinetic measurement procedure, 117  
Mannich quaternary of poly(acrylamide dimer) formation, 126,127*t*  
poly(acrylamide dimer) formation, 121,126  
poly(acrylamide dimer) Mannich derivative preparation and quaterization procedure, 117  
solvent effect, 121,124*f*  
temperature effect on conversion of acrylamide to acrylamide dimer and oligomer, 121–124*f*  
VTN–3 oligomer preparation and synthesis, 116,118–120*t*  
Weakly charged polyelectrolyte structure and stability at solid–liquid interface  
approximate treatment for charged surface, 428,430–432  
charged surfaces, 423–432  
layer thickness for charged surface, 428,429*f*,431*f*  
numerical solution for charged surfaces, 424–426*f*,429*f*  
scaling analysis for charged surfaces, 425,427,428*t*  
theoretical formation, 422–423  
uncharged surfaces, 432–434  
Weakly ionized poly(acrylic acid) in deuterated water  
dynamic properties, 290,292–295  
experimental procedure, 288–289  
static structure factor, 289–291*f*

**American Chemical  
Society Library**  
1155 16th St., N.W.  
Washington, D.C. 20036